UNIVERSITY OF BIRMINGHAM

Advancing high-recovery desalination with free-piston batch reverse osmosis (RO) technology

by

Ebrahim Hosseinipour

The thesis submitted to the University of Birmingham

for the degree of

DOCTOR OF PHILOSOPHY

Department of Civil Engineering
School of Engineering
College of Engineering and Physical Sciences
University of Birmingham
November 2024

Abstract

Reverse osmosis (RO) dominates desalination industry, yet achieving high recovery is energy-intensive and costly. Batch RO represents a promising approach to desalination, theoretically capable of achieving minimum thermodynamic specific energy consumption (SEC) at high recovery rates. Its applicability covers various domains including brackish and seawater desalination, brine mining, solute recovery, and industrial effluent treatment. Nonetheless, rigorous pilot-scale experimental studies on batch RO performance are currently lacking. This thesis bridges this gap by conducting seven research studies using two free-piston batch RO systems in the laboratory. Each system utilizes an 8-inch spiral wound membrane module: one operates at pressures up to 25 bar, while the other reaches up to 120 bar. The research programme encompassed various feed solutions, including sodium chloride, sparingly soluble salts representative of groundwater, seawater, and metal plating wastewater. The system was adopted to operate in batch, semi-batch, and hybrid modes, allowing comparisons to be made among these modes. Experimental data were used to develop analytical models capturing key factors such as membrane characteristics, pump efficiencies, salt retention, and concentration gradient effects. The modelling was used to design systems at larger scale and using improved membrane and pump properties, demonstrating favourable performance compared to state-of-the-art semi-batch RO systems.

Keywords: Batch RO, High recovery, Energy efficiency, Scale-up, Membrane permeability.

DEDICATION

"I may not have gone where I intended to go, but I think I have ended up where I needed to be."

Douglas Adams

The Long Dark Tea-time of the Soul

This thesis is dedicated to my parents, **Mohammad and Setareh**, whose unwavering love, support, and belief in me have been the foundation of all my achievements. To my friends, whose encouragement and companionship have made this journey both meaningful and memorable—thank you for always being there.

ACKNOWLEDGEMENTS

I would like to express my deepest gratitude to Professor Philip Davies for his unwavering support, patience, and confidence in me over the years. The opportunities he provided to work with brilliant research teams and the supportive work environment he fostered have been invaluable. His guidance and professionalism are deeply woven into the fabric of this thesis, and I am especially indebted to him for his exceptional mentorship.

I would like to extend my sincere gratitude to the co-authors of the seven publications included in this thesis. Their insightful contributions and exceptional research skills have greatly enriched this work. I have strived to match their expertise and am deeply appreciative of the collaborative spirit that made these studies possible. Special thanks are extended to Salinity Solutions LTD, especially to Tim Naughton and Liam Burlace, for their invaluable support and contribution.

Finally, I am thankful to the European Union's Horizon 2020 research and innovation programme under grant agreement No 820906 and 958454, the UK Engineering and Physical Sciences Research Council (EPSRC, Grant Ref: EP/T025867/1) and the British Council Newton Fund Institutional Links programme (STDF project ID:42703). Their substantial support over several years has been crucial for transdisciplinary research, and I am confident that it has significantly enhanced the quality and impact of this thesis.

Contents

Lis of illustrations

1. Introduction

Water scarcity presents a pressing global challenge that is projected to escalate in the foreseeable future. More than two billion individuals lack access to safe and clean water sources [1]. The surge in population growth and subsequent agricultural demands have led to a twofold increase in water usage by humans in recent decades [2]. Moreover, rapid urbanization has exacerbated water stress by intensifying demand in populated settings [3] and polluting water bodies with industrial effluents [4]. Additionally, human-induced climate change is altering water availability patterns and heightening the likelihood of drought [5-7]. These combined contributors strain the world's water resources, impacting the availability of health and sanitation services, as challenges associated with sanitation continue to rise in parallel.

The growing strain on freshwater resources necessitates alternative methods of water supply, such as desalination. Desalination technology has emerged as a solution to address water scarcity by harnessing freshwater from non-conventional sources including seawater, brackish groundwater, and industrial effluents [8, 9]. With the relative abundance of these resources, desalination technology holds the potential to provide freshwater to fulfil municipal and irrigation requirements [10]. The increasing number of desalination plants globally is evidence of this trend, as they are constructed daily to alleviate freshwater scarcity. Desalination technology is poised for continued growth across numerous regions worldwide. Nevertheless, while desalination offers a reliable source of fresh, clean water, the disposal of rejected brine by-products poses environmental concerns [11].

Presently, the majority of desalination processes fall into two primary categories: thermal-based or membrane-based desalination processes. Thermal desalination involves the evaporation of salty water followed by converting the resulting steam into freshwater through condensation [2]. In membrane-based desalination, salts and minerals are removed from water solutions as they pass through a semipermeable membrane. In the past two decades, the cost-effectiveness and efficacy of membrane-based desalination have undergone substantial enhancements, owing to advancements in membrane technology, pumps, and energy recovery devices (ERDs) [12-14]. Consequently, membrane-based technology is swiftly replacing the older thermal methods such as multi-stage flash and multi-effect distillation, becoming the leading approach in desalination today. Membrane-based desalination represents more than 65% of the global desalination capacity and now dominates the seawater desalination market [15].

Reverse osmosis (RO) is the predominant membrane desalination technology. Thanks to its simplicity, scalability, and relatively high energy efficiency compared to other desalination methods, the RO process is widely utilized [2, 14, 16]. However, despite its efficiency, the specific energy consumption (SEC) of RO still exceeds significantly the theoretical minimum work of water-salt separation dictated by the second law of thermodynamics. This gap primarily arises from irreversibility linked to the high pumping pressure in continuous RO processes [8, 17, 18]. The necessity to consistently surpass the osmotic pressure at the system outlet, which is significantly higher compared to the inlet, contributes significantly to the elevated pumping pressure or energy consumption, particularly at high recovery rates.

Apart from the need for more energy-efficient RO systems, there is a huge drive for high recoveries ($r \geq 0.9$) in RO desalination, particularly in waste and brackish water for the following key reasons:

- Water conservation and reuse: High recovery RO is essential for conserving water sources, particularly in scenarios where resources are limited, such as groundwater, industrial effluents, and other finite supplies. By maximizing water recovery, this process supports sustainable water management and reduces the strain on these critical resources.
- Environmental Benefits: Conventional desalination processes produce a significant amount of high-salinity waste brine, which is difficult to dispose of. High recovery RO contributes to environmental protection by reducing waste and minimizing the discharge of pollutants. This aligns with stricter wastewater regulations and supports sustainable practices in water management.
- Lowering costs: High recovery desalination technologies aim to maximize the amount of fresh water produced from a given volume of feed water. This reduces the costs associated with intake, pretreatment, and brine disposal infrastructure, lowering overall desalination expenses.
- Energy efficiency: Desalination is an energy-intensive process. By increasing the recovery rate, the amount of energy required for the pre-treatment is reduced, improving the overall energy efficiency and sustainability of the process. Additionally, by minimizing concentrate volume, high recovery RO systems reduce energy consumption and operational costs, which is crucial in energy-intensive industries like brine mining and nutrient valorization.
- Resource recovery: High recovery RO systems facilitate the extraction of valuable resources from wastewater streams. These resources can include nutrients, metals, and other valuable compounds that can be reused or sold, contributing to a circular economy. This process, known as waste valorization, helps offset the costs of wastewater treatment and reduces harmful discharges.
- Issues regarding inland applications: For inland brackish water desalination plants, high recovery is crucial to minimize the volume of concentrated brine that needs to be disposed of, as options like ocean discharge are not available. The rejected brine must be disposed in accordance with local ordinances, via means including sewer discharge, deep-well injection, evaporation ponds and so on [19]. Brine management is costly, especially in inland areas. Thus, increasing the recovery rate not only enhances the water supply but also reduces the brine volume.

Brackish water, with its lower salinity compared to seawater, enables a significantly higher recovery rate before reaching saturation; for instance, recovery of $r = 0.8–0.85$, utilizing 2-3 stages compared to $r = 0.35–0.5$ for seawater [14]. Increasing the recovery to $r > 0.9$ enhances water supply and substantially cuts brine management expenses, which can exceed the energy costs for pumping in inland locations [20]. Nevertheless, in certain situations, the potential for scaling by sparingly soluble minerals (e.g., $CaCO_3$, $CaSO_4$, $BaSO_4$, $SrSO_4$, CaF_2, and SiO_2) in the feed may limit the recovery rate [21-23].

Seawater desalination is vital for freshwater production, with predicted supply expected to reach 192 million m^3/day by 2050. However, the discharge of seawater brine, estimated at 51.7

billion m^3 annually, raises environmental concerns. The brine rejected by seawater RO desalination systems typically includes a variety of salts and ions, with concentrations around ~70,000 mg/L (assuming a recovery rate of $r = 0.5$) [24]. Recent advancements in resource recovery technology offer economic benefits by extracting valuable minerals from this brine [25]. This approach not only reduces production costs (by creating extra revenue through the extraction of valuable minerals) and environmental impacts but also provides an alternative to land-based mining, which encounters sustainability concerns [26, 27]. Moreover, the cost of mining has significantly increased. Yet, cost-effective extraction of minerals from seawater RO brine remains a challenge, necessitating strategies to increase recovery rates in seawater RO desalination. Achieving high recovery enhances mineral extraction feasibility by increasing the concentration of minerals in the brine stream, thereby making the process more economical [28]. It also boosts freshwater production.

In addition to traditional desalination applications, there are other industries with unique processes that demand high recovery rates. Waste valorization is such an example which aims to convert waste into valuable resources that can be reused or sold. Resource recovery helps offset the cost of wastewater treatment by extracting valuable materials from waste streams. This process reduces harmful discharges and supports a circular economy by turning waste into resources. For instance, the metal plating industry generates wastewater containing toxic components that exceed permissible discharge limits. Despite the high costs associated with chemical usage and disposal, electroplating facilities are exploring methods to recover and reuse these components [29]. Current approaches are chemical- and energy-intensive and only remove components from wastewater without facilitating reuse. Given the high osmotic pressure of this specialized wastewater and the need for a high concentration factor of components for reuse, RO systems capable of achieving very high recoveries ($r > 0.9$) are essential. Other applications include the treatment processes in the semiconductor [30] and textile industries [31], as well as mineral recovery, such as lithium extraction [32-34], which are of significant interest in high-recovery desalination methods.

2. High recovery desalination

As explained in the previous section, high recovery desalination is gaining interest in various application domains including brackish groundwater to preserve the limited groundwater resources, seawater desalination to increase water production as well as using brine mining and mineral recovery. In industrial settings, they constitute a critical component of Zero or Minimal Liquid Discharge (ZLD/MLD) systems Focused on preventing environmental harm caused by brine discharges [8, 9]. However, high recovery often leads to elevated energy consumption [10, 11]. Hence, urgent efforts are needed to create solutions that combine high recovery with energy efficiency including continuous multi-stage RO, semi-batch and batch RO.

2.1. Conventional continuous RO systems

In a continuous single-stage RO system, the osmotic pressure is consistent over time, increasing along the length of the RO membrane. The applied feed pressure must exceed the brine osmotic pressure, which is much higher than that of the feed. This results in an unbalanced system where the permeate flux is significantly higher at the front compared to the back of RO systems. A more balanced system, like a continuous multi-stage RO, can generate the same quantity of fresh water with less energy [35, 36].

Continuous single-stage RO operates far from the optimal condition due to relatively constant feed pressure and permeate pressure along the channel length (see Fig. 1). While the pressure difference remains relatively constant, the osmotic pressure of the feed stream increases as it becomes more concentrated along the length of RO module, while the osmotic pressure of the permeate is nearly zero. Thus, according to the solution-diffusion model, the driving force for pure water flux ($\Delta P - \Delta\pi$) peaks close to the inlet and decreases constantly along the membrane length [37]. This results in a gradual decrease in flux along the membrane length, leading to increased entropy generation and reduced energy efficiency [35].

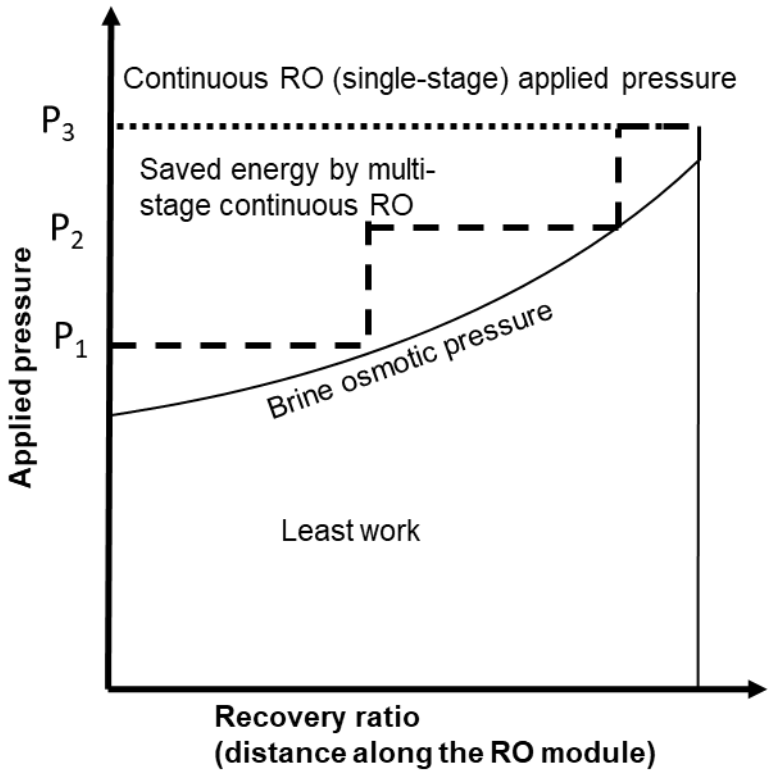

Fig. 1. Illustration of the theoretical minimum energy required for desalination (represented by the area under the brine osmotic pressure curve), compared to a single-stage continuous RO system (where the area under the dashed line P3 represents the applied e energy), and a three-stage continuous RO system, which conserves energy by optimizing pressure at each stage.

To achieve a more uniform distribution of membrane flux, multi-staging the RO process is a viable approach. Multi-stage RO is frequently utilized for high-recovery brackish water desalination [36]. In multi-stage RO, the retentate from each stage serves as the feed stream for the subsequent stage (see Fig. 2). In this method, the feed pressure is initially adjusted to a low value under conditions of low feed salinity. Subsequently, booster pumps are employed in subsequent stages to increase the feed pressure as the salinity of the feed stream increases. Following the final stage, in many cases the ERD retrieves the remaining pressure energy from the final brine to optimize energy efficiency. In theory, an infinite multi-stage RO setup would eliminate irreversible work (exergy destruction). However, this is impractical due to the enormous capital cost associated with such a system [8].

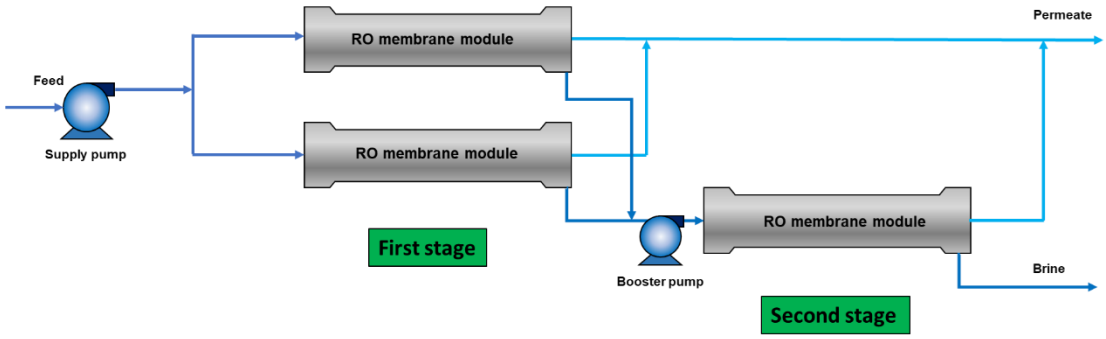

Fig. 2. Schematic of a multi-stage RO design (2-stage).

Designing a continuous multi-stage RO with a recovery rate exceeding about 0.9 presents significant challenges. As the recovery (r) approaches 100%, the concentration factor (CF) and osmotic pressure escalate. For instance, an increase in recovery from 0.8 to 0.95 leads to a rise in CF from 5 to 20 as CF = 1/(1-r). Assuming a 5000 mg/L of NaCl feed solution corresponding to the osmotic pressure of approximately 4 bar, brine osmotic pressure increases from 20 to 80 bar (assuming 100% salt rejection). Moreover, the lead elements in the first stage experience higher fluxes, which can intensify concentration polarization and fouling. Conversely, elements in the final stage contribute significantly less to total permeate output as the hydraulic pressure could only marginally exceed the brine pressure. One approach to mitigating flux variations at ultra-high recoveries like 0.95 is to increase the number of stages, potentially up to 4 or 5, and incorporate interstage booster pumps. As a result, although multi-stage configurations are effective in reducing energy consumption and achieving high water recovery, they come with drawbacks such as the need for a larger membrane surface area, additional high-pressure pumps, pressure vessels, valves, piping, process control-related equipment, and increased system footprint and capital cost [38]. Moreover, in small-scale RO applications, the practicality of multi-stage configurations, considering the system size and the needed number of membrane elements, can be challenging and costly [39].

In a traditional steady-state multi-stage RO design, the RO elements at the end of the system encounter the highest concentration of minerals and salts, including gypsum, calcite and silica persistently, unless interrupted by clean-in-place (CIP) or permeate flushing. Relying solely on antiscalants at high recovery rates is often insufficient, as they only delay salt precipitation rather than prevent it, and overdosing can exacerbate fouling issues [40]. An alternative approach to mitigate scaling at ultra-high recoveries is through transient and cyclic operations, such as semi-batch RO, batch RO, and flow reversal RO. These non-steady processes include cyclic phases, typically involving a pressurization (production) phase followed by a shorter purge (flushing) phase [41, 42]. This method is ideal for attaining high recovery while keeping the system footprint to a minimum [39, 43]. These processes can reach recoveries as high as 0.98, limited by the feed water's scaling potential and the membrane’s operational pressure constraints [44].

2.2. Semi-batch RO

A semi-batch RO configuration has been proposed as an alternative to an infinite multistage RO system for high recovery desalination [45]. The schematic diagram of the semi-batch RO is shown in Fig. 3. The semi-batch RO is a cyclic process with a filtration step followed by a brief purging step. During filtration, the brine stream is fully recycled and mixed with the raw feed, requiring increased pressure over time to maintain a positive driving force as feed salinity rises. The permeate rate matches the raw feed rate (100% recovery). After reaching the desired permeate amount, a short flushing step purges the concentrate solution trapped in the membranes, and the cycle repeats. The system uses a recirculation pump to boost the retentate pressure and supply it to the RO system without employing ERDs [46].

The semi-batch RO process offers multiple benefits compared to traditional RO systems, including reduced energy consumption, higher recovery rates, increased resistance to fouling and scaling, and optimal operational flexibility [44]. The relatively stable flow and flux conditions of semi-batch RO are especially beneficial for ultra-high recovery applications [47]. Additionally, research indicates that semi-batch RO is less prone to fouling than traditional steady-state systems, as the cycle duration is shorter than the crystallization induction time for most sparingly soluble salts [48]. Furthermore, a semi-batch RO can replicate the benefits of a multistage RO system without the need for complex installations, leading to reduced capital costs compared to traditional multistage configurations [49].

Several studies have explored the practical feasibility and energy efficiency of the semi-batch RO process [39, 42, 50-53]. Traditional brackish water RO systems with high recovery rates often do not feature ERDs because of their high capital costs and limited return on investment. Consequently, semi-batch RO has emerged as a competitive alternative for energy-efficient brackish water desalination at high recovery rates [39, 52]. However, the mixing of low-salinity feed with high-salinity concentrate leads to undesired entropy generation and negatively impacts the energy efficiency of semi-batch RO systems [54]. Its effect on energy usage becomes more pronounced with higher recovery rates [55]. As a result, the suitability of semi-batch RO for seawater desalination remains uncertain. While pilot tests have been conducted with seawater feeds, a full-scale implementation of semi-batch RO for seawater RO has not yet been realized [49].

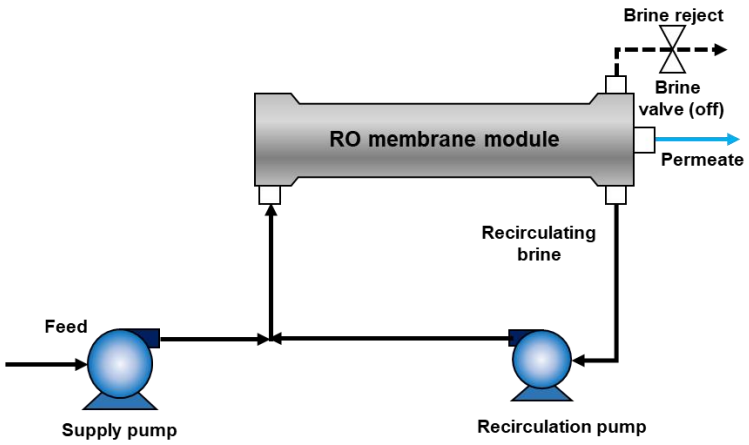

Fig. 3. Schematic of a standard semi-batch RO design.

2.3. Batch RO

The batch RO system has emerged as a leading candidate for reducing the irreversibility linked to the high applied pressures utilized in continuous RO systems. The anticipated expansion of batch RO as an expanding area of research is fuelled by the demand for novel approaches aimed at reducing SEC, enhancing recovery rates, and mitigating fouling risks across diverse applications.

Theoretically, the batch RO process achieves the lowest practical energy consumption [54]. Conventional single-stage continuous RO applies a uniform pressure to the feed solution to provide the necessary driving force for water permeation. This constant pressure operation results in inevitable irreversible exergy loss in the membrane module, causing increased energy usage. In contrast, batch RO minimizes this loss by gradually increasing pressure in response to changing feed concentration over time [56]. The high-pressure pump starts with low pressure at the beginning of the batch RO process and incrementally increases it as the salinity of the feed inside the system rises [41]. Unlike continuous RO systems, this process maintains a balanced permeate flux over time. In an ideal batch RO process, achieving a uniform permeate flux over space is desirable but not practically achievable. However, considerable energy savings can still be obtained if the variation in osmotic pressure (and consequently flux) along the length of a RO membrane module is minimized [43].

An illustrative diagram of the batch RO process showcases the fundamental features of a batch RO system (see Fig. 4). It involves applying a constant net driving pressure to maintain a steady permeate flux. Additionally, a high-pressure, variable-volume tank is essential to accommodate the decreasing volume of saline solution. Stirrers are employed to mitigate the impacts of concentration polarization.

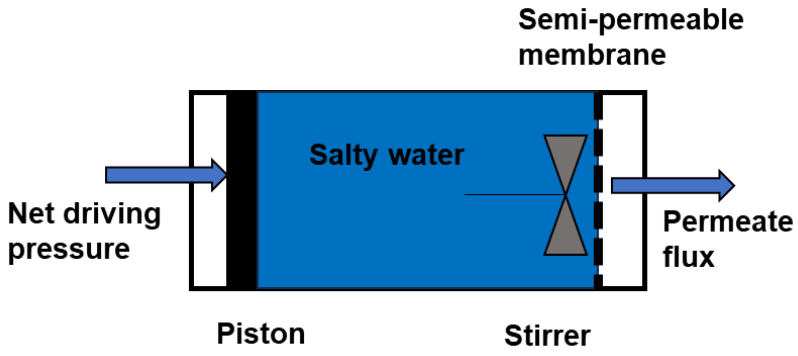

Fig. 4. Essential aspects of a free-piston batch RO system.

In practical batch RO designs, a recirculation pump generates crossflow, serving as the stirrer in the conceptual design [57, 58]. Without this pump, higher pressures would be needed to drive permeate flow because of salt buildup at the membrane surface, known as concentration polarization. This feature distinguishes batch RO from continuous RO systems, offering an additional operational aspect but also requiring extra energy [51, 54], which may offset potential energy savings of batch RO. Thus, optimization of the recirculation pump flow seems vital in terms of energy savings of batch RO systems. The utilization of a recirculation pump in batch RO offers flexibility in operating at various crossflow velocities, influencing levels of concentration polarization [58]. Unlike continuous RO, where maximum and minimum

crossflow velocities are dictated by initial feed flow and overall recovery ratio, in batch RO, the maximum crossflow velocity can be set by the recirculation pump flow rate, independent of initial feed mass and applied pressure. The minimum crossflow velocity typically occurs at the membrane module's end, yet in batch RO systems, it should approximate the maximum crossflow velocity due to the relatively low per-pass recovery ratio (i.e., high recirculation flow compared to the feed flow).

Most research on batch RO has been conducted primarily by groups at Aston University [18, 54, 58-60], followed by a continuation at the University of Birmingham [41, 43, 61], Yale University [42], Massachusetts Institute of Technology [48, 51, 62, 63], Purdue University [56, 64, 65], and California State Polytechnic University, Pomona [47, 55, 66]. This collective effort aims to advance the fundamental understanding and development of batch RO systems. The main distinction between semi-batch and batch RO designs lies in the former's use of undesired mixing between incoming feed and the recirculating brine solution already present in the system. In contrast, batch RO typically involves high-pressure vessels with variable volumes, which increases the complexity of both design and operation. Moreover, unlike traditional steady-state RO systems, in batch and semi-batch RO processes, raw feed is supplied to the RO unit under time-varying pressures.

So far, the main approaches to batch RO design have primarily involved either: (1) atmospheric vessels with ERDs [42, 62, 65], or (2) pressurized work exchanger vessels [41, 43, 54, 60, 63]. To the author’s best knowledge, the former design has not been put into practice yet. Nevertheless, theoretical investigations have indicated that batch RO utilizing atmospheric vessels with ERDs consumes more energy compared to pressurized vessels [65]. Energy is partially lost as the feed repeatedly passes through the ERDs, which have inherent inefficiencies [63].

To implement batch RO with a pressurized vessel, one approach involves utilizing a flexible bladder to partition the pressure vessel into two compartments. In their pioneering study, Wei et al. [63] constructed and operated the first batch RO prototype employing a flexible bladder in a bench-scale setup. They advocated for the bladder design over the piston design, claiming its ease of fabrication and reduced vulnerability to leaks.

Another proposed batch RO design utilizing a pressurized vessel involves a free piston, which partitions the vessel into two compartments [54]. One compartment contains the feed intended for treatment during the batch RO process, while the other starts empty. A pump introduces makeup fluid, such as water, into the empty compartment to initiate permeate production. This makeup fluid accommodates the reduction in feed volume and remains separated from the feed by the piston, thus avoiding direct interaction with the membrane. As the pressure vessel is already fully filled, pressure in both compartments rapidly increases because of water's near-incompressibility. Upon surpassing the feed osmotic pressure, permeate exits through the membrane, reducing the feed volume and causing the piston to move accordingly. Consequently, the makeup fluid flow rate approximately matches the permeate flow rate [54].

Batch RO is a cyclical process, and each cycle usually involves three phases: pressurization, purge, and refill. Pressurization initiates filtration or permeate production, gradually increasing the concentration of feed water until desired recovery rates are achieved. Subsequently, the purge phase flushes out the concentrate, replaced by feed water with lower salinity. The final

refill stage refills the batch of saline water [54]. Some designs enable simultaneous execution of stages [56, 60].

To facilitate the transition between stages, the batch-RO system relies on valves. Various implementations of free-piston batch RO designs, including single-acting 2- and 3-stage configurations as well as double-acting 4-stage configurations, were demonstrated in [59].

While batch RO offers theoretical efficiency advantages over continuous RO, a drawback is that some phases of the cyclic operation are not productive. Only the pressurization phase generates output, while subsequent purge and refill phases do not. Thus, in a comparison between batch and continuous RO with equal output per membrane area, batch processes will exhibit higher permeate water flux, leading to increased SEC and slightly diminishing the batch RO's advantage [41, 63]. Minimizing downtime associated with non-productive phases is crucial. Hence, simultaneous conduct of the purge and refill phases proves advantageous in reducing downtime [59]. Therefore, the two pilots used in this thesis were constructed based on single-acting 2-stage design (see Fig. 5). Yet, an even more favourable approach would involve operating in the double-acting mode rather than single-acting. In the double-acting free-piston batch RO design, the pressure exchange vessel operates with one side refilling while the other side is pressurizing. This setup ensures continuous output during the refill phase, leading to an increase in water output compared to single-acting design with an equivalent membrane area [60]. However, the complexity of operational control philosophy presents the main drawback of the double-acting mode compared to the single-acting [56].

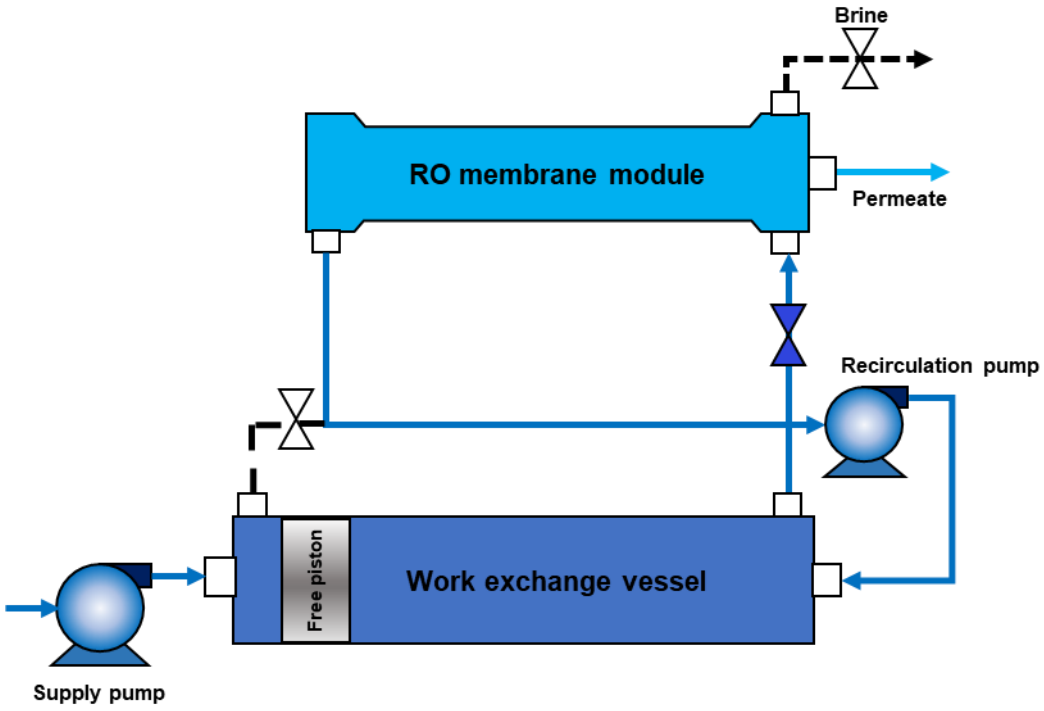

Fig. 5. Schematic of a single-acting free-piston batch RO system operating in 2 stages, incorporating pressurization and purge-and-refill, taken from paper 2.

Over the past decade, several modelling studies have focused on batch RO [41-43, 51, 56, 67], consistently highlighting its superiority in many applications, particularly at high recoveries. Firstly, it is theoretically the most energy-efficient technology, as the applied pressure closely follows the feed osmotic pressure. Secondly, batch RO can achieve very high

recoveries with a compact design. Lastly, it offers resistance against fouling and scaling through periodic flushing, salinity cycling, and osmotic backflow. While these theoretical studies have underscored the importance of this new RO configuration for energy savings and high recoveries in a compact design, experimental studies are essential. Such studies are necessary not only to refine and validate theoretical predictions but also to improve our understanding of the system's design and facilitate advancements for industrial applications. The primary goal of this technology is to address the limitations of conventional RO technologies, especially for specialized applications or remote areas that require low-energy, high-recovery RO desalination. This underscores the critical need for designing and constructing batch RO pilots and conducting rigorous experimental studies to mature the technology and prepare it for market adoption.

The essence of batch RO technology lies in maintaining pressure and energy at the lowest thermodynamic threshold possible during the separation process. However, achieving this ideal minimum is prevented by thermodynamic irreversibilities. Hence, a primary aim of this project is to quantify and comprehend the disparity between ideal and observed performance. This understanding will inform the conceptualization, implementation, and assessment of design improvements.

The review of the literature has revealed many theoretical studies of batch RO but only a few rigorous experimental studies. Moreover, despite the attractive simplicity of the single-acting free-piston design, there are few studies beyond preliminary laboratory studies that were not yet thoroughly characterised, modelled or validated [54, 59]. In this thesis, therefore, the author further investigated and developed the batch RO technology with a single-acting free-piston design through comprehensive experiments using two different pilots– one low and the other high pressure (see Fig. 6). These prototypes were employed to modify and validate theoretical models of energy consumption and water production. The thesis examined practical losses associated with free-piston batch RO operation to validate the model against experimental measurements. This included modifying the control philosophy of the system to enable experiments in different operational modes: batch, semi-batch, and hybrid semi-batch/batch. This approach allowed variable recovery rates, achieving values ranging from 0.66 to 0.99, depending on the feed concentrations. The results predict that the free-piston batch RO design is practical and efficient for achieving very high recoveries with energy efficiency in a very compact design compared to its counterparts, particularly for outputs ranging from 100 to 300 m^3/day. This technology could provide excellent solutions for various applications, including supplying safe drinking water to remote areas and irrigation water for agriculture where extensive piping networks are costly and impractical. It is also suitable for treating industrial effluents, where high concentration factors (i.e., substantially high recovery rates) are needed for component reuse. Additionally, it can be applied in areas such as mineral recovery from salt-lake brines (e.g., lithium and magnesium) and nutrient recovery from sources like animal waste.

(A)

(B)

Fig. 6. Photographs of the two pilot systems designed, built, modified, and used in this thesis. (A) Low-pressure single-acting free-piston batch RO system (maximum pressure: 25 bar), used in papers 1 to 4; (B) High-pressure single-acting free-piston batch RO system (maximum pressure: 120 bar), used in papers 5 to 7.

3. Objectives

The key aims of this thesis were to:

- Develop and enhance a single-acting free-piston batch RO system for achieving high recovery rates with energy efficiency.
- Create and validate an analytical model capable of predicting the performance of the free-piston batch RO, applicable for pilot design, system scaling, and assessing the performance of new membranes.
- Conduct a fair comparison between batch RO and semi-batch RO systems.
- Evaluate fouling and scaling mitigation strategies in cyclic processes like batch RO.
- Address the challenge of large work exchanger requirements in batch RO through the implementation of hybrid semi-batch/batch RO systems, aiming for Minimal Liquid Discharge (MLD) or Zero Liquid Discharge (ZLD).
- Implement high-pressure batch RO for seawater desalination applications.

I believe that the papers comprising this thesis have effectively fulfilled each of these goals.

4. Paper summaries

This thesis is built upon seven papers, which are reproduced with permission (refer to Appendix A). These papers primarily, though not exclusively, contribute to four key research initiatives:

- **European Horizon 2020 Funded Project: intelWATT (Grant agreement No: 958454):** Intelligent Water Treatment Technologies for water preservation combined with simultaneous energy production and material recovery in energy intensive industries (Case study 3: Simultaneous metal recovery and wastewater treatment in plastic electroplating production).
- **European Horizon 2020 Funded Project: INDIA-H_2O (Grant Agreement No: 820906):** Bio-mimetic and Phyto-technologies designed for low-cost purification and recycling of water. (Workpackage 1: Drinking Water from High Salinity Brackish Groundwater).
- **British Council Newton-Mosharafa funded project in collaboration with the Science and Technology Development Fund, Egypt:** Investigation and optimization of design parameters for reverse osmosis (RO) and photo-catalytic water desalination and treatment systems to protect groundwater.
- **Engineering and Physical Sciences Research Council (EPSRC) grant EP/T025867/ 1:** Batch Reverse Osmosis (RO): Desalination with minimum wastage of energy and water.

All seven papers are published in the Journal of *Desalination*. They are closely connected in terms of advancing the understanding and development of batch RO technology, particularly the free-piston design. A list of the papers and a short summary of them are as follows:

1. Hosseinipour E, Park K, Burlace L, Naughton T, Davies PA. A free-piston batch reverse osmosis (RO) system for brackish water desalination: Experimental study and model validation. Desalination. 2022 Apr 1;527:115524. https://doi.org/10.1016/j.desal.2021.115524.

2. Hosseinipour E, Davies PA. Effect of membrane properties on the performance of batch reverse osmosis (RO): The potential to minimize energy consumption. Desalination. 2024 May 18;577:117378. https://doi.org/10.1016/j.desal.2024.117378.
3. Hosseinipour E, Harris E, El Nazer HA, Mohamed YM, Davies PA. Desalination by batch reverse osmosis (RO) of brackish groundwater containing sparingly soluble salts. Desalination. 2023 Nov 15;566:116875. https://doi.org/10.1016/j.desal.2023.116875.
4. Hosseinipour E, Karimi S, Barbe S, Park K, Davies PA. Hybrid semi-batch/batch reverse osmosis (HSBRO) for use in zero liquid discharge (ZLD) applications. Desalination. 2022 Dec 15;544:116126. https://doi.org/10.1016/j.desal.2022.116126.
5. Karimi S, Engstler R, Hosseinipour E, Wagner M, Heinzler F, Piepenbrink M, Barbe S, Davies PA. High-pressure batch reverse osmosis (RO) for zero liquid discharge (ZLD) in a Cr (III) electroplating process. Desalination. 2024 Jul 1;580:117479. https://doi.org/10.1016/j.desal.2024.117479.
6. Hosseinipour E, Davies PA. Direct experimental comparison of batch reverse osmosis (RO) technologies. Desalination. 2024 Aug 19;583:117717. https://doi.org/10.1016/j.desal.2024.117717.
7. Hosseinipour, E., & Davies, P. Free-piston batch reverse osmosis (RO): Modelling and scale-up. *Available at SSRN 4854851*. https://doi.org/10.1016/j.desal.2024.117980.

Note that the papers are not necessarily summarized in chronological order of publication, as the order in which studies were conducted was not always the same as the order in which they were reported.

The focus of **paper 1** was to conduct in-depth experimental investigations on an automated free-piston batch RO system for the first time, building on previous works and designs [41, 54, 57-59]. The study aimed to achieve energy-efficient desalination of brackish water (NaCl solution of up to 5000 mg/L was used as a representative of brackish water) using a single-acting free-piston batch RO at a pilot scale with one 8-in RO membrane at a recovery rate of $r = 0.8$. It involved measuring the total hydraulic SEC to validate an updated model and, for the first time in batch RO research, precisely measuring electrical SEC for different salinities, water fluxes, and recirculation flow rates. Additionally, the study quantified salt retention, and osmotic backflow for the first time in batch RO studies, achieving higher output and recovery compared to previous experimental studies [54, 59, 63]. This pilot-scale system demonstrated significant progress towards practical applications of batch RO technology and greatly assisted in the design of the pilot for the INDIA-H_2O project, which was subsequently deployed in rural India.

Promising predictions suggest that the use of high-permeability membranes could enhance performance in batch RO systems [67, 68]. It was predicted that compared to continuous RO, high-permeability membranes have a greater effect on SEC reduction in batch RO, particularly at lower feed salinities and high recoveries. However, there was no experimental research in this area to prove the claim. Thus, **paper 2** addressed this gap by assessing a batch RO system with a selection of advanced RO membranes, including a newly introduced membrane using biomimetic aquaporin technology. Four 8-inch RO modules with low and high permeability were tested in a single-acting free-piston batch RO pilot. The study measured salt rejection and SEC to evaluate the trade-off between membrane permeability and selectivity. The study revealed a significant difference in osmotic backflow among high and low permeability membranes– this being the first time that backflow has been systematically quantified. The

findings provide insights into the potential SEC improvements achievable through enhanced membrane permeability, considering salt rejection, while also underscoring the limitations of current commercial membranes. Thus, it was predicted that up to a 30% reduction in SEC will be achieved when permeability is increased from about 5 (current brackish RO membranes) to 20 L/m²/h/bar.

To test the hypothesis that novel cyclic processes such as batch RO reduce fouling, as suggested by numerous studies [39, 48, 69], **paper 3** reports laboratory experiments using a free-piston batch RO pilot with features such as periodic flushing, osmotic backwash, feed flow reversal, and salinity cycling. These features have proven effective in mitigating fouling in various RO systems separately [70-73]. Unlike prior batch RO experiments, this study used feedwater prone to mineral scaling instead of only sodium chloride solution. The feed solution was simulated based on analysis of field samples taken from two locations in Egypt and India where desalination is needed to improve the poor quality of groundwater for drinking and irrigation applications. Key performance parameters, such as SEC, peak pressure, and rejection, were measured and compared to previous results with sodium chloride. The study showed no significant drop in membrane performance after testing the system with simulated groundwater, indicating effective scaling resistance. The system maintained functionality for over 100 hours of operation despite the high scaling potential, with a Langelier Saturation Index (LSI) for calcite reaching 2.6 in the brine. The paper also compared results to other research that employed similar anti-scaling methods in different RO systems. Nonetheless, it is essential to conduct long-term pilot testing using abundant sources of real feed water that are prone to different types of fouling encountered in the field.

Paper 3 had established that batch RO is highly suitable for high-recovery and energy-efficient desalination. However, a significant obstacle remained which was the sharp increase in system size when recovery exceeds about $r = 0.8$, due to the large volume required for the work exchanger vessel. To address this issue, **paper 4** introduces the hybrid semi-batch/batch RO concept, which allows for a much smaller work exchanger vessel volume at very high recoveries like $r = 0.95$, with only a minor increase in SEC. The primary goal of this paper was to experimentally validate this concept and update the modelling to enable the subsequent design of a high-pressure (120 bar) pilot for electroplating wastewater treatment. A series of experiments were conducted with different feed salinities (up to 1500 mg/L NaCl feed solution) and water fluxes, studying system performance metrics including hydraulic and electrical SEC, salt retention, permeate and batch conductivity variation, concentration factor, and recovery. Then the model was adjusted based on experimental findings to predict hybrid RO performance at higher salinities and pressures, beyond the 25-bar peak pressure limit of the pilot used in this study. These findings, thus, informed the design of the 120-bar system for electroplating wastewater treatment, which was designed to achieve ZLD by reusing both concentrate and permeate streams in the electroplating process.

Paper 5 concentrated on water reuse in the metal plating industry through the hybrid semi-batch/batch RO configuration, previously (paper 4) proven efficient for ZLD in **paper 4**. The goal was to develop and test a full-scale high-pressure high-recovery batch RO system for chromium recovery and water reuse in the electroplating industry. The main goals included: developing a 120-bar batch RO system to process chromium rinse water (diluted from chromium electroplating bath) simulated in the laboratory with an SEC of less than 2.5 kWh/m³ and achieving chromium concentration factors of 10-20; presenting a precise approach for

determining the switch point from semi-batch to batch phase in hybrid operation, necessary for process automation; measuring main performance parameters such as concentration factor, rejection of main electroplating compounds, pressure, SEC and permeate quality; and finally, assessing the fouling and durability of the RO membrane in this system, especially since substantial fouling was observed on the membrane surface in a continuous RO system study using the same feed solution. The system effectively recovered chromium to electrolyte bath levels, suitable for reuse in the electroplating process. Most species had a rejection rate of over 99.8%, making the permeate fit for reuse as rinse water. However, boric acid rejection was < 80%, possibly necessitating a second RO pass. The system also achieved a 50-fold energy saving in comparison to the existing industrial treatment method.

Although several modelling studies exist [18, 42, 51], comparing batch, semi-batch, and hybrid RO systems fairly has been challenging due to differences in feed water composition, recovery rates, rejection rates, membrane types, water flux, recirculation flow rates, pump types, and pipework designs across various studies. These factors impact energy efficiency and SEC, making side-by-side comparisons based solely on literature impractical. Furthermore, studies often lack uniform reporting of essential information. **Paper 6** aimed to bridge this research gap through direct experimental comparison among batch, semi-batch and hybrid semi-batch/batch RO using an identical pilot. The main objectives were to:

- present a single system that can operate in semi-batch, batch, or hybrid mode using the same feed composition, membrane, pumps, and pipework.
- run the system to compare performance parameters such as SEC, peak pressure, recovery, rejection, and permeate quality.

Both seawater and brackish water feed were used to address different operational conditions. In addition to being the first direct experimental evaluation of batch RO technologies, this study was also the first experimental investigation of batch RO using seawater, providing valuable insights for selecting and designing batch RO technologies for various applications. Furthermore, the study examined the effect of work exchanger volume. Using seawater feed, batch RO achieved a recovery of 0.655 and reduced electrical SEC by 10% compared to semi-batch RO at a peak pressure of 110 bar. While for brackish water feed, hybrid mode was used; a 20 L work exchanger volume reduced SEC by 23%, while a 40 L volume reduced SEC by 32% at $r = 0.94$. Additionally, permeate conductivity decreased by as much as 50% when using batch and hybrid RO compared to semi-batch RO, indicating improved quality of the product water.

Paper 6 showed batch RO can achieve excellent energy efficiency at high recovery, but practical systems have so far been limited to outputs under 25 m^3/day, while many applications require larger outputs. The methodology for scaling up traditional RO plants is well-documented, but batch RO presents unique challenges when scaling up. Large-scale batch RO systems require design predictions regarding performance and cost, with major challenges including selecting an appropriate work exchanger vessel and determining the optimal membrane arrangement in parallel or series, both impacting capital and operational costs. Thus, in **paper 7** we calibrated a performance model of batch RO against experiments conducted at pressures up to 112 bar with brackish and seawater feed solutions. The results were used to modify a model predicting performance for scaled-up systems using multiple RO modules and larger work exchangers. For instance, an industrial-sized vessel (16-inch diameter and 4 m

long) was used to design a hybrid semi-batch/batch RO system with twelve 8-inch RO modules, projected to deliver 128 m^3/day at an SEC of 1.19 kWh/m^3 and $r = 0.97$ for a feed concentration of 3000 mg/L NaCl solution, compared to 2.18 kWh/m^3 for semi-batch RO. The study concluded that hybrid semi-batch/batch RO is highly suitable for brackish water desalination at recoveries greater than 0.9 and outputs up to 165 m^3/day, while batch RO is viable for small-scale seawater desalination at a high recovery of 0.65. Additionally, the study predicted that the efficiency of batch or hybrid operations improves with larger work exchanger sizes, though this increases capital cost. High-permeability membranes have the potential to substantially improve the performance of batch RO systems; increasing permeability from 0.8 to 2 L/m^2/h/bar, for instance, could almost double permeate output. Thus, the study provided a comprehensive and reliable guide for scaling up free-piston batch RO systems and offered essential insights for design selection and optimization, enabling outputs of up to approximately 300 m^3/day, which is over ten times larger than current implementations.

5. Conclusions

In this thesis, a single-acting free-piston batch RO design was developed to achieve high recovery and energy efficiency and was subjected to rigorous experiments to address gaps in the existing literature. Two pilot systems were designed, constructed, and modified in the laboratory at the University of Birmingham, each comprising an 8-inch spiral wound RO membrane, giving an approximate permeate output of 10-25 m^3/day. The first pilot operated at pressures up to 25 bar and was initially constructed solely for batch RO processes at a recovery rate of $r = 0.8$. It was later modified to operate in a hybrid semi-batch/batch mode, allowing for recovery rates up to 0.96 at low feed salinities (up to 1500 mg/L). This modification informed the design of the second pilot, which was built to withstand pressures up to 120 bar and initially designed for hybrid mode operation to treat electroplating wastewater. Additionally, it facilitated a direct comparison of batch, semi-batch, and hybrid operations. The pilot studies employed a range of feed solutions, including NaCl solutions representative of brackish water (up to 5000 mg/L), synthesized groundwater containing sparingly soluble salts, seawater, and chromium rinse bath from the electroplating industry. Six different RO membranes with special features for various applications were also used in this study.

Experimental data and findings were used to develop and modify analytical models, incorporating inefficiencies such as salt retention, concentration polarization, longitudinal concentration gradient, recirculation flow rate, and other minor inefficiencies to accurately measure the SEC. The model was then applied to predict the system's performance under different operational conditions, including increased membrane permeability. Additionally, the model was used to forecast the performance of scaled-up batch RO systems, when utilizing a 500-L work exchanger volume. The key findings of this thesis are as follows:

- The batch RO system performs competitively with conventional continuous RO, particularly for small-scale industrial applications. It achieves hydraulic SEC of 0.2 to 1.2 kWh/m^3 at recoveries from 0.8 to 0.95 and outputs around 20 m^3/day using feed concentrations of 1000-5000 mg/L, which typically requires a larger multi-stage RO system.
- The batch RO system has significant potential for further SEC reduction compared to continuous RO. Enhancing membrane permeability could reduce hydraulic SEC by

up to 50%. Additionally, introducing a pump optimized for pressure variations in batch RO could further improve SEC, as current pump efficiencies measured in this study were only 10-65%.

- The batch RO system resisted scaling for over 100 hours of operation with synthesized groundwater containing sparingly soluble salts, which are typically expected to cause scaling on RO membranes. The absence of scaling was attributed to mechanisms such as periodic flushing, flow reversal, osmotic backwash, and salinity cycling, all occurring within a single cycle of batch RO.
- The first experimental investigation of a hybrid semi-batch/batch RO demonstrated the potential to achieve recoveries up to 0.99 in a very compact design with only a minor SEC penalty compared to batch RO, which requires a much larger system for such high recoveries. Very high concentration factors were achieved with low electrical SEC, making hybrid RO an attractive option for ZLD in various industries, particularly for extracting valuable components from effluents.
- The first direct experimental comparison among batch, semi-batch, and hybrid semi-batch/batch systems using a high-pressure RO system (120-bar) showed batch and hybrid RO superiority against semi-batch RO. With brackish water (5000 mg/L NaCl solution), the hybrid mode achieved up to 32% savings in SEC over the semi-batch mode at a recovery of 0.94, with potential for even greater savings at lower feed salinities and higher recoveries. Batch and hybrid RO systems also achieved superior permeate quality compared to semi-batch RO, a finding not revealed by previous models or experiments.
- The first experimental evaluation of seawater desalination by batch RO demonstrated a high recovery rate of 0.66 with a hydraulic SEC of less than 2.3 kWh/m³, a 13% reduction compared to semi-batch RO. However, osmotic backflow negatively affected recovery and permeate output in seawater batch RO.
- The high-pressure batch RO system proved to be an energy-efficient, compact, and robust solution for industrial ZLD applications, specifically in treating electroplating rinse water, reducing the current method's electrical SEC by about 50 times.
- An approach for setting the switch point from semi-batch to batch phase in hybrid mode was introduced and experimentally validated, enabling automatic operation and maintaining peak pressure within 2.2% of the target value.
- A model was developed and refined using experimental data and new findings step by step. Validation at the final stage showed agreement in SEC with an error of less than 4% for both brackish and seawater.
- The work exchanger volume should ideally be 1 to 2 times the volume of the membrane pressure vessels, as this results in significant SEC savings (31-54%) compared to semi-batch systems without a work exchanger. Although increasing the work exchanger volume further marginally reduces SEC, it also raises the capital cost.
- Predictions indicate that arranging up to 4 membrane elements in series results in a minimal increase in SEC (less than 10%), as long as the recirculation flow does not exceed 4 times the flow from the supply pump. However, when using 5 or 6 elements in series, SEC becomes more sensitive to increased recirculation flow. Nevertheless, electrical SEC can be kept below 1.5 kWh/m^3 with brackish water (at r = 0.97) and 3.0 kWh/m^3 with seawater (r = 0.66) at such high recoveries.

- Predictions indicate that for scaled-up systems using brackish water feed, three parallel vessels (equivalent to 12 membrane elements) with XLE and XUS membranes can achieve permeate outputs of 165 and 128 m^3/day respectively. These systems reach recoveries of 0.93 and 0.97 with hydraulic SEC of 0.69 and 1.19 kWh/m^3, using a 500-L work exchanger vessel. For seawater using a similar configuration with 12 XUS membranes, batch RO can provide 105 m^3/day permeate output at r = 0.66, with hydraulic SEC of 2.37 kWh/m^3.

6. Areas for future research

Paper 2 indicates that unlike previous studies on continuous RO [3,16,17,19], increasing membrane permeability to values of 10 or 20 L/m^2/h/bar remains beneficial for reducing SEC in batch RO. This underscores the ongoing significance of researching new materials and membrane fabrication techniques to enhance water permeability. Additionally, economic studies are needed to evaluate the costs and benefits associated with the development and adoption of future high-permeability membranes in batch RO applications.

Paper 3 focused on treating groundwater containing sparingly soluble salts that could lead to scaling issues in RO processes. However, there are other types of fouling such as particulate, organic, and biofouling that are equally important for future research. Therefore, conducting extensive pilot testing using various real-world feed water sources prone to different forms of fouling is essential for a comprehensive evaluation of the system. This approach will allow for a thorough assessment of fouling mitigation strategies in batch RO, comparing them with continuous RO systems, and providing valuable insights into real-world performance, practical feasibility, and reliability.

Paper 5 proposes that conducting a comparative experimental study between batch RO and continuous RO systems, including single-stage and multi-stage configurations using identical equipment, would offer a more precise evaluation of energy savings and performance parameters.

Paper 6 recommends conducting a life cycle assessment (LCA) to comprehensively evaluate the environmental impacts and benefits of high-pressure high-recovery batch RO technology.

Paper 7 suggests that conducting experimental studies on scaled-up systems using real-world water sources is essential to validate the model when multiple modules are arranged in parallel or series. Additionally, long-term monitoring of batch RO system operations is necessary to observe its performance over time, considering it is a novel process.

Furthermore, a study is recommended to optimize the duration of the purge phase, which significantly impacts performance parameters such as SEC, recovery, and peak pressure. Insufficient purging may increase SEC while potentially reducing peak pressure at the set recovery level, whereas excessive purging can elevate both SEC and peak pressure.

Future studies should consider hybridizing batch RO with other membrane technologies, such as forward osmosis or nanofiltration, to effectively address challenges associated with high salinity in feed water sources and mitigate fouling potential across diverse applications.

7. References

[1] Unicef, Progress on drinking water, sanitation and hygiene, (2017).
[2] F.E. Ahmed, A. Khalil, N. Hilal, Emerging desalination technologies: Current status, challenges and future trends, Desalination, 517 (2021) 115183.
[3] M. Flörke, C. Schneider, R.I. McDonald, Water competition between cities and agriculture driven by climate change and urban growth, Nature Sustainability, 1 (2018) 51-58.
[4] M.S. Babel, S.M. Wahid, Freshwater under threat South Asia: vulnerability assessment of freshwater resources to environmental change: Ganges-Brahmaputra-Meghna River Basin, Helmand River Basin, Indus River Basin, UNEP, 2009.
[5] R.S. Padrón, L. Gudmundsson, B. Decharme, A. Ducharne, D.M. Lawrence, J. Mao, D. Peano, G. Krinner, H. Kim, S.I. Seneviratne, Observed changes in dry-season water availability attributed to human-induced climate change, Nature Geoscience, 13 (2020) 477-481.
[6] X. Yuan, L. Wang, P. Wu, P. Ji, J. Sheffield, M. Zhang, Anthropogenic shift towards higher risk of flash drought over China, Nature communications, 10 (2019) 4661.
[7] G. Konapala, A.K. Mishra, Y. Wada, M.E. Mann, Climate change will affect global water availability through compounding changes in seasonal precipitation and evaporation, Nature communications, 11 (2020) 3044.
[8] M. Elimelech, W.A. Phillip, The future of seawater desalination: energy, technology, and the environment, science, 333 (2011) 712-717.
[9] J. Kim, K. Park, D.R. Yang, S. Hong, A comprehensive review of energy consumption of seawater reverse osmosis desalination plants, Applied Energy, 254 (2019) 113652.
[10] U. Caldera, C. Breyer, Assessing the potential for renewable energy powered desalination for the global irrigation sector, Science of the total environment, 694 (2019) 133598.
[11] A.S. Bello, N. Zouari, D.A. Da'ana, J.N. Hahladakis, M.A. Al-Ghouti, An overview of brine management: Emerging desalination technologies, life cycle assessment, and metal recovery methodologies, Journal of Environmental Management, 288 (2021) 112358.
[12] N. Voutchkov, Energy use for membrane seawater desalination–current status and trends, Desalination, 431 (2018) 2-14.
[13] C. Wang, S. Wang, K. Wang, Y. Xiao, Q. Ma, D. Song, R. Wang, Y. Zhang, Developmental impediment and prospective trends of desalination energy recovery device, Desalination, (2024) 117465.
[14] Y. Okamoto, J.H. Lienhard, How RO membrane permeability and other performance factors affect process cost and energy use: A review, Desalination, 470 (2019) 114064.
[15] K. Sumesh, D. Roshan, Reverse Osmosis Membrane Market by Material Type, Filter Module, and Application: Global Opportunity Analysis and Industry Forecast, 2025 (2018).
[16] M. Qasim, M. Badrelzaman, N.N. Darwish, N.A. Darwish, N. Hilal, Reverse osmosis desalination: A state-of-the-art review, Desalination, 459 (2019) 59-104.
[17] A. Shrivastava, S. Rosenberg, M. Peery, Energy efficiency breakdown of reverse osmosis and its implications on future innovation roadmap for desalination, Desalination, 368 (2015) 181-192.
[18] T. Qiu, P.A. Davies, Comparison of configurations for high-recovery inland desalination systems, Water, 4 (2012) 690-706.
[19] A. Panagopoulos, K.-J. Haralambous, M. Loizidou, Desalination brine disposal methods and treatment technologies-A review, Science of the Total Environment, 693 (2019) 133545.
[20] M. Li, B. Noh, Validation of model-based optimization of brackish water reverse osmosis (BWRO) plant operation, Desalination, 304 (2012) 20-24.
[21] P. Sanciolo, N. Milne, K. Taylor, M. Mullet, S. Gray, Silica scale mitigation for high recovery reverse osmosis of groundwater for a mining process, Desalination, 340 (2014) 49-58.
[22] A. Matin, F. Rahman, H.Z. Shafi, S.M. Zubair, Scaling of reverse osmosis membranes used in water desalination: Phenomena, impact, and control; future directions, Desalination, 455 (2019) 135-157.
[23] J. Rolf, T. Cao, X. Huang, C. Boo, Q. Li, M. Elimelech, Inorganic scaling in membrane desalination: models, mechanisms, and characterization methods, Environmental Science & Technology, 56 (2022) 7484-7511.
[24] A. Kumar, G. Naidu, H. Fukuda, F. Du, S. Vigneswaran, E. Drioli, J.H. Lienhard, Metals recovery from seawater desalination brines: technologies, opportunities, and challenges, ACS Sustainable Chemistry & Engineering, 9 (2021) 7704-7712.
[25] V. Lundaev, A. Solomon, U. Caldera, C. Breyer, Material extraction potential of desalination brines: A technical and economic evaluation of brines as a possible new material source, Minerals Engineering, 185 (2022) 107652.
[26] K. Park, J. Kim, S. Hong, Brine management systems using membrane concentrators: Future directions for membrane development in desalination, Desalination, 535 (2022) 115839.
[27] M.S. Diallo, M.R. Kotte, M. Cho, Mining critical metals and elements from seawater: opportunities and challenges, Environmental science & technology, 49 (2015) 9390-9399.

[28] I. Ihsanullah, J. Mustafa, A.M. Zafar, M. Obaid, M.A. Atieh, N. Ghaffour, Waste to wealth: A critical analysis of resource recovery from desalination brine, Desalination, 543 (2022) 116093.
[29] R. Engstler, J. Reipert, S. Karimi, J.L. Vukušić, F. Heinzler, P. Davies, M. Ulbricht, S. Barbe, A reverse osmosis process to recover and recycle trivalent chromium from electroplating wastewater, Membranes, 12 (2022) 853.
[30] Z. Lv, R. Chen, B. Shen, H. Tao, Y. Ding, Y. Xia, Y. He, Y. Zhang, H. Feng, Simultaneous removal of fluorine and dissolved silica from semiconductor wastewater by an in-situ crystal nucleation method towards near-zero liquid discharge, Desalination, 586 (2024) 117831.
[31] N. Jahan, M. Tahmid, A.Z. Shoronika, A. Fariha, H. Roy, M.N. Pervez, Y. Cai, V. Naddeo, M.S. Islam, A comprehensive review on the sustainable treatment of textile wastewater: zero liquid discharge and resource recovery perspectives, Sustainability, 14 (2022) 15398.
[32] X. Liu, J. Ma, E. Li, J. Zhu, H. Chu, X. Zhou, Y. Zhang, Multistage membrane-integrated zero liquid discharge system for ultra-efficient resource recovery from steel industrial brine: Pilot-scale investigation and spatial membrane fouling, Journal of Membrane Science, 699 (2024) 122655.
[33] A. Panagopoulos, V. Giannika, Decarbonized and circular brine management/valorization for water & valuable resource recovery via minimal/zero liquid discharge (MLD/ZLD) strategies, Journal of Environmental Management, 324 (2022) 116239.
[34] A. Khalil, S. Mohammed, R. Hashaikeh, N. Hilal, Lithium recovery from brine: Recent developments and challenges, Desalination, 528 (2022) 115611.
[35] G.P. Thiel, R.K. McGovern, S.M. Zubair, Thermodynamic equipartition for increased second law efficiency, Applied energy, 118 (2014) 292-299.
[36] Q.J. Wei, R.K. McGovern, Saving energy with an optimized two-stage reverse osmosis system, Environmental Science: Water Research & Technology, 3 (2017) 659-670.
[37] J.G. Wijmans, R.W. Baker, The solution-diffusion model: a review, Journal of membrane science, 107 (1995) 1-21.
[38] A. Zhu, P.D. Christofides, Y. Cohen, Effect of thermodynamic restriction on energy cost optimization of RO membrane water desalination, Industrial & Engineering Chemistry Research, 48 (2009) 6010-6021.
[39] T. Lee, A. Rahardianto, Y. Cohen, Multi-cycle operation of semi-batch reverse osmosis (SBRO) desalination, Journal of membrane science, 588 (2019) 117090.
[40] M. Li, Analysis and Design of Membrane Processes: A Systems Approach, (2020).
[41] K. Park, L. Burlace, N. Dhakal, A. Mudgal, N.A. Stewart, P.A. Davies, Design, modelling and optimisation of a batch reverse osmosis (RO) desalination system using a free piston for brackish water treatment, Desalination, 494 (2020) 114625.
[42] J.R. Werber, A. Deshmukh, M. Elimelech, Can batch or semi-batch processes save energy in reverse-osmosis desalination?, Desalination, 402 (2017) 109-122.
[43] K. Park, P.A. Davies, A compact hybrid batch/semi-batch reverse osmosis (HBSRO) system for high-recovery, low-energy desalination, Desalination, 504 (2021) 114976.
[44] R.L. Stover, High recovery, low fouling, and low energy reverse osmosis, Desalination and Water Treatment, 57 (2016) 26501-26506.
[45] A. Efraty, in, 2010.
[46] J. Kim, L. Dong, H.K. Shon, K. Park, Current progress in semi-batch reverse osmosis for brackish water desalination, Desalination, (2024) 117434.
[47] M. Li, Effect of cylinder sizing on performance of improved closed-circuit RO (CCRO), Desalination, 561 (2023) 116688.
[48] D.M. Warsinger, E.W. Tow, L.A. Maswadeh, G.B. Connors, J. Swaminathan, Inorganic fouling mitigation by salinity cycling in batch reverse osmosis, Water research, 137 (2018) 384-394.
[49] S. Hong, K. Park, J. Kim, A.B. Alayande, Y. Kim, Seawater Reverse Osmosis (SWRO) Desalination: Energy consumption in plants, advanced low-energy technologies, and future developments for improving energy efficiency, IWA Publishing, 2023.
[50] Z. Gal, A. Efraty, CCD series no. 18: record low energy in closed-circuit desalination of ocean seawater with nanoH2O elements without ERD, Desalination and Water Treatment, 57 (2016) 9180-9189.
[51] D.M. Warsinger, E.W. Tow, K.G. Nayar, L.A. Maswadeh, Energy efficiency of batch and semi-batch (CCRO) reverse osmosis desalination, Water research, 106 (2016) 272-282.
[52] B. Sutariya, H. Raval, Analytical study of optimum operating conditions in semi-batch closed-circuit reverse osmosis (CCRO), Separation and Purification Technology, 264 (2021) 118421.
[53] S. Li, K. Duran, S. Delagah, J. Mouawad, X. Jia, M. Sharbatmaleki, Energy efficiency of staged reverse osmosis (RO) and closed-circuit reverse osmosis (CCRO) desalination: a model-based comparison, Water Supply, 20 (2020) 3096-3106.
[54] P.A. Davies, J. Wayman, C. Alatta, K. Nguyen, J. Orfi, A desalination system with efficiency approaching the theoretical limits, Desalination and Water Treatment, 57 (2016) 23206-23216.

[55] M. Li, Cyclic simulation and energy assessment of closed-circuit RO (CCRO) of brackish water, Desalination, 545 (2023) 116149.
[56] S. Cordoba, A. Das, J. Leon, J.M. Garcia, D.M. Warsinger, Double-acting batch reverse osmosis configuration for best-in-class efficiency and low downtime, Desalination, 506 (2021) 114959.
[57] T. Qiu, P.A. Davies, Longitudinal dispersion in spiral wound RO modules and its effect on the performance of batch mode RO operations, Desalination, 288 (2012) 1-7.
[58] T. Qiu, P. Davies, Concentration polarization model of spiral-wound membrane modules with application to batch-mode RO desalination of brackish water, Desalination, 368 (2015) 36-47.
[59] H. Abu Ali, M. Baronian, L. Burlace, P.A. Davies, S. Halasah, M. Hind, A. Hossain, C. Lipchin, A. Majali, M. Mark, Off-grid desalination for irrigation in the Jordan Valley, Desalination and Water Treatment, 168 (2019) 143-154.
[60] P. Davies, A. Afifi, F. Khatoon, G. Kuldip, S. Javed, S. Khan, Double-acting batch-RO system for desalination of brackish water with high efficiency and high recovery, Desalination for the Environment–Clean Energy and Water, Rome, (2016) 23-25.
[61] L. Burlace, P. Davies, Fouling and fouling mitigation in batch reverse osmosis: review and outlook, Desalination Water Treatment, 249 (2022) 1-22.
[62] J. Swaminathan, E.W. Tow, R.L. Stover, Practical aspects of batch RO design for energy-efficient seawater desalination, Desalination, 470 (2019) 114097.
[63] Q.J. Wei, C.I. Tucker, P.J. Wu, A.M. Trueworthy, E.W. Tow, Impact of salt retention on true batch reverse osmosis energy consumption: experiments and model validation, Desalination, 479 (2020) 114177.
[64] A. Das, A.N. Beni, C. Bernal-Botero, D.M. Warsinger, Temporally multi-staged batch counterflow reverse osmosis, Desalination, 575 (2024) 117238.
[65] A. Das, A.K. Rao, S. Alnajdi, D.M. Warsinger, Pressure exchanger batch reverse osmosis with zero downtime operation, Desalination, 574 (2024) 117121.
[66] M. Li, N. Chan, J. Li, Novel dynamic and cyclic designs for ultra-high recovery waste and brackish water RO desalination, Chemical Engineering Research and Design, 179 (2022) 473-483.
[67] J. Swaminathan, R. Stover, E.W. Tow, D.M. Warsinger, J.H. Lienhard, Effect of practical losses on optimal design of batch RO systems, (2017).
[68] D.M. Warsinger, J. Swaminathan, J.H. Lienhard, Ultrapermeable membranes for batch desalination: maximum desalination energy efficiency, and cost analysis, (2017).
[69] A. Efraty, J. Septon, Closed circuit desalination series no-5: high recovery, reduced fouling and low energy nitrate decontamination by a cost-effective BWRO-CCD method, Desalination and Water Treatment, 49 (2012) 384-389.
[70] Y. Chen, Y. Cohen, Calcium sulfate and calcium carbonate scaling of thin-film composite polyamide reverse Osmosis membranes with surface-tethered polyacrylic acid chains, Membranes, 12 (2022) 1287.
[71] Y.-H. Cai, C.J. Burkhardt, A.I. Schäfer, Renewable energy powered membrane technology: Impact of osmotic backwash on organic fouling during solar irradiance fluctuation, Journal of Membrane Science, 647 (2022) 120286.
[72] H. Gu, A.R. Bartman, M. Uchymiak, P.D. Christofides, Y. Cohen, Self-adaptive feed flow reversal operation of reverse osmosis desalination, Desalination, 308 (2013) 63-72.
[73] T. Lee, J.Y. Choi, Y. Cohen, Gypsum scaling propensity in semi-batch RO (SBRO) and steady-state RO with partial recycle (SSRO-PR), Journal of membrane science, 588 (2019) 117106.

Papers

List of papers

1. Hosseinipour E, Park K, Burlace L, Naughton T, Davies PA. A free-piston batch reverse osmosis (RO) system for brackish water desalination: Experimental study and model validation. Desalination. 2022 Apr 1;527:115524. https://doi.org/10.1016/j.desal.2021.115524.
2. Hosseinipour E, Davies PA. Effect of membrane properties on the performance of batch reverse osmosis (RO): The potential to minimize energy consumption. Desalination. 2024 May 18;577:117378. https://doi.org/10.1016/j.desal.2024.117378.
3. Hosseinipour E, Harris E, El Nazer HA, Mohamed YM, Davies PA. Desalination by batch reverse osmosis (RO) of brackish groundwater containing sparingly soluble salts. Desalination. 2023 Nov 15;566:116875. https://doi.org/10.1016/j.desal.2023.116875.
4. Hosseinipour E, Karimi S, Barbe S, Park K, Davies PA. Hybrid semi-batch/batch reverse osmosis (HSBRO) for use in zero liquid discharge (ZLD) applications. Desalination. 2022 Dec 15;544:116126. https://doi.org/10.1016/j.desal.2022.116126.
5. Karimi S, Engstler R, Hosseinipour E, Wagner M, Heinzler F, Piepenbrink M, Barbe S, Davies PA. High-pressure batch reverse osmosis (RO) for zero liquid discharge (ZLD) in a Cr (III) electroplating process. Desalination. 2024 Jul 1;580:117479. https://doi.org/10.1016/j.desal.2024.117479.
6. Hosseinipour E, Davies PA. Direct experimental comparison of batch reverse osmosis (RO) technologies. Desalination. 2024 Aug 19;583:117717. https://doi.org/10.1016/j.desal.2024.117717.
7. Hosseinipour, E., & Davies, P. Free-piston batch reverse osmosis (RO): Modelling and scale-up. *Available at SSRN 4854851*. https://doi.org/10.1016/j.desal.2024.117980.

Paper 1: A free-piston batch reverse osmosis (RO) system for brackish water desalination: experimental study and model validation

Ebrahim Hosseinipour[1], Kiho Park[2], Liam Burlace[1], Tim Naughton[1] and Philip A. Davies[1*]

1. School of Engineering, University of Birmingham, Edgbaston, Birmingham, B15 2TT, UK
2. School of Chemical Engineering, Chonnam National University, 77 Yongbong-ro, Buk-gu, Gwangju, 61186, Republic of Korea

* p.a.davies@bham.ac.uk

Graphical abstract

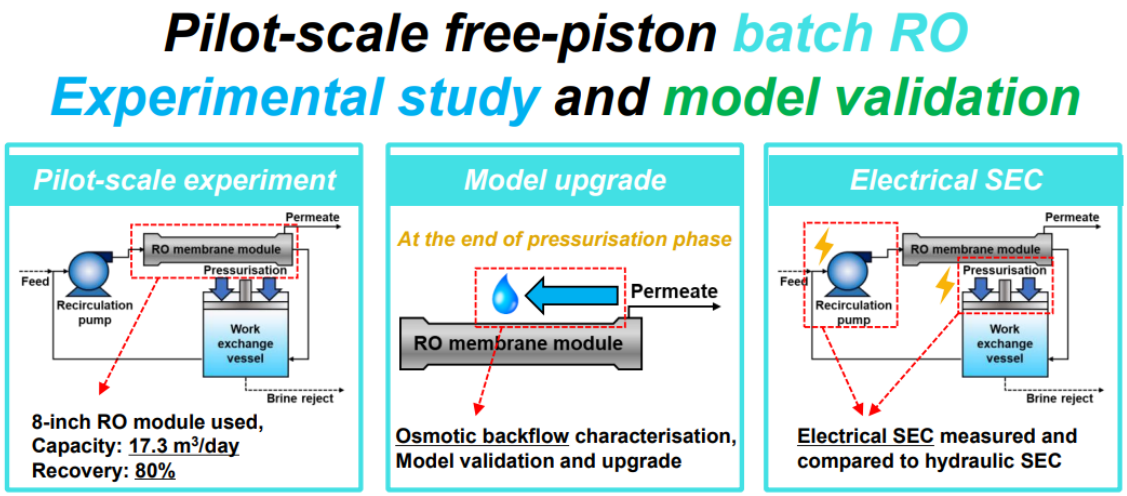

Abstract

Batch RO is designed to achieve high energy efficiency and high recovery in desalination. However, so far relatively few experiments on batch RO have been reported. Here we present an extensive experimental study of a single-acting, free-piston batch RO system using an 8-inch spiral wound membrane. The system was tested in the laboratory with brackish feed water containing up to 5 g/L NaCl. The objective was to quantify system performance in terms of Specific Energy Consumption (SEC), recovery, rejection, and output. Sensitivity to permeate flux and recirculation flow rate was also investigated. Performance was compared against the predictions of a theoretical model that accounts for salt retention, concentration polarization, and longitudinal concentration gradient in the RO module. For the first time, osmotic backflow was measured and incorporated into the model. For feed concentrations ranging from 1–5 g/L and recovery of 0.8, hydraulic *SEC* was measured in the range 0.22–0.48 kWh/m^3 and electrical *SEC* in the range 0.48–0.83 kWh/m^3. With improvements to the membrane permeability from 4.4 to 8 LMH/bar, selection of more efficient pumps, and reduction of valve friction losses, the model predicts that hydraulic *SEC* will be lowered to 0.14–0.39 kWh/m^3.

Keywords: Batch reverse osmosis, high recovery, energy efficiency, brackish water, osmotic backflow.

Highlights:

- A batch RO system operating over only two phases to reduce downtime.
- In-depth experimental study validates model with 3% accuracy in hydraulic SEC.
- Osmotic backflow of 2.5–5 L measured and included in modelling.
- Electrical SEC in the range 0.48–0.83 kWh/m^3 measured at recovery of 0.8.
- Model predicts electrical SEC of 0.14–0.39 kWh/m^3 through improvements to membrane, valves and pump.

1. Introduction

Water scarcity has become a serious problem in many world regions and is expected to worsen with population growth, water pollution, improved standards of living, and rising demand from the industrial and agricultural sectors. To help address this issue, individual countries and regions are increasingly using desalination technologies. The two main categories of desalination technology are thermal and membrane-based systems. Thermal desalination methods, however, have high capital and operational costs and are energy-intensive [1]. Thanks to advances in membrane science, membrane-based processes – particularly reverse osmosis (RO) – are the more promising and viable option today, enabling potable water production from various sources [2-4]. Compared to thermal desalination, these processes are energy efficient, offering excellent prospects to help tackle the growing water crisis [2].

In recent years, the energy consumption of RO systems has steadily decreased thanks to enhancements in the fabrication of membranes with higher permeability and selectivity [5], improved pump efficiency, better energy recovery devices [6], and new feed spacer designs [7, 8]. Despite these improvements, RO desalination remains energy intensive compared to conventional potable water treatments such as coagulation and filtration [9]. There is still potential to lower the SEC of desalination systems, to get closer to the thermodynamic minimum as represented by the following expression for the ideal Specific Energy Consumption (SEC_{ideal}) needed to desalinate a dilute feed solution [10]:

$$SEC_{\text{ideal}} = \frac{\pi_{\text{feed}}}{r} ln \frac{1}{1-r} \quad (1)$$

where π_{feed} is the osmotic pressure of the feed solution and r is recovery ($0 \leq r \leq 1$). For seawater with salinity 35 g/l and recovery of 50%, SEC_{ideal} is thus calculated to be about 1 kWh/m^3, while the most efficient state-of-the-art RO desalination plants can achieve real SEC just under twice this value [11]. For brackish water systems, however, the gap between real and ideal efficiency is much greater, such that typically a tenfold reduction in SEC is theoretically possible [12, 13].

Another drawback associated with RO desalination is depletion of groundwater and rejection of a high-salinity by-product (i.e. brine) that must be disposed of carefully. This means that RO systems having both low energy consumption and high recovery are desirable to overcome

these limitations. Nevertheless, these two requirements conflict. Eq. 1 illustrates that *SEC* tends to increase with recovery and at an increasing rate.

This conflict has prompted researchers to investigate alternative system configurations to minimize *SEC*. Conventional single-stage RO configuration cannot achieve the ideal minimum *SEC*, because the applied feed pressure must overcome the osmotic pressure of the brine, which at high recovery, is several times above π_{feed} [11]. This problem can be mitigated by spatial or temporal separation [14]. In spatial separation, the system is divided into multiple stages, each working at progressively higher pressure. In temporal separation, only one stage is employed – but the pressure varies with time to overcome the changing osmotic pressure of the water being desalinated [10, 14, 15]. Time-varying pressure makes it possible, in theory, to achieve the theoretical minimum SEC_{ideal}; whereas multi-stage systems require an infinite number of stages to attain such ideal performance [14]. Batch RO is a prominent example of a time-varying desalination system [10, 15-18]. Batch RO operates in a cyclic manner, consisting of a pressurization (or permeate production) phase, during which the pressure increases, followed by purge (or flush) and refill (or recharge) phases.

Over the last decade, there have been several studies about batch RO. Two main types of design have been built and experimentally tested: one using a free piston and the other a bladder. Davies et al. [10] proposed and implemented a free-piston design and reported a hydraulic *SEC* of 0.31 kWh/m^3 for feed concentration of 5 g/L NaCl and r = 0.69. However, this *SEC* did not include the recirculation pump energy and included only the pressurization phase. In a more detailed theoretical study, a single-acting free-piston batch RO for brackish water treatment was designed, modelled, and optimized by the same group. Non-ideal correction factors including salt retention, concentration polarization, and longitudinal concentration gradient were identified and used in the calculation of *SEC* [19]. To reduce the downtime of the batch system during refill, double-acting free-piston designs have also been proposed [15, 20].

The bladder type of batch RO design has been studied by Wei et al. [17]. These authors experimented with a bench top system and used the results to validate a numerical model which achieved 2.7% accuracy. The experiments included measurements of hydraulic work by both supply and recirculation pumps. Salt retention was also quantified, to show that salt retention decreases energy savings previously expected by researchers. Their experiments were limited to brackish water with operating pressures below 10 bar and recovery < 0.55. For example, at 3.5 g/L feed concentration, recovery of 0.52, and flux of 15 LMH, hydraulic *SEC* was 0.28 kWh/m^3. Model projections showed that, at higher recoveries, batch RO could save more energy. It was also predicted that with a seawater feed of 35 g/L salinity and recovery of 0.5, batch RO could save 11 % energy compared to a single-stage continuous RO plant [17].

Apart from the examples above, the potential advantages of batch RO over its conventional rivals have been investigated mainly by modelling and design studies [15, 16, 21-25], with relatively few detailed experimental studies reported [10, 17]. Therefore, in-depth experimental studies are needed to achieve a rigorous understanding of the process, and to identify optimal operating conditions that are critical for the practical implementation of the system. In this new study, an automated free-piston batch RO system, designed based on our previous study [19], has been experimentally investigated. The aim of the study is to achieve, using this system, energy-efficient desalination of brackish water at pilot scale with recovery of around 0.8. By

measuring the hydraulic work of the pumps, we have measured the total *SEC* and used it to validate an updated model. Moreover, for the first time in the study of batch RO systems, electrical *SEC* is precisely measured for various salinities, water fluxes, and recirculation flow rates – thus giving a complete picture of system energy consumption and losses. Further, salt retention, rejection, and osmotic backflow are accurately quantified. Table 1 compares the current study against the two earlier experimental studies, showing that it achieves higher output and recovery, and that it examines a wider range of phenomena, than covered previously. With output more than 10 times greater than in previous studies, this pilot-scale system brings batch RO closer to the size needed in many practical applications.

Table 1. Comparison of experimental studies conducted on batch RO performance.

	Davies et al. [10]	Wei et al. [17]	Current study
Design type	Free-piston Single-acting, 3-phase	Bladder 3-phase	Free-piston Single-acting, 2-phase
Membrane type	FilmTec, BW30-2540	Hydranautics, ESPA-2514	FilmTec, Eco Pro-440
Membrane area (m^2)	2.6	0.47	41
Feed concentration (g/L) of NaCl	2–5	2–5	0.1–5
Flux (LMH)	7-24	10, 15, 20	11–22
Recovery	0.17–0.7	0.29–0.53	0.8
Approximate maximum output (m^3/day)	1	0.12	17.3
Number of experimental runs reported	15	15	53
Type of *SEC* measured	Hydraulic *SEC* of supply pump during pressurization phase	Hydraulic *SEC* of supply and recirculation pumps over a whole cycle	Electrical and hydraulic *SEC* of supply and recirculation pumps over a whole cycle
Key comments	Manual operation. First experimental study on batch RO.	Automatic operation. Salt retention measured. Model verification for hydraulic *SEC* measurement.	Automatic operation. Osmotic backflow and salt retention measured. Model verification for hydraulic *SEC*, pressure measurement, and for longitudinal concentration gradient measurement.

The paper is structured as follows: section 2 describes the design concept, while section 3 presents the modified model. Section 4 describes the experimental equipment and procedure. Section 5 presents and discusses the results, including osmotic backflow, salt rejection, validation of model predictions and experimental measurements regarding hydraulic and *SEC*, average and peak pressure, and concentration vs time inside the recirculation loop. In section 6, the model is used to predict the system's performance with improved membranes and pump efficiencies. Finally, the overall findings of this study are summarised in section 7.

2. Batch RO design concept and operating principle

The concept of free-piston batch RO evolved from an earlier design in which the force to move the piston was provided by a mechanical linkage driven by a Rankine cycle [26, 27]. In the current design, the force is provided by pressurized water supplied from a motorized pump. This results in the concept of the free piston. Though various free-piston designs have been described [28], some of these are quite complex requiring numerous pumps and valves. In this study, the single-acting 2-phase design has been chosen as it minimizes this complexity in the

sense that it requires just two pumps (recirculation and supply pump) and three 2-port valves. This is the first in-depth experimental study of the single-acting 2-phase batch RO design.

The recirculation pump is an important feature of batch RO, needed to homogenize the solution in the pressurized loop and reduce concentration polarization, thus reducing supply pump energy consumption [22]. Nevertheless, the recirculation pump itself adds to the energy consumption of the batch RO system, thus raising the real *SEC* above the theoretical minimum of Eq. (1). This study looks in detail at the energy consumption and savings associated with the recirculation pump.

Of the three typical phases of the typical batch RO cycle (i.e. pressurization, purge, and refill), only the pressurization phase produces output of permeate. To compensate for the lost output during the other two phases, a larger operating flux is needed to achieve the same daily output as a conventional continuous desalination system. This incurs a penalty in *SEC* [24]. In the single-acting 2-phase design, purge and refill phases occur simultaneously as one phase, thus achieving higher output and reduced penalty as the non-productive time is minimized.

The resulting two phases of the free-piston batch RO cycle are shown in Fig. 1. In the pressurization phase, the recirculation valve is open while the bypass and brine valves are closed. Initially, the free piston is at the left-hand end of the work exchanger vessel. The supply pump generates high pressure, which is transferred to the feed water inside the work exchanger via the free piston. Once the pressure exceeds the osmotic pressure of feed water, permeate exits the system, while brine flows back to the work exchanger via the recirculation pump, thus completing the batch RO loop. As more permeate exits, concentration inside the loop gradually rises. Therefore, the supply pump must apply higher pressure to overcome the increased osmotic pressure and maintain constant permeate flow rate. Pressurization finishes when the piston reaches the right end of the work exchanger.

At the end of the pressurization phase, the RO module contains concentrated brine. The purge-and-refill phase is now required to flush the brine from the system and refill the right compartment of the work exchanger. In this phase, the bypass and brine valves are open while the recirculation valve is closed. The recirculation pump transfers feed solution from the left to the right end of the work exchanger, displacing the piston from right to left. Simultaneously, the supply pump supplies feed solution (without applying high pressure) to purge the remaining brine inside the RO module and pipes via the brine valve. The direction of flow inside the RO module is reversed with respect to the pressurization phase, with the inlet now on the left. Typically, purging continues until the volume collected at the brine outlet equals the volume of brine contained inside the RO module [29]. Once the brine is purged from the system, and the piston has moved back to the left, the brine and bypass valves are closed automatically and the recirculation valve is opened, thus starting the next cycle.

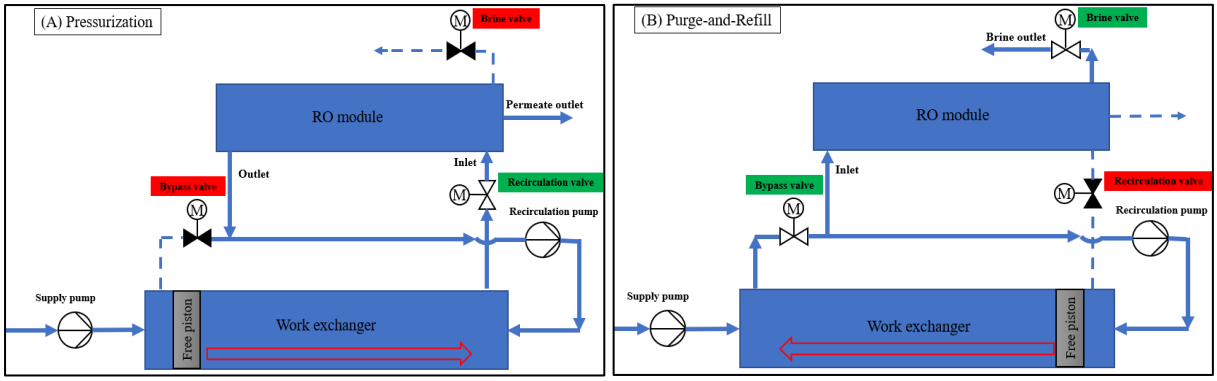

Fig. 1. (A) Pressurization and (B) purge-and-refill phases of the free-piston batch RO cycle (single-acting, 2-phase design). Phases are changed by opening and closing the three on-off valves. During the pressurization phase, bypass and brine valves are closed while the recirculation valve is open. During the purge-and-refill phase, bypass and brine valves are open and the recirculation valve is closed. (Black shading and white shading indicate respectively closed and open valves. Solid and dashed lines represent flow and no flow respectively).

3. Theory

Our previous study modelled the main parameters of the free-piston batch RO system including recovery, energy consumption, average and peak pressures, and rejection [19]. The modelling approach used here is similar but with certain differences. The main difference is that osmotic backflow, neglected in previous studies [17, 19], is now included. Osmotic backflow occurs at the end of the pressurization phase when the hydraulic pressure falls to zero, allowing the salinity gradient to draw permeate back across the membrane.

The design intention of the free-piston batch RO was to set the recovery based on the system geometry. Therefore, recovery was calculated previously by Eq. (2) based on internal volumes i.e.

$$r = \frac{\text{permeate output}}{\text{feed input}} = \frac{V_{\text{b0}}}{V_{\text{b0}} + V_{pg}} \tag{2}$$

where V_{b0} is the swept volume of the work exchanger, and the V_{pg} is the nominal volume needed to purge the system (comprising the internal volume of the membrane channel and associated connecting pipes and ports). However, pilot experiments showed and that the permeate volume was less than V_{b0} because of osmotic backflow, resulting in a lower recovery. Thus, we modified Eq. (2) by subtracting the osmotic backflow volume (V_{backflow}) from V_{b0} to calculate the permeate output and thus recovery:

$$r = \frac{V_{\text{b0}} - V_{\text{backflow}}}{V_{\text{b0}} + V_{\text{pg}}} \tag{3}$$

The energy consumption model includes the energy used by the supply pump and recirculation pump. It neglects, however, auxiliary loads of valves and instrumentation, as these are considered circumstantial to the nature of the experimental set up, and not fundamental to the batch RO concept. Furthermore, the energy used by the valves is estimated at <0.5% of the total consumption and as such negligible [19].

Following the above assumptions, the *SEC* is calculated as the energy consumption (E) in each cycle divided by the permeate output (taking into account V_{backflow}). E is broken down by

phase of operation, resulting in the energy of pressurization (E_{P}) and energy of purge-and-refill ($E_{\mathrm{P\&R}}$). *SEC* is broken down similarly as follows:

$$SEC = \frac{E}{V_{\mathrm{b0}} - V_{\mathrm{backflow}}} = \frac{E_{\mathrm{P}} + E_{\mathrm{P\&R}}}{V_{\mathrm{b0}} - V_{\mathrm{backflow}}} = SEC_{\mathrm{P}} + SEC_{\mathrm{P\&R}} \quad (4)$$

For each respective phase, *SEC* can be further broken down between the supply pump (SP) and recirculation pump (RP) contributions. Using the corresponding subscripts,

$$SEC_{\mathrm{P}} = SEC_{\mathrm{P,SP}} + SEC_{\mathrm{P,RP}} \quad (5)$$

$$SEC_{\mathrm{P\&R}} = SEC_{\mathrm{P\&R,SP}} + SEC_{\mathrm{P\&R,RP}} \quad (6)$$

The hydraulic energy consumption of each pump is calculated by multiplying the differential pressure by the volume of water displaced by that pump, i.e. $P\Delta V$ (or $\int PdV$ when P varies with V). Pressure is needed to overcome osmotic pressure and to compensate frictional losses related to the membrane, pipework, and the piston seal. Because osmotic pressure changes through the pressurization phase, it is appropriate to use the average pressure $\bar{P}$ (such that $\bar{P}\Delta V = \int PdV$) in calculating $SEC_{\mathrm{P,SP}}$.

Of the four *SEC* contributions in equations (5) and (6), the largest is generally $SEC_{\mathrm{P,SP}}$; therefore, this contribution is analysed in the greatest detail. The analysis uses a top-down approach in calculating $\bar{P}$ (and therefore $SEC_{\mathrm{P,SP}}$), which starts from the ideal minimum *SEC* as presented in Eq. (1) and brings in terms to represent non-ideal behaviour and losses in the system. This approach enables us to quantify the causes of non-ideality and to pinpoint readily the scope for improving the system towards the ideal case. Accordingly, the average pressure is given by:

$$\bar{P} = S_{\mathrm{p}} S_{\mathrm{L}} S_{\mathrm{R}} \pi_{\mathrm{feed}} \frac{1}{r_{\mathrm{p}}} ln \frac{1}{1 - r_{\mathrm{p}}} + \frac{J_{\mathrm{w}}}{A_{\mathrm{w}}} + \frac{\Delta P_{\mathrm{m}}}{2} + \Delta P_{\mathrm{V2}} + \Delta P_{\mathrm{S}} \quad (7)$$

where the pressurisation recovery r_p is given by:

$$r_p = \frac{V_{\mathrm{b0}}}{V_{\mathrm{b0}} + V_{\mathrm{pg}} + V_{\mathrm{pipe,R}}} \quad (8)$$

This refers to the gross volume of water recovered before osmotic backflow, as a fraction of the total initial internal volume including the volume of the unpurged pipe section ($V_{\mathrm{pipe,R}}$) [19]. Note that r_{p} is the variant of the recovery relevant for calculating the pressure in the system. It differs slightly from the overall system recovery, r, which is relevant for comparing performance against other desalination systems.

The non-ideal correction factors, S_{p}, S_{L}, and S_{R} represent respectively the concentration polarization factor, the longitudinal concentration gradient, and salt retention – following the same calculation procedures as in [19]. S_{L} is a function of the ratio of recirculation flow to feed flow ratio ($Q_{\mathrm{r}}/Q_{\mathrm{f}}$) as explained in the Supplementary Information (SI) section 4. The membrane pressure losses comprise two components: a major component of the hydrodynamic friction of flow through the membrane (second term in Eq. 7) and a minor component of pressure drop ΔP_{m} along the membrane channel caused by friction with the membrane surface and spacer element (third term in Eq. (7)). The correlation developed by Haidari *et al.* [30] has been used for ΔP_{m} [kPa].

$$\Delta P_{\mathrm{m}} = 791 \times v^{1.63} \times L \quad (9)$$

where v is the cross-flow velocity [m/s] and L is the module length [m]. Eq. (7) also includes, unlike in the previous work, terms representing the valve loss ΔP_{V2} in the supply path, and the piston seal friction, ΔP_{S} , as explained next.

Pipework friction losses may in general include losses in pipes, fittings and valves. According to the construction of the rig used in this study, however, only the valves contribute a significant loss. The pipes and fittings are sized to ensure negligible losses in comparison. The pressure loss in the valves is calculated based on the Torricelli equation for flow through an orifice [31]:

$$\Delta P_{\mathrm{Valves}} = (\frac{\rho}{2})(\frac{v}{C_{\mathrm{d}}})^2 \quad (10)$$

where v is the velocity at the valve orifice, and C_{d} is the coefficient of discharge. According to Massey [31], C_{d} typically has values in the range of 0.6 to 0.7. The precise value has to be determined by experiment. All three valves used in this study are of the same type; therefore, only one value of C_{d} is needed.

The piston friction ΔP_{S} arises because, although the piston in this design is theoretically a free piston, in practice it uses a seal that presents a small amount of friction. This results in a finite pressure drop which is approximately constant and opposing the direction of motion.

Besides $SEC_{\mathrm{P,SP}}$, the other three *SEC* contributions on the right-hand side of Eqs. (5) and (6) depend only on friction, such that the corresponding pressure drops remain constant throughout the respective phase. Analysis of these pressure drops requires consideration of the flow path, flow rates and displaced volume in each case, the details of which are included in SI section 1. The resulting *SEC* calculation is implemented in a spreadsheet appended as a supplementary file. The above equations provide the hydraulic *SEC*, which is divided by the pump efficiency (including the motor efficiency) to provide the electrical *SEC*.

Peak pressure ($\hat{P}$) is another important factor in the design of RO systems since materials and components must be selected to withstand it. It is calculated by using Eq. (11). Maximum peak pressure occurs at the end of the pressurization cycle, at which time longitudinal concentration gradient becomes zero (see SI, section 4). Thus, the term S_{L} is excluded from this equation.

$$\hat{P} = S_{\mathrm{p}} S_{\mathrm{R}} \pi_{\mathrm{feed}} \frac{1}{1 - r_{\mathrm{p}}} + \frac{J_{\mathrm{w}}}{A_{\mathrm{w}}} + \frac{\Delta P_{\mathrm{m}}}{2} + \Delta P_{\mathrm{V2}} + \Delta P_{\mathrm{s}} \quad (11)$$

Salt rejection in the batch RO system is calculated by using Eq. (12), where B is the salt permeability of the membrane calculated from the manufacturer's datasheet (B=J_{w}[1-R_{s}], where R_{s} is the salt rejection).

$$R_s = 100\% \left(1 - \frac{C_{\mathrm{perm}}}{C_{\mathrm{feed}}}\right) = 100\% \left(1 - \frac{J_{\mathrm{s}}}{J_{\mathrm{w}}}\right) = 100\% (1 - \frac{B.A_{\mathrm{m}}}{Q_{\mathrm{perm}}} S_{\mathrm{p}} S_{\mathrm{L}} S_{\mathrm{R}} \frac{1}{r_{\mathrm{p}}} ln \frac{1}{1 - r_{\mathrm{p}}}) \quad (12)$$

This equation uses the ratio of the salt flux J_{s} through the membrane divided by the water flux J_{w}. The salt flux is driven by the concentration difference across the membrane, averaged over time and over the duration of the pressurization phase. Thus, the driving concentration takes into account the increase of concentration during the phase, as well as concentration

polarisation, longitudinal gradient, and salt retention effects – giving Eq. (12) a similar form to the first term in Eq. (7). As this study deals with high rejection systems (R_s>90%), salt concentration on the permeate side is approximated to zero in calculating the concentration difference.

4. Experimental

4.1. General description of system

The experimental free-piston batch RO system is shown in Figs. 2 and 3 and its main design parameters are listed in Table 2. Major components of this system are a work exchanger vessel housing the free piston, a RO module, a high-pressure pump, a recirculation pump, and three motorized ball valves. These components are connected by 1.25-inch diameter stainless steel pipework. The system control panel allows for both manual and automated operation. For automated operation, a Programmable Logic Controller (PLC) controls the pumps and valves in a cyclic sequence. The PLC receives feedback signals from pressure, conductivity, and flow sensors. A one-way valve installed on the permeate line prevents permeate from returning to the RO module when osmotic backflow occurs. An 8-inch spiral-wound RO module has been selected since most industries use this size for various applications [3]. The system is designed to be used for pressures up to 20 bar nominally. If pressure exceeds 25 bar, the system automatically shuts down to avoid damage. SI section 2 contains a detailed list of the components and instruments employed.

Fig. 2. High-recovery batch RO prototype installed in the laboratory.

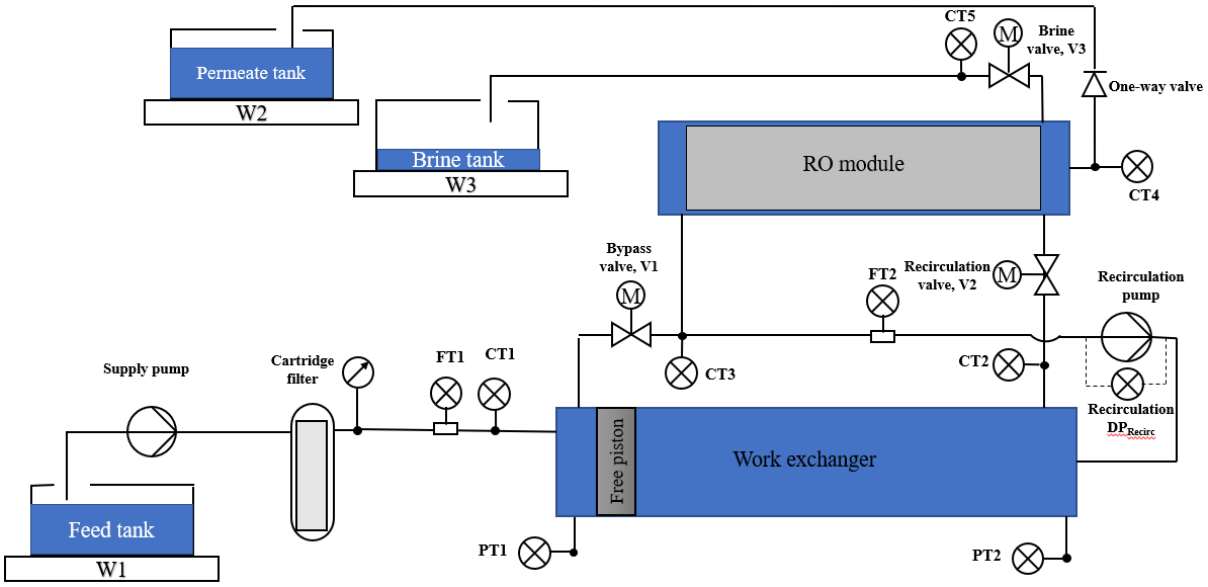

Fig. 3. Schematic diagram of high-recovery batch RO system (PT, CT and FT are pressure, conductivity and flow transmitters, respectively. W1, W2, and W3 are weighing platforms for feed, permeate and brine tanks. M indicates motorised valves).

Table 2. General parameters of the experimental system and model.

Membrane Characteristics			
Parameter	symbol	unit	value
Membrane area	A_m	m^2	41.0
Membrane channel height	H	m	7.11×10^{-4}
Membrane length	L	m	1.0
Membrane permeability (A value)	A_w	LMH/bar	4.4
Membrane salt diffusion coefficient (B value)	B	m/s	8.13×10^{-8}
Feed Solution Properties			
Density	ρ	kg/m^3	1000
Viscosity	μ	Pa·s	8.9×10^{-4}
Diffusivity of NaCl in water	D	m^2/s	1.47×10^{-9}
Gas constant	R	kJ/kmol.K	8.314
NaCl dissociation constant	i	-	1.865
Molecular mass of NaCl	M	kg/kmol	58.44
Vessel and pipework			
Valve orifice diameter	d	m	0.015
Coefficient of discharge	C_d	-	0.62
Piston seal friction pressure	ΔP_s	kPa	3.5
Work exchanger swept volume	V_{b0}	L	69.0
Membrane volume	V_m	L	14.5
Pipe volume (purged)	$V_{pipe,pg}$	L	0.11
Pipe volume (retained)	$V_{pipe,R}$	L	1.66
Port dead volume	V_{ports}	L	1.87
Nominal purge volume ($V_m + V_{pipe,pg} + V_{ports}$)	V_{pg}	L	16.5

4.2. Detailed description of equipment

4.2.1. Supply and recirculation pumps

During pressurization, the supply pump must provide steadily increasing pressure up to about 20 bar. During purge-and-refill, in contrast, it operates at pressures of less than 1 bar. To cover

this range of pressure, a positive displacement pump is preferred (Lorenz Solar Submersible Pump PS2-1800 HR-05HL, helical rotor type pump). The high-pressure supply pump is powered by a DC power supply (Keysight N5770A) which enables measurement of electrical power consumption with error <2%. The pump is connected to the RO system by a hydraulic hose. To remove any suspended particles, a 5-micron cartridge pre-filter is used at the inlet of the RO system.

The recirculation pump is used to recirculate the batch during the pressurization phase and to restore the piston to its initial position during the refill phase. A centrifugal pump is a suitable choice since it works over a smaller range of differential pressures, contrary to the supply pump. A special pump was designed and made with a maximum flow of 60 l/min and system pressure rating up to 25 bar gauge. It uses a 24 V DC power supply and current is logged to monitor its power consumption. Both pumps allow for speed adjustment via manual or PLC control.

4.2.2. Membrane and work exchanger

The RO membrane element is an 8-inch spiral wound type (Eco Pro-440, manufactured by DuPont Filmtec^{TM}) with 41 m^2 active area. Two fibre-reinforced polymer pressure vessels are used, with pressure rating of 30 bar, and dimensions 8 inch × 1.5 m (for the RO module) and 9.45 inch × 2 m (for the work exchanger). The free-piston is machined from polyoxymethylene to provide a clearance fit inside the work exchanger vessel, and it is fitted with a two C-seals to ensure sealing in both directions.

4.2.3. Sensors

Nine sensors are used with continuous data logging. Two pressure transmitters (PT) measure supply and batch pressure on corresponding sides of the piston; five conductivity transmitters (CT) measure conductivity of supply, batch, brine, permeate, and RO outlet in the recirculation loop; and two flow transmitters (FT) measure supply and recirculation flow rate. Refer to SI for detailed specifications and accuracies.

4.2.4. Weighing platforms and tanks

For precise measurements of flow, weighing platforms are used with the accuracy of 0.2, 0.1, and 0.05 kg for feed, permeate, and brine tanks respectively, allowing automatic logging of mass change throughout the experiment. The capacities of the feed, permeate, and brine tanks are 1500, 1000, and 600 L, respectively. A mixing pump ensures and uniforms feed water solution inside the feed tank at the start of each experiment. A thermostatic immersion heater provides a constant temperature of 25 ± 0.5°C in the feed tank.

4.3. Experimental Procedure

Feed solution was prepared using tap water (salt concentration ~0.1 g/L) and analytical grade sodium chloride (Fisher Scientific, purity > 99.5%). Feed solutions were made up with concentrations of 1–5 g/L, to represent brackish water salinity. To prevent membrane oxidation, 3 g sodium metabisulfite was added per m^3 of feed solution to counteract free chlorine.

The control sequence is as follows. Operation starts with an extra purge-and-refill phase which is not part of the typical cycle. This clears any concentrated salts from the system and

thus ensures a consistent starting condition. The first pressurization phase is then run, followed by the first purge-and-refill phase, thus completing the first cycle. Pilot experiments showed that stable repetitive cyclic conditions were reached after 3–4 cycles (see SI section 3). Therefore at least 3 cycles are performed before the test cycle (i.e. the cycle that is used for collecting and analysing results). All parameters, including time, weight of the tanks, conductivities, differential pressure of recirculation pump, power consumption of pumps, pressures, and flow rates are logged at a frequency of at least once per second, resulting in at least 470 sets of readings per cycle.

5. Results and Discussion

This section discusses the experimental results for recovery, salt retention, hydraulic and electrical *SEC*, and compares them against the model results. In total, 53 tests have been conducted, each representing a different set of experimental conditions. The raw experimental data are included as electronic appendices and indexed in SI section 5.

5.1. Mass balance and recovery

The design intention of the batch RO system was that the recovery would be determined purely by the geometry of the machine (as in Eq.2, giving a recovery of r=0.807 with parameters from Table 2). The system would be fed at constant flow, such that the recovery would correspond to the duration of the pressurization phase (expected to provide output V_{b0}) divided by the total cycle duration. Therefore, initial experiments were carried out to test the system with constant supply flow, using a flux of J_w=17.3 LMH and salinities of 0.1, 1, 2, 3, 4, and 5 g/L. Table 3 compares the observed recovery against expected recovery. The *observed* recovery is the permeate volume collected divided by the total feed volume supplied over the whole cycle; whereas the *expected* recovery is the feed supplied during the pressurization phase divided by the total feed volume supplied over the whole cycle. The observed recovery was substantially less than expected in all cases except at 0.1 g/L feed concentration.

This discrepancy was caused by osmotic backflow at the end of the pressurization phase when the system de-pressurized. Because of osmotic backflow, about 2.5–5 L of the batch volume failed to leave the system as permeate, instead remaining inside the system at the end of pressurization. This backflow volume corresponded to 0.07–0.12 L per m^2 of membrane area, equivalent to 0.07–0.12 mm of water distributed over the membrane surface. This volume can be explained by water retained in the permeate side spacer, which has a thickness of about 0.3 mm.

Table 3. Observed and expected recoveries obtained at different salinities – constant flow operation (J_w = 17.3, Q_r/Q_f = 2.1).

Feed salinity (g/L)	Observed recovery	Expected recovery based on feed amounts	Osmotic backflow volume $V_{backflow}$ (L)
0.1	0.794	0.803	0.6
1	0.767	0.803	2.6
2	0.749	0.799	4.2
3	0.74	0.799	4.8
4	0.74	0.799	4.8
5	0.74	0.799	4.8

The mass balance of the batch RO system over pressurization and purge-and-refill phases at different feed salinities is further detailed in Fig. 4. The total input and output to the rig over each cycle was consistently 86.4±0.2 L. During the pressurization phase, however, input exceeded output by the amount $V_{backflow}$ (see Table 3). Conversely, during purge-and-refill, output exceeded input by the same amount.

Observations of the weighing tanks with time gave further insight into the mass balance of the system over the cycle, as shown in Fig. 5. The feed tank mass decreased linearly with time over the whole cycle (R^2 = 0.999). The mass changes of the permeate and brine tanks, though mostly linear, showed non-linearity at the start and end of the pressurization and purge-and-refill phases respectively. The permeate output was delayed for the first 20 s of pressurization, during which time about 4.2 L of water was fed to the rig but no permeate came out. Afterwards, the permeate tank gained mass linearly up to the end of the pressurization phase. At the start of the purge-and-refill phase, there was a surge of brine leaving the rig for the first 20 s, before the brine outlet settled to a constant flow.

Fig. 5 also shows the total mass of the tanks against time, as a change from the initial total mass. A net loss of about 4 kg in total tank mass occurred during the pressurization phase, corresponding to a net gain in 4 kg of the RO rig itself. It was also observed that a vacuum formed in the permeate tube upstream of the one-way valve at the end of the pressurization cycle, as permeate was sucked back across the RO module and into the feed channel. This loss of permeate can explain the difference in the net weight of the rig. These observations confirm that, for feed salinities higher than 2 g/L, around 4–5 L of permeate were sucked back through the membrane, creating a vacuum on the permeate side upstream of the one-way valve, at the beginning of purge-and-refill phase. The vacuum had to be refilled at the start of pressurization phase before output recommences. For lower salinities, the backflow was smaller (e.g. only 2.6 L at 1 g/L).

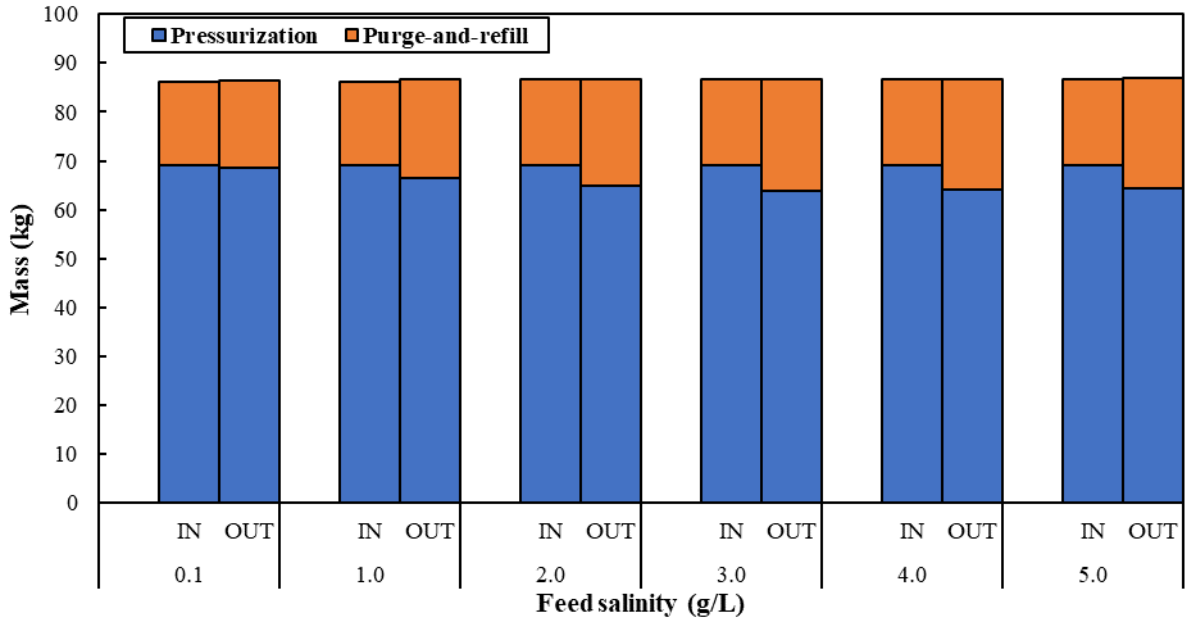

Fig. 4. Mass balance: total input and output to the batch RO system over pressurization and purge-and-refill phases at different feed salinities when supply pump was operating at a constant flow rate (J_w = 17.3 LMH, Q_r/Q_f = 2.1).

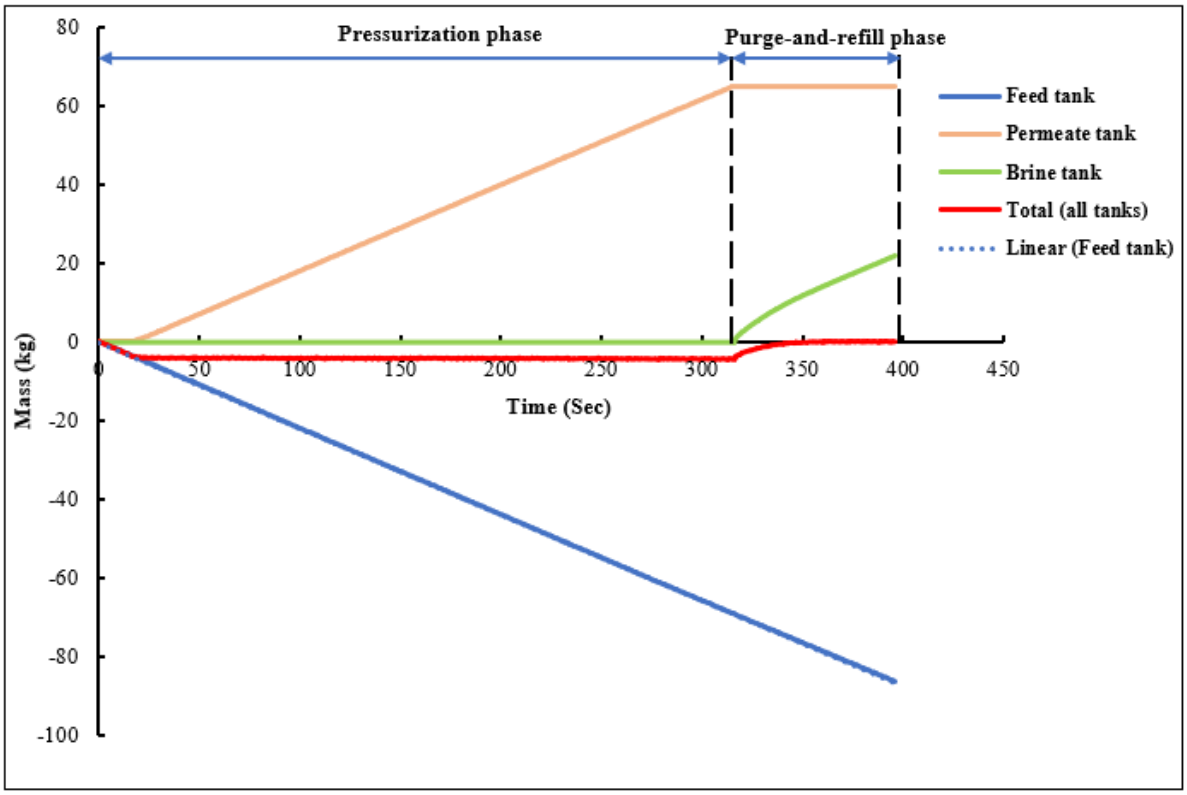

Fig. 5. Mass changes of feed, permeate, and brine tanks over a cycle. Red line shows total of mass changes of feed, permeate and brine tank. The experiment was conducted at 2 g/L feed concentration, and constant feed flow rate (water flux J_w = 17.3 LMH).

5.2. Salt retention

Salt retention plays an important role in the performance of batch and semi-batch RO systems. When the pressurization phase ends, concentrated brine inside the RO module and pipes must be purged and a new feed solution is introduced to prepare the system for the next cycle. In an ideal case, during purge, the incoming feed would displace the brine with zero mixing. However, in practice, dispersion causes unwanted mixing of incoming feed with the concentrated brine. Moreover, a minor volume of our system ($V_{pipe,R}$) is not purged by the feed solution, causing additional salt retention. Thus, the initial concentration for the next cycle rises, increasing the required pressure and *SEC* of the system.

A series of experiments was carried out to measure directly salt retention in the free-piston batch RO. The experiments were conducted with 2 g/L feed solution and at flux J_w =17.9 LMH. In each experiment, a different volume of brine was purged, from 80% to 150% of the nominal purge volume (V_{pg} =16.5 L), corresponding to V = 13.4–25.4 L of brine collected at the outlet. In each experiment, we ran the system for 4 cycles to reach the steady-state condition. At the end of the fourth cycle, after turning off the supply pump and opening the bypass valve, the whole solution inside the membrane and work exchanger was thoroughly mixed for 10 minutes by the recirculation pump. The solution inside the system was then sampled and its conductivity was compared to that of the feed tank. Fig. 6 demonstrates the effect of the purge volume V on salt retention and recovery. When the purge volume was equal to the volume of brine inside the membrane and piping (V/V_{pg} = 1), the salt retention factor was 1.159 ± 0.023 and recovery was 0.8, which agrees with the theoretical value of 1.155 using the method of [19].

At larger purge volumes, salt retention decreased markedly. However, increased purge also lowered recovery as more feed was supplied for the same permeate output over the cycle. For example, on increasing the purge volume by 12, 30, and 54%, the salt retention factor was reduced to 1.10, 1.06, and 1.02 respectively; while recovery fell to 0.78, 0.75, and 0.72 respectively. Conversely, although recovery was higher with less purge, greater salt retention was observed. Salt retention rose sharply when purging with $V < V_{pg}$ whereas recovery rose less sharply (see Fig. 6A).

Though higher salt retention increased energy consumption by the supply working at increased pressure, this was largely compensated by the shorter purge time, and therefore, reduced energy consumption during purge and refill. Thus, overall *SEC* increased only marginally as purge volume decreased and recovery increased, as seen in Fig. 6(B).

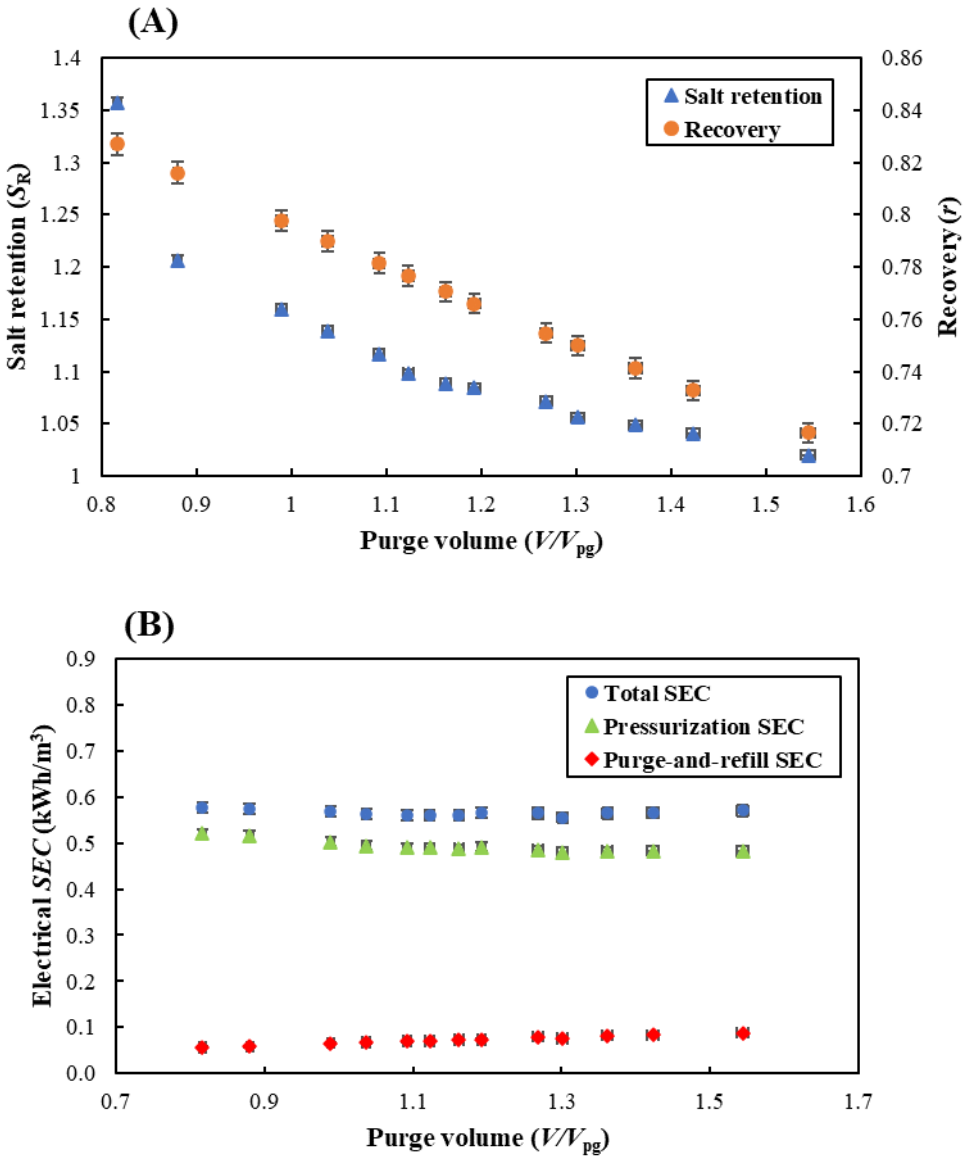

Fig. 6. (A) Observed salt retention and recovery *vs.* normalized purge volume. (B) Electrical SEC, total and by phase, *vs.* normalized purge volume. (Experimental conditions: 2 g/L feed concentration, J_w = 17.9 LMH, and Q_r/Q_f = 2.1).

Qiu and Davies [29] previously studied salt retention in a RO module by observing concentration *vs*. volume at the brine outlet during purge. They did not, however, conduct the experiment under the real conditions of a batch RO process in the sense that they did not apply pressure to the RO module. Therefore, we repeated their test but under real condition, with high pressure falling to low pressure at the beginning of purge. The results in Fig. 7 show the normalized concentration at the brine outlet as a function of normalized purge volume. These experiments were conducted at 2 g/L feed concentration and at various feed flow rates.

Concentration curves were almost the same at different flow rates under the pressurized condition, indicating that salt retention is almost independent of the flow rate. However, there was a substantial difference between the cases of unpressurized and pressurized operation. Under zero pressure (Test 1 and 2 in Fig. 7) the concentration curve was very similar to that reported in [29]. However, under pressurized conditions (initial high pressure, then falling to zero, as in the real batch RO process) the concentration curves initially fall more suddenly and then tail off more slowly. This is attributed to the osmotic backflow that enters the RO module, not just near the inlet, but over its whole length, allowing the low-concentration solution to break through sooner at the outlet.

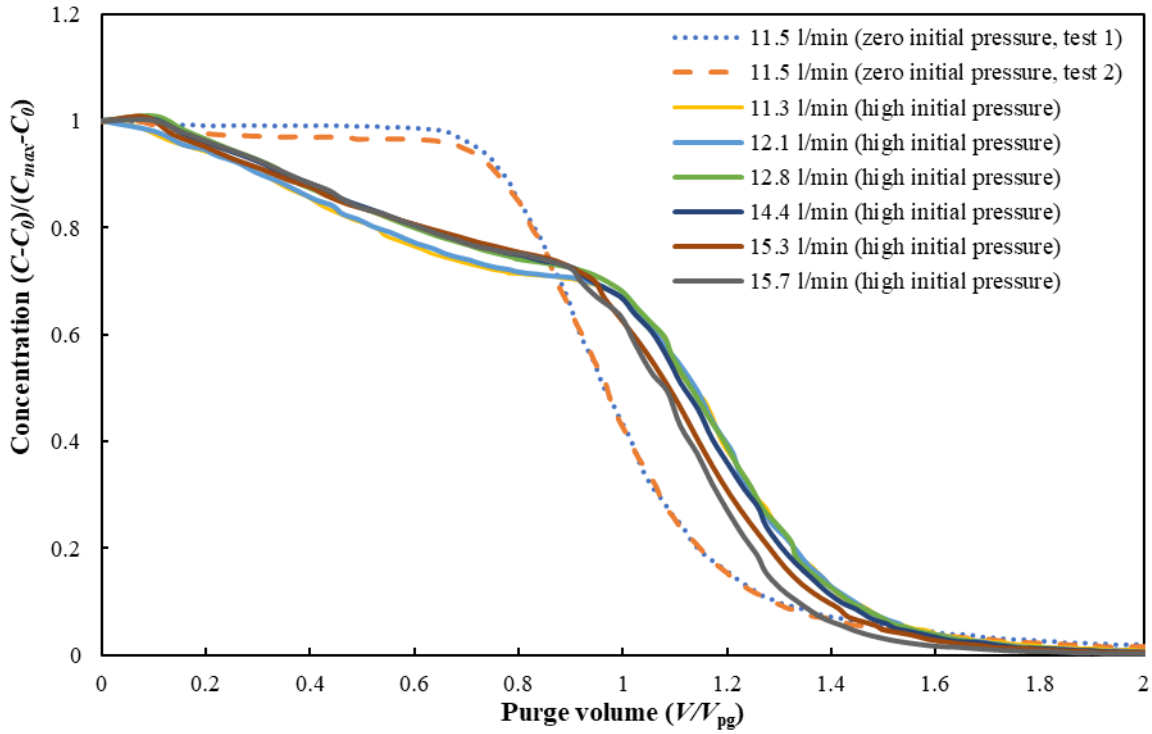

Fig. 7. Normalized concentration at RO brine outlet vs. normalized purge volume. Tests 1–2 (11.5 L/min) were conducted without applying pressure, using a similar procedure to [29]. The remaining tests used an initial high pressure condition, as occurring in the real batch RO process. C_0 is the feed water concentration, and C_{max} is the initial concentration of brine leaving the system at the start of the purge phase.

5.3. Salt passage and rejection

At the beginning of the pressurization phase, permeate quality was poor, but it improved after initially saline permeate left the system. Fig. 8 shows the permeate conductivity as a function of time at 1 g/L feed concentration, r = 0.8, and J_w = 18.1 LMH. The results were taken from the fifth cycle such that the system was at the steady-state condition. Permeate conductivities

were measured and logged 10 times per second for increased resolution. Over the first 30 seconds of the pressurization phase, permeate conductivity peaked sharply, dropped, and then increased again slowly. The initial peak may be attributed to the salt diffusion during the purge-and-refill phase. Because of the concentration gradient across the membrane, salt passed through it and reached the permeate spacer, even in the absence of permeate flux. The salt accumulated and exited the system shortly after the next pressurization phase commenced. Similarly, Wei et al. [17] reported that permeate was relatively poor at the start of each pressurization phase, but then improved quickly. Further, Davies et al. [10] observed that permeate concentration decreased 4 times from 0.4 to 0.1 g/L after 50 seconds of pressurization (at 2 g/L feed concentration).

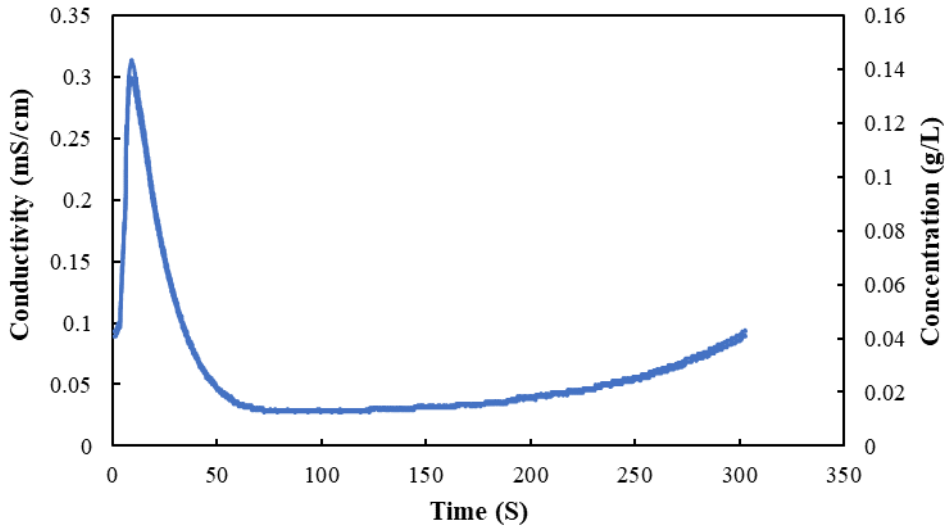

Fig. 8. Permeate conductivity and concentration *vs*. time after start of pressurization, at 1 g/L feed solution, r = 0.8 and J_w = 18.1 LMH.

Regarding salt rejection over the whole cycle, Fig. 9 compares model predictions (based on Eq.12), against experimental measurements at different water fluxes ranging from 11 to 22 LMH. Experiments were conducted at 3 g/L feed concentration and Q_r/Q_f = 2.1. Model predictions were 2 to 2.5% higher than the experimental results. This is because of the low quality permeate at the start of each pressurization phase, as discussed above. The difference between experimental and theoretical rejection decreased slightly as flux increased.

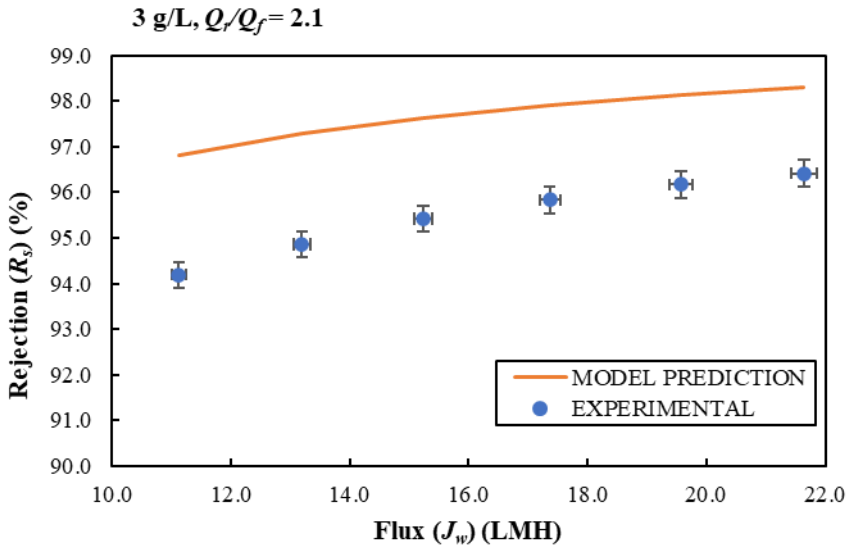

Fig. 9. Model predictions and experimental rejection values at various water fluxes and 3 g/L feed concentration (Q_r/Q_f = 2.1).

5.4. Hydraulic SEC

Though there have been several modelling studies on the energy consumption of batch RO systems [15, 16, 18, 19, 21, 23, 25, 32, 33], most studies did not consider all losses in such systems; and only Wei et al. [17] reported model validation by experiment. In the current study, the experimental hydraulic work of the batch RO system was calculated by integrating, at each measurement time step, the differential pressure of each pump by the amount of water displaced by that pump. Hydraulic *SEC* was thus measured and compared against model predictions. The model used two adjustable parameters: (1) the discharge coefficient of the valves, C_d, which was adjusted to 0.62 (within the expected range of 0.6 to 0.7 [31]); and (2) the permeability of the membrane, which was adjusted to A_w = 4.4 LMH/bar. This permeability value was consistent with readings taken in separate tests using tap water without salt added. In addition, piston friction was determined at ΔP_s = 3.5 kPa from the difference in readings between the pressure sensors at either side of the piston.

The experiments in this section were conducted at recovery of 0.8 in accordance with the design intention of the system. Though the results of section 5.1 showed that recovery was, at constant feed flow, less than 0.8, this shortfall was corrected by slowing the supply pump during the purge-and-refill phase so as to compensate for the secondary purge effect of the osmotic backflow. Thus, the target recovery of 0.8 was achieved.

Fig. 10 illustrates hydraulic *SEC* measured experimentally and predicted by our model at different salinities, recirculation flow ratios and water fluxes. Experimental hydraulic *SEC* at r = 0.8, J_w =17.3 LMH, and feed salinities of 2, 3, 4, and 5 g/L were 0.3, 0.37, 0.43, and 0.48 kWh/m^3 respectively, giving a maximum error of 2% against model predictions (see Fig. 10 (A)). Hydraulic work of the recirculation pump in both phases and supply pump in the purge-and-refill phase were approximately the same for all feed concentrations. Only in the case of the supply pump in the pressurization phase did the hydraulic work increase with concentration, because of the increased osmotic pressure.

The hydraulic *SEC* measured in this study was consisted with previous batch RO studies, although the recovery was higher than before. Wei et al. [17] reported hydraulic *SEC* of 0.25 kWh/m^3 at 2 g/L feed concentration, and J_w = 20 LMH in their bladder system. In comparison, this study measured slightly higher hydraulic *SEC* of 0.31 kWh/m^3 at similar flux and concentration, which may be explained by the higher recovery of this study (r = 0.8 compared to r = 0.5 in [17]). Davies et al. [10] reported hydraulic *SEC* of 0.22, 0.24, and 0.27 kWh/m^3 at the recovery of 0.4, 0.57, and 0.7, respectively in a free-piston batch RO design using 4-inch membrane at similar flux and concentration. However, those results only included supply pump work during pressurization. Our corresponding result was slightly higher at $SEC_{P,SP}$ = 0.28 kWh/m^3 which again may be explained by the higher recovery of 0.8. Variations in membrane permeability and pipework details may also contribute to the observed differences.

Total hydraulic *SEC* increased from 0.42 to 0.47 kWh/m^3 on increasing recirculation flow ratio, Q_r/Q_f, from 1.55 to 3.92 at flux of J_w = 17.3 LMH (Fig. 10B). As expected, higher recirculation flow increased recirculation pump *SEC* but decreased supply pump *SEC*. Experimental hydraulic *SEC* for Q_r/Q_f =1.55, 2.13, and 2.73 was roughly constant at 0.43 kWh/m^3. However, at Q_r/Q_f = 3.35 and 3.92, the drawback of using a larger recirculation flow rate outweighed the benefit. The largest error between model predictions and experimental measurements of *SEC* was 3.1% at Q_r/Q_f = 1.55. This may be because of inaccuracy of the longitudinal concentration gradient model at low recirculation flow. At higher recirculation flow, the error was less than 2.5%.

We also investigated the model accuracy at different water fluxes (see Fig. 10C). The biggest error of 2.8% occurred at the highest flux of 21.2 LMH, when the experimental value and model predictions were 0.477 and 0.463 kWh/m^3, respectively.

Overall, with osmotic backflow included, we obtained a good agreement (<3% error in *SEC*) between model and experiments at different salinities, recirculation flow rates, and water fluxes. Thus, our model can be used to predict the free-piston batch RO performance under various conditions in the treatment of the brackish water. Further, since the model uses only explicit algebraic equations, it is readily implemented as a spreadsheet and made accessible here for general use.

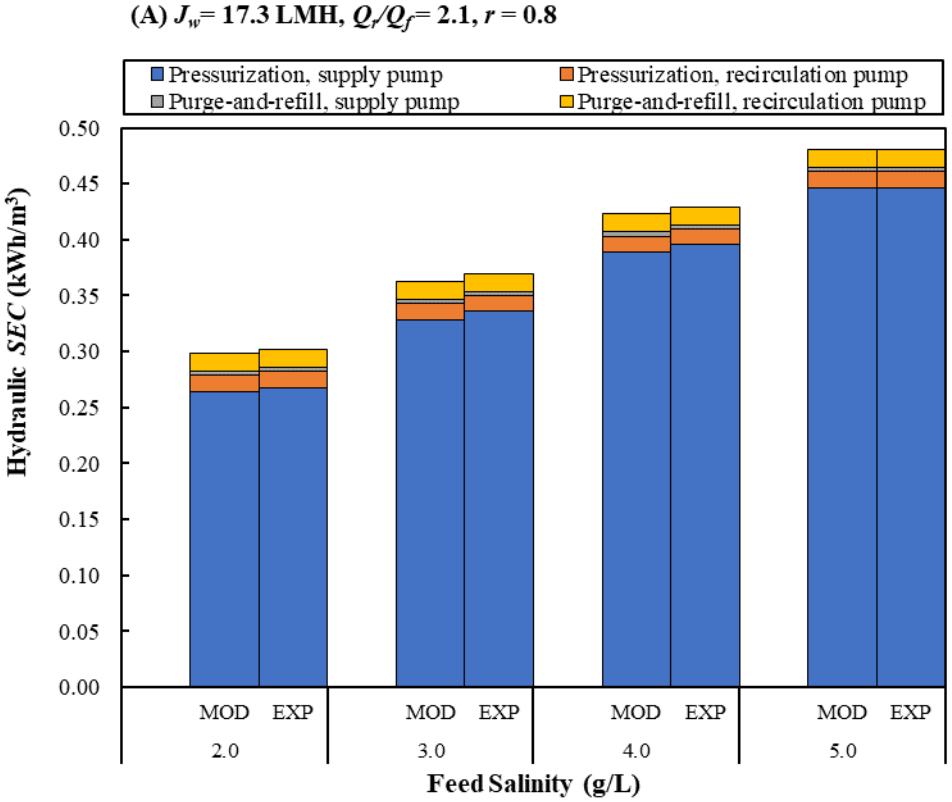
(A) J_w= 17.3 LMH, Q_r/Q_f= 2.1, r = 0.8
Pressurization, supply pump
Pressurization, recirculation pump
Purge-and-refill, supply pump
Purge-and-refill, recirculation pump
Hydraulic SEC (kWh/m3)
0.50
0.45
0.40
0.35
0.30
0.25
0.20
0.15
0.10
0.05
0.00
MOD EXP
2.0
3.0
4.0
5.0
Feed Salinity (g/L)

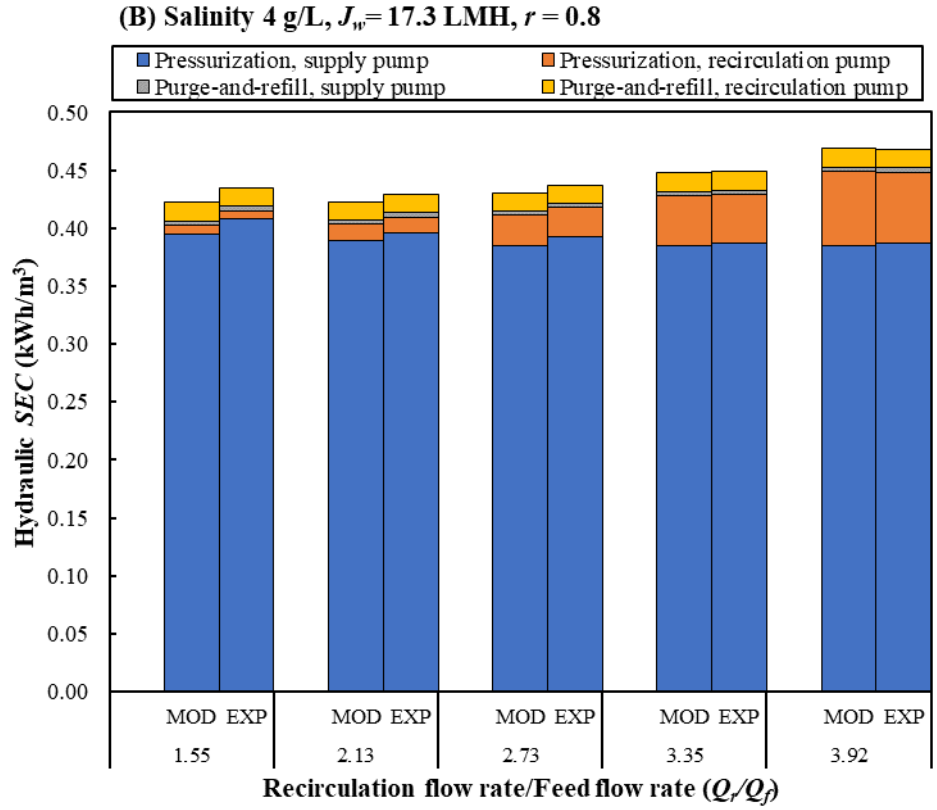
(B) Salinity 4 g/L, J_w= 17.3 LMH, r = 0.8
Pressurization, supply pump
Pressurization, recirculation pump
Purge-and-refill, supply pump
Purge-and-refill, recirculation pump
Hydraulic SEC (kWh/m3)
0.50
0.45
0.40
0.35
0.30
0.25
0.20
0.15
0.10
0.05
0.00
MOD EXP
1.55
2.13
2.73
3.35
3.92
Recirculation flow rate/Feed flow rate (Q_r/Q_f)

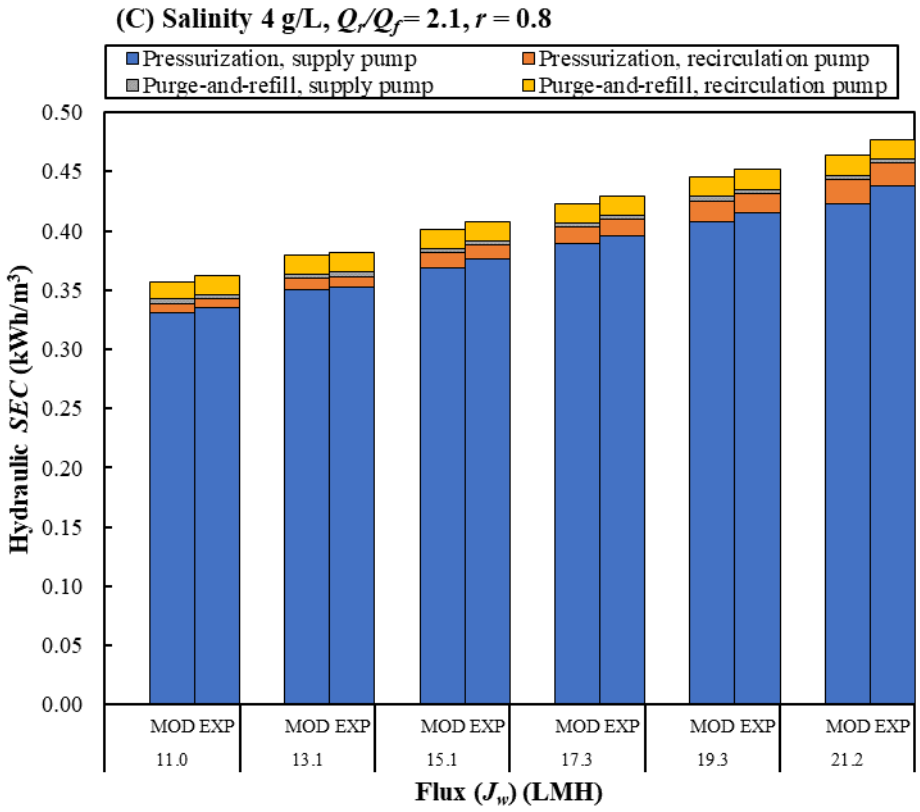

Fig. 10. Model predictions (MOD) and experimental measurements (EXP) of hydraulic *SEC* of free-piston batch RO at various: (A) feed salinities, (B) recirculation flow ratios, and (C) water fluxes.

5.5. Electrical SEC

For the first time in batch RO studies, we measured electrical *SEC* and compared it to hydraulic *SEC*. Whereas hydraulic *SEC* is of academic interest in understanding and improving the fundamental system, industries will be more interested in electrical *SEC* as it determines the cost of operation.

5.5.1. Comparison of electrical and hydraulic SEC

Electrical *SEC* was determined by integrating measured power over time for each pump, and dividing by water output. Fig. 11 compares the hydraulic and electrical *SEC* breakdown of the batch RO system at different salinities, recirculation flow ratios, and water fluxes. The total measured electrical *SEC* at salinities of 2, 3, 4, and 5 g/L were respectively 0.57, 0.67, 0.74, and 0.83 kWh/m^3 at flux J_w = 17.3 LMH and Q_r/Q_f = 2.1 (Fig. 11A). The difference between electrical and hydraulic *SEC* becomes smaller when concentration increases; e.g. the electrical *SEC* was 1.9 and 1.7 times higher than the hydraulic *SEC* at 2 and 5 g/L respectively, showing an increase of the supply pump efficiency with pressure.

Regarding the effect of recirculation flow on *SEC* (Fig. 11B), at Q_r/Q_f = 1.55 and 2.13, both electrical *SEC*s and hydraulic *SEC*s were unchanged (0.43 kWh/m^3 for hydraulic *SEC*s and 0.73 kWh/m^3 for electrical *SEC*s); whereas electrical *SEC* increased at a higher rate than hydraulic *SEC* at larger recirculation flow rates. Thus, electrical *SEC* increased from 0.73 to 0.85 kWh/m^3, whereas hydraulic *SEC* rose from 0.43 to 0.47 kWh/m^3 when Q_r/Q_f increased to 3.92.

Measurement of electrical and hydraulic *SEC* at different water fluxes (Fig. 11C) showed that, by increasing water flux from 11 to 21.2 LMH, both *SEC*s increased, giving a 31% and 20% rise in hydraulic and electrical *SEC*, respectively. This was because of the greater membrane friction loss represented by the 2nd term in Eq. (7). On the other hand, the higher flux gave a 74% increase in system output (an increase from 9.6 to 16.7 m^3/day).

The electrical *SEC* of the system is greatly affected by the supply and recirculation pump efficiencies. Table 4 shows measured pumps efficiencies (i.e. hydraulic *SEC*/electrical *SEC*). Supply pump efficiency was acceptable (mostly >60%) during the pressurization phase, but poor during the purge-and-refill phase (<15%). This is because the supply pump was not optimised for low-pressure operation.

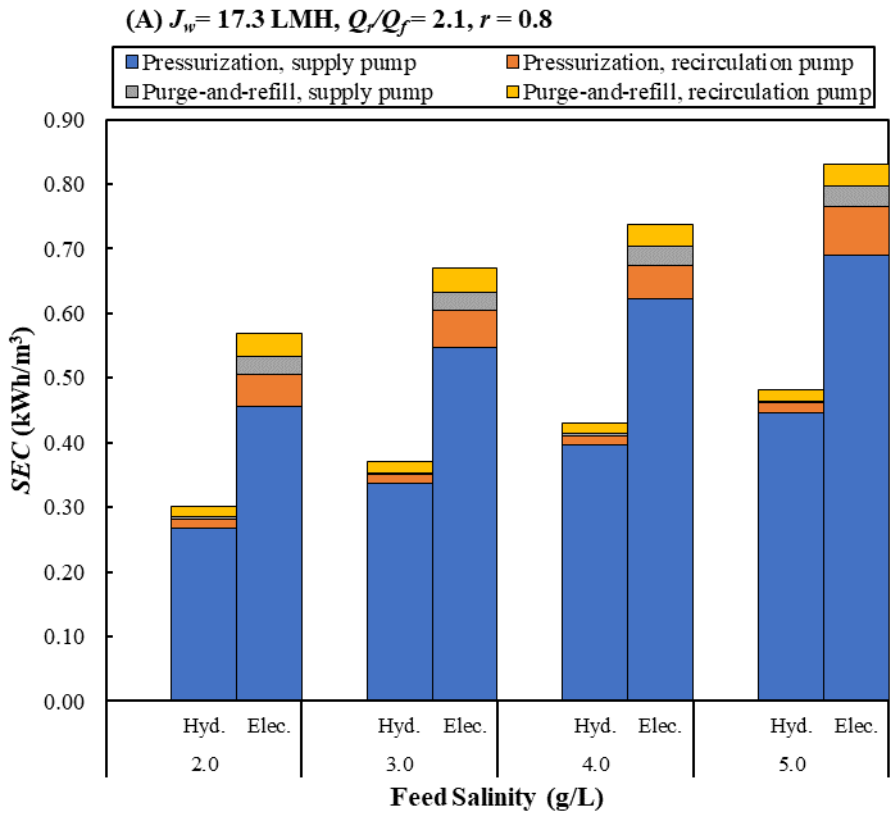

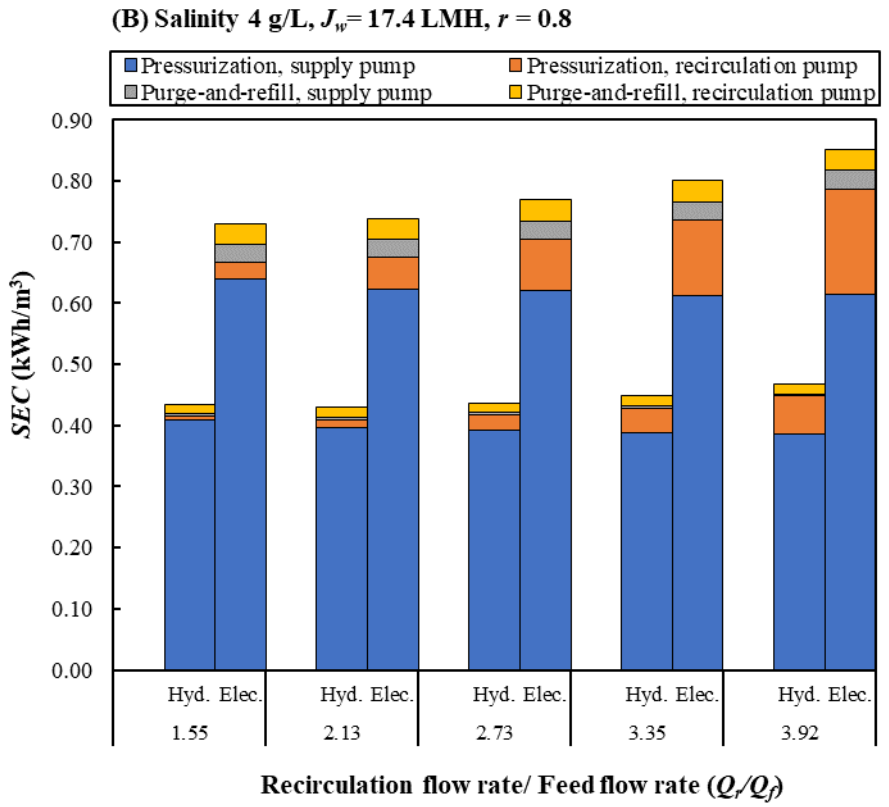

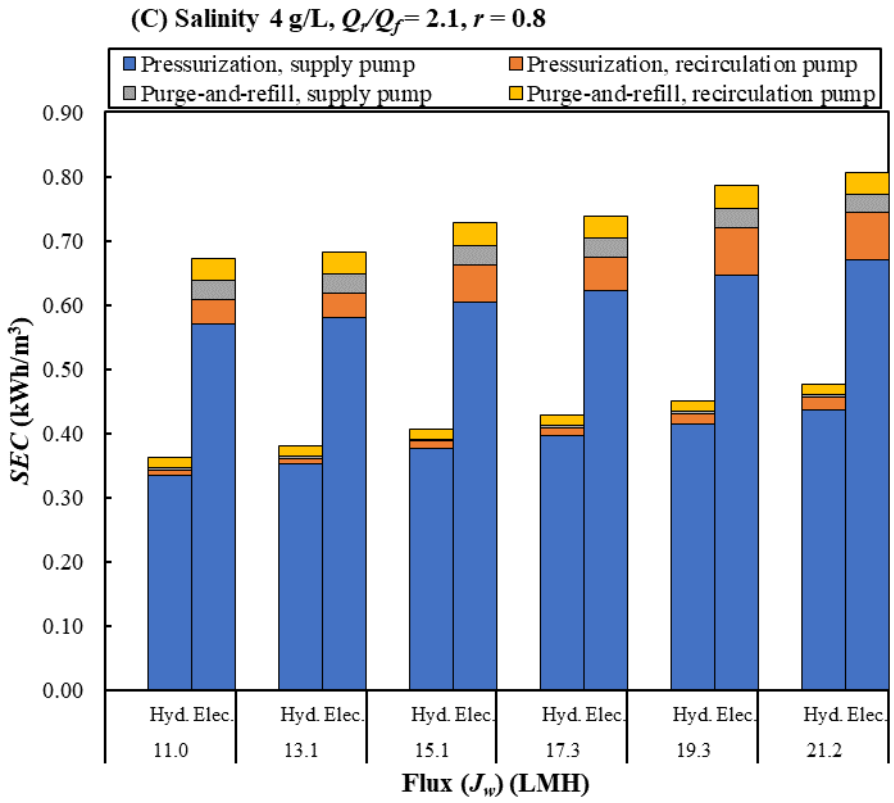

Fig. 11. Hydraulic and electrical *SEC* of the free-piston batch RO system over a cycle at various: (A) salinities, (B) recirculation flow ratios, and (C) water fluxes.

Table 4. Feed and recirculation pump efficiencies over a cycle for pressurization and purge-and-refill phases at various water fluxes, 4 g/L feed concentration and $Q_r/Q_f = 2.1$.

Flux J_w (LMH)	Pump efficiency (%)			
	Supply pump		Recirculation pump	
	Pressurization	Purge-and-refill	Pressurization	Purge-and-refill
11.0	58.7	11.9	19.5	47.1
13.1	60.6	13.3	25.4	47.7
15.0	62.3	10.8	20.2	44.4
17.3	63.6	12.6	26.5	47.6
19.3	64.3	11.4	21.9	44.6
21.2	65.3	12.6	26.0	48.1

5.5.2. Breakdown of electrical SEC

The electrical *SEC* breakdowns of each pump during the pressurization and purge-and-refill phases are shown in Fig. 12. In general, the main contribution to *SEC* came from the supply pump during the pressurization phase, contributing 75 to 85% of total *SEC*. At increased feed salinity, the supply pump contributed a greater fraction. For example, supply pump pressurization *SEC* at 1, 2, 3, 4, and 5 g/L salinity contributed 75, 79, 82, 84, and 85% respectively. In contrast, *SEC* in the purge-and-refill phase for both pumps, and during the pressurization phase for the recirculation pump, are independent of feed salinity. Therefore, as salinity increases, the supply pump must apply higher pressure and its energy consumption increases, while other *SEC* components remain constant.

About 6% of *SEC* came from the supply pump in the purge-and-refill phase, as needed to flush the brine out of the system. This significant fraction is not favourable since it reduces the system's potential to minimize *SEC*. The main cause is the low efficiency of the supply pump (< 15%) in the purge-and-refill phase.

The recirculation pump contributed 10 to 20 % to the total *SEC*, with lower percentage contribution at higher salinities. Thus, this contribution dropped from 19 to 11% when feed salinity increased from 1 to 5 g/L. The lower the recirculation *SEC*, the closer the system comes to achieving the theoretical minimum *SEC*.

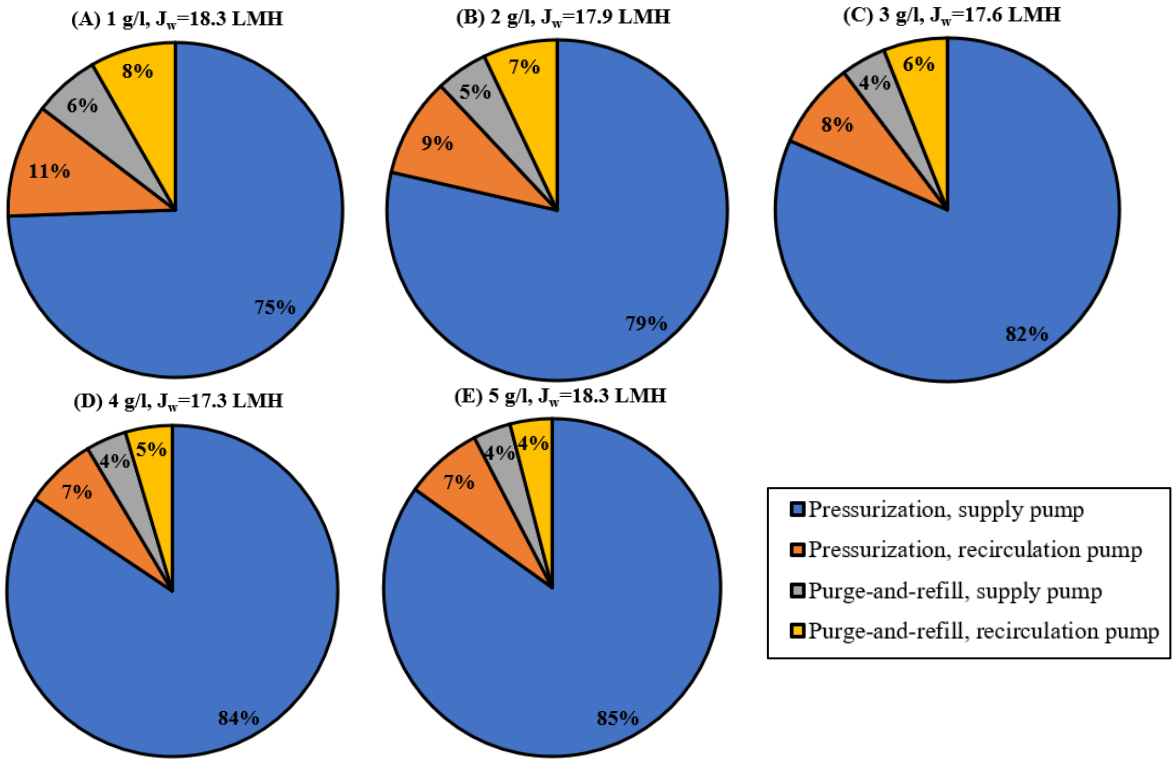

Fig. 12. Electrical *SEC* breakdown (percentage) for the feed and recirculation pumps over the pressurization and purge-and-refill phases at feed salinity of (A) 1g/L, (B) 2 g/L, (C) 3 g/L, (D) 4 g/L, and (E) 5 g/L.

5.5.3. Sensitivity of electrical SEC to recirculation flow rate

Table 5 presents the effect of increasing recirculation flow rate on the electrical *SEC* breakdown. On increasing the ratio Q_r/Q_f while keeping other parameters constant, the recirculation pump provided higher flow during pressurization and consequently the *SEC* of this pump rose (Table 5). On the other hand, at low recirculation flow, concentration polarization (S_p) and longitudinal concentration gradient (S_L) inside the RO module increase and the supply pump must apply a slightly higher pressure to compensate. For example, when Q_r/Q_f increased from 1.55 to 3.92, $SEC_{P,RP}$ increased by 0.146 kWh/m^3 while $SEC_{P,SP}$ decreased by 0.026 kWh/m^3. Overall, as recirculation flow increased, recirculation pump *SEC* rose at a higher rate than the reduction in supply pump *SEC*. Meanwhile, *SEC* of pumps in the purge-and-refill phase were approximately constant and insignificant. Therefore, it is better to operate with Q_r/Q_f between 1.5 and 2.2, as concluded in our previous theoretical study [19]. Fig. 13 also shows the effect of recirculation rate on the total electrical *SEC* at various feed salinities.

Table 5. Effect of varying recirculation flow rate ratio on the *SEC* breakdown and total *SEC* over a cycle at 4 g/L feed salinity and J_w = 17.3 LMH.

	Electrical *SEC* (kWh/m^3)				
	Pressurization phase		Purge-and-refill phase		
Q_r/Q_f	Supply pump ($SEC_{P,SP}$)	Recirculation pump ($SEC_{P,RP}$)	Supply pump ($SEC_{P\&R,SP}$)	Recirculation pump ($SEC_{P\&R,RP}$)	Total
1.55	0.640	0.028	0.029	0.034	0.731
2.13	0.623	0.052	0.029	0.034	0.738
2.73	0.620	0.084	0.029	0.035	0.769
3.35	0.613	0.125	0.029	0.034	0.801
3.92	0.614	0.174	0.029	0.034	0.851

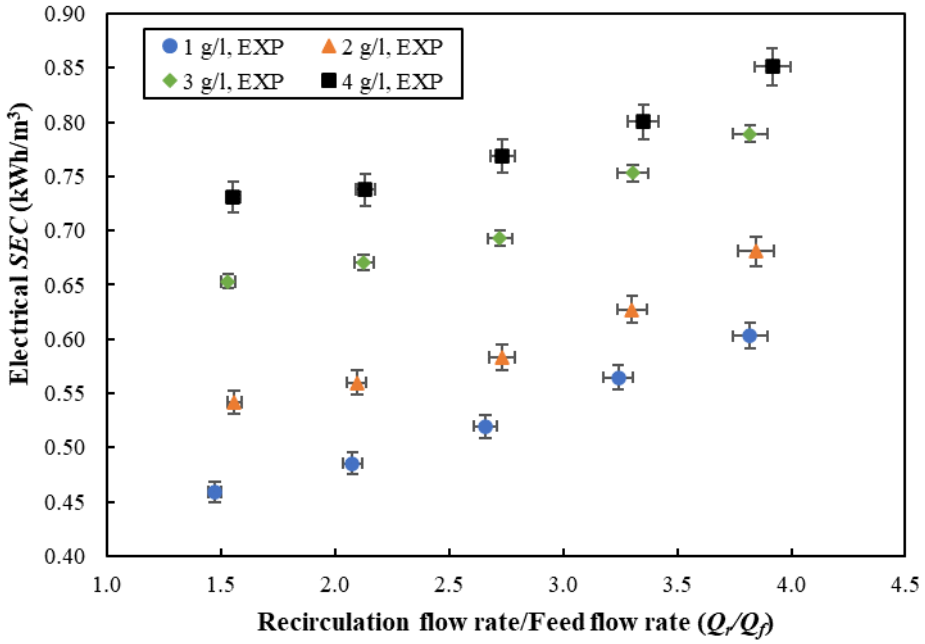

Fig. 13. Recirculation flow rate effect on the total electrical *SEC* of the batch RO system over a cycle at various salinities, and J_w = 17.3 LMH.

5.5.4. Sensitivity of electrical SEC to permeate flux

Another factor having an important effect on the performance of RO systems is permeate flux. We measured the effect of permeate water flux on the main factors of the system including electrical *SEC* (see Table 6). Electrical *SEC* increased with flux as expected from Eq. (7). However, at higher fluxes, the system output was higher in direct proportion to the flux. Thus, there was a trade-off between *SEC* and output. For example, when flux was doubled, electrical *SEC* increased by 28% while output rose by 74%. Additionally, at lower fluxes, permeate quality worsened, and by increasing the system flux, rejection of batch RO system slightly improved. System flux is always lower than the permeate flux because of the reset time in the purge-and-refill phase when permeate is not produced.

The effect of feed salinity on the total electrical *SEC* at various water fluxes is also illustrated in Fig. 14. Higher feed salinity resulted in higher electrical *SEC*.

Table 6. The effect of varying flux on the important factors of batch RO system at 2 g/L feed salinity and Q_r/Q_f = 2.1. System flux is the flux averaged over the whole cycle.

Flux during Press. J_w, (LMH)	System Flux (LMH)	Rejection R_s	Output (m^3/day)	Peak Pressure $\hat{P}$ (bar)	Electrical *SEC* (kWh/m^3)
11.42	9.90	0.946	9.74	11.63	0.482
13.59	11.49	0.953	11.30	12.32	0.498
15.63	12.92	0.957	12.71	13.06	0.518
17.89	14.44	0.960	14.21	13.56	0.560
20.11	15.80	0.963	15.54	14.43	0.581
22.35	17.22	0.966	16.94	15.11	0.618

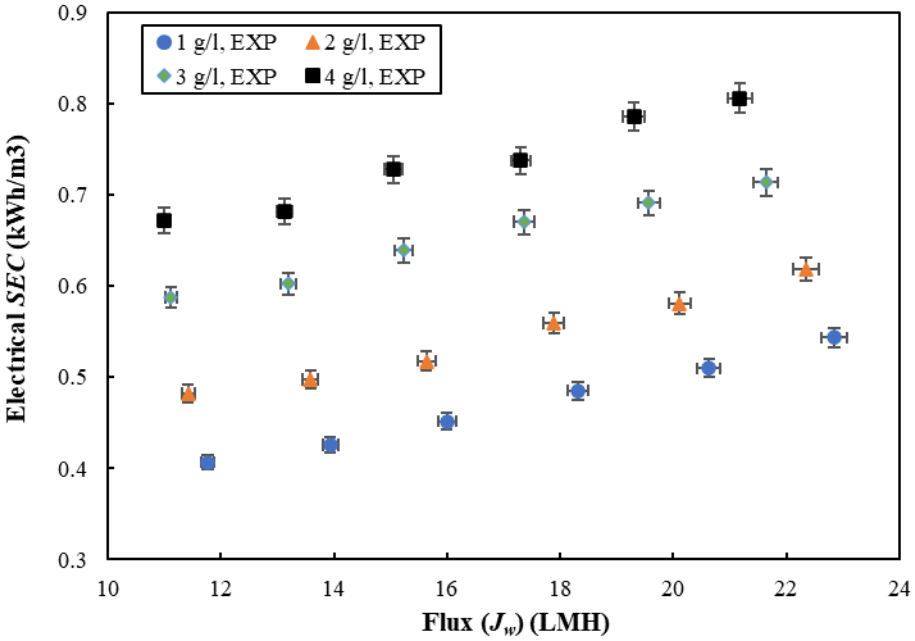

Fig. 14. Effect of the permeate flux on the total electrical *SEC* at various salinities ($Q_r/Q_f = 2.1$).

5.6. Concentration in the recirculation loop

Concentration difference from the inlet to outlet of a RO module tends to increase system pressure and energy consumption. We have measured how the concentration at both inlet and outlet vary against time, how these concentrations were affected by the recirculation flow rate, and how they compared to model predictions (see SI Section 4 for details of the Ordinary Differential Equation model used). The concentration difference becomes zero at infinite recirculation flow, which represents the ideal case as regards minimizing the work done by the supply pump, but overall SEC minimisation requires a finite optimum recirculation rate as seen in section 5.4.

Fig. 15 shows experimental and theoretical results for concentration *vs.* time with recirculation flow of $Q_r/Q_f = 2.1$. The experimental results are for two cases: A) constant feed flow over both phases of operation (such that the total purge volume equalled the nominal purge volume V_{pg} plus the osmotic backflow, as in section 5.1, giving recovery r<0.8); and B) reduced feed flow and volume (such that the purge volume equalled just V_{pg} and recovery of r=0.8 was achieved). The time axis is normalized to the duration of the pressurization phase. In case A, there was good agreement between the theoretical and experimental values during the first half of the phase, except for the initial peak in the experimental outlet concentration. This peak

reflected salt retention inside the RO module at the end of the purge-and-refill phase. As the flow reversed to start the pressurization phase, a portion of concentrated brine inside the RO module flowed back towards the outlet (which was the inlet during purge-and-refill) causing this initial peak to be detected. Subsequently, this portion of brine entered the work exchanger to become mixed with the bulk of recirculating solution. In the second half of the pressurization phase, experimental inlet and outlet concentrations were slightly lower than the theoretical predictions.

In case B, the initial peak was larger due to the higher salt retention associated with less purging. The experimental outlet concentration was slightly above the theoretical prediction mostly, except over the last 20% of the pressurization phase where there was a good agreement. The outlet concentration was higher than the ideal concentration in both cases. Furthermore, the difference between the experimental outlet concentration and ideal concentration varied through the phase, being higher at the beginning and lower at the end. Thus, a varying recirculation (faster in the first half of the pressurization phase) may be helpful to reduce this gap.

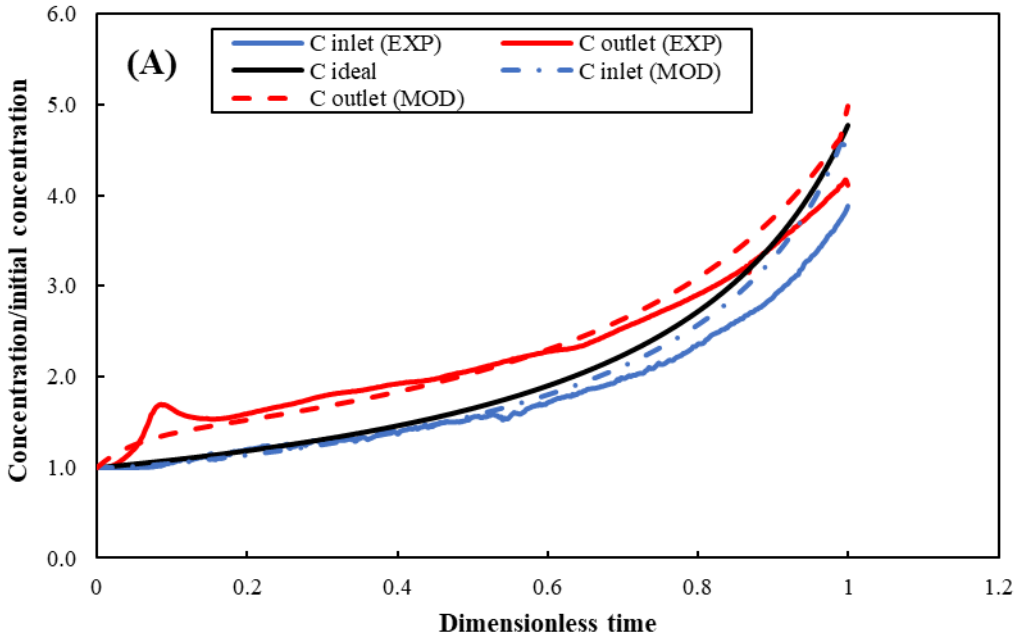

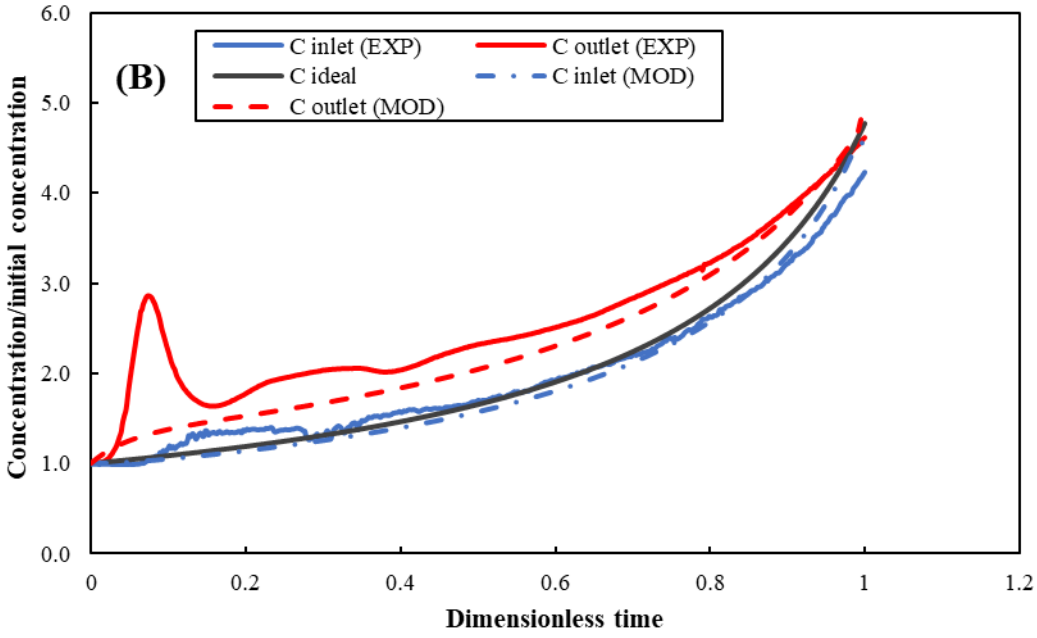

Fig. 15. Comparison of model predictions (MOD) and experimental (EXP) salt concentration vs. time (normalised to duration of pressurization phase) at the inlet and outlet of the RO module. (A) constant feed flow, purging the nominal purge volume V_{pg} plus the osmotic backflow ($r = 0.74$), and (B) purging V_{pg} exactly ($r = 0.8$). Experiments were conducted at 4 g/L feed concentration, $Q_r/Q_f = 2.1$ and $J_w = 17.3$ LMH. The ideal concentration corresponds to that expected at infinite recirculation flow and therefore homogeneous concentration.

5.7. Pressure

Experimental and theoretical supply pump pressures over a pressurization phase of the free-piston batch RO system are shown in Fig. 16. The calculation of theoretical pressure considers all the inefficiencies and losses including concentration polarization, salt retention, longitudinal concentration gradient, net driving pressure to overcome the hydrodynamic resistance in the pores of the RO membrane, pressure drop in the RO module, pressure drop caused by piston seal, and frictional pressure drop over the recirculation valve (see SI section 4). Therefore, a good agreement between model predictions and experimental measurements was achieved (Fig. 16). However, there are still some minor differences. First, at the beginning of the pressurization phase, the model predicted instantaneous pressure rise and permeate production; whereas in reality, it took 15–20 seconds for the pressure to rise to the predicted value and for production to begin. This corresponded to about 5% of the total duration of the pressurization phase and to a supplied volume of 3–4 L. Second, corresponding to the initial concentration peak discussed above, we observed a small peak in the pressure at the start of the pressurization phase. This peak increased with feed solution salinity, as shown in Fig. 16 at 4 g/L feed concentration. Furthermore, the theoretical peak pressure at the end of the pressurization phase was about 1 bar higher than the experimental measurement. This may be because the internal volume of the RO channel expanded under pressure, resulting in a slightly lower final concentration and lower peak osmotic pressure than predicted. Such expansion could also explain the slow initial rise in pressure, as incoming feed pressure gets cushioned as the membrane deforms.

Deformation of RO membranes under pressure (i.e. compaction) has been observed in several studies [34, 35], especially under high pressure operation. For example, Davenport et al. [36]

reported 60% compressive strain in a seawater RO membrane at 150 bar. In our study, to accommodate 4 L of supplied fluid, the membrane would need to compress by 0.1 mm, approximately equivalent to the thickness of the membrane itself – and the operating pressure is lower (<25 bar). This suggests that compressive strain is not the only cause of the slow pressure rise. Additional causes may include compression of the permeate-side spacer, and wavy deformation of the membrane within the spacer-membrane-spacer sandwich. Dilation of other components like the pressure vessels, and the hose connecting the supply pump to the rig, may also contribute – though these contributions are estimated to be individually small. If, as is likely, the membrane springs back upon release of pressure, this could contribute to the apparent backflow described in section 5.1 above. The phenomena of membrane deformation and osmotic backflow may be interlinked in batch RO.

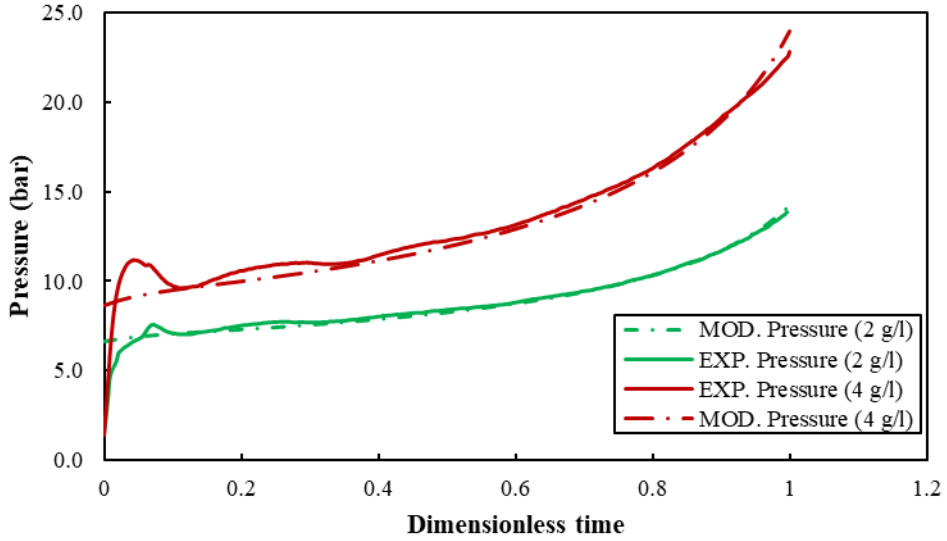

Fig. 16. Comparison of model predictions (MOD) and experimental (EXP) pressure over the pressurization phase at feed concentrations of 2 and 4 g/L (J_w = 17.3 LMH, Q_r/Q_f = 2.1, and r = 0.8).

At the end of the pressurization phase, pressure peaks again at a maximum value. Fig. 17 compares experimental final peak pressure against the value predicted by Eq. (11), at different water fluxes. At all water fluxes, experimental measurements were lower than model predictions, most likely because of membrane compliance as noted above. Nonetheless, error was less than 6%. In addition, the error was bigger at the lowest tested flux of 11 LMH and decreased by increasing the flux; the smallest difference was 3% at J_w = 22 LMH.

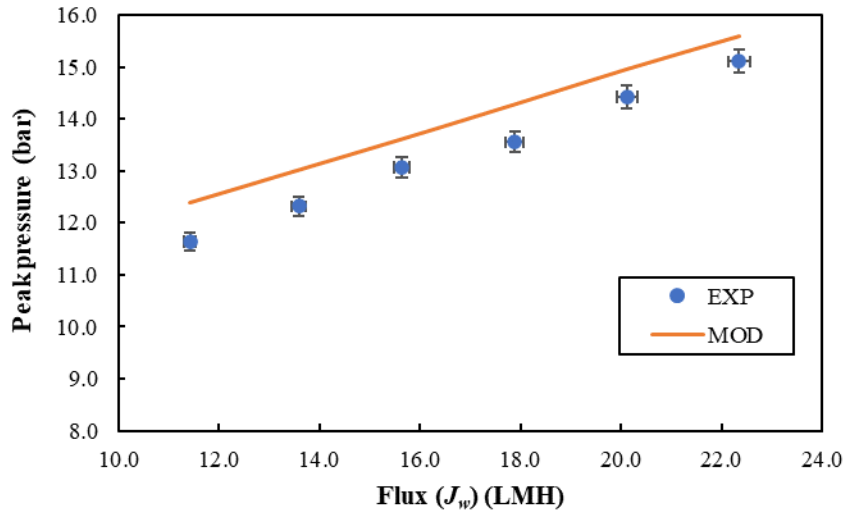

Fig. 17. Peak pressure at end of pressurisation phase *vs* water flux. Model predictions (MOD) and experimental values (EXP), at 2 g/L feed concentration, and $Q_r/Q_f = 2.1$.

6. Potential future improvements

The experiments have shown promising electrical *SEC* values of 0.40–0.84 kWh/m^3 at 1–5 g/L feed salinities. These values compare well with many brackish water desalination systems available today, but are above the predictions of our earlier theoretical study [19]. For example, we predicted 0.39 kWh/m^3 for high-flux membrane (DuPont XLE-440) at 3 g/L feed concentration (with J_w = 22.06 LMH, and Q_r/Q_f = 2.03) [19]. The main reasons for this discrepancy are that: (1) the theoretical study assumed efficiencies of 70% for the supply pump and 50% for the recirculation pump, whereas actual efficiencies are in the range of only 10–65% (Table 4); (2) it assumed membrane permeability of A_w=8.32 LMH/bar compared to only 4.4 LMH/bar determined experimentally.

By using our modified model for such a high-permeability membrane, and assuming pump efficiencies of 70% and 50%, we now predict *SEC* of 0.48 kWh/m^3 at the same feed concentration and flux. The remaining discrepancy with the earlier value of 0.39 kWh/m^3 is due mainly to osmotic backflow and also to differences in friction losses associated with detailed pipework and valve design.

6.1. Effect of membrane permeability on SEC

Membrane permeability has a significant effect on the energy consumption and performance of RO systems. Several studies have shown that *SEC* decreases with increasing permeability [23, 37, 38]. We used our validated model to study further the potential of using high-permeability membranes in the current batch RO system (Fig. 18). The Eco Pro-440 element used in the experiments had a permeability of 4.4 LMH/bar. On increasing membrane permeability to 6, 8, and 10 LMH/bar, hydraulic *SEC* will decrease by 8.0, 13.5, and 16.8%, respectively (at 4 g/L feed concentration, r = 0.8, J_w = 17.3 LMH, and Q_r/Q_f = 2.1).

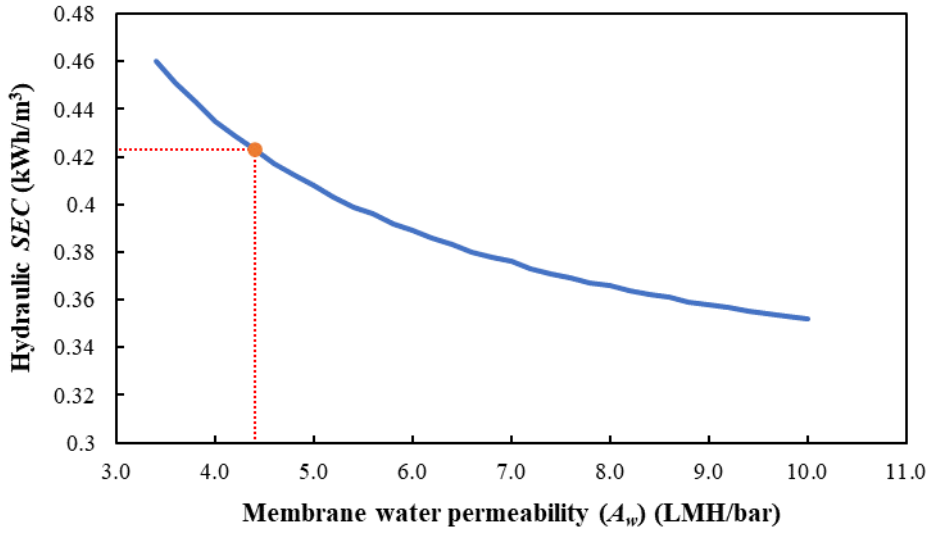

Fig. 18. Model predictions of hydraulic *SEC* as a function of membrane water permeability (A value) at 4 g/L feed solution, r=0.8, J_w = 17.3 LMH, and Q_r/Q_f = 2.1. The orange point is the value measured experimentally for the Eco Pro-440 membrane.

6.2. Effect of pump efficiency

More efficient pumps will improve system performance considerably. In these experiments, pump efficiencies were mostly below 65% (Table 4). Table 7 shows how electrical *SEC* of the free-piston batch RO will improve using pumps with higher efficiencies, assuming that both pumps have the same efficiency over both phases of operation. If the pump efficiency were 80%, *SEC* would decrease to 0.37, 0.45, 0.54, and 0.6 kWh/m^3 at 2, 3, 4, and 5 g/L feed concentration, respectively. Therefore, pumps that are better matched to the system will significantly improve energy performance.

Table 7. Predicted electrical *SEC* according to pump efficiencies at various feed salinities (J_w = 17.3 LMH, and Q_r/Q_f = 2.1). In these experiments, the efficiencies are those in Table 4.

Feed salinity (g/L)	Pump efficiencies (%)	Electrical *SEC* (kWh/m^3)
2	These experiments	0.56
	60	0.49
	70	0.42
	80	0.37
3	These experiments	0.64
	60	0.6
	70	0.51
	80	0.45
4	These experiments	0.74
	60	0.72
	70	0.61
	80	0.54
5	These experiments	0.83
	60	0.8
	70	0.69
	80	0.6

6.3. Effect of valve size

We also investigated the effect of valve orifice diameter on *SEC* (Fig. 19). By increasing the orifice diameter from 15 to 20 or 25 mm, we predict energy savings of 6 or 7.5% respectively. This results from the reduction of velocity in Eq.10 and consequent reduction in friction losses.

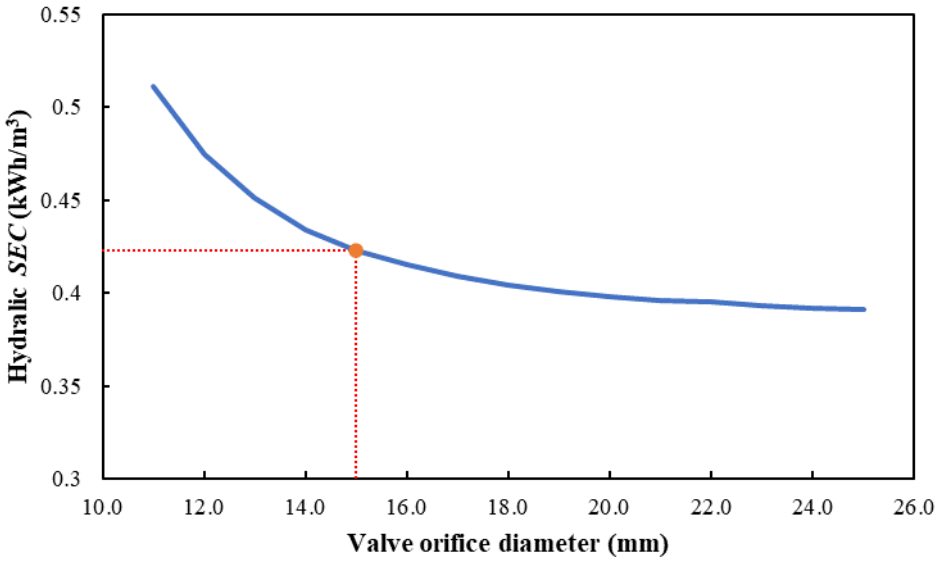

Fig. 19. Predicted hydraulic *SEC* as a function of valves diameter in the free-piston batch RO at 4 g/L feed solution, J_w = 17.3 LMH, r = 0.8, and Q_r/Q_f = 2.1. The orange point is the valve diameter used in the current prototype.

6.4. Overall scope for improvement and comparison with existing systems

The above improvements may be implemented together to reduce further *SEC*. Table 8 shows predicted *SEC* after making improvements in membrane permeability (i.e. A_w = 8 LMH/bar), pump efficiencies (i.e. 70% for both supply and recirculation pumps) and in valve orifice diameter (i.e. 25 mm) at different feed concentrations. On implementing all these changes, electrical *SEC* should substantially decrease from the range of 0.48–0.83 to that of 0.2–0.56 kWh/m^3 for feed concentration of 1–5 g/L. However, there is still a gap between predicted *SEC* of the improved system and the ideal minimum SEC_{ideal}, indicating further theoretical scope for improvement (see Table 8).

Table 8. Comparison of theoretical minimum *SEC* (based on Eq. 1) with the measured results, and with predicted electrical *SEC* following improvements in membrane water permeability (A_w = 8 LMH/bar), pump efficiencies (70% for both supply and recirculation pumps) and valve orifice diameter (25 mm) at various feed salinities (water flux J_w = 17.3 LMH). The corresponding 2nd law efficiency (SEC_{ideal}/SEC) is also shown.

Feed salinity (g/L)	Ideal system	Current batch RO system		Model predictions after improvements	
	SEC_{ideal} (kWh/m^3)	Electrical *SEC* (kWh/m^3)	2nd law efficiency (%)	Electrical *SEC* (kWh/m^3)	2nd law efficiency (%)
1.0	0.044	0.485	9.1	0.204	21.6
2.0	0.088	0.560	15.7	0.297	29.6
3.0	0.132	0.637	20.7	0.389	33.9
4.0	0.176	0.738	23.8	0.478	36.8
5.0	0.220	0.831	26.5	0.563	39.1

The batch RO system has low energy consumption compared to conventional RO systems reported in the literature, as shown in Fig. 19 which compares its *SEC* against the results collated by Zhao et al. [39]. Even before applying any improvement, the current system has lower *SEC* than the earlier studies at all feed salinities. Nonetheless, care must be taken when making such comparisons, as *SEC* can be affected by several parameters, especially by recovery which is not always reported in the literature. To correct for both feed water salinity and recovery, 2nd law efficiency is a good criterion to use. Though not many studies provide 2nd law efficiency directly, Ahdab and Lienhard [40] have found that the 2nd law efficiency of conventional brackish water desalination is in the range 4–20%. This also suggests that batch RO compares favourably, as the 2nd law efficiency achieved here is 9.1–26.5% and is predicted to increase to 21.6–39.1% with the improvements proposed above (see Table 8).

One of the reasons for the typically low efficiency of brackish water RO is the absence of any Energy Recovery Device (ERD) in many existing systems. Greater use of ERDs would improve the 2nd law efficiency of conventional systems, perhaps making them compare more favourably against batch RO. Nonetheless, the typical ERDs (i.e. isobaric pressure exchangers and Pelton wheels) are mostly designed for larger systems (>100 m^3/day capacity) compared to this study where the capacity is only 10–20 m^3/day [41]. This suggests that batch RO is particularly promising for high recovery brackish water desalination at small to medium scale.

There are further considerations about the practical and comparative performance of brackish water RO. Real systems usually contain several treatment steps, such as pre- and post-treatment besides the RO – which have to be considered in overall *SEC* and running costs. These may or may not be included in reported values. In addition, the long-term performance is likely to deteriorate compared to short term tests. For example, after 80000 hours of operation, the *SEC* of a system installed in Gran Canaria rose from 0.8 to 2 kWh/m^3 [42]. This deterioration was attributed to fouling and aging of the membranes. Laboratory and modelling studies suggest that batch RO has advantages regarding resistance to fouling in seawater and brackish water applications [43]. Long term testing and fouling in pilot batch RO systems is certainly an important topic for future research.

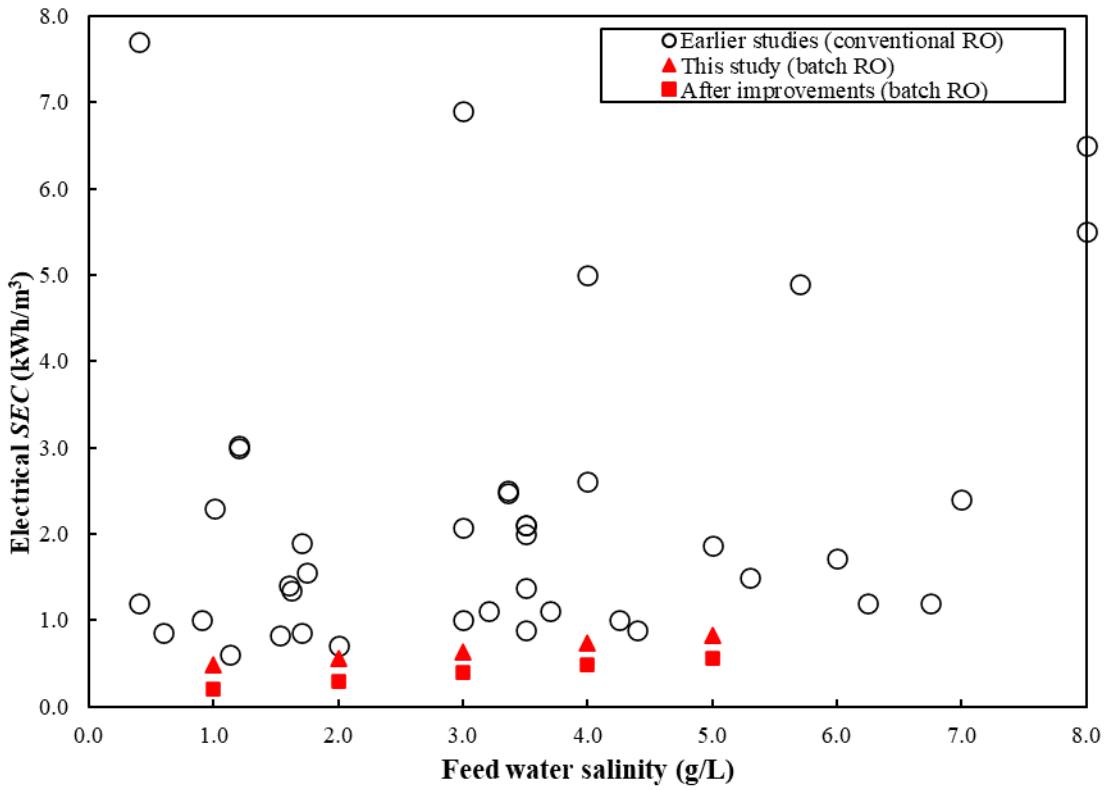

Fig. 20. The batch RO system studied here has lower *SEC* than that reported for many conventional brackish water RO systems [39], and future improvements are expected to lower further its *SEC*.

7. Conclusions

In this study, the performance of a high-recovery batch RO system using a free-piston has been experimentally investigated and modelled. The system has been designed for treating brackish water up to 5 g/L feed salinity and at recovery of 0.8, which is the highest recovery reported in practical batch RO studies so far. Using an 8-inch RO, an output of 10–17.3 m^3/day, and rejection > 94% was achieved. In total, 53 experimental runs have been conducted over a wide range of operating parameters, making this the most thorough and detailed experimental study of a high-recovery batch RO system reported in the literature. Key conclusions are:

- Batch RO is subject to osmotic backflow when depressurization occurs during each cycle. Backflow volume increases with feed salinity and amounts to 2.5–5 L for the 8-inch spiral wound membrane element.
- Osmotic backflow tends to reduce system recovery, but this can be offset by limiting the amount of purge, thus maintaining a high recovery of 0.8.
- Batch RO reaches steady-state cyclic operation after 3–4 cycles.
- Once a steady state is reached, salt retained between cycles tends to increase the salinity at the beginning of each cycle by 16%, thus increasing system pressure and energy consumption.
- Salt retention causes a minor peak in concentration at the outlet of the RO module shortly after the start of pressurisation.
- Both supply and recirculation pumps consume energy over both phases of operation. The greatest consumption is that of the supply pump during the pressurization phase,

which contributes 75–85% to total *SEC*, while the recirculation pump contributes only 10–20% over the whole cycle.

- *SEC* depends weakly on recirculation flow, such that any recirculation flow (as a ratio to feed flow) from 1.5 to 3 allows minimal *SEC*. At higher recirculation flows, *SEC* increases significantly.
- At a flux of 17.3 LMH, depending on feed salinity over the range 1–5 g/L, hydraulic *SEC* is 0.22–0.48 kWh/m^3 and electrical *SEC* is 0.48–0.83 kWh/m^3. The flux of 17.3 LMH gives an output of 13.9 m^3/day. Higher water fluxes give higher outputs up to 17.3 m^3/day but at the expense of slightly higher *SEC*.
- A simple spreadsheet model using explicit algebraic equations predicts hydraulic *SEC* with accuracy better than 3%.
- During the pressurization phase, there is an initial delay in pressure rise, and the final pressure is slightly below the model prediction. This may be because of compliance of the membrane channel increasing its internal volume in response to the supply pressure.

The batch RO system performs competitively against conventional systems, especially for small-scale industrial applications. It can achieve electrical *SEC* < 0.8 kWh/m^3 at 4 g/L feed concentration with an output of 16.4 m^3/day, which would normally require a much larger, multistage system. The batch RO system also has great potential for *SEC* minimization through future improvements. For example, though the pump efficiencies measured here were only 10–65%, if this were uniformly improved to 70% for both pumps and phases of operation, electrical *SEC* would reduce to 0.60 kWh/m^3 at 4 g/L. With membrane permeability increased from 4.4 to 8 LMH/bar and improvements to the valves used in this system, we expect hydraulic *SEC* of 0.14–0.39 kWh/m^3 and electrical *SEC* of 0.20–0.56 kWh/m^3 for feed concentrations of 1–5 g/L. Therefore, future work should focus on: testing with innovative high-permeability membranes, developing or sourcing high-efficiency pumps, and refining the valves and pipework to optimize the trade-off between friction and salt retention. In addition to these modifications, hybrid batch/semi-batch RO designs [44] can be the next step towards improving energy efficiency at recoveries higher than 0.9 which will be advantageous especially for minimum liquid discharge applications. At such high recoveries, testing and research into fouling will become especially important.

Acknowledgements

This project has received funding from the European Union's Horizon 2020 research and innovation programme under grant agreement No 820906 and the Department of Biotechnology (Government of India), project no: BT/IN/EU-WR/40/AM/2018. LB acknowledges support from the Douglas Bomford Trust. The authors would like to thank Somayeh Karimi for her comments on the manuscript.

Nomenclature

Roman and Greek symbols

A_w	LMH/bar, Water permeability
A_m	m^2, Membrane area

B	m/s, Salt permeability
C	g/L (kg/m^3), Concentration
C_0	g/L (kg/m^3), Feed concentration
C_{max}	g/L (kg/m^3), Initial concentration leaving the system at the start of the purge phase
C_d	-, Coefficient of discharge
E	kJ (kWh), Energy consumption
J_w	m/s (l/m2 /h), Permeate flux
P	kPa (bar), Pressure
$\bar{P}$	kPa (bar), Volume-weighted average pressure
$\hat{P}$	kPa (bar), Maximum peak pressure
Q	m^3/s, Flow rate
Q_f	m^3/s, Feed flow rate
Q_r	m^3/s, Recirculation flow rate
R_s	–, Salt rejection
r	–, Recovery
r_p	–, Recovery in pressurization phase
S_L	–, Longitudinal concentration gradient factor
S_p	–, Concentration polarization factor
S_R	–, Salt retention factor
SEC	kWh/m^3, Specific Energy Consumption
V	m^3, Volume
V_{b0}	m^3, Work exchanger swept volume
$V_{backflow}$	m^3, Backflow volume
V_{pipe}	m^3, Pipe volume
V_{pg}	m^3, Nominal purge volume
$V_{pipe,R}$	m^3, Retained solution volume in pipes
V_{ports}	m^3, Port dead volume
V_m	m^3, Membrane volume
v	m/s, Velocity
α	–, Ratio of recirculation flow rate to the feed flow rate
ΔP	kPa, Pressure drop
ΔP_s	kPa, Piston seal pressure drop
ΔP_v	kPa, Valve pressure drop
ΔP_{v1}	kPa, Bypass valve pressure drop
ΔP_{v2}	kPa, Recirculation valve pressure drop
ΔP_{v3}	kPa, Brine valve pressure drop
Π_{feed}	kPa, Feed osmotic pressure
ρ	kg/m^3, Density
τ	–, Dimensionless time

Abbreviations

CT	Conductivity transmitter
EXP	Experimental
FT	Flow transmitter
LMH	Litres per m^2 per hour
MOD	Model
P	Pressurization
P&R	Purge-and-refill
PT	Pressure transmitter

RO	Reverse osmosis
RP	Recirculation pump
SI	Supporting Information
SP	Supply pump
W1	Weighing platform (feed tank)
W2	Weighing platform (permeate tank)
W3	Weighing platform (brine tank)

References

[1] M. Qasim, M. Badrelzaman, N.N. Darwish, N.A. Darwish, N. Hilal, Reverse osmosis desalination: A state-of-the-art review, Desalination, 459 (2019) 59-104.
[2] H. Nassrullah, S.F. Anis, R. Hashaikeh, N. Hilal, Energy for desalination: A state-of-the-art review, Desalination, 491 (2020) 114569.
[3] S.S. Shenvi, A.M. Isloor, A. Ismail, A review on RO membrane technology: Developments and challenges, Desalination, 368 (2015) 10-26.
[4] Z. Yang, Y. Zhou, Z. Feng, X. Rui, T. Zhang, Z. Zhang, A review on reverse osmosis and nanofiltration membranes for water purification, Polymers, 11 (2019) 1252.
[5] D.L. Zhao, S. Japip, Y. Zhang, M. Weber, C. Maletzko, T.-S. Chung, Emerging thin-film nanocomposite (TFN) membranes for reverse osmosis: A review, Water research, 173 (2020) 115557.
[6] J. Kim, K. Park, D.R. Yang, S. Hong, A comprehensive review of energy consumption of seawater reverse osmosis desalination plants, Appl. Energy, 254 (2019) 113652.
[7] A. Haidari, S. Heijman, W. Van Der Meer, Optimal design of spacers in reverse osmosis, Separation and purification technology, 192 (2018) 441-456.
[8] Y. Wang, W. He, J.-D. Müller, Sensitivity analysis and gradient-based optimisation of feed spacer shape in reverse osmosis membrane processes using discrete adjoint approach, Desalination, 449 (2019) 26-40.
[9] C. Skuse, A. Gallego-Schmid, A. Azapagic, P. Gorgojo, Can emerging membrane-based desalination technologies replace reverse osmosis?, Desalination, (2020) 114844.
[10] P.A. Davies, J. Wayman, C. Alatta, K. Nguyen, J. Orfi, A desalination system with efficiency approaching the theoretical limits, Desalin. Water Treat., 57 (2016) 23206-23216.
[11] M. Elimelech, W.A. Phillip, The future of seawater desalination: energy, technology, and the environment, Science, 333 (2011) 712-717.
[12] M. Li, Optimal plant operation of brackish water reverse osmosis (BWRO) desalination, Desalination, 293 (2012) 61-68.
[13] P.A. Davies, J. Orfi, Self-powered desalination of geothermal saline groundwater: technical feasibility, Water, 6 (2014) 3409-3432.
[14] T. Qiu, P.A. Davies, Comparison of configurations for high-recovery inland desalination systems, Water, 4 (2012) 690-706.
[15] S. Cordoba, A. Das, J. Leon, J.M. Garcia, D.M. Warsinger, Double-acting batch reverse osmosis configuration for best-in-class efficiency and low downtime, Desalination, 506 (2021) 114959.
[16] J.R. Werber, A. Deshmukh, M. Elimelech, Can batch or semi-batch processes save energy in reverse-osmosis desalination?, Desalination, 402 (2017) 109-122.
[17] Q.J. Wei, C.I. Tucker, P.J. Wu, A.M. Trueworthy, E.W. Tow, J. Lienhard, Impact of salt retention on true batch reverse osmosis energy consumption: Experiments and model validation, Desalination, 479 (2020) 114177.
[18] A. Das, D.M. Warsinger, Batch counterflow reverse osmosis, Desalination, 507 (2021) 115008.
[19] K. Park, L. Burlace, N. Dhakal, A. Mudgal, N.A. Stewart, P.A. Davies, Design, modelling and optimisation of a batch reverse osmosis (RO) desalination system using a free piston for brackish water treatment, Desalination, 494 (2020) 114625.
[20] P. Davies, A. Afifi, F. Khatoon, G. Kuldip, S. Javed, S. Khan, Double-acting batch-RO system for desalination of brackish water with high efficiency and high recovery, Desalination for the Environment–Clean Energy and Water, Rome, (2016) 23-25.
[21] A. Chougradi, F. Zaviska, A. Abed, J. Harmand, J.-E. Jellal, M. Heran, Batch Reverse Osmosis Desalination Modeling under a Time-Dependent Pressure Profile, Membranes, 11 (2021) 173.
[22] T. Qiu, P. Davies, Concentration polarization model of spiral-wound membrane modules with application to batch-mode RO desalination of brackish water, Desalination, 368 (2015) 36-47.

[23] J. Swaminathan, R.L. Stover, E.W. Tow, D.M. Warsinger, J. Lienhard, Effect of practical losses on optimal design of batch RO systems, in: The International Desalination Association World Congress, International Desalination Association, 2017, pp. 15-20.
[24] J. Swaminathan, E.W. Tow, R.L. Stover, Practical aspects of batch RO design for energy-efficient seawater desalination, Desalination, 470 (2019) 114097.
[25] D.M. Warsinger, E.W. Tow, K.G. Nayar, L.A. Maswadeh, J.H. Lienhard, Energy efficiency of batch and semi-batch (CCRO) reverse osmosis desalination, Water Res., 106 (2016) 272-282.
[26] P.A. Davies, A solar-powered reverse osmosis system for high recovery of freshwater from saline groundwater, Desalination, 271 (2011) 72-79.
[27] A. Mudgal, P. Davies, A cost-effective steam-driven RO plant for brackish groundwater, Desalination, 385 (2016) 167-177.
[28] H. Abu Ali, M. Baronian, L. Burlace, P.A. Davies, S. Halasah, M. Hind, A. Hossain, C. Lipchin, A. Majali, M. Mark, Off-grid desalination for irrigation in the Jordan Valley, Desalin. Water Treat., 168 (2019) 143-154.
[29] T. Qiu, P.A. Davies, Longitudinal dispersion in spiral wound RO modules and its effect on the performance of batch mode RO operations, Desalination, 288 (2012) 1-7.
[30] A. Haidari, S. Heijman, W. van der Meer, Visualization of hydraulic conditions inside the feed channel of Reverse Osmosis: A practical comparison of velocity between empty and spacer-filled channel, Water Res., 106 (2016) 232-241.
[31] B. Massey, Mechanics of Fluids 4. th Edition, The English Language Book Society, (1980).
[32] M. Li, Dynamic operation of batch reverse osmosis and batch pressure retarded osmosis, Industrial & Engineering Chemistry Research, 59 (2020) 3097-3108.
[33] M. Li, Effects of finite flux and flushing efficacy on specific energy consumption in semi-batch and batch reverse osmosis processes, Desalination, 496 (2020) 114646.
[34] M. Aghajani, M. Wang, L.M. Cox, J.P. Killgore, A.R. Greenberg, Y. Ding, Influence of support-layer deformation on the intrinsic resistance of thin film composite membranes, Journal of membrane science, 567 (2018) 49-57.
[35] J.A. Idarraga-Mora, A.D. O'Neal, M.E. Pfeiler, D.A. Ladner, S.M. Husson, Effect of mechanical strain on the transport properties of thin-film composite membranes used in osmotic processes, Journal of Membrane Science, 615 (2020) 118488.
[36] D.M. Davenport, C.L. Ritt, R. Verbeke, M. Dickmann, W. Egger, I.F. Vankelecom, M. Elimelech, Thin film composite membrane compaction in high-pressure reverse osmosis, Journal of Membrane Science, 610 (2020) 118268.
[37] D. Cohen-Tanugi, R.K. McGovern, S.H. Dave, J.H. Lienhard, J.C. Grossman, Quantifying the potential of ultra-permeable membranes for water desalination, Energy & Environmental Science, 7 (2014) 1134-1141.
[38] A. Shrivastava, S. Rosenberg, M. Peery, Energy efficiency breakdown of reverse osmosis and its implications on future innovation roadmap for desalination, Desalination, 368 (2015) 181-192.
[39] R. Zhao, S. Porada, P. Biesheuvel, A. Van der Wal, Energy consumption in membrane capacitive deionization for different water recoveries and flow rates, and comparison with reverse osmosis, Desalination, 330 (2013) 35-41.
[40] Y.D. Ahdab, J.H. Lienhard, Desalination of brackish groundwater to improve water quality and water supply, in: Global Groundwater, Elsevier, 2021, pp. 559-575.
[41] R.L. Stover, B. Andrews, Isobaric energy-recovery devices: past, present, and future, IDA Journal of Desalination and Water Reuse, 4 (2012) 38-43.
[42] A. Ruiz-García, E. Ruiz-Saavedra, 80,000 h operational experience and performance analysis of a brackish water reverse osmosis desalination plant. Assessment of membrane replacement cost, Desalination, 375 (2015) 81-88.
[43] D.M. Warsinger, E.W. Tow, L.A. Maswadeh, G.B. Connors, J. Swaminathan, Inorganic fouling mitigation by salinity cycling in batch reverse osmosis, Water Res., 137 (2018) 384-394.
[44] K. Park, P.A. Davies, A compact hybrid batch/semi-batch reverse osmosis (HBSRO) system for high-recovery, low-energy desalination, Desalination, 504 (2021) 114976.

Paper 2: Effect of membrane properties on the performance of batch reverse osmosis (RO): the potential to minimize energy consumption

E. Hosseinipour, P.A. Davies*

School of Engineering, University of Birmingham, Edgbaston, Birmingham, UK

* p.a.davies@bham.ac.uk

Graphical Abstract

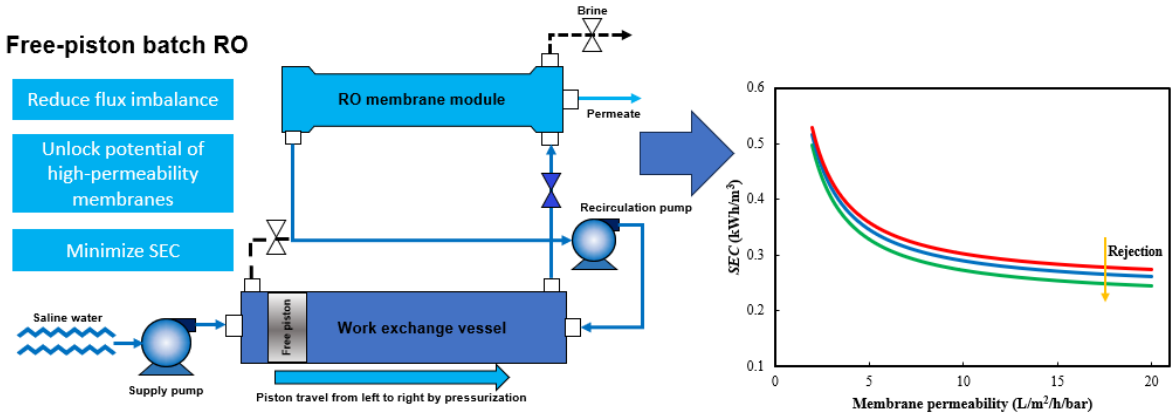

Abstract

Efforts to improve the performance of RO desalination include new membranes and new system configurations. Batch RO is an innovative configuration which helps to minimize Specific Energy Consumption (*SEC*) at high recovery. However, there is a lack of experimental studies regarding the performance of different membranes in batch RO. In this study, we tested four 8-inch RO membranes of different permeabilities in a free-piston batch RO system to assess how membrane properties affect performance. Tests were conducted with brackish feed water containing 1000-5000 mg/L of NaCl, at recovery of 0.8. Performance in terms of *SEC*, permeate quality and salt rejection was quantified. *SEC* and salt rejection varied considerably from low-permeability to high-permeability membranes. For the lowest permeability membrane rejection was >95%, whereas for the higher permeability membranes it was only 82-96%. *SEC* with high-permeability membranes was approximately 25-29% lower than with the lowest permeability membrane. Using a verified model, we predict that on increasing the permeability from 5 to 20 L/m^2/h/bar, hydraulic *SEC* would go down further by 17-28% using ultra high-permeability membranes. Though this study shows the potential for *SEC* reduction, it also underlines the limitations of current commercial membranes and therefore the need for membranes with even higher permeability.

Keywords: Batch RO, Membrane permeability, *SEC* minimization, Salt rejection, Brackish water

Highlights:

- Four 8-inch RO membranes of differing permeabilities tested in free-piston batch RO at recovery of 0.8.
- High-permeability membranes gave 25-29% lower *SEC* than the low-permeability membrane.
- Predictions indicate up to 30% *SEC* reduction when permeability further increased from 5 to 20 L/m^2/h/bar.
- Significant differences in osmotic backflow also observed, from 2.6 to 5.2 L.

Nomenclature

Symbols

c_{feed}	mg/L, Feed concentration to the batch RO system
c_{perm}	mg/L, Permeate concentration
r	-, Recovery
J_{w}	L/m^2/h, Water flux
R_{s}	-, Salt rejection
η	-, Second law efficiency
π_{feed}	bar, Feed osmotic pressure

Abbreviations

Aq-U	Aquaporin-Ultra membrane
BWRO	Brackish Water Reverse Osmosis
CF	Concentration Factor
D-HR	Dupont-BW30HR membrane
D-XLE	Dupont-XLE membrane
ICP	Internal Concentration Polarization
RO	Reverse Osmosis
SEC	Specific Energy Consumption
SI	Supporting Information
TDS	Total Dissolved Solids
TFC	Thin Film Composite
T-TMHA	Toray-TMH20A membrane

1. Introduction

Membrane reverse osmosis (RO) dominates the desalination industry today, providing nearly 100 million m^3 of clean water per day globally [1]. Since its introduction in the 1950s, RO desalination has undergone substantial advances in materials science, process refinement, system optimization, techniques for membrane synthesis, and membrane surface modifications [2]. Over the last 3 decades, the specific energy consumption (*SEC*) of RO has almost halved [3]. Driven by the large uptake of RO desalination, research efforts to achieve further advances are on-going.

1.1. Membrane materials and structures

One important research area aims to develop new membrane materials and structures with improved properties such as water permeability and salt selectivity. The polyamide thin-film composite (TFC) is the most common type of membrane, thanks to its high permeability, high salt rejection, stability and low cost [4]. Typically, permeability of current TFC membranes ranges from 1-2 L/m^2/h/bar for seawater membranes and 2-8 L/m^2/h/bar for brackish water RO (BWRO) membranes [5]. Conversely, salt rejection is about 99% for seawater [2, 6] and 95-99% for brackish water [7].

Though the structure of TFC membranes can be modified to enable faster water permeation, this also tends to increase the ease of salt passage [8]. This trade-off between permeability and salt rejection, along with the issue of membrane fouling, has posed challenges to the efficient use of RO technology – thus prompting research into alternative membranes. Examples include inorganic membranes consisting of ceramics or 2D-carbon-based materials such as carbon nanotubes and graphene oxides [9]. Inorganic membranes offer advantages including improved chemical and physical stability, as well as high tunability and reusability compared to polymeric membranes. However, their commercialization has been hindered by challenges in preparation, high manufacturing costs, and their thickness and bulkiness [4]. Combining the advantages of both polymeric and ceramic membranes, mixed matrix membranes are another option [10]. In this hybrid organic–inorganic approach, the properties of a polymeric matrix are enhanced by the addition of inorganic fillers. The fillers can be a porous and/or nonporous material such as zeolite, activated carbon, carbon nanotubes, silica, alumina, silver, and/ or titanium oxide nanoparticles. However, the application of mixed-matrix membranes is restricted by factors like identification of filler material for synthesis, complex fabrication process, high cost, agglomeration, and phase separation [11].

A further alternative is biomimetic membranes. Biological water channels based on aquaporin proteins promise to enable membranes with exceptional permeability and salt rejection capabilities [12, 13]. For instance, Sharma et al. [14] reported membrane permeability in the range of 3-10 L/m^2/h/bar and salt rejection ranging from 90-95% for aquaporin-based membranes fabricated using *E. coli* aquaporin Z proteoliposomes immobilized in a polyamide layer formed by interfacial polymerization. However, current research has yet to provide performance data surpassing that of conventional state-of the-art TFC desalination membranes [15].

The extent to which membrane properties influence system performance varies among studies. For example, in a theoretical study, Cohen-Tanugi et al. [16] found that increasing permeability from 1.5 to 4.5 L/m^2/h/bar resulted in a large decrease (46%) in the feed pump pressure and *SEC* in conventional single-stage BWRO at recovery of 0.65. However, beyond this point, further increases in permeability yielded diminishing returns, with 5 L/m^2/h/bar being considered as the upper limit for meaningful reduction in *SEC* for BWRO.

In another theoretical study, Werber et al. [17] assessed the effect of increasing permeability on energy efficiency in BWRO (at feed concentration of 5844 mg/L NaCl and recovery of 0.75). In a single-stage continuous RO process, a permeability increase from 4 to 10 L/m^2/h/bar yielded a marginal 2.2% decrease in *SEC*. In contrast, in a two-stage RO configuration (where the energy requirement at 4 L/m^2/h/bar was already 22% lower than in single-stage RO) an increase in permeability from 4 to 10 L/m^2/h/bar led to a more significant 12% reduction in *SEC*.

1.2. Configurations for minimal SEC

Traditionally, a single-stage configuration was the norm for RO. However, in the past twenty years, there has been a shift towards multi-stage RO to minimize *SEC* [18]. Wei et al. [19], theoretically assessed the potential energy savings in a two-stage BWRO system using high-permeability membranes (3 and 10 L/m^2/h/bar) at a feed concentration of 3000 mg/L NaCl and recovery rate ranging from 0.60 to 0.98. They found that at lower recoveries, the *SEC* reduction achieved by employing a 10 L/m^2/h/bar membrane is limited (0.02 kWh/m^3 at recovery of 0.6). At very high recoveries (>98%), *SEC* became almost insensitive to permeability. The highest *SEC* savings due to increased permeability were predicted at recovery of 0.91. They explained that raising the membrane water permeability from 3 to 10 L/m^2/h/bar does not notably enhance energy efficiency, because of growing concentration polarization. They also concluded that the energy savings derived from increased membrane water permeability decline as feed concentration rises.

Although *SEC* tends to bottom out at high permeability, this tendency varies with process factors like feed concentration, recovery, pump efficiency, and system configuration. Nevertheless, according to Okamoto and Lienhard [3], across all scenarios, any further reduction in energy becomes marginal once the water permeability surpasses approximately 3 and 8 L/m^2/h/bar in seawater and brackish water RO, respectively. This is almost the upper value for the BWRO membranes in the market today, suggesting that improvement in this area is unnecessary for conventional continuous RO.

In contrast to continuous RO, batch RO is a new configuration developed to achieve high recovery with reduced energy consumption [20-23]. In a batch RO system, concentration at the membrane varies over time. Meanwhile, applied pressure follows the osmotic pressure helping to minimize *SEC* [24-27]. This contrasts with continuous RO where the constant applied pressure must be maintained at a maximum value as needed to at least overcome the osmotic pressure of the brine corresponding to the recovery of the system (see Fig. 1 below) [28]. Not only does this excess pressure correspond to wasted energy, but it also results in loss of membrane permeability since several studies have shown decrease of permeability with pressure [29-32].

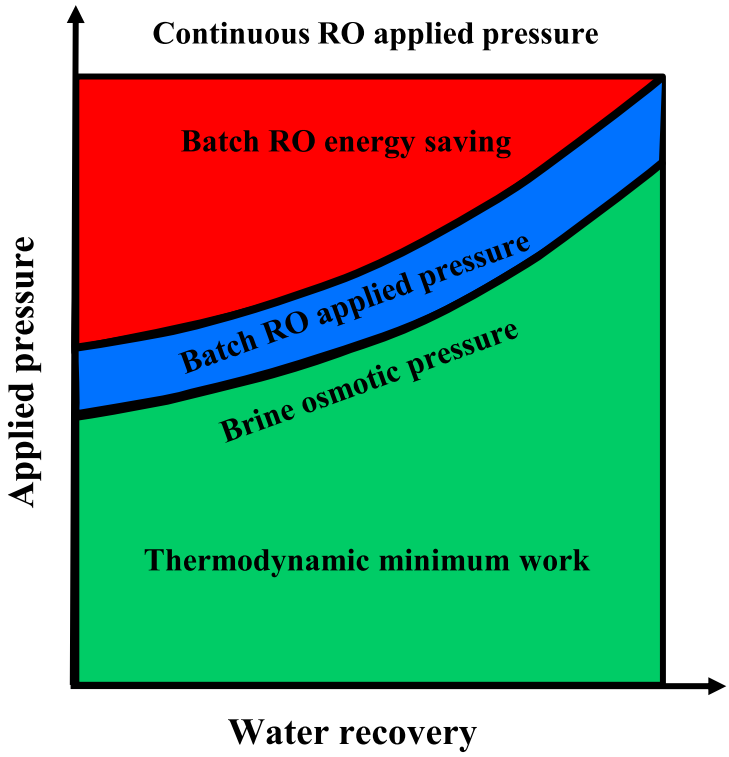

Fig. 1. Comparison of applied pressure vs. water recovery ratio between batch RO and single-stage continuous RO (adapted from [33]). The areas beneath the green, blue, and red curves represent energy.

Understanding factors, such as membrane permeability, that affect *SEC* in batch RO systems is vital for optimizing system performance and energy efficiency. Further research and investigation in this area will contribute to the development of better membrane materials and improved operational strategies for batch RO system designs. To date only a few studies have addressed these issues.

For example, Warsinger et al. [34] theoretically evaluated the impact of permeability on *SEC* in batch RO for seawater (recovery of 0.50 and concentration of 35000 mg/L) and brackish water (concentration of 5000 mg/L and recovery of 0.66). They assumed an 80% pump efficiency, and an average membrane flux of 14.5 L/m^2/h. For seawater, most energy savings (~13%) resulting from more permeable membranes were observed up to a permeability of 4 L/m^2/h/bar. In the case of brackish water, energy savings (37%) remained significant up to about 7 L/m^2/h/bar. Beyond these permeability values, a 10% increase in membrane water permeability yielded less than 2% energy saving.

Swaminathan et al. [35] similarly illustrated the impact of increased permeability on *SEC* in seawater batch RO as compared to traditional continuous seawater RO. They predicted a drop in *SEC* of approximately 10% (0.2 kWh/m^3) when permeability increases from 2 to 10 L/m^2/h/bar. In continuous RO, the decrease in *SEC* was a more modest 5% (0.11 kWh/m^3). The study anticipated that batch RO systems may benefit more than continuous RO from the use of ultra-permeable membranes such as those based on graphene or aquaporins.

Hosseinipour et al. [27] tested a batch RO system using an Eco Pro-440 membrane with brackish water at recovery of 0.80 and used the results to calibrate a model. By increasing the

permeability from the experimental baseline of 4.4 L/m^2/h/bar up to 10 L/m^2/h/bar, they predicted a *SEC* reduction of 17% (0.352 down from 0.423 kWh/m^3). These predictions assumed a feed concentration of 4000 mg/L and flux of 17.3 L/m^2/h.

In summary, there have been promising predictions concerning the use of high-permeability membranes to improve performance in batch RO. Compared to the continuous RO, high permeability membranes have a more significant impact on *SEC* in batch RO and the relative impact is even larger at lower feed salinities. However, still there is a lack of experimental research in this area. This study sets out to address this gap by testing a batch RO system with a series of state-of-the-art RO membranes, including a recently introduced membrane using biomimetic aquaporin technology. Four 8-inch RO modules with varying permeability were assessed in a single-acting free-piston batch RO pilot. Salt rejection and *SEC* were measured to analyse the trade-off between permeability and selectivity. The validated model was then employed to assess potential *SEC* improvements by enhancing membrane permeability, considering salt rejection within the range of 87-97%.

2. Experimental equipment and procedure

This study used a free-piston batch RO system housing a single 8-inch spiral wound membrane (Fig. 2). The system has a maximum rated pressure of 25 bar. Detailed information about the equipment and experimental procedure has been documented in an earlier study [27] and is not repeated here. The earlier study established that, for feed concentrations ≤ 5000 mg/L, the optimal ratio of recirculation to feed flow is approximately 2 to minimize the *SEC*. To avoid repetition, we used the same ratio here and did not re-evaluate the effect of varying it. This helped to rationalize the number of experiments and provide comparable results.

Four different 8-in spiral-wound RO membranes were tested. Henceforth, these membranes are referred according to the abbreviations in Table 1, which also shows important manufacturers' data. All four membranes are intended for brackish water treatment with maximum pressure of 41 bar (except the T-TMHA membrane which is rated at only 25 bar). Three of these membranes are regarded as high-permeability membranes (Aq-U, D-XLE and T-TMHA) and one as low-permeability and high-rejection (D-HR).

Feed solutions were prepared by dissolving approximately 1.5 to 7.5 kg of reagent grade NaCl (Fisher Scientific, ACS grade, 99.5% purity) in tap water with total dissolved solids (TDS) < 100 mg/L in a 1500 L polyethylene feed tank, representing brackish water with TDS ranging from 1000 to 5000 mg/L. To remove free chlorine, 4.5 mg of sodium metabisulfite was added to the feed tank. The feed water temperature was kept constant at 25 ± 0.5°C throughout. A 5-micron 10-in cartridge pre-filter was used to remove small particles and protect the RO membrane.

The system was operated at the design recovery of 0.80 ± 0.01. Experiments were conducted at fluxes ranging from approximately 11-23 L/m^2/h, resulting in an output of 10-17 m^3/day. This translated to a complete cycle duration ranging from 330 to 580 seconds (including a 75-second purge-and-refill phase), with shorter durations correlating with higher water fluxes. Hence, the overall duration for each run (four cycles) varied from 22 to 44 minutes. During the experiments, all relevant parameters (shown in Table S1) including conductivities, pressure, flow rates, power consumption of the pumps, and weights of the tanks were monitored and recorded using a data logger and LabVIEW® software. These data were used to calculate

results, including *SEC*, salt rejection, and permeate quality – following the calculation methods previously described [27].

The main measurement equipment used in this study (shown in Fig. S8), including pressure sensors, conductivity sensors, power supply, and scales, have errors of less than 1% of their respective ranges (0.25%, 1.0%, 0.1%, and 0.3%, respectively). When considering the cumulative errors, the calculation error for parameters such as salt rejection, hydraulic and electrical *SEC*, and flux falls within the range of 1-3% in all cases.

Table 1. Specifications of the 8-inch spiral wound membranes used in this study according to the manufacturers' datasheets. All membranes had area of 41 m^2 and feed spacer thickness of 0.71 mm (0.028 inch). All reported test conditions were at 25 °C, pH = 7-8 and water recovery of 0.15.

Membrane manufacturer and type	Abbreviation	Salt rejection %	Product flow rate (m^3/day)	Maximum operating pressure (bar)	Membrane test conditions		
					Feed concentration, c_{feeed} (mg/L)	Pressure, P_f (bar)	Flux, J_w (L/m^2/h)
Aquaporin-Ultra	Aq-U	99.0	51	41.4	500	6.9	52.1
Dupont-XLE	D-XLE	99.0	53	41.4	2000	8.6	53.9
Dupont-BW30HR	D-HR	99.7	48	41.4	2000	15.5	48.8
Toray-TMH20A	T-TMHA	99.3	45.7	25.1	500	6.9	46.4

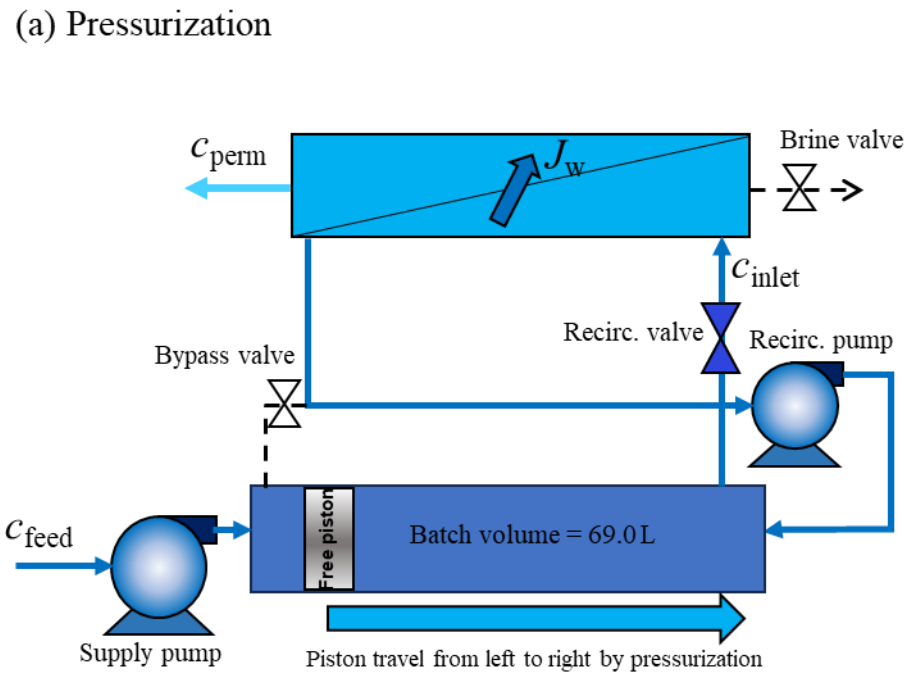

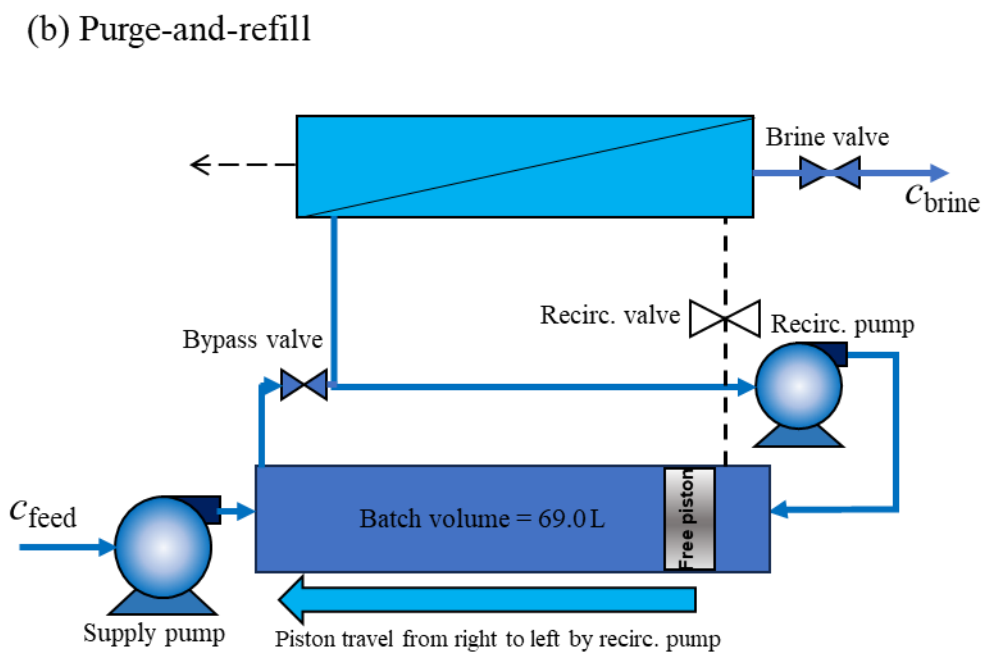

Fig. 2. Schematic of the free-piston batch RO, a) pressurization, and b) purge-and-refill phase. The phases involve switching three on-off valves. In the pressurization phase, the bypass and brine valves are closed while the recirculation valve remains open. Conversely, in the purge-and-refill phase, the bypass and brine valves are open, and the recirculation valve is closed. For more details refer to [27]. Solid and dashed lines represent flow and no flow respectively.

3. Result and discussions

3.1. Membrane water permeability

We measured the permeability for each membrane under similar conditions. To eliminate osmotic pressure, RO permeate with a conductivity of approximately 0.1 mS/cm was collected and then used as feed. The pressure and flow rate during the tests were stable, with minimal fluctuations of no more than ± 0.1 bar or ± 0.1 L/min respectively. These tests were done in the continuous RO mode operation with the brine valve fully closed (i.e., as a dead-end flow system).

To determine flux, we measured the mass of the produced permeate over a period of 600 s, using a precision scale with an accuracy of ± 0.1 kg. The test was repeated over a range of flow and pressure, and the permeability was determined from the slope of the straight-line fit of flux vs. pressure (see SI section 2 for detailed results). For the high-permeability membranes, measured permeability ranged from 4.6 to 5.7 L/m^2/h/bar, while the high-rejection membrane (D-HR) exhibited a permeability of only 2.7 L/m^2/h/bar (Table 2).

Table 2. Membrane water permeabilities measured experimentally and calculated using manufacturer's datasheet. The permeability was calculated using $A = \frac{J_w}{P_f - \pi_f}$ (where P_f and J_w are taken from Table 1 and π_f is calculated using the van 't Hoff expression).

Permeability, A (L/m^2/h/bar)

Membrane	Experimental	Calculated
T-TMHA	5.7	7.1
Aq-U	5.4	8.0
D-XLE	4.6	7.7
D-HR	2.7	3.5

Table 2 shows that the experimental values for permeability are lower than those inferred from the manufacturers' datasheets. Nonetheless, such differences are also found elsewhere in the literature. For example, Khunnonkwao et al. [36] mentioned permeability of about 5 L/m^2/h/bar for the D-XLE membrane, while in another study the D-XLE membrane permeability was reported in the range of 3.6 to 6.8 L/m^2/h/bar depending on the experimental conditions such as pressure [37]. These differences could be due to quality variations in membranes and variations in operating conditions and testing arrangement. In the case of the Aq-U membrane, we note that this is a newly available membrane so its specifications may not yet have been firmly established.

3.2. Permeate conductivity variation over the pressurization phase

Fig. 3 compares permeate conductivity over a pressurization phase. There is an initial delay of about 10-20 seconds before permeate production commences. During this period, the applied pressure rapidly increases above the feed solution's osmotic pressure, before driving water through the membrane. Simultaneously, the permeate spacer and permeate tube, which were previously evacuated during the purge phase due to osmotic backflow, are re-filled with water. Next there is a sharp peak in permeate conductivity, like that reported in previous studies [24-27]. This peak indicates that the stagnant salt that had diffused into the permeate spacer during the purge phase is now leaving the system, causing a temporary increase in permeate conductivity. After the peak, the permeate conductivity drops to a minimum, and then it starts to increase steadily as the process continues. This second rise is attributed to the increasing concentration in the recirculation loop of the batch RO system.

The Aq-U membrane showed the largest initial peak whereas the D-HR showed the smallest. Following the initial peak, the permeate conductivity of the D-HR increased from 0.07 to 0.19 mS/cm during a test at c_{feed} = 3000 mg/L and J_w = 17.8 L/m^2/h. In contrast, D-XLE, T-TMHA, and Aq-U experienced greater increases in permeate conductivity from 0.22 to 0.56, 0.32 to 0.91, and 0.4 to 1.43 mS/cm respectively.

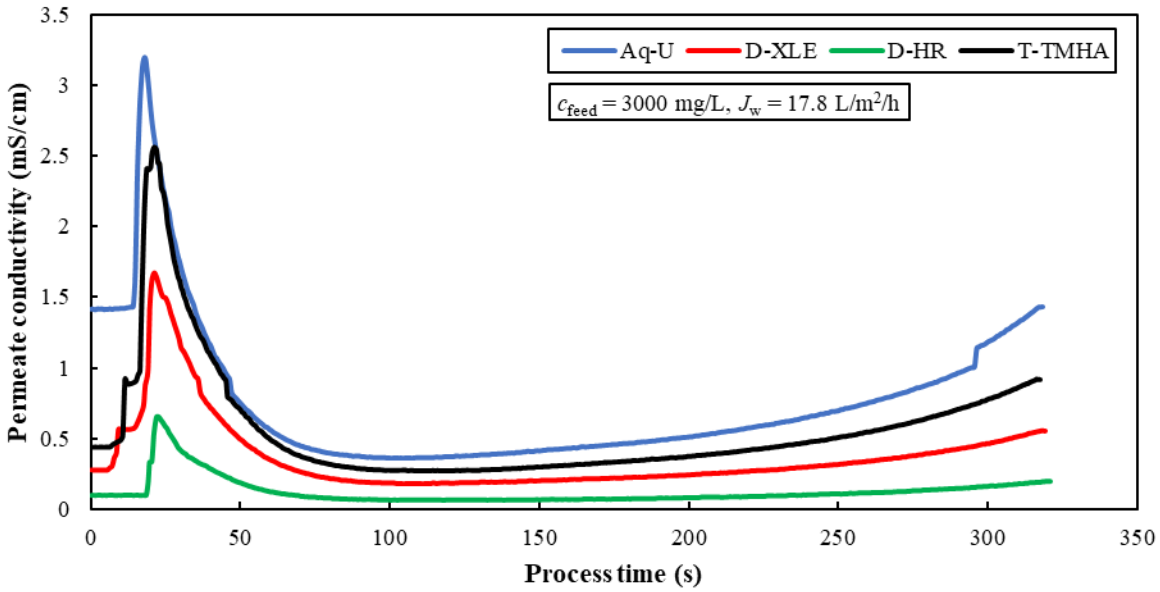

Fig. 3. Permeate conductivity vs. time over the pressurization phase in batch RO at c_{feed} = 3000 mg/L and J_w = 17.8 L/m^2/h for different RO membranes.

The World Health Organization (WHO) generally considers water with a TDS level of less than approximately 600 mg/L to have good palatability [38]. Thus, in our study, it was essential to compare the membranes against this limit. Fig. 4 shows the average permeate concentration over a cycle at different feed concentrations ranging from 1000 to 4000 mg/L, and three different fluxes. The permeate water produced by all membranes at feed concentrations up to c_{feed} = 4000 mg/L met acceptable water quality standards for drinking applications.

Permeate TDS increased with both flux and feed concentration (see Fig. 4). The high-rejection D-HR membrane stood out by consistently producing water with TDS levels below 100 mg/L. This suggests that this membrane offers significant flexibility, allowing for operation at higher feed concentrations and lower fluxes without having to worry about exceeding the TDS limit for drinking applications. Additionally, the D-XLE produced permeate with TDS < 300 mg/L under the same conditions. Both the T-TMHA and Aq-U membranes demonstrated good performance at low feed concentrations ($c_{feed} \leq$ 2000 mg/L). Nonetheless, as the feed concentration increased, the difference in permeate TDS between these two membranes and the D-HR and D-XLE membranes became more noticeable, increasing the risk of failing to meet drinking quality standards. This suggests that the selection of the right membrane should be based on the feed concentration and the final permeate quality required in each application.

The best permeate quality was observed at the highest flux and the lowest feed concentration (J_w = 22.2 L/m^2/h and c_{feed} = 1000 mg/L), resulting in TDS < 60 mg/L for all membranes. The worst permeate quality was seen at the highest feed concentration and the lowest flux. Flux had a big effect on the permeate quality; for example, at c_{feed} = 4000 mg/L and J_w = 13.4 L/m^2/h the average permeate TDS levels were 104, 298, 487, and 655 mg/L for D-HR, D-XLE, T-TMHA, and Aq-U respectively. On increasing flux to J_w = 22.2 L/m^2/h these values reduced by approximately 25%.

Moreover, the initial conductivity peak (as shown in Fig. 3) has a negative impact on the permeate quality. This peak tends to become more prominent at higher fluxes and feed

concentrations. If it did not occur, the permeate TDS levels for the D-XLE, T-TMHA, and Aq-U membranes would have been lower. For instance, at c_{feed} = 4000 mg/L and J_w = 22.2 L/m^2/h, the permeate TDS would have decreased from 215, 366, and 500 mg/L to about 173, 297, and 437 mg/L, respectively. These estimated decreases are based on comparing with a hypothetical situation where the initial permeate concentration were at the minimum concentration observed, which is a plausible assumption if osmotic backflow were absent.

Considering the trade-off between permeate quality and energy efficiency when varying the flux, for the high-permeability membranes, it is recommended to operate the system at higher fluxes whenever possible, even though it may lead to higher energy consumption. By doing so, the improved water quality and permeate output achieved at higher fluxes justifies the increase in energy usage and offers a practical approach to obtain desirable permeate quality for drinking water applications.

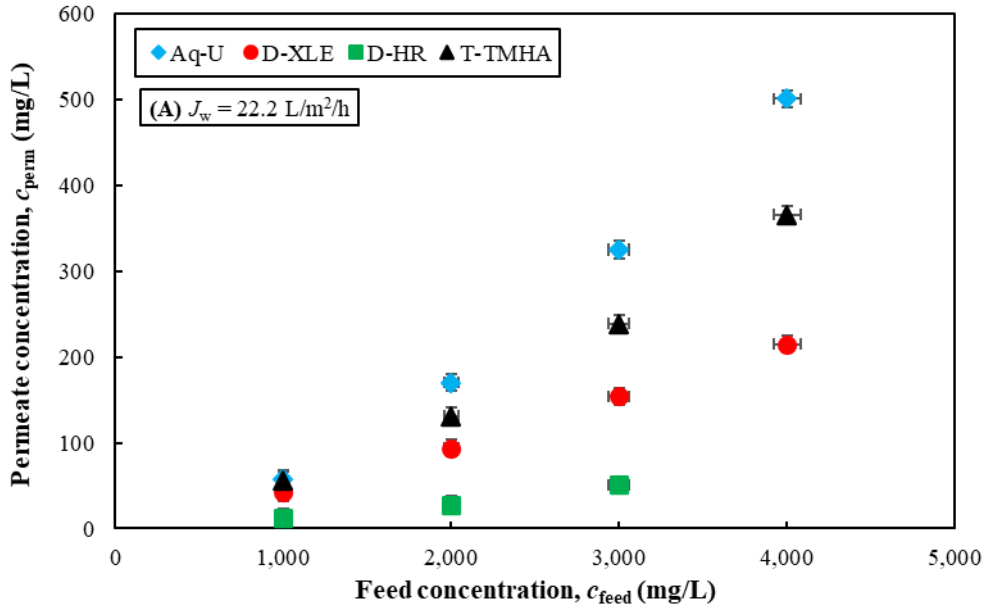

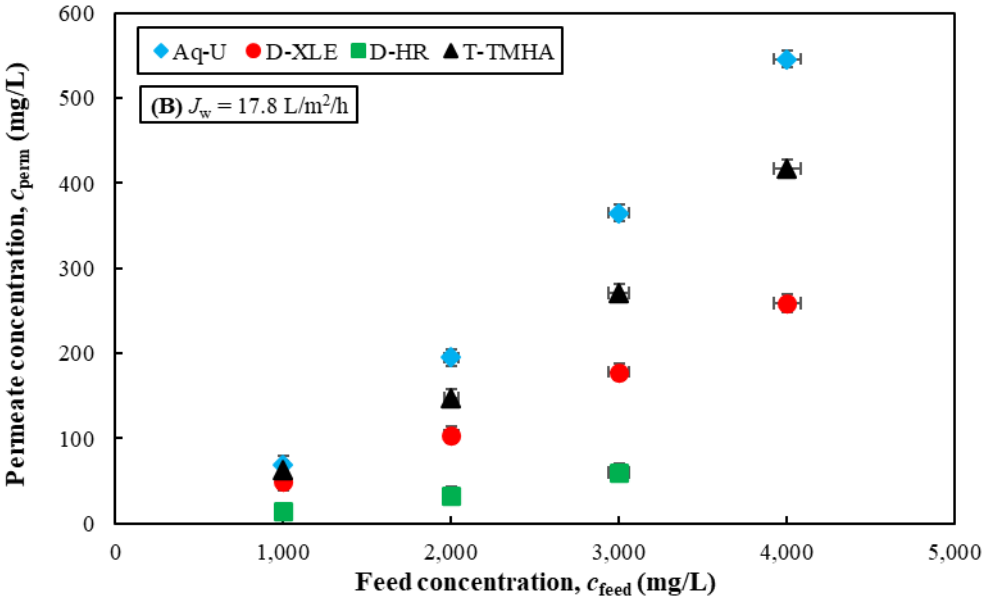

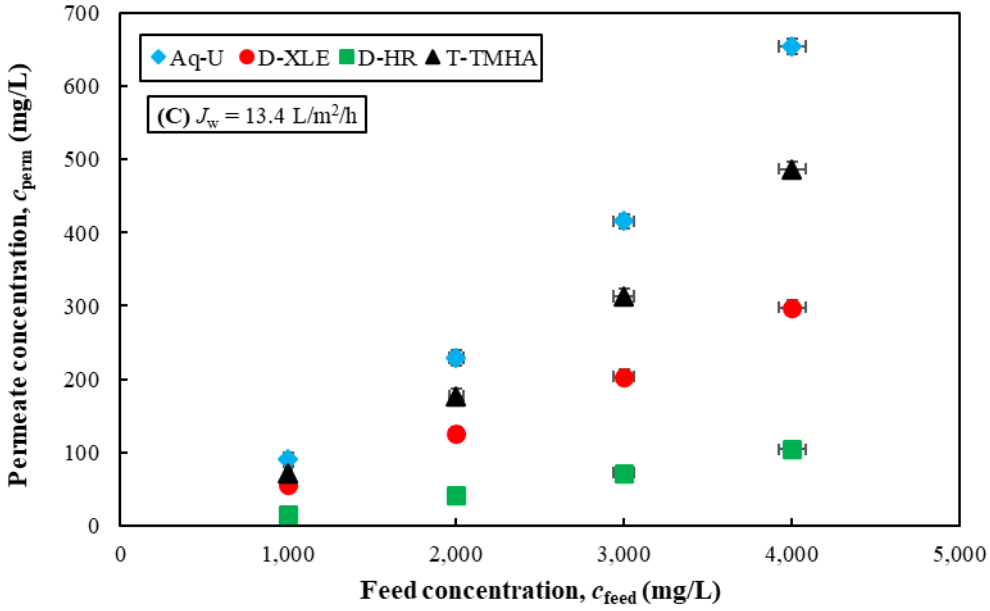

Fig. 4. Average permeate concentration over a cycle in batch RO vs. feed concentration for different RO membranes at A) J_w = 22.2 L/m^2/h, B) J_w = 17.8 L/m^2/h, and C) J_w = 13.4 L/m^2/h.

3.3. Salt rejection

The above permeate concentrations c_{perm} were used to calculate the salt rejection R_s of the system using the equation:

$$R_s = \frac{c_{feed} - c_{perm}}{c_{feed}} \quad (1)$$

The D-HR membrane showed the highest rejection, ranging from 97-99% according to flux and feed concentration. In the case of D-XLE, rejection ranged from 91.5-96%. With T-TMHA and Aq-U, the range widened considerably varying from 86-94.5% and from 81.5-94% respectively. As an example, at c_{feed} = 2000 mg/L and J_w = 17.8 L/m^2/h, rejections were 98.3, 94.8, 92.6, and 90.2% respectively. Figures showing the rejection for each membrane at different feed concentrations and fluxes can be found in the SI.

Rejection increased with flux but decreased with feed concentration. However, the sensitivity with the D-HR and D-XLE membranes was less than with the T-TMHA and Aq-U membranes (see Fig. 5). For instance, at J_w = 17.8 L/m^2/h, on increasing feed concentration from 1000 to 3000 mg/L, rejection of D-HR dropped by only 0.6% while that of the Aq-U fell by 5.6%. Additionally, at c_{feed} = 3000 mg/L, on decreasing flux from 22.2 to 11.4 L/m^2/h, rejection decreased by 1.0 and 5.4% for D-HR and Aq-U respectively. Therefore, it may be better to operate the Aq-U and T-TMHA membranes at higher fluxes to reach higher rejection values (albeit at higher energy cost).

The rejection in the batch RO system is negatively affected by the initial peak in permeate concentration, as explained in section 3.2 above. Moreover, in comparing against the rejection values stated by the manufacturers' datasheets (Table 1) we note that, in our experiments, the flux is lower (11 to 23 L/m^2/h as opposed to 45 to 55 L/m^2/h), and the recovery is much higher (0.8 as opposed to 0.15). The feed concentration is also different. All these factors contribute to the lower rejection in the current study.

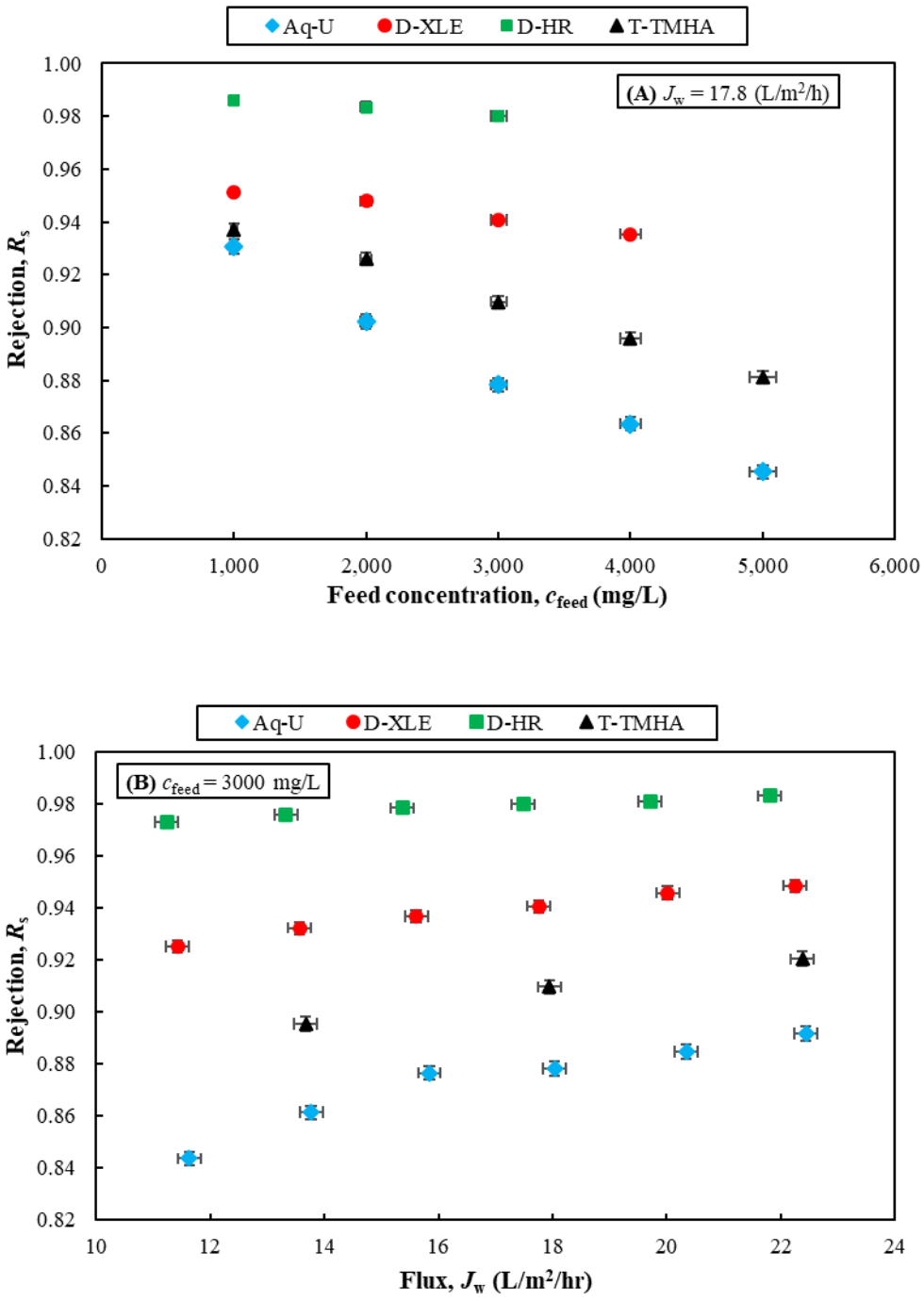

Fig. 5. Salt rejection comparison of different RO membranes, A) at J_w = 17.8 L/m²/h and different feed concentrations, B) at c_{feed} = 3000 mg/L and different fluxes.

3.4. Osmotic backflow

When a batch RO system depressurizes at the beginning of the purge-and-refill phase, a small volume of permeate water fails to exit because of the osmotic backflow due to the concentration gradient [24-27]. A check valve on the permeate line helped to reduce osmotic backflow but did not eliminate it entirely.

The batch volume in this study is 69.0 L. Subtracting the batch volume by the produced permeate volume yields the osmotic backflow, as shown in Table 3. Osmotic backflow increased with feed concentration and varied significantly among the four membranes. The Aq-U membrane exhibited the lowest osmotic backflow volume of 2.6-3.4 L; whereas the D-HR exhibited the highest osmotic backflow volume of 3.7-5.2 L.

Comparing with the results of section 3.3, it is interesting that membranes giving lower rejection also give lower backflow. The likely explanation is as follows. Lower rejection membranes allow more salt to pass through to the permeate. At the beginning of the purge cycle, when backflow occurs, the salt in the permeate is drawn back into the membrane support layer where it builds up as an internal concentration polarisation (ICP) layer. Momentarily, the membrane is behaving as a forward osmosis (not reverse osmosis) membrane. It is known that the flux in forward osmosis is detrimentally affected by ICP which (unlike external concentration polarisation) is not removed by convection [39]. In the case of batch RO, ICP is beneficial to reduce the backflow albeit with the penalty of lower overall salt rejection. ICP reduces the concentration gradient between the feed and permeate sides which is the driver of osmotic backflow.

This explanation is supported by Fig. 7 which correlates the initial peak in concentration at the beginning of the permeate production against osmotic backflow. It is seen that a higher peak (associated with lower salt rejection) correlates consistently with decreased backflow. The peak reflects salt accumulation and ICP on the permeate side. The explanation is also supported by the fact that the initial peak in Fig. 3 is higher than the final peak – suggesting a multiplication of the permeate concentration by ICP during backflow prior to permeate production recommencing.

An alternative explanation could be related to the construction of the membrane element. Although the feed spacer thickness for all the membranes was the same (0.71 mm), no details were available about the permeate carrier which could hold more or less permeate according to its thickness or porosity. Nonetheless, it seems unlikely that the correlation with rejection would occur just by coincidence, so the first explanation above seems much more probable.

Table 3. Permeate and osmotic backflow volume in every batch cycle for different membranes at different feed concentrations, $r = 0.8$ and $J_w = 17.8$ L/m^2/h.

	Membrane type							
	Aq-U		D-XLE		D-HR		T-TMHA	
Feed concentration (mg/L)	Permeate volume (L)	Osmotic backflow volume (L)	Permeate volume (L)	Osmotic backflow volume (L)	Permeate volume (L)	Osmotic backflow volume (L)	Permeate volume (L)	Osmotic backflow volume (L)
1000	66.4	2.6	65.7	3.3	65.3	3.7	65.7	3.3
2000	65.7	3.3	64.9	4.1	64.3	4.7	65.2	3.8
3000	65.6	3.4	64.6	4.4	64	5	65	4
4000	65.6	3.4	64.3	4.7	63.8	5.2	65	4
5000	65.6	3.4	64.3	4.7	-	-	64.8	4.2

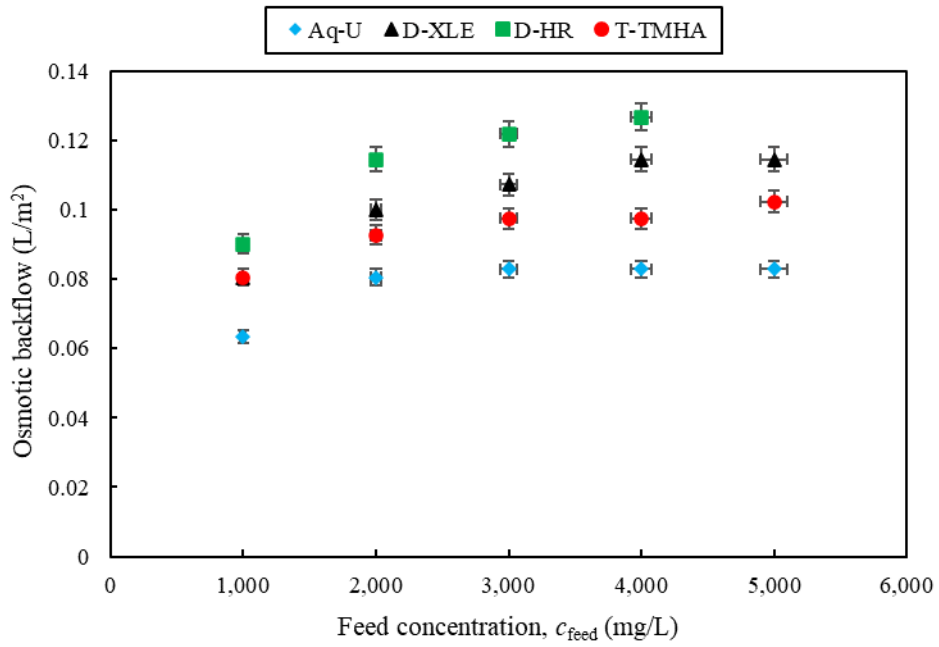

Fig. 6. Comparison of osmotic backflow per m^2 of membrane area as a function of feed concentration for different membranes at r = 0.8 and J_w = 17.8 L/m^2/h.

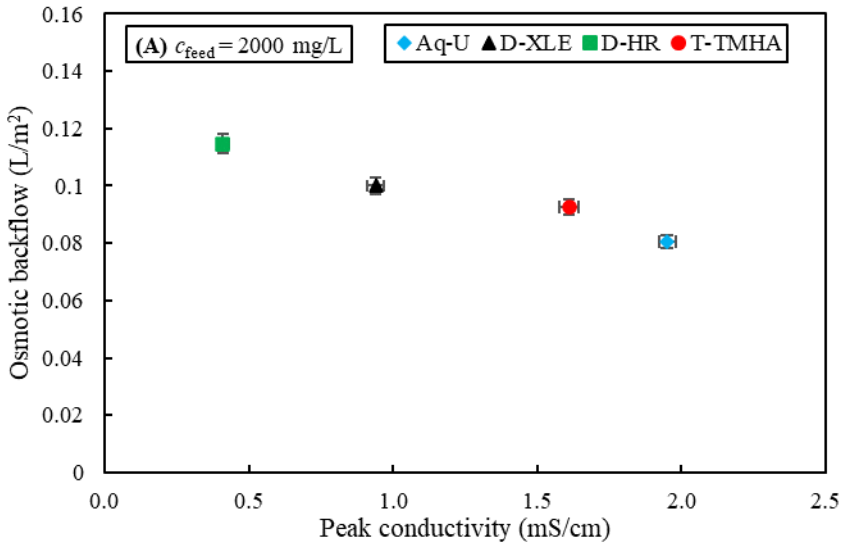

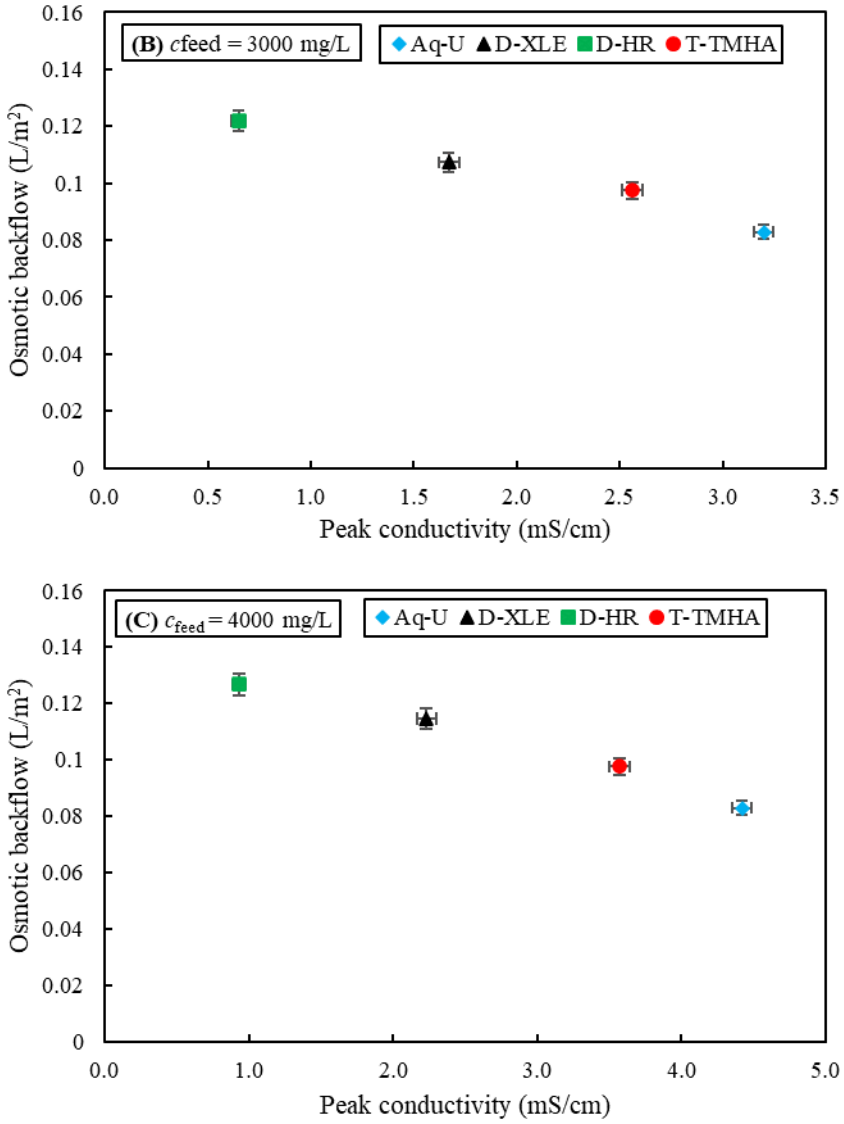

Fig. 7. Comparison of osmotic backflow per m^2 of membrane area as a function of peak conductivity for different membranes at A) c_{feed} = 2000 mg/L, B) c_{feed} = 3000 mg/L, and C) c_{feed} = 4000 mg/L, r = 0.8 and J_w = 17.8 L/m^2/h.

3.5. Pressure changes over a pressurization cycle

Fig. 8 shows how supply pump hydraulic pressure and conductivity at the RO membrane inlet varies over a batch pressurization phase at c_{feed} = 3000 mg/L and J_w = 17.8 L/m^2/h. Both variables, shown in Fig. 8(A) and (B), exhibit a similar increasing trend over the duration of the cycle as the supply pump pressure increases with inlet concentration and the associated osmotic pressure.

The T-TMHA and Aq-U membranes demonstrated almost identical pressure trends, with average values of 9.6 and 9.7 bar, respectively. The D-XLE membrane had a slightly higher average pressure of 10.1 bar, while the high-rejection D-HR had considerably higher pressure, averaging at 13.2 bar (Fig. 8(A)). This higher pressure was caused by the lower permeability of the D-HR membrane (see Table 2).

Inlet conductivity among the four membranes was almost the same with slightly higher in the case of D-HR. This can be explained by the higher rejection, which resulted in more salt remaining in the recirculating loop during pressurization.

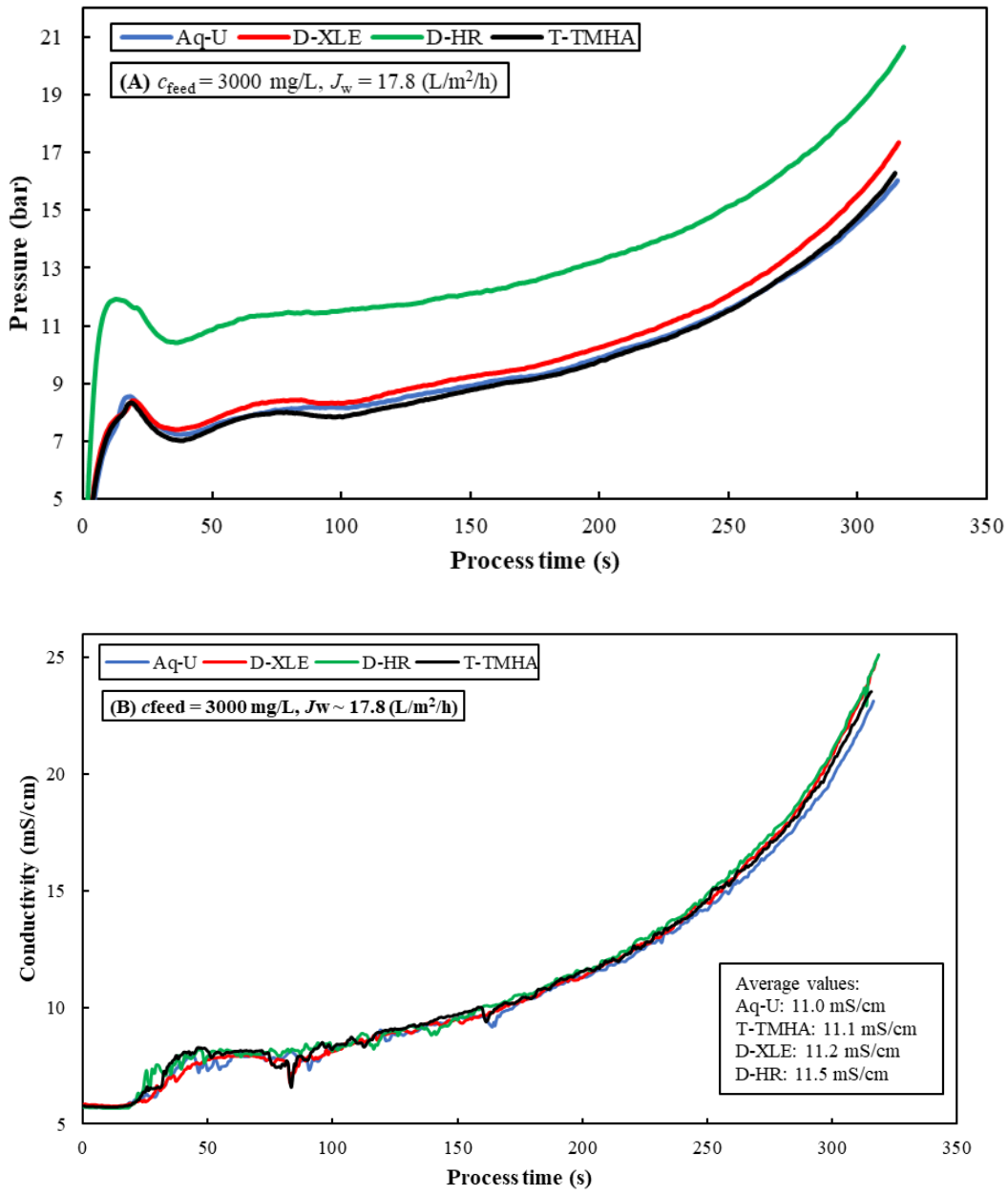

Fig. 8. Observed A) pressure, and B) inlet RO conductivity variations over a pressurization phase for different RO membranes at c_{feed} = 3000 mg/L and J_w = 17.8 L/m²/h.

3.6. Comparison of peak and average applied pressure with brine osmotic pressure

Fig. 9 compares the brine osmotic pressure, average applied pressure and peak pressure of different RO membranes at different feed concentrations and J_w = 17.8 L/m²h. Brine osmotic pressure was calculated by multiplying the concentration factor (Eq. 2, derived from mass

balance) by the osmotic pressure of NaCl solution calculated using the van 't Hoff expression (e.g., 0.79 bar for 1000 mg/L NaCl solution at 25 ◦C).

$$CF = \frac{[1 - r(1 - R_s)]}{1 - r} \quad (2)$$

Batch RO allows operation at lower average applied pressure than conventional RO. Thus, average applied pressure in batch RO can be less than the brine osmotic pressure (or exceed it by only a small margin). In contrast, in conventional RO the applied pressure must exceed the brine pressure substantially, to maintain a net driving pressure.

For the three high-permeability membranes, at low feed concentration (c_{feed} < 2000 mg/L), the average applied pressure equalled or exceeded the brine osmotic pressure. This observation deviates from the design intention – suggesting that batch RO is not so efficient in this case at recovery of 0.80. It indicates that the applied pressure requirement was dominated by membrane hydrodynamic resistance. In contrast, at feed concentration c_{feed} > 2000 mg/L, average applied pressure was greater than the brine osmotic pressure, suggesting an efficiency advantage.

For the low-permeability D-HR membrane, the average applied pressure was always higher than the brine osmotic pressure, but the gap became smaller on increasing the feed concentration. However, because of the system pressure limitation of 25 bar, we were unable to test at c_{feed} > 4000 mg/L which may have resulted in applied pressure dropping below the brine osmotic pressure.

Extending the comparison to include different fluxes (at c_{feed} = 3000 mg/L, see Fig. 9B) showed that, at decreased flux, the average applied pressure almost equalled the brine osmotic pressure with the D-HR membrane because of lower hydrodynamic resistance. All membranes showed a similar trend. Thus, on decreasing flux from 22.2 to 13.4 L/m^2/h, the difference of average applied pressure minus brine osmotic pressure decreased from -0.1, 0.0, +3.7, and -0.5 bar, to -2.1, -2.1, +0.2, -2.3 bar for Aq-U, D-XLE, D-HR and T-TMHA membranes respectively.

Another important consideration is peak pressure, as this may limit the choice of membrane. Higher pressures also require more robust and expensive pressure vessels, pipework, valves, instrumentation, and other accessories. As expected, peak pressure increased with flux and feed concentration (see Fig. 9). Aq-U and T-TMHA membranes had almost similar peak pressure at different experimental conditions, slightly lower than that of D-XLE membrane, while that of D-HR membrane was much higher. For instance, at c_{feed} = 3000 mg/L and J_w = 22.2 L/m^2/h, peak pressure was about 17.7 bar when using Aq-U and T-TMHA membranes; while it increased by 5.6% to 18.7 bar with the D-XLE membrane. The D-HR membrane gave the highest peak pressure at 21.8 bar (17% above D-XLE and 23% above Aq-U and T-TMHA).

(A)

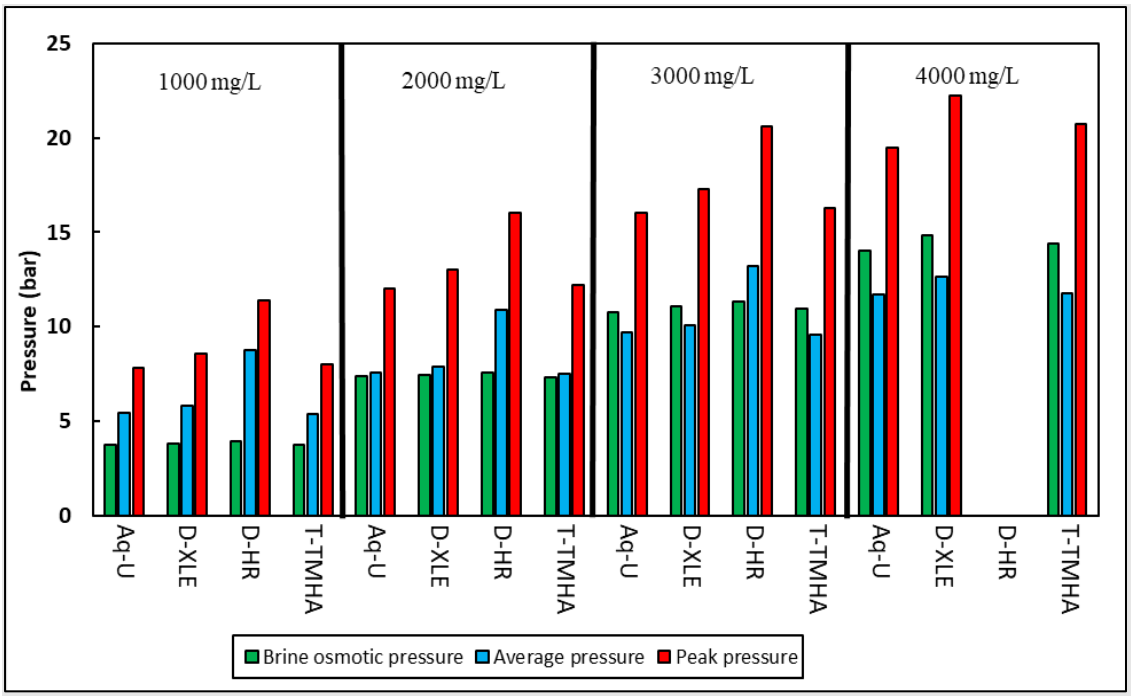

(B)

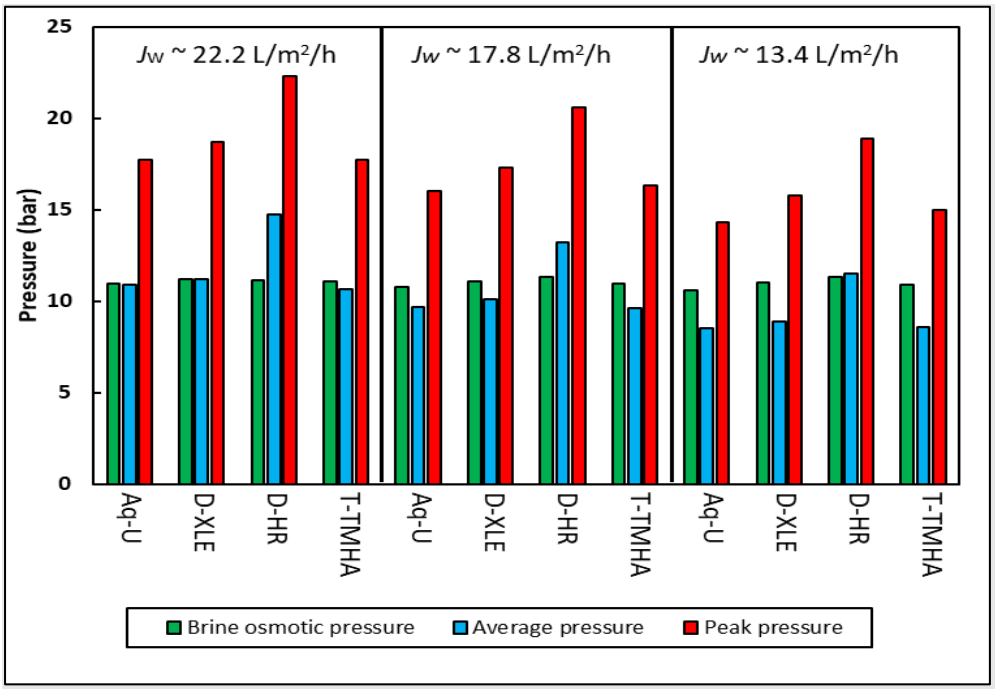

Fig. 9. Comparison of brine osmotic pressure, average applied pressure and peak pressure of different RO membranes at A) different feed concentrations and J_w = 17.8 L/m^2/h, and B) different fluxes and c_{feed} = 3000 mg/L.

3.7. Specific Energy Consumption (SEC)

Hydraulic *SEC* was measured based on the integration of differential pressure vs. discharged volume for each pump, and then totalled over the two pumps (supply and recirculation pumps) and two phases (pressurization and purge-and-refill) as carried out previously [27]. Fig. 10 presents hydraulic *SEC* of different RO membranes at various feed concentrations and fluxes. As expected, along with the applied pressure, hydraulic *SEC* increased with flux and feed

concentration. Hydraulic *SEC* was in the range 0.15-0.47 kWh/m^3 among the high-permeability membranes with only slight differences. For the high-rejection D-HR membrane, it increased to 0.21-0.48 kWh/m^3 at $c_{feed} \leq 4000$ mg/L (and fluxes < 15.5 L/m^2/h) and would likely have been higher if c_{feed} = 5000 mg/L and fluxes > 15.5 L/m^2/h at c_{feed} = 4000 mg/L had been possible.

The Aq-U and T-TMHA membranes had the lowest hydraulic *SEC,* whereas that of the D-XLE membrane was slightly higher due to the lower permeability and higher rejection. The D-HR membrane had the highest hydraulic *SEC*. For example, at flux of J_w = 17.8 L/m^2/h and c_{feed} = 2,000 mg/L, hydraulic *SEC* of D-HR was 0.362 kWh/m^3 while that of D-XLE was 25% less at 0.271 kWh/m^3. That of Aq-U and T-TMHA membranes was almost the same at 0.256 kWh/m^3 (29% lower than D-HR and 6% lower than D-XLE). On increasing the feed concentration, the gap among the membranes slightly widened, such that the hydraulic *SEC* of the T-TMHA membrane became slightly higher than that of the Aq-U because of its greater rejection.

On almost doubling the flux, system output increased by 70% from around 10 to 17 m^3/day. However, hydraulic *SEC* did not rise proportionately with only 35-40% increase at c_{feed} = 3000 mg/L. Therefore, this trade-off between output and energy saving should be considered during the design and operation. Additionally, as mentioned in section 3.2, at higher fluxes, better permeate quality is achieved.

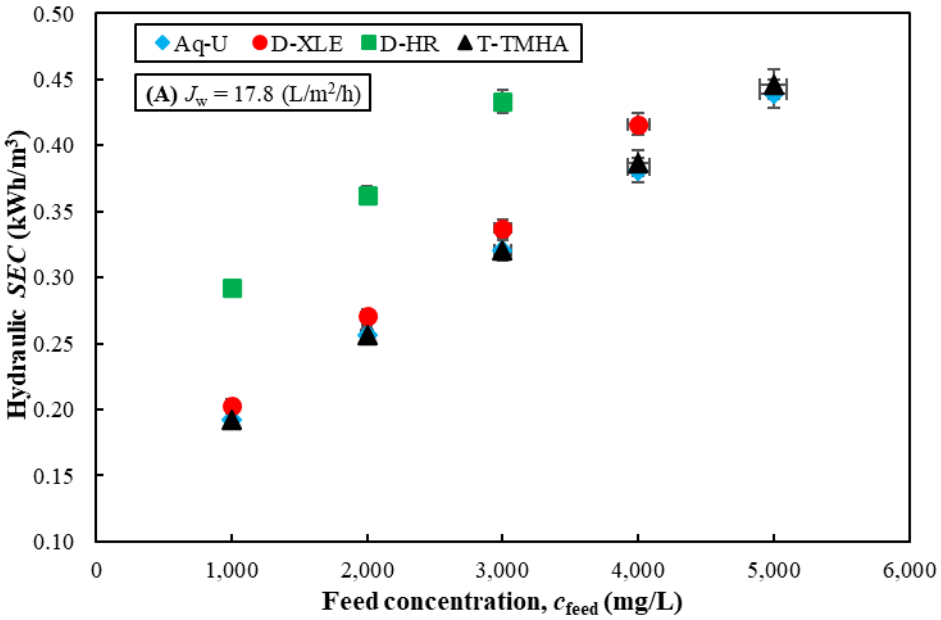

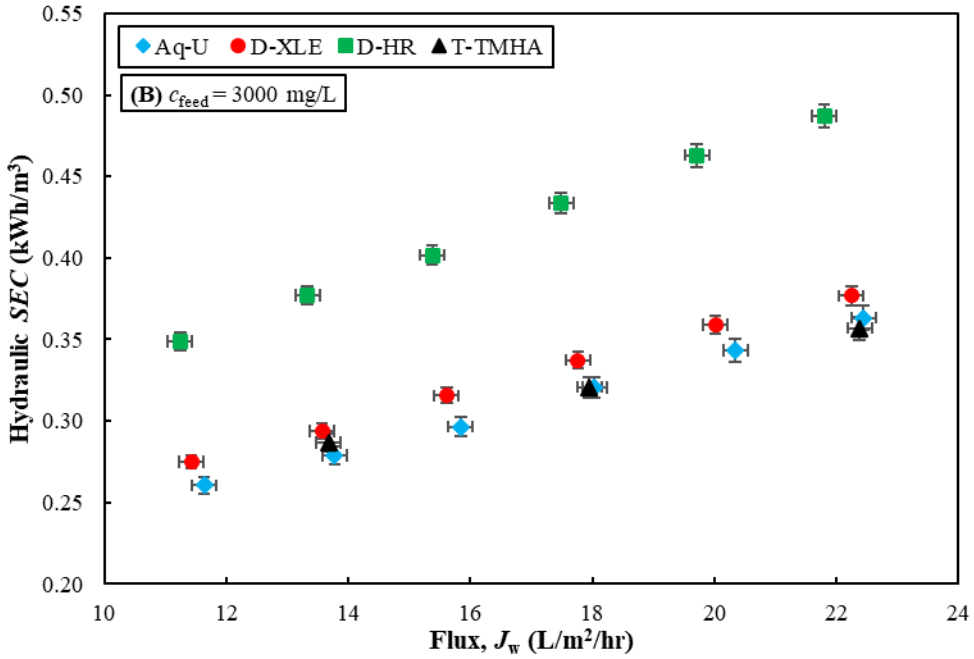

Fig. 10. Hydraulic *SEC* comparison of different RO membranes, A) at J_w = 17.8 L/m^2/h and different feed concentrations, B) at c_{feed} = 3000 mg/L and different fluxes.

Fig. 11 shows the electrical and hydraulic *SEC* breakdown of different RO membranes by pump and phase of operation. Most energy is used by the supply pump in the pressurization phase, providing enough pressure to overcome the osmotic pressure of feed solution and other losses in the system including major losses due to salt retention, concentration polarization, longitudinal concentration gradient and hydrodynamic resistance in the membrane pores.

Only 9-17% of the total energy was consumed by the recirculation pump, with a higher percentage contribution at lower feed concentrations and fluxes when the required applied pressure is smaller. The total electrical *SEC* of the recirculation pump in all cases was around 0.06-0.065 kWh/m^3. The electrical *SEC* of the supply pump in the purge-and-refill phase was constant at around 0.03 kWh/m^3 while it varied a lot in the pressurization phase with feed concentration and flux because of variations in osmotic pressure and membrane pore resistance, respectively. As recirculation pump energy consumption is a loss in batch RO, reducing this loss is desirable for improved system performance. The loss became less significant at higher fluxes and feed concentrations.

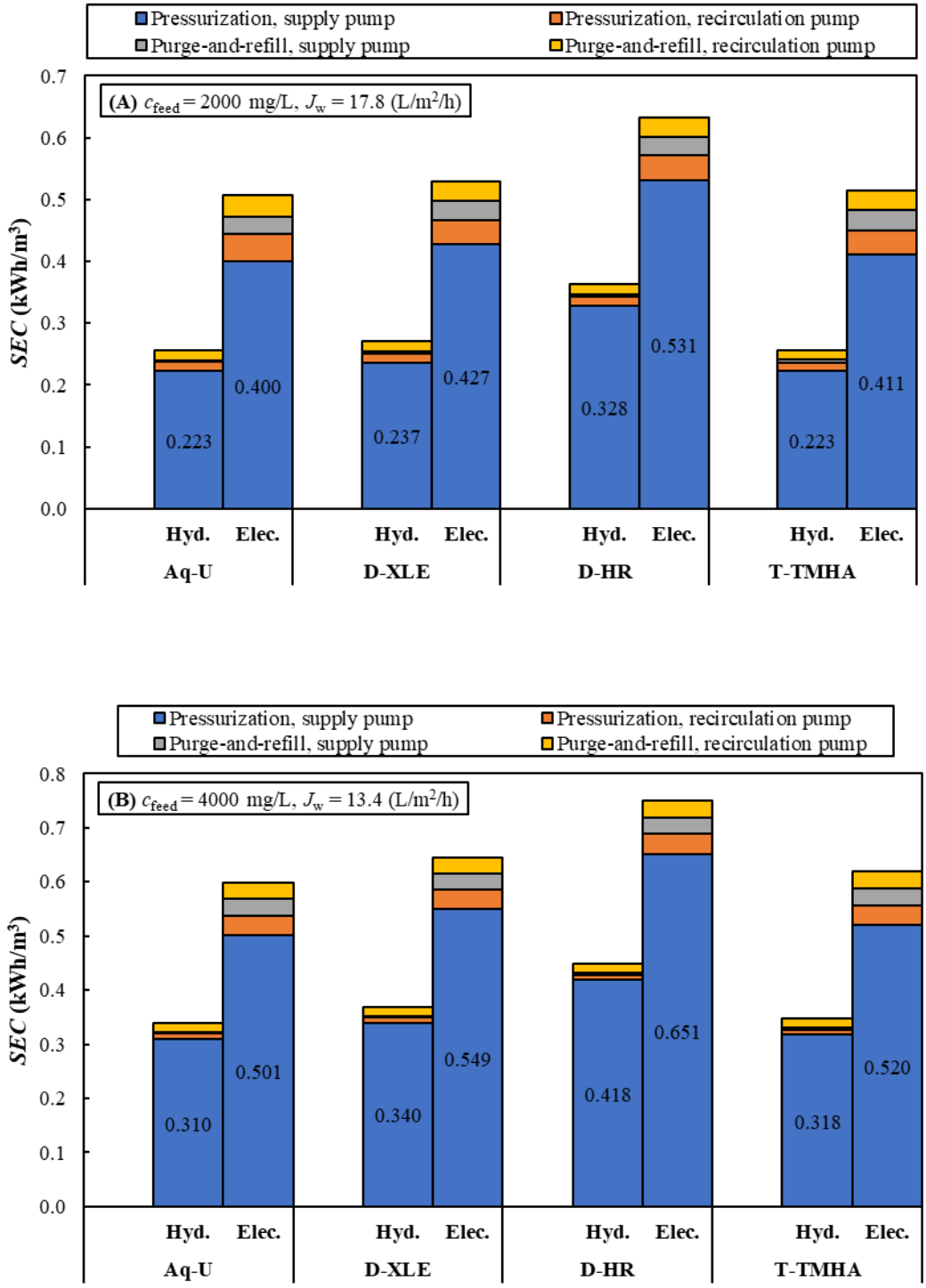

Fig. 11. Comparison of hydraulic and electrical *SEC* breakdown in batch RO system for both phases of operation and both pumps when using different RO membranes, A) at c_{feed} = 2000 mg/L, J_w = 17.8 L/m²/h, and B) at c_{feed} = 4000 mg/L, J_w = 13.4 L/m²/h.

3.8. Second law efficiency

Second law efficiency expresses the water output of a desalination system as fraction of the maximum output thermodynamically possible for a fixed energy input, while working at given

operating conditions such as feed concentration, water recovery, salt rejection and temperature. As such, it enables a fair comparison among systems, regardless of the technology used and allowing for variations in operating conditions. The following equation was used to calculate second law efficiency:

$$\eta = \frac{SEC_{min}}{SEC} = \frac{\pi_{\text{feed}} \left[\frac{1}{r} \ln\left(\frac{1 - r[1 - R_s]}{1 - r}\right) - (1 - R_S) \ln\left(\frac{1 - r[1 - R_s]}{(1 - r)(1 - R_s)}\right)\right]}{SEC} \quad (3)$$

where electrical *SEC* is used in the denominator (*SEC* and π should be expressed in similar units [e.g. MPa] for dimensional consistency). This equation applies to a desalination system treating brackish water as used in this study [40].

Fig. 12 compares second law efficiency among the different membranes as a function of flux and feed concentration. At c_{feed} = 3000 mg/L, second-law efficiencies with the Aq-U, T-TMHA and D-XLE membranes were approximately the same (21.9-22.3%) while that of the D-HR membrane was slightly lower (18.4%). Thus, the energy performance with the D-HR membrane lagged that of the others even with its higher rejection taken into account.

Second law efficiency increased with feed concentration and decreased with flux. Over the whole range of concentrations and fluxes in this study, the lowest second law efficiency of 7% occurred with D-HR at the lowest feed concentration and highest flux (c_{feed} = 1000 mg/L and J_w = 22.2 L/m^2/h); the highest was about 31% at the highest feed concentration and lowest flux (c_{feed} = 5000 mg/L and J_w = 11.4 L/m^2/h) for the high permeability membranes.

As reported in [26], second law efficiency of some of the existing brackish RO plants [41-44] are in the range of 1.5 to 4.5% when they supplied with feed concentrations of 900-2500 mg/L and operate at high recoveries (ranging from 0.6 to 0.8). Compared to these plants, under nearly similar conditions, batch RO showed higher second law efficiency, ranging between 8-22% with high-permeability membranes and 7-19% with low-permeability membranes.

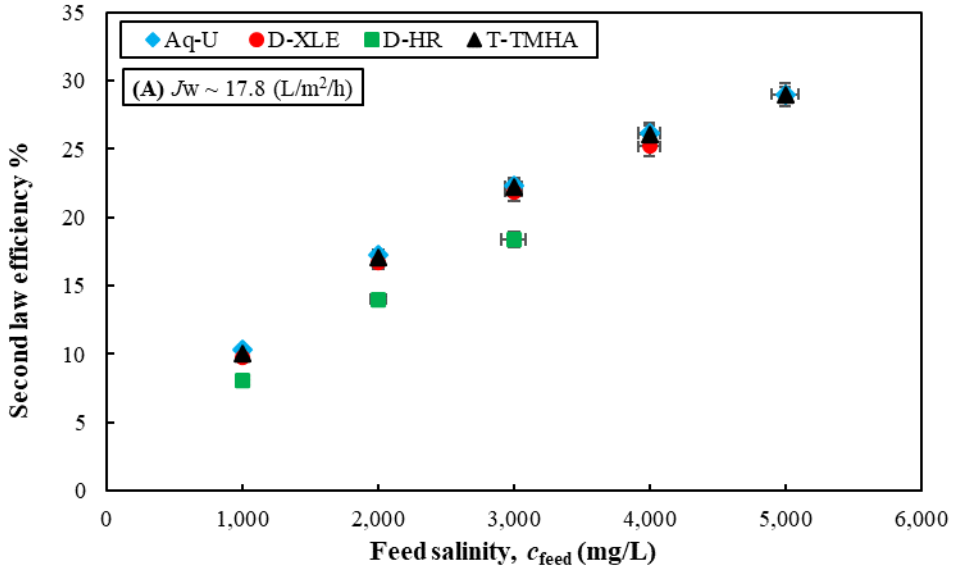

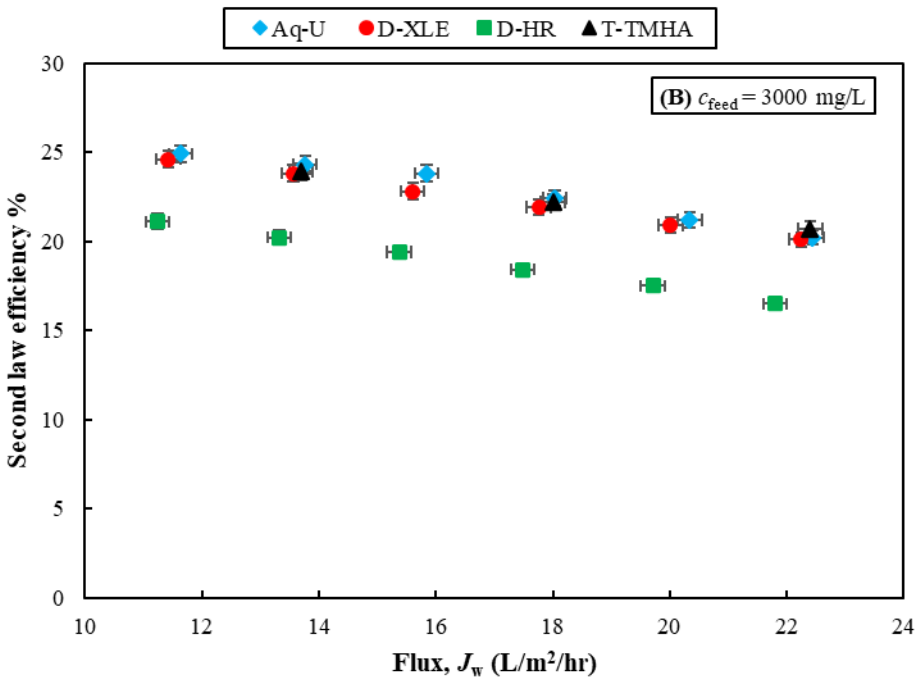

Fig. 12. Comparison of the second law efficiency of different RO membranes as a function of A) feed concentration at J_w = 17.8 L/m^2/h, and B) flux at c_{feed} = 3,000 mg/L.

4. Reduction in *SEC* through future membrane improvements

RO membranes have undergone a steady enhancement in permeability over the past few decades while maintaining their selectivity [4, 45]. This trend is anticipated to continue with further advances in membrane materials and manufacturing techniques. In this section, a verified model [25, 27] is used to project reductions in *SEC* that would result from future ultra-high permeability membranes. Details of the modelling assumptions and verification can be found in the SI and the model spreadsheet is provided as a supplementary file.

Projections are made of *SEC* with increasing permeability for different cases of rejection and osmotic backflow. Recovery is kept at 0.8, with feed concentrations of 3000 and 5000 mg/L and fluxes of 17.8 and 22.2 L/m^2/h. For a high-rejection membrane with R_s = 0.975 and osmotic backflow of 5.0 L (i.e., similar to the D-HR membrane) predictions at J_w = 17.8 L/m^2/h show that increasing permeability from 2.7 to 10 and 20 L/m^2/h/bar would reduce *SEC* by 34% and 40% respectively, giving *SEC*s of 0.302 and 0.273 kWh/m^3 compared to 0.456 kWh/m^3 at 2.7 L/m^2/h/bar. This *SEC* reduction will be even greater at higher fluxes. For instance, at slightly higher flux (J_w = 22.2 L/m^2/h), *SEC* would be 37% and 44% less at 10 and 20 L/m^2/h/bar, compared to that at 2.7 L/m^2/h/bar (see Fig. 13). This corresponds to an increase in the second law efficiency from 22.3% to 35.1% and 38.7% (assuming 80% efficiency for both pumps).

For a high-permeability low-rejection membrane with R_s = 0.87 and osmotic backflow of 3.4 L (i.e., similar to the Aq-U membrane) predictions at J_w = 17.8 L/m^2/h indicate that doubling the water permeability from 5 to 10 L/m^2/h/bar, results in approximately 17% *SEC* reduction. At 20 L/m^2/h/bar, *SEC* is predicted to drop further by 25%. At higher flux (J_w = 22.2 L/m^2/h) these reductions are enhanced further to 19% and 28% respectively (see Fig. 13), corresponding to second law efficiencies of 37.7 and 42%.

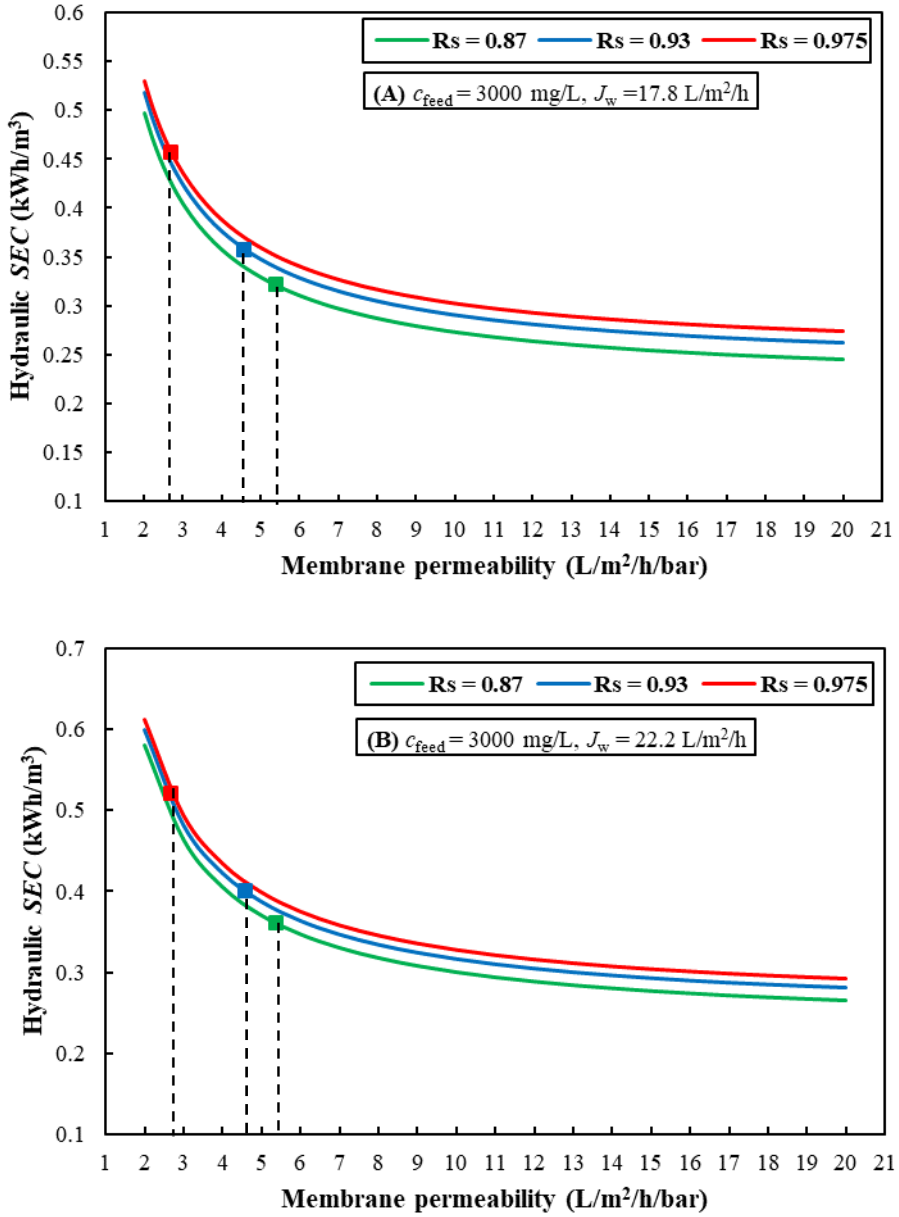

Fig. 13. Hydraulic *SEC* predictions as a function of membrane water permeability at r = 0.8, c_{feed} = 3000 mg/L and A) J_w = 17.8 L/m^2/h, and B) J_w = 22.2 L/m^2/h. The dashed lines indicate the adjusted values in model through experimental validation found in this study for D-HR, D-XLE, and Aq-U respectively from left to right.

Predictions also show that energy savings resulting from enhanced membrane water permeability decrease as the feed concentration increases. For instance, on permeability increase from 2.7 to 10 L/m^2/h/bar in the case of the low-permeability high-rejection membrane (R_s = 0.975), *SEC* falls by 29% at c_{feed} = 5000 mg/L (see Fig. 14), compared to 37% at 3000 mg/L. In the case of the high-permeability low-rejection membrane (R_s = 0.87), increasing permeability from 5 to 10 L/m^2/h/bar results in 14% *SEC* reduction at c_{feed} = 5000 and 19% reduction at c_{feed} = 3000 mg/L.

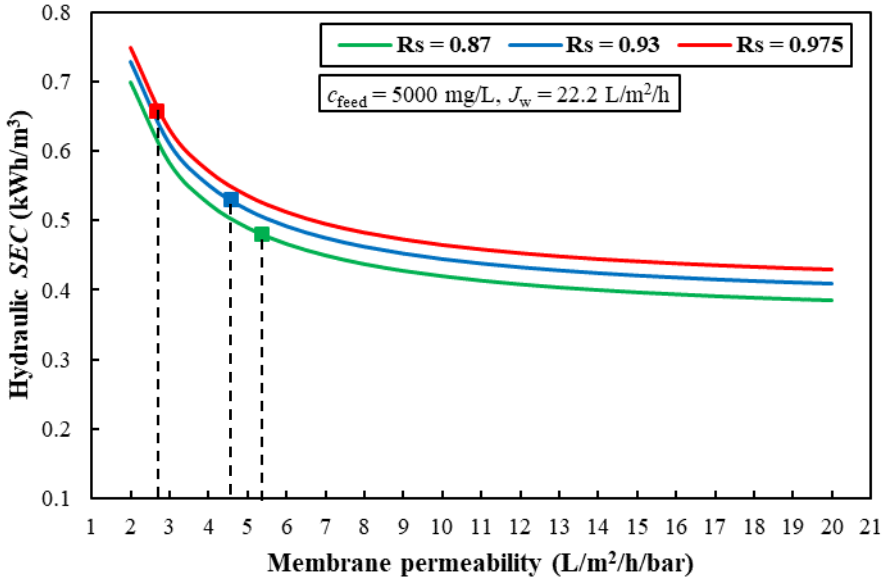

Fig. 14. Hydraulic *SEC* predictions as a function of membrane water permeability at r = 0.8, c_{feed} = 5000 mg/L and J_w = 22.2 L/m^2/h. The dashed lines indicate the adjusted values in model through experimental validation found in this study for D-HR, D-XLE, and Aq-U respectively from left to right.

Predictions in this study show that, in contrast to previous studies regarding continuous RO, increasing permeability still has an important role in the *SEC* reduction in batch RO. When using single-stage ROs, 5 and 8 L/m^2/h/bar was predicted as the upper limit of the membrane water permeability for the *SEC* reduction in BWRO by Cohen-Tanugi et al. [16] and Okamoto and Lienhard [3] respectively. However, we predict about 16% *SEC* reduction at 20 L/m^2/h/bar compared to 8 L/m^2/h/bar.

Moreover, Werber et al. [17] reported only a 2.2% energy saving on increasing permeability from 4 to 10 L/m^2/h/bar in single-stage BWRO while the energy saving was about 12% (0.05 kWh/m^3) in a two-stage RO system. In contrast, our predictions suggest a more substantial reduction in *SEC* (up to 20%, equivalent to 0.11 kWh/m^3) in the batch RO system under almost similar conditions.

Comparing to previous studies of batch RO, Warsinger et al. [34] reported a 40% reduction in energy consumption when increasing membrane permeability from 1 to 10 L/m^2/h/bar, with a 37% saving observed before reaching 7 L/m^2/h/bar. Our predictions indicate a slightly higher 59% reduction in *SEC* on going from 1 to 10 L/m^2/h/bar. Both studies agree, however, that the *SEC* reduction in the range of 7 to 10 L/m^2/h/bar is less than 10%.

Table 4 summarises and compares the most relevant studies on *SEC* reduction resulting from use of higher permeability membranes. We note that caution is needed in comparing the studies because of the variations in operating conditions and assumptions used among the studies.

Table 4. Simulation conditions from various references assessing the relationship between membrane permeability and SEC in brackish water RO desalination.

Author	Configuration	Feed concentration (mg/L)	Recovery	Flux ($L/m^2/h$)	Rejection (%)	Pump efficiency (%)	ERD efficiency (%)	Key findings	Reference
Cohen-Tanugi et al.	Continuous RO	2000	0.65	13.2	99.8	75	97	47% decrease in feed pump pressure when permeability increases from 1.5 to 4.5 $L/m^2/h/bar$. 5 $L/m^2/h/bar$ was considered as a meaningful limit for SEC reduction.	[16]
Shrivastava et al.	Continuous RO	804	0.85	N.D.	N.D.	85	95	30% decrease in SEC when permeability increases from 2.5 to 5 $L/m^2/h/bar$.	[46]
Werber et al.	Continuous RO	5844	0.75	15	N.D.*	100	100	2.2 % SEC reduction in single-stage while 12 % SEC reduction in two-stage when permeability increases from 4 to 10 $L/m^2/h/bar$. They stated that the reason for minor SEC reduction is that the hydraulic overpressure is small.	[17]
Wei et al.	Continuous RO	3000	0.6-0.98	15	100	100	100	SEC saving of 0.02 kWh/m^3 at low recovery of 0.6 when permeability increases from 1 to 10 $L/m^2/h/bar$. At very high recoveries of 0.98, SEC became almost insensitive to permeability.	[19]
Karabelas et al.	Continuous RO	2000	0.7	N.D.	N.D.	85	95	51.2 % of SEC is related to membrane filtration resistance and can be reduced by improved membrane permeability.	[47]
Warsinger et al.	Batch RO	5000	0.66	14.5	N.D.**	80	N.D.	About 40 % SEC reduction when increasing permeability from 1 to 10 $L/m^2/h/bar$.	[34]
Current study	Batch RO	3000 & 5000	0.8	17.8 & 22.2	0.87 and 0.93 and 0.975	100	N.A.	59-67 % SEC reduction when increasing permeability from 1 to 10 $L/m^2/h/bar$.	-

*B-value was used. **All scenarios were assumed to have the same permeate qualit

5. Conclusion

We experimentally investigated the performance of a free-piston batch RO system while using four different 8-inch RO membranes of differing water permeability, to evaluate the effect on salt rejection, permeate quality, *SEC,* and efficiency. Permeability of the membranes was measured and found to be in the range of 2.7-5.7 L/m^2/h/bar.

The system was tested at recovery of 0.8 with brackish water feed containing 1000-5000 mg/L of NaCl, at fluxes of about 11-23 L/m^2/h. Whereas salt rejection with the low-permeability membrane varied little from 97 to 99%, that with the three high-permeability membranes varied more widely from 82 to 96%, with the lowest rejections seen at lowest fluxes and greatest feed concentrations. All membranes achieved an acceptable permeate quality for drinking and irrigation applications. However, for high-permeability membranes, operation at higher fluxes (> 14 L/m^2/h) is necessary at high feed concentrations (> 5000 mg/L) to ensure water quality standards are met - albeit at the expense of slightly higher energy consumption.

We observed significant variations in osmotic backflow volume among the membranes and according to the feed salinity. The lower backflow (of 2.6 L) occurred with the lowest rejection membrane at low feed salinity of 1000 mg/L, whereas the highest (of 5.2 L) occurred with the highest rejection membrane at feed salinity of 4000 mg/L.

When comparing the hydraulic *SEC* among the four membranes, that obtained using the high-permeability membranes was considerably lower than with the low-permeability membrane (D-HR). For example, at feed concentration of 2000 mg/L and flux of 17.8 L/m^2/h, hydraulic *SEC* using the high-permeability membranes was 25-29% lower than obtained using the D-HR membrane.

Second law efficiency of up to 31% was achieved, comparing favourably to existing brackish water RO plants. This could increase to 42% with improvements in membrane permeability. At higher feed concentrations, the average applied pressure was lower than the brine osmotic pressure exiting the system - thus indicating improved energy performance against single-stage continuous RO.

Unlike several earlier studies of continuous RO [3, 16, 17, 19], this study predicts that increasing permeability to values of 10 or 20 L/m^2/h/bar will continue to have benefits in reducing *SEC* in batch RO. On increasing permeability from the baseline value of 2.7 L/m^2/h/bar to 10 and 20 L/m^2/h/bar, we predict *SEC* reductions of 37 and 44% respectively for a high-rejection membrane (R_s = 0.975). For a low-rejection membrane (R_s = 0.87), with baseline permeability of 5.4 L/m^2/h/bar, we predict corresponding reductions of 17 and 28% (at 10 and 20 L/m^2/h/bar respectively) at feed concentration of 3000 mg/L and flux of 22.2 L/m^2/h. The energy savings would be even greater at higher fluxes and lower feed concentrations. This highlights the on-going importance of research into new materials and techniques of membrane fabrication to increase water permeability. There is also a need for economic studies to assess the costs and benefits of developing and implementing future high-permeability membranes.

Acknowledgements

This project has received funding from the European Union's Horizon 2020 research and innovation programme under grant agreement No 820906. We would also like to acknowledge valuable contributions by Dr Jörg Vogel of Aquaporin A/S (Denmark) in advising about and supplying membranes. The authors would also like to thank Rubén Rodríguez Alegre for his comments and corrections on the manuscript.

References

[1] A. Yusuf, A. Sodiq, A. Giwa, J. Eke, O. Pikuda, G. De Luca, J.L. Di Salvo, S. Chakraborty, A review of emerging trends in membrane science and technology for sustainable water treatment, Journal of cleaner production, 266 (2020) 121867.
[2] S.S. Shenvi, A.M. Isloor, A. Ismail, A review on RO membrane technology: Developments and challenges, Desalination, 368 (2015) 10-26.
[3] Y. Okamoto, J.H. Lienhard, How RO membrane permeability and other performance factors affect process cost and energy use: A review, Desalination, 470 (2019) 114064.
[4] R.H. Hailemariam, Y.C. Woo, M.M. Damtie, B.C. Kim, K.-D. Park, J.-S. Choi, Reverse osmosis membrane fabrication and modification technologies and future trends: A review, Advances in colloid and interface science, 276 (2020) 102100.
[5] Z. Yang, X.-H. Ma, C.Y. Tang, Recent development of novel membranes for desalination, Desalination, 434 (2018) 37-59.
[6] D. Li, Y. Yan, H. Wang, Recent advances in polymer and polymer composite membranes for reverse and forward osmosis processes, Progress in polymer science, 61 (2016) 104-155.
[7] L.F. Greenlee, D.F. Lawler, B.D. Freeman, B. Marrot, P. Moulin, Reverse osmosis desalination: water sources, technology, and today's challenges, Water research, 43 (2009) 2317-2348.
[8] H.B. Park, C.H. Jung, Y.M. Lee, A.J. Hill, S.J. Pas, S.T. Mudie, E. Van Wagner, B.D. Freeman, D.J. Cookson, Polymers with cavities tuned for fast selective transport of small molecules and ions, Science, 318 (2007) 254-258.
[9] M. Bekbolet, C. Uyguner, H. Selcuk, L. Rizzo, A. Nikolaou, S. Meric, V. Belgiorno, Application of oxidative removal of NOM to drinking water and formation of disinfection by-products, Desalination, 176 (2005) 155-166.
[10] D. Qadir, H. Mukhtar, L.K. Keong, Mixed matrix membranes for water purification applications, Separation & Purification Reviews, 46 (2017) 62-80.
[11] M. Aroon, A. Ismail, T. Matsuura, M. Montazer-Rahmati, Performance studies of mixed matrix membranes for gas separation: A review, Separation and purification Technology, 75 (2010) 229-242.
[12] M. Wang, Z. Wang, X. Wang, S. Wang, W. Ding, C. Gao, Layer-by-layer assembly of aquaporin Z-incorporated biomimetic membranes for water purification, Environmental science & technology, 49 (2015) 3761-3768.
[13] M. Grzelakowski, M.F. Cherenet, Y.-x. Shen, M. Kumar, A framework for accurate evaluation of the promise of aquaporin based biomimetic membranes, Journal of membrane science, 479 (2015) 223-231.
[14] L. Sharma, L. Ye, C. Yong, R. Seetharaman, K. Kho, W. Surya, R. Wang, J. Torres, Aquaporin-based membranes made by interfacial polymerization in hollow fibers: Visualization and role of aquaporin in water permeability, Journal of Membrane Science, 654 (2022) 120551.
[15] J.R. Werber, C.O. Osuji, M. Elimelech, Materials for next-generation desalination and water purification membranes, Nature Reviews Materials, 1 (2016) 1-15.
[16] D. Cohen-Tanugi, R.K. McGovern, S.H. Dave, J.H. Lienhard, J.C. Grossman, Quantifying the potential of ultra-permeable membranes for water desalination, Energy & Environmental Science, 7 (2014) 1134-1141.
[17] J.R. Werber, A. Deshmukh, M. Elimelech, The critical need for increased selectivity, not increased water permeability, for desalination membranes, Environmental Science & Technology Letters, 3 (2016) 112-120.
[18] A. Zhu, P.D. Christofides, Y. Cohen, Energy consumption optimization of reverse osmosis membrane water desalination subject to feed salinity fluctuation, Industrial & Engineering Chemistry Research, 48 (2009) 9581-9589.
[19] Q.J. Wei, R.K. McGovern, Saving energy with an optimized two-stage reverse osmosis system, Environmental Science: Water Research & Technology, 3 (2017) 659-670.
[20] P.A. Davies, J. Wayman, C. Alatta, K. Nguyen, J. Orfi, A desalination system with efficiency approaching the theoretical limits, Desalination and Water Treatment, 57 (2016) 23206-23216.
[21] K. Park, L. Burlace, N. Dhakal, A. Mudgal, N.A. Stewart, P.A. Davies, Design, modelling and optimisation of a batch reverse osmosis (RO) desalination system using a free piston for brackish water treatment, Desalination, 494 (2020) 114625.
[22] D.M. Warsinger, E.W. Tow, K.G. Nayar, L.A. Maswadeh, Energy efficiency of batch and semi-batch (CCRO) reverse osmosis desalination, Water research, 106 (2016) 272-282.

[23] J.R. Werber, A. Deshmukh, M. Elimelech, Can batch or semi-batch processes save energy in reverse-osmosis desalination?, Desalination, 402 (2017) 109-122.
[24] Q.J. Wei, C.I. Tucker, P.J. Wu, A.M. Trueworthy, E.W. Tow, Impact of salt retention on true batch reverse osmosis energy consumption: experiments and model validation, Desalination, 479 (2020) 114177.
[25] E. Hosseinipour, E. Harris, H.A. El Nazer, Y.M. Mohamed, P.A. Davies, Desalination by batch reverse osmosis (RO) of brackish groundwater containing sparingly soluble salts, Desalination, 566 (2023) 116875.
[26] E. Hosseinipour, S. Karimi, S. Barbe, K. Park, P.A. Davies, Hybrid semi-batch/batch reverse osmosis (HSBRO) for use in zero liquid discharge (ZLD) applications, Desalination, 544 (2022) 116126.
[27] E. Hosseinipour, K. Park, L. Burlace, T. Naughton, P.A. Davies, A free-piston batch reverse osmosis (RO) system for brackish water desalination: Experimental study and model validation, Desalination, 527 (2022) 115524.
[28] M. Elimelech, W.A. Phillip, The future of seawater desalination: energy, technology, and the environment, science, 333 (2011) 712-717.
[29] D.M. Davenport, C.L. Ritt, R. Verbeke, M. Dickmann, W. Egger, I.F. Vankelecom, M. Elimelech, Thin film composite membrane compaction in high-pressure reverse osmosis, Journal of membrane science, 610 (2020) 118268.
[30] M. Aghajani, M. Wang, L.M. Cox, J.P. Killgore, A.R. Greenberg, Y. Ding, Influence of support-layer deformation on the intrinsic resistance of thin film composite membranes, Journal of membrane science, 567 (2018) 49-57.
[31] J.A. Idarraga-Mora, A.D. O'Neal, M.E. Pfeiler, D.A. Ladner, S.M. Husson, Effect of mechanical strain on the transport properties of thin-film composite membranes used in osmotic processes, Journal of Membrane Science, 615 (2020) 118488.
[32] M. Askari, C.Z. Liang, L.T.S. Choong, T.-S. Chung, Optimization of TFC-PES hollow fiber membranes for reverse osmosis (RO) and osmotically assisted reverse osmosis (OARO) applications, Journal of Membrane Science, 625 (2021) 119156.
[33] S. Cordoba, A. Das, J. Leon, J.M. Garcia, D.M. Warsinger, Double-acting batch reverse osmosis configuration for best-in-class efficiency and low downtime, Desalination, 506 (2021) 114959.
[34] D.M. Warsinger, J. Swaminathan, J.H. Lienhard, Ultrapermeable membranes for batch desalination: maximum desalination energy efficiency, and cost analysis, (2017).
[35] J. Swaminathan, R. Stover, E.W. Tow, D.M. Warsinger, J.H. Lienhard, Effect of practical losses on optimal design of batch RO systems, (2017).
[36] P. Khunnonkwao, K. Jantama, S. Kanchanatawee, S. Galier, H. Roux-de Balmann, A two steps membrane process for the recovery of succinic acid from fermentation broth, Separation and Purification Technology, 207 (2018) 451-460.
[37] P.A. Davies, A.K. Hossain, Development of an integrated reverse osmosis-greenhouse system driven by solar photovoltaic generators, Desalination and Water Treatment, 22 (2010) 161-173.
[38] W.H. Organization, Guidelines for drinking-water quality: incorporating the first and second addenda, World Health Organization, 2022.
[39] M. Mohammadifakhr, J. de Grooth, H.D. Roesink, A.J. Kemperman, Forward osmosis: A critical review, Processes, 8 (2020) 404.
[40] L. Wang, C. Violet, R.M. DuChanois, M. Elimelech, Derivation of the theoretical minimum energy of separation of desalination processes, Journal of Chemical Education, 97 (2020) 4361-4369.
[41] N. Kahraman, Y.A. Cengel, B. Wood, Y. Cerci, Exergy analysis of a combined RO, NF, andEDR desalination plant, Desalination, 171 (2005) 217-232.
[42] I.H. Aljundi, Second-law analysis of a reverse osmosis plant in Jordan, Desalination, 239 (2009) 207-215.
[43] M.H. Sharqawy, S.M. Zubair, Second law analysis of reverse osmosis desalination plants: An alternative design using pressure retarded osmosis, Energy, 36 (2011) 6617-6626.
[44] A.A. Alsarayreh, M.A. Al-Obaidi, A. Ruiz-García, R. Patel, I.M. Mujtaba, Thermodynamic limitations and exergy analysis of brackish water reverse osmosis desalination process, Membranes, 12 (2021) 11.
[45] Y.J. Lim, K. Goh, M. Kurihara, R. Wang, Seawater desalination by reverse osmosis: Current development and future challenges in membrane fabrication–A review, Journal of Membrane Science, 629 (2021) 119292.
[46] A. Shrivastava, S. Rosenberg, M. Peery, Energy efficiency breakdown of reverse osmosis and its implications on future innovation roadmap for desalination, Desalination, 368 (2015) 181-192.
[47] A. Karabelas, C. Koutsou, M. Kostoglou, D. Sioutopoulos, Analysis of specific energy consumption in reverse osmosis desalination processes, Desalination, 431 (2018) 15-21.

Paper 3: Desalination by batch reverse osmosis (RO) of brackish groundwater containing sparingly soluble salts

Ebrahim Hossseinipour[1], Ellie Harris[1], Hossam A. El Nazer[2], Yasser M. A. Mohamed[2], Philip A. Davies[1*]

[1]School of Engineering, University of Birmingham, Edgbaston, Birmingham B15 2TT, UK

[2]Photochemistry Department, National Research Centre, P.O. 12622, Egypt.

* p.a.davies@bham.ac.uk

Graphical Abstract

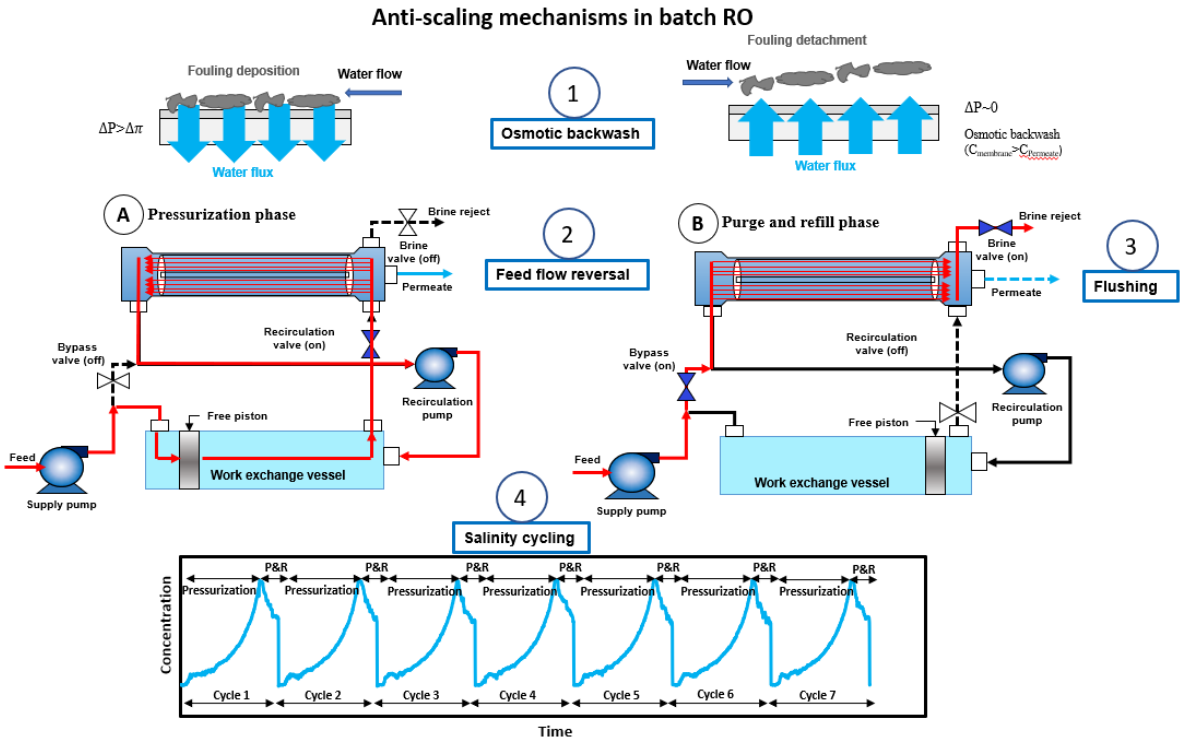

Abstract

Batch RO desalination is a new approach to high-recovery, energy-efficient desalination. So far, however, batch RO has been tested mostly with pure sodium chloride solutions. An important application of batch RO is desalination of brackish groundwater which, besides sodium chloride, contains sparingly soluble salts. In this experimental study of a batch RO system, we used simulated groundwater (with total dissolved solids ranging from 1180 to 3637 mg/L) following compositions of samples taken from a location in Egypt and a location in India. The groundwater contained high levels of salts which could be expected to cause scaling on the RO membrane surface. For example, the Langelier Saturation Index (*LSI*) for calcite reached 2.6 in the brine. Nonetheless, the system resisted scaling throughout >100 hours of operation. Membrane permeability remained almost unchanged, as demonstrated by tests conducted before and after the experiments. Induction time calculations showed that salinity cycling did not fully explain the scaling inhibition. Other anti-scaling mechanisms – such as periodic flushing, osmotic backwash, and feed flow reversal – were also likely contributors. At

recovery of 0.8, hydraulic specific energy consumption (*SEC*) was <0.5 kWh/m^3 and close to that obtained with sodium chloride solution at equivalent osmotic pressure.

Keywords: Scaling, Osmotic backwash, Periodic flushing, Feed flow reversal, Salinity cycling.

Highlights:

- Batch RO successfully treated brackish groundwater at high recovery (80 %) and with low energy consumption (*SEC* < 0.5 kWh/m^3).
- Despite a high risk of scaling in the simulated groundwater (*LSI* of 1.7–2.6) no scaling was observed.
- Four anti-scaling mechanisms: periodic flushing, feed flow reversal, osmotic backwash, and salinity cycling.
- *SEC* was comparable (within 7 %) to that of batch RO treating pure NaCl solutions.

1. Introduction

Batch RO is a relatively new approach to desalination that has gained interest because it achieves high efficiency and recovery rates in a compact design [1]. However, much of the research on batch RO has been done with feed water containing a solution of a single salt – typically sodium chloride (NaCl). For example, using NaCl solution, Wei et al [2] studied a batch RO system to conclude that (compared to standard continuous RO) batch RO could save about 11% of energy in the desalination of seawater at recovery of 0.55. In a study of brackish water desalination, Hosseinipour et al. [3] measured the performance of a batch RO system, fed by NaCl solution of concentration 1000-5000 mg/L and obtained electrical *SEC* of 0.48–0.83 kWh/m^3 at a recovery of 0.8. This was better than achieved by most existing brackish RO systems. Compared to standard RO, batch RO allows recovery to increase without large penalties in *SEC*. Thus, by operating in hybrid semi-batch/batch mode, batch RO achieved recovery of 0.94 with *SEC* of just 0.54 kWh/m^3 using NaCl feed solution of concentration 1500 mg/L [1].

Though these studies have shown batch RO to be a promising technology, for practical applications it is important to understand how it will perform with realistic feed water compositions containing multiple components as opposed to simple NaCl solution. One important category of feed water is brackish groundwater which occurs in many aquifers exploited by humans across the world. Brackish water desalination accounts for about 25% of the RO desalination output globally [4]. Typically, brackish groundwater contains many other salts besides sodium chloride, dependent on the geology of the aquifer from which it is extracted [5]. Because of its high energy efficiency at high recovery, batch RO is envisaged as a good solution to desalinate groundwater. However, given the many and varied groundwater compositions occurring worldwide, testing batch RO with every possible composition is not practical. Therefore, if experiments and models based on sodium chloride are a good representation of performance with more complex compositions, this will be a very useful simplification when it comes to developing and testing batch RO technology.

Unlike sodium chloride, some of the other salts in groundwater may be sparingly soluble. Such salts are prone to precipitate on the membrane surface, thus causing mineral fouling (i.e., scaling) which can lead to loss of performance, manifested as decreased permeate output or increased pumping pressure and energy consumption. Sparingly soluble salts common in groundwater include $CaCO_3$, $CaSO_4$, $BaSO_4$, $SrSO_4$, CaF_2, and $Ca_3(PO_4)_2$. According to Liu et al. [6], calcium carbonate ($CaCO_3$) and calcium sulfate ($CaSO_4$) are the most prevalent sources of scaling in RO desalination. To mitigate scaling, acid [7] and anti-scalants [8-10] are often dosed to the feed of groundwater RO plants. The required dosing volume depends highly on the recovery of the plant which is constrained by the presence of the sparingly soluble salts. Thus, to reduce the usage, cost, and environmental impact of the anti-scalant chemicals, designers may prefer to decrease the plant's recovery in some cases [11]. Even with anti-scalant dosing, Ruiz-Garcia et al. [12] reported a limitation in recovery to a maximum of 76% using Genesys anti-scalants, depending on the feed composition of a brackish water source. However, the cost-efficient operation of inland brackish water RO favours high recovery [12-14].

The cyclic nature of the batch RO process provides four mechanisms that could provide advantages over standard continuous RO when it comes to avoiding fouling and scaling at high recovery. Each mechanism has been used individually in other RO or other membrane separation processes, but all four are brought together in batch RO [15].

The first mechanism is flushing, which occurs towards the end of each cycle of the batch RO operation. During the initial phase of the cycle (i.e., pressurisation) the concentration in the RO channel gradually increases above the feed concentration. Precipitation and scaling by salts could be expected at these elevated concentrations. Then, during subsequent flushing, the concentration falls back down close to the feed concentration – providing an opportunity to redissolve any precipitated salts and remove them from the membrane surface. Permeate output flow is paused such that precipitates are no longer drawn towards the membrane; while tangential flow continues and provides a cleaning action to sweep away deposits. Flushing is already a common method to remove scaling and fouling in many types of membrane processes. It is regularly used, for example, in clean-in-place procedures in standard RO plants [16]. In batch RO, however, the role of flushing is less well known and understood.

The second mechanism is osmotic backwash, which occurs at the end of the pressurisation phase of each batch RO cycle. At this moment, the feed pressure falls suddenly, such that the osmotic pressure of the brine causes permeate to flow back through the membrane and into the feed channel [2]. This backflow continues until enough flushing has taken place to lower the osmotic pressure in the feed channel. Osmotic backwash has a downside in that it reduces output and recovery slightly, but the upside is that it may help to restore membrane permeability by lifting scaling species off the membrane. Many studies have confirmed the foulant removal potential and flux restoration of cleaning RO membranes using the osmotic backwash method [17-23]. For example, in a UF-RO pilot system treating secondary treated effluent, a direct osmosis backwash using high-salinity solution injection (varying from 100-136 g/L) was studied [17]. The study reported a five-fold increase in brine turbidity (3 NTU) compared to the normal process without osmotic backwash (0.6 NTU), showing that foulants were effectively removed and carried away in the brine stream. Osmotic backwash is not unique to batch RO, as it can occur in other types of RO where permeate flow is intermittent. For example, battery-less solar-powered RO systems experience starting and stopping of permeate production as solar radiation varies over the diurnal cycle or more frequently [24]. Even grid-

connected continuous RO systems could be controlled to provide osmotic backwash through deliberate stopping and starting. Nevertheless, the periodic and frequent (i.e., every few minutes) occurrences of osmotic backwash in batch RO makes it particularly relevant for this technology.

Thirdly, feed flow reversal occurs in some batch RO systems, which can also be beneficial to delay nucleation and thus counter scaling. In a standard continuous RO system, scaling normally begins near the brine outlet end of the RO module, where the concentration of minerals is highest [25, 26]. Feed flow reversal could mitigate scaling by periodically introducing fresh feed at the outlet (i.e., by swapping the inlet and outlet), thus disrupting precipitation and preventing or redissolving scale before it builds up significantly. Again, this is not unique to batch RO. Feed flow reversal RO exists as a non-batch RO technology designed to take advantage of this effect and reduce anti-scalant dosage [27, 28]. In 2012, for example, Gu et al. [29] demonstrated feed flow reversal at recovery up to 0.81 without anti-scalant, despite calcium sulfate (gypsum) saturation index reaching 0.54 at the RO outlet. Batch RO may provide varying degrees of feed flow reversal, depending on the configuration chosen. For example, double-acting batch RO systems can provide full flow reversal, meaning that equal operation time is spent running in either flow direction [30, 31]. Some single-acting batch RO systems use no feed flow reversal; whereas others use partial feed flow reversal, meaning that flow is reversed for a shorter period corresponding to the purge phase of operation only [32] – as is the case in the current study.

Fourthly, salinity cycling in the batch RO may also help reduce scaling. Although, for a given recovery, the final concentration in batch RO must reach the same maximum as in continuous RO, the maximum is only reached momentarily during the batch RO cycle. Supersaturated conditions are therefore only transient, such that scaling may be avoided if they do not persist sufficiently for salt crystals to nucleate [33, 34]. In a study of salinity cycling, Warsinger et al. [33] used a model of crystal nucleation to predict promising anti-scaling performance of batch or semi-batch RO processes treating $CaCO_3$ and $CaSO_4$ solutions. The study used the following correlation between the nucleation induction time and saturation index of $CaCO_3$ which crystalises as calcite:

$$t_{ind,CaCO_3} = 10^{\left(4.22 - \frac{13.8}{LSI} - \frac{1876.4}{T} + \frac{6259.6}{LSI.T}\right)} \quad (1)$$

where $t_{ind,CaCO_3}$ is the nucleation induction time [s], *LSI* is the Langelier saturation index, and *T* is the absolute temperature [K]. For $CaSO_4$, which crystallises as gypsum, the following correlation was used [33]:

$$t_{ind,CaSO_4} = 55.5\, SI^{-4.701} \qquad SI < 0.2 \quad (2)$$

where *SI* is the saturation index. By comparing the residence time of the water to the nucleation induction times calculated, the study predicted the scaling of the salts based on residence times in typical RO systems and predicted the maximum possible recovery for batch *vs*. standard continuous RO, assuming saturated feed solutions. In the case of $CaCO_3$, it predicted significant bulk nucleation starting at recovery $r = 0.87$ in batch RO, compared to only $r = 0.74$ in standard continuous RO [33]. In the case of $CaSO_4$, the corresponding thresholds were $r = 0.87$ (batch) *vs* $r = 0.54$ (continuous). Thus, batch RO should be able to operate at $r = 0.87$

when challenged with either of these sparingly soluble salts. This is a high recovery compared to many current groundwater desalination systems.

To investigate the hypothesis that batch RO helps to reduce fouling, this paper reports laboratory experiments with a single-acting batch RO system that includes these four features of periodic flushing, osmotic backwash, feed flow reversal, and salinity cycling. Unlike most previous experimental studies which used only sodium chloride, the experiments have been performed with feedwater which poses a risk of mineral scaling. The feedwater was made up to replicate samples taken in the field in two case study locations, one in Egypt and the other in India. In both cases, groundwater quality is poor, and desalination is required to upgrade it for drinking and irrigation purposes. Therefore, the use of batch RO is of practical interest to address the scarcity of good-quality water in both locations. Using these groundwater compositions, this paper quantifies important performance parameters, including *SEC*, peak pressure and rejection and compares these to the experimental and modelling results obtained previously with sodium chloride. By testing performance before and after the series of tests, we show that no significant drop in performance occurred. The Discussion section analyses the results in comparison to other studies that used similar approaches to avoid scaling in various types of RO system.

2. Case Study Locations

2.1. Siwa Oasis, Egypt

The first location is Siwa Oasis, Egypt, where samples have been taken from the Tertiary Carbonate Aquifer System. This is a shallow limestone aquifer, of depth 10-200 m, characterized by its medium to high salinity: the samples contained total dissolved solids (TDS) of 1300-8600 mg/L (with an average of 4200 mg/L). Siwa Oasis is considered among the most promising locations in the Western Desert of Egypt for future agricultural expansion projects because of the availability of groundwater. Currently, the aquifer is exploited mainly for the irrigation of crops such as dates and olives. The use of irrigation, together with the high rate of evaporation during the summer, leads to the development of a thick salty layer that hampers such agricultural activities [35]. The uncontrolled withdrawal of groundwater and agricultural expansion in the last decades have led to the decline of piezometric head levels and the deterioration of groundwater quality [36]. Consequently, Siwa Oasis suffers from environmental problems including water logging, soil salinization, inefficiency of disposed drainage water systems, and loss of agricultural productivity. As a result of the increased salinity in the groundwater wells, it has been suggested to construct RO desalination systems to enhance the water quality for irrigation [37]. Nonetheless, the presence of limestone in the aquifer is likely to present a challenge for RO because of calcite scaling.

2.2. Saurashtra region, Gujarat, India

The second location is the semi-arid Saurashtra region of the Indian state of Gujarat, where the coastal strip has become severely affected by saline intrusion. A recent field study focused on Lodhva, a village of about 8500 inhabitants that has relied on groundwater for domestic, agricultural, and industrial uses [38]. There are limestone reserves in this area, and numerous cement businesses engage in open-pit mining. The coastal aquifer is more susceptible to

seawater intrusion because of open-cast mining. Deterioration in groundwater quality, which now typically contains 2000-3500 mg/L of dissolved solids, effectively renders it unfit for human consumption. Consequently, piped water has been introduced to provide drinking water from distant reservoirs. Nevertheless, the supply of such water is intermittent and not accessible to all villagers; and its quality cannot be guaranteed. As regards the disposal of wastewater, Lodhva has no infrastructure or treatment systems for this purpose. Domestic wastewater is mostly discharged to simple soak pits adjacent to buildings. The problems at Lodhva are typical of those in Saurashtra and more broadly across Gujarat – which has over 3500 km^2 of salinized land in total [38].

3. Materials and methods

3.1. Feedwater composition

The feedwater compositions used in this study are based on the analysis of field samples from the above two locations, as reported in [37] and [38]. In total, 54 sample compositions were reported from Siwa (Egypt) and 20 from Lodhva (India) – henceforth referred to simply as Egypt (E) and India (I) samples, respectively. Each sample was taken from a different well. Four sample compositions have been chosen from each location, giving eight in total. The TDS of the chosen compositions ranged from 1138-3492 mg/L (see Table A1). These compositions represent a range of salinities at each location (though some higher salinities had to be excluded because of the 25-bar pressure limit of the batch RO equipment used in this study). At these TDS levels, none of these compositions meets general water quality requirements for drinking. The levels would also exceed the acceptable limits of many irrigated crops.

A Piper diagram has been used to classify groundwater quality (Fig. 1). In the cation plot (left triangle), the Egypt samples lie towards the alkali metal ($Na^+ + K^+$) vertex, indicating the dominance of these cations. The India samples lie more towards the Ca^{2+} vertex, showing a greater abundance of calcium, which may be problematic for scaling. In the anion plot (right triangle), all samples fall close to the halide ($Cl^- + F^-$) vertex. The diamond plot shows that the Egypt samples are dominant in (Na^+– K^+– Cl^-–SO_4^{2-} type) indicating the prevalence of alkali metal ions ($Na^+ + K^+$) and stronger acidic anions ($Cl^- + SO_4^{2-}$) over the alkaline earth ($Ca^{2+} + Mg^{2+}$) and weaker acidic anions (CO_3^{2-}+HCO_3^-). The India samples are dominated by cations (Ca^{2+} and Mg^{2+}) and anions (SO_4^{2-} and Cl^-), which indicates permanent hardness in the water (Ca^{2+}- Mg^{2+}-Cl^-- SO_4^{2-} type). The Na/Cl ratio indicates that all the India samples (I1-I4) have a ratio of less than 0.86, confirming that the wells are affected by seawater intrusion.

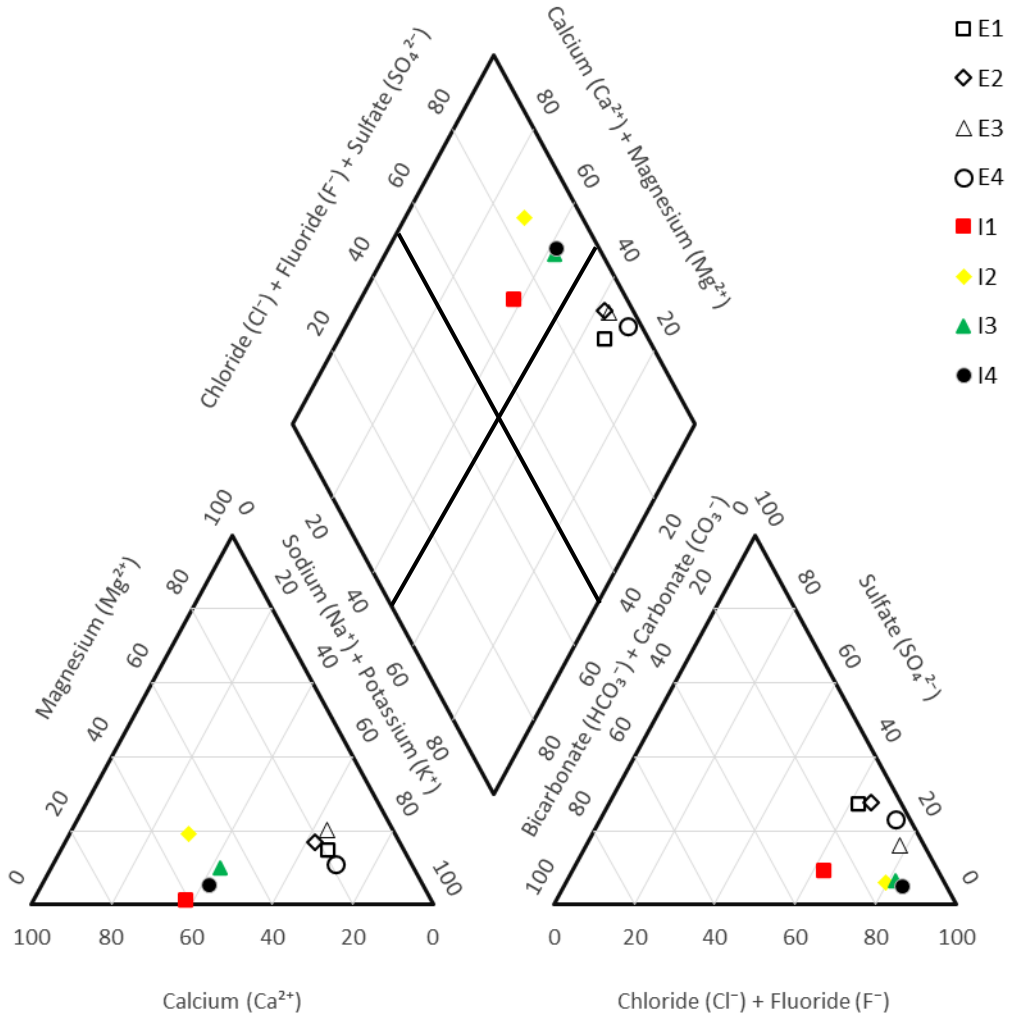

Fig. 1. Piper diagram for groundwater quality in Egypt (E1-E4) and India (I1-I4).

The compositions were checked for charge neutrality (ignoring minor ions at concentrations <1 mg/L). The discrepancy in the Egypt samples was less than 0.4%; whereas in the India samples it was as high as 6 and 9% in the case of samples I1 and I2, respectively (that of I3 and I4 was less than 1%). Adjustments to charge balance were therefore necessary before making up the feedwater. The adjustments were made preferentially to the higher concentrations of ions present to follow the reported compositions as closely as possible. For example, Table 1 shows the adjustments for sample E2. The total amount of cations reported was $\sum C^{z+} = 30470\ \mu eq/L$, while the total amount of anions was $\sum A^{z-} = 30310\ \mu eq/L$. Therefore, we balanced them to the average value of $\sum C^{z+} = \sum A^{z-} = 30390$ mainly by adjusting the concentrations of Na^+ and Cl^- which were the most concentrated ions in this case. Table 2 shows the ionic compositions used for the experiments, following similar adjustments in each of the 8 cases.

Table 1. Charge balance adjustments for sample E2 (see Appendix for similar details for other samples).

Ions	Measured value (mg/L)	Measured value (µeq/L)	Adjustments (µeq/L)	Balanced Concentration (µeq/L)	Balanced Concentration (mg/L)
Ca^{2+}	128	6384	-17	6367	127.7
Mg^{2+}	62.4	5136	-13	5122	62.2

Na^+	423.2	18408	-48	18360	422.1
K^+	20.28	519	-1	517	20.2
NH_4^+	0.42	23	0	23	0.4
$\sum C^{Z+}$		30470	-80	30390	-
HCO_3^-	131.76	2160	6	2166	132.1
Cl^-	700	19774	52	19826	701.8
SO_4^{2-}	401.28	8351	22	8373	402.3
NO_3^-	1.51	24	0	24	1.5
$\sum A^{Z-}$	-	30310	80	30390	

Table 2. Ionic composition of feed water used in the experiments, following adjustment of change balance. The pH was that measured after making up the tanks, without any adjustment.

	Sample number	pH	TDS (mg/L)	Ca^{2+} (mg/L)	Mg^{2+} (mg/L)	Na^+ (mg/L)	K^+ (mg/L)	NH_4^+ (mg/L)	HCO_3^- (mg/L)	Cl^- (mg/L)	SO_4^{2-} (mg/L)	NO_3^- (mg/L)	F^- (mg/L)
Egypt	E1	7.8	1319	79.6	38.2	315.1	9.3	0.3	136.6	462	276.5	0.8	-
	E2	7.9	1871	127.7	62.2	422.1	20.2	0.4	132.1	701.8	402.3	1.5	-
	E3	7.9	2788	151.5	114.8	669.7	25.8	0.6	171.3	1292	359.3	2.1	-
	E4	7.9	3637	223.2	81.3	951.7	28.3	0.7	120	1560	669	1.9	-
India	I1	7.9	1180	217.4	2.7	153	4.4	-	278.2	364.1	72.9	85.5	0.6
	I2	7.9	1994	338.1	77.4	222.4	5.6	-	277.2	885.5	89	96.2	0.6
	13	7.9	2576	411.8	52.7	407.8	11	-	305.4	1226	133	26	0.6
	I4	7.9	2811	507.1	15	439.2	32	-	296.3	1360	109.8	50.5	0.6

The scaling potential of these compositions was analysed with the help of PHREEQC software [39] applied to the feed and brine composition. The brine composition was based on a recovery of $r = 0.8$, corresponding to a fivefold increase in the concentration of all species with respect to the feed. By calculating the saturation indices of the various salts, PHREECQ identified three species at risk of scaling: $CaCO_3$, $CaSO_4$ and CaF_2. In the case of CaF_2, we took into account the background concentration of 0.6 mg/L fluoride ions in the tap water used to prepare the feed water. This was significant as the solubility of CaF_2 is only 15 mg/L at 25°C, such that the addition of just small amounts of fluoride can affect saturation. For $CaCO_3$, solubility is pH-dependent, and the Langelier Saturation Index (*LSI*) is used instead of the simple saturation index (*SI*). A value of *LSI* or *SI* greater than zero indicates supersaturation of the respective salt and thus a risk of scaling [40].

As seen in Table 3, all brine compositions had a high calcium carbonate scaling potential (*LSI* > 0 with values up to 2.6) which may cause calcite to precipitate on the membrane. For comparison, Ruiz-Garcia et al. [12] found that, even using anti-scalants, the maximum allowable *LSI* was in the range of 2.4 to 3 and this placed an important limitation on the recovery achievable in their standard RO system. The *LSI* values of the India compositions were much higher than those of the Egypt compositions, sometimes exceeding 0 in the feed and not only the brine. Calcium fluoride was also saturated in the brine, especially in the India compositions. In contrast, there is little risk of calcium sulfate scaling because the corresponding *SI* is negative except for a small positive value in the brine for E4.

Overall, the brine has a high scaling potential. Scaling could be expected to occur towards the outlet of an RO module in standard, continuous flow RO desalination. Anti-scalant chemicals would normally be used in such applications. According to proprietary software, dosing of 2 mg of anti-scalant per L of feedwater would be recommended in all eight cases. This confirms that these are suitable compositions to evaluate batch RO for the possible occurrence of scaling.

Table 3. Scaling potential of calcium carbonate (as calcite), calcium sulfate (as gypsum), and calcium fluoride (as fluorite) in different feed compositions (by PHREEQC software) at 25 °C. Saturation index $SI_y = \log (IAP_y/KP_{sp,y})$, where IAP_y and $KP_{sp,y}$ are the ion activity and solubility products of mineral scalant y, respectively.

Origin	Composition	Langelier Saturation Index, *LSI* ($CaCO_3$)		Saturation Index			
				SI ($CaSO_4.2H_2O$)		*SI* (CaF_2)	
		Feed	Brine	Feed	Brine	Feed	Brine
Siwa Oasis, Egypt	E1	0.35	1.66	-1.23	-0.31	-1.54	0.21
	E2	0.46	1.79	-1.01	-0.1	-1.45	0.32
	E3	0.69	1.88	-1.09	-0.21	-1.48	0.33
	E4	0.63	1.81	-0.74	0.11	-1.35	0.45
Gujarat, India	I1	1.15	2.42	-1.35	-0.39	-0.83	0.87
	I2	1.25	2.47	-1.28	-0.34	-0.82	0.94
	I3	1.35	2.55	-1.09	-0.19	-0.75	0.99
	I4	1.41	2.6	-1.08	-0.19	-0.64	1.07

3.2. Feedwater preparation

The method of Smith et al. [41] was used to formulate and prepare the feed water solutions. Low solubility salts such as calcium sulfate and magnesium carbonate were avoided since they are difficult to dissolve and may precipitate (for example, Table 4 shows low solubility salts avoided in the case E2). We grouped the required salts in compatible combinations into the minimum number of stock solutions. Thus, Table 5 shows the eight recipes used for feedwater preparation.

Table 4. Matrix of the salts used for the preparation of composition E2 using the balanced concentrations calculated in Table 1 (see Appendix for similar data for other samples). The red highlighted cells indicate possible salt combinations that would result in insoluble salts and were therefore avoided.

Ions	HCO_3^-(µeq/L)	Cl^- (µeq/L)	SO_4^{2-} (µeq/L)	NO_3^- (µeq/L)	$\sum C^{Z+}$
Ca^{2+} (µeq/L)		6367		_	6367
Mg^{2+} (µeq/L)		_	5122	_	5122
Na^+ (µeq/L)	1673	13436	3251	_	18360
K^+ (µeq/L)	493	_	_	24	517
NH_4^+ (µeq/L)		23	_		23
$\sum A^{Z-}$	2166	19826	8373	24	_

Table 5. Recipes for preparation of the feed water compositions representative of Egypt (E1-E4) and India (I1-I4) groundwater samples.

Required salts	Concentration															
	E1		E2		E3		E4		I1		I2		I3		I4	
	µeq/L	mg/L	µeq/L	mg/L	µeq/L	mg/L	µeq/L	mg/L	µeq/L	mg/L	µeq/L	mg/L	µeq/L	mg/L	µeq/L	mg/L
$CaCl_2$	3979	441.6	6367	706.6	7557	838.7	11132	1235.4	10306	1143.8	16848	1869.8	20524	2277.8	25280	2805.6
$MgSO_4$	3152	379.4	5122	616.5	-	-	6692	805.5	219	26.4	1854	223.2	2771	333.5	-	-
NaCl	8866	518.1	13436	785.2	19458	1137.1	32886	1921.9	-	-	3678	214.9	12554	733.7	11947	698.2
$NaHCO_3$	2246	188.7	1673	140.5	2183	183.4	1273	106.9	4559	434	4545	381.8	5006	420.6	4858	408.1
Na_2SO_4	2617	371.7	3251	461.8	7480	1062.5	7231	1027.1	1213	172.3	-	-	-	-	2285	324.6
$KHCO_3$	-	-	493	49.4	626	62.7	694	69.5	-	-	-	-	-	-	-	-
NH_4Cl	14	0.75	23	1.2	33	1.8	37	2	-	-	-	-	-	-	-	-
KNO_3	12	1.2	24	2.4	34	3.4	30	3	-	-	109	11	-	-	789	79.8
KCl	227	16.9	-	-	-	-	-	-	-	-	-	-	-	-	-	-
$MgCl_2$	-	-	-	-	9452	899.9	-	-	-	-	4511	429.5	1569	149.4	1195	113.8
$NaNO_3$	-	-	-	-	-	-	-	-	871	74	1445	122.8	166	14.1	118	10
K_3PO_4	-	-	-	-	-	-	-	-	17	3.6	23	4.9	16	3.4	18	3.8
K_2SO_4	-	-	-	-	-	-	-	-	86	15	-	-	-	-	-	-
$Ca(NO_3)_2$	-	-	-	-	-	-	-	-	512	84	-	-	-	-	-	-
$Mg(NO_3)_2$	-	-	-	-	-	-	-	-	-	-	-	-	-	-	26	3.9
KF	-	-	-	-	-	-	-	-	10	0.6	10	0.6	11	0.65	10	0.6

All chemicals were of analytical grade (purity > 99%) and purchased from Sigma-Aldrich. The recipes were used to make up the feed tank volume of 1200 L for each test, using tap water with TDS less than 100 mg/L. To ensure dissolution and mixing, each salt was mixed with hot tap water (at 50-60 °C) in smaller volumes before being added to the main feed tank. Once all salts had been added, the feed tank was topped up to a final volume of 1200 L as indicated by a weighing scale underneath the tank (accuracy of ±0.2 kg). Using a recirculating pump, the feed solution in the tank was further mixed for about an hour before the start of each experiment. At the same time, using submersible titanium heaters (D-D Premium Aqua Supply GmbH) and a thermostat, the temperature was raised to 25 ± 0.1 °C and then kept constant during the experiments.

3.3. Experimental equipment and procedure

The batch RO laboratory equipment used a single-acting free piston design (see Fig. 2). A description of the equipment and experimental procedure, as used previously to treat NaCl solution, has already been provided [3] and is not therefore repeated here. Based on the earlier findings, a ratio of recirculation flow to feed flow of Q_{recirc}/Q_{feed} ~2 was chosen to minimise *SEC*. Like in [3], the membrane used was a Dupont Eco Pro-440 8-inch module with an active membrane area of 41 m^2. The flux varied from 11 to 23 L/m^2/h (corresponding to feed flow rates of about 8.4 to 16.4 L/min), giving an output of about 10 to 17 m^3/day. The system was operated at the design recovery of r = 0.8.

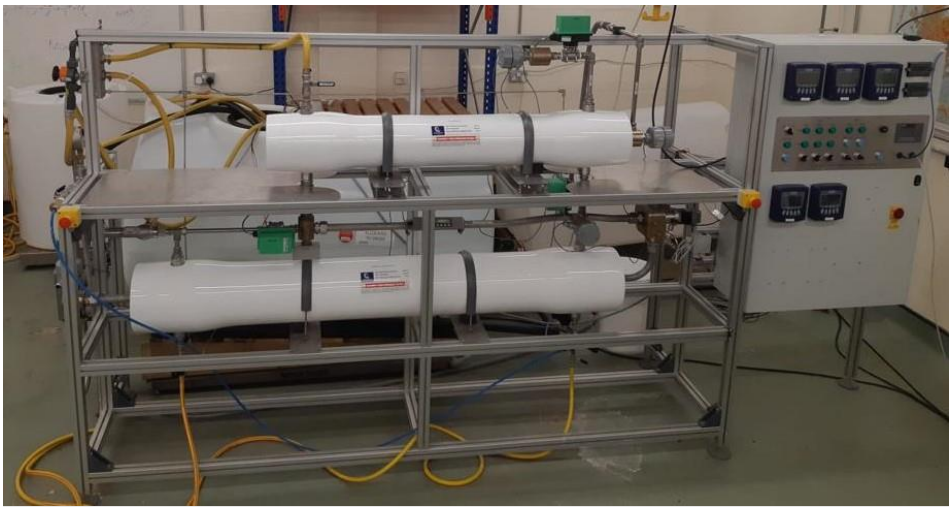

Fig. 2. Photo of the batch RO pilot system at the University of Birmingham.

As reported in [3], salt retention causes an increase in concentration during the initial cycles. The system reaches a stable condition after 3-4 cycles. Therefore, the recorded data of the fourth cycle (including changes in the weight of the tanks, conductivities, pressures, flow rates, and power consumption of the two feed and recirculation pumps) was used for the calculation of the results. This corresponded to a total duration of 330 to 580 s for each cycle (including a purge-and-refill phase of about 75 s), with shorter durations corresponding to higher water fluxes. Therefore, the total duration of each run was 26 to 44 minutes. Each of the eight compositions was tested at six water fluxes (11-23 L/m^2/h) and each test was repeated in duplicate (giving a total of 8×6×2 = 96 tests). After each test, the system was completely flushed by circulating the feed solution for 30 min to ensure that the solution inside the system

and feed tank reached a uniform concentration in preparation for the next test (the work exchanger was also drained to remove retained salts from the previous test). Overall, including preliminary tests to debug the system, about 100 hours of testing were conducted over a period of one month. Before and after the entire series of tests, a standard performance test was carried out with sodium chloride feed to compare performance and detect any membrane deterioration due to scaling or fouling.

4. Results and discussion

This section first presents the main results in comparison to the results with the NaCl solution. It then compares the performance in standard tests, using NaCl, before and after the whole series of tests with simulated groundwater. To interpret further the findings, the nucleation induction time is compared to the experimental residence times, thus helping to assess the extent to which induction time is a useful predictor of scaling in batch RO. All detailed results from the experiments and the raw experimental data are provided in the supporting information and appended data files.

4.1. Performance comparison: groundwater vs NaCl feed water

4.1.1. Specific energy consumption

Specific energy consumption was measured as the total hydraulic work done by the supply and recirculation pumps per m^3 of permeate (*i.e.,* hydraulic *SEC*). The work was calculated as the integral of pressure with volume at the outlet of each pump. For comparison with the NaCl solution, we used solutions of equivalent osmotic pressure. Since all the samples had low concentrations (< 5000 mg/L), the osmotic pressures of the simulated groundwater compositions were calculated using the van't Hoff expression, with the help of published osmotic coefficients [42], and were found to be in the range of 1.1 to 3.2 bar [3].

Because the resulting osmotic pressures did not correspond exactly to the concentrations at which the NaCl tests were carried out previously, we used our validated model of the batch RO system to work out the *SEC* values with NaCl. (This model gave hydraulic *SEC* to 3% accuracy and enabled us to interpolate experimental results based on feed salinity and flux [3]; membrane permeability was adjusted to 4.1 $L/m^2/h/bar$ in the model according to the results of the NaCl performance tests in section 4.2). Table 6 compares *SEC* at constant flux of 15.6 $L/m^2/h$. Although groundwater *SEC* was slightly lower than for NaCl, the discrepancy was less than 7% (averaging 3.5%) between the groundwater compositions and pure NaCl solution. This confirmed that tests and models obtained with NaCl were a useful representation of groundwater in all eight cases.

Table 6. Hydraulic *SEC* with groundwater compared to that with NaCl at equivalent osmotic pressure, at flux J_w~ 15.6 $L/m^2/h$.

	Composition	Osmotic pressure (bar)	Equivalent NaCl concentration (mg/L)	Hydraulic *SEC* (kWh/m^3)		
				Groundwater	NaCl	Error (%)
Egypt	E1	1.12	1420	0.228	0.241	5.4
	E2	1.62	2050	0.286	0.281	1.8
	E3	2.55	3228	0.338	0.352	4

	E4	3.15	3987	0.376	0.398	5.5
India	I1	1.17	1476	0.253	0.253	0.0
	I2	2.11	2673	0.296	0.318	6.9
	I3	2.46	3342	0.351	0.355	1.1
	I4	2.89	3662	0.357	0.383	6.8

Fig. 3 compares the hydraulic *SEC* measured using the eight groundwater compositions against the NaCl equivalent values at different fluxes. The model predictions agree well with almost all the experimental measurements. Hydraulic pressure caused by hydrodynamic friction in a RO membrane is approximately proportional to the flux ($P \propto J_w/A_w$). Thus, SEC increased with water flux because of greater applied pressure by the supply pump – as has previously been reported in both standard and batch RO systems [1, 43]. For both Egypt and India compositions, the total hydraulic *SEC* varied from around 0.19 to 0.46 kWh/m^3. The highest *SEC* was measured at the highest tested water flux (J_w~22.1 L/m^2/h) and the greatest feed concentrations (E4 and I4); whereas the lowest *SEC* was measured at the lowest tested water flux (J_w~11.4 L/m^2/h) and the lowest feed concentrations (E1 and I1).

Depending on the target specifications, we could choose to achieve higher water output at the cost of higher *SEC*, or lower *SEC* at the cost of less output. For instance, on increasing the water flux from 11.4 to 22.1 L/m^2/h when using sample E4 as the feed solution, the hydraulic *SEC* increased by 37% while system output rose by 73% from 9.6 to 16.7 m^3/day (see **Fig. 4**). Since the *SEC* values are low in all cases, this suggests that a higher water output may be preferred in practice.

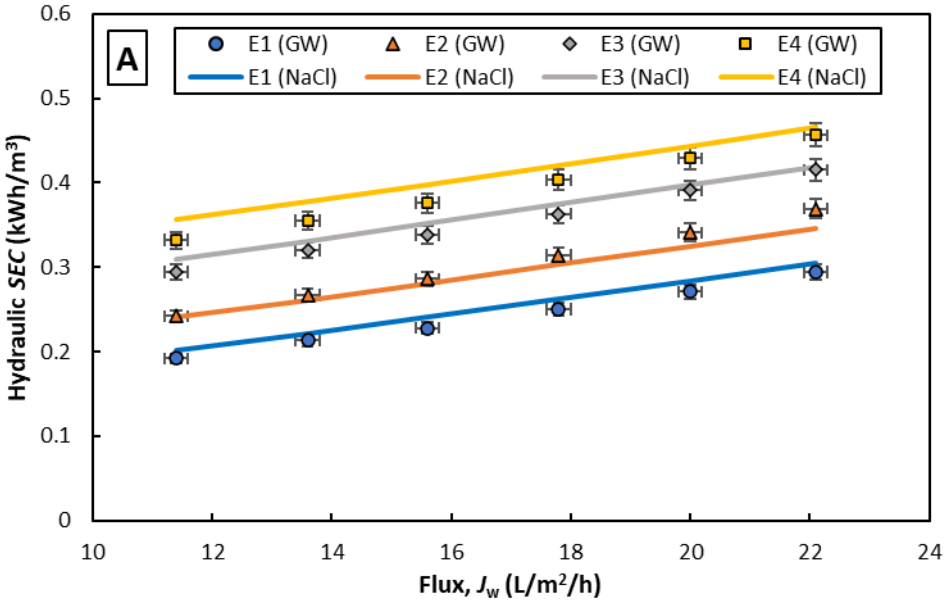

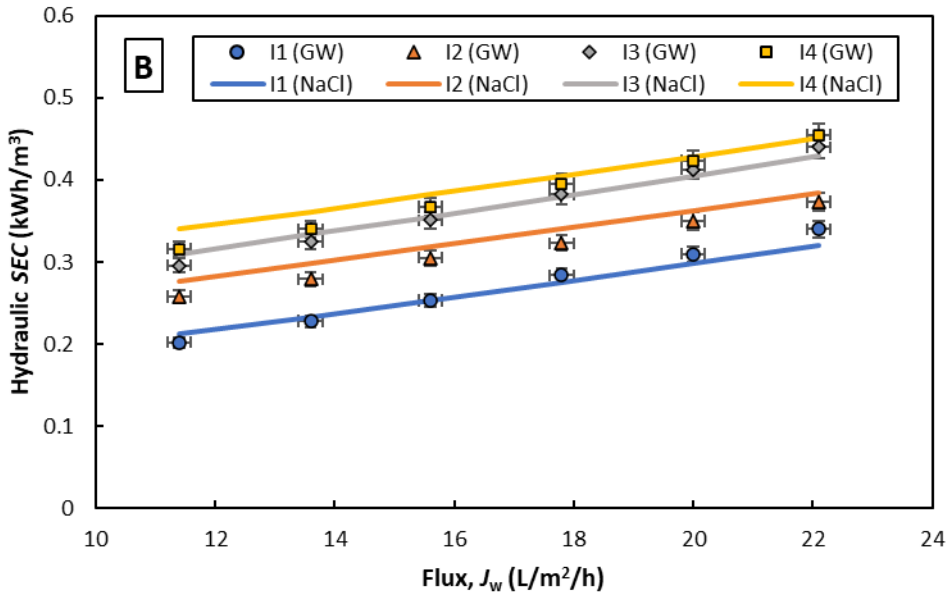

Fig. 3. Total hydraulic *SEC* for A) Egypt and B) India water samples (GW and NaCl represent experimental results for groundwater compositions and modeling values using equivalent NaCl feed respectively) at various water fluxes and $r = 0.8$.

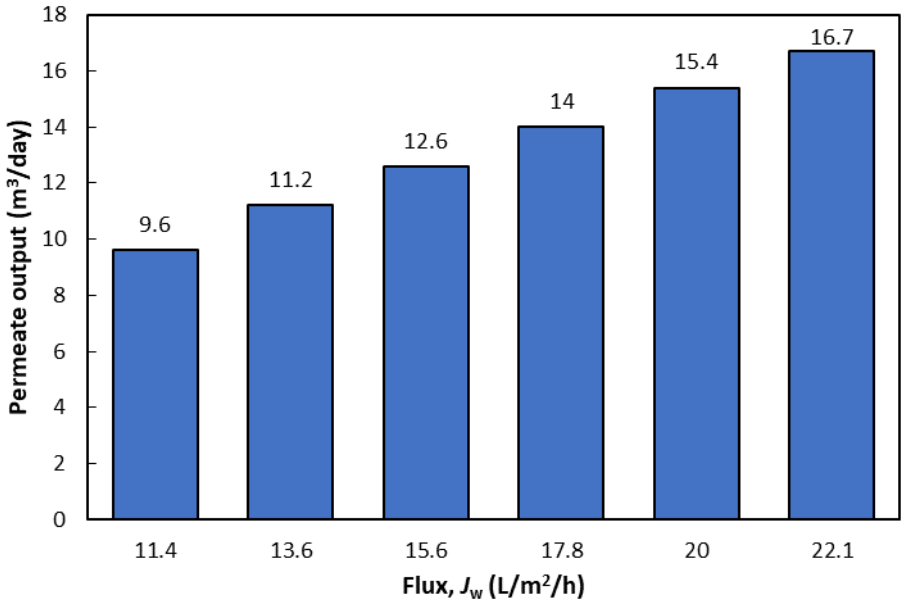

Fig. 4. Total permeate output as a function of water flux using batch RO system, at $r = 0.8$.

4.1.2. Peak pressure

In batch RO, the peak pressure is an important parameter regarding the system design and pressure ratings of the equipment needed; it also limits the final brine concentration achievable. The peak pressures in this study were in the range of 8 to 22 bar, which was within the 25-bar pressure limit of the equipment used. Peak pressure increased with the feed concentration, as shown in Fig. 5. Comparing the peak pressure observed in this study (for both groundwater tests and the performance tests of section 4.2) against NaCl solutions in [3] at a water flux of approximately 15.6 L/m^2/h revealed similar values, with only minor differences. These differences may be attributed to the membrane's permeability loss, which occurred over a year

of membrane use, resulting in a lower water permeation rate of about 4.1 L/m^2/h/bar in this study compared to 4.4 L/m^2/h/bar reported in [3].

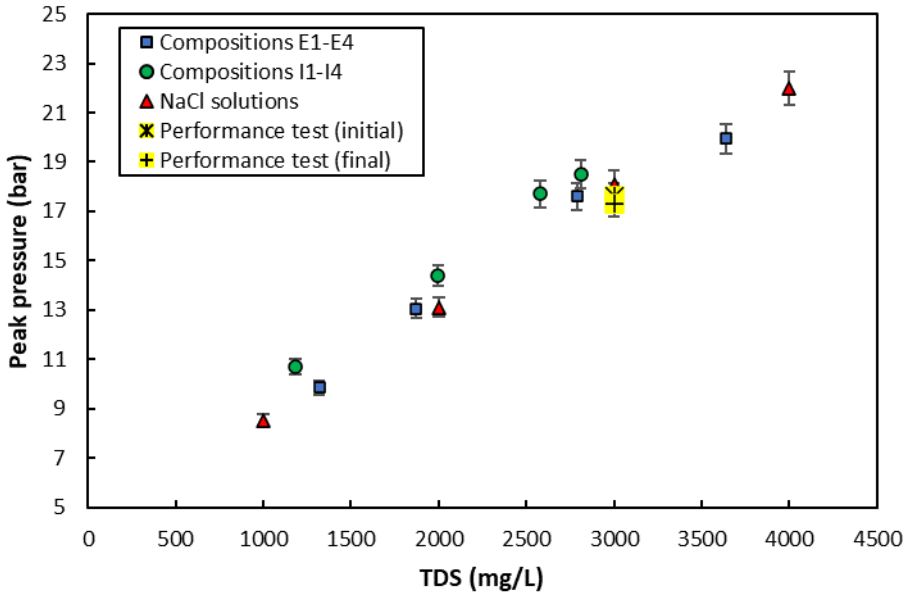

Fig. 5. Comparison of observed peak pressure at various feed samples, simulated groundwater of Egypt (E1-E4) and India (I1-I4) and NaCl solution (1000-4000 mg/L) at r = 0.8, and J_w~15.6 L/m^2/h. Performance tests refer to those described in section 4.2.

4.1.3. Rejection

We also compared the salt rejection results against those in our previous study using NaCl feed (see Fig. 6). In all cases, salt rejection varied between 0.94 to 0.97 with low concentration samples having better salt rejection. This may be due to the lower concentration difference across the membrane [43]. However, it is interesting to note that, the salt rejection was slightly higher with NaCl solution. This may have been due to a drift in membrane properties among the different tests. The higher rejection with NaCl corresponds to a higher differential osmotic pressure which is consistent with the observation of slightly higher *SEC* in section 4.1.1. above.

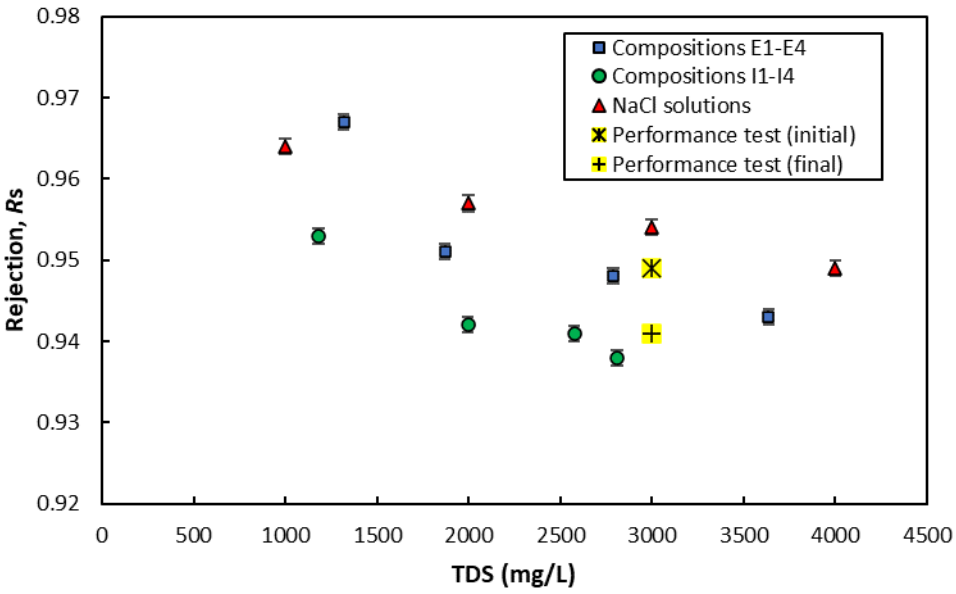

Fig. 6. Comparison of observed salt rejection at various feed samples, simulated groundwater of Egypt (E1-E4) and India (I1-I4) and NaCl solution (1000-4000 mg/L) at r = 0.8, and J_w~15.6 L/m^2/h.

4.2. Performance test before and after experiments

Before and after the 100-hour series of experiments, we performed a test using a feed solution containing 3000 mg/L of NaCl to determine whether membrane performance had deteriorated. If fouling or scaling occurs at the membrane surface, it will likely cause additional hydraulic resistance and applied pressure will rise, for a fixed water flux and recovery. Fig. 7A shows how pressure changed over the pressurisation phase for the NaCl performance at r = 0.8 and J_w~22.1 L/m^2/h, comparing the situation before and after the series of experiments. The applied pressure in both tests followed the same pattern with a minor discrepancy (the average pressure values for the performance test before and after trials were 12.44 and 12.36 bar respectively). Fig. 7B also compares the average applied pressure before and after the experiments, as measured by the NaC performance test at different water fluxes. Surprisingly, a slight decrease (as much as 0.2 bar) in applied pressure was consistently observed. To investigate the possible cause of this decrease, the permeate quality was studied in more detail.

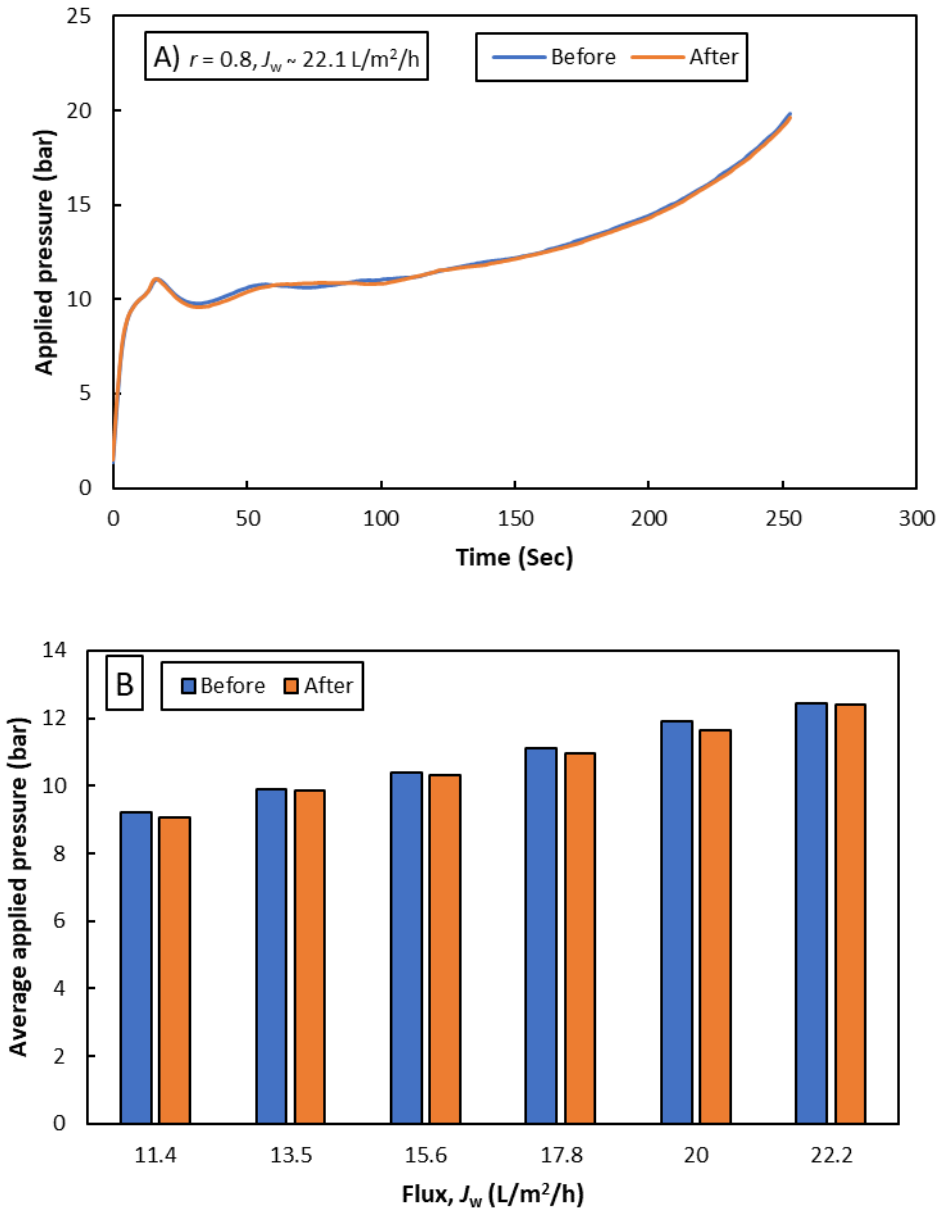

Fig. 7. Performance in NaCl test before and after the simulated groundwater experiments in the batch RO system, A) pressure changes over time in the pressurisation phase and B) Average pressure in the pressurisation phase vs. water flux for a cycle. All the tests were conducted at $r = 0.8$.

Fig. 8A and B show the conductivity of the RO module inlet and permeate over the pressurisation phase during the NaCl performance tests (at J_w~ 22.1 L/m^2/h). Inlet RO conductivity was almost unchanged before and after, with average values of 11.05 and 11.14 mS/cm respectively, *i.e.,*<1% difference. However, the permeate conductivity after the series of experiments test was slightly increased at 0.29 mS/cm average compared to 0.24 mS/cm before (see Fig. 8B). Similarly, Fig. 8C compares salt rejection at different fluxes showing that rejection deteriorated. This decrease in rejection is consistent with the decrease in applied pressure, as it corresponds to a slightly decreased osmotic pressure difference across the membrane. This may have been due to some membrane oxidation (despite the use of sodium metabisulphite to neutralise free chlorine) which can cause higher salt passage and loss of rejection. For example, the salt rejection reduced from 0.96 to 0.952 at J_w~22.1 L/m^2/h after a month of trials.

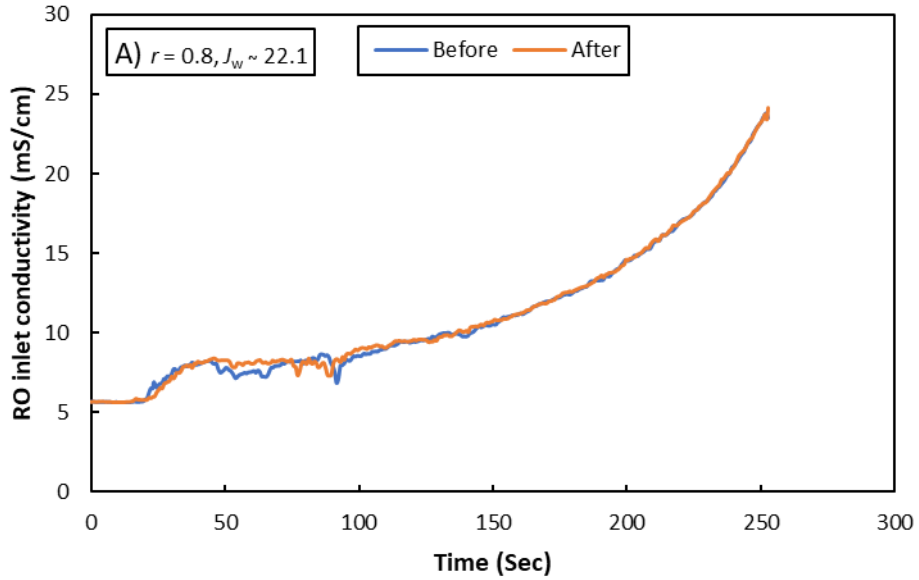
A) r = 0.8, J_w ~ 22.1
Before
After
RO inlet conductivity (mS/cm)
Time (Sec)
0
5
10
15
20
25
30
0
50
100
150
200
250
300

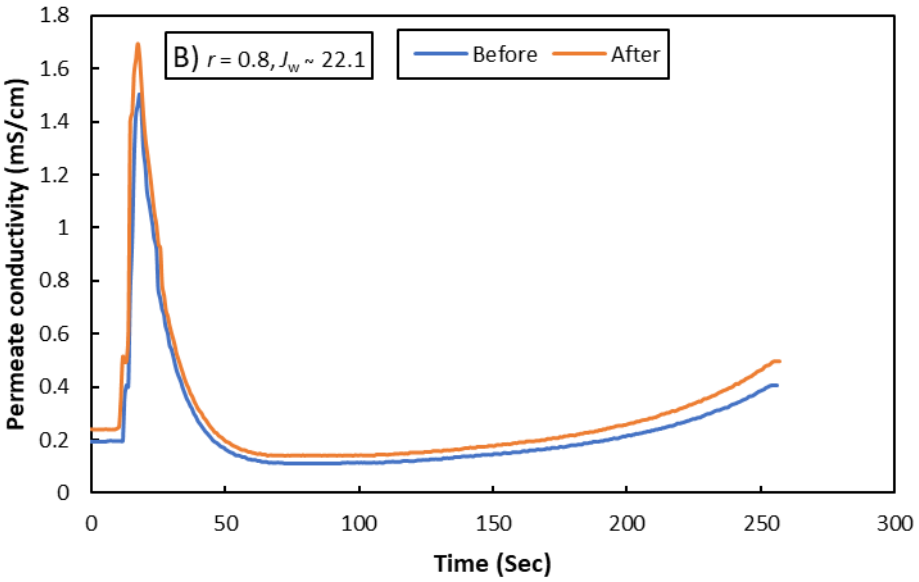
B) r = 0.8, J_w ~ 22.1
Before
After
Permeate conductivity (mS/cm)
Time (Sec)
0
0.2
0.4
0.6
0.8
1
1.2
1.4
1.6
1.8
0
50
100
150
200
250
300

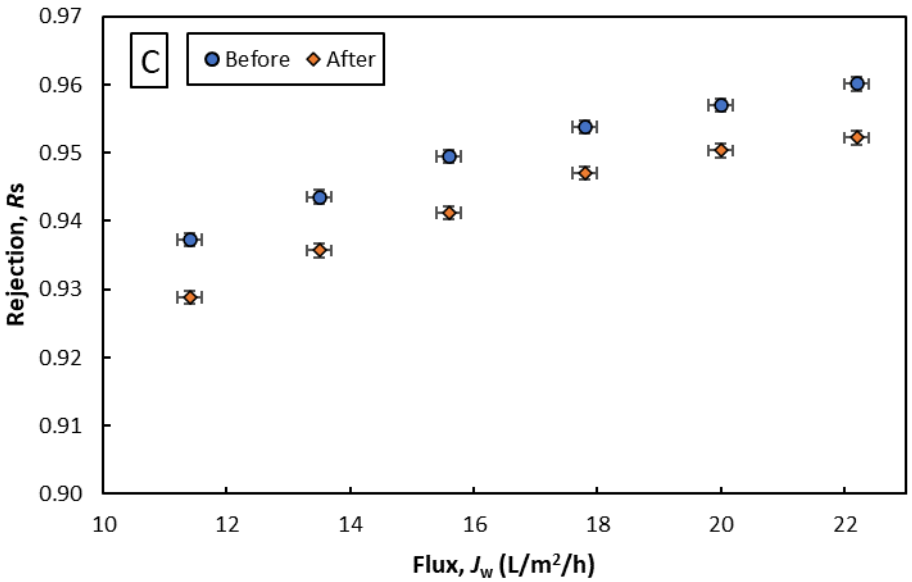

Fig. 8. Results of NaCl performance tests before and after the simulated groundwater experiments, A) RO inlet conductivity variation vs. time over the pressurisation phase, B) permeate conductivity variation vs. time over the pressurisation phase and C) Salt rejection as a function of water flux. All the tests were conducted at $r = 0.8$.

4.3. Anti-scaling mechanisms

Fig. 9 is a sample of results recorded over two cycles of batch RO operation, showing the flow and conductivity at the inlet to the RO module, and the permeate flow. It illustrates how the four anti-scaling mechanisms occur during each cycle. Each of these mechanisms will next be discussed individually.

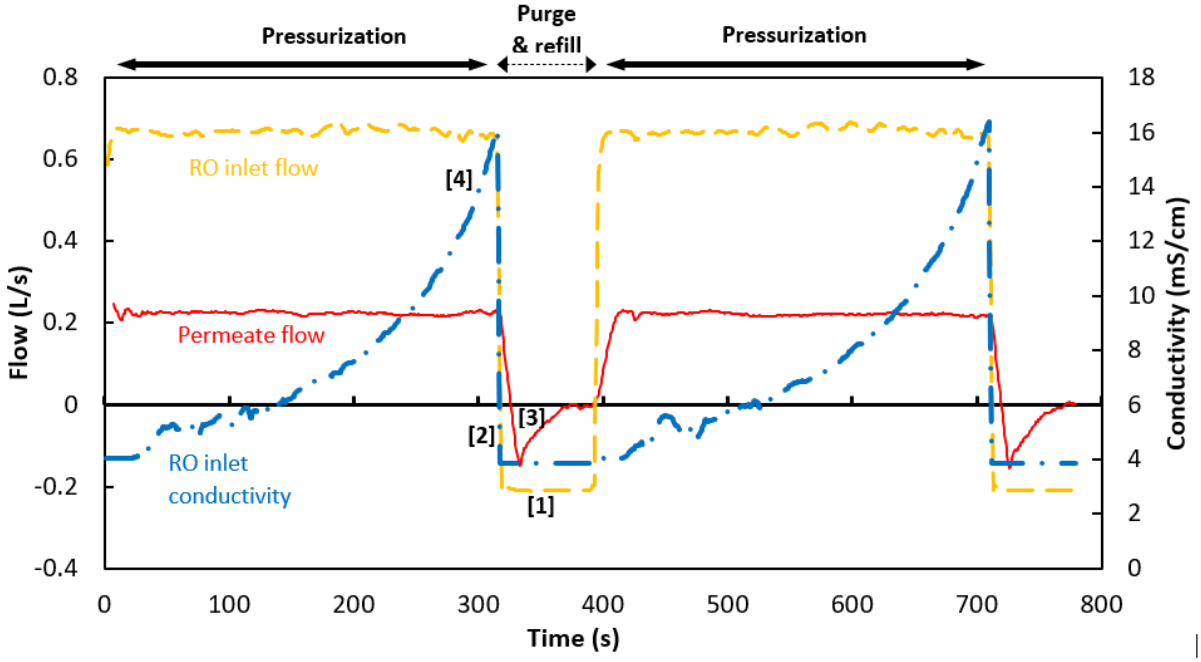

Fig. 9. Mechanisms of scaling inhibition in the batch RO cycle: **[1] periodic flushing** occurs during each purge-and-refill phase: permeate output pauses while tangential flow over the membrane (represented by RO inlet flow) continues at low salinity (represented by conductivity); **[2] flow reversal,** shown as a negative RO inlet flow,

during purge-and-refill; **[3] osmotic backwash**, evident as a negative permeate flow; **[4] salinity cycling** evident from the saw tooth pattern of conductivity at the RO inlet. Data measured with composition E2 at J_w~17.8 L/m^2/h. Note: The permeate flow was measured as the rate of decrease of the sum of feed and brine tank weights. A decrease in this sum indicates an outflow via the permeate, whereas an increase indicates the osmotic backwash. A moving average trendline was used to smooth the data.

4.3.1 Flushing

Flushing in batch RO differs from flushing in standard continuous RO plants as feed water, rather than permeate or clean-in-place chemicals, are used to carry out the flushing. Additionally, since flushing is a necessary step in batch RO to remove the highly concentrated solution from the RO module at the end of the pressurization phase, it is considerably more frequent than in standard continuous systems, which typically only flush before the startup or during a shutdown.

The flushing volume in each cycle in our experiments was about 16.5±0.3 L, corresponding to the volume of concentrated solution trapped in the RO module (V_m=A_m*H/2= 14.6 L, where A_m and H are membrane area and membrane channel height) plus piping and port dead volumes (about 2 L in total). Relative to the total feed supplied to the system at each cycle, which is 85.5±0.3 L, flushing comprises about 20% of the total feed supplied in each cycle.

Many studies have confirmed that membrane fouling can be alleviated by flushing [44-48]. However, the membrane flushing process detaches the particles from the membrane surface only, not from the pores. Chen et al. [48] showed 92-100% water permeability recovery of seawater and brackish water RO membranes fouled with gypsum and calcite when they were flushed with deionized (DI) water. In another study, Chen et al. [46] examined anti-fouling techniques on membranes fouled in pressure retarded osmosis (PRO) process using retentate from a municipal water recycling plant. Without pH correction or antiscalant addition, they observed 85 and 95% flux recovery using DI water flushing and air bubbling, respectively, under a high cross-flow velocity of 0.23 m/s for 30 minutes. Flux recovery improved with pH adjustment, reaching 94.6 and 100% by DI water flushing and air bubbling, respectively. When using antiscalant, flux recovery was almost 100% with both DI water flushing and air bubbling. De Vries et al. [45] reported the flushing effectiveness on membrane fouling removal using a stop period mechanism. Membranes were flushed at flow velocities of 0.1 and 0.2 m/s at a stop period of four minutes, twenty-four hours, or four weeks. They found that longer stop-periods improved the fouling removal rate at low feed flow velocities (0.1 m/s), but this effect became less significant at higher flow velocities. It is important to remember, however, that stop periods have the drawback of requiring more membrane surface area to maintain output in compensation for downtime.

In comparison to the studies mentioned, our batch RO system had a much higher frequency of flushing, occurring for 75 seconds after every 4-8 minutes of operation at high feed flow velocities (0.8-1.6 m/s). However, in our system, flushing was conducted with feed solution instead of DI water. It is important to note that in the aforementioned studies, flushing was the sole cleaning mechanism, whereas in batch RO a combination of different cleaning mechanisms occurred in the same process. This made it challenging to assess the individual contribution of each mechanism.

4.3.2 Osmotic backwash

The amount of osmotic backwash in the batch RO pilot was determined by subtracting the permeate output from the amount of feedwater supplied to the system during the pressurisation phase (see Table 7). Since osmotic backwash is driven by the brine osmotic pressure, which increases with the feed osmotic pressure, we have correlated in Fig. 10 the osmotic backwash volume against feed osmotic pressure, comparing also against experimental values with NaCl solution [3].

Table 7. Permeate and osmotic backwash volume in every batch cycle (69 L) for all the compositions tested.

Composition	TDS (mg/L)	Permeate volume (L)	Osmotic backwash volume (L)
E1	1319	65.4	3.6
E2	1871	65.3	3.7
E3	2788	64.6	4.4
E4	3637	64.4	4.6
I1	1180	65.9	3.1
I2	1994	65.0	4.0
I3	2576	64.7	4.3
I4	2811	64.6	4.4

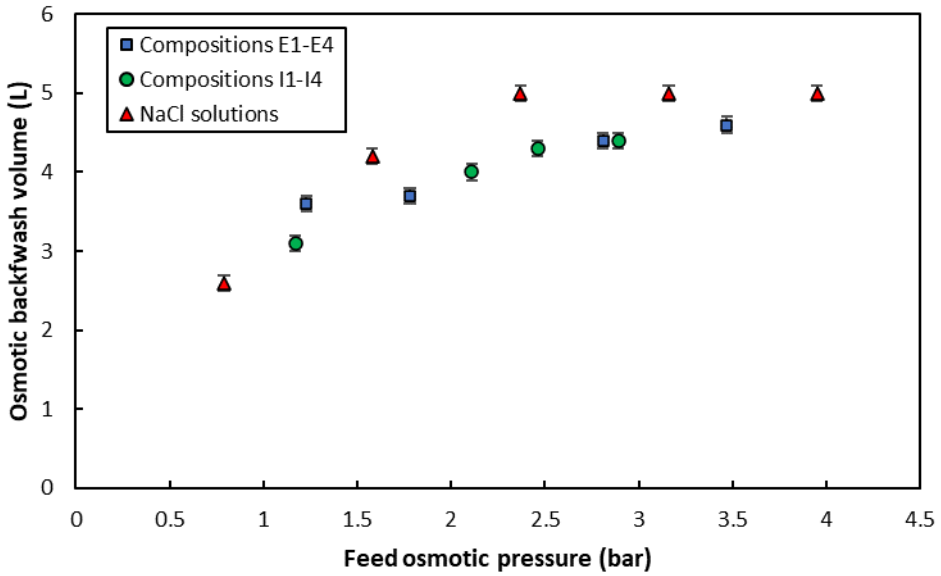

Fig. 10. Osmotic backwash volume vs. osmotic feed pressure, for groundwater compositions and pure NaCl feed solution at recovery $r = 0.8$.

Thus, 3.1-4.6 L of osmotic backwash volume in each cycle in our batch RO pilot could be another cause of scaling inhibition. The amount of osmotic backwash was lower than that occurring with pure NaCl solution as feed [3]. This might be because the salt rejection of NaCl solutions was slightly higher than the groundwater compositions; thus, the concentration difference inside the RO module in the case of NaCl solutions was slightly higher and caused more osmotic-backwash volume.

Cai et al. [49] reported that, with a membrane fouled by organics, periodic osmotic backwash caused by solar irradiance fluctuation restored 46–98% of the permeate flux, demonstrating the effectiveness of osmotic backwash in reducing membrane fouling. Nevertheless, they observed 2-2.5×10^{-3} L of backwash volume with a membrane active area of 4.7×10^{-3} m^2 compared to the current 3.1-4.6 L backwash volume with the membrane active area of 41 m^2 at almost the same feed osmotic pressure. Expressed per membrane area, Cai et al., therefore used about 0.5 L/m^2 of backwash which compares to only 0.1 L/m^2 in this study, suggesting the contribution in countering fouling may be less in this study. Nonetheless, an increased backwash would decrease system output which is undesirable.

4.3.3 Feed flow reversal

In the batch RO system of this study, the flow direction was reversed during the purge phase with feed water replacing the supersaturated solution inside the RO module. The duration of reversed flow was about one fifth that of forward flow in the pressurisation phase. The reversal feed flow velocity ranged from 0.8-1.6 m/s and the flow was reversed for a duration of 1.2 min every 4-8 minutes. It is interesting to compare these parameters against previous studies using non-batch RO systems.

In one such study, Gilron et al. [28] tested a calcium sulfate feed solution with *SI* of 0.54-0.73 and also a calcium carbonate solution with *LSI* of 1.0 at recoveries ranging from 0.67-0.82. In the case of calcium sulfate, when applying flow reversal every half hour at recoveries around 0.8, they observed no scaling over the total 18 h of the experiment. In the case of calcium carbonate, when operating at recovery of 0.7 (concentrate *LSI* of 1.5), they observed little sign of scaling when the flow was reversed every hour.

In another previous study, Gu et al. [29] evaluated the technical feasibility and performance of reversal feed flow in a RO pilot system also using calcium sulfate in the feed. Scale detection in an external membrane monitor (MeMo) triggered the reversal of feed flow in their pilot. Scale-free operation was observed while the RO pilot was operated in cyclic reversal flow mode at a recovery of 0.69-0.81 with *SI* reaching 0.54 at the tail element membrane surface. When the pilot was operated without flow reversal at r = 0.69, the membrane surface in the MeMo became fully covered by scale in 1.5 h, with 50% coverage occurring in just 45 min. At the same recovery, and with reversal feed flow triggered when coverage reached 50%, the 45 min was extended some eight times to 6 h, thus confirming a substantial retardation of scaling.

In summary, the above two studies [28, 29] reported significant improvements using feed flow reversal that was substantially less frequent than in the current study, i.e., reversing the flow direction only every 30-360 minutes as opposed to just 4-8 minutes in the current batch RO experiments. Therefore, it is likely that feed flow reversal has a useful effect in batch RO also.

4.3.4. Salinity Cycling

Fig. 11 shows the variation of *LSI* and the corresponding nucleation induction time of calcium carbonate (as calcite) calculated using Eq. (1) over the process time during pressurisation, for compositions I3 and I4 at J_w~15.6 L/m^2/h and r = 0.8. As time passes, the concentration of the solution inside the system increases and consequently the *LSI* also increases, causing the nucleation induction time to decrease. For example, for composition I4, at r = 0.5 the *LSI* has

risen from the initial value of 1.35 to 1.87 causing the calculated induction nucleation time to drop from 1803 to 59 s. Meanwhile, the process needs to continue for another 135 s to reach the recovery of $r = 0.8$. Thus, severe calcite scaling could be expected to occur before the end of the pressurisation phase. Similar analysis of other tests, corresponding to the other 6 feed compositions, also suggested the risk of scaling due to short nucleation induction time compared to the remaining process time. Nevertheless, such scaling was not evident in our experiments.

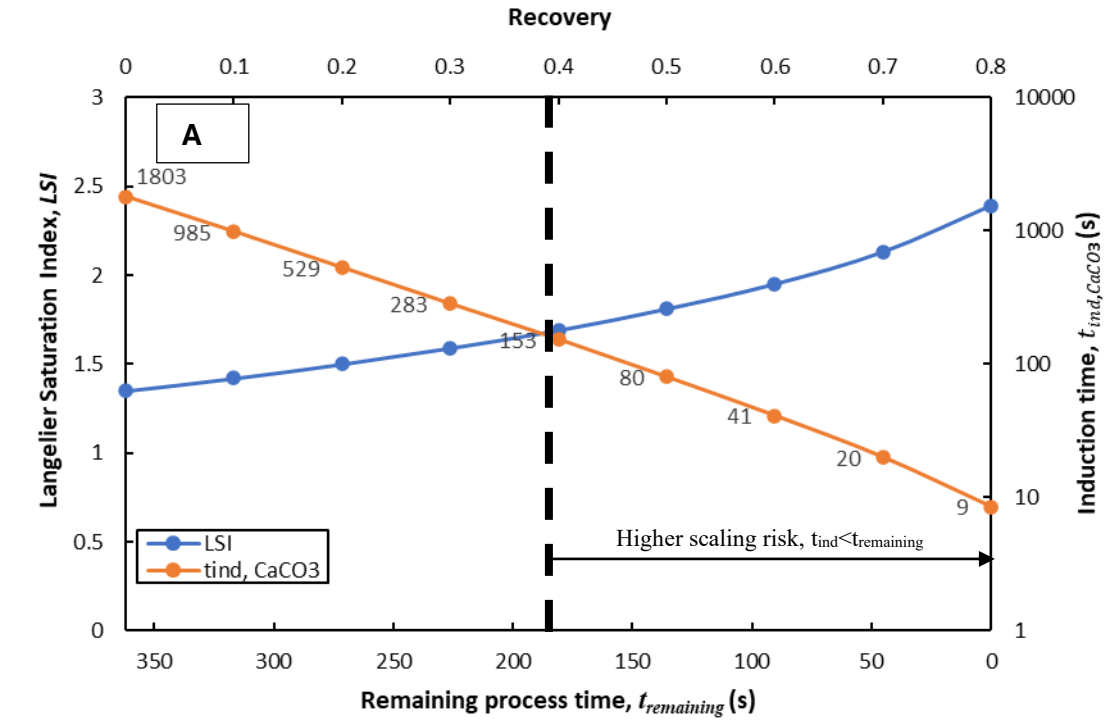

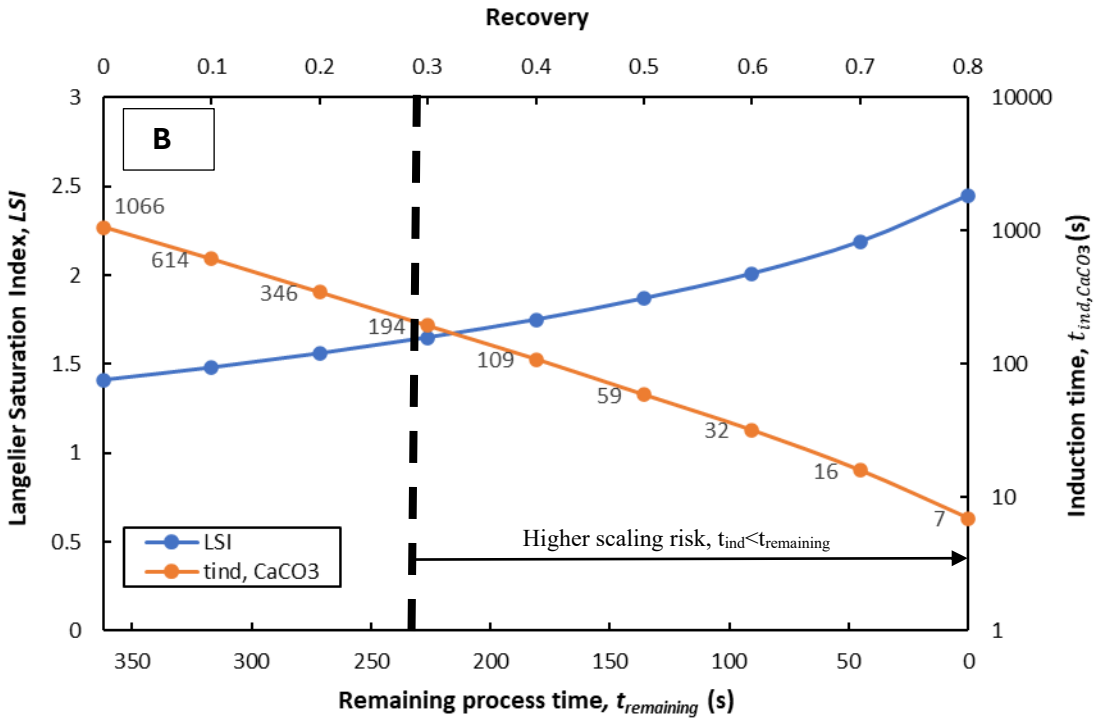

Fig. 11. Progress of Langelier saturation index and corresponding nucleation induction time for $CaCO_3$ (as calcite) as a function of remaining process time and recovery at J_w~15.6 L/m^2/h. A) composition I3, and B) composition I4. The vertical dashed line indicates the threshold where the calculated induction time becomes less than the remaining process time ($t_{ind}<t_{remaining}$), indicating the risk of scaling.

Scaling of calcite and gypsum on RO membrane occurs through two routes: bulk deposition or homogenous nucleation, and surface crystallization or heterogeneous nucleation. In general, the time required in heterogenous crystalization (on the membrane surfaces and in the presence of the seeds) is significantly shorter compared to the crystallization induction time in solutions which is the basis for equations 1 and 2 [50]. Thus, scaling might be expected to occur even earlier than indicated in Fig. 11.

Purging at each salinity cycle of the batch RO could be more effective at the initial stage of the formation of crystals since they are smaller and may be removed with a shorter purging interval. Surface crystals can become larger with each cycle if they are not entirely removed, which could make purging less effective than anticipated. Therefore, it would be desirable to completely remove any crystals and nuclei that may have developed on the membrane surface during the water production phase.

Over the purging period, the brine salinity and saturation indices both drop to below saturation. After each filtration phase, which took about 250-500 s in the batch RO pilot in this study, flow was reversed during the purging phase for about 75 s. As a result, the saturation index could be consistently reset at the end of the purge phase to the values slightly higher than the initial values of the feed solution (due to the salt retention).

4.4. Future work

Regarding further work, although the current study showed that batch RO can maintain performance even without the use of anti-scalant chemicals, it will be worth investigating performance when an anti-scalant is used. Batch RO may decrease the anti-scalant dosage needed with highly supersaturated feed solutions and high recoveries, reducing the operational cost and environmental impact of dosing anti-scalants. It would also be interesting to carry tests with salts such as calcium phosphate against which anti-scalants have been shown to be ineffective in conventional RO [51].

Another critical consideration is whether this concept can be successfully applied to scaled-up systems using more than one RO element. A system can be scaled up either by adding elements in series, in parallel, or a combination of series and parallel. Parallel configurations are expected to behave the same as the 1-element system as the flow conditions in each element will be unchanged. However, it would be costly to scale up using a parallel-only configuration because of the large number of vessels, end caps, and piping connections [52]. Use of elements in series is therefore desirable. Considering the presence of the four mechanisms of scaling mitigation in batch RO, we are of the opinion systems using 2-4 elements [32] would indeed continue to exhibit resistance to fouling. However, to confirm whether the behaviour of a multi-module batch RO system aligns with that of a single module, further studies are necessary.

Based on the findings presented in our previous studies [1, 3], it was determined that, for low concentrations (< 5000 mg/L) and low applied pressures (< 25 bar), the optimal recirculation to feed flow ratio is approximately 2 to minimize the overall *SEC*. This corresponds to a recovery per pass of approximately 0.33 which is somewhat higher than the typical range of

0.12-0.2 used in industrial standard RO systems [53]. In future research, it would be intriguing to expand the study to encompass higher recirculation flows along with more challenging fouling feed compositions. By employing larger ratios, the concentration polarization can be reduced, which may offer advantages in terms of fouling prevention. *SEC* would increase slightly but, based on previous studies, the penalty in increasing the flow ratio from 2 to say 3 would only be about 4% [3].

This study has focused on desalination of groundwater containing high levels of sparingly soluble salts, causing scaling. However, in RO processes, there are various types of fouling that can be encountered, including particulate fouling, organic fouling, biofouling, and scaling that are important for future research. For instance, natural water often contains a certain level of silica, causing colloidal fouling which is often challenging to control [54]. Additionally, apart from scaling (which usually starts in the tail element) other forms of fouling commonly occur in the lead element [55]. Among the fouling removal methods mentioned in Section 4.3, osmotic backwash is thought to have the highest potential for minimizing or preventing these types of fouling. Nevertheless, conducting future studies that consider each type of fouling would greatly contribute to a better understanding of the potential of batch RO in fouling minimization. Moreover, studies have shown interactions among the various foulants [56] such that studies of combined (and not just individual) foulants will also be important.

Overall, conducting long-term pilot testing using ample sources of real feed water that have a high likelihood of experiencing various forms of fouling in the field is imperative to comprehensively evaluate the system. This approach will allow for a thorough assessment of the impact of the aforementioned fouling mitigation mechanisms in batch RO and a comparison against standard continuous RO systems. Such testing will provide valuable insights into the system's performance and effectiveness in real-world scenarios and help evaluate its practical viability and reliability.

5. Conclusion

An experimental investigation has been undertaken in a free-piston batch RO pilot to compare the performance in treating brackish groundwater at high recovery (r = 0.8) against the performance of the same system treating pure NaCl solution. Eight feedwater compositions were replicated in the lab, using field data taken from two locations (one in Egypt and one in India) where raw groundwater quality is not acceptable. The *SEC* of the system was within 7% of that obtained with NaCl solutions having equivalent osmotic pressure. This confirmed that studies conducted with pure NaCl solutions are a reasonable representation of the more complex salt mixtures in the groundwater.

The saturation level of sparingly soluble salts suggested a significant risk of calcite ($CaCO_3$) and fluorite (CaF_2) scaling at the RO outlet. Nonetheless, over the duration of these tests (totalling >100 hours), the batch RO system resisted scaling. This was confirmed by two performance tests with a 3000 mg/L NaCl feed solution, conducted before and after the entire test series. No increase in transmembrane pressure was observed. Absence of scaling is attributed to mechanisms of periodic flushing, flow reversal, osmotic backwash, and salinity cycling. Flushing occurred during 15-20% of the operation time, after the end of each pressurisation phase, in the reverse direction to the feed flow during pressurisation. Osmotic backwash of 3.1-4.6 L occurred (a similar amount to that observed with pure NaCl feed). A

careful study of the saturation and expected nucleation induction for crystallisation of calcite and gypsum during each batch RO cycle showed that, in all the tests conducted, there was theoretically sufficient time for crystallisation to begin. Nevertheless, no deterioration in performance was observed suggesting that no crystallization and scaling occurred. Comparisons against the literature suggest that the other three mechanisms (i.e., flushing, osmotic backwash, and flow reversal) were also likely contributors to scaling inhibition.

Acknowledgements

The authors acknowledge funding from the British Council Newton Fund Institutional Links programme (STDF project ID:42703) and the Engineering and Physical Sciences Research Council (Grant Ref: EP/T025867/1). The authors thank the National Research Centre (Egypt) for its valuable support. They also thank Paris Pasqualin for his comments on the manuscript.

References

[1] E. Hosseinipour, S. Karimi, S. Barbe, K. Park, P.A. Davies, Hybrid semi-batch/batch reverse osmosis (HSBRO) for use in zero liquid discharge (ZLD) applications, Desalination, 544 (2022) 116126.
[2] Q.J. Wei, C.I. Tucker, P.J. Wu, A.M. Trueworthy, E.W. Tow, J.H. Lienhard, Impact of salt retention on true batch reverse osmosis energy consumption: experiments and model validation, Desalination, 479 (2020) 114177.
[3] E. Hosseinipour, K. Park, L. Burlace, T. Naughton, P.A. Davies, A free-piston batch reverse osmosis (RO) system for brackish water desalination: Experimental study and model validation, Desalination, 527 (2022) 115524.
[4] E. Jones, M. Qadir, M.T. van Vliet, V. Smakhtin, S.-m. Kang, The state of desalination and brine production: A global outlook, Science of the Total Environment, 657 (2019) 1343-1356.
[5] J.W. Delleur, The handbook of groundwater engineering, CRC press, 2006.
[6] Q. Liu, G.-R. Xu, R. Das, Inorganic scaling in reverse osmosis (RO) desalination: Mechanisms, monitoring, and inhibition strategies, Desalination, 468 (2019) 114065.
[7] S. Oren, L. Birnhack, O. Lehmann, O. Lahav, A different approach for brackish-water desalination, comprising acidification of the feed-water and CO2 (aq) reuse for alkalinity, Ca2+ and Mg2+ supply in the post treatment stage, Separation and purification technology, 89 (2012) 252-260.
[8] S. Shirazi, C.-J. Lin, D. Chen, Inorganic fouling of pressure-driven membrane processes—A critical review, Desalination, 250 (2010) 236-248.
[9] J. Benecke, J. Rozova, M. Ernst, Anti-scale effects of select organic macromolecules on gypsum bulk and surface crystallization during reverse osmosis desalination, Separation and Purification Technology, 198 (2018) 68-78.
[10] C. Fritzmann, J. Löwenberg, T. Wintgens, T. Melin, State-of-the-art of reverse osmosis desalination, Desalination, 216 (2007) 1-76.
[11] X. Xu, J.E. Ness, A. Miara, K.A. Sitterley, M. Talmadge, B. O'Neill, K. Coughlin, S. Akar, E.T. Edirisooriya, P. Kurup, Analysis of brackish water desalination for municipal uses: case studies on challenges and opportunities, ACS ES&T Engineering, 2 (2022) 306-322.
[12] A. Ruiz-García, I. Nuez, M. Carrascosa-Chisvert, J. Santana, Simulations of BWRO systems under different feedwater characteristics. Analysis of operation windows and optimal operating points, Desalination, 491 (2020) 114582.
[13] A. Matin, F. Rahman, H.Z. Shafi, S.M. Zubair, Scaling of reverse osmosis membranes used in water desalination: Phenomena, impact, and control; future directions, Desalination, 455 (2019) 135-157.
[14] A. Ruiz-García, J. Feo-García, Antiscalant cost and maximum water recovery in reverse osmosis for different inorganic composition of groundwater, Desalination and Water Treatment, 73 (2017) 46-53.
[15] L. Burlace, P. Davies, Fouling and fouling mitigation in batch reverse osmosis: review and outlook, Desalination and Water Treatment, 249 (2022) 1-22.
[16] A. Matin, T. Laoui, W. Falath, M. Farooque, Fouling control in reverse osmosis for water desalination & reuse: Current practices & emerging environment-friendly technologies, Science of the total Environment, 765 (2021) 142721.
[17] J.-J. Qin, M.H. Oo, K.A. Kekre, B. Liberman, Development of novel backwash cleaning technique for reverse osmosis in reclamation of secondary effluent, Journal of membrane science, 346 (2010) 8-14.

[18] E. Bar-Zeev, M. Elimelech, Reverse osmosis biofilm dispersal by osmotic back-flushing: cleaning via substratum perforation, Environmental science & technology letters, 1 (2014) 162-166.
[19] J. Park, W. Jeong, J. Nam, J. Kim, J. Kim, K. Chon, E. Lee, H. Kim, A. Jang, An analysis of the effects of osmotic backwashing on the seawater reverse osmosis process, Environmental technology, 35 (2014) 1455-1461.
[20] W. Jiang, Y. Wei, X. Gao, C. Gao, Y. Wang, An innovative backwash cleaning technique for NF membrane in groundwater desalination: Fouling reversibility and cleaning without chemical detergent, Desalination, 359 (2015) 26-36.
[21] J.W. Nam, J.Y. Park, J.H. Kim, Y.S. Lee, E.J. Lee, M.J. Jeon, H.S. Kim, A. Jang, Effect on backwash cleaning efficiency with TDS concentrations of circulated water and backwashing water in SWRO membrane, Desalination and Water Treatment, 43 (2012) 124-130.
[22] E.W. Tow, M.M. Rencken, In situ visualization of organic fouling and cleaning mechanisms in reverse osmosis and forward osmosis, Desalination, 399 (2016) 138-147.
[23] S. Daly, A. Allen, V. Koutsos, A.J. Semião, Influence of organic fouling layer characteristics and osmotic backwashing conditions on cleaning efficiency of RO membranes, Journal of Membrane Science, 616 (2020) 118604.
[24] Y.-A. Boussouga, B.S. Richards, A.I. Schäfer, Renewable energy powered membrane technology: System resilience under solar irradiance fluctuations during the treatment of fluoride-rich natural waters by different nanofiltration/reverse osmosis membranes, Journal of Membrane Science, 617 (2021) 118452.
[25] M.N. Mangal, S.G. Salinas-Rodriguez, J. Dusseldorp, B. Blankert, V.A. Yangali-Quintanilla, A.J. Kemperman, J.C. Schippers, W.G. van der Meer, M.D. Kennedy, Foulant identification and performance evaluation of antiscalants in increasing the recovery of a reverse osmosis system treating anaerobic groundwater, Membranes, 12 (2022) 290.
[26] L. Fortunato, A.H. Alshahri, A.S. Farinha, I. Zakzouk, S. Jeong, T. Leiknes, Fouling investigation of a full-scale seawater reverse osmosis desalination (SWRO) plant on the Red Sea: Membrane autopsy and pretreatment efficiency, Desalination, 496 (2020) 114536.
[27] M. Li, N. Chan, J. Li, Novel dynamic and cyclic designs for ultra-high recovery waste and brackish water RO desalination, Chemical Engineering Research and Design, 179 (2022) 473-483.
[28] J. Gilron, M. Waisman, N. Daltrophe, N. Pomerantz, M. Milman, I. Ladizhansky, E. Korin, Prevention of precipitation fouling in NF/RO by reverse flow operation, Desalination, 199 (2006) 29-30.
[29] H. Gu, A.R. Bartman, M. Uchymiak, P.D. Christofides, Y. Cohen, Self-adaptive feed flow reversal operation of reverse osmosis desalination, Desalination, 308 (2013) 63-72.
[30] S. Cordoba, A. Das, J. Leon, J.M. Garcia, D.M. Warsinger, Double-acting batch reverse osmosis configuration for best-in-class efficiency and low downtime, Desalination, 506 (2021) 114959.
[31] P. Davies, A. Afifi, F. Khatoon, G. Kuldip, S. Javed, S. Khan, Double-acting batch-RO system for desalination of brackish water with high efficiency and high recovery, Desalination for the Environment–Clean Energy and Water, Rome, (2016) 23-25.
[32] H. Abu Ali, M. Baronian, L. Burlace, P.A. Davies, S. Halasah, M. Hind, A. Hossain, C. Lipchin, A. Majali, M. Mark, Off-grid desalination for irrigation in the Jordan Valley, Desalination and Water Treatment, 168 (2019) 143-154.
[33] D.M. Warsinger, E.W. Tow, L.A. Maswadeh, G.B. Connors, J. Swaminathan, J.H. Lienhard, Inorganic fouling mitigation by salinity cycling in batch reverse osmosis, Water research, 137 (2018) 384-394.
[34] M. Li, Cyclic simulation and energy assessment of closed-circuit RO (CCRO) of brackish water, Desalination, 545 (2023) 116149.
[35] M. El Hossary, Evaluation and management of groundwater resources in Siwa area with emphasis on the Nubia Sandstone aquifer, Geology Department, 138 (1999).
[36] S. Salman, E.A. El Ella, E. Seleem, A. Elnazer, Groundwater quality and environmental investigations in Siwa Oasis, Egypt, International Journal of Recent Advances in Multidisciplinary Research, 5 (2018) 3951-3958.
[37] A.A. Elnazer, S.A. Salman, Y. Mohamed, J. Stafford, P. Davies, H.A. El Nazer, Siwa Oasis groundwater quality: factors controlling spatial and temporal changes, Environmental Monitoring and Assessment, 195 (2023) 1-14.
[38] R.P. Pujari, N. Labhsetwar, G.C Quesada, C.Y Lopez, Deliverable 5.2 of the EU H2020 project bio-mimetic and photo technologies designed for low-cost purification and recycling of water: Geo-hydrological Ecological Status of Microwatersheds., in, https://cordis.europa.eu/project/id/820906/results, 2020.
[39] D.L. Parkhurst, C. Appelo, Description of input and examples for PHREEQC version 3—a computer program for speciation, batch-reaction, one-dimensional transport, and inverse geochemical calculations, US geological survey techniques and methods, 6 (2013) 497.
[40] N. AlSawaftah, W. Abuwatfa, N. Darwish, G. Husseini, A comprehensive review on membrane fouling: Mathematical modelling, prediction, diagnosis, and mitigation, Water, 13 (2021) 1327.
[41] E. Smith, W. Davison, J. Hamilton-Taylor, Methods for preparing synthetic freshwaters, Water research, 36 (2002) 1286-1296.

[42] R.A. Robinson, R.H. Stokes, Electrolyte solutions, Courier Corporation, 2002.
[43] L. Wang, T. Cao, J.E. Dykstra, S. Porada, P. Biesheuvel, M. Elimelech, Salt and water transport in reverse osmosis membranes: Beyond the solution-diffusion model, Environmental Science & Technology, 55 (2021) 16665-16675.
[44] J. Zhang, K. Northcott, M. Duke, P. Scales, S.R. Gray, Influence of pre-treatment combinations on RO membrane fouling, Desalination, 393 (2016) 120-126.
[45] H.J. de Vries, E. Kleibusch, G.D. Hermes, P. van den Brink, C.M. Plugge, Biofouling control: the impact of biofilm dispersal and membrane flushing, Water Research, 198 (2021) 117163.
[46] S.C. Chen, G.L. Amy, T.-S. Chung, Membrane fouling and anti-fouling strategies using RO retentate from a municipal water recycling plant as the feed for osmotic power generation, Water research, 88 (2016) 144-155.
[47] G.Z. Ramon, T.-V. Nguyen, E.M. Hoek, Osmosis-assisted cleaning of organic-fouled seawater RO membranes, Chemical engineering journal, 218 (2013) 173-182.
[48] Y. Chen, Y. Cohen, Calcium Sulfate and Calcium Carbonate Scaling of Thin-Film Composite Polyamide Reverse Osmosis Membranes with Surface-Tethered Polyacrylic Acid Chains, Membranes, 12 (2022) 1287.
[49] Y.-H. Cai, C.J. Burkhardt, A.I. Schäfer, Renewable energy powered membrane technology: Impact of osmotic backwash on organic fouling during solar irradiance fluctuation, Journal of Membrane Science, 647 (2022) 120286.
[50] T. Lee, J.Y. Choi, Y. Cohen, Gypsum scaling propensity in semi-batch RO (SBRO) and steady-state RO with partial recycle (SSRO-PR), Journal of Membrane Science, 588 (2019) 117106.
[51] M.N. Mangal, S.G. Salinas-Rodriguez, J. Dusseldorp, A.J. Kemperman, J.C. Schippers, M.D. Kennedy, W.G. van der Meer, Effectiveness of antiscalants in preventing calcium phosphate scaling in reverse osmosis applications, Journal of membrane science, 623 (2021) 119090.
[52] H. Kotb, E. Amer, K. Ibrahim, On the optimization of RO (Reverse Osmosis) system arrangements and their operating conditions, Energy, 103 (2016) 127-150.
[53] DuPont, FilmTec reverse osmosis membranes technical manual, in, DuPont Wilmington, DE, USA, 2020.
[54] Y.-M. Park, K.-M. Yeon, C.-h. Park, Silica treatment technologies in reverse osmosis for industrial desalination: A review, Environmental Engineering Research, 25 (2020) 819-829.
[55] W. Jiang, X. Xu, L. Lin, H. Wang, R. Shaw, D. Lucero, P. Xu, A pilot study of an electromagnetic field for control of reverse osmosis membrane fouling and scaling during brackish groundwater desalination, Water, 11 (2019) 1015.
[56] A. Karanasiou, A. Karabelas, S. Mitrouli, Incipient membrane scaling in the presence of polysaccharides during reverse osmosis desalination in spacer-filled channels, Desalination, 500 (2021) 114821.

Appendix

Table A1. Reported analyses of samples on which feed compositions are based. Ion concentrations below 1 mg/L are neglected.

	Composition	Sample*	pH	TDS (mg/L)	EC (µS/cm)	Ca^{2+} (mg/L)	Mg^{2+} (mg/L)	Na^{+} (mg/L)	K^{+} (mg/L)	NH_4^{+} (mg/L)	HCO_3^{-} (mg/L)	Cl^{-} (mg/L)	SO_4^{2-} (mg/L)	NO_3^{-} (mg/L)
Egypt	E1	SN52	7.5	1367	2229	80	38.4	316.5	9.4	0.3	136.6	462	276.5	0.8
	E2	SN11	7.3	1853	2793	128	62.4	423.2	20.3	0.4	131.8	700	401.3	1.5
	E3	SN29	7.3	2961	4540	152	115.2	671.6	25.9	0.6	170.8	1288	358.3	2.1
	E4	SN33	7.2	3492	5149	224	81.6	955.0	28.4	0.7	119.6	1554	666.6	1.9
India	I1	LG14	6.3	1138	1897	196	2.4	138	4	-	310	400	80	94
	I2	LG13	6.3	2090	3490	304	69.6	200	5	-	305	975	98	106
	13	LG12	6.3	2600	4330	412	52.8	408	11	-	305	1225	133	26
	I4	LG2	6.5	3080	5130	492	28.8	426	31	-	305	1400	113	52

* Sample numbering as used in source references [37, 38].

Paper 4: Hybrid semi-batch/batch reverse osmosis (HSBRO) for use in Zero Liquid Discharge (ZLD) applications

Ebrahim Hosseinipour[a], Somayeh Karimi[a], Stéphan Barbe[b], Kiho Park[c] and Philip A. Davies[a]*

a. School of Engineering, University of Birmingham, Edgbaston, Birmingham B15 2TT

b. Faculty of Applied Natural Sciences, Technische Hochschule Köln, Kaiser-Wilhelm-Allee, Gebäude E39, 51373 Leverkusen, Germany

c. School of Chemical Engineering, Chonnam National University, 77 Yongbong-ro, Buk-gu, Gwangju 61186, Republic of Korea

* p.a.davies@bham.ac.uk

Graphical Abstract

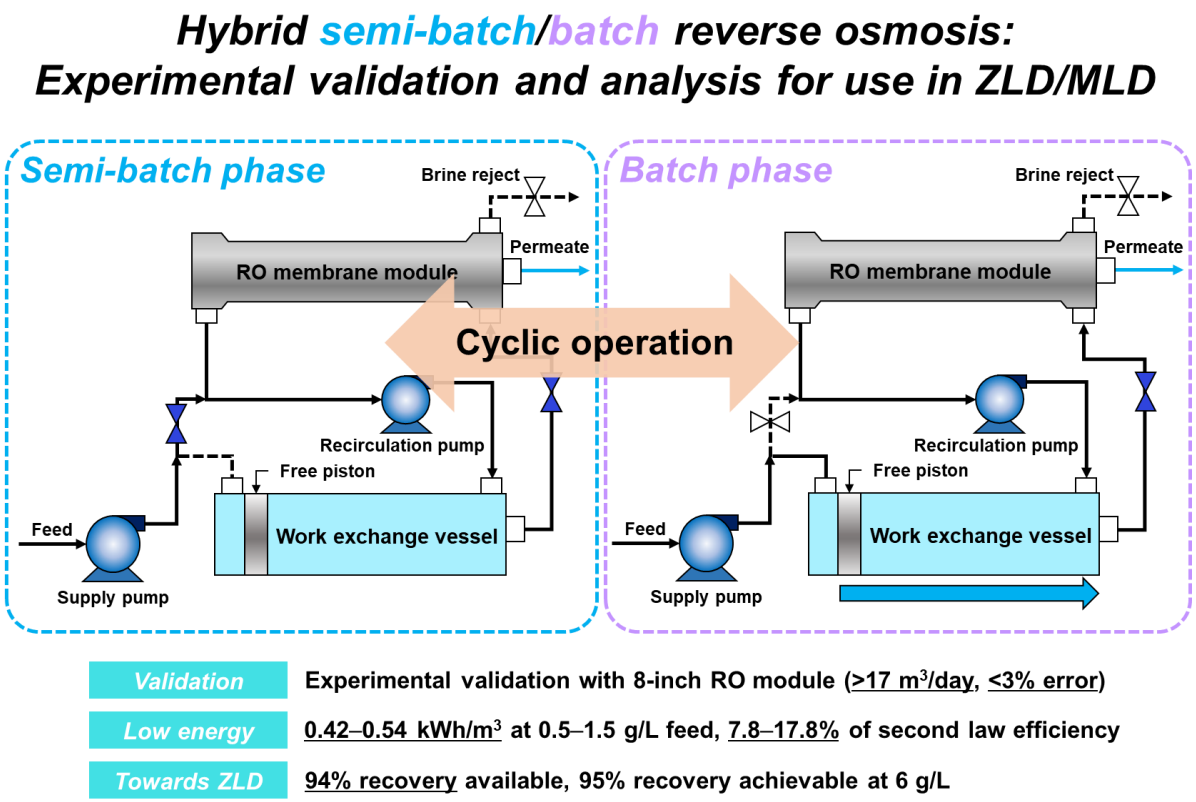

Abstract

Hybrid semi-batch/batch reverse osmosis (HSBRO) is a new method of high-recovery desalination that provides low Specific Energy Consumption (*SEC*) in a compact design. In this first experimental study on HSBRO, we report *SEC* over a range of operating parameters using brackish feed water. For example, at 500–1,500 mg/L feed concentration, and recovery of 0.94, we measured hydraulic and electrical *SEC* of 0.20–0.31 kWh/m^3 and 0.42–0.54 kWh/m^3 respectively, using a flux of 18.9 L/m^2/h and obtaining an output of 17.5 m^3/day. Second law efficiency was 7.8–17.8% thus improving on available multistage and semi-batch

RO systems. A model of the system, that includes the effect of finite salt rejection, predicts *SEC* with accuracy of 1–3%. With improvements in membrane permeability, valves, and pump efficiency, we predict electrical *SEC* lowered to 0.14–0.28 kWh/m^3 and second law efficiency elevated to 22.8–34.5%. Though simple batch RO can achieve comparable *SEC* to HSBRO, for recovery as high as 0.94 it would require an impractically large work exchanger. The model shows that feed of salinity up to 6,000 mg/L may be treated with recovery of 0.95 and peak system pressure <120 bar, indicating great potential in ZLD and MLD applications.

Keywwords: High recovery, Energy efficiency, Batch reverse osmosis, Salt retention, Zero liquid discharge.

Highlights:

- HSBRO is more efficient than semi-batch RO and more compact than batch RO.
- Specific energy consumption of 0.54 kWh/m^3 at recovery of 0.94 with 1.5 g/L feed salinity.
- Model agrees with experiments within 3 % error.
- 2nd law efficiency of 7.8–17.8 % obtained, with 22.8–34.5 % predicted after technical improvements.
- Feed of salinity up to 6 g/L may be treated with recovery of 0.95 and system pressure < 120 bar.

1. Introduction

The worldwide demand for new sources of water has increased in recent decades because of rapid population growth, climate change, increased per capita domestic usage, and increasing industrial and agricultural water requirements [1-4]. Desalination is being increasingly adopted to address this problem. The two most common approaches to desalination are thermal- and membrane-based technologies. Thermal technologies are highly energy-intensive, requiring many times the theoretical minimum energy of separation. In contrast, membrane technologies are becoming more popular due to their greater energy efficiency, reduced equipment size, and more flexible capacity [3, 5-9].

Reverse osmosis (RO), the most common membrane desalination technology, currently dominates the desalination industry [10-12]. But despite its benefits, RO also has drawbacks. First, like other desalination technologies, RO plants discharge highly saline brine and chemicals which pose a risk to the environment [11]. Second, the energy consumption of RO systems is still higher than the theoretical minimum and efforts to reduce energy consumption are therefore ongoing.

To address the first drawback, the zero liquid discharge (ZLD) approach has been proposed. As the growing concerns about waste disposal increase, ZLD is becoming more important to eliminate liquid waste and maximize water recovery [13]. ZLD is attracting significant interest in recent years in sustainable desalination and wastewater treatment, to overcome waste disposal hazards and concerns [10, 14, 15]. In particular, ZLD has a crucial role in the desalination of brackish groundwater, where high recovery of water and elimination of brine discharge is needed in inland agricultural and municipal applications [16, 17]. However, ZLD processes tend to be energy-intensive since they attempt to separate all impurities from the

effluent stream [13, 14]. Therefore, minimal liquid discharge (MLD) has also been put forward as an approach to minimize (though not completely eliminate) brine discharge, while incurring lower energy consumption than ZLD [18].

ZLD and MLD schemes use either membrane or non-membrane technologies. Non-membrane technologies include mechanical/thermal evaporation methods such as MVC (mechanical vapour compression). This traditional technique is highly energy-intensive with a reported *SEC* of 20–40 kWh/m^3 [14, 19-21]. Such methods have mostly been used for feeds with high salinities such as concentrated brines and seawater. Among the membrane-based methods, including electrodialysis and membrane distillation, RO is an energy-efficient and cost-effective method with energy consumption as low as 2-4 kWh/m^3 with seawater [20]. However, the application of RO in ZLD/MLD systems is limited by membrane burst pressure and fouling at high salinity. Therefore, RO has mostly been used as the initial concentration step before a thermal process to achieve ZLD/MLD [22]. High recovery RO, with its superior energy efficiency, would offer great promise in ZLD/MLD by helping to reduce the size of downstream thermal treatment units [13]. Recently, new RO technologies such as osmotically-assisted reverse osmosis (OARO) [19, 23-27], high pressure reverse osmosis (HPRO) [28], low-salt-rejection reverse osmosis (LSRRO) [18, 19], and cascading osmotically mediated RO (COMRO) [19, 29, 30] were shown to be technically and economically favourable in high-recovery applications for ZLD and MLD. However, only a few experimental works have been reported using such methods [30-33].

In response to the second drawback of RO, over the last few decades a number of approaches have helped to improve energy efficiency, including energy recovery devices (ERDs), more efficient pumps, osmotic pre-dilution to reduce feed salinity, the use of technologies to recover osmotic energy in the form of pressure-retarded osmosis (PRO) or reverse electrodialysis (RED), multi-stage RO, and novel RO configurations [3, 5, 15]. Nevertheless, the RO process still requires further research to reduce the energy consumption [3]. To this end, several innovative concepts have been proposed. For example, energy-efficient reverse osmosis (EERO) has been developed to overcome the problem of excessively high pressure in RO when targeting increased water recovery [34-39]. Centrifugal RO (CRO) was also proposed to reduce energy consumption relative to single-stage RO [40]. Moreover, several configurations of staged RO, batch RO and semi-batch RO (or closed-circuit desalination) have been proposed to enhance the energy efficiency of RO as well as enhancing water recovery. Some proposals were based on modelling [8, 9, 13, 15, 41-50]; and others on experimental studies [17, 41, 44, 45, 47, 50-56]. Table 1 summarizes the experimental performance of some RO-based treatment technologies with high recovery (>0.7) which can be considered for use in ZLD and MLD applications.

Table 1. Comparison of experimental performances of RO-based technologies operating at high recovery. In general, the *SEC* values are electrical energy per m^3 of output. However, ref [57] and [58] do not distinguish between hydraulic and electrical *SEC*; ref [58] gives *SEC* per m^3 of input.

Technology	Feed TDS (mg/L)	Recovery (%)	*SEC* (kWh/m^3)	System Output (m^3/day)	Reference
Batch RO	1,000-5,000	80	0.48–0.83	17.3	Hosseinipour et al. [44]
	2,000-5,000	70	0.6	1	Davies et al. [47]
Semi-batch RO	98-197[a]	90	0.42	97	Efraty et al.[52][b]
	Not reported [c]	80 and 88	0.82 and 0.8	586 and 840	Efraty [17]
	Not reported [d]	82.9	0.94	737	Efraty [53]

Multiple stage RO	5,000	91–95	15.8–20.9	6	Cingolani et al. [58]
	900	72	0.71	2,595	Kahraman et al. [54]
	2,450	71	1.89	1,584	Aljundi [59]
New RO technologies (COMRO-OARO)	50,000	75	15	156	Hyrec [57]
	41,000	75	7.4	307	Martinez et al. [30]

a total NO_3 concentration, **b** Plug flow desalination (PFD) –Semi-batch RO, **c** Salinity of 6,800 and 4,000 µS/cm, **d** Salinity of 6,800 µS/cm

Several researchers have carried out comparisons among different configurations of RO in terms of performance and energy consumption [9, 13, 42, 49]. At recovery up to about 0.7, semi-batch RO offers comparable energy consumption to three-stage RO but in a more practical, compact and economical configuration [42, 49]. However, batch RO is an even more promising method for improving the energy efficiency of RO systems when high recovery is needed [15].

Using batch RO technology, desalination can be achieved with minimal energy consumption, even at high recoveries [46]. For example, Davies et al. [47] constructed a batch RO prototype and achieved a hydraulic *SEC* of 0.31 kWh/m^3 and recovery of 0.69 with feedwater salinity of 5,000 mg/L. Park et al. [46] modelled the design and operation of a single-acting batch RO system that operates cyclically in two phases, using a work exchanger to transfers pressure from the feed fluid to the recirculating side. Their batch RO model showed promising results including water recovery of 0.8 and low energy consumption with second law efficiency of 33.2%. Recently, Hosseinipour et al. [44] presented an extensive experimental study of a batch RO system for brackish water treatment and modified the model in [46] by addition of osmotic backflow effect. The experiments showed a recovery of 0.8, hydraulic *SEC* in the range 0.22–0.48 kWh/m^3 and electrical *SEC* in the range 0.48–0.83 kWh/m^3. Cordoba et al. [48] modelled a double-acting batch RO configuration that used a high-pressure tank with a reciprocating piston. The study calculated a specific energy consumption of 1.88 kWh/m^3 for seawater with a salinity of 35,000 mg/L, recovery of 0.5, and a permeate flux of 15 L/m^2/h. Wei et al. [50] experimentally studied a batch RO system using a flexible bladder as the work exchanger, and predicted a 11% energy saving compared to a single-stage RO for seawater at recovery of 0.5.

Although batch RO is an excellent candidate for high-recovery and energy-efficient desalination, the system size increases sharply as recovery increases above about 0.7, because of the large volume required of the work exchanger vessel. To overcome this practical drawback, Park et al. [15] introduced a hybrid semi-batch/batch reverse osmosis (HSBRO) concept as a high-recovery, compact, and energy-efficient system. This hybrid design was predicted to approach the energy efficiency of batch RO in a more compact format. With the proposed novel design of HSBRO, the volume of work exchange vessel is several times smaller than in batch RO at the recovery of 0.95, whereas only a small energy penalty (less than 5%) is incurred compared to batch RO.

However, this hybrid concept has yet to be validated experimentally [15]. Therefore, the main objective of the present study is to investigate the HSBRO system at pilot scale and evaluate its performance in treating brackish feed water. A series of experiments has been performed at several feed salinities and water permeate fluxes. The system performance is studied including hydraulic and electrical *SEC*, salt retention effect, permeate and batch conductivity, concentration factor and recovery. Moreover, the model developed by Park et al. [15] has been modified and adjusted in light of the experimental findings. This study further aims to use the

validated mathematical model to predict the HSBRO system performance in applications at higher salinities and pressures. Although the RO system of this study is limited to 25 bar, the experiments validate the HSBRO concept as a preconcentration stage for ZLD/MLD that will be applicable for a higher range of pressures and concentrations. For example, besides treating brackish water, the concept may in the future be applied to the concentration of metal plating wastewater where pressures up to 120 bar are needed. In such applications, the system will recover both water and valuable minerals. In the electroplating wastewater treatment application, a high recovery is needed (>65%) and both concentrate and permeate streams are reused in the electroplating process resulting in no discharge or waste thus meeting the objectives of a ZLD system. The high-pressure (up to 120 bar) design of HSBRO has now been constructed by the authors at the University of Birmingham and the detailed results will be reported in a forthcoming paper.

The structure of this paper is as follows. Section 2 explains the description and working principles of the HSBRO system. Section 3 describes the improvements made to the mathematical models for the HSBRO system. Section 4 describes the experimental procedures using brackish water as the feed. Section 5 presents the results from the experiments, and discusses the findings of experiments and validation of the mathematical model. Section 6 discusses the results and compares them against other experimental studies reported in the literature. Moreover, in section 6, the validated model is used to predict system performance at higher pressures and higher salinities. Section 7 summarizes major findings of this study regarding the modelling and experimental results.

2. Operating principle of HSBRO system

Hybrid semi-batch/batch reverse osmosis (HSBRO) operates cyclically over three consecutive phases: 1) semi-batch pressurization, 2) batch pressurization, and 3) purge-and-refill – as shown in Fig. 1.

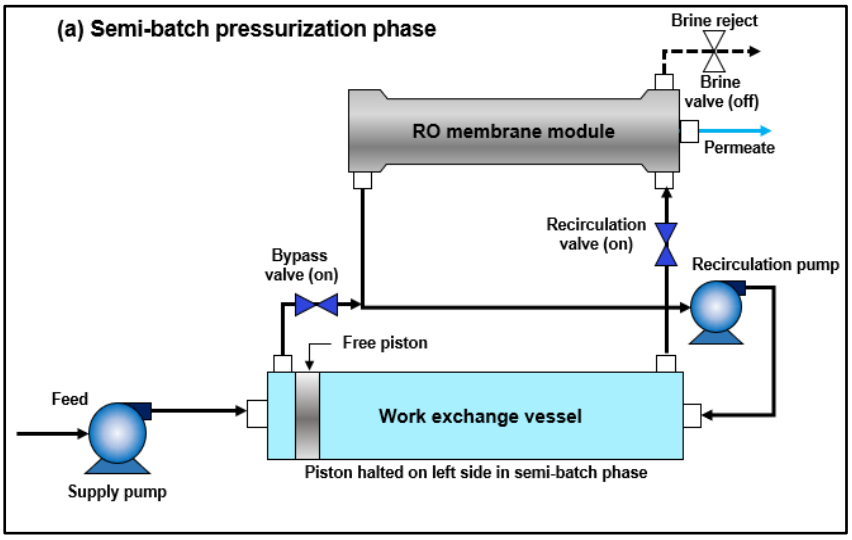

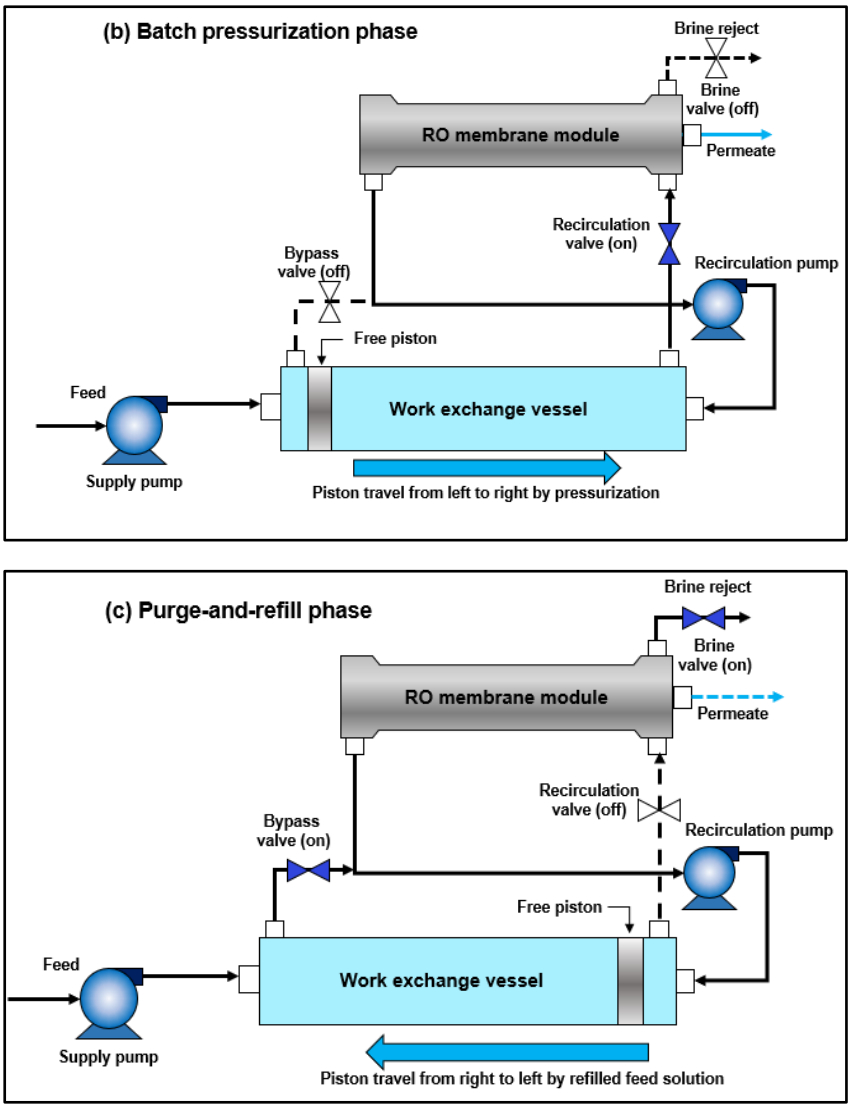

Fig. 1. Hybrid semi-batch/batch reverse osmosis (HSBRO), showing the three phases of cyclic operation. Flow and no flow are depicted by solid and dashed lines, respectively.

The process starts with a preliminary purge-and-refill phase, used only in the first cycle to purge any retained salt from previous operations and ensure that the piston starts at the left end of the work exchanger. This prepares the system for the pressurization phases. During the semi-batch pressurization phase (Fig. 1a) the brine valve is closed (off) while the bypass and recirculation valves are open (on). The free piston remains at the left of the work exchanger with no pressure driving it, since the bypass valve is open. The supply pump feeds the system and provides adequate pressure to overcome the osmotic pressure of the feed solution. Permeate is thus produced, while the concentrated brine stream exiting the RO module is recirculated, mixed with the incoming feed, and sent back to the RO module. As salt is added steadily to the system via the feed, concentration and pressure increase linearly with time. The switch point to the next phase can be set either according to a fixed time duration or according to a threshold pressure.

For the next phase (i.e., batch pressurization) the bypass valve is shut while the other valves remain unchanged (Fig. 1b). Now, unlike in the previous phase, there is no mixing between the incoming feed and recirculation stream. The free piston transfers the high pressure generated

by the supply pump to the batch volume of water on the right side of the piston. Permeate is produced from the RO module while the concentrated stream is recirculated to the work exchanger by the recirculation pump. In this phase, the concentration inside the system increases at a higher and increasing rate in comparison to the semi-batch pressurization phase. When the piston reaches the right end of the work exchanger, batch pressurization finishes, and purge-and-refill begins.

During the purge-and-refill phase (Fig. 1c), the recirculation valve is closed, while the brine and bypass valves are open. Because the brine valve vents into the atmosphere, the internal pressure drops and water production ceases. Through the bypass and brine valves, the supply pump purges the remaining brine inside the RO module from the system and replaces it with fresh feed water. Purging ends when a volume approximately equal to the volume of water inside the RO module and connecting pipes is flushed out. The end of the refill is detected by zero flow rate through the recirculation pump, indicating that the piston has returned to the left end and cannot move any further.

For further explanation of the rationale and operating principle of the HSBRO system, the reader is referred to reference [15].

3. Theory

A recent study successfully modelled and validated the performance of a batch RO system, including the effect of osmotic backflow which had not been considered previously [44]. This current study extends that approach to the hybrid system, by including also the initial semi-batch phase preceding the batch pressurization phase. The assumptions and equations mostly resemble those used earlier by Park et al. to model the hybrid system [15]; however, the current study uses an analytical rather than numerical approach to solving the equations.

The approach to modelling salt retention has also been improved here. Salt retention determines the initial concentration at the beginning of each pressurization phase and is thus important for the calculation of energy consumption. The above two studies assumed an ideal 100% rejection in the salt retention calculation, thus ignoring the effect of salt loss across the membrane. Incorporation of a non-ideal salt rejection value (<100%) means that a lower salt retention is calculated, thus giving a more accurate prediction of *SEC* in the hybrid system.

Because several aspects of the modelling were covered in previous works [15, 44], this theory section covers mainly the new aspects. Further details may be found in the Supporting Information (SI).

3.1. Salt retention model

In semi-batch and batch RO generally, salt retention increases the initial osmotic pressure of the solution, resulting in higher energy demand and decreased energy saving compared to conventional RO [44, 50]. This phenomenon also affects the hybrid system. To avoid salt retention completely, prolonged purging would be needed between cycles, which would waste feedwater and therefore conflict with achieving higher recovery.

Salt retention S_R refers to the initial concentration in the system at the start of the cycle divided by the feed concentration. Calculation of S_R requires two steps: (1) external mass balance followed by (2) internal mass balance. In the first step, the system is considered as a control

volume such that the mass inputs and outputs are balanced at the system boundary over the whole cycle (Fig. 2A). This first step is identical for semi-batch, batch, and HSBRO systems.

(A)

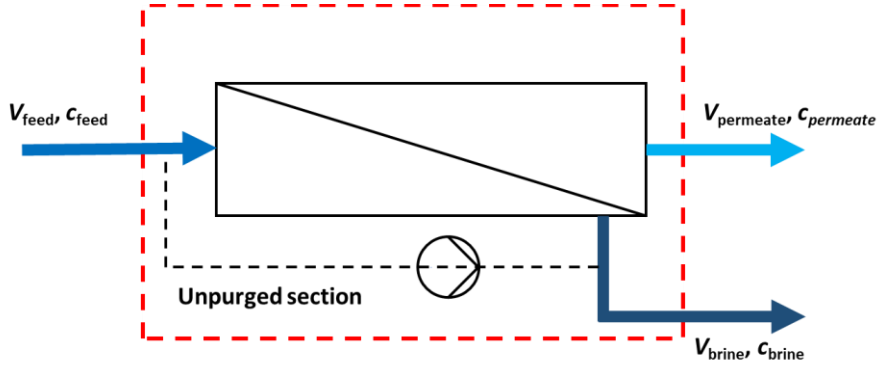

(B)

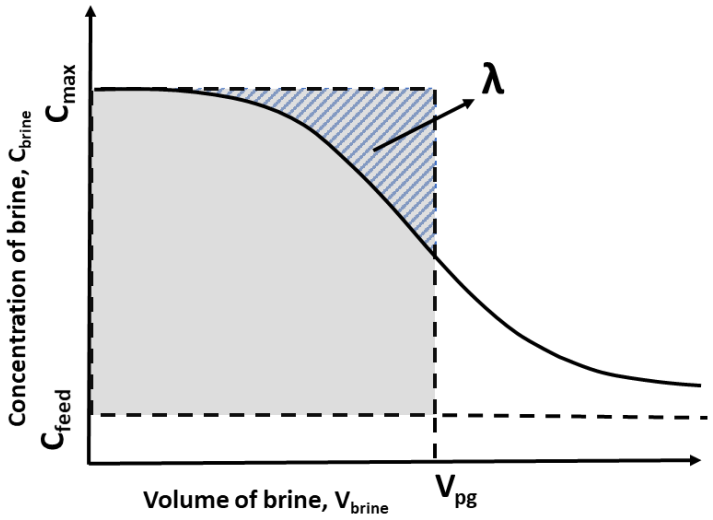

(C)

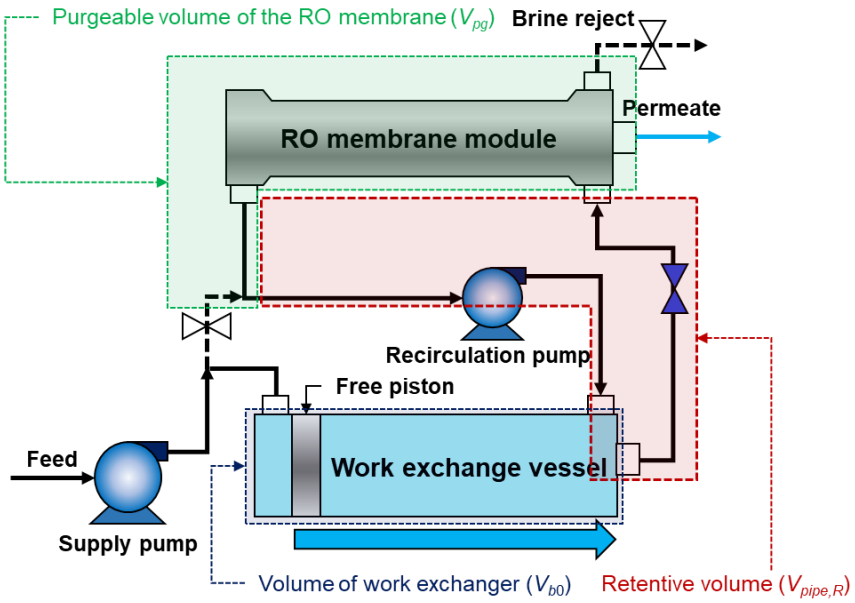

Fig. 2. (A) Sketch of RO system (semi-batch, batch or HSBRO) relevant to external mass balance. The dashed red line shows the system boundary. The unpurged section indicates pipe sections which are not in the purge path, and therefore contribute substantially to salt retention. (B) Concentration at brine outlet *vs* brine volume during purging, showing longitudinal dispersion parameter λ. This parameter represents the ratio of the hatched area over the larger rectangular area shaded in grey – it remains approximately constant over a range of concentrations and flow conditions. (C) Details of the HSBRO and labelling of volumes, as needed for the analysis of salt retention and recovery.

Assuming a constant density of the solution, the input volume equals the total output volume i.e.,

$$V_{\text{feed}} = V_{\text{permeate}} + V_{\text{brine}} \tag{1}$$

where V indicates the volume of each stream crossing the boundary (feed, permeate or brine respectively).

By definition, the recovery r is the amount of permeate per amount of feed:

$$r = \frac{V_{\text{permeate}}}{V_{\text{feed}}} \tag{2}$$

After several cycles, the system reaches a steady repetitive condition regarding concentrations c. Then, over each complete cycle, there is no accumulation of salt inside the system, such that input and output mass of salt balance. Accordingly:

$$V_{\text{feed}}c_{\text{feed}} = V_{\text{brine}}c_{\text{max}} - V_{\text{brine}}(c_{\text{max}} - c_{\text{feed}})\lambda + V_{\text{permeate}}c_{\text{permeate}} \tag{3}$$

The first term on the right-hand side is the output of salt that would occur in the absence of dispersion in the RO module. The next term represents salt retained due to dispersion, shown in terms of the maximum concentration c_{max} and the longitudinal dispersion parameter λ (retained salt as a fraction of the salt that could be purged from the module after purging indefinitely with the feed solution [60]). The last term is the salt leaving via the permeate, where its concentration is c_{permeate} which, in terms of the system rejection R_s, is given by:

$$c_{\mathrm{permeate}} = (1 - R_{\mathrm{s}})c_{\mathrm{feed}} \tag{4}$$

Eq. (3) shows that a larger value of λ requires a larger maximum brine concentration c_{max} to balance with the salt fed into the system. In other words, more dispersion results in higher salt retention (see Fig. 2B).

Substituting $V_{brine} = V_{feed} - V_{permeate}$ from Eq. (1) into Eq. (3), and dividing through by V_{feed} and by c_{feed}, gives (using also Eqs. (2) and (4)):

$$1 = (1 - r)\left(\frac{c_{\mathrm{max}}}{c_{\mathrm{feed}}}\right) - (1 - r)\left(\frac{c_{\mathrm{max}}}{c_{\mathrm{feed}}} - 1\right)\lambda + (1 - R_{\mathrm{s}})r \tag{5}$$

This can be rearranged as:

$$\frac{c_{\mathrm{max}}}{c_{\mathrm{feed}}} = \frac{1 - \lambda(1 - r) - (1 - R_{\mathrm{s}})r}{(1 - r)(1 - \lambda)} \tag{6}$$

In the second step, the internal mass balance applies to the recirculation loop during the two pressurization phases (but excluding the purge-and-refill phase). It equates the net mass of salt supplied to the mass accumulated in this loop, taking into account the decrease in loop volume:

$$V_{\mathrm{sb}}c_{\mathrm{feed}} - V_{\mathrm{permeate}}c_{\mathrm{permeate}} = (V_{\mathrm{pg}} + V_{\mathrm{pipe,R}})c_{\mathrm{max}} - V_0 c_0 \tag{7}$$

where V_{sb} is volume supplied during the initial semi-batch phase, c_0 is the initial concentration and V_0 is the initial volume of the system, given by:

$$V_0 = V_{\mathrm{b0}} + V_{\mathrm{pg}} + V_{\mathrm{pipe,R}} \tag{8}$$

where V_{b0} is the volume of the work exchanger (i.e., the volume supplied during the batch phase), V_{pg} is the purgeable volume of the RO module (including connecting pipes and ports) and $V_{\mathrm{pipe,R}}$ is the retentive volume of the pipework connected to the work exchanger vessel (i.e. the volume that is not in the purge path). Refer to Fig. 2C for explanation of the volumes in the HSBRO system.

Earlier experiments have shown that the volume of permeate collected is equal to the total volume supplied during pressurization, minus the backflow (V_{back}) [44]:

$$V_{\mathrm{permeate}} = V_{\mathrm{sb}} + V_{\mathrm{b0}} - V_{\mathrm{back}} \tag{9}$$

Dividing Eq. (7) by c_{feed}, and substituting from Eqs. (4), (8) and (9), leads to the following expression for salt retention:

$$S_{\mathrm{R}} = \frac{c_0}{c_{\mathrm{feed}}} = \frac{1}{V_0}\left[\left(V_{\mathrm{pg}} + V_{\mathrm{pipe,R}}\right)\frac{c_{\mathrm{max}}}{c_{\mathrm{feed}}} + (V_{\mathrm{sb}} + V_{\mathrm{b0}} - V_{\mathrm{back}})(1 - R_{\mathrm{s}}) - V_{\mathrm{sb}}\right] \tag{10}$$

To calculate S_{R}, therefore, the value of $c_{\mathrm{max}}/c_{\mathrm{feed}}$ is calculated from Eq. (6) and substituted in Eq. (10).

The above yields the initial concentration c_0, but it is also important to know the concentration c_1 at the end of semi-batch pressurization (i.e., the beginning of the batch pressurization phase).

For this purpose, the internal mass balance is applied to the semi-batch pressurization phase only. The result is similar to Eq. (7), but with the loop volume remaining constant:

$$V_{\mathrm{sb}}c_{\mathrm{feed}} - V_{\mathrm{sb}}c_{\mathrm{feed}}(1 - R_{\mathrm{s}}) = V_0(c_1 - c_0) \tag{11}$$

Rearranging, and substituting for c_0 in terms of S_{R}, gives:

$$c_1 = c_{\mathrm{feed}}\left[S_{\mathrm{R}} + \frac{V_{\mathrm{sb}}}{V_0}R_{\mathrm{s}}\right] \tag{12}$$

Eq. (12) shows that, unlike in the case of the batch pressurization stage, the salt retention does not have a multiplicative effect on concentration and pressure throughout the semi-batch pressurization phase. Salt retention is important for the initial concentration but has less effect on the final concentration in this phase.

Note that, in this analysis, a uniform value of rejection R_{s} has been used over the cycle whereas, in fact, it may vary. This approximation is useful to minimize the number of input parameters in the model but could be revised in future works.

3.2. Recovery and backflow

Considering that backflow subtracts from the permeate output, the recovery for the whole system becomes:

$$r = \frac{\text{permeate output}}{\text{feed input}} = \frac{V_{\mathrm{sb}} + V_{\mathrm{b0}} - V_{\mathrm{back}}}{V_{\mathrm{sb}} + V_{\mathrm{b0}} + (V_{\mathrm{pg}} - V_{\mathrm{back}})} \tag{13}$$

where $V_{\mathrm{sb}}, V_{\mathrm{b0}}$ and $V_{\mathrm{pg}} - V_{\mathrm{back}}$ are, respectively, the amount fed in the semi-batch, batch and purge-and-refill phases. Previous work showed that it was appropriate to limit the feed during the purge-and-refill stage, to compensate for backflow; hence V_{back} is subtracted in the last term. Previous experiments [44] showed that, except at very low concentrations, V_{back} = 5 L with an 8-inch RO module and this value is therefore used here.

3.3. Energy consumption

Hydraulic *SEC* is calculated as the hydraulic energy consumption (*E*) divided by the permeate output (with V_{back} subtracted). For one complete cycle, *E* is broken down by phase of operation (i.e., semi-batch pressurization, batch pressurization, and purge-and-refill) giving components of E_{P1} , E_{P2} and $E_{\mathrm{P\&R}}$ respectively. Similarly, *SEC* is broken down as follows:

$$SEC = \frac{E}{V_{\mathrm{sb}} + V_{\mathrm{b0}} - V_{\mathrm{back}}} = \frac{E_{\mathrm{P1}} + E_{\mathrm{P2}} + E_{\mathrm{P\&R}}}{V_{\mathrm{sb}} + V_{\mathrm{b0}} - V_{\mathrm{back}}} = SEC_{\mathrm{P1}} + SEC_{\mathrm{P2}} + SEC_{\mathrm{P\&R}} \tag{14}$$

where

$$SEC_{\mathrm{P1}} = \frac{E_{\mathrm{P1}}}{V_{\mathrm{sb}} + V_{\mathrm{b0}} - V_{\mathrm{back}}}, SEC_{\mathrm{P2}} = \frac{E_{\mathrm{P2}}}{V_{\mathrm{sb}} + V_{\mathrm{b0}} - V_{\mathrm{back}}}, SEC_{\mathrm{P\&R}} = \frac{E_{\mathrm{P\&R}}}{V_{\mathrm{sb}} + V_{\mathrm{b0}} - V_{\mathrm{back}}} \tag{15}$$

For each phase, *SEC* can be further broken down between the supply pump and recirculation pump contributions. Using the corresponding subscript for each pump:

$$SEC_{\mathrm{P1}} = SEC_{\mathrm{P1,supply}} + SEC_{\mathrm{P1,recirc}} \tag{16}$$

$$SEC_{\mathrm{P2}} = SEC_{\mathrm{P2,supply}} + SEC_{\mathrm{P2,recirc}} \tag{17}$$

$$SEC_{\mathrm{P\&R}} = SEC_{\mathrm{P\&R,supply}} + SEC_{\mathrm{P\&R,recirc}} \tag{18}$$

The hydraulic energy consumption is calculated as the product of differential pressure and pumped volume V, i.e.

$$E = \int PdV = \bar{P}\Delta V \tag{19}$$

where $\bar{P}$ is the differential pressure averaged over the phase (when P is constant, as is the case during the purge-and-refill phase, no averaging is needed). Pressure is needed to overcome osmotic pressure and to compensate for frictional losses related to the membrane, pipework, and the piston seal. Major pressure terms occur in the pressurization phases. During the semi-batch pressurization phase, concentration and pressure increase linearly as feed is supplied to the system [9] such that the average osmotic pressure is determined by the average of the initial and final concentrations which, using Eq. (12), is given by:

$$\bar{c} = c_{\mathrm{feed}}\left(S_{\mathrm{R}} + \frac{V_{\mathrm{sb}}}{2V_0}R_{\mathrm{s}}\right) \tag{20}$$

With other losses included, the expression for total average pressure required of the supply pump becomes

$$\bar{P_1} = S_{\mathrm{p}}S_{\mathrm{L1}}R_{\mathrm{S}}\pi_{\mathrm{feed}}\frac{\bar{c}}{c_{\mathrm{feed}}} + \frac{J_{\mathrm{w}}}{A_{\mathrm{w}}} - \frac{1}{2}\Delta P_m + \Delta P_{V1} \tag{21}$$

where J_{w} is the water flux through the membrane, A_{w} is the membrane water permeability, ΔP_{m} is the cross-flow pressure drop in the RO module, which is calculated using the correlation of Haidari *et al.* [61]; S_{p} is the concentration polarization factor calculated as in [62]; and ΔP_{V1} the pressure drop across the bypass valve which is calculated by the Toricelli equation using a discharge coefficient C_{d}, as in [44]. During batch pressurization, the pressure increases at an increasing rate such that a simple average can no longer be used. Instead, integration under the relevant pressure-volume curve gives [46]:

$$\bar{P}_2 = S_{\mathrm{p}}S_{\mathrm{L2}}R_{\mathrm{S}}\pi_{\mathrm{feed}}\frac{c_1}{c_{\mathrm{feed}}}\frac{1}{r_{\mathrm{p}}}ln\frac{1}{1-r_{\mathrm{p}}} + \frac{J_{\mathrm{w}}}{A_{\mathrm{w}}} + \frac{\Delta P_{\mathrm{m}}}{2} + \Delta P_{\mathrm{V2}} + \Delta P_{\mathrm{S}} \tag{22}$$

Note that Eqs. (21) and (22) rely on the assumption of linear correlation between concentration and osmotic pressure (i.e., van't Hoff approximation). This linear assumption is accurate for the brackish water concentrations used in the experiments of this study but may be reconsidered in future works covering higher concentrations or differing feed compositions.

The terms ΔP_{V2} and ΔP_{S} are the pressure drop across the recirculation valve and piston seal respectively; and the pressurization recovery r_{p} is given by:

$$r_{\mathrm{p}} = \frac{V_{\mathrm{b0}}}{V_{\mathrm{b0}} + V_{\mathrm{pg}} + V_{\mathrm{pipe,R}}} \tag{23}$$

The multiplier R_{s} in Eq. (22) is used to account for the concentration on the permeate side, due to finite salt rejection, which lowers the salt gradient and differential osmotic pressure to be overcome. The term S_{p} is the concentration polarization factor, which is calculated exactly as previously [44]. The terms S_{L1} and S_{L2} are the longitudinal concentration factors in the semi-batch and batch pressurization phases respectively, which are calculated based on ordinary differential equation (ODE) models. The model used for S_{L1} is new, and included in the SI section 4. The model for S_{L2} is the same as that used previously for the non-hybrid batch RO process [46]. As such, the model for S_{L2} assumes uniform concentration at the start of the batch RO pressurization phase. In fact, the concentration would be slightly non-uniform according to the conditions reached during the preceding semi-batch pressurization phase. Nonetheless, this simplifying assumption is preferred, as it allows the energy contribution of each phase to be modelled independently.

For the purge-and-refill phase, only minor frictional losses are encountered, including the losses in valves and piston seal friction. The corresponding calculations are included in the SI section 1, which explains in detail the flow paths and pressure drops for each pump and phase of operation.

The above calculations give the hydraulic *SEC*. The electrical *SEC* equals the hydraulic *SEC* divided by the overall pump efficiency (i.e. the efficiency of the pump and electric motor).

3.4. Peak Pressure

Finally, the peak pressure at the end of the batch pressurization phase is calculated as in reference [46], but taking into account the elevated concentration c_1 at the start of this phase and salt rejection R_{S}:

$$\hat{P} = S_{\mathrm{p}} R_{\mathrm{S}} \pi_{\mathrm{feed}} \frac{c_1}{c_{\mathrm{feed}}} \frac{1}{1 - r_{\mathrm{p}}} + \frac{J_{\mathrm{w}}}{A_{\mathrm{w}}} + \frac{\Delta P_{\mathrm{m}}}{2} + \Delta P_{\mathrm{V2}} + \Delta P_{\mathrm{s}} \tag{24}$$

3.5. Second law efficiency

Second law efficiency is useful for comparing desalination systems working at different feed salinities and recoveries. It is defined as the ideal *SEC* divided by that really obtained.

The ideal *SEC* corresponds to the change in Gibbs energy between the inlet and outlet streams. For a generalized desalination system treating a dilute solution [63], this is given by:

$$SEC_{min} = \pi_{\mathrm{feed}} \left[\frac{1}{r} \ln\left(\frac{1 - r[1 - R_s]}{1 - r} \right) - (1 - R_{\mathrm{S}}) \ln\left(\frac{1 - r[1 - R_s]}{(1 - r)(1 - R_s)} \right) \right] \tag{25}$$

3.6. Concentration factor (CF)

Concentration factor refers to the concentration of the brine divided by that of the feed. It is related to the recovery and rejection of the RO system by:

$$CF = \frac{1 - r[1 - R_s]}{1 - r} \tag{26}$$

4. Experimental

4.1. Experimental equipment

The HSBRO system investigated in this study is the same as described in [44]. Only the sequence of valve operation is modified. Fig. 3 shows a schematic of the HSBRO prototype.

The system uses a single-acting free piston and an 8-inch RO module to obtain an output up to 22 m^3/day. Experiments were conducted using an Eco Pro-440 membrane element (Dupont) with 41 m^2 active area. The output is limited by the maximum operating pressure of 25 bar, which limits the flux J_w to about 24 L/m^2/h with this membrane. Major parts include two pumps (supply and recirculation pumps), three motorized on-off valves, two pressure vessels (one housing the free piston and the other an 8-inch RO membrane) and nine sensors to measure pressure, flow rates and conductivities. A stainless-steel housing holding a 10-inch length cartridge filter (5 μm pores) is also used to remove the particulates inside the feed water for membrane protection. Additionally, a one-way valve installed on the permeate outlet reduces backflow when the system depressurizes at the end of the batch pressurization phase. SI section 2 includes details of parts and instruments used, as well as constant parameters of the system.

The system is controlled by a Programmable Logic Controller (PLC) which uses timers and feedback from pressure, flow, and conductivity sensors to control the pumps and the valves. The PLC program can be adjusted to achieve the desired recovery at various water fluxes. The recovery was determined by dividing the mass of water collected in the permeate tank, by the mass of water leaving the feed tank.

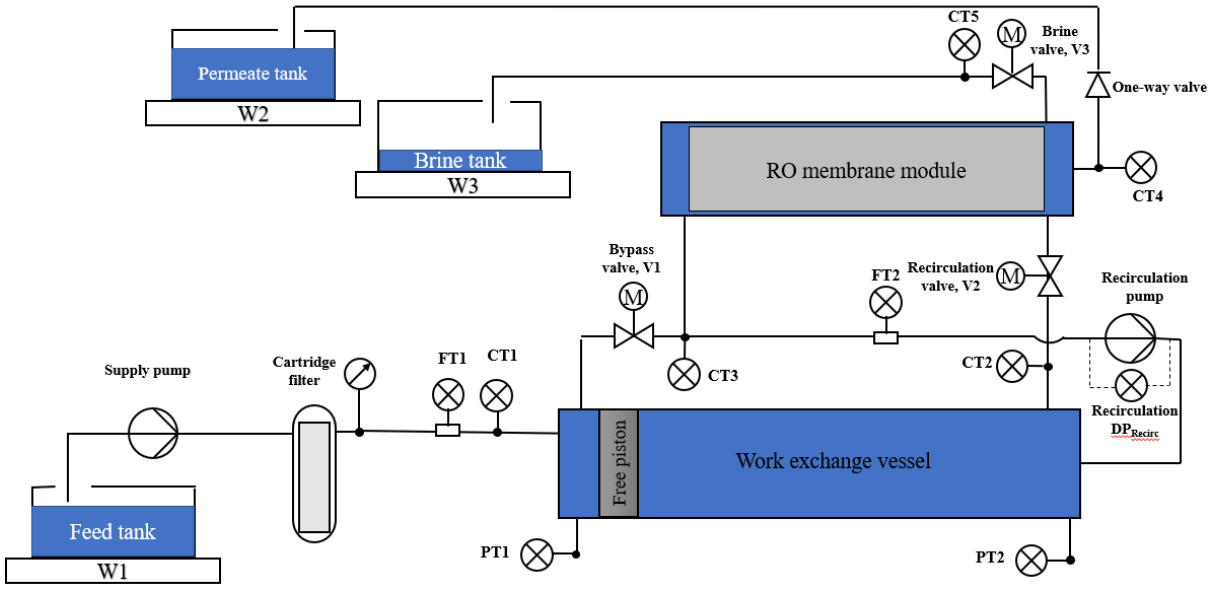

Fig. 3. Schematic diagram of high-recovery hybrid semi-batch/batch RO (HSBRO) system (PT, CT and FT are pressure, conductivity and flow transmitters, respectively; W1, W2, and W3 are weighing platforms for feed, permeate and brine tanks; M indicates motorized valves).

4.2. Experimental procedure

To evaluate the HSBRO performance, a series of experiments were carried out at various feed salinities and water permeate fluxes, at recovery $r \geq 0.94$. Because the system was designed for brackish water treatment, its operating pressure was limited to 25 bar. We therefore used feed solutions with maximum concentration of 1,500 mg/L to avoid exceeding this limit. Thus, concentrations of 500, 1,000, and 1,500 mg/L and water permeate fluxes of 10–24 L/m^2/h were selected. These concentrations corresponded to conductivities of 1.019, 1.995 and 2.945 mS/cm respectively (see SI section 5 for conversion factors from conductivity to concentration).

The feed solution was prepared using tap water (salinity of ~100 mg/L) and analytical grade sodium chloride (purity>99.5%). 4.5 mg/L of sodium metabisulfite (SMBS) was also added to the feed tank to counteract free chlorine in the tap water and prevent membrane oxidization. Experiments were conducted at a constant temperature (25 ℃) maintained by a thermostatic immersion heater. An external mixing pump was used to homogenize the water inside the feed tank before and during the tests.

Because of salt retention, initial cycles gave a different pattern of concentration *vs.* time. After two cycles the system stabilized; thus, we took the third cycle as representative of continued operation. All the parameters including time, supply and batch pressure, conductivities in supply, entry to the RO module, the exit of the RO module, brine, and permeate streams, differential pressure of the recirculation pump, electrical energy consumption of both supply and recirculation pumps, and weight of the feed, permeate and brine tanks were recorded at a frequency of at least once per second, resulting in at least 3,000–8,000 sets of readings per cycle. The data files are indexed in the SI section 5 and included as electronic appendices. These data were used to calculate results such as hydraulic and electrical *SEC*, recovery, rejection, and concentration factor and thus evaluate system performance.

5. Results

5.1 Salt retention

Salt retention has an important influence on the initial salt concentrations c_0 and c_1 at the start of the semi-batch and the batch pressurization phases respectively. According to the theory above, the concentration should increase linearly from the c_0 to c_1 as predicted by Eqs. (10) and (12). To verify the theory, Fig. 4 presents the experimental and theoretical variations of salt concentration (measured at the inlet of the RO module) from the start to the end of the semi-batch pressurization phase. Experiments were conducted at 1,000 mg/L feed concentration and J_w = 18.9 L/m^2/h. Except for some initial fluctuation in concentration, there was good agreement between experimental measurements and theoretical values.

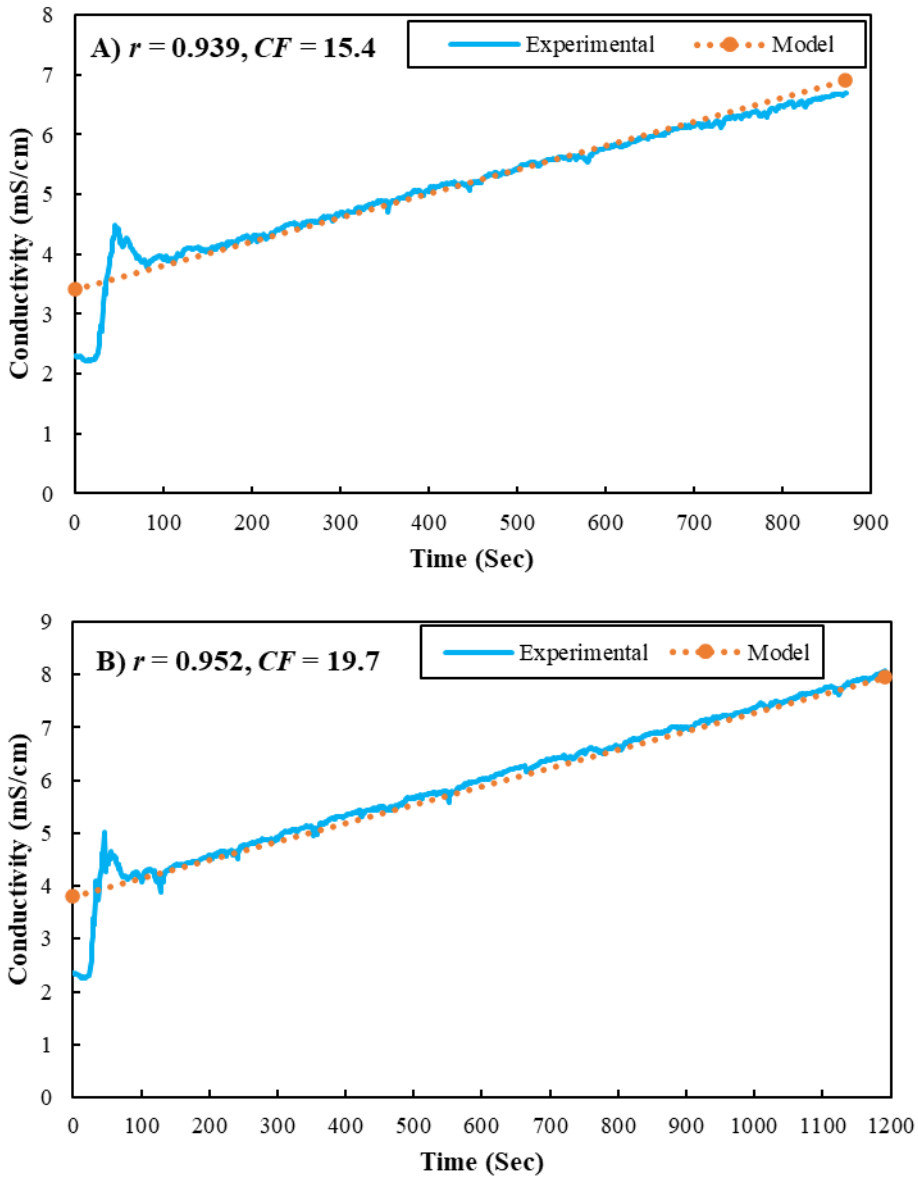

Fig. 4. Comparison of model predictions and experimental inlet conductivity into the RO module vs. time in semi-batch pressurization phase at feed salinity c_{feed} = 1,000 mg/L, flux J_w = 18.9 L/m^2/h A) recovery r = 0.939 and concentration factor CF= 15.4, B) recovery r = 0.952 and concentration factor CF= 19.7. See SI section 5 for conversion between conductivity and concentration.

The above theory and experiments correspond to the case where the purged brine volume V_{brine} (collected at the outlet) equals the purgeable volume V_{pg} of the batch RO system. But it is also interesting to study the case of smaller or larger brine volumes during purging. For this purpose, we carried out some tests to measure the salt retention inside the HSBRO system over a range of V_{brine}/V_{pg}. These tests were conducted at 1,000 mg/L feed salinity, and J_w = 18.9 L/m^2/h. At each value of V_{brine}/V_{pg}, the system was operated for three cycles. Once the third cycle purge-and-refill phase finished, we mixed the water inside the whole system (including membrane and work exchanger) for 10 minutes using the recirculation pump and then measured the solution concentration and divided it by the feed concentration to calculate the salt retention ($S_R = c_0/c_{feed}$).

Fig. 5 demonstrates the effects of varying purged brine volume on salt retention and recovery. At V_{brine}/V_{pg} = 1 (i.e. brine volume equal to the purgeable volume of solution inside the membrane and pipes) and r = 0.94, salt retention was 1.89 ± 0.03, slightly higher than the theoretical prediction of S_R = 1.78. As expected, by increasing the purged brine volume, salt retention decreased but at expense of lower recovery since the permeate production was constant. Therefore, there is a trade-off between either (1) higher recovery and higher salt retention, or (2) lower recovery and lower salt retention. Salt retention dropped substantially when purging more; for example, on increasing V_{brine} from 16.5 (V_{brine}/V_{pg} = 1) to 24.6 L (V_{brine}/V_{pg} = 1.5), salt retention dropped 24% from 1.89 to 1.44. Alongside, however, the recovery fell from 0.940 to 0.913. In the case of less purging, salt retention increased sharply. For instance, when V_{brine}/V_{pg} = 0.9, salt retention was 2.26 which is 20% larger than when V_{brine}/V_{pg} = 1, while the recovery was only slightly higher at r = 0.945 compared to r = 0.94.

Electrical *SEC* decreased with increasing purged brine volume. Fig. 6 presents the effect of V_{brine} on the electrical *SEC* at 1,000 mg/L feed salinity and J_w = 18.9 L/m^2/h. Total electrical *SEC* decreased from 0.502 to 0.468 kWh/m^3 when we increased V_{brine}/V_{pg} from 0.9 to 1.5. As we saw in Fig. 5, longer purges lead to less salt retention, which in turn decreases the applied pressure and energy requirements.

In the non-hybrid batch RO studied previously, we observed almost constant electrical *SEC* over the same range of purged brine volumes [44]. However, in HSBRO we observed about a 7% decrease in electrical *SEC* at larger volumes. The main reason is that salt retention in HSBRO is much larger than in batch RO (1.89 compared to 1.16 at V_{brine}/V_{pg} = 1), and it has a greater effect on energy consumption. As can be seen in Fig. 6, larger purged brine volume caused a reduction in the supply pump *SEC* in both semi-batch and batch pressurization phases, which dominated over the increase during the purge-and-refill phase.

Fig. 7 shows concentration inside the recirculation loop over the semi-batch pressurization phase, for different values of V_{brine}/V_{pg}. As in Fig. 4, concentration increased linearly over time. Smaller amounts of purging (V_{brine}/V_{pg} <1) led to higher initial and final concentrations.

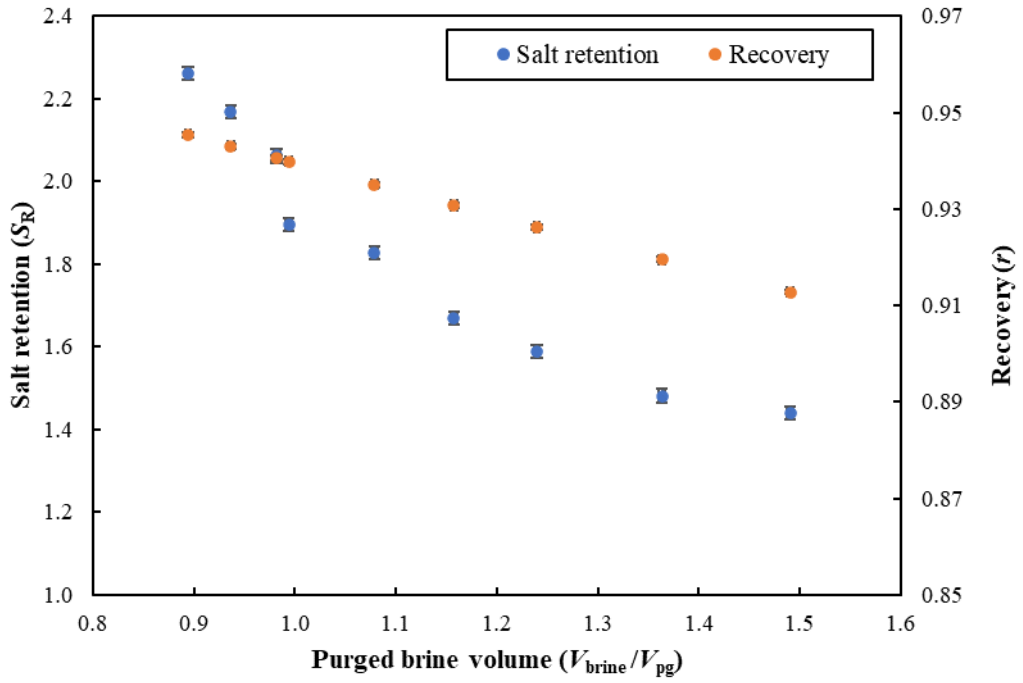

Fig. 5. Observed salt retention and recovery as a function of normalized purge volume at feed salinity c_{feed} = 1,000 mg/L and J_w = 18.9 L/m^2/h.

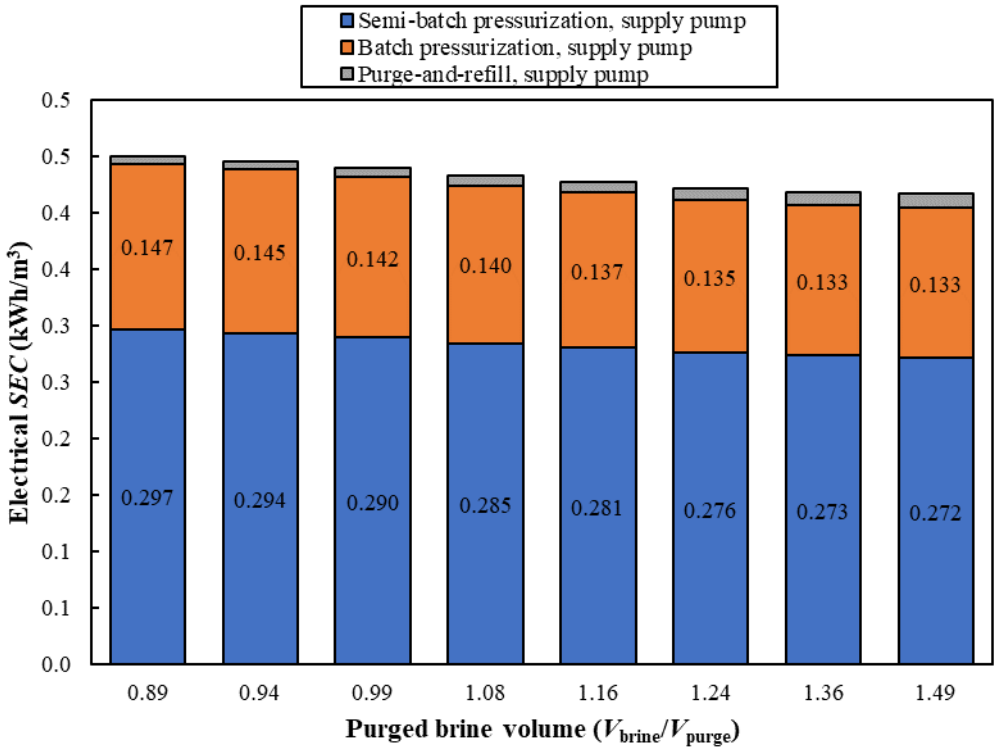

Fig. 6. Electrical *SEC*, supply pump breakdown as a function of normalized purged brine volume at feed salinity c_{feed} = 1,000 mg/L and flux J_w = 18.9 L/m^2/h.

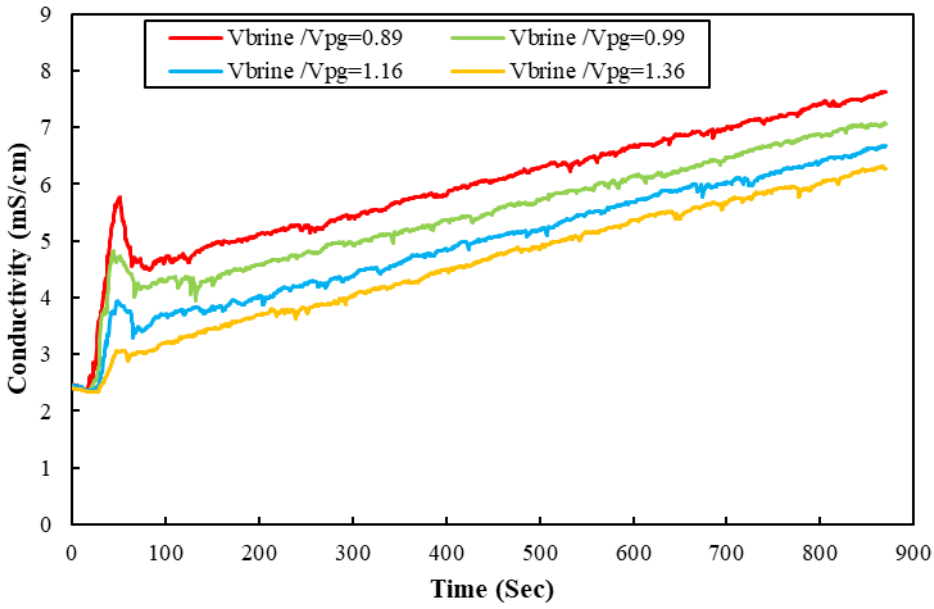

Fig. 7. Effect of varying purge volume on recirculation loop concentration (represented by conductivity) over a semi-batch pressurization phase (r = 0.94, J_w = 18.9 L/m^2/h, c_{feed} = 1,000 mg/L). See SI section 5 for conversion between conductivity and concentration.

5.2 Hydraulic SEC

The hydraulic energy consumption for each pump was measured by integrating the amount of water transferred by that pump with respect to the differential pressure. The integration was carried out over successive time steps using the trapezoidal rule. Then, experimental hydraulic *SEC* was obtained by dividing the consumed energy by the permeate volume output as measured by the weighing tank (W2). For the model predictions of SEC, the model input parameters are included in Table S3. The discharge coefficient of C_d = 0.62 is consistent with the range of 0.61 to 0.66 reported for orifices generally [64] and only a has minor influence on the total energy consumption within this range. The dispersion parameter was determined as λ = 0.15 based on an analysis of exit brine concentration during purge under conditions of osmotic backflow (see SI section 3). Note that this value differs from the previous study, where the influence of osmotic backflow was not rigorously included in the salt retention calculation [44]. The backflow volume was assigned a value of V_{back} = 5 L, according to the backflow typically observed in this and the previous study. The piston friction of $\Delta P_s = 3.5$ kPa was observed from measurements of the differential pressure (see SI section 6).

To match the model and experimental results, two important adjustable parameters were used, as follows. The membrane permeability was assigned the same value of A_w = 4.4 L/m^2/h/bar as in the previous study [44]. In this new study, the salt rejection was assigned the value of R_s = 0.94, consistent with the observed permeate salt concentration. The dispersion parameter was determined as λ = 0.15 based on an analysis of exit brine concentration during purge under conditions of osmotic backflow (see SI section 3). Note that this value differs from the previous study, where the influence of osmotic backflow was not rigorously included in the salt retention calculation [44].

Fig. 8A compares experimental values of hydraulic *SEC* against the model predictions at different feed salinities for each pump and phase of operation (r = 0.94, and J_w = 18.9 L/m^2/h). Total experimental hydraulic *SEC* increased with feed salinity from 0.202 to 0.308 kWh/m^3 at 500 and 1,500 mg/L respectively. Since recovery and permeate water flux were kept constant at different tested feed salinities, the amount of water displaced by each pump was the same. However, at increased feed salinity, supply pressure increased with osmotic pressure. As a result, the hydraulic *SEC* of the semi-batch and batch pressurization phases increased; whereas the energy consumed by both the recirculation and supply pumps during the purge-and-refill phase remained constant. For example, measured supply pump *SEC* during pressurization phases ($SEC_{P1,supply}$+$SEC_{P2,supply}$) was 0.181, 0.239, and 0.287 kWh/m^3 at 500, 1,000, and 1,500 mg/L feed solutions respectively, while other *SEC* contributions totalled only 0.021 kWh/m^3 regardless of feed concentration. As expected, most of the energy was consumed by the supply pump during the two pressurization phases. The model predicted well the hydraulic *SEC* (Fig. 8A). The highest error was around 2% with the 1,000 mg/L feed solution while at 500 and 1,500 mg/L the error between experimental results and model values was less than 1%.

Fig. 8B compares experimental measurements of hydraulic *SEC* against predicted values at various water fluxes, r = 0.94, and 1,000 mg/L feed salinity c_{feed}. It shows an increase of hydraulic *SEC* with flux. This is because more pumping pressure was needed to overcome hydrodynamic resistance in the RO membrane pores ($P \propto J_w/A_w$). Thus, the *SEC* of the supply pump over the two pressurization phases, $SEC_{P1,supply}$+$SEC_{P2,supply}$, increased from 0.187 to 0.28 kWh/m^3 as flux almost doubled from 12.1 to 23.6 L/m^2/h. However, unlike in Fig. 8A, the recirculation pump *SEC* was not constant. To achieve higher permeate flux, we needed to increase the feed flow rate; then to maintain an optimum value of $Q_r/Q_f \approx 2$, we had to increase the recirculation flow rate proportionately which led to an increase in recirculation pump *SEC*. For instance, on increasing water flux from 12.1 to 23.6 L/m^2/h, the experimental recirculation pump *SEC* over the two pressurization phases, $SEC_{P1,recirc}$+$SEC_{P2,recirc}$, increased from 0.008 to 0.022 kWh/m^3. Overall, by almost doubling the water flux, we observed a 54% increase in total hydraulic *SEC* from 0.2 to 0.308 kWh/m^3. Fig. 8B also shows model predictions of hydraulic *SEC* at different water fluxes. The model again agrees well with the experimental results, with less than 3% error.

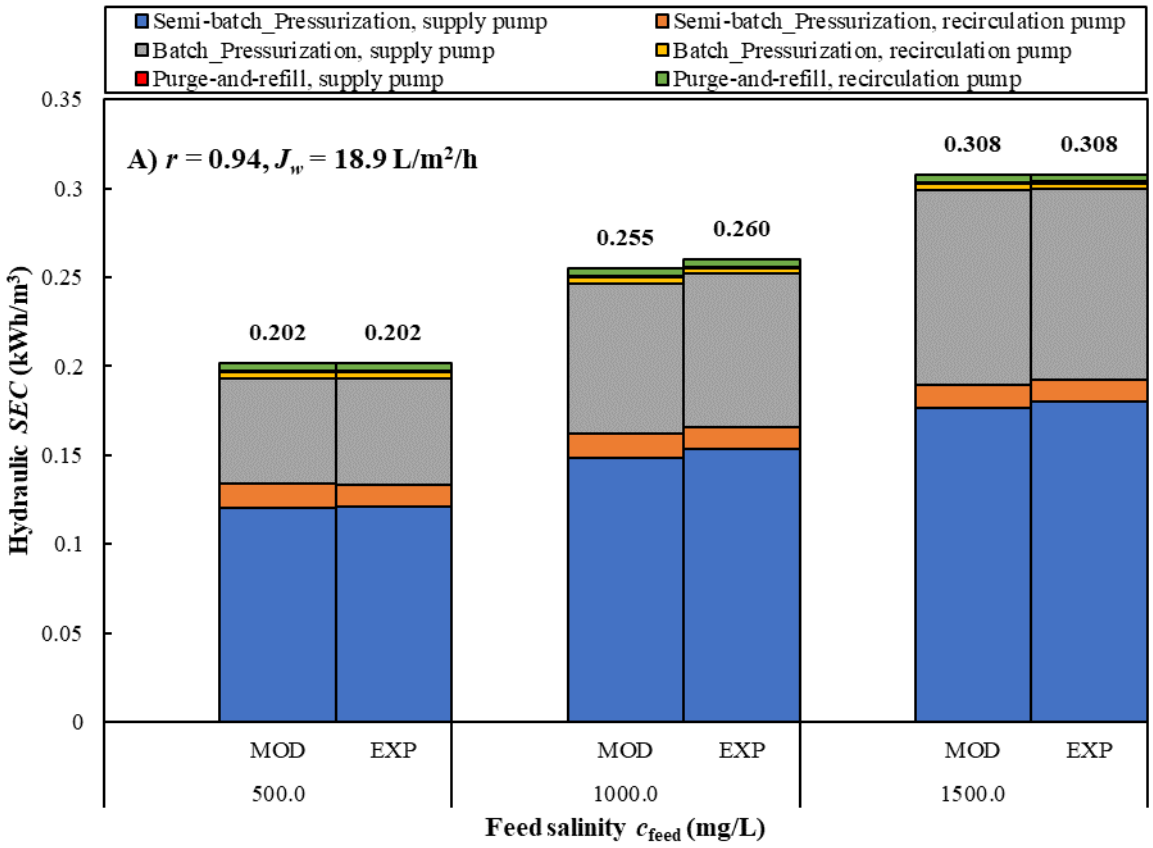
Semi-batch_Pressurization, supply pump
Semi-batch_Pressurization, recirculation pump
Batch_Pressurization, supply pump
Batch_Pressurization, recirculation pump
Purge-and-refill, supply pump
Purge-and-refill, recirculation pump
A) r = 0.94, J_w = 18.9 L/m²/h
Hydraulic SEC (kWh/m³)
0.35
0.3
0.25
0.2
0.15
0.1
0.05
0
0.202
0.202
0.255
0.260
0.308
0.308
MOD
EXP
MOD
EXP
MOD
EXP
500.0
1000.0
1500.0
Feed salinity c_feed (mg/L)

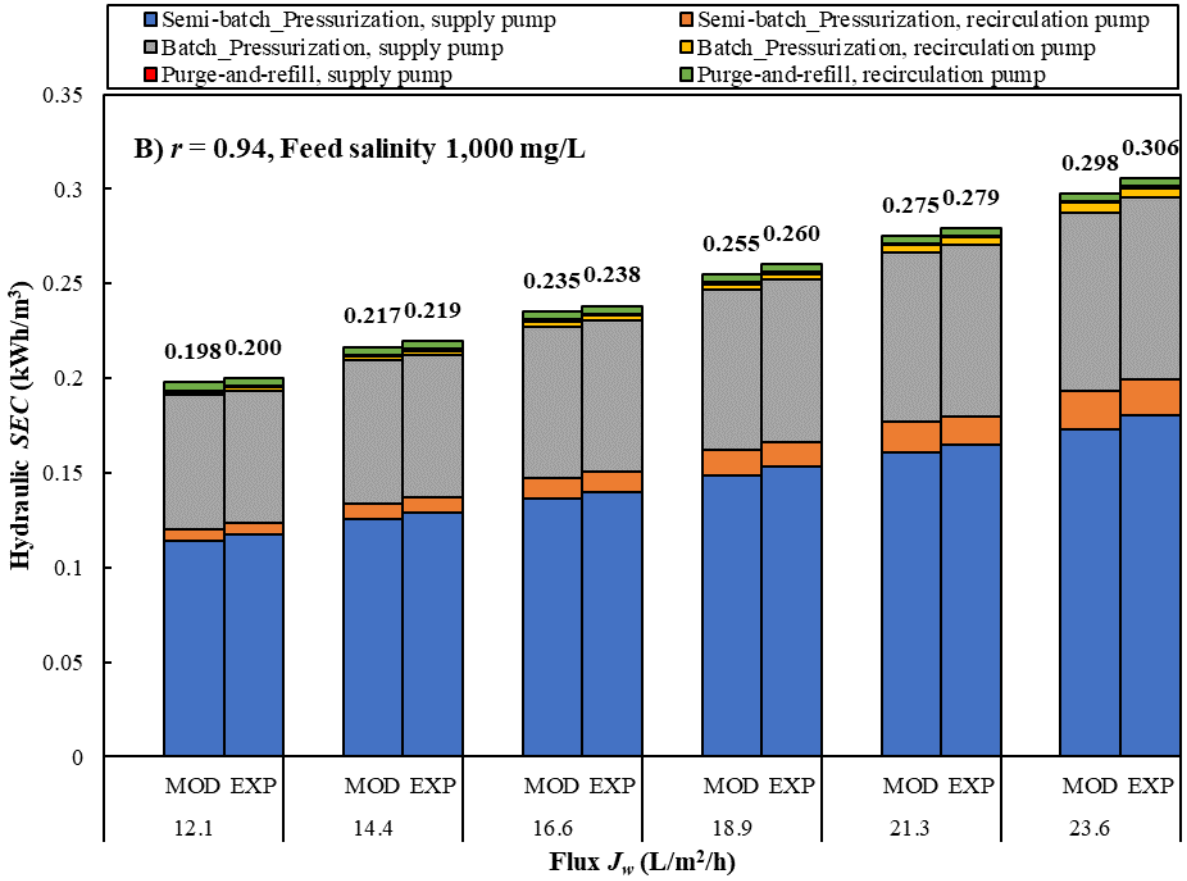

Fig. 8. Comparison of hydraulic *SEC* breakdown between experimental measurements (EXP) and model predictions (MOD) at recovery r = 0.94. A) different feed salinities at J_w = 18.9 L/m^2/h, and B) different water fluxes at c_{feed} = 1,000 mg/L.

5.3 Electrical SEC

We calculated electrical *SEC* of the HSBRO system by integrating, over time, the electrical power (current × voltage) consumed by both pumps and then dividing by the amount of permeate water produced.

Fig. 9A compares electrical and hydraulic *SEC* breakdown at different water salinities, at r = 0.94 and J_w = 16.5 L/m^2/h. As feed salinity increased, both electrical and hydraulic *SEC* increased, but the increase in electrical *SEC* was less marked. At 500, 1,000, and 1,500 mg/L, total electrical *SEC* was 0.394, 0.458, and 0.501 kWh/m^3 respectively compared to hydraulic *SEC* of 0.181, 0.238, and 0.278 kWh/m^3 with the main contribution coming from the supply pump. Total electrical *SEC* was respectively 118, 92, and 80% higher than the hydraulic *SEC*. As seen in Table 2, the lower increase in electrical *SEC* was associated with supply pump efficiency increasing from 45.9 to 55.5% (while the recirculation pump efficiency remained constant at about 35%).

Fig. 9B compares hydraulic and electrical *SEC* at various water fluxes, at r = 0.94 and 1,000 mg/L feed concentration. By increasing water flux from 12.1 to 23.6 L/m^2/h, both *SECs* increased: hydraulic *SEC* by 53% from 0.2 to 0.306 kWh/m^3, and electrical *SEC* by 31% from 0.419 to 0.549 kWh/m^3. Again, the increase in electrical *SEC* was smaller, because of increased

pump efficiency at higher pressures associated with the higher fluxes. As water flux doubled, supply pump efficiency increased by a factor of 1.18 (from 47.7% to 56.1%) in semi-batch and by 1.11 (from 57.5% to 63.9%) in batch pressurization phases respectively (see Table 3). The recirculation pump *SEC* also increased with flux. Again, electrical *SEC* increased less than hydraulic *SEC* because recirculation pump efficiency increased with flow. For example, when flux increased from 12.1 to 23.6 L/m^2/h, we observed an increase in efficiency by a factor of 1.73 (from 24.5% to 42.5%) and by 1.82 (from 18.9% to 34.4%) during semi-batch and batch pressurization phases respectively (Table 3). However, since the recirculation pump consumes less than 12% of total energy, it had a minor impact on total *SEC* in all cases.

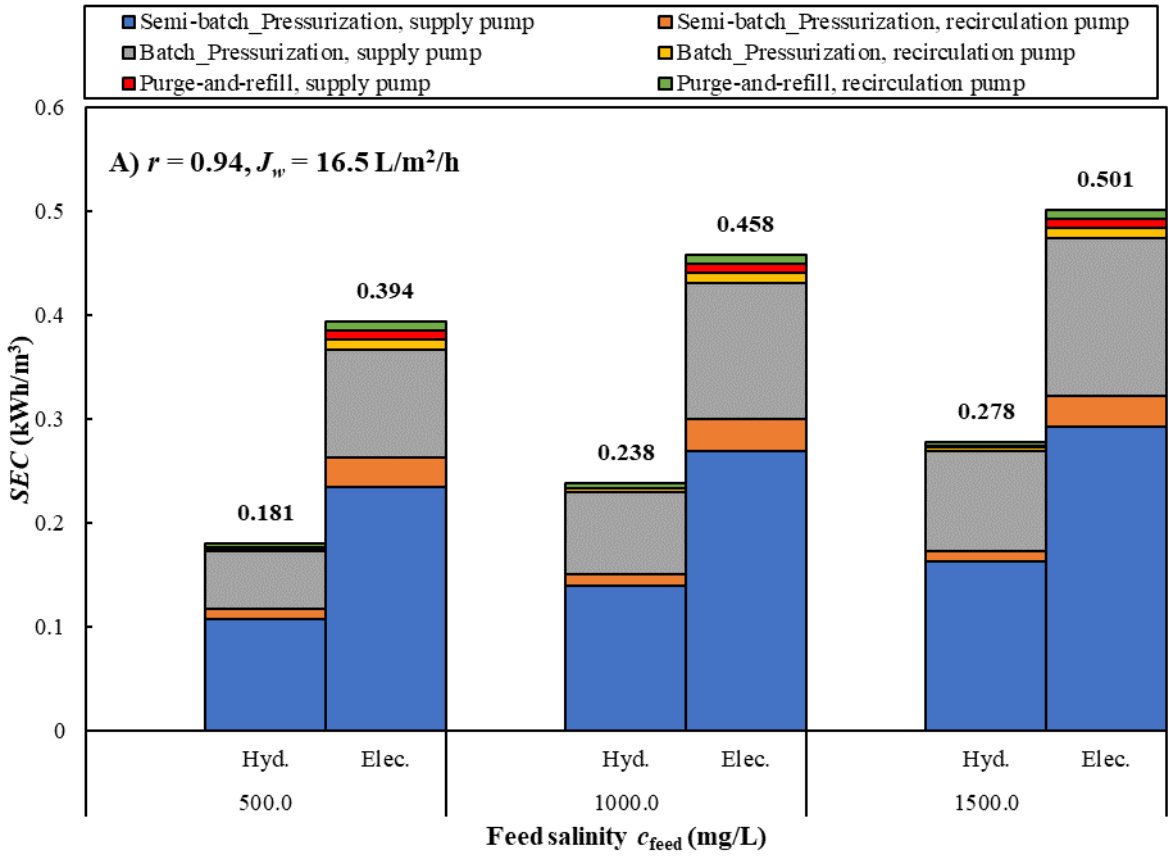

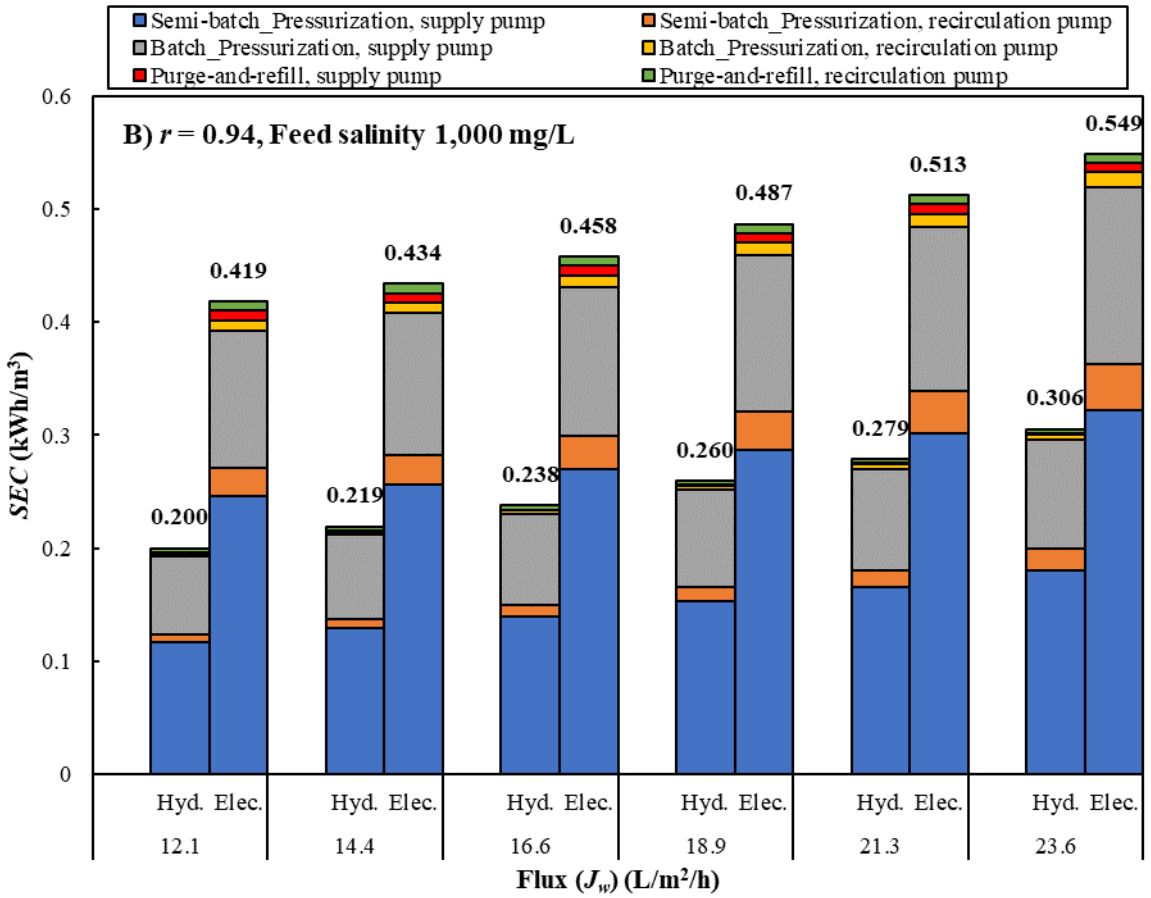

Fig. 9. Comparison of hydraulic and electrical *SEC* breakdown at $r = 0.94$. A) different feed salinities at $J_w = 16.5$ L/m^2/h, and B) different water fluxes at $c_{feed} = 1{,}000$ mg/L.

Table 2. Supply and recirculation pump efficiencies for semi-batch pressurization, batch pressurization, and purge-and-refill phases at various feed salinities (flux J_w=16.5 L/m^2/h).

Feed salinity c_{feed} (mg/L)	Pump efficiency (%)					
	Supply pump			Recirculation pump		
	Semi-batch pressurization	Batch pressurization	Purge-and-refill	Semi-batch pressurization	Batch pressurization	Purge-and-refill
500	45.9	53.2	10.3	35.3	28.3	48.6
1,000	51.9	60.9	10.8	34.4	27.3	48.7
1,500	55.5	63.9	12.2	34.6	27.3	48.3

Table 3. Supply and recirculation pump efficiencies for semi-batch pressurization, batch pressurization, and purge-and-refill phases at various water fluxes and c_{feed} = 1,000 mg/L.

Flux J_w (L/m^2/h)	Pump efficiency (%)					
	Supply pump			Recirculation pump		
	Semi-batch pressurization	Batch pressurization	Purge-and-refill	Semi-batch pressurization	Batch pressurization	Purge-and-refill
12.1	47.7	57.5	12.9	24.5	18.9	47.7
14.4	50.3	59.3	12.4	32.0	24.7	47.6
16.6	51.9	60.9	10.8	34.4	27.3	48.7
18.9	53.4	61.8	10.6	37.7	30.5	48.1
21.3	54.6	62.6	10.9	40.0	33.2	48.3
23.6	56.1	63.9	11.9	42.5	34.4	48.1

Fig. 10 shows the percentage contribution of each pump to the total electrical *SEC* during different phases of operation at different feed salinities, at r = 0.94 and J_w = 18.9 L/m^2/h. The largest fraction (about 60%) of electrical *SEC* came from the supply pump during semi-batch pressurization. Over both phases of pressurization, this fraction increased to 86–89%. The fraction slightly increased with feed salinity, as the absolute contribution from the recirculation pump remained constant. In total, about 10–12% of *SEC* came from the recirculation pump.

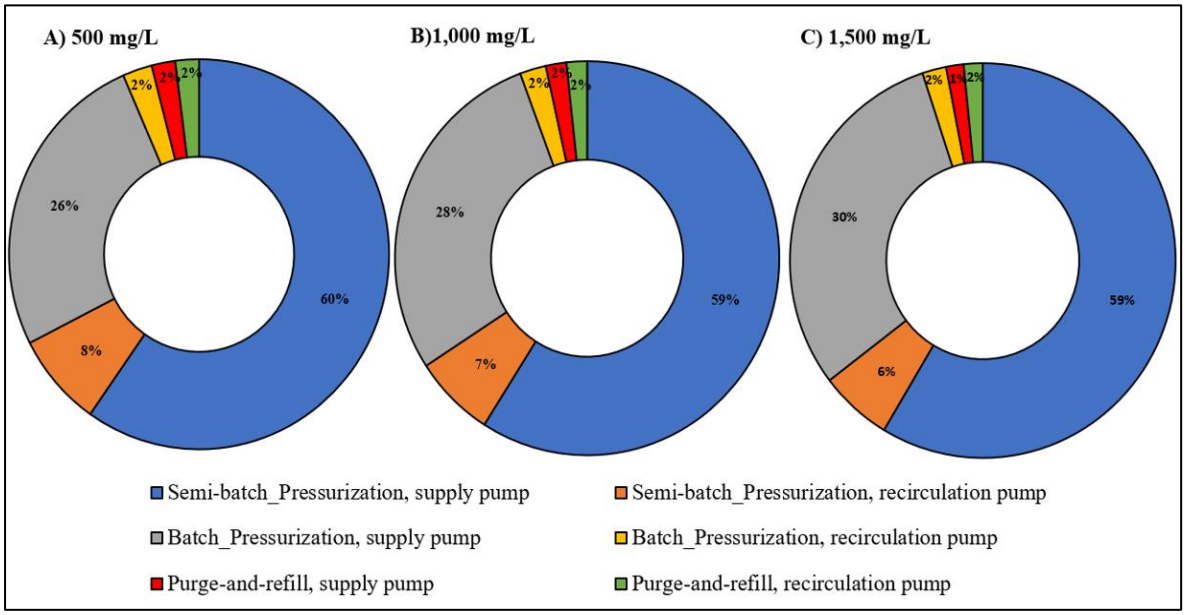

Fig. 10. Percentage contribution of each pump to total electrical *SEC* at each operation phase at feed salinity A) c_{feed} = 500 mg/L, B) c_{feed} = 1,000 mg/L, and C) c_{feed} = 1,500 mg/L. (r = 0.94 and J_w = 18.9 L/m^2/h).

A useful feature of HSBRO is the ability to achieve different recoveries by changing the duration of the semi-batch pressurization phase. Fig. 11 compares electrical *SEC* breakdown at two different recoveries for 500 mg/L feed solution and J_w = 23.6 L/m^2/h. At r = 0.979, semi-batch pressurization share of *SEC* was around 77% while this was 59% at r = 0.94. This is because the operation time at r = 0.979 was much longer; this increased the concentration inside the system and consequently more pressure was needed. To reach r = 0.979, semi-batch duration was 2,580 s (about 88% of process time) while for r = 0.94 it was 690 s (about 68% of process time). The batch and purge-and-refill durations for both recoveries were about the same at 259 and 76 s respectively. In addition, at r = 0.94, the contributions of semi-batch and

batch phases to the total recovery were r_{sb} = 0.704 and r_b = 0.236 respectively, while at r = 0.979 these values were r_{sb} = 0.898, r_b = 0.081. Although, in theory, operating longer at semi-batch mode increases the energy penalty, it reduces the need for having a large work exchanger which becomes impractical at such high recoveries. The unfavourable *SEC* portion (purge-and-refill phase and recirculation pump over pressurization phase) was 12 and 15% at r = 0.979 and r = 0.94 respectively. Recirculation pump *SEC* was the same in both cases (11%) while at higher recoveries the purge-and-refill *SEC* portion was much smaller, around 1% at r = 0.979 compared to 4% at r = 0.94.

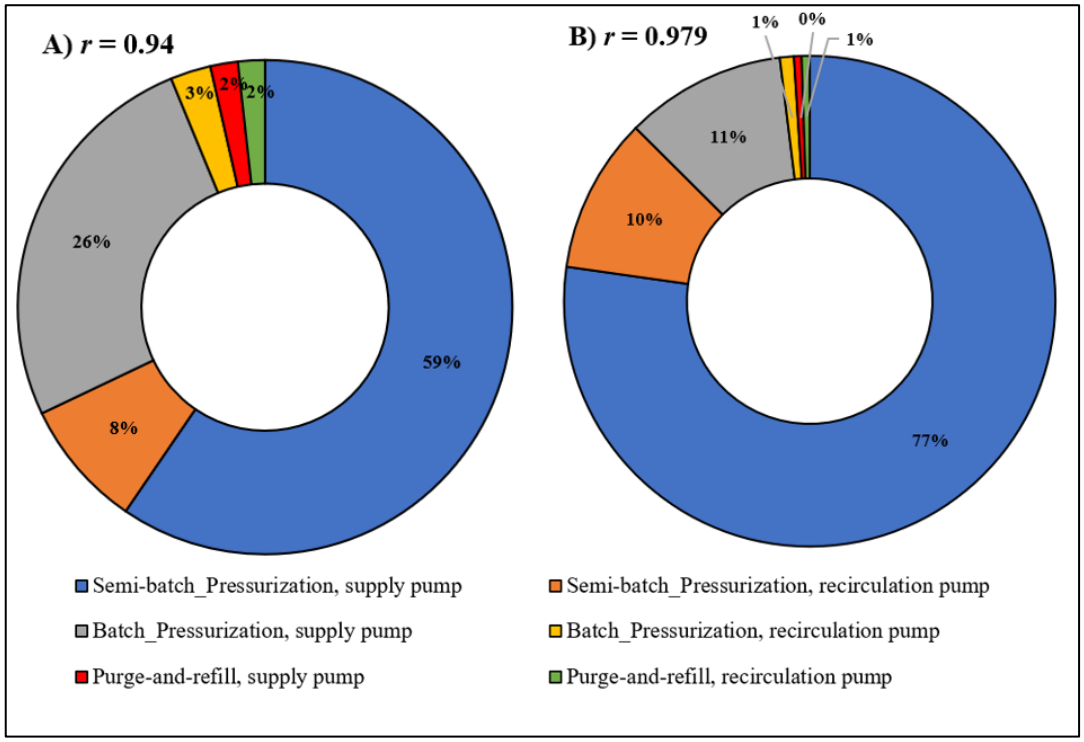

Fig. 11. Percentage contribution of each pump to total electrical *SEC* at each operation phase at feed salinity c_{feed} = 500 mg/L, flux J_w = 23.6 L/m^2/h, and recovery A) r = 0.94, and B) r = 0.979.

5.4. Permeate conductivity changes over a cycle

Fig. 12 shows how permeate quality changed over the semi-batch and batch pressurization phases at r = 0.94, J_w = 21.3 L/m^2/h, and different feed salinities. At the start of water production, permeate conductivity rose sharply, peaked after 30 s, and dropped quickly. It then increased again slowly as the recirculation stream concentration increased. The initial peak is attributed to salt diffusion after the system depressurizes. During the purge-and-refill phase, the RO module is filled with brine and, due to the concentration gradient, salt continues to pass through the membrane. When the next pressurization phase starts, this salty water leaves in the permeate thus causing this peak.

The pattern was similar to that seen in batch RO [44], but in HSBRO the peak was higher. For example, at 1,000 mg/L feed, in batch RO, conductivity peaked at only 0.3 mS/cm whereas in HSBRO it peaked at around 1.5 mS/cm. This was because of the higher recovery and concentration factor in the HSBRO case, which provided a larger concentration gradient to drive salt passage into the permeate. At 500, 1,000 and 1,500 mg/L feed concentration, permeate conductivity peaked at around 0.6, 1.5 and 2.0 mS/cm, respectively (Fig. 12A-C).

The initial conductivity peak has a detrimental effect on the overall rejection of the system. For instance, in cases A, B, and C (Fig. 12A-C), the rejection was 95.4, 94.3, and 93.9% respectively. However, if the initial peak had not occurred, rejection would have increased to 96.1, 95.2, and 94.7% respectively. In another words, salt passage (1-R_s) of the system would have decreased by 15%.

The rate of permeate conductivity increase in batch mode is higher than semi-batch mode. For example, after the initial peak, permeate conductivity increased from around 0.04 to 0.09 mS/cm in semi-batch while it increased from around 0.09 to 0.43 mS/cm in the batch phase. The reason is that in semi-batch mode the concentration at the entrance of the RO module increased linearly with time, whereas in batch mode it grew at an increasing rate.

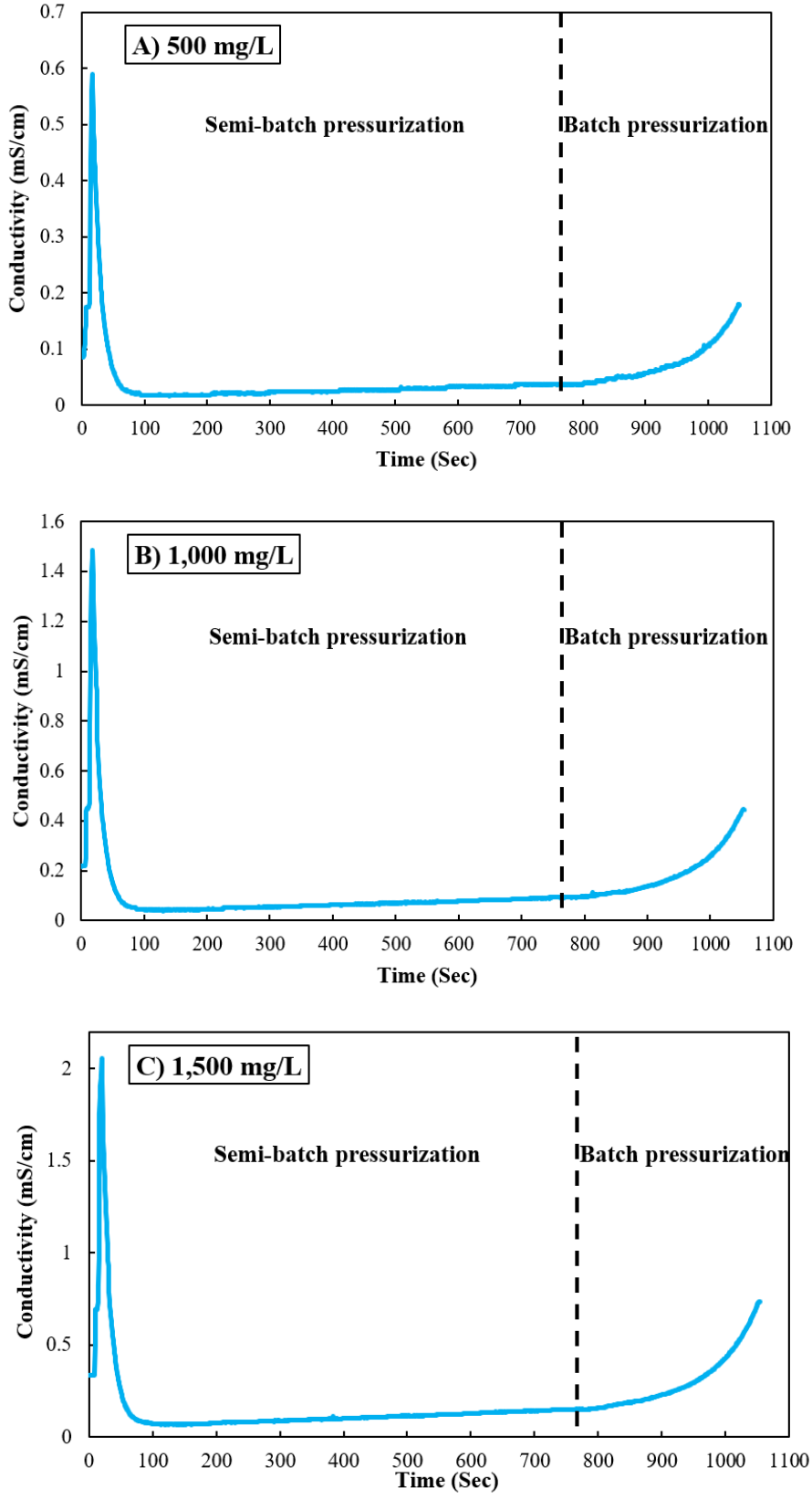

Fig. 12. Permeate conductivity vs. time over the semi-batch and batch pressurization phases at recovery $r = 0.94$, flux $J_w = 21.3$ L/m^2/h, and feed salinity A) $c_{feed} = 500$ mg/L, B) $c_{feed} = 1{,}000$ mg/L, and C) $c_{feed} = 1{,}500$ mg/L. See SI section 5 for conversion between conductivity and concentration.

5.5. Pressure and conductivity changes over a cycle

Fig. 13 shows variations against time of applied pressure and incoming solution conductivity to the RO module at r = 0.94, J_w = 18.9 L/m^2/h and feed salinity of 1,000 mg/L. Because pressure tends to increase with concentration, these two variables show similar trends over the cycle. In the semi-batch pressurization phase, with an assumption of constant rejection, concentration increases linearly since the internal loop volume is constant while solute is added at a constant rate. Therefore, the permeate that leaves the loop is replaced by the same amount of feed. However, during batch pressurization, the internal loop volume decreases linearly with time while the contained mass of solute remains constant. Consequently, concentration increases at an increasing rate as seen in Fig. 13.

We also compared the experimental peak pressure with the predicted values by the model at different water fluxes, r = 0.94, and 1,000 mg/L feed salinity (Fig. 14). Predicted values exceeded slightly the experimental results. One possible cause for the discrepancy is membrane deformation and compaction at high pressure. This may lead to increased internal volume, lower concentration, and hence lower final osmotic pressure. Another factor may be the variation in salt rejection which, though considered constant in our model, in fact increases with flux. Higher salt rejection results in higher salt retention, thus increasing the peak pressure and causing the measured peak pressure to approach the predicted one at higher fluxes.

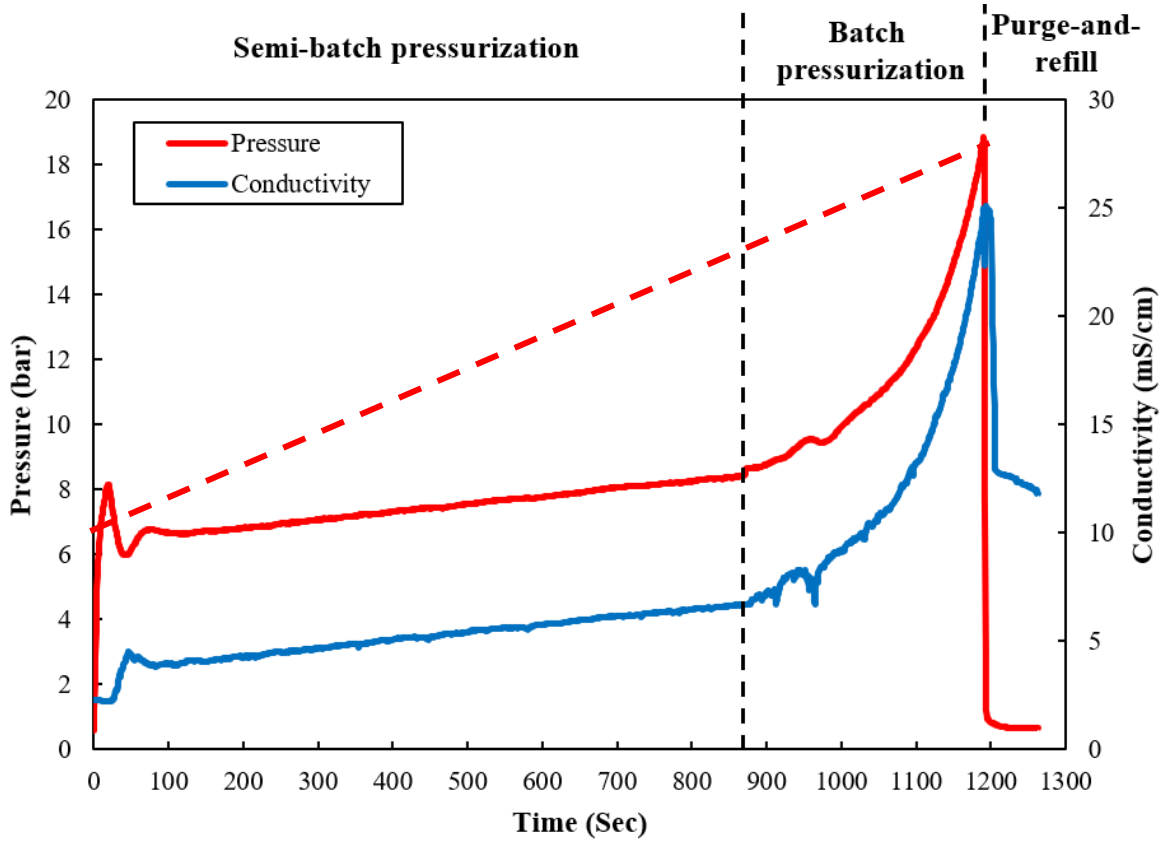

Fig. 13. Pressure and batch conductivity variations over a cycle in HSBRO system at feed salinity c_{feed} = 1,000 mg/L (r = 0.94, J_w = 18.9 L/m^2/h). The dashed line shows the linear pressure variation that would occur in non-hybrid semi-batch mode, corresponding to a higher energy consumption. See SI section 5 for conversion between conductivity and concentration.

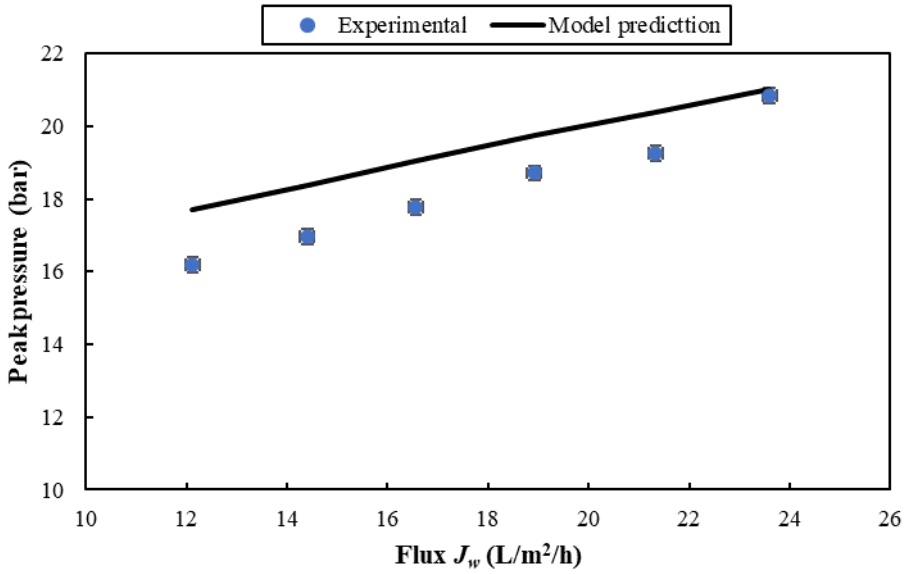

Fig. 14. Peak pressure at end of batch pressurization phase vs water flux. Model predictions and experimental values at feed salinity c_{feed} = 1,000 mg/L and recovery r = 0.94.

5.6. Recirculation flow optimization

Table 4 shows the effect of recirculation flow Q_r at the brine exit of the RO module, as a ratio to feed flow Q_f, on important parameters including pressurization *SEC* in the HSBRO system. On increasing Q_r/Q_f, recirculation pump *SEC* over the two pressurization phases increased because of the higher flow rate, while the corresponding supply pump *SEC* decreased due to lower concentration polarization and longitudinal concentration gradient. This trend is also shown by the average pressure required for the process, which decreased with Q_r/Q_f. For example, on increasing Q_r/Q_f from 1.5 to 3.7, the average required pressure decreased from 9.08 to 8.23 bar which directly reduced supply pump *SEC* during pressurization by 0.026 kWh/m^3 from 0.441 to 0.415 kWh/m^3; while the corresponding recirculation pump *SEC* increased by 0.124 kWh/m^3 from 0.027 to 0.151 kWh/m^3. Thus, by comparing total *SEC*, we found out that operation at Q_r/Q_f = 1.5 or 2.0 consumed the least energy. However, Q_r/Q_f = 1.5 gave higher peak pressure: 19.9 bar compared to only 18.8 bar at Q_r/Q_f = 2.0. Therefore, Q_r/Q_f = 2.0 was preferred as the optimum operating point. Moreover, the membrane rejection slightly improved with Q_r/Q_f which may be due to lower concentration polarization at high Q_r/Q_f. Note that the average measured rejection of 0.936 is consistent with the value of 0.94 used in the modelling.

Table 4. Effect of varying recirculation flow rate ratio (Q_r/Q_f) on the pressurization *SEC* breakdown (by pump) and on rejection, peak pressure, and average pressure over a cycle at 1,000 mg/L feed salinity, r = 0.94, and J_w = 18.9 L/m^2/h. *SEC* includes energy consumed in both semi-batch and batch pressurization phases (but not purge-and-refill phase).

Recirc. flow/feed flow Q_r/Q_f	Average pressure (bar)	Start batch pressure (bar)	Peak pressure (bar)	Rejection R_s	Electrical *SEC* over two pressurization phases (kWh/m^3)		
					Supply pump	Recirculation pump	Total
1.5	9.08	9.3	19.9	0.926	0.441	0.027	0.468
2.0	8.54	8.7	18.8	0.936	0.425	0.043	0.468
2.6	8.37	8.6	18.7	0.94	0.42	0.067	0.487
3.2	8.28	8.6	18.7	0.942	0.416	0.103	0.519
3.7	8.23	8.5	18.7	0.943	0.415	0.151	0.566

5.7. Effect of permeate flux

Besides increasing *SEC*, permeate flux affects other parameters in the HSBRO system including rejection, peak pressure and output. We investigated a range of fluxes at r = 0.952, and 1,000 mg/L feed salinity, to evaluate the effect on such parameters (Table 5). On increasing flux by nearly double, from 12.1 to 23.6 L/m^2/h, total pressurization *SEC* increased by 31% (contributed mainly by the supply pump) while system output rose by 90% from 11.56 to 21.9 m^3/day. Thus, there is a trade-off between lowered *SEC* or increased output.

Associated with this flux increase, the average pressure required during the pressurization phase increased by 46% (from 7.07 to 10.32 bar). Alongside, peak pressure increased by 27% (from 18.7 to 23.8 bar), and the switch pressure (from semi-batch to batch pressurization) increased by 114% from 7.5 to 11 bar. However, semi-batch and batch pressurization duration approximately halved. Salt rejection also increased by 4%, confirming that we can achieve higher permeate quality at high fluxes but at the expense of higher *SEC* – as in a conventional RO system.

Table 5. Effect of varying flux on measured parameters of HSBRO system at 1,000 mg/L feed salinity and recovery r = 0.952. System flux averaged over the whole cycle, including the purge-and refill phase which is non-productive.

Flux during Press. J_w (L/m^2/h)	System Flux (L/m^2/h)	Semi-batch duration (s)	Batch duration (s)	Purge-and-refill duration (s)	Transition pressure semi-batch to batch (bar)	Average pressure during pressurization phase (bar)	Rejection R_s	Output (m^3/day)	Peak Pressure $\hat{P}$ (bar)	Electrical *SEC* over two pressurization phases (kWh/m^3)		
										Supply pump	Recirculation pump	Total
12.1	11.7	1,858	504	77	7.5	7.07	0.9	11.56	18.7	0.38	0.035	0.415
14.4	13.9	1,559	424	77	8.2	7.70	0.91	13.65	19.7	0.398	0.035	0.433
16.6	15.9	1,358	367	77	8.8	8.28	0.919	15.62	20.6	0.417	0.039	0.456
18.9	18.0	1,191	322	77	9.5	8.95	0.925	17.74	21.5	0.441	0.044	0.485
21.3	20.2	1,059	286	77	10.2	9.63	0.931	19.87	22.5	0.465	0.049	0.514
23.6	22.3	946	257	76	11.0	10.32	0.936	21.91	23.8	0.49	0.055	0.544

5.8. Effect of varying switch pressure

We investigated the effect of changing the switch pressure on concentration factor, *SEC*, and peak pressure. The switch pressure determines when the system switches from semi-batch to batch pressurization. Increased switch pressure resulted in a longer semi-batch pressurization phase. These experiments were carried out at constant flux J_w = 16.5 L/m^2/h and 1,000 mg/L feed salinity.

5.8.1. Effect of switch pressure on Concentration Factor

HSBRO is a promising technology not only for water production but also for valuable component extraction from water sources. In such applications, it is desirable to concentrate maximally the feed water. Therefore, we studied the concentration factor (*CF*) which was calculated using Eq. (26). Fig. 15A shows the increase of *CF* and recovery with switch pressure. A longer semi-batch pressurization phase resulted in a higher concentration at the onset of batch pressurization and thus a higher final concentration. When switch pressure rose from 8.1 to 10.2 bar, semi-batch duration increased from 1,117 to 1,976 s, *CF* increased by 51% from 16.3 to 24.6, and recovery increased from r = 0.943 to r = 0.963.

5.8.2. Effect of switch pressure on SEC

SEC also increased with switch pressure. Hydraulic *SEC* increased by 13% from 0.242 to 0.274 kWh/m^3 while electrical *SEC* increased by 7% from 0.459 to 0.491 kWh/m^3 (Fig. 15B). As explained in section 5.3, electrical *SEC* increased less because of the higher efficiency of the supply pump at higher operating pressures.

5.8.3. Effect of switch pressure on peak pressure

Fig. 15C shows that peak pressure increased alongside *CF*, reaching a maximum of 24.8 bar at a switch pressure of 10.2 bar, while the average pressure was 9.14 bar. As 25 bar was the design limit of our experimental system, this peak pressure limited the *CF* that could be achieved. However, future systems with higher pressure ratings will enable even higher *CF*.

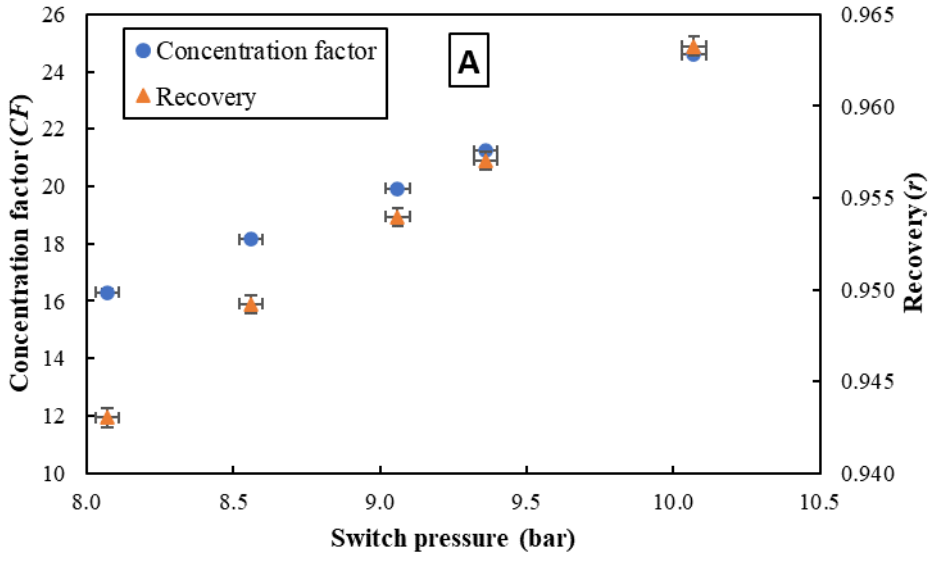

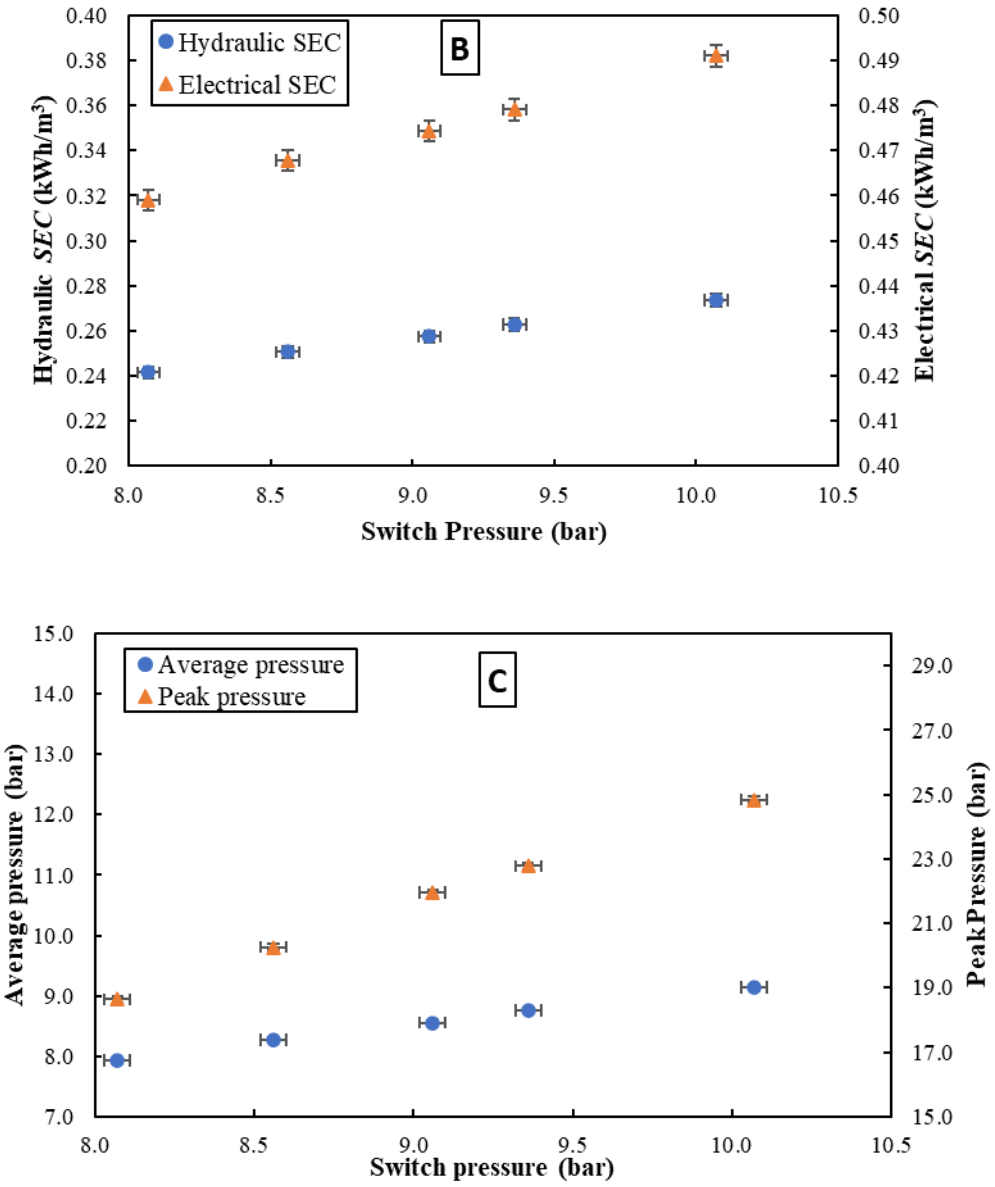

Fig. 15. Effect of varying switch pressure on: A) concentration factor (*CF*) and recovery (*r*), B) hydraulic and electrical *SEC*, C) Average and peak pressure. Feed salinity 1,000 mg/L and J_w = 16.5 L/m^2/h.

6. Discussion

6.1. Comparison with non-hybrid systems

To compare the HSBRO system against the options of non-hybrid semi-batch RO or batch RO, we used our validated model to compare the three options in achieving a recovery of 0.94 (see Table 6).

Table 6. Comparison of HSBRO against non-hybrid options (r = 0.94, J_w = 18.9 L/m^2/h, feed concentration of 1,000 mg/L, 60% pump efficiencies assumed throughout all phases; 8-inch Eco Pro-440 membrane as in this study).

Option	Hydraulic *SEC* (kWh/m^3)	Electrical *SEC* (kWh/m^3)	Work exchanger volume V_{b0} (L)	Notes
Semi-batch RO	0.415	0.692	0	
Batch RO	0.254	0.423	265.0	
HSBRO	0.255	0.425	69.0	Current study
HSBRO	0.273	0.455	40.0	Reduced work exchanger volume

The results show that the *SEC* of the HSBRO is close to that of the batch RO, while the work exchanger volume (V_{b0}) is around four times smaller; 69 L for HSBRO compared to 265 L for batch RO. This confirms that the HSBRO option is advantageous in achieving a low *SEC* (almost as low as with batch RO) with a much more compact work exchanger. In semi-batch RO, although there is no need for a work exchanger, the *SEC* is almost 63% higher than HSBRO and batch RO. The fourth row in Table 6 shows that a further reduction in work exchanger may also be acceptable to make the system even more compact. A reduction in V_{b0} from 69 to 40 L increases *SEC* by just 7%.

6.2. Comparisons against existing systems

In this section, we compare our results against earlier studies with the help of second law efficiency. Second law efficiency is defined as the ratio of the minimum work of separation to the total actual work consumed in the desalination process. It illustrates how closely systems work to the reversible thermodynamic limit (a fully reversible system has a second law efficiency of 100%) and can help identify potential for improvement. We use second law efficiency to make a fair comparison against other studies, taking into account variations in recovery and feed concentration.

To ensure a fair comparison, we have applied certain criteria in selecting those studies against which to compare. Firstly, the systems should be high recovery. At recovery below about 70%, the HSBRO system is probably not needed; a non-hybrid batch RO system would be adequate, as described previously [44]. Secondly, we have selected systems using brackish feed, rather than seawater feed, as seawater systems typically provide a significantly higher 2nd law efficiency [65] such that direct comparison with brackish water systems could be misleading. In addition, seawater systems rarely achieve recovery above 70%. Thirdly, we have selected only experimental (not theoretical) studies, in which the systems have been piloted at least at laboratory scale. Fourthly, the systems selected are ones where second law efficiency is reported, or where sufficient information is given for second law efficiency to be calculated. The studies selected are mostly multi-stage RO systems, or batch or semi-batch RO systems.

Although batch RO is theoretically the most efficient configuration in RO systems, comparison of HSBRO and batch RO at 1,000 mg/L showed that second law efficiency of HSBRO is actually slightly higher than batch RO: 13.1% (see Table 6) against 9.2% (calculated using Eq. 25 and data in [44]). Electrical *SEC* for both systems were nearly the same around 0.49 kWh/m^3, even though the HSBRO achieves much higher recovery. This finding is consistent with [15] and explained by reduction in minor losses in the refill stage of HSBRO. The SEC_{ideal} of HSBRO is slightly larger than for batch RO, because of the higher recovery, resulting in improved second law efficiency.

Semi-batch RO (or closed-circuit RO) is another configuration that attracted much attention over the last decade. Efraty et al. [17] reported electrical *SEC* of 0.77 kWh/m^3 for two cases using semi-batch RO. In the first case, the feed conductivity was 6.8 mS/cm, recovery r was 0.8, flux J_w = 19 L/m^2/h, the high-pressure pump efficiency was 55%, and rejection of 90.8% was achieved. In the second case, feed conductivity was 4.0 mS/cm, recovery r was 0.88, flux J_w was 27 L/m^2/h, the high-pressure pump efficiency was 60%, and rejection of the system was 88%. Since the authors did not mention the feed analysis, by assuming that the feed source is like a NaCl solution, we calculated the osmotic pressure and then second law efficiency. The latter had values of 20.5 and 13.6% for the first and second cases respectively. Considering the same feed salinity, fluxes, and pump efficiencies as cases 1 and 2 but at a higher recovery of r = 0.94 in HSBRO, we predict electrical *SEC* of 0.93 and 0.69 kWh/m^3 for these two cases in the HSBRO system. These values correspond to second law efficiencies of approximately 24.4 and 18.4% respectively – as such considerably better than the values of 20.5 and 13.6% mentioned above for semi-batch RO. Additionally, considering the same recovery as cases 1 and 2, we predict electrical *SEC* of 0.69 and 0.49 kWh/m^3 in the HSBRO system respectively. Corresponding second law efficiency values were 22.9 and 21.3%.

Kahraman et al. [54] reported second law efficiency of 8% for a two-stage brackish RO plant at a feed concentration of 900 mg/L and recovery r = 0.72. However, using their data and Eq. (25), second law efficiency was calculated 3.8% which is around three times lower than the value of 13.1% for the HSBRO system at 1,000 mg/L feed. Second law efficiency of only 4.1% was reported for a two-stage RO plant in Jordan using actual plant data [59]. This plant was fed with brackish water of 2,450 mg/L salinity (electrical conductivity of 3.95 mS/cm) and a combined pump-motor efficiency of 75% was used in the calculations. In another case study, Sharqawy et al. [66] analysed the performance of a RO plant in California (USA) fed with underground brackish water at a salinity of about 1,550 mg/L. The value reported for the second law efficiency was 1.51% considering pump efficiency of 100%. At similar feed salinity in the HSBRO system, we achieved second law efficiency of 17.8%. It is also interesting that they calculated how much second law efficiency would increase by adding an energy recovery device; the predicted increase was marginal from 1.51 to 1.73%. More recently, a medium-sized two-stage brackish RO plant of the Arab Potash Company with r = 0.68 was analysed. This plant was fed with brackish water with a salinity of 1098.6 mg/L and second law efficiency of 4.48% was reported for the whole RO plant [67].

We also believe that HSBRO can improve second law efficiency for more saline feeds including seawater. This will be evaluated in future studies.

6.3. Potential improvements

In this section, we use our validated model to assess the benefits of future improvements to the HSBRO system.

6.3.1. Effect of membrane water permeability on hydraulic SEC

Thanks to advances in membrane material and manufacturing technology, the water permeability of RO membranes has gradually improved over the last few decades, while high salt rejection has been maintained [68]. We expect this trend to continue. Therefore, we have predicted the effect of improved water permeability on hydraulic *SEC* (see Fig. 16). We assumed 1,000 mg/L feed concentration, J_w = 18.9 L/m^2/h, and r = 0.94. We project that, by increasing membrane water permeability from 3 to 6 and 9 L/m^2/h/bar, the hydraulic *SEC* will decrease by 29.1 and 39.0% respectively (from 0.313 to 0.222 and 0.191 kWh/m^3). The membrane element used in this study (Eco Pro-440) had a water permeability of A_w = 4.4 L/m^2/h/bar, as measured experimentally using RO permeate water and confirmed throughout this study.

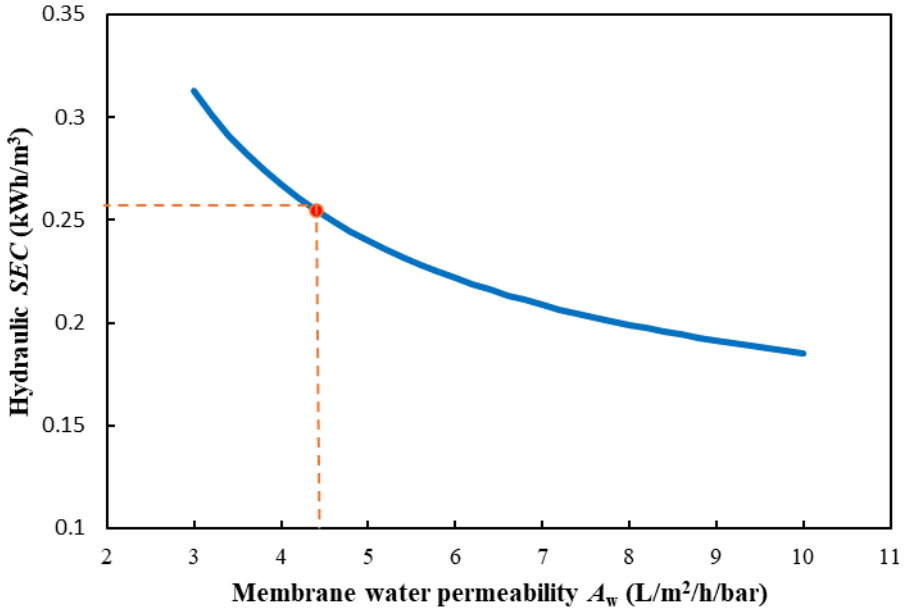

Fig. 16. Predicted hydraulic *SEC* as a function of membrane water permeability (*A* value) at 1,000 mg/L feed concentration, r = 0.94, and J_w = 18.9 L/m^2/h. The orange point indicates the experimental value for the Eco Pro-440 membrane used in this study.

6.3.2. Effect of valve size on hydraulic SEC

Fig. 17 shows the effect of valve orifice diameter on hydraulic *SEC* in the HSBRO system. The model predicted how hydraulic *SEC* will change on changing the valve size at 1,000 mg/L feed concentration, J_w = 18.9 L/m^2/h, and r = 0.94. On increasing the valve orifice diameter from 15 (current study) to 20 and 25 mm, hydraulic *SEC* will reduce by 5.4 and 6.9%. This energy saving results from a reduction in friction losses [44].

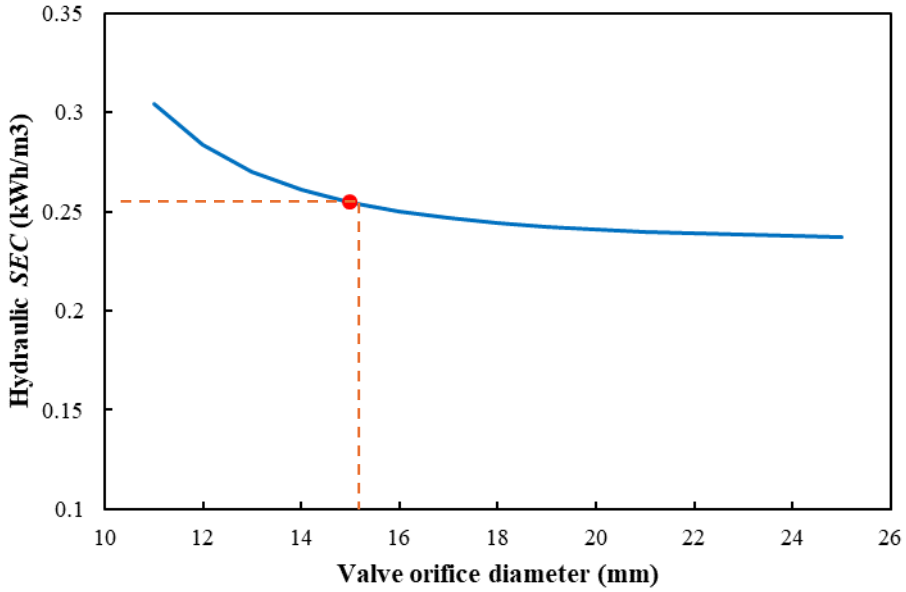

Fig. 17. Model predictions of hydraulic SEC as a function of valves diameter in the HSBRO system at 1,000 mg/L feed concentration, J_w = 18.9 L/m^2/h, and r = 0.94. The orange point is the valve diameter used in the current prototype.

6.3.3. Effect of pump efficiency on hydraulic SEC

As discussed in section 5.3, pump efficiencies have a considerable impact on the total electrical energy consumed by the HSBRO system. More efficient pumps will lower electrical *SEC*, making the HSBRO system even more attractive for various industries and applications. Fig. 18 compares electrical *SEC* of the current HSBRO against some hypothetical cases (assuming the same efficiency for both pumps during all three operation phases) at different feed salinities, J_w = 18.9 L/m^2/h, and r = 0.94. As can be seen, with pump efficiency uniformly improved to 60%, electrical *SEC* would decrease by 20, 12.7, and 4.3% at 500, 1,000, and 1,500 mg/L feed concentrations respectively. However, by implementing pumps with 80% efficiency, electrical *SEC* would reduce by 40% (from 0.42 to 0.252 kWh/m^3), 34.7% (from 0.487 to 0.318 kWh/m^3), and 28.4% (from 0.536 to 0.384 kWh/m^3) at 500, 1,000, and 1,500 mg/L respectively.

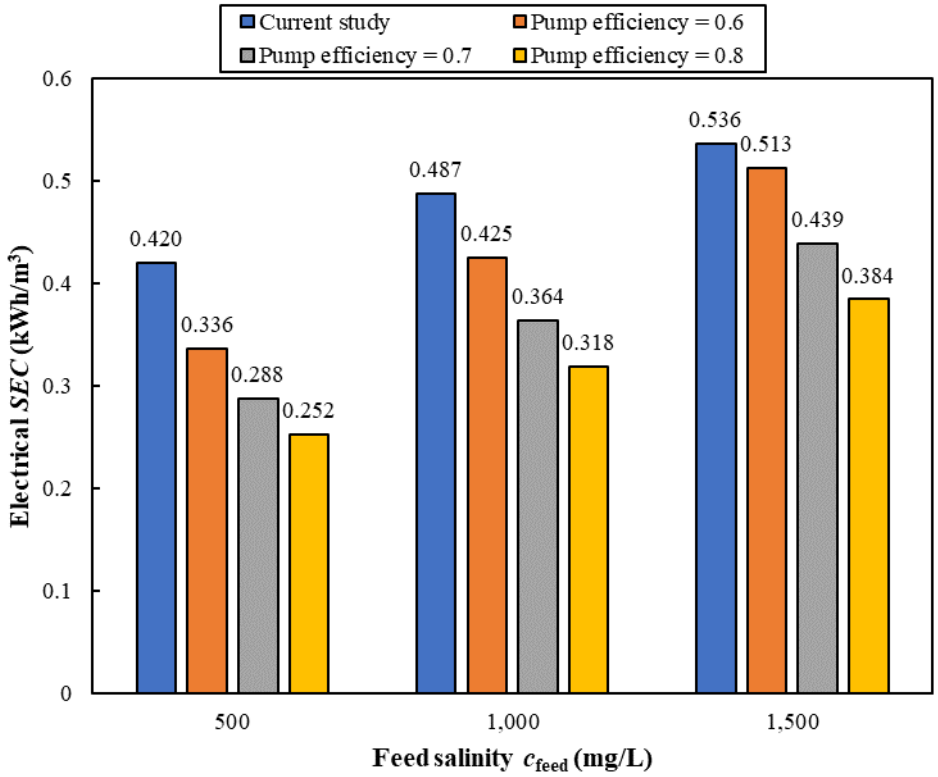

Fig. 18. Projection of electrical *SEC* according to pump efficiencies at various feed salinities, J_w = 18.9 L/m^2/h, and r = 0.94.

6.3.4. Combined improvements

To reduce overall *SEC* further, the above improvements of high-permeability membranes, more efficient pumps, and bigger valve size can be combined for the best overall performance. Accordingly, we modelled the overall electrical *SEC* of the HSBRO system assuming membranes with a permeability of A_w = 10 L/m^2/h/bar, valve orifice diameter of 25 mm, and 80% efficiency for both pumps. Table 7 shows the predicted results at different feed salinities, with J_w = 18.9 L/m^2/h, and r = 0.94. These predictions are also compared with the ideal system (calculated by Eq. 25) and the experimental measurements for the current system. Furthermore, Table 7 shows second law efficiency (SEC_{ideal}/SEC) for general comparison against existing RO plants.

With all three improvements implemented, electrical *SEC* of the HSBRO system would decrease by 66.0%, 56.9%, and 48.5% at 500, 1,000, and 1,500 mg/L feed concentrations respectively. This corresponds to a considerable electrical *SEC* decrease from the range of 0.42-0.536 to that of 0.143-0.276 kWh/m^3 at 500-1,500 mg/L feed concentration. Nevertheless, the predicted *SEC* after improvements remains higher than SEC_{ideal}, showing that there is still room for improvement.

Table 7. Theoretical minimum *SEC* comparison with the experimental results for the current HSBRO system, and with predicted electrical *SEC* after improvements in membrane water permeability (A_w = 10 L/m^2/h/bar), pump efficiencies (80% for both supply and recirculation pumps) and valve orifice diameter (25 mm) at various feed salinities, J_w = 18.9 L/m^2/h, and r = 0.94. The corresponding second law efficiency (SEC_{ideal}/SEC) is also shown.

Feed salinity	Ideal system	Current HSBRO system	Model predictions after improvements

c_{feed} mg/L	SEC_{ideal} (kWh/m^3)	Electrical *SEC* (kWh/m^3)	Second law efficiency (%)	Electrical *SEC* (kWh/m^3)	Second law efficiency (%)
500	0.0325	0.420	7.8	0.143	22.8
1,000	0.0640	0.487	13.1	0.210	30.5
1,500	0.0953	0.536	17.8	0.276	34.5

6.4. Operation at higher salinities

Today's RO systems are limited to about 120 bar, as determined by the maximum allowable pressure specified by membrane manufacturers. Therefore, peak pressure is an important consideration if the HSBRO system is to operate at high recovery, such as $r = 0.95$, and at high feed salinity. The Eco Pro-440 module used for treating brackish water in this study is limited to 41 bar. Using this membrane specification in our experimentally validated model, we predicted the performance of the HSBRO system up to 4,000 mg/L feed concentration at two recoveries, $r = 0.90$ and 0.95 (see Table 8). Electrical *SEC* was calculated assuming 60% pump efficiency for both pumps. Additionally, for higher concentrations, we applied XUS180808 module specifications *i.e.* membrane area of 30.6 m^2 and permeability of $A_w = 1.39$ L/m^2/h/bar based on the manufacturer's datasheet. This module can withstand pressures up to 120 bar.

Using the Eco Pro-440 module, HSBRO can desalinate feed sources up to around 4,000 mg/L at $r \geq 0.9$ and $J_w = 18.9$ L/m^2/h, while staying within the peak pressure limitation of 41 bar. Although peak pressure seems to be a major limitation for HSBRO, in all cases presented in Table 8 for this module, average pressure during semi-batch and batch phases will not exceed 11.7 and 21 bar respectively, meaning that the operating pressure is lower than the 41 bar limit during most of the cycle. Operation at pressures near the limit occur only during the last seconds of the batch pressurization phase and last for a short period of time (less than 3% of process time). Thus, we do not expect that the module would be damaged since this limitation applies to continuous operation normally. Nonetheless, by reducing the duration of semi-batch pressurization (resulting in lower recovery), we can decrease the peak pressure and eliminate this risk. For example, at 3,000 mg/L feed concentration, although the average batch pressure is 29.1 bar, the peak pressure reaches 60 bar, clearly exceeding the 41 bar limit. Therefore, by reducing the recovery to $r = 0.923$, we predict that the peak pressure will decrease to 40.7 bar, which is within the limit for the Eco Pro-440 module.

Regarding *SEC* using the Eco Pro-440 module, hydraulic *SEC* ranges from 0.268–0.431 kWh/m^3 and electrical *SEC* ranges from 0.446–0.718 kWh/m^3 at 1,000–3,000 mg /l feed salinity, with $J_w = 18.9$ L/m^2/h, and $r = 0.95$ (except at 3,000 mg/L feed solution where recovery is reduced to $r = 0.923$). However, at $r = 0.9$, these values decrease to 0.234–0.398 kWh/m^3 for the hydraulic *SEC,* and 0.391–0.663 kWh/m^3 for electrical *SEC.* Maximum achievable recovery at 4,000 mg/L (observing the pressure limit) is $r = 0.9$ and gives hydraulic and electrical *SEC* of 0.48 and 0.799 kWh/m^3, respectively. Additionally, for this module at $r \geq 0.9$ and $R_s = 0.94$, we predict second law efficiency ranging from 14.2% at 1,000 mg/L to 27.8% at 4,000 mg/L – a substantial improvement on earlier studies mentioned in section 6.2.

We also predict that the HSBRO system using an ultra-high pressure XUS180808 module can treat water sources with salinity up to 10,000 mg/L while operating at recoveries higher than $r \geq 0.9$, at flux $J_w = 18.9$ L/m^2/h, without exceeding the pressure limit of 120 bar. For instance, when operating at $r = 0.9$, peak pressure varies from 57–115 bar at feed salinities

ranging from 4,000–10,000 mg/L while semi-batch and batch average pressure is in the range of 30–37 and 35–60 bar, respectively. Hydraulic *SEC* is in the range 0.9–1.41 kWh/m^3 while electrical *SEC* is 1.5–2.35 kWh/m^3. Furthermore, second law efficiency ranges from 14.8–23.7%. Such high feed salinity and high recovery is important for ZLD applications.

Comparing the two membranes at r = 0.9 and 4,000 mg/L feed salinity, the hydraulic *SEC* of the XUS180808 module is almost twice that of the Eco Pro-440 module; 0.9 against 0.48 kWh/m^3. The main reason for this increase is the lower permeability of the XUS180808 compared to the Eco Pro-440 membrane. Future work will include verifying the performance with the XUS180808 or similar membranes, noting that there are several practical challenges to address in implementing such high-pressure RO systems [69].

Table 8. Prediction of hydraulic and electrical *SEC* (assuming 60% pump efficiency for both pumps), peak and average pressure for the HSBRO system at a wide range of feed salinities, J_w = 18.9 L/m^2/h, and two different recoveries. The prediction is based on the properties of the Eco Pro-440 membrane (41 bar limit) and the ultra-high pressure XUS180808 membrane (120 bar limit). Second law efficiency was calculated assuming rejection of R_s = 0.94. The italicized values (marked not applicable, NA) of peak pressure show where the limit is exceeded and therefore recovery must be decreased to lower the peak pressure. Recoveries corresponding to operation near the pressure threshold are marked *.

Membrane type	Feed salinity (mg/L)	Recovery	Hydraulic *SEC* (kWh/m^3)	Electrical *SEC* (kWh/m^3)	Peak pressure (bar)	Average semi-batch pressure (bar)	Average batch pressure (bar)	Second law efficiency (%)
BW Eco Pro-440	1,000	0.95	0.268	0.446	23.1	7.6	12.8	15.2
		0.9	0.234	0.391	13.9	6.2	8.7	14.2
	2,000	0.95	0.390	0.649	41.6	10.9	20.9	20.9
		0.9	0.316	0.527	23.2	8.1	12.8	21.1
	3,000	0.95 *(NA)*	0.512 *(NA)*	0.853 *(NA)*	*60 (NA)*	14.2 *(NA)*	29.1 *(NA)*	*(NA)*
		0.923*	0.431	0.718	40.7	11.2	20.5	25.1
		0.9	0.398	0.663	32.4	9.9	16.9	25.2
	4,000	0.95 *(NA)*	0.633 *(NA)*	1.056 *(NA)*	*78.6 (NA)*	17.4 *(NA)*	37.3 *(NA)*	*(NA)*
		0.9	0.480	0.799	41.5	11.7	21	27.8
XUS 180808 (Ultra-high pressure)	4,000	0.95	1.043	1.738	95.1	31.5	51.3	15.6
		0.9	0.900	1.501	57.4	25.9	35.2	14.8
	5,000	0.95	1.167	1.945	114.2	34.7	59.4	17.4
		0.9	0.985	1.642	67	27.7	39.3	16.9
	6,000	0.95 *(NA)*	1.291 *(NA)*	2.152 *(NA)*	*133.3 (NA)*	37.9 *(NA)*	67.6 *(NA)*	*(NA)*
		0.94*	1.217	2.028	114.8	35.2	59.7	19.1
		0.9	1.070	1.783	76.7	29.6	43.4	18.7
	7,000	0.95	NA	NA	NA	NA	NA	NA
		0.93*	1.264	2.107	114.6	35.5	59.6	20.5
		0.9	1.155	1.925	86.4	31.4	47.6	20.2
	8,000	0.95	NA	NA	NA	NA	NA	NA
		0.92*	1.316	2.193	115.7	36.1	60	21.7
		0.9	1.240	2.067	96.1	33.2	51.7	21.5
	9,000	0.95	NA	NA	NA	NA	NA	NA
		0.91*	1.362	2.270	115.3	36.5	59.9	22.8
		0.9	1.325	2.208	105.7	35.1	55.8	22.7
	10,000	0.95	NA	NA	NA	NA	NA	NA
		0.9	1.410	2.350	115.4	36.9	60	23.7

Fig. 19 gives an overall summary of the above findings regarding second law efficiency of the HSBRO and other comparable systems. For HSBRO, it shows experimental values and those predicted after improvements to the system. It also includes model predictions at higher feed salinities using two different RO modules. For comparison, Fig.19 further includes experimental results from batch RO and other experimental studies in high-recovery RO. Second law efficiency in HSBRO and batch RO generally increases with feed salinity. At similar salinity, HSBRO gave the highest second law efficiency compared to other studies (even batch RO) and this can be increased further by implementing some improvements such as more efficient pumps and high permeability membranes.

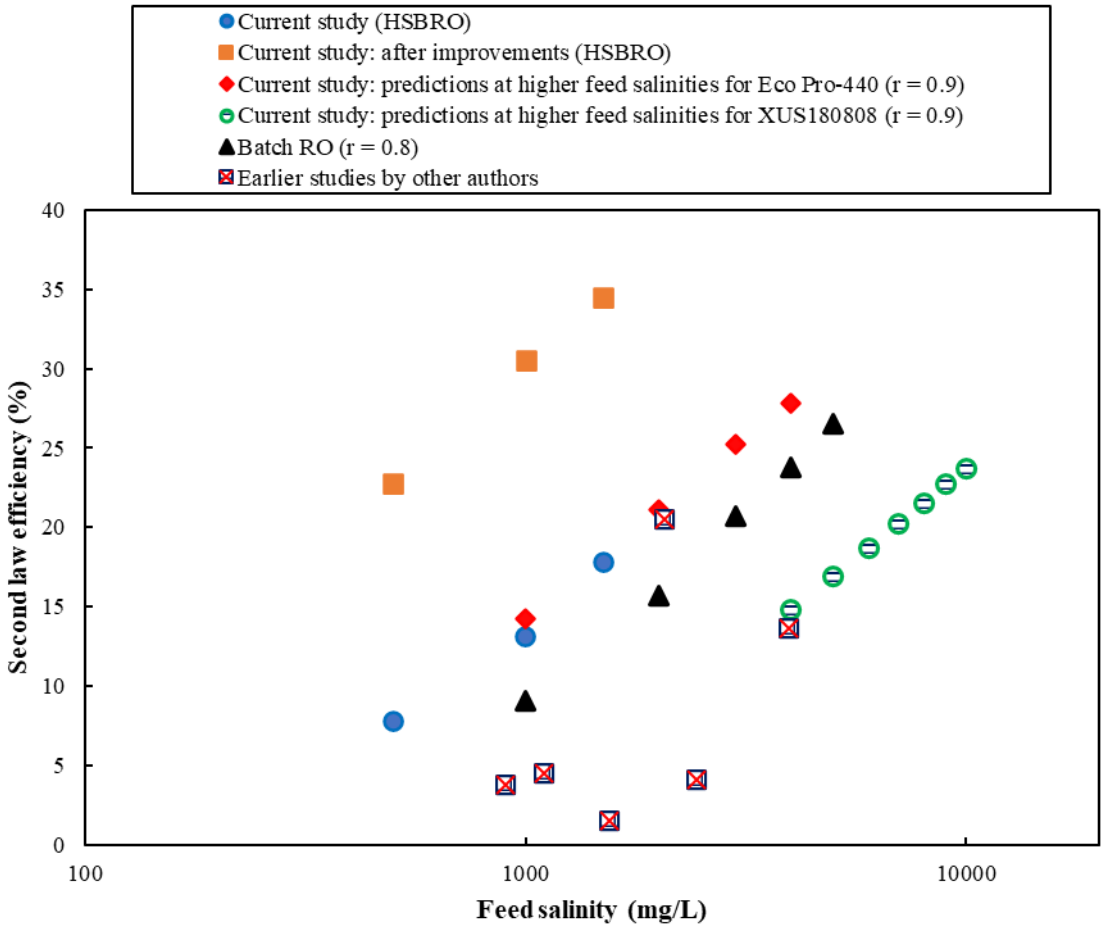

Fig. 19. Comparison of second law efficiency in the current study against batch RO and other earlier experimental RO studies, as a function of feed salinity.

6.5. Further improvements and future research

Future developments of the HSBRO system could also include modifications at the brine outlet to retard the pressure surge at the beginning of the purge-and-refill phase. It is possible that such an arrangement could reduce the amount of osmotic backflow and recover a small amount of energy. Based on an initial estimate of the hydraulic energy contained in the pressure surge, the potential for energy recovery is limited to about 2% of overall SEC but may be worth considering for future optimization.

Another development may concern the design of the supply pump arrangement. As seen in Table 3 above, the efficiency of the supply pump dropped from about 60% to only ~10% during

purge and refill. This is because the supply pump is a positive displacement pump that is not optimized to run at low pressure. A centrifugal pump would likely achieve efficiency >50%, thus substantially reducing the electrical *SEC* contribution during purge and refill, which currently accounts for about 1–5% of total *SEC*. Therefore, it may be beneficial to use a combination of a positive displacement pump (for pressurization) and a centrifugal pump (for purge and refill) – albeit at the cost of added complexity.

In future research, the inherent advantages and energy losses of HSBRO may further be investigated based on theoretical analyses. It would be valuable to carry out a complete exergy analysis (in comparison to multi-stage RO, semi-batch RO, and advanced system designs such as EERO) and to present the results with the help of Sankey and Grassman diagrams.

7. Conclusions

For the first time in RO studies, we experimentally investigated the performance of a hybrid semi-batch/batch RO (HSBRO) system. Using a single-acting free-piston design and an 8-inch RO module (Eco Pro-440), HSBRO achieves an output of 15–22 m^3/day at recovery of 0.94. The HSRBO is no more complex than batch RO, requiring only a modification to the controller program to alter the sequence of valve operation. The main conclusions are:

- Operating at flux J_w = 18.9 L/m^2/h, recovery r = 0.94, and feed concentrations c_{feed} of 500 to 1,500 mg/L, HSBRO gives hydraulic and electrical *SEC* in the range of 0.2–0.31 and 0.42–0.54 kWh/m^3 respectively, with an output of 17.5 m^3/day, and salt rejection of R_S = 93–94%.
- The greatest component of energy consumption comes from the supply pump during the pressurization phases, which contributes 86–89% of the total *SEC*; whereas the recirculation pump contributes only 10–12% over the whole cycle. Optimum recirculation flow (at the RO module brine outlet) to the feed pump flow is around 2; at higher flow ratios, the total *SEC* increases substantially (although slightly higher salt rejection is achieved).
- An updated and validated model gives *SEC* agreement of 1–3% with experiment, using explicit algebraic equations thus avoiding the need for numerical algorithms. Two important adjustable parameters were used in the model: membrane permeability and system salt rejection.
- When the system reaches a stable condition, salt retention between cycles causes the initial concentration to be around 89% higher than the feed concentration, increasing the applied pressure and energy consumption. This can be reduced to 44% by purging for longer, thus saving 7% in electrical *SEC* (but at the expense of system recovery falling from 94 to 91.3%). The updated model accurately represents salt retention, taking into account both salt rejection and osmotic backflow.
- Due to salt diffusion during the purge-and-refill phase, there is an initial peak in the permeate quality which has a negative effect on salt rejection, causing a 0.6–0.9% decrease in the total rejection of the system.
- A concentration factor of 24.6 and recovery r = 0.96 are achieved at feed salinity c_{feed} = 1,000 mg/L with electrical *SEC* <0.5 kWh/m^3, making HSBRO an attractive option that can be implemented in many industries particularly for extraction of valuable components from effluents. Using ultra high-pressure RO membranes that have recently become available, we will be able to achieve even higher concentration factors.

- Compared to semi-batch RO under similar conditions, HSBRO consumes 63% less energy. Compared to batch RO, although HSBRO energy consumption is almost the same, the HSBRO work exchanger size is almost four times smaller at recovery r = 0.94. HSBRO can achieve recovery up to r = 0.98 at low feed salinities, just by operating for longer in semi-batch mode.
- Second law efficiency is in the range of 7.8–17.8% for feed concentrations of 500–1,500 mg/L. The second law efficiencies measured equal or exceed those for other high-recovery experimental systems reported in the literature (not only multi-stage RO systems but also the batch and semi-batch RO).
- The validated model enables us to predict the effect of improvements, such as using high-permeability membranes and more efficient pumps, to lower electrical *SEC* to 0.14–0.28 kWh/m^3 and improve second law efficiency up to 34.5% for feed salinities of c_{feed} = 500–1,500 mg/L
- With ultrahigh-pressure RO membranes, the model predicts that feed solutions with concentration c_{feed} = 10,000 mg/L can be treated, with recovery $r \geq 0.9$, hydraulic $SEC < 1.4$ kWh/m^3 and second law efficiency up to 23.7%.

The hybrid concept allows energy efficiency close to that of batch RO, even at very high recoveries $r \geq 0.94$, in a much more compact arrangement. Nonetheless, there are still challenges in scaling this solution to larger systems with output greater than about 100 m^3/day. Therefore, future work should focus on this scale up challenge. There is also a need for experimental work at higher pressures to validate the predictions for highly concentrated feed and brine solutions, as needed for ZLD and MLD applications. This should include studies of organic and inorganic fouling using substances encountered in such applications.

Nomenclature

Roman and Greek symbols

A_w	L/m^2/h/bar, Water membrane permeability
A_m	m^2, Membrane area
c	mg/L, Concentration
$\bar{c}$	mg/L, Average of initial and final concentration
c_0	mg/L, Initial concentration of semi-batch phase
c_1	mg/L, Initial concentration of batch phase
c_{feed}	mg/L, Feed concentration
c_{max}	mg/L, Initial concentration leaving the system at the start of the purge phase
$c_{permeate}$	mg/L, Permeate concentration
C_d	-, Coefficient of discharge
E	kJ (kWh), Energy consumption
E_{P1}	kJ (kWh), Energy consumption of semi-batch pressurization phase
E_{P2}	kJ (kWh), Energy consumption of batch pressurization phase
$E_{P\&R}$	kJ (kWh), Energy consumption of purge-and-refill phase
J_w	m/s (L/m^2/h), Permeate flux
P	kPa (bar), Pressure
$\bar{P}$	kPa (bar), Volume-weighted average pressure
$\bar{P}_1$	kPa (bar), Volume-weighted average pressure during semi-batch phase

$\overline{P_2}$	kPa (bar), Volume-weighted average pressure during batch phase
$\hat{P}$	kPa (bar), Maximum peak pressure
Q	m^3/s, Flow rate
Q_f	m^3/s, Feed flow rate
Q_r	m^3/s, Recirculation flow rate
R_s	–, Salt rejection
r	–, Recovery
r_b	–, Recovery in batch phase
r_p	–, Recovery in pressurization phase
r_{sb}	–, Recovery in semi-batch phase
S_{L1}	–, Longitudinal concentration gradient factor during semi-batch phase
S_{L2}	–, Longitudinal concentration gradient factor during batch phase
S_P	–, Concentration polarization factor
S_R	–, Salt retention factor
V	m^3, Volume
V_0	m^3, Initial volume of the system
V_{b0}	m^3, Work exchanger swept volume
V_{back}	m^3, Backflow volume
V_{brine}	m^3, Brine volume
V_{feed}	m^3, Feed volume
$V_{permeate}$	m^3, Permeate volume
V_{pg}	m^3, Nominal purge volume
$V_{pipe,R}$	m^3, Retained solution volume in pipes
V_{sb}	m^3, Volume supplied during the semi-batch phase
ΔP	kPa, Pressure drop
ΔP_m	kPa, Cross-flow pressure drop in the RO module
ΔP_s	kPa, Piston seal pressure drop
ΔP_v	kPa, Valve pressure drop
ΔP_{v1}	kPa, Bypass valve pressure drop
ΔP_{v2}	kPa, Recirculation valve pressure drop
ΔP_{v3}	kPa, Brine valve pressure drop
Π_{feed}	kPa, Feed osmotic pressure
λ	–, Longitudinal dispersion parameter

Abbreviations

CF	Concentration factor
COMRO	Cascading osmotically mediated reverse osmosis
CRO	Centrifugal Reverse Osmosis
CT	Conductivity transmitter
EERO	Energy Efficient Reverse Osmosis
ERD	Energy recovery device
EXP	Experimental
FT	Flow transmitter
HPRO	High pressure reverse osmosis
HSBRO	Hybrid semi-batch/batch reverse osmosis
LSRRO	Low salt rejection reverse osmosis
MLD	Minimum Liquid Discharge
MOD	Model
MVC	Mechanical vapour compression
OARO	Osmotically assisted reverse osmosis

P	Pressurization
PFD	Plug flow desalination
P&R	Purge-and-refill
PT	Pressure transmitter
RO	Reverse osmosis
FO	Forward osmosis
UF	Ultrafiltration
RP	Recirculation pump
SEC	Specific energy consumption
SI	Supporting Information
W1	Weighing platform (feed tank)
W2	Weighing platform (permeate tank)
W3	Weighing platform (brine tank)
ZLD	Zero liquid discharge

Acknowledgements

This project has received funding from the European Union's Horizon 2020 research and innovation programme under grant agreements No 820906 and No 958545, and from the National Research Foundation of Korea (NRF) grant funded by the Korean government (MSIT) (No. NRF-2021R1F1A1055769).

Supplementary material

The supplementary material includes the Supporting Information (SI), the files of raw experimental data (as indexed and explained and SI section 5), and the spreadsheet containing the model presented in this paper.

References

[1] M. Elimelech, A. Phillip William, The Future of Seawater Desalination: Energy, Technology, and the Environment, Science, 333 (2011) 712-717.
[2] P.S. Goh, H.S. Kang, A.F. Ismail, N. Hilal, The hybridization of thermally-driven desalination processes: The state-of-the-art and opportunities, Desalination, 506 (2021) 115002.
[3] K. Park, J. Kim, D.R. Yang, S. Hong, Towards a low-energy seawater reverse osmosis desalination plant: A review and theoretical analysis for future directions, Journal of Membrane Science, 595 (2020) 117607.
[4] E. Jones, M. Qadir, M.T.H. van Vliet, V. Smakhtin, S.-m. Kang, The state of desalination and brine production: A global outlook, Science of The Total Environment, 657 (2019) 1343-1356.
[5] J. Kim, K. Park, D.R. Yang, S. Hong, A comprehensive review of energy consumption of seawater reverse osmosis desalination plants, Applied Energy, 254 (2019) 113652.
[6] N.C. Darre, G.S. Toor, Desalination of Water: a Review, Current Pollution Reports, 4 (2018) 104-111.
[7] A. Garciadiego, T. Luo, A.W. Dowling, Molecular design targets and optimization of low-temperature thermal desalination systems, Desalination, 504 (2021) 114941.
[8] B. Sutariya, H. Raval, Analytical study of optimum operating conditions in semi-batch closed-circuit reverse osmosis (CCRO), Separation and Purification Technology, 264 (2021) 118421.
[9] D.M. Warsinger, E.W. Tow, K.G. Nayar, L.A. Maswadeh, J.H. Lienhard V, Energy efficiency of batch and semi-batch (CCRO) reverse osmosis desalination, Water Research, 106 (2016) 272-282.
[10] A. Yusuf, A. Sodiq, A. Giwa, J. Eke, O. Pikuda, G. De Luca, J.L. Di Salvo, S. Chakraborty, A review of emerging trends in membrane science and technology for sustainable water treatment, Journal of Cleaner Production, 266 (2020) 121867.

[11] M.T. Mito, X. Ma, H. Albuflasa, P.A. Davies, Reverse osmosis (RO) membrane desalination driven by wind and solar photovoltaic (PV) energy: State of the art and challenges for large-scale implementation, Renewable and Sustainable Energy Reviews, 112 (2019) 669-685.
[12] R.H. Hailemariam, Y.C. Woo, M.M. Damtie, B.C. Kim, K.-D. Park, J.-S. Choi, Reverse osmosis membrane fabrication and modification technologies and future trends: A review, Advances in Colloid and Interface Science, 276 (2020) 102100.
[13] J.R. Werber, A. Deshmukh, M. Elimelech, Can batch or semi-batch processes save energy in reverse-osmosis desalination?, Desalination, 402 (2017) 109-122.
[14] T. Tong, M. Elimelech, The Global Rise of Zero Liquid Discharge for Wastewater Management: Drivers, Technologies, and Future Directions, Environmental Science & Technology, 50 (2016) 6846-6855.
[15] K. Park, P.A. Davies, A compact hybrid batch/semi-batch reverse osmosis (HBSRO) system for high-recovery, low-energy desalination, Desalination, 504 (2021) 114976.
[16] R.Y. Ning, T.L. Troyer, Tandom reverse osmosis process for zero-liquid discharge, Desalination, 237 (2009) 238-242.
[17] A. Efraty, Closed circuit desalination series no-4: high recovery low energy desalination of brackish water by a new single stage method without any loss of brine energy, Desalination and water treatment, 42 (2012) 262-268.
[18] Z. Wang, A. Deshmukh, Y. Du, M. Elimelech, Minimal and zero liquid discharge with reverse osmosis using low-salt-rejection membranes, Water Research, 170 (2020) 115317.
[19] A.A. Atia, N.Y. Yip, V. Fthenakis, Pathways for minimal and zero liquid discharge with enhanced reverse osmosis technologies: Module-scale modeling and techno-economic assessment, Desalination, 509 (2021) 115069.
[20] Y. Muhammad, W. Lee, Zero-liquid discharge (ZLD) technology for resource recovery from wastewater: A review, Science of The Total Environment, 681 (2019) 551-563.
[21] Y. Oren, E. Korngold, N. Daltrophe, R. Messalem, Y. Volkman, L. Aronov, M. Weismann, N. Bouriakov, P. Glueckstern, J. Gilron, Pilot studies on high recovery BWRO-EDR for near zero liquid discharge approach, Desalination, 261 (2010) 321-330.
[22] R. Schwantes, K. Chavan, D. Winter, C. Felsmann, J. Pfafferott, Techno-economic comparison of membrane distillation and MVC in a zero liquid discharge application, Desalination, 428 (2018) 50-68.
[23] C.D. Peters, N.P. Hankins, Osmotically assisted reverse osmosis (OARO): Five approaches to dewatering saline brines using pressure-driven membrane processes, Desalination, 458 (2019) 1-13.
[24] C.D. Peters, N.P. Hankins, The synergy between osmotically assisted reverse osmosis (OARO) and the use of thermo-responsive draw solutions for energy efficient, zero-liquid discharge desalination, Desalination, 493 (2020) 114630.
[25] T.V. Bartholomew, L. Mey, J.T. Arena, N.S. Siefert, M.S. Mauter, Osmotically assisted reverse osmosis for high salinity brine treatment, Desalination, 421 (2017) 3-11.
[26] A.T. Bouma, J.H. Lienhard, Split-feed counterflow reverse osmosis for brine concentration, Desalination, 445 (2018) 280-291.
[27] K. Park, D.Y. Kim, D.R. Yang, Cost-based feasibility study and sensitivity analysis of a new draw solution assisted reverse osmosis (DSARO) process for seawater desalination, Desalination, 422 (2017) 182-193.
[28] D.M. Davenport, A. Deshmukh, J.R. Werber, M. Elimelech, High-Pressure Reverse Osmosis for Energy-Efficient Hypersaline Brine Desalination: Current Status, Design Considerations, and Research Needs, Environmental Science & Technology Letters, 5 (2018) 467-475.
[29] X. Chen, N.Y. Yip, Unlocking High-Salinity Desalination with Cascading Osmotically Mediated Reverse Osmosis: Energy and Operating Pressure Analysis, Environmental Science & Technology, 52 (2018) 2242-2250.
[30] J. Martínez, E. León, F.M. Baena-Moreno, M. Rodríguez-Galán, F. Arroyo-Torralvo, L.F. Vilches, Techno-economic analysis of a membrane-hybrid process as a novel low-energy alternative for zero liquid discharge systems, Energy Conversion and Management, 211 (2020) 112783.
[31] J. Kim, J. Kim, J. Kim, S. Hong, Osmotically enhanced dewatering-reverse osmosis (OED-RO) hybrid system: Implications for shale gas produced water treatment, Journal of Membrane Science, 554 (2018) 282-290.
[32] N. Togo, K. Nakagawa, T. Shintani, T. Yoshioka, T. Takahashi, E. Kamio, H. Matsuyama, Osmotically Assisted Reverse Osmosis Utilizing Hollow Fiber Membrane Module for Concentration Process, Industrial & Engineering Chemistry Research, 58 (2019) 6721-6729.
[33] N.S. Siefert, J. Arena, M. Mauter, Dewatering of high salinity brines by osmotically assisted reverse osmosis (ASME 2017 power conference), in, NETL, 2017.
[34] T.H. Chong, S.-L. Loo, W.B. Krantz, Energy-efficient reverse osmosis desalination process, Journal of Membrane Science, 473 (2015) 177-188.
[35] T.H. Chong, S.-L. Loo, A.G. Fane, W.B. Krantz, Energy-efficient reverse osmosis desalination: Effect of retentate recycle and pump and energy recovery device efficiencies, Desalination, 366 (2015) 15-31.

[36] S. Kürklü, S. Velioğlu, M.G. Ahunbay, S.B. Tantekin-Ersolmaz, W.B. Krantz, A novel energy-efficient concurrent desalination and boron removal (CDBR) process, Desalination, 423 (2017) 79-94.
[37] M.G. Ahunbay, S.B. Tantekin-Ersolmaz, W.B. Krantz, Energy optimization of a multistage reverse osmosis process for seawater desalination, Desalination, 429 (2018) 1-11.
[38] T.H. Chong, W.B. Krantz, Process economics and operating strategy for the energy-efficient reverse osmosis (EERO) process, Desalination, 443 (2018) 70-84.
[39] K. Jeong, M. Park, T.H. Chong, Numerical model-based analysis of energy-efficient reverse osmosis (EERO) process: Performance simulation and optimization, Desalination, 453 (2019) 10-21.
[40] W.B. Krantz, T.H. Chong, Centrifugal reverse osmosis (CRO)− a novel energy-efficient membrane process for desalination near local thermodynamic equilibrium, Journal of Membrane Science, 637 (2021) 119630.
[41] R.L. Stover, Industrial and brackish water treatment with closed circuit reverse osmosis, Desalination and Water Treatment, 51 (2013) 1124-1130.
[42] S. Lin, M. Elimelech, Staged reverse osmosis operation: Configurations, energy efficiency, and application potential, Desalination, 366 (2015) 9-14.
[43] P.A. Davies, A solar-powered reverse osmosis system for high recovery of freshwater from saline groundwater, Desalination, 271 (2011) 72-79.
[44] E. Hosseinipour, K. Park, L. Burlace, T. Naughton, P.A. Davies, A free-piston batch reverse osmosis (RO) system for brackish water desalination: Experimental study and model validation, Desalination, 527 (2022) 115524.
[45] M. Barello, D. Manca, R. Patel, I.M. Mujtaba, Operation and modeling of RO desalination process in batch mode, Computers & Chemical Engineering, 83 (2015) 139-156.
[46] K. Park, L. Burlace, N. Dhakal, A. Mudgal, N.A. Stewart, P.A. Davies, Design, modelling and optimisation of a batch reverse osmosis (RO) desalination system using a free piston for brackish water treatment, Desalination, 494 (2020) 114625.
[47] P.A. Davies, J. Wayman, C. Alatta, K. Nguyen, J. Orfi, A desalination system with efficiency approaching the theoretical limits, Desalination and Water Treatment, 57 (2016) 23206-23216.
[48] S. Cordoba, A. Das, J. Leon, J.M. Garcia, D.M. Warsinger, Double-acting batch reverse osmosis configuration for best-in-class efficiency and low downtime, Desalination, 506 (2021) 114959.
[49] T. Qiu, P.A. Davies, Comparison of Configurations for High-Recovery Inland Desalination Systems, Water, 4 (2012).
[50] Q.J. Wei, C.I. Tucker, P.J. Wu, A.M. Trueworthy, E.W. Tow, J.H. Lienhard, Impact of salt retention on true batch reverse osmosis energy consumption: Experiments and model validation, Desalination, 479 (2020) 114177.
[51] Z. Gal, A. Efraty, CCD series no. 18: record low energy in closed-circuit desalination of Ocean seawater with nanoH2O elements without ERD, Desalination and Water Treatment, 57 (2016) 9180-9189.
[52] A. Efraty, J. Septon, Closed circuit desalination series no-5: high recovery, reduced fouling and low energy nitrate decontamination by a cost-effective BWRO-CCD method, Desalination and Water Treatment, 49 (2012) 384-389.
[53] A. Efraty, Closed circuit desalination series no-3: high recovery low energy desalination of brackish water by a new two-mode consecutive sequential method, Desalination and Water Treatment, 42 (2012) 256-261.
[54] N. Kahraman, Y.A. Cengel, B. Wood, Y. Cerci, Exergy analysis of a combined RO, NF, andEDR desalination plant, Desalination, 171 (2005) 217-232.
[55] I.H. Aljundi, Second-law analysis of a reverse osmosis plant in Jordan, Desalination, 239 (2009) 207-215.
[56] A.A. Alsarayreh, M.A. Al-Obaidi, A. Ruiz-García, R. Patel, I.M. Mujtaba, Thermodynamic Limitations and Exergy Analysis of Brackish Water Reverse Osmosis Desalination Process, Membranes, 12 (2022).
[57] Hyrec., www.hyrec.co., See report on https://www.bluetechforum.com/wp-content/uploads/Hyrec-BlueTech-Forum-2018-Innovation-Showcase_HYREC_GM-version-2.pdf,

access on 25/04/2022.

High recovery, membrane based, non thermal concentration technology to treat produced water, in.
[58] D. Cingolani, F. Fatone, N. Frison, M. Spinelli, A.L. Eusebi, Pilot-scale multi-stage reverse osmosis (DT-RO) for water recovery from landfill leachate, Waste Management, 76 (2018) 566-574.
[59] I.H. Aljundi, Second-law analysis of a reverse osmosis plant in Jordan, Desalination, 239 (2009) 207-215.
[60] T. Qiu, P.A. Davies, Longitudinal dispersion in spiral wound RO modules and its effect on the performance of batch mode RO operations, Desalination, 288 (2012) 1-7.
[61] A. Haidari, S. Heijman, W. van der Meer, Visualization of hydraulic conditions inside the feed channel of Reverse Osmosis: A practical comparison of velocity between empty and spacer-filled channel, Water research, 106 (2016) 232-241.
[62] C.P. Koutsou, S.G. Yiantsios, A.J. Karabelas, A numerical and experimental study of mass transfer in spacer-filled channels: Effects of spacer geometrical characteristics and Schmidt number, Journal of Membrane Science, 326 (2009) 234-251.

[63] L. Wang, C. Violet, R.M. DuChanois, M. Elimelech, Derivation of the theoretical minimum energy of separation of desalination processes, Journal of Chemical Education, 97 (2020) 4361-4369.
[64] B. Massey, Mechanics of Fluids 4. th Edition, The English Language Book Society, (1980).
[65] J.H. Lienhard, G.P. Thiel, D.M. Warsinger, L.D. Banchik, Low carbon desalination: status and research, development, and demonstration needs, report of a workshop conducted at the Massachusetts Institute of Technology in association with the Global Clean Water Desalination Alliance, (2016).
[66] M.H. Sharqawy, S.M. Zubair, Second law analysis of reverse osmosis desalination plants: An alternative design using pressure retarded osmosis, Energy, 36 (2011) 6617-6626.
[67] A.A. Alsarayreh, M.A. Al-Obaidi, A. Ruiz-García, R. Patel, I.M. Mujtaba, Thermodynamic Limitations and Exergy Analysis of Brackish Water Reverse Osmosis Desalination Process, Membranes, 12 (2021) 11.
[68] H. Shimura, Development of an advanced reverse osmosis membrane based on detailed nanostructure analysis, Polymer Journal, 54 (2022) 767-773.
[69] D.M. Davenport, L. Wang, E. Shalusky, M. Elimelech, Design principles and challenges of bench-scale high-pressure reverse osmosis up to 150 bar, Desalination, 517 (2021) 115237.

Paper 5: High-pressure Batch Reverse Osmosis (RO) for Zero Liquid Discharge (ZLD) in a Cr(III) electroplating process

S. Karimi[a], R. Engstler[b], E. Hosseinipour[a], M. Wagner[c], F. Heinzler[c], M. Piepenbrink[c], S. Barbe[b], P.A. Davies[a*]

a. School of Engineering, University of Birmingham, Edgbaston, Birmingham, UK

b. Faculty of Applied Natural Sciences, Technische Hochschule Köln, Campus Leverkusen, Campusplatz 1, 51379 Leverkusen, Germany

c. BIA Kunststoff- und Galvanotechnik GmbH & Co. KG, Solingen, Germany

Graphical Abstract

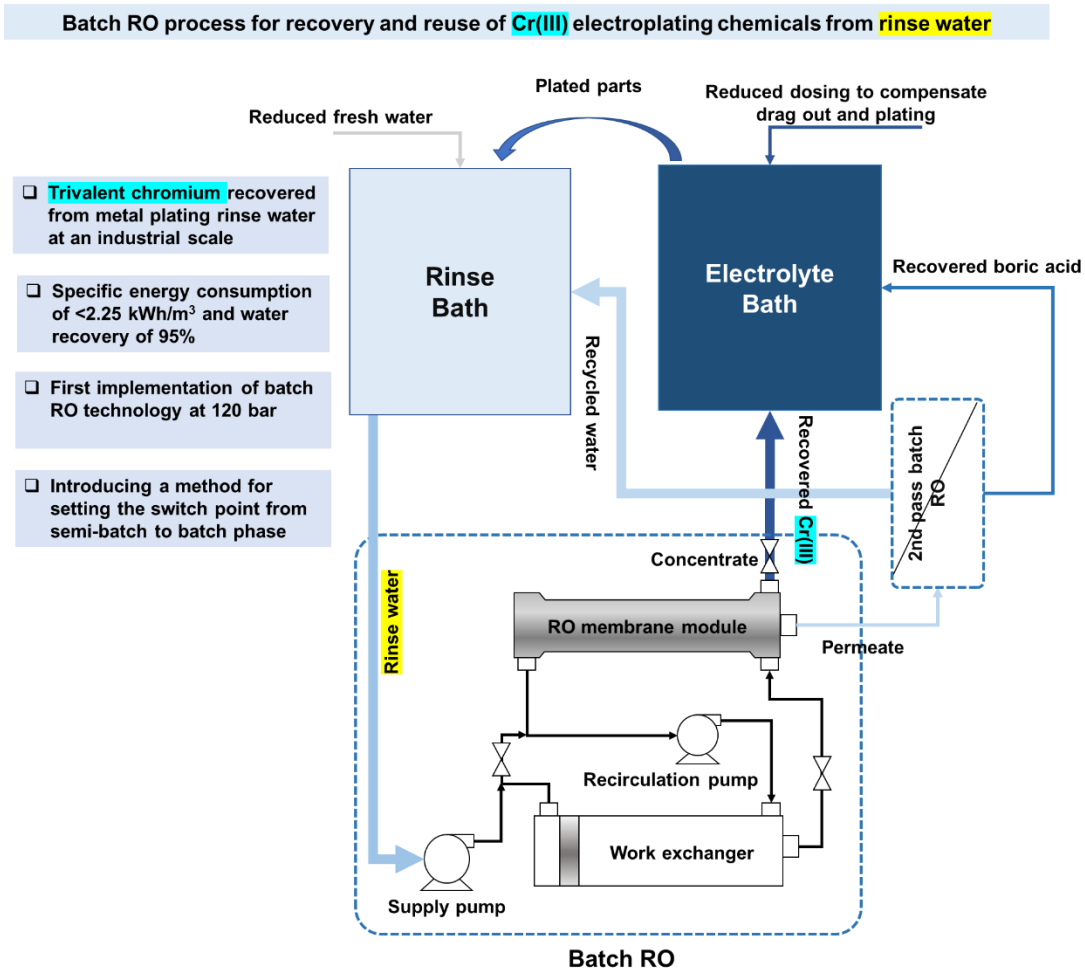

Abstract

A batch RO system was designed and built for high-pressure (120 bar) operation. The system was developed for a ZLD application involving treatment of metal plating wastewater from a Cr(III) electroplating process at a major industrial plant. Hybrid semi-batch/batch operation enabled a compact design to be achieved. To maximize water recovery without exceeding a set

peak pressure, a method for controlling the switch point between semi-batch and batch phases was developed. The system was tested with feed representative of rinse water from the electroplating process. A range of feed concentrations (at 10-20× dilution of the plating bath), feed flows (0.21-0.46 m^3/h), water fluxes (6-14 LMH) and water recoveries (87-95.7%) were investigated. The system successfully recovered Cr(III) and restored its concentration to that of the electrolyte bath, thus meeting the requirements for reuse in the electroplating process. Rejection of most species was >99.8%, sufficient for reuse of the permeate as rinse. However, rejection of boric acid was only 69-80% such that a second RO pass may be needed to remove boric acid. Specific Energy Consumption was <2.25 kWh per m^3 of treated rinse water, representing a 50-fold saving compared to the current method of treatment and disposal at the industrial plant.

Keywords: Batch RO, High-pressure RO, Energy saving, Metal plating wastewater, Trivalent chromium, Zero liquid discharge.

Highlights:

- First implementation of batch RO technology at high pressure of 120 bar.
- Method for setting switch pressure in hybrid semi-batch/batch RO operation.
- Cr(III) recovered from metal plating rinse water at industrial scale.
- Concentration factor of 10-23 for Cr(III) achieved in a single process step.
- Specific energy consumption of <2.25 kWh/m^3 and water recovery of 95%.

Nomenclature

Symbols

A	m^2, Membrane area
A_m	LMH/bar, Membrane permeability
a_w	-, Water activity
c	mg/L, Concentration
c_f	mg/L, Feed concentration
c_p	mg/L, Permeate concentration
c_c	mg/L, Concentrate concentration
E_rp	kWh, Energy consumption of recirculation pump
E_sp	kWh, Energy consumption of supply pump
J	LMH (L/m^2/h), Water flux
k	bar.L/mg, Osmotic pressure coefficient
n	osmol/kg, Osmolality
P	bar, Pressure
$P_\mathrm{0,I}$	bar, Initial pressure for the first cycle
P_m	bar, Hydrodynamic friction of the membrane pores
P_max	bar, Maximum pressure
P_switch	bar, Switch pressure
pK_a	-, Acid dissociation constant
Q_p	L/min, Permeate flowrate
r	%, Water recovery
R_s	%, Rejection
R	J/(gmol.K), Universal gas constant

T	K, Temperature
V_0	L, Internal volume
V_{b0}	L, Feed volume during the batch phase
V_{back}	L, Osmotic backflow
V_{conc}	L, Purge volume
V_f	L, Feed volume
V_p	L, Permeate volume
V_s	m^3/gmol, Partial molar volume of water
V_{sb}	L, Feed volume during the semi-batch phase
η	-, Empirical pressure correction factor
π	bar, Osmotic pressure
ρ_w	kg/L, Water density

Abbreviations

CF	Concentration Factor
LMH	Litre per square Meter per Hour
MVC	Mechanical Vapour Compression
NF	Nanofiltration
PLC	Programmable Logic Controller
REACH	Registration, Evaluation, Authorisation and Restriction of Chemicals
RO	Reverse Osmosis
SEC	Specific Energy Consumption, electrical kWh per m^3 of treated wastewater
SI	Supporting Information
TOC	Total Organic Carbon
UF	Ultrafiltration
UV	Ultraviolet
ZLD	Zero Liquid Discharge

1. Introduction

Batch RO is an innovative approach to desalination that enables high recoveries to be achieved with modest energy consumption [1-5]. This makes it especially interesting for separation and recovery processes where zero or liquid minimal discharge is required. Several configurations of batch RO have been presented in the literature [6, 7]. In principle, batch RO can achieve the theoretical ideal minimum specific energy consumption (SEC) of desalination [8]. In practice, however, there are several losses that affect its efficiency. Taking into account frictional losses and concentration polarization, Werber et al. [9] carried out a theoretical study to compare the performance of batch RO against several other RO configurations. These configurations included batch, semi-batch, and conventional staged RO processes. The study confirmed that, even considering losses, batch RO incurs the least SEC. However, true batch RO requires a large-pressurised vessel of variable volume, making it difficult to scale up. The size of this vessel increases with recovery ratio. Thus, while batch RO has been demonstrated at recovery of 80% [2], at higher recovery practical implementation becomes difficult unless some modifications are introduced.

To overcome this difficulty, Park et al. [10] recently proposed a hybrid mode of operating batch RO that achieved similar SEC to true batch RO, while using a smaller pressurized vessel

(*i.e.*, work exchanger). Hybrid batch RO uses a preliminary semi-batch phase followed by a batch phase. The hybrid approach was later validated experimentally using brackish water feed, achieving in a single stage 95% water recovery with SEC <0.6 kWh/m^3 [11]. Such high recovery has great potential for ZLD applications. Nonetheless, this experimental study [11] had some important limitations, namely: (1) because the batch RO system was rated at only 25 bar, it could not achieve high final concentrations, thus limiting its use in ZLD; and (2) no systematic method was presented for controlling the switch point between semi-batch and batch phases of operation, which (as this study will show) is an important consideration in high-pressure operation. In this study, we present a high-pressure (120 bar) batch RO system with water recoveries >95% and we apply it to a challenging ZLD application in electroplating of chromium.

In general, electroplating processes tend to produce large amounts of environmentally-hazardous wastewater [12]. In the case of chromium, strict regulations limit concentrations in wastewater in most European countries. Limits range from 0.05-0.3 mg/L for hexavalent chromium, Cr(VI), and from 0.3-10 mg/L for total chromium content in effluents. Germany has especially strict regulations, limiting Cr(VI) to 0.1 mg/L and total chromium to 0.5 mg/L [13]. Electroplating also faces economic challenges [14]. According to the German Central Association for Surface Technology, the cost of chromium electroplating had increased by 52% in 2021 compared to the mean over 2015-2017, reaching 11.98 €/m². This increase was driven by a 37% increase in energy costs and a 63% increase in metal costs [15]. The cost has recently increased further, reaching 17.17 €/m² [16]. Cr(VI) is carcinogenic and is being phased out in favour of trivalent chromium, Cr(III), as a less harmful alternative [17, 18]. Nevertheless, Cr(III) still presents a significant environmental hazard. Moreover, it is more expensive than Cr(VI) in terms of the whole electrolyte composition and its maintenance, thus giving a strong incentive to recover and reuse Cr(III) waste.

In the Cr(III) plating process, parts are immersed in an electrolyte bath for the electrodeposition of chromium layers. The electrolyte contains a chromium source together with organic acids as complexing agents, boric acid as buffer, sulfates as conducting salts, plus other organic additives and surfactants to increase plating performance [19-21]. The parts are then rinsed of excess plating chemicals, generating a stream of wastewater.

Traditional thermal technologies consume substantial energy to treat such electroplating wastewater [22]. For example, Yang et al. [23] used mechanical vapor compression (MVC) and reported a SEC of 58 kWh/m^3. Common chemical treatment methods include hydroxylic precipitation which produces an insoluble metal sludge, which is separated by filtration [14]. Coagulation or flocculation agents are often used to improve the sedimentation or flotation of the sludge and reduce its settling time, which further increase the costs. Other treatments include adsorption on powdered activated carbon or ion exchange resins. Electrochemical methods have also been investigated, including electrocoagulation, electrodeposition and electrodialysis; nonetheless, these may incur high capital and energy costs, and create new waste streams [24-26].

Membrane separation technologies have the potential to overcome such limitations. Their advantages include simplicity, cost-effectiveness, energy efficiency, and scalability. Membrane technologies – including ultrafiltration (UF), nanofiltration (NF) and reverse osmosis (RO) – have received increased attention for the removal of various metal ions [14, 27]. Although RO

has been used to remove Cr(VI) from wastewater [28-32], its use for Cr(III) rinse water treatment is quite new. To our knowledge, the only relevant study on Cr(III) is that of Engstler et al. [19] which used a conventional bench-top RO system in the laboratory. The study achieved the concentration factor needed for direct reuse of the electroplating chemicals. Nonetheless, the system was much too small for industrial implementation, comprising just 160 cm^2 of membrane and processing only a few litres of wastewater over several weeks. No measurements of SEC were taken or reported. Moreover, severe membrane fouling was observed which led to a halving of the membrane permeability, such that this system did not provide an industrial solution for Cr(III) wastewater treatment.

Because electroplating rinse water is very dilute, most of the water (~90-95%) must be removed to restore the electrolyte concentration sufficiently for reuse. In the field of desalination, such a high percentage of water recovery is quite unusual and challenging. In seawater desalination by RO, for example, the water recovery is typically only about 45% [33]. Increased recovery tends to increase the SEC of RO [34]. Meanwhile, energy saving is ever more important to the metal plating industry. This makes an energy-efficient approach, such as batch RO, attractive in this application.

Batch RO has been evaluated for seawater [35], brackish groundwater [2] and for agricultural runoff water [36]. But to our knowledge, it has not been studied for water reuse in the metal plating industry, nor has it been implemented at high pressure. Therefore, the goal here is to develop and test a full-scale batch RO system for Cr(III) recovery and water reuse. The specific objectives are:

(1) Develop an efficient, 120-bar batch RO system that can process industrial quantities of Cr(III) rinse water with SEC <2.5 kWh/m^3 and water recovery up to ~95%.

(2) Present a method for setting the switch point from semi-batch to batch phase in hybrid operation, as needed for the automation of the process.

(3) Test the system with metal plating rinse water made up in the laboratory, and measure key performance parameters including concentration factor and rejection of the main electroplating chemicals, pressure, SEC, water recovery, permeate quality and flux.

(4) Assess fouling and durability of the RO membrane in this system.

These objectives are guided by an application that is representative of modern Cr(III) plating industry, as described in section 2. Then, section 3 explains the concept and development of the high-pressure batch RO technology. Section 4 presents the theory of the methods used to set the switch point. The experimental procedure, equipment and characterisation methods are given in section 5 while section 6 presents the results (including the assessment of fouling) and discusses how the findings compare with earlier works. Section 7 states the main conclusions of the study.

2. Industrial electroplating plant

The batch RO system has been designed to meet the requirements of the state-of-the-art Cr(III) plating process of BIA Kunststoff- und Galvanotechnik GmbH & Co. In the BIA plant, parts of ABS (acrylonitrile-butadiene-styrene) undergo several successive process steps separated by dedicated rinsing baths. Etching, activation, and acceleration steps first prepare

the parts for metal electroplating by rendering the surface conductive. A thin 1-2 µm nickel layer is then applied to reinforce the surface, followed by a thick 20-30 µm copper layer to correct any unevenness and provide ductility. Next, another 7-10 µm of semi bright nickel is plated for corrosion resistance. Nickel is electroplated in two further steps to make the surface bright or satin and for more corrosion protection. To avoid cross contamination, thorough rinsing is applied to ensure that virtually all soluble nickel is removed from the parts. Finally, electroplating of a 0.3-0.8 µm layer of chromium generates a hard and chemically resistant surface. The finished parts are supplied mainly to the automotive industry.

The plant has three Cr(III) plating lines each including a 1.5-m^3 rinse bath (Fig. 1) which is emptied twice weekly, thus generating in total about 9 m^3 of chromium-contaminated rinse water per week. As the rinse water becomes contaminated by drag out from the electrolyte bath, it has similar composition to the electrolyte bath but diluted by a factor of 10-20 typically. As such, it contains 500-1000 mg/L of Cr(III) which greatly exceeds the allowed discharge limit of 0.5 mg/L. Despite the high cost of the plating chemicals and their disposal, BIA (like other electroplating factories) has not yet been able to implement any effective recovery process. Currently, the rinse is disposed of by hydroxylic precipitation to form a $Cr(OH)_3$ sludge. However, an initial treatment by UV/H_2O_2 oxidation is needed to destroy the complexing agents. The UV lamps are energy intensive, and for this reason disposal currently incurs a SEC of 118 kWh of electricity per m^3 of wastewater. As shown in Fig. 1, it is now proposed to recycle both water and chemicals in this process, with the help of batch RO to achieve much lower SEC.

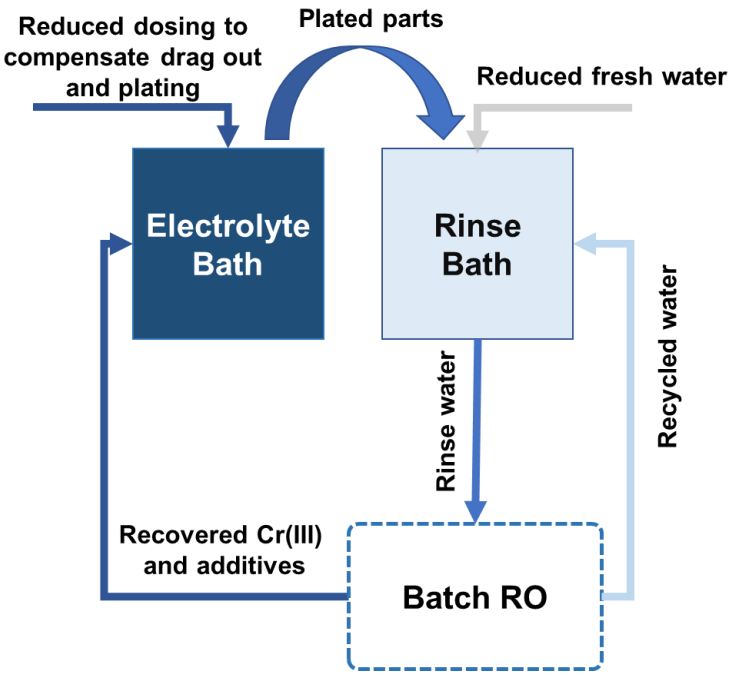

Fig. 1. Schematic of Cr(III) plating line at BIA, showing the electrolyte bath and rinse bath. The dashed box indicates the proposed recycling system using batch RO.

3. Batch RO system

The batch RO system was supplied by ETS Design Ltd, London (model number 477) and installed in the laboratory at the University of Birmingham (Fig. 2). The design was based on

an earlier system also installed at the university [2] but with upgrades for the high-recovery and high-pressure operation needed for the metal plating wastewater treatment.

Fig. 2. The installed pilot scale 120-bar batch RO system at the University of Birmingham, UK, showing 8-inch RO module (top) and work exchanger (bottom) inside safety enclosure.

Unlike the earlier system, this system was designed from the outset to be operated in hybrid semi-batch/batch mode, thus avoiding the need for an excessively large work exchanger [10, 11, 37]. If non-hybrid batch mode had been specified, a work exchanger volume of about 300 L would have been needed to achieve the required water recovery of 95%. In hybrid operation, this volume is reduced to just 38.5 L without significant penalty in SEC [10]. This size reduction is especially important because of the space restrictions at the BIA factory where a similar system will later be installed. Moreover, though multi-stage conventional RO may be another option to achieve 95% recovery, in practice this would likely require a 3-stage system with a large footprint and of capacity exceeding the requirements of this application. In contrast, the hybrid batch RO system provides a compact solution at the required scale.

Fig. 3 illustrates the concept of the system operating in hybrid mode. It includes two pumps: a supply pump, that increases the feed pressure from 0 to 120 bar, and a recirculation pump that operates under a high pressure but provides a low pressure rise to overcome internal pressure losses. It also includes three valves: the bypass, recirculation, and concentrate valve. Operation is cyclic involving three phases, *i.e.,* semi-batch pressurization, batch pressurization, and purge-and-refill. The phase is determined by the state of the valves. In the semi-batch phase (Fig. 3a) the bypass and recirculation valves are open while the concentrate valve is closed. The piston is stationary at the left end of the work exchanger, resulting in a fixed internal volume. Wastewater is fed via the supply pump and mixed with concentrate returning from the RO membrane module, while the recirculation pump sends the mixed solution to the work exchanger. The solution then passes through the recirculation valve and the membrane module where permeate water exits such that the recirculating solution gradually becomes more concentrated.

At the end of the semi-batch phase, the system is switched to batch phase by closing the bypass valve while the other two valves remain in the same state (Fig. 3b). The switch causes

the pressure to rise more sharply. In the absence of the bypass path, the high-pressure supply forces the piston to the right, thus decreasing the internal volume. This phase continues until the piston reaches the other end of the work exchanger. With the concentrate valve closed, the volume of permeate corresponds to that displaced by the piston. Finally, the purge-and-refill phase (Fig. 3c) is started by opening the concentrate and bypass valves and closing the recirculation valve. Now, the supply branches in two directions after the bypass valve. It displaces the concentrate from the RO module, which leaves the system via the concentrate valve. It also passes through the recirculation pump and refills the work exchanger. Pressure variations in semi-batch and batch phases of hybrid operation are shown in Fig. 4.

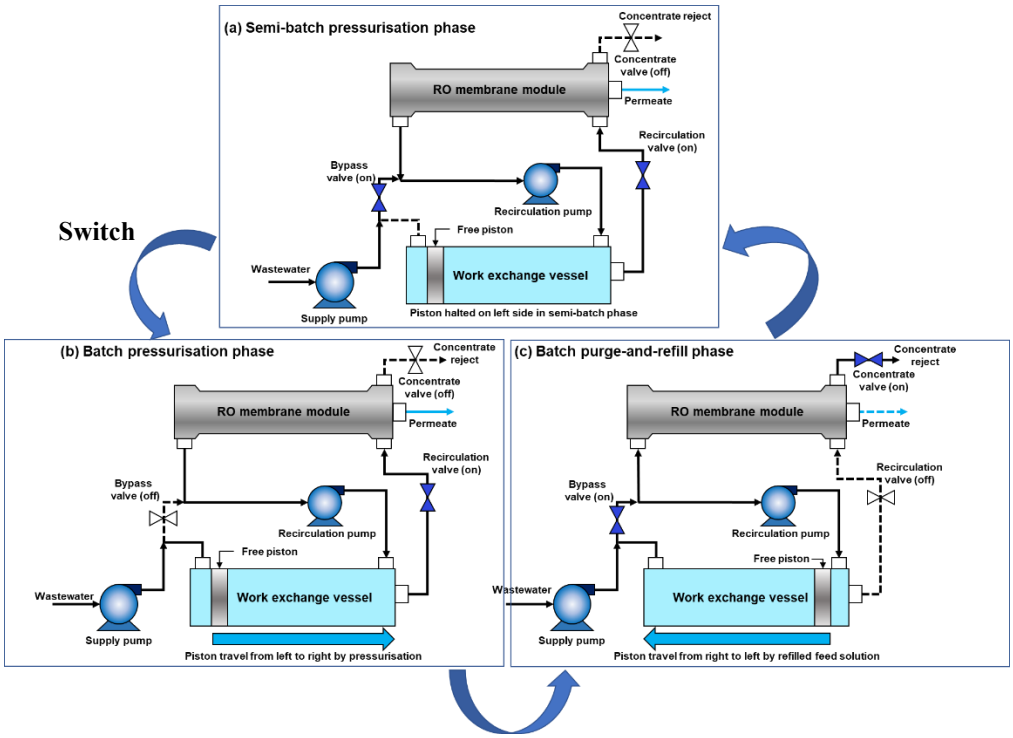

Fig. 3. Flow diagram and the working principle of the hybrid semi-batch/batch RO, showing the three phases of cyclic operation. The solid and dashed lines show flow and no flow, respectively.

Preliminary measurements indicated that, depending on the type of electrolyte, the osmotic pressure of the electrolyte bath could reach 78 bar. To overcome this while providing sufficient net driving pressure, it was estimated that an applied pressure exceeding 100 bar may be required. In contrast, the earlier system was rated at only 25 bar because it was designed to treat only brackish water [11]. Even seawater RO systems and membranes are normally rated at only 80 bar. Nonetheless, some membrane manufacturers have recently introduced membranes rated at high pressures for ZLD applications. The membrane selected for this study is rated at 120 bar (a DuPont™ XUS180808, an 8-inch diameter, 1.016m long spiral-wound polyamide thin-film composite membrane with active area of 30.6 m^2). This kind of high-pressure RO membrane and process is a recent innovation that introduces several challenges with respect to, for example, safety, sealing and membrane compaction [38].

To ensure operator safety and system integrity at such high pressure, the design includes several features. A pressure relief valve actuates at 120 bar, releasing pressure and tripping a safety relay. The relay then cuts off power to the supply pump and opens two pneumatic drain

valves, thus releasing system pressure at three points. All pressurised components are housed in a transparent polycarbonate enclosure with doors interlocked to the safety relay (Fig. 2). The safety relay also responds to other fault conditions including manual intervention via the emergency stop buttons. All these features are designed to be failsafe, such that loss of electrical or pneumatic supply, or an open-circuit fault condition, will cause the equipment to default to its safe state in which the drain valves are open. The Supporting Information (SI) provides a detailed schematic of the batch RO system (Fig. S1) and lists its main components including the pumps, valves, sensors, and controls (Table S1). The system is controlled by a programmable logic controller (PLC).

4. Theory

An important consideration in the operation of the batch RO system is the criterion for switching from semi-batch to batch pressurization phase (see Fig. 3). If the switch is too early, insufficient concentration will occur for reuse of the electrolyte. If too late, the pressure will rise above the safe working pressure and the system will automatically shut down and require restarting. To avoid such difficulties, the following theory provides two methods for setting switch point.

4.1. Concentration factor method

The first method sets the switch point according to a target concentration factor *CF*. This factor refers to the chromium concentration in the concentrate divided by that in the rinse water feed. Because the chromium is thoroughly rejected by the high-pressure RO membrane (as confirmed in section 6.1) virtually all the chromium is collected in the concentrate. Thus, provided that the system is operating in a steady cyclic condition such that no chromium accumulates internally, CF is calculated by dividing the volume V_f of rinse water fed to the system by the volume of concentrate, V_conc, collected from the system, *i.e.*

$$CF = \frac{V_\mathrm{f}}{V_\mathrm{conc}} = \frac{V_\mathrm{sb} + V_\mathrm{b0} + (V_\mathrm{conc} - V_\mathrm{back})}{V_\mathrm{conc}} \tag{1}$$

where V_sb, V_b0 and $(V_\mathrm{conc} - V_\mathrm{back})$ are the feed volumes during the semi-batch, batch, and purge-and-refill phases respectively. V_back is the osmotic backflow [11]. Table 5 shows the volumes used in this study as determined by the design of the system.

Table 5. Volumes of the high-pressure batch RO rig used in this study [L]. The osmotic backflow was based on the maximum value observed in an earlier study [2].

Feed volume batch phase (work exchanger swept volume)	V_b0	38.5
Concentrate volume	V_conc	16.0
Osmotic backflow	V_back	5.0
Internal volume	V_0	54.9

Based on these volumes, equation (1) becomes

$$CF = 3.1 + \frac{V_{sb}}{16} \quad (2)$$

Equation (2) provides a criterion for the switch point based on setting V_{sb}, which is known from the change in mass (or level) of the feed tank. In other words, to achieve a target CF we need to supply:

$$V_{sb} = 16\,(CF - 3.1) \quad (3)$$

Equation (2) shows that *CF* increases with V_{sb} from the minimum value of 3.1 at V_{sb}=0.

4.2. Peak pressure method

The second method addresses the risk of excessive pressure. The method relies on a minimum number of input parameters, making it simple to implement. It avoids the need for accurate characterization of the rinse water feed.

According to the solution-diffusion theory, the applied pressure (P) in RO has two components, one corresponding to the hydrodynamic friction of the membrane pores (P_m) and the second corresponding to osmotic pressure (π). Thus:

$$P = P_m + \pi \quad (4)$$

The first component (P_m) is equivalent to the permeate flux (J) divided by the membrane permeability (A_m), *i.e.*

$$P_m = J/A_m \quad (5)$$

J is defined as the ratio of permeate flowrate (Q_p) to the membrane area (A).

$$J = \frac{Q_p}{A} \quad (6)$$

where the permeate flowrate (Q_p) is the permeate volume (V_p) divided by the total duration of the semi-batch and batch pressurization phases. Therefore, P_m is proportional to the feed flow and is considered a constant for a series of cycles of the batch RO system (normally lasting less than one day) during which the feed flow and flux remain constant.

The osmotic pressure component in equation (4) is related to the concentration, c, of the solute inside the batch RO system. Osmotic pressure increases with concentration and, at low concentrations such as those occurring during the semi-batch phase, the relation is expected to be linear according to a constant k. This constant lumps together factors such as the osmotic coefficient of the solute, temperature, rejection, and concentration polarization effects which are assumed approximately constant for a given series of cycles. Thus equation (4) becomes:

$$P = P_m + kc \quad (7)$$

During the semi-batch phase, the internal volume of the system remains fixed at V_0 and solute is gradually added at concentration c_f via the feed stream which arrives at a flow rate of dV_f/dt

where V_f is the volume of feed that has been added since the beginning of the phase. This accumulation of mass causes the concentration to rise with time, *i.e.*

$$V_0 \frac{dc}{dt} = \frac{dV_f}{dt} c_f \tag{8}$$

This may be written as:

$$\frac{dc}{dV_f} = \frac{c_f}{V_0} \tag{9}$$

Because P_m is constant, equation (7) can be differentiated with respect to V_f to give:

$$\frac{dP}{dV_f} = k \frac{dc}{dV_f} \tag{10}$$

Substituting from equation (9) gives:

$$\frac{dP}{dV_f} = k \frac{c_f}{V_0} \tag{11}$$

Equation (11) shows that the pressure is expected to rise linearly with feed volume at a rate proportional to the feed concentration (c_f). At the beginning of the first cycle of the batch RO operation, the system is initially filled with solution at the feed concentration. Therefore, the initial pressure ($P_{0,I}$) according to equation (7) will be:

$$P_{0,I} = P_m + k c_f \tag{12}$$

Where the second subscript 'I' indicates 'the first cycle'. Substituting from equation (11) and rearranging for P_m provides:

$$P_m = P_{0,I} - V_0 \frac{dP}{dV_f} \tag{13}$$

Equation (13) allows the value of P_m to be determined from the slope and intercept of the pressure *vs* volume curve during the first cycle (see Fig. 4).

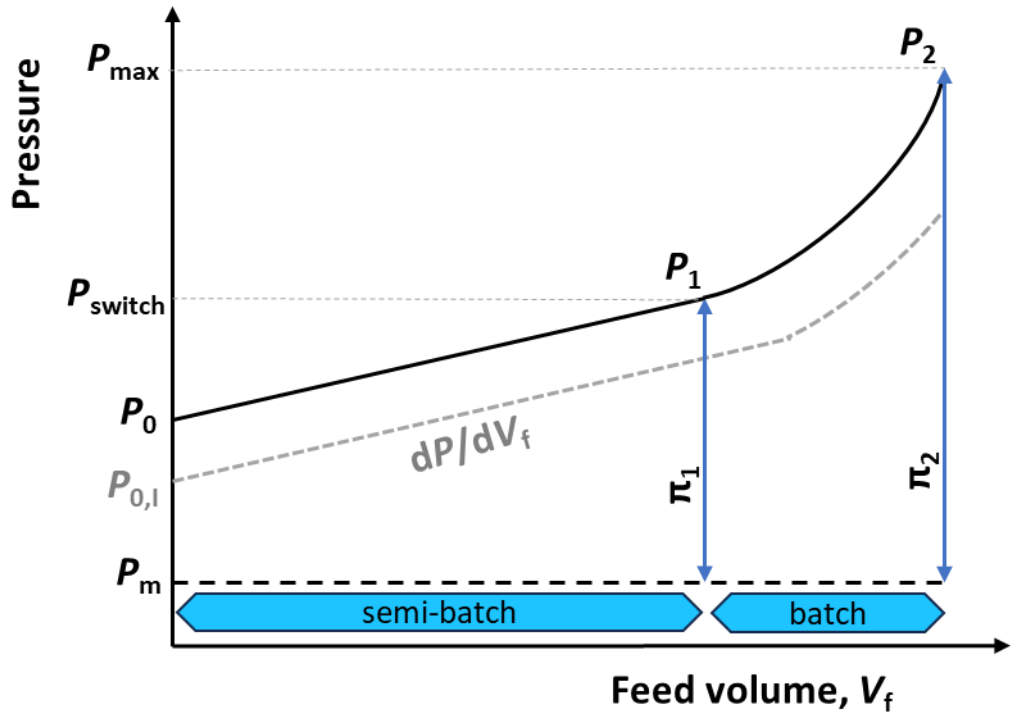

Fig. 4. Principle of determination of switch pressure based on pressure *vs.* feed volume. The dashed grey curve indicates the first cycle. Also showing the semi-batch and batch phases of hybrid operation, with the switch occurring at the end of the semi-batch phase.

Next the batch phase is considered. During this phase, the volume of the system is decreased from V_0 by the swept volume V_{b0} of the work exchanger to give a final volume of $V_0 - V_{b0}$. Applied pressure increases from P_1 to P_2. This phase is approximately a constant mass phase, whereby the same amount of solute is compressed into a smaller volume, and osmotic pressure is expected to rise in inverse proportion to the volumetric ratio $(V_0 - V_{b0})/V_0$. Nonetheless, experiments have shown that the observed rise in pressure is slightly less than expected [11]. Reasons for this may include: (1) less than 100% rejection such that the mass of solute decreases; (2) deflection of the membrane and dilation of the pressurised system; (3) sub-linear increase of osmotic pressure with concentration. Therefore, an empirical correction η (slightly less than one) is applied to account for these factors, as follows:

$$\frac{\pi_2}{\pi_1} = \eta \frac{V_0}{(V_0 - V_{b0})} \tag{14}$$

where π_1 and π_2 are the osmotic pressures at the beginning and end of the batch phase, respectively. Like P_m, η is initially unknown, but it can be found after each cycle based on measured pressures as follows:

$$\eta = \frac{(P_2 - P_m)}{(P_1 - P_m)} \frac{(V_0 - V_{b0})}{V_0} \tag{15}$$

η is assumed to remain approximately constant from one cycle to the next. The maximum osmotic pressure that can be utilised is the difference between the maximum allowable pressure and the hydrodynamic friction pressure, *i.e.*

$$\pi_2 = P_{\max} - P_{\mathrm{m}} \tag{16}$$

The corresponding switch pressure is given by:

$$P_{\mathrm{switch}} = P_{\mathrm{m}} + \pi_1 \tag{17}$$

Combining equations (14), (16), and (17) gives the following equation for the switch pressure according to the maximum pressure $P_{\max}$:

$$P_{\mathrm{switch}} = P_{\mathrm{m}} + \frac{(P_{\max} - P_{\mathrm{m}})}{\eta}\frac{(V_0 - V_{\mathrm{b0}})}{V_0} \tag{18}$$

Alternatively, this can be rearranged to calculate $P_{\max}$ resulting from a given switch pressure:

$$P_{\max} = \frac{\eta V_0 (P_{\mathrm{switch}} - P_{\mathrm{m}})}{(V_0 - V_{\mathrm{b0}})} + P_{\mathrm{m}} \tag{19}$$

Equation (19) confirms the importance of precise adjustment of P_{switch}. This is because of the sensitive dependence of $P_{\max}$ on P_{switch} due to the multiplying factor of $V_0/(V_0 - V_{\mathrm{b0}})$ which equals 3.35 in this study. For example, using typical values of $\eta = 0.8$, P_{m}=12 bar and the volumes in Table 5, a modest increase in P_{switch} from 35 to 55 bar increases $P_{\max}$ greatly from 70 to 120 bar.

To summarize, the peak pressure method is implemented as follows:

1. For the first cycle, a conservatively low value of P_{switch} is chosen to ensure that $P_{\max}$ is not exceeded. P_{switch} is calculated by equation (18) with η=1 and P_{m} based on previous tests carried out at similar feed flow. If no such test result is available, equation (5) may be used to estimate P_{m} using permeability based on data from the membrane manufacturer. The PLC program controls the system to switch phase when the applied pressure reaches P_{switch}.
2. At the end of the first cycle, equations (13) and (15) are used to find more precise values of P_{m} and η respectively (for example, η=0.8) based on the measured data of pressure *vs.* feed volume. Equation (18) is then used to determine P_{switch} for the second cycle.
3. Following each subsequent cycle, an updated value of η is found using equation (15) while P_{m} remains constant. Equation (18) is again used to determine P_{switch} for the next cycle.

The two approaches to determining switch point (*i.e.,* based on concentration factor or based on peak pressure) will be evaluated and compared in the experimental part of this study.

5. Materials and methods

7.1. *5.1. Experimental setup*

Fig. 5 shows the experimental set up including the batch RO rig, supply pump (CAT pumps, model 3CP1241G), plastic tanks (1500 L for feed and permeate and 425 L for the concentrate tank), cartridge filter (Amazon Filters Ltd, Superpleat II 20×4.5-inch filter, 1 um) and sensors (see SI). The feed, permeate and concentrate tanks had scales (Mettler Toledo) to record the weight changes. Temperature of the feed tank was kept constant at 25±0.5 °C using a thermostat and four immersed 650W titanium heaters. The energy consumption of the supply pump was monitored using a power sensor (Multitek M100-WA4). Pressure was measured using a sensor on the feed line (Applied Measurements LTD, P600). The peak pressure of each cycle was recorded at the end of the batch pressurisation phase, when the highest concentration of concentrate leaves the membrane module. A data logger recorded measurements from the sensors and scales at intervals of approximately one second. Raw experimental data are included as supplementary files (see SI section 4).

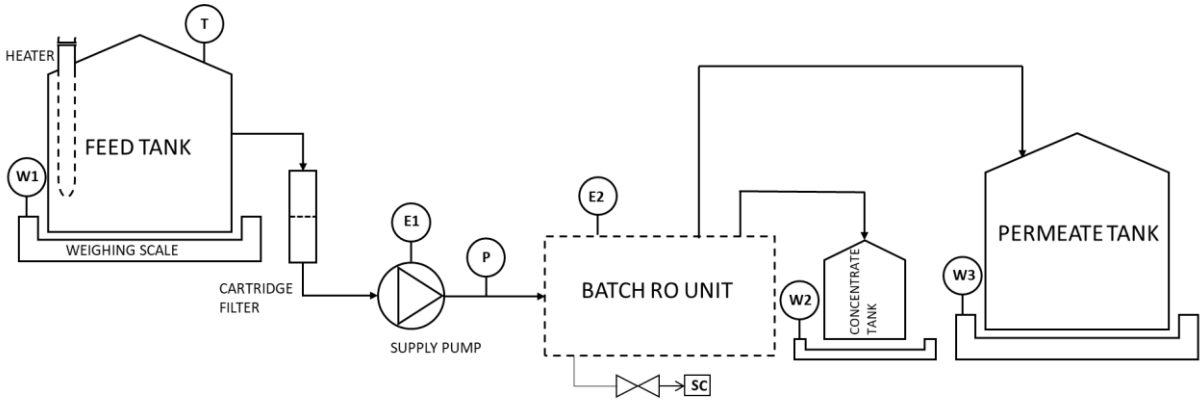

Fig. 5. Experimental set up. Symbols T, W, E and P indicate respectively temperature, weight, power, and pressure sensors.

5.2. Rinse water preparation

The rinse wastewater was prepared by dilution of the electrolyte bath solution to replicate the composition at the BIA plant. The electrolyte bath solution was synthesized using the TRILYTE® FLASH SF-POP products and procedure supplied by MacDermid Enthone (Birmingham , UK) [39]. TRILYTE® FLASH SF-POP is a REACH compliant, corrosion resistant Cr(III) plating process providing a direct substitute for Cr(VI)-based solutions. It is used for the deposition of a bright decorative chromium layer over bright or satin nickel layers [40]. The products are listed in Table 2 together with their functions and the quantities used.

Table 6. Commercial products used to make up 120 L of the TRILYTE® FLASH SF-POP electroplating bath solution, based on [39].

Commercial product	Quantity	Main function
TRILYTE FLASH SF Makeup	36 L	Source of chromium (III) and complexing agent [41]
TRILYTE FLASH SF Buffer	23 kg	Source of conductive salts and pH stabiliser (boric acid) [19-21, 42, 43]
TRILYTE FLASH SF Replenisher	2.4 L	Provides bright deposits [42, 44]
TRILYTE WETTING AGENT	0.12 L	Reduces surface tension [42, 45]

The electrolyte bath solution was synthesized first by adding 65 L of tap water to the feed tank. Then, the TRILYTE FLASH SF Makeup was added followed by heating the solution using the immersion heaters to 65-70 °C. Next, 23 Kg of TRILYTE FLASH SF Buffer was added in portions while vigorously stirring using a recirculation pump. This step was done very carefully to ensure that all the salts are dissolved. 2 kg of potassium hydroxide 50% wt. (Fisher Scientific) was then added to the solution to adjust the pH to 3.5-3.9. Thereafter TRILYTE FLASH SF, Replenisher and TRILYTE WETTING AGENT were added and the water level topped up to 120 L. The measuring was done using the weighing platform beneath the tank (component density values were used to convert volumes to mass). Finally, a series of representative electroplating rinse water bath compositions were prepared by dilution with tap water by a factor of 10, 15, and 20× respectively. These compositions were used as the feed to the batch RO in the experiments described next.

5.3. Experimental procedure

To investigate performance over a range of feed concentrations, fluxes, and recoveries, two series of experiments were carried out: the first at set concentration factor and the second at set peak pressure (following sections 4.1 and 4.2 respectively). Experiments were conducted for at least three cycles and the measurement were done on the third cycle, as three cycles were enough to approximate steady state (see Fig. S2). Fluxes were adjusted over a range of 6-16 LMH by varying the speed of the supply pump. The recirculation flow, as measured by the flow sensor at the inlet to the recirculation pump, was adjusted to 6 times the supply flow. For further details of the experimental procedure the reader is referred to previous work [2].

The results from the experiments were obtained as follows. The permeate volume (V_p) and feed volume (V_f) were measured according to weight changes of the tanks, dividing by the solution density. The density of 1 kg/L was used throughout because the dilute nature of the feed and permeate caused their densities to be within 2% that of pure water. Water recovery r was calculated as the ratio:

$$r = \frac{V_\mathrm{p}}{V_\mathrm{f}} \tag{20}$$

For components where rejection is nearly 100%, the mass balance gives the concentration factor *CF* as the ratio of the volume of concentrate ($V_\mathrm{f} - V_\mathrm{p}$) to the volume of feed (V_f). Therefore, *CF* was calculated by:

$$CF = \frac{1}{1 - r} \tag{21}$$

The electrical SEC was calculated as the sum of the energy consumption of the supply pump (E_{sp}) and recirculation pump $\left(E_{\mathrm{rp}}\right)$, divided by the feed volume over a whole cycle:

$$SEC = \frac{E_{\mathrm{sp}} + E_{\mathrm{rp}}}{V_{\mathrm{f}}} \tag{22}$$

Rejection (R) was calculated by:

$$R = \frac{c_{\mathrm{f}} - c_{\mathrm{p}}}{c_{\mathrm{f}}} \tag{23}$$

where c_{f} and c_{p} are the concentrations of a given ion in the feed and permeate respectively.

5.4. Analytical methods

Inductively coupled plasma optical emission spectroscopy (ICP-OES) was used to determine concentrations of chromium, sulfate, boric acid in the feed and permeate. Further details are given in SI section 2, which also describes the determination of Total Organic Carbon (TOC) and measurement of osmotic pressure.

6. Results and Discussion

6.1. Permeate concentrations and rejection

Chromium, sulfate, and TOC were detected in only small amounts in the permeate with maximum concentrations of 1.13, 13.28, and 0.053 mg/L respectively, as such well within the recycling limits for the rinsing bath of 10, 150, 100 mg/L respectively (see Table 3). In contrast, the concentration of boric acid in the permeate was ca. 1000-2000 mg/L, as such above the estimated allowed limit of 1000 mg/L.

Fig. 6. Feed (dilution of 15×), permeate and concentrate samples (water recovery of 94.1%, flux 6.6 LMH).

Corresponding to these concentrations, the average rejections of chromium, sulfate, boric acid and TOC were 99.88, 99.85, 74.97, and 100 % respectively (see Table 3). Except for boric acid, all these rejections were therefore >99.8%, as expected in RO for such multivalent ions and large organic molecules. Due to the high rejection of chromium, the permeate appeared very clear, whereas the concentrate was dark blue, compared to the mild blue colour of the rinse water feed (see Fig. 6).

Table 3. Rejections of chromium (III), sulfate, TOC and boric acid as a function of water recovery and flux, for dilution of 15×. Feed concentrations of chromium (III), sulfate, TOC and boric acid were 672.5, 6133, 575.1, and 6495 mg/L respectively.

Water recovery (%)	Flux (LMH)	Permeate concentration (mg/L)				Rejection (%)			
		Cr(III)	Sulfate	TOC	Boric acid	Cr(III)	Sulfate	TOC	Boric acid
88.4	6.5	0.68	7.12	0.053	1708.7	99.90	99.88	99.98	73.69
90.4	6.6	0.96	11.63	0.002	1805.2	99.86	99.81	100.00	72.20
94.1	6.6	1.13	13.28	0.000	2008.2	99.83	99.78	100.00	69.08
87.9	8.3	0.61	5.88	0.000	1480.9	99.91	99.90	100.00	77.20
90.3	8.3	0.82	8.82	0.000	1609.0	99.88	99.86	100.00	75.23
87.6	10	0.75	8.74	0.000	1285.4	99.89	99.86	100.00	80.21
90	10	0.69	6.98	0.000	1482.7	99.90	99.89	100.00	77.17

Rejection of boric acid was, however, only 69-80%. This can be explained by the neutral character of the boric acid molecules at the working pH of 3.0-3.9 which is well below the pKa of 9.22. Therefore, the small uncharged and non-hydrated boric acid molecules can pass through the membrane to some extent [46]. Additionally, boric acid forms hydrogen bridges with the active groups of membranes and diffuses like water [47]. To ensure the required purity of the rinse water for reuse, the rejection needs to be improved to about 85%. This could be achieved by adding a second RO pass (as indicated in the Graphical Abstract).

6.2. Performance at set concentration factor

The results of this section were obtained using the switch point method based on target concentration factor, as described in section 4.1. Because of the high rejection (except for boric acid) concentration factor is directly related to water recovery via equation (21).

(a)

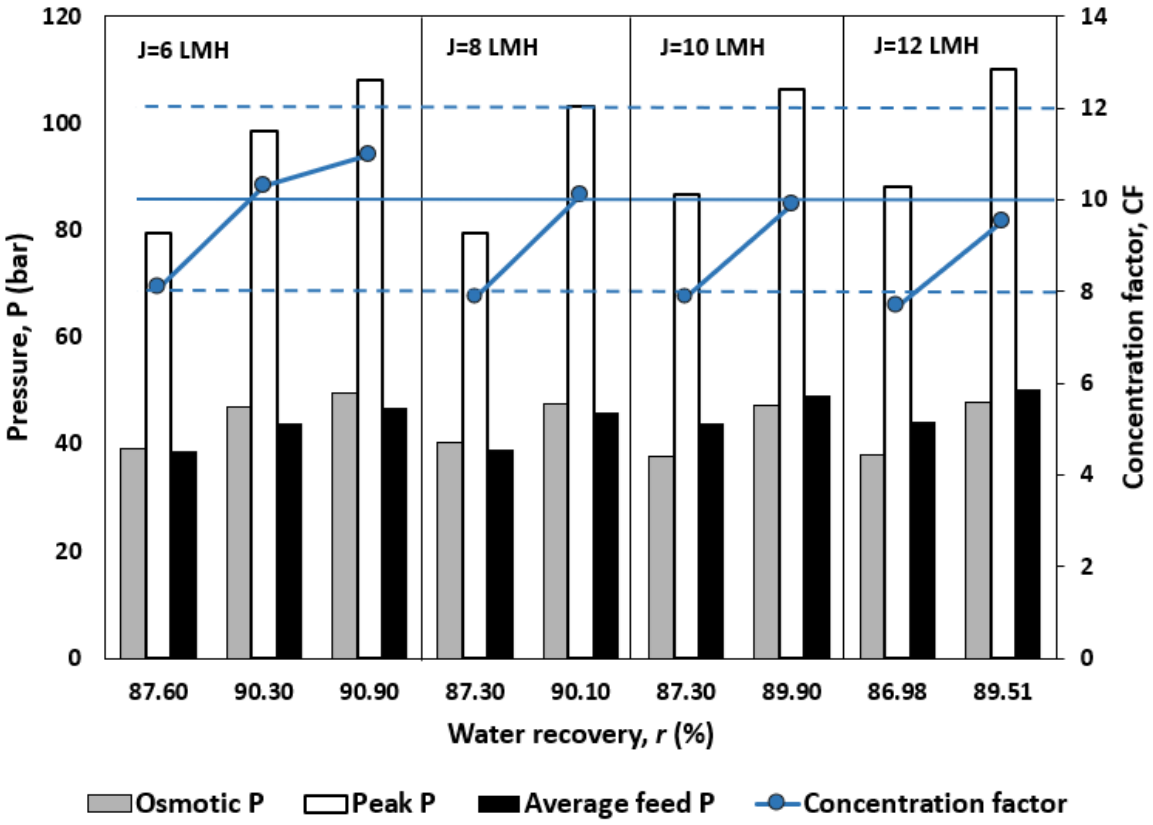

(b)

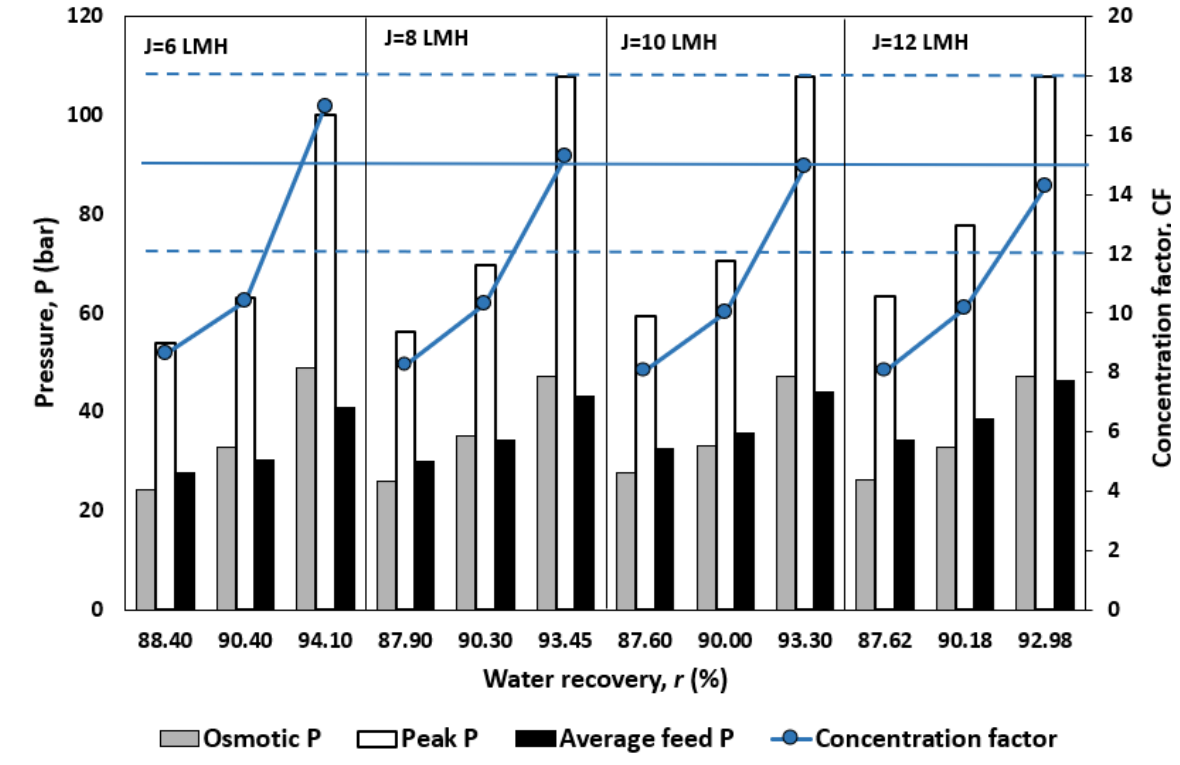

(c)

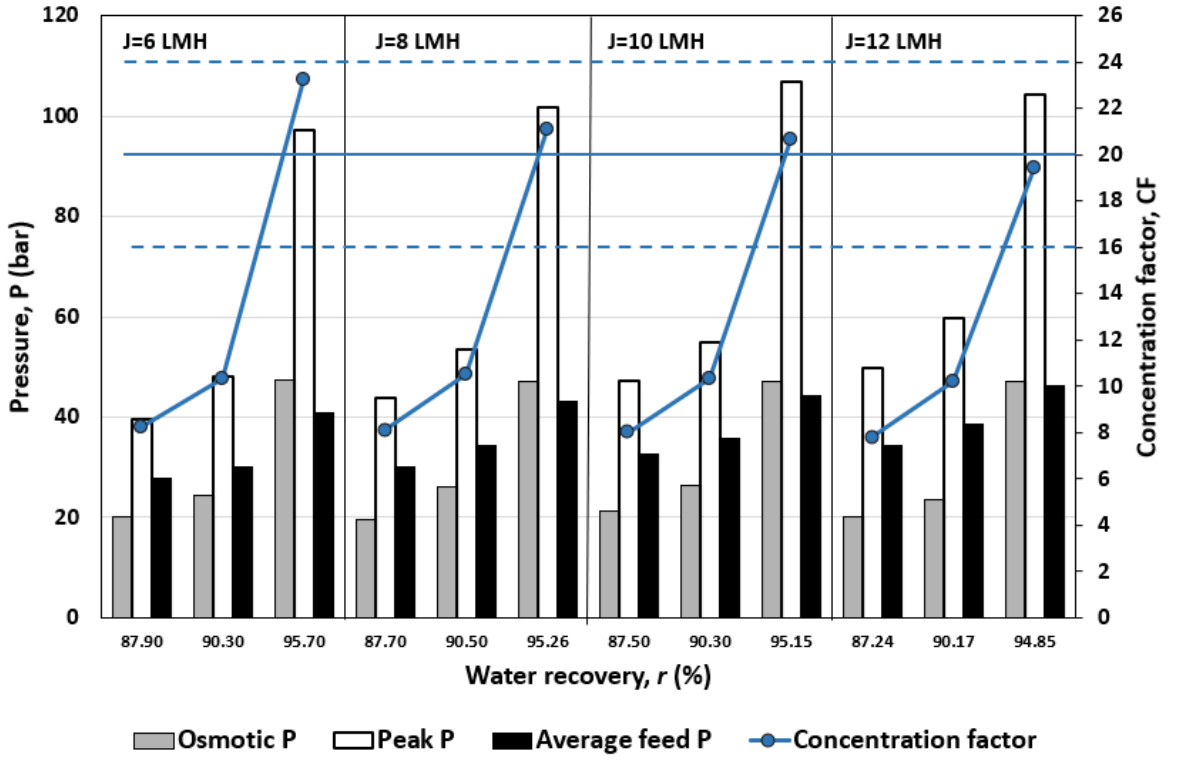

Fig. 7. Osmotic pressure of concentrate, peak feed pressure (P_{max}), and average feed pressure, at different water recoveries from 87-95% and fluxes from 6-12 LMH for dilution of (a) 10×, (b) 15×, and (c) 20×. Osmotic pressure of feed was measured to be 7.55, 5.23 and 4.13 bar for dilutions of 10×, 15×, and 20× respectively. Also shows concentration factor, with dashed horizontal blue lines showing the lower and upper limits for recycling to the electrolyte bath, and the solid blue line showing the optimum value for recycling to the electrolyte bath.

Feed pressures (peak and average) and concentration factor as a function of recoveries of 87-95% and at fluxes of 6-12 LMH are illustrated in Fig. 7a, b and c for dilutions of 10×, 15× and 20× respectively. To meet the requirement for recycling as defined by the plating industry, the target is 80-120% of the initial concentration of the electrolyte bath [39]. Therefore, concentration factors of 8-12, 12-18, and 16-24 are needed for dilutions of 10, 15, and 20× respectively. These limits are shown by dashed horizontal blue lines in Fig. 7. The concentration factors presented are for the fully rejected components *i.e.,* all components except boric acid, where lower concentration was achieved due to only partial rejection being achieved. Based on mass balance, boric acid concentration reached only 30-78 g/L – below the 80-110 g/L required for the electrolyte bath [39]. Boric acid would therefore need to be replenished or recovered further in a second RO pass. For the other components, sufficient concentration factors were achieved by working at high recovery, at fluxes up to 12 LMH.

Note that, with this method of controlling switch point, there was no systematic way to ensure that the maximum system pressure of 120 bar was not exceeded. The maximum water recoveries and concentration factors had to be determined by trial and error.

As expected, peak and average pressure increased with water recovery and flux. At the highest recoveries and concentration factors, the average feed pressure was about half the peak pressure, and below the osmotic pressure of the concentrate. In contrast, a conventional single-stage RO system would require a constant feed pressure above the concentrate osmotic pressure to maintain a positive net driving pressure and transmembrane flux. These results suggest that the batch RO system has a significant energy advantage compared to conventional single-stage RO. Nonetheless, further experimental studies will be needed to make a complete and fair comparison, considering factors such as flux distribution, membrane friction, and salt retention in each system [48]. In addition, pump efficiency has an important effect on overall performance and may vary between batch and continuous systems.

The osmotic pressure of the final concentrate is an indication of the total concentration of final concentrate product, and it is higher than 47 bar for the samples that met the concentration requirement (Fig. 7). This osmotic pressure is more than 10 bar below that of the electrolyte bath (63 bar) mainly because of the loss of boric acid to the permeate.

(a)

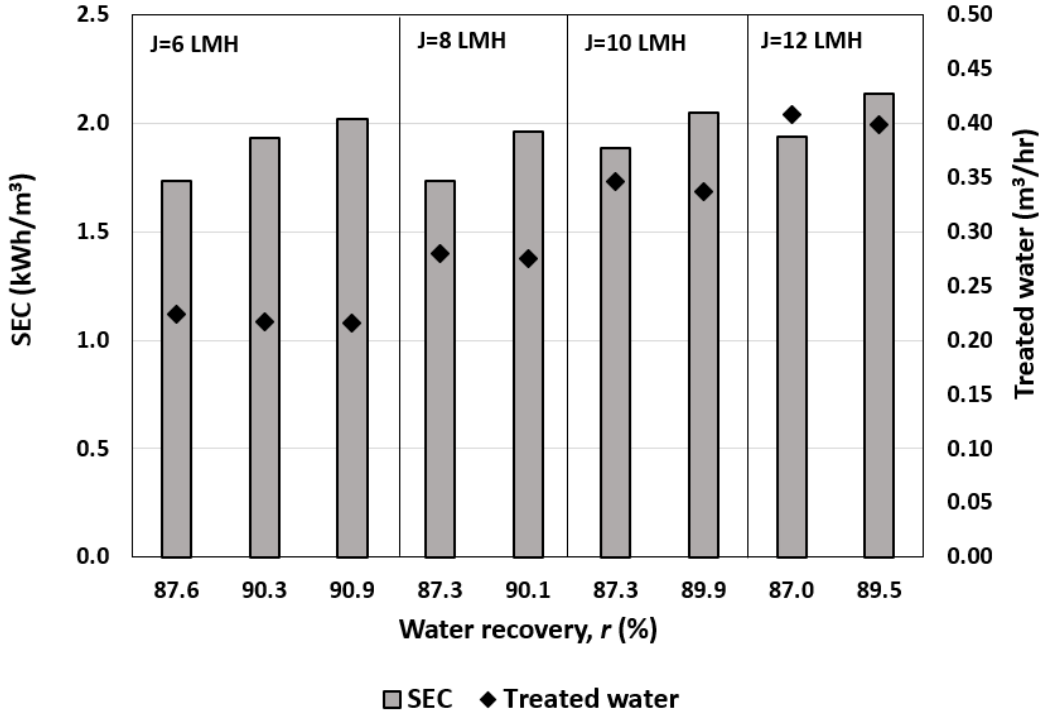
J=6 LMH
J=8 LMH
J=10 LMH
J=12 LMH
SEC (kWh/m³)
Treated water (m³/hr)
2.5
2.0
1.5
1.0
0.5
0.0
0.50
0.45
0.40
0.35
0.30
0.25
0.20
0.15
0.10
0.05
0.00
87.6 90.3 90.9 87.3 90.1 87.3 89.9 87.0 89.5
Water recovery, r (%)
SEC
Treated water

(b)

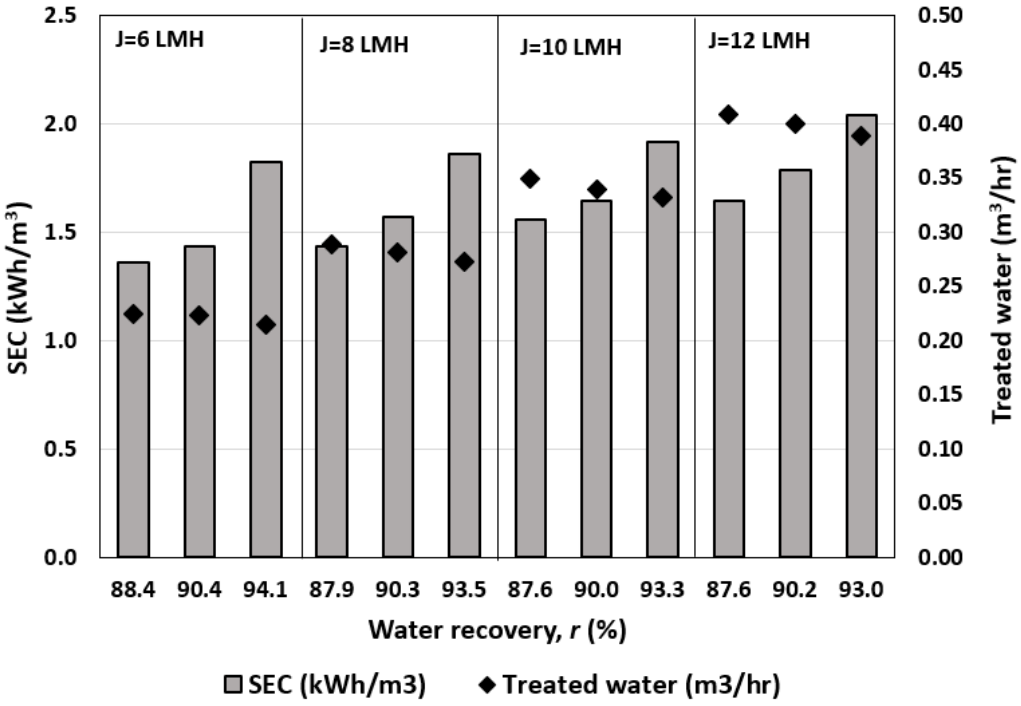
J=6 LMH
J=8 LMH
J=10 LMH
J=12 LMH
SEC (kWh/m³)
Treated water (m³/hr)
2.5
2.0
1.5
1.0
0.5
0.0
0.50
0.45
0.40
0.35
0.30
0.25
0.20
0.15
0.10
0.05
0.00
88.4 90.4 94.1 87.9 90.3 93.5 87.6 90.0 93.3 87.6 90.2 93.0
Water recovery, r (%)
SEC (kWh/m3)
Treated water (m3/hr)

(c)

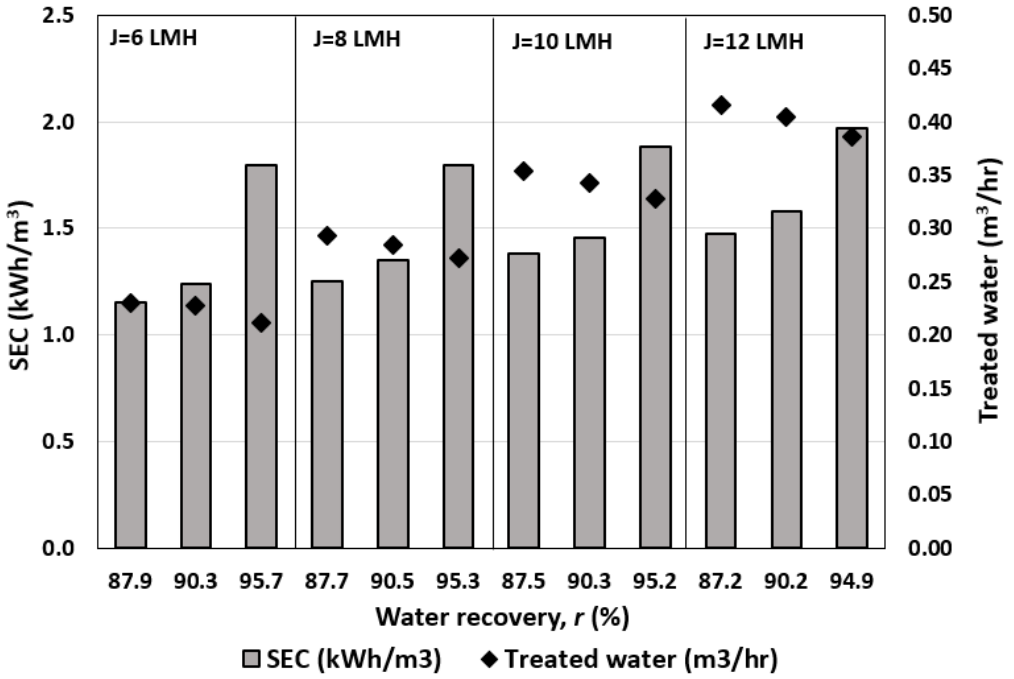

Fig. 8. Specific energy consumption (SEC) and flowrate of treated water at recoveries of 87-95% and fluxes of 6-12 LMH for dilution of (a) 10×, (b) 15×, and (c) 20×.

Fig. 8 shows SEC<2.15 kWh/m^3 when treating rinse water at a rate of 0.21-0.42 m^3/h. Thus, it will be possible to treat 1.7-3.4 m^3 of rinse water in an 8-hour working shift, meeting the requirement of the industrial process at BIA. SEC increased with water recovery and flux.

6.3. Analysis of results against the switch pressure theory

To assess the accuracy of the theory described in section 4, the theory was used to analyse the above data. In total, 24 experiments were analysed covering fluxes of 6-12 LMH, water recoveries of 87-95% and dilutions of 10, 15 and 20×.

The P_{m} value was calculated using equation (13) (based on the recorded pressures in cycle 1) and is shown as a function of flux in Fig. 9a. In the semi-batch phase, dP/dV_{f} values were calculated for all three cycles. There was less than 10% deviation in dP/dV_{f} at cycle 3 compared to cycles 1 and 2. The value at cycle 3 was plotted as a function of feed concentration as presented in Fig. 9b which clearly shows the linear dependency of the dP/dV_{f} value to the feed concentration as predicted by equation (11).

The peak pressure of the third cycle is predicted using equation (19), based on the measured switch pressure and the value of η calculated from the previous cycle using equation (15). This predicted peak pressure is compared against the measured value at cycle 3 to give a model error of less than 3% (see Fig. 10). Fig. 10 also confirms that η has values consistently just below one (from 0.75 to 0.82) as assumed in the theory of section 4.

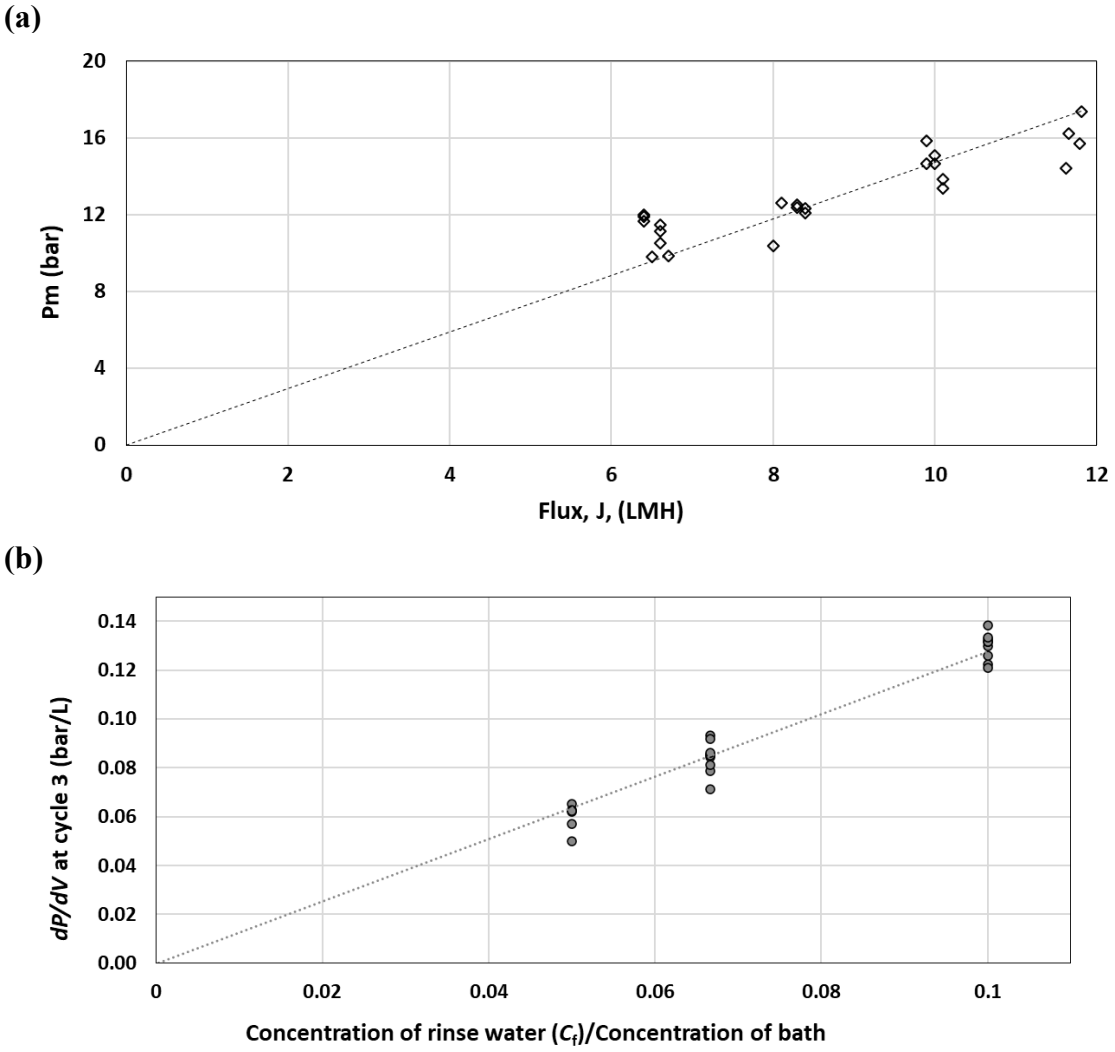

Fig. 9. Verification of theory of switch point determination, using results from section 6.2: (a) Hydrodynamic pore friction pressure P_m as a function of flux J. (b) Slope dP/dV during cycle 3 of the semi-batch phase versus the relative feed concentration.

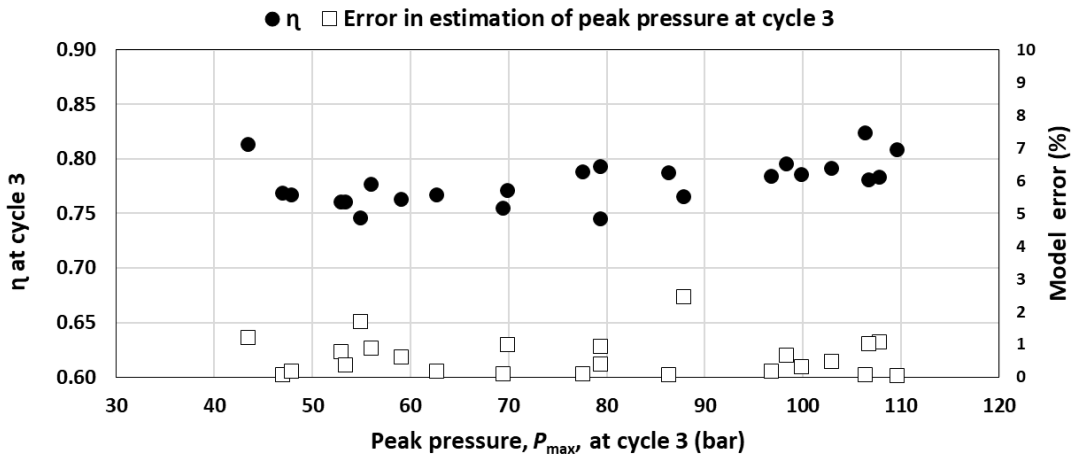

Fig. 10. Empirical pressure correction factor η and error of modelling peak pressure at cycle 3, at different peak pressures (cycle 3).

6.4. Performance at set peak pressure

This section evaluates the method of setting switch pressure for a target peak pressure, as described in section 4.2. In addition, the method is used to compare batch RO performance at 80 bar *vs*. 120 bar.

Experiments were carried out at dilutions of 15 and 20×, fluxes of 8-16 LMH, and two target peak pressures: (1) 108 bar to provide a 10% safety margin below the maximum allowable pressure of 120 bar; (2) 72 bar to represent 80 bar maximum pressure as allowed by standard seawater RO membranes. Table 4 shows the results, including maximum obtained pressure at each cycle. In all cases, the peak pressure converged quickly from cycle 2 on, with ≤2.2% deviation from the set peak pressure.

Table 4. The summary of the results obtained from the RO experiments operated using the methodology of switch pressure determination for a target peak pressure.

Dilution	Pressure limit (bar)	Target pressure (bar)	Flux (LMH)	Observed peak pressure (bar) at cycle:				Max deviation of peak pressure from target Cycles 2-4 (%)	Switch pressure Cycle 3 (bar)	SEC Cycle 3 (kWh/m^3)
				1	2	3	4			
15×	120	108	8	88.4	108.5	109.0	105.8	2.20	47.9	1.97
15×	120	108	10	90.0	107.7	107.2	107.5	0.50	48.8	2.00
15×	120	108	12	92.6	106.3	106.3	108.9	1.70	50.6	2.05
15×	120	108	14	89.5	108.9	107.7	107.6	0.87	51.0	2.22
15×	120	108	16	90.9	108.0	107.7	107.7	0.32	53.1	2.21
15×	80	72	8	58.3	72.0	71.5	71.7	0.50	34.6	1.54
15×	80	72	10	58.8	70.4	71.7	72.0	1.55	36.1	1.63
15×	80	72	12	63.1	71.3	71.6	71.7	0.65	36.8	1.71
15×	80	72	14	61.1	70.6	70.6	70.4	1.53	37.8	1.89
20×	120	108	12	88.6	109.2	107.7	-	1.24	49.9	2.04
20×	120	108	14	93.4	108.9	107.4	-	0.91	51.4	2.19

Fig. 11 presents three examples of pressure *vs*. feed volume, showing the value of η for each cycle. Cycle 1 had lower peak pressure due to the conservative setting of η_1=1 and the absence of salt retention, but the rapid convergence of η from cycle 2 onward means that switch pressure, water recovery, and concentration factor all converged rapidly. The linear increase of pressure in the semi-batch phase agrees with equation (11).

(a)

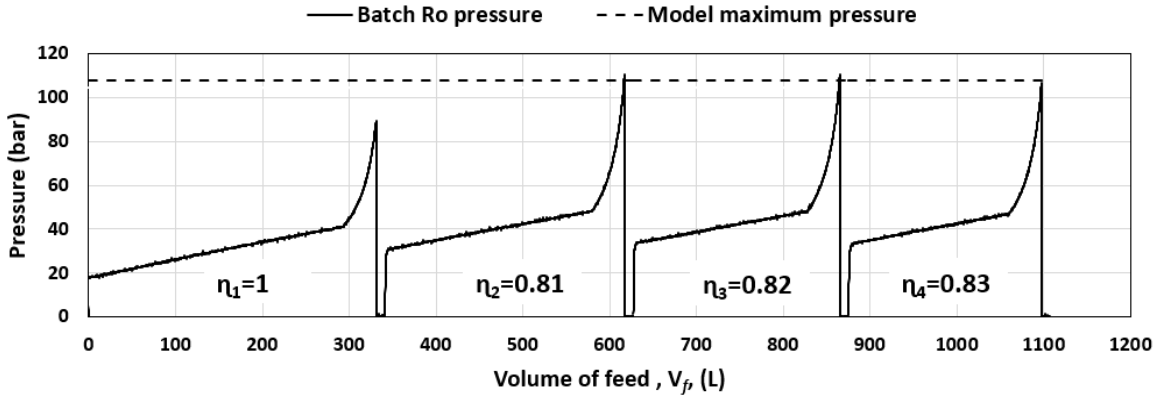

(b)

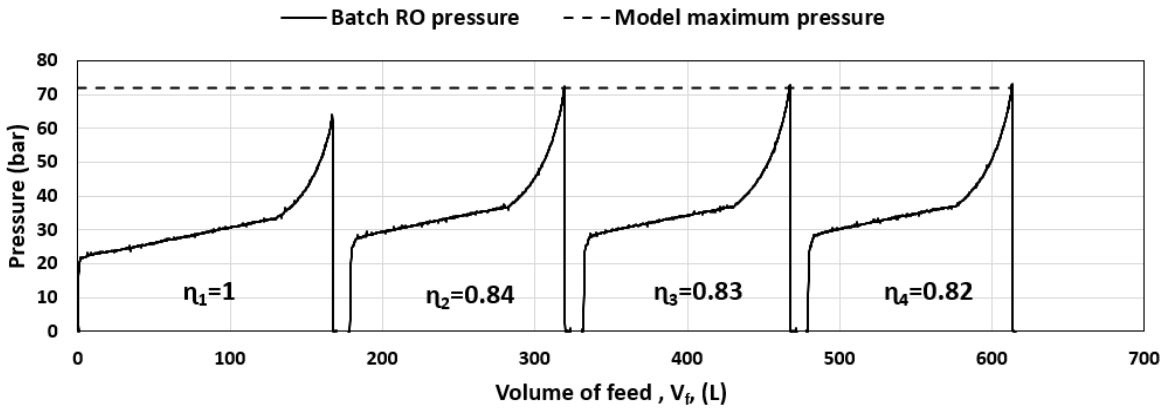

(c)

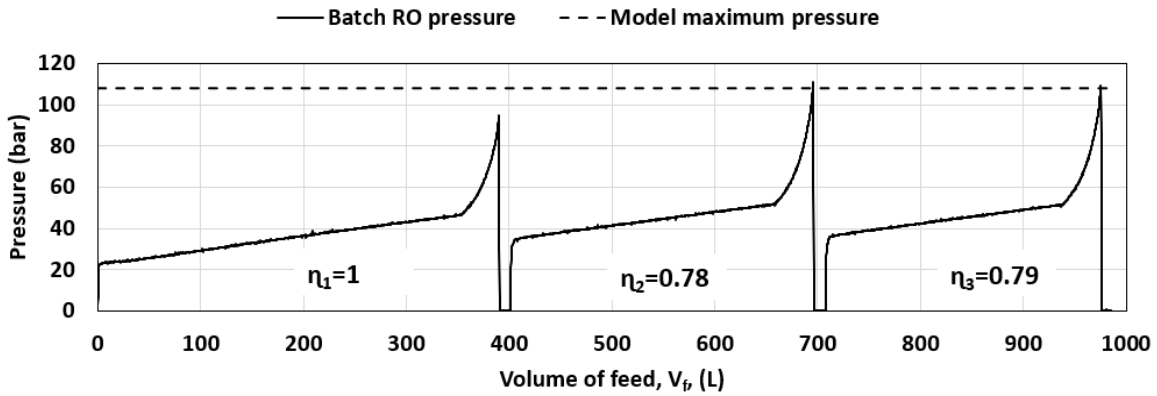

Fig. 11. Pressure variation vs. supplied feed volume for three experiments, using switch point setting based on peak pressure. (a) dilution of 15×, flux of 8 LMH, concentration factor of 15.48, set peak pressure of 108 bar (b) dilution 15×, flux 12 LMH, concentration factor 9.12, set peak pressure 72 bar, (c) dilution 20×, flux 12 LMH, concentration factor 18.34, set peak pressure 108 bar. Dashed horizontal lines show the set peak pressures.

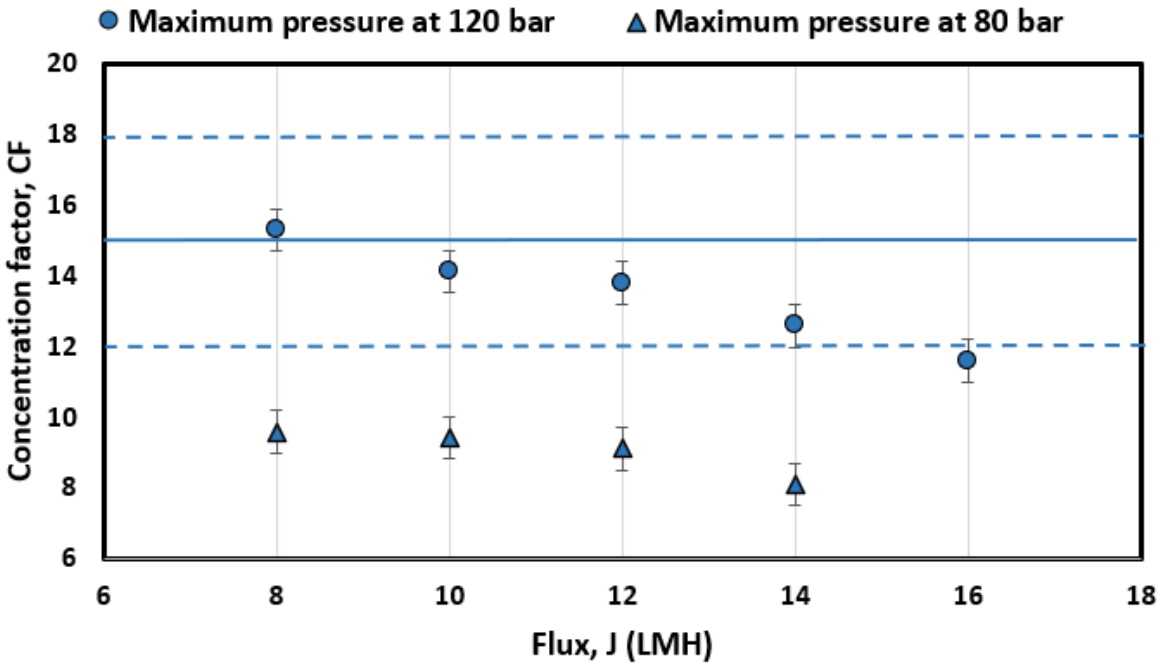

Fig. 12. Concentration factor *vs*. flux at 80 and 120 bar operation, for feed concentration of 15×. Dashed horizontal blue lines show the lower and upper limits for recycling to the electrolyte bath; the solid blue line shows the optimum for recycling to the electrolyte bath.

The concentration factor at feed concentration of 15× is plotted versus flux, at both 80 and 120 bar maximum pressure, in Fig. 12. The optimum concentration factor of 15, needed to restore the electrolyte bath concentration, is shown by the solid blue line. The desired range of concentration factor of 12-18, corresponding to 80-120% of the electrolyte bath concentration, is shown by dashed blue lines. The results show that batch RO was able to concentrate the Cr(III) rinse water sufficiently at fluxes up to 14 LMH at 120 bar operation, but unable to do so at 80 bar operation even at lower flux.

Compared to the method of 4.1, where switch point is set for a target concentration factor, this method automatically concentrates the wastewater to the maximum extent possible for a given flux and pressure limit, without the need for trial and error. It also avoids the need for accurate characterisation of the wastewater, as the concentration is effectively detected from the slope of pressure *vs*. feed volume during the semi-batch phase. This method is therefore recommended whenever there is a risk of approaching the maximum operating pressure of the system. In fact, the two methods of switch point control are complementary and can be used together. Thus, we recommend that the first method can be used to determine a supply volume in the semi-batch phase for a target concentration factor, while the second method is simultaneously used to set a safeguard on the switch pressure to ensure maximum system pressure is not exceeded. In this way, the switch will occur at whichever point is reached earlier (i.e., according to the target concentration factor or according to the pressure limit). If, however, the aim is simply to achieve the maximum concentration factor, then the first method is not needed.

6.5. Membrane fouling and durability

Total organic carbon (TOC) was present in significant quantities in the Cr(III) rinse water (at 926, 575, and 445 mg/L for feed dilution of 10,15, and 20× respectively) and could cause fouling of the RO membrane, as was previously observed in benchtop RO experiments with Cr(III) rinse water [19]. Membrane fouling can generally be detected by a decrease in flux, a decrease in permeability, and an increase in working pressure [49].

Membrane fouling and durability were investigated through two tests, each conducted before and after the entire series of Cr(III) experiments which lasted about 100 hours in total. The first test was for permeability, using tap water in continuous flow mode at water flux of 17 LMH. The permeability tests showed negligible change in permeability and average pressure which were constant at 1.15 LMH/bar and 14.9 bar respectively. The second test was for salt rejection, using a feed solution of 4500 mg/L sodium chloride in hybrid semi-batch/batch mode, with water flux of 16.8 LMH and set water recovery of 0.94. The rejection showed a reduction of just 0.1% from 96.7% to 96.6%. These results indicated negligible fouling and negligible deterioration in membrane performance. The absence of fouling tends to confirm previous work describing mechanisms of fouling avoidance in batch RO. These mechanisms may include periodic flushing, feed flow reversal, osmotic backflow, and salinity cycling [4, 50].

6.6. Comparison against earlier studies

Table 5 compares the findings of this study against earlier studies on chromium plating rinse water treatment using RO technology. The comparison is limited to studies using the real composition of rinse water as occurring in modern metal plating plants, as opposed to simplified compositions that may omit important components.

Only this study used a RO membrane rated at 120 bar, whereas earlier studies used standard membranes limited to 80 bar or less. This higher working pressure enabled the process to achieve the required concentration for reuse while working at flux up to 14 LMH. The high water recovery of 87-95% resulted in a chromium concentration factor of 8-23 thus going above the range of earlier studies. In addition, this study produced the highest output compared to other studies, making the system suitable for direct industrial application. Most earlier studies used Cr(VI), which is less challenging than the Cr(III) rinse water, because of the absence of other chemicals such as boric acid.

Table 5. Performance comparison among relevant studies on chromium plating wastewater treatment using RO technology.

Main component and concentration in feed (mg/L)	**Treatment method**	**Specific Energy Consumption (kWh/m^3)**	**Chromium concentration factor**	**Water output (m^3/h)**	**Flux (LMH)**	**Max Pressure (bar)**	**Reusability of concentrate**	**Reference**	**Comments**
Cr(VI) 1800	UF/RO	Not reported	13.26	0.03	-	46	Yes	[31]	Rejection of 98.6% for chromium. Flux not reported.
Cr(VI) 1.9	RO	Not reported	3.33	0.07	5-15	8	No	[30]	UF pretreatment. Metal, organic/inorganic compounds removed by RO with effectiveness 91.3-99.8%. RO permeate reuse investigated.
Cr(VI) 100-1000	RO	Not reported	4.5	0.125	30-60	60	No	[29]	Rejection < 98% for concentration of 1000 mg/L. RO concentrate used to enable recovery of heavy metals through the ferrite process and ion exchange. Severe scaling observed.
Cr(VI) 84-228	NF/RO	Not reported	20	0.1	40-55	30	No	[28]	UF pretreatment. Permeate met requirements for reuse in rinsing bath.
Cr(III) 770	RO	Not reported	10.9	1.2×10^{-4}	3.75-7.5	80	Yes	[19]	Severe fouling observed.
Cr(III) 520-1080	Batch RO	<2.25	8-23	0.2-0.46	6-14	120	Yes	This study	Rejection >99.8% for chromium. No fouling

This study resulted in a SEC of 1.15-2.22 kWh per m^3 of treated wastewater corresponding to <2.42 kWh per m^3 of permeate water. None of the above studies reported SEC against which to compare. However, the SEC of traditional RO used in ZLD systems is reported to be 2-6 kWh/m^3. MVC, the most common thermal technique for ZLD, is highly energy intensive with SEC of 20–25 kWh/m^3 [51, 52].

The flux in this study was higher than in the other Cr(III) study, but lower than in the Cr(VI) studies. This is because of the need to overcome higher osmotic pressures of the Cr(III) solution caused by the presence of additional components.

6.7. Future research

Longer term testing is needed to assess fouling and durability in the industrial application and to define clean-in-place procedures that may be required. Post treatment for improved boron rejection may be investigated using a second RO pass. Another important area of future study is modelling of the boron permeability in RO membranes in the batch RO process. Advances in membranes could be useful to improve to boron rejection. They could also be useful to reduce further the SEC of the batch RO process [53].

It will also be useful to update the previous mathematical model [2, 11] of batch RO to predict behaviour and to design systems for a range of metal plating processes involving complex solutions. The simplified modelling presented here is only for the purpose of setting the switch point, and does not predict performance parameters such as SEC and rejection. Future research should also investigate the use of batch RO to treat rinse water containing other metals used in electroplating, such as copper and nickel. Moreover, future modelling and experimental studies may also address the issue of comparison between batch RO and multi-stage continuous RO systems that can also be used to achieve high recovery.

A further area of future research should be to explore the economic feasibility of batch RO in the metal plating wastewater application. In addition, a life cycle assessment (LCA) should be carried out to assess fully the environmental impacts and benefits of this technology.

7. Conclusions

In this study, a high-pressure batch RO system has been developed for an industrial ZLD application involving the treatment of Cr(III) rinse water. The main conclusions are:

- The system was designed for safe and reliable operation at 120 bar. Hybrid semi-batch/batch operation avoided the need for an excessively large work exchanger, thus enabling a compact design.
- An approach to setting the switch point from semi-batch to batch phase was introduced and experimentally validated. This enabled the peak pressure to be controlled to within 2.2% of a target value.
- The system provided >99.8% rejection of Cr(III), sulfate, and organics, such that the permeate was sufficiently free of these species for reuse in the rinse bath.
- Nonetheless, rejection of boric acid was only about 75%, such that a second RO pass may be needed to avoid boric acid contamination in the recycled rinse water.

- The batch RO system concentrated the rinse water sufficiently for reuse of Cr(III), sulfate, and organics in the electrolyte bath, providing 99.8% rejection of these species. At 120 bar, a concentration factor up to 23 was achieved, thus meeting the target for reuse. In comparison, 80 bar operation did not reliably achieve a sufficient concentration factor.
- Working at fluxes of 6-14 LMH, the system treated 0.21-0.46 m^3/hr of rinse water, meeting the requirements of the industrial electroplating process.
- SEC was 1.15-2.22 kWh per m^3 of treated wastewater, which is very competitive in the field of RO, and greatly superior to thermal methods, or to alkaline precipitation with UV pretreatment. In the industrial plant considered in this study, the new batch-RO process will reduce energy consumption by a factor of 50.
- No deterioration in membrane permeability or rejection occurred after 100 hours of testing, indicating absence of fouling.

In summary, the high-pressure batch RO process provides an energy-efficient, compact and robust solution to the previously unsolved problem of treating and recycling Cr(III) waste at industrial scale.

Acknowledgement

This project has received funding from the European Union Horizon 2020 research and innovation programme under grant agreement No 958454. We also acknowledge the assistance of Marcus Allard of ETS Design Ltd.

References

[1] D.M. Warsinger, E.W. Tow, K.G. Nayar, L.A. Maswadeh, Energy efficiency of batch and semi-batch (CCRO) reverse osmosis desalination, Water research, 106 (2016) 272-282.
[2] E. Hosseinipour, K. Park, L. Burlace, T. Naughton, P.A. Davies, A free-piston batch reverse osmosis (RO) system for brackish water desalination: Experimental study and model validation, Desalination, 527 (2022) 115524.
[3] A. Das, A.K. Rao, S. Alnajdi, D.M. Warsinger, Pressure exchanger batch reverse osmosis with zero downtime operation, Desalination, 574 (2024) 117121.
[4] E. Hosseinipour, E. Harris, H.A. El Nazer, Y.M.A. Mohamed, P.A. Davies, Desalination by batch reverse osmosis (RO) of brackish groundwater containing sparingly soluble salts, Desalination, 566 (2023) 116875.
[5] A. Das, A. Naderi Beni, C. Bernal-Botero, D.M. Warsinger, Temporally multi-staged batch counterflow reverse osmosis, Desalination, 575 (2024) 117238.
[6] H. Abu Ali, M. Baronian, L. Burlace, P.A. Davies, S. Halasah, M. Hind, A. Hossain, C. Lipchin, A. Majali, M. Mark, T. Naughton, Off-grid desalination for irrigation in the Jordan Valley, Desalinaation and Water Treatment, 168 (2019) 143-154.
[7] S. Cordoba, A. Das, J. Leon, J.M. Garcia, D.M. Warsinger, Double-acting batch reverse osmosis configuration for best-in-class efficiency and low downtime, Desalination, 506 (2021) 114959.
[8] P.A. Davies, J. Wayman, C. Alatta, K. Nguyen, J. Orfi, A desalination system with efficiency approaching the theoretical limits, Desalination and Water Treatment, 57 (2016) 23206-23216.
[9] J.R. Werber, A. Deshmukh, M. Elimelech, Can batch or semi-batch processes save energy in reverse-osmosis desalination?, Desalination, 402 (2017) 109-122.
[10] K. Park, P.A. Davies, A compact hybrid batch/semi-batch reverse osmosis (HBSRO) system for high-recovery, low-energy desalination, Desalination, 504 (2021) 114976.
[11] E. Hosseinipour, S. Karimi, S. Barbe, K. Park, P.A. Davies, Hybrid semi-batch/batch reverse osmosis (HSBRO) for use in zero liquid discharge (ZLD) applications, Desalination, 544 (2022) 116126.
[12] B.R. Babu, S.U. Bhanu, K.S. Meera, Waste Minimization in Electroplating Industries: A Review, Journal of Environmental Science and Health, Part C, 27 (2009) 155-177.
[13] E. Vaiopoulou, P. Gikas, Regulations for chromium emissions to the aquatic environment in Europe and elsewhere, Chemosphere, 254 (2020) 126876.

[14] S.S. Hosseini, E. Bringas, N.R. Tan, I. Ortiz, M. Ghahramani, M.A.A. Shahmirzadi, Recent progress in development of high performance polymeric membranes and materials for metal plating wastewater treatment: A review, Journal of Water Process Engineering, 9 (2016) 78-110.
[15] https://www.zvo.org/publikationen/jahresbericht/, access date: 12-02-2024.
[16] https://www.zvo.org/indizes/rohstoffpreisindex-verchromung, access date: 12-02-2024.
[17] Commission Regulation (EU) No. 348/2013 of 17 April 2013 amending Annex XIV to regulation (EC) No. 1907/2006 of the European parliament and of the council on the registration, evaluation, authorisation and restriction of chemicals (REACH). Off. J. Eur. Union 2013, L108, 1–5.
[18] A. Pechova, L. Pavlata, Chromium as an essential nutrient: a review, Veterinární medicína, 52 (2007) 1.
[19] R. Engstler, J. Reipert, S. Karimi, J.L. Vukušić, F. Heinzler, P. Davies, M. Ulbricht, S. Barbe, A reverse osmosis process to recover and recycle trivalent chromium from electroplating wastewater, Membranes, 12 (2022) 853.
[20] M. Leimbach, C. Tschaar, D. Zapf, M. Kurniawan, U. Schmidt, A. Bund, Relation between Color and Surface Morphology of Electrodeposited Chromium for Decorative Applications, Journal of The Electrochemical Society, 166 (2019) D205.
[21] L. Büker, R. Dickbreder, R. Böttcher, S. Sadowski, A. Bund, Investigation of The Reaction Kinetics of Chromium(III) Ions with Carboxylic Acids In Aqueous Solutions and The Associated Effects on Chromium Deposition, Journal of The Electrochemical Society, 167 (2020) 162509.
[22] Y. Xia, J. Yu, S. Jin, Q. Cheng, Performance analysis of electroplating wastewater treatment system combining air compression expansion cycle with spray drying tower, Applied Thermal Engineering, 184 (2021) 116257.
[23] J. Yang, C. Zhang, Z. Zhang, L. Yang, Electroplating Wastewater Concentration System Utilizing Mechanical Vapor Recompression, Journal of Environmental Engineering, 144 (2018) 04018053.
[24] M.T. Kamar, H. Elattar, A.S. Mahmoud, R.W. Peters, M.K. Mostafa, A critical review of state-of-the-art technologies for electroplating wastewater treatment, International Journal of Environmental Analytical Chemistry, (2022) 1-34.
[25] A.A. Azmi, J. Jai, N.A. Zamanhuri, A. Yahya, Precious Metals Recovery from Electroplating Wastewater: A Review, IOP Conference Series: Materials Science and Engineering, 358 (2018) 012024.
[26] K. Staszak, I. Kruszelnicka, D. Ginter-Kramarczyk, W. Góra, M. Baraniak, G. Lota, M. Regel-Rosocka, Advances in the Removal of Cr(III) from Spent Industrial Effluents—A Review, in: Materials, 2023.
[27] I. Frenzel, D.F. Stamatialis, M. Wessling, Water recycling from mixed chromic acid waste effluents by membrane technology, Separation and Purification Technology, 49 (2006) 76-83.
[28] E. Piedra, J.R. Álvarez, S. Luque, Hexavalent chromium removal from chromium plating rinsing water with membrane technology, Desalination and Water Treatment, 53 (2015) 1431-1439.
[29] S. Chung, S. Kim, J.-O. Kim, J. Chung, Feasibility of Combining Reverse Osmosis–Ferrite Process for Reclamation of Metal Plating Wastewater and Recovery of Heavy Metals, Industrial & Engineering Chemistry Research, 53 (2014) 15192-15199.
[30] I. Petrinic, J. Korenak, D. Povodnik, C. Hélix-Nielsen, A feasibility study of ultrafiltration/reverse osmosis (UF/RO)-based wastewater treatment and reuse in the metal finishing industry, Journal of Cleaner Production, 101 (2015) 292-300.
[31] J. Schoeman, J. Van Staden, H. Saayman, W. Vorster, Evaluation of reverse osmosis for electroplating effluent treatment, Water Science and Technology, 25 (1992) 79-93.
[32] J. Walker Jr, J. Wilson, C. Brown Jr, Minimization of chromium-contaminated wastewater at a plating facility in the Eastern United States, Environmental progress, 9 (1990) 156-160.
[33] N. Voutchkov, Energy use for membrane seawater desalination – current status and trends, Desalination, 431 (2018) 2-14.
[34] D. Cingolani, F. Fatone, N. Frison, M. Spinelli, A.L. Eusebi, Pilot-scale multi-stage reverse osmosis (DT-RO) for water recovery from landfill leachate, Waste Management, 76 (2018) 566-574.
[35] Q.J. Wei, C.I. Tucker, P.J. Wu, A.M. Trueworthy, E.W. Tow, J.H. Lienhard, Impact of salt retention on true batch reverse osmosis energy consumption: Experiments and model validation, Desalination, 479 (2020) 114177.
[36] https://buttondown.email/harmonyDesalting/archive/harmony-team-demonstrates-batch-ro-in-the-field/, access date: 12-02-2024.
[37] T.N. Philip Davies, Liam Burlace, Kiho Park, Desalination system and method, in: Internation application published under the patent cooperation treaty (PCT) 2022.

[38] D.M. Davenport, A. Deshmukh, J.R. Werber, M. Elimelech, High-Pressure Reverse Osmosis for Energy-Efficient Hypersaline Brine Desalination: Current Status, Design Considerations, and Research Needs, Environmental Science & Technology Letters, 5 (2018) 467-475.
[39] TRILYTE (R) FLASH SF, MacDermid Enthone, MDS number: 997301019/2, Process code: 081009/001 in: Technical data sheet, MacDermid Enthone, 2019.

[40]https://industrial.macdermidenthone.com/application/files/5215/7061/3130/TRILYTE_FLASH_SF_MEIS_B76_2018_1804.pdf, access date: 12-02-2024.
[41] Regulatory.DE@Macdermid.com, SAFETY DATA SHEET for TRILYTE Flash SF Make-Up

in: Safety data sheet, MacDermid Performance Solutions UK Limited, 2020.
[42] R.E. Stéphan Barbe, Sven Johann Bohr, Philip Davies, Somayeh Karimi, Ibrahim Hosseinipour, Andreas Sapalidis, Deliverable 3.3- Lab scale HRRO/IX unit, in: Project title: Intelligent Water Treatment for water preservation combined with simultaneous energy production and material recovery in energy intensive

industries, Grant Agreement Number: 958454, 2021.
[43] Regulatory.DE@Macdermid.com, TRILYTE Flash SF Buffer in: Safety data sheet, MacDermid Performance Solutions UK Limited, 2021.

[44] Regulatory.DE@Macdermid.com, TRILYTE Flash SF Replenisher in: Safety data sheet, MacDermid Performance Solutions UK Limited, 2021TRILYTE Flash SF Replenisher.

[45] Regulatory.DE@Macdermid.com, TRILYTE Wetting Agent in: Safety data sheet, MacDermid Performance Solutions UK Limited, 2021.

[46] X. Jin, C.Y. Tang, Y. Gu, Q. She, S. Qi, Boric Acid Permeation in Forward Osmosis Membrane Processes: Modeling, Experiments, and Implications, Environmental Science & Technology, 45 (2011) 2323-2330.
[47] Y. Cengeloglu, G. Arslan, A. Tor, I. Kocak, N. Dursun, Removal of boron from water by using reverse osmosis, Separation and Purification Technology, 64 (2008) 141-146.
[48] M. Li, Effects of finite flux and flushing efficacy on specific energy consumption in semi-batch and batch reverse osmosis processes, Desalination, 496 (2020) 114646.
[49] S. Nakaya, A. Yamamoto, T. Kawanishi, N. Toya, H. Miyakawa, K. Takeuchi, M. Endo, Detection of dynamic biofouling from adenosine triphosphate measurements in water concentrated from reverse osmosis desalination of seawater, Desalination, 518 (2021) 115286.
[50] D.M. Warsinger, E.W. Tow, L.A. Maswadeh, G.B. Connors, J. Swaminathan, J.H. Lienhard V, Inorganic fouling mitigation by salinity cycling in batch reverse osmosis, Water Research, 137 (2018) 384-394.
[51] T. Tong, M. Elimelech, The Global Rise of Zero Liquid Discharge for Wastewater Management: Drivers, Technologies, and Future Directions, Environmental Science & Technology, 50 (2016) 6846-6855.
[52] Y. Muhammad, W. Lee, Zero-liquid discharge (ZLD) technology for resource recovery from wastewater: A review, Science of The Total Environment, 681 (2019) 551-563.

[53] E. Hosseinipour and P. A. Davies, Effect of membrane properties on the performance of batch reverse osmosis (RO): The potential to minimize energy consumption, Desalination (2024): 117378.

Paper 6: Direct experimental comparison of batch reverse osmosis (RO) technologies

E. Hosseinipour[1*], P.A. Davies[1*]

[1]School of Engineering, University of Birmingham, Edgbaston, Birmingham, B15 2TT, UK

* e.hosseinipour@bham.ac.uk

* p.a.davies@bham.ac.uk

Graphical Abstract

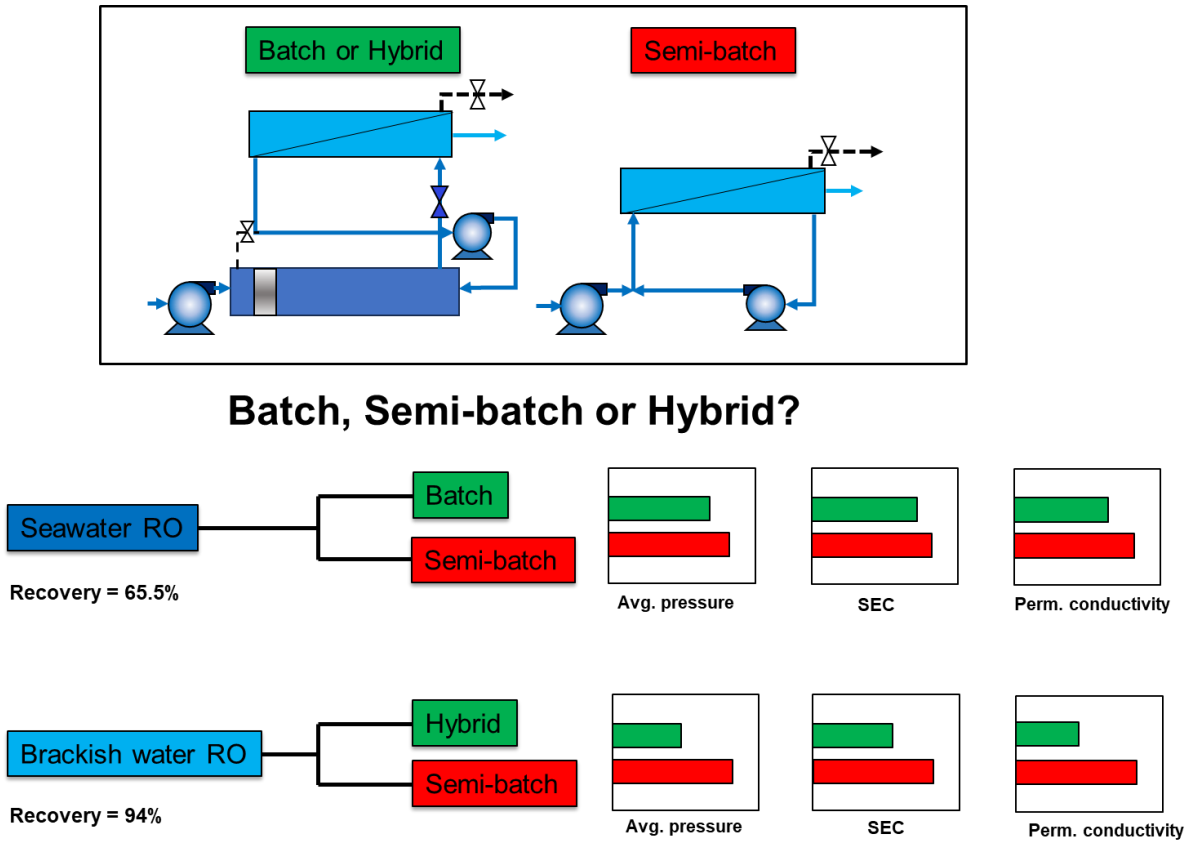

Abstract

Batch RO technologies can help fulfil the growing need for high-recovery desalination. Several experimental studies have given results for batch and semi-batch RO processes individually, but under differing conditions. There is a lack of side-by-side comparisons. Here we report, for the first time, experiments with a high-pressure RO system that can be operated in batch, semi-batch, or hybrid semi-batch/batch mode. Using the same membrane and supply pump at pressures up to 110 bar, we compare performance against semi-batch mode as the baseline throughout. With seawater feed, batch RO reduces electrical *SEC* by 10% at recovery of 0.655. With brackish water feed, we use hybrid mode to avoid an excessively large work exchanger volume. Working at recovery of 0.94, a work exchanger volume of 20 L reduced *SEC* by 23%. A work exchanger volume of 40 L reduced *SEC* further, resulting

in *SEC* of 1.81, 1.89 and 2.02 kWh/m^3 at recoveries of 0.9, 0.92 and 0.94 respectively, thus representing a 22-32% reduction against the semi-batch baseline. The results also showed permeate conductivity reduced by up to 50%. The study confirms the advantages of batch and hybrid RO over semi-batch RO, especially for brackish water desalination at high recovery.

Keywords: Batch RO, Semi-batch RO, High recovery, Energy efficiency, Permeate quality.

Highlights:

- First direct experimental comparison among batch, semi-batch and hybrid RO.
- First experimental investigation of seawater desalination with 120 bar batch RO.
- Tests also included brackish water feed.
- Effect of work exchanger volume investigated.
- Hybrid mode achieved up to 32% saving in *SEC* over semi-batch mode.

Nomenclature

Symbols

J_w	L/m^2/h, Flux
r	-, Water recovery
V_b	L, Swept volume of work exchanger
V_{b0}	L, Swept volume to achieve defined recovery in batch mode

Abbreviations

CF	Concentration Factor
ERD	Energy Recovery Device
HSBRO	Hybrid Semi-batch/Batch Reverse Osmosis
PLC	Programmable Logic Controller
RO	Reverse Osmosis
SEC	Specific Energy Consumption
SI	Supporting Information
TDS	Total Dissolved Solids

1. Introduction

Interest in high-recovery desalination is increasing in several application areas. For example, in the desalination of brackish groundwater, there is an increasing need for high-recovery desalination to conserve limited groundwater resources [1-3]. In seawater desalination, high-recovery desalination is interesting for brine mining and mineral recovery [4-7]. For industrial applications, it is an important aspect of Zero or Minimal Liquid Discharge systems needed to protect the environment against harmful brine discharges [8, 9]. Nevertheless, high recovery typically results in high specific energy consumption (*SEC*) [10, 11]. For this reason, there is a need to develop approaches that allow both high recovery and high energy efficiency.

An innovative approach to achieving low *SEC* in high-recovery desalination is the use of semi-batch and batch RO processes [12-14]. These processes are unsteady and cyclic, including at least two phases i.e., a pressurization (production) followed by a shorter purge (flushing) phase [12, 14]. This approach is well-suited to achieving high recovery while minimizing the system footprint [15, 16]. Such processes can achieve recoveries up to 0.98, subject to the scaling potential of the feed water and

operational pressure limit of the membrane [17]. They help to overcome the problems of flux imbalance that are detrimental to the efficiency of conventional, continuous flow RO systems when working at high recovery [18].

Semi-batch and batch RO are closely related technologies addressing similar applications, but the choice between them is not straightforward. The fundamental advantage of batch is that it avoids the mixing of low-salinity feed and high-salinity concentrate, which results in undesirable entropy generation and lower *SEC* than in the semi-batch case [14, 16]. The impact of this mixing becomes more pronounced as recovery increases [19]. Nonetheless, batch RO also has downsides: for example, it may require a large work exchanger vessel that increases the capital cost and makes the system relatively difficult to scale up. Therefore, to inform the choice of technology, it is important to have a reliable comparison of key performance parameters such as *SEC* and permeate quality. Nonetheless, direct experimental comparisons are missing in the literature.

Earlier studies compared batch vs semi-batch RO based on modelling alone. For example, Qiu and Davies [20] compared several configurations, including batch and semi-batch, while considering only the essential losses in each system. They calculated that batch would save about 34% energy compared to semi-batch when treating brackish water (4000 mg/L NaCl) at recovery of 0.8. Similarly, Werber et al. [13] showed that, for brackish water treatment at high recovery ($r > 0.75$), batch RO is the most energy-efficient configuration. Though they considered frictional losses in membrane and piping as well as concentration polarization, Werber et al. ignored the effects of osmotic backflow and salt retention in consecutive cycles. To reduce the need for a large work exchanger, Park et al. [16] introduced and modelled hybrid semi-batch/batch RO (HSBRO) using a free piston. For this hybrid arrangement, they predicted *SEC* even lower than batch RO at $r > 0.90$, considering non-idealities, such as salt retention, concentration polarization and frictional losses. Simplified assumptions about pipework losses were made. All three studies above ignored osmotic backflow and assumed 100% salt rejection. Either they ignored pump efficiency [20] or assumed it to be constant [13, 16].

In summary, theoretical studies have not consistently accounted for all factors affecting the performance of batch and semi-batch RO such as salt retention, friction losses, and osmotic backflow. They did not always give accurate predictions about rejection, permeate quality, and peak pressure – leaving uncertainties in comparing batch against semi-batch and hybrid operation. To remove these uncertainties, it is desirable to make a comparison based on experiments.

Since the above theoretical studies were written, more batch RO prototypes have been built and reported on, making more experimental comparisons possible in principle. Table 1 summarises the most relevant experimental studies, each of which has been conducted on either a batch, semi-batch or hybrid system (but not comparing all three). Nonetheless, these studies do not easily enable a fair comparison, because of variations in the:

(1) Feed water composition, which affects osmotic pressure, affecting in turn the feed pressure and *SEC*.

(2) Recovery, which also affects osmotic pressure, feed pressure and *SEC*.

(3) Rejection, which affects the differential osmotic pressure across the membrane.

(4) Type of membrane (including its age and condition) which affects transmembrane pressure drop, which also contributes to *SEC*.

(5) Transmembrane water flux (as determined by the supply pump flow rate) which also affects transmembrane pressure drop.

(6) Pipework design which affects salt retention and friction losses, which further minor contributions to *SEC*. These losses are also related to the flows of the supply and recirculation pumps.

(7) The type of feed pump and recirculation pump (including electric motor, any gearing and variable frequency drive) the efficiencies of which have a multiplying effect on overall energy efficiency.

(8) The ratio of the recirculation flow to the supply flow, which determines the single-pass recovery. This influences the concentration polarization factor: a higher single-pass recovery exacerbates concentration polarization, leading to increased energy usage by the supply pump. Conversely, a lower single-pass recovery necessitates higher flow rates for the recirculation pump, thereby elevating its energy consumption. Hence, optimizing this factor involves a trade-off in the energy consumption between the two pumps, which is also affected by the pump efficiencies (see point 7 above).

Thus, all these eight factors affect energy efficiency and *SEC*. Second law efficiency may be used as an energy performance measure to correct for feedwater composition, recovery and rejection [21] but it does not account for the remaining four factors above. The data in Table 1 shows that a fair side-by-side comparison is not possible based on review of the literature alone, because of the non-comparable design and operating conditions. Moreover, studies did not report all the necessary information or report it in a uniform manner. For example, studies reported feedwater compositions differently – some as single salt concentration, others as total dissolved solids (TDS), and others as conductivity – making osmotic pressure corrections indirect and of limited accuracy. Details of pipework design were not reported in any of the semi-batch RO studies. At least 5 types of membrane were used in the studies and pump efficiencies were not always provided. Given that the above eight factors are mostly interrelated, it is especially difficult to draw accurate conclusions by comparing these experimental studies.

This paper sets out to address this research gap by making a direct experimental comparison. The objectives are to: (1) present a single system that can be run in semi-batch, batch or hybrid mode while using identical feed composition, membrane, pumps, and pipework; (2) run the system to provide a comparison of performance parameters (*SEC*, peak pressure, recovery, rejection, and permeate quality). To cover a range of operating conditions, both seawater and brackish water feeds are used. Besides being the first direct experimental comparison among batch RO technologies, to our knowledge, this is the first experimental study of batch RO using seawater. Therefore, this study is expected to be of value in selecting and designing batch RO technologies to address a range of applications.

Table 1. Comparison of experimental studies regarding batch and semi-batch RO performance.

Technology	Feed water composition	Overall Recovery	Single pass recovery	Permeate flux ($L/m^2/h$)	Salt rejection	*SEC* (kWh/m^3)	Membrane type	Pump efficiency	Notes	Reference
Free-piston batch RO	NaCl solution: 1000-5000 mg/L	0.8	0.2-0.4	11-21	93-98%	Hydraulic: 0.22-0.48, Electrical: 0.48-0.83	FilmTec™: Eco-Pro 440	High-pressure: 55-65%, Recirculation: 25-40%	The pilot system includes one 8-in RO module and a work exchanger volume of 69 L (9.5-in × 2 m pressure vessel), housing the free-piston.	[22]
Free-piston batch RO	Synthesised groundwater with TDS of 1180-3637 mg/L	0.8	0.3	11-22	94-97%	Hydraulic: 0.2-0.45	FilmTec™: Eco-Pro 440	Not stated	As above.	[23]
Free-piston batch RO	NaCl solution: 1000-5000 mg/L	0.8	0.3	11-23	86-99%	Hydraulic: 0.15-0.48 Electrical: 0.38-0.79	Aquaporin: Ultra Dupont: XLE Dupont: BW30HR Toray: TMH20A	High-pressure: 55-65%, Recirculation: 25-40%	As above.	[24]
Hybrid semi-batch/batch RO	NaCl solution: 500-1500 mg/L	0.94-0.95	0.2-0.4	12-24	93-94%	Hydraulic: 0.2-0.31, Electrical: 0.48-0.83	FilmTec™: Eco-Pro 440	High-pressure: 50-60%, Recirculation: 25-40%	As above.	[14]
Bladder-type batch RO	NaCl solution: 2000-5000 mg/L	0.3-0.5	Not stated	10-20	87-97%	Hydraulic: 0.24-0.31	Hydranautics: ESPA-2514	Not stated	Bench-scale prototype, a pressure vessel houses a custom-moulded silicone bladder and a 2.5-in spiral wound membrane element.	[25]
Semi-batch RO	Brackish water sources: 4.0-6.8 mS/cm	0.8 and 0.88	Not stated	19 and 27	91 and 88%	Electrical: 0.82 and 0.8	Hydranautics: ESPA2+	High-pressure: 55-60% Recirculation: not stated	A pilot of eight 4-element pressure vessels. Brine was replaced with fresh feed through a side conduit.	[26]
Semi-batch RO	NaCl solution: 1000-5000 mg/L	0.7-0.9	0.15-0.2	17-44	Not stated	Hydraulic: 0. 4-1.7	FilmTec™: BW30-2540	Not stated	The pilot consists of two parallel pressure vessels each containing one 2.5-in module. There is a holding tank, similar to work exchanger in batch RO. Measurements were done in the	[27]

									first cycle (maximum recovery), ignoring the salt retention effect.	
Semi-batch RO	3rd-stage RO concentrate used as feed with a mean TDS of 6500 mg/L	0.4-0.66	Not stated	11-13.6	98-99%	Not stated	Hydranautics: ESPA2-LD, followed by FilmTec™: BW30 XFRLE-400	Not stated	Semi-batch RO was operated as the fourth stage RO. The industrial pilot called Desalitech ReFlex™ Max was used.	[28]
Semi-batch RO	Seawater: TDS of 33,800-37,200 (EC of 48.8–54.6 mS/cm)	0.42-0.53	Not stated	9.2-13.4	98-99%	Electrical: 1.45–1.78	NanoH_2O (LG): SW-400-ES	High-pressure: 80-82%, Recirculation: 38-45%	A pilot of four 4-element pressure vessels. The brine was replaced with fresh feed through a side conduit.	[29]

2. Materials and methods

2.1. Batch RO system and experimental method

The batch RO system and its method of operation has been described in earlier publications [14, 22, 23]. Here it has been upgraded for 120 bar operation and fitted with a high-pressure spiral-wound RO element (Dupont XUS180808, see Table 2). The supply pump is a plunger type (manufactured by CAT PUMPS, model: 3CP1241G with a pressure range of 6.9 to 138 bar) driven by a 3-phase AC induction motor. The recirculation pump is a bespoke centrifugal pump driven by a 24V DC motor. The work exchanger is a free-piston type. Fig. 1 shows this system in the laboratory at the University of Birmingham. Further experimental details, including a list of the main components are included in the Supporting Information (SI). The high-pressure RO system has been tested in applications including metal plating wastewater recovery, and has been described elsewhere [30]. The system is controlled by a Programmable Logic Controller (PLC).

Table 2. Specifications of the RO membrane element used in this study.

Membrane type	Active area (m^2)	Feed spacer thickness (mm)	Element diameter (inch)	Maximum operating pressure at 30°C (bar)
DuPont™ XUS180808	30.6	0.864	8	120

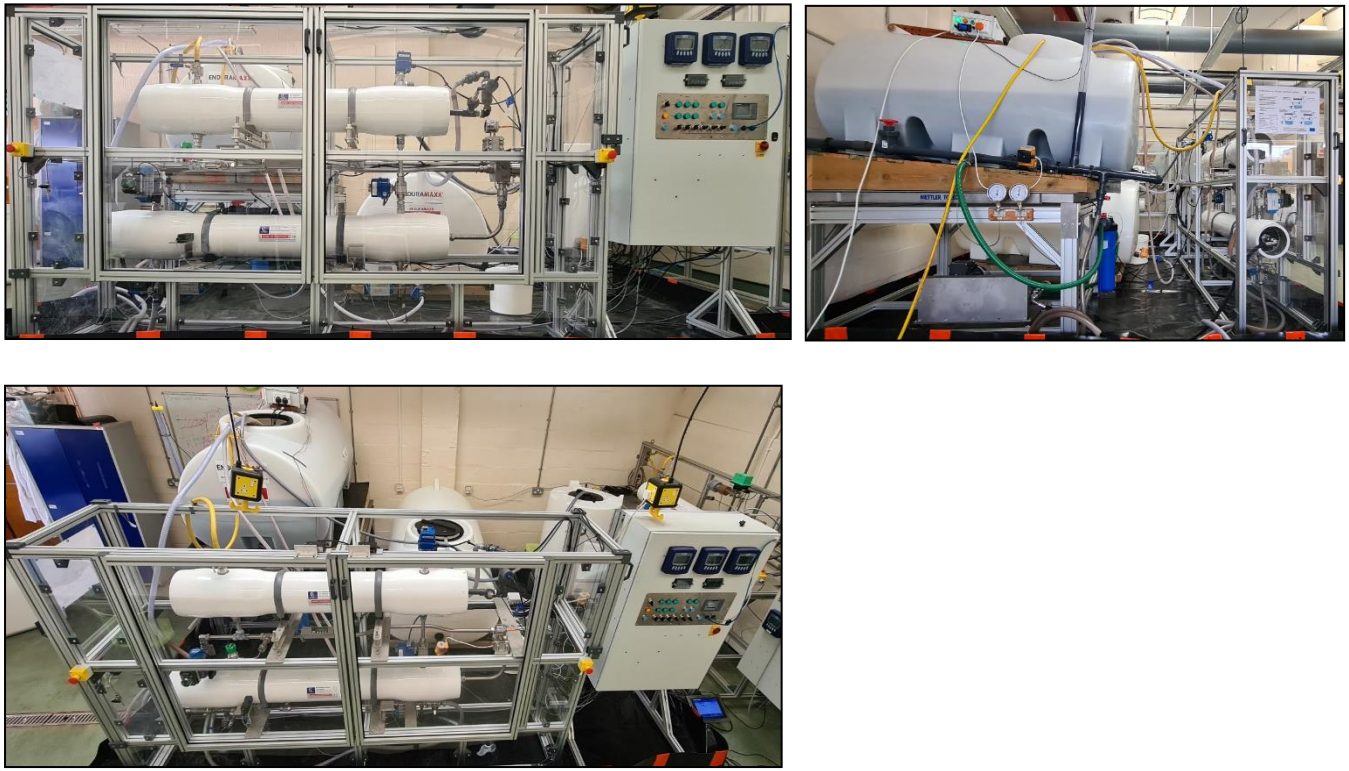

Fig. 1. High-pressure (120 bar) batch RO system. The feed tank was elevated to ensure positive pressure for the high-pressure pump.

2.2. Modes of operation

Fig. 2 shows the three cyclic modes: semi-batch, batch, and hybrid semi-batch/batch RO. The mode is determined by the valve sequence (Table 3) and using extension rods to restrict the movement of the piston (see Fig. 3 and Table 4). A longer extension rod locked the piston fully to the right making the work exchanger non-operational, such that the equipment operated in semi-batch mode only (Fig. 3A). Using a shorter extension rod, the swept volume was restricted to 20 L (Fig. 3B). Without any extension, it was 40 L approximately (Fig. 3C).

The extension rod gives the same effect as a smaller work exchanger vessel. It was used here for experimental convenience, as it was not feasible or necessary to swap out work exchanger vessels in the experimental set-up. Nonetheless, in a practical application, a smaller work exchanger vessel would be used in place of a piston extension rod, once the work exchanger volume is determined.

(A)

Semi-batch mode	Batch mode	Hybrid mode
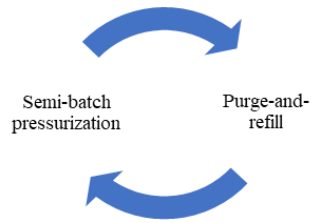	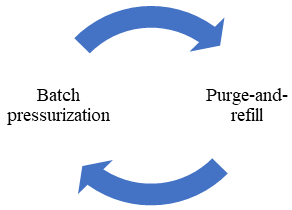	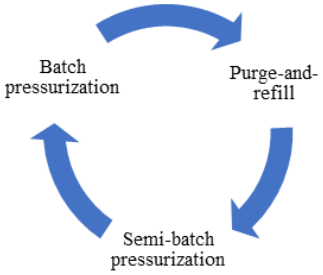

(B)

Phase	Schematic
Semi-batch pressurization (in semi-batch mode)	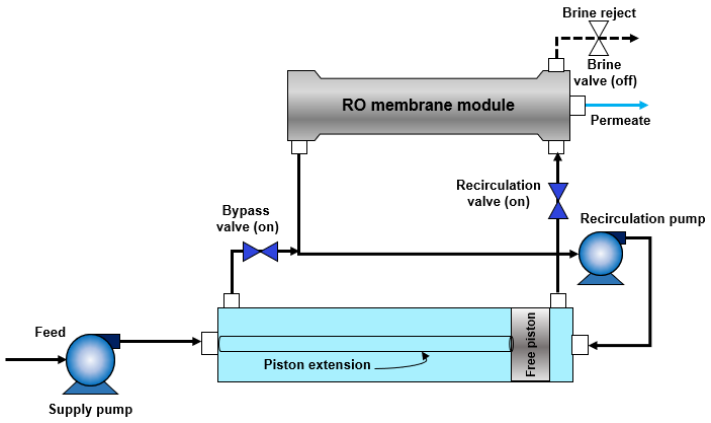

Semi-batch pressurization (in hybrid mode)	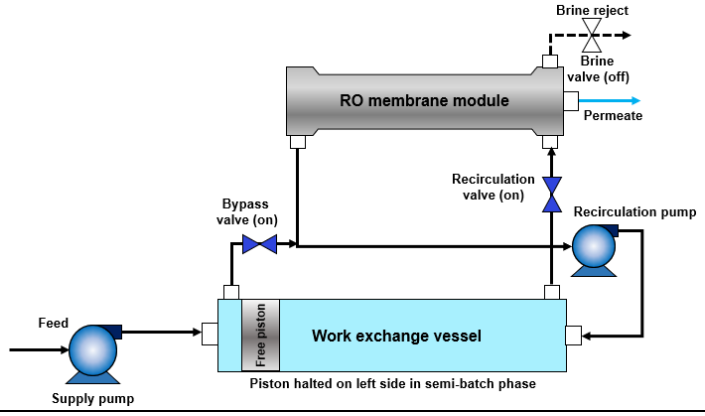
Batch pressurization (full stroke, 40 L swept volume)	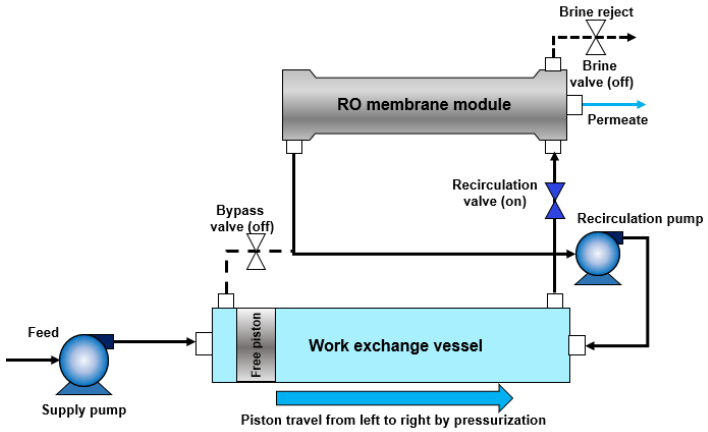
Batch pressurization (reduced stroke, 20 L swept volume)	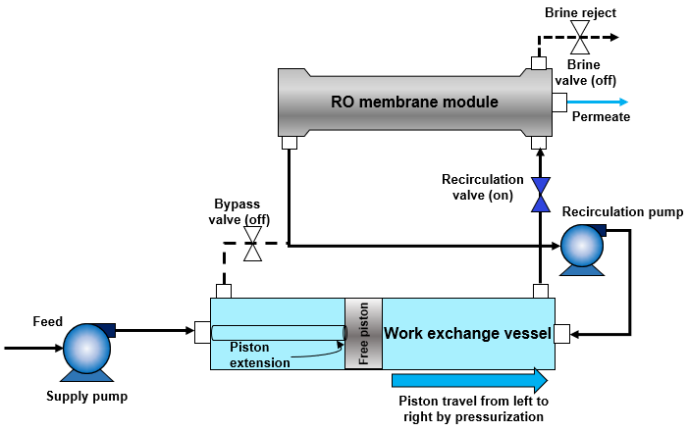
Purge-and-refill	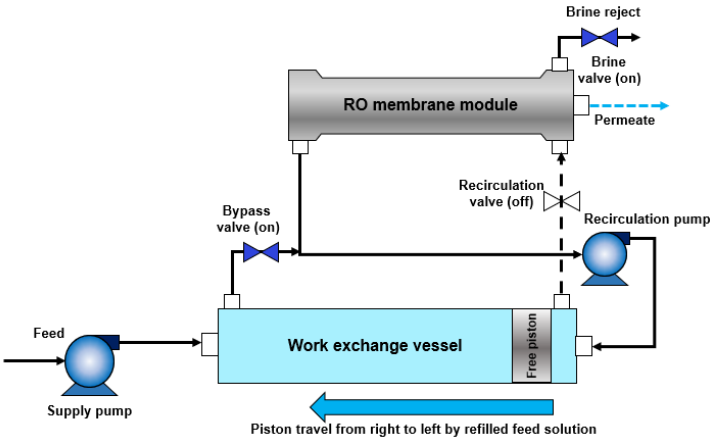

Fig. 2. Illustration of how semi-batch, batch and hybrid modes of operation are achieved in the batch RO system. (A) Phases of cyclic operation in each mode; (B) Schematics of each phase – including the option of reduced stroke in the batch pressurization phase which is achieved by restricting the leftward movement of the piston using an extension rod. Solid and dashed lines indicate flow and no-flow, respectively.

Table 3. Position of the valves in different phases of operation in the free-piston batch RO pilot, as determined by the PLC program.

	Valve		
	Bypass	Recirculation	Brine
Semi-batch phase	Open	Open	Closed
Batch phase	Closed	Open	Closed
Purge-and-Refill phase	Open	Closed	Open

Fig. 3. Photo of piston variants with extension rods, providing different work exchanger swept volumes of A) $V_b = 0$ (longer extension rod) B) $V_b = 20$ L (shorter extension rod) and C) $V_b = 40$ L (full stroke, no extension rod).

Table 4. Details of piston variants used in work exchanger (internal diameter of 202 mm) to achieve different swept volumes.

Variant (Fig. 3)	Nominal swept volume, V_b (L)	Actual swept volume (L)	Stroke (mm)	Mode where used
(A)	0	0	0	Semi-batch
(B)	20	19.6	545	Hybrid
(C)	40	38.5	1130	Hybrid and batch

2.3. Feed water

Approximately 1 m^3 of seawater, originating from the English Channel, was procured from Shirley Aquatics, Birmingham. The electrical conductivity at 25 °C was measured as 50 mS/cm. The analysis of anion and cation content, determined by ion chromatography, is shown in Table S2 in the SI.

For the tests with brackish feed, brackish water of concentration 5000 mg/L was prepared by dissolving reagent grade NaCl (Fisher Scientific, ACS grade, 99.5% purity) in 1500 L of tap water with TDS < 100 mg/L. To protect the RO membrane against oxidation, 4.5 mg of sodium metabisulfite was added to remove free chlorine.

During experiments, the feed tank was kept mixed, and the temperature was maintained at a constant 25 ± 0.5°C. Prior to entering the high-pressure supply pump, the feed solution passed through a 1-micron 20-in cartridge filter to remove small particles and protect the RO module.

Table 5 summarises the operating conditions used in the seawater and brackish water experiments. While the operating limit of the system was 120 bar, a 110 bar limit was adopted to provide a safety margin. This pressure limit imposed some constraints in the case of seawater because of its high concentration and osmotic pressure compared to brackish water. Thus, lower flux and recovery were used with seawater, and the brine volume per cycle was increased slightly to lower salt retention and moderate the peak pressure.

Table 5. Summary of experimental parameters.

		Seawater feed	**Brackish water feed**
Feed TDS (mg/L)		32000	5000
Feed conductivity (mS/cm)		50	9.1
Brine volume/cycle (L)		18	16
Swept volume, V_b (L)	Semi-batch mode	0	0
	Hybrid mode	Not used	20, 40
	Batch mode	40	Not used
Feed flow (L/min)		6.2	8.8
Recirculation flow (L/min)		30-35	30-35
Flux, J_w (L/m^2/h)		10.5	16.8
Recovery, r		0.655	0.9 – 0.94
Maximum allowable system pressure (bar)		120	
Peak pressure used in experiments (bar)		110	

2.4. Data logging and analysis

Data were recorded at intervals of approximately 1 s, including weights of the feed, permeate, and brine tanks, electrical conductivities of the feed, permeate, and brine streams, feed pressure before and after the piston, permeate pressure, power consumption of the feed and recirculation pumps, recirculation flow rate, and differential pressure measuring the pressure drop across the recirculation pump.

Hydraulic *SEC* [kWh/m^3] was calculated by integrating and summing, over an entire cycle, the differential pressure p [kPa] of each pump (supply and recirculation pump, indicated by subscripts 'S' and 'R' respectively) with respect to the volume of water displaced V [m^3] by that pump at each measurement time step (~1 s), and dividing by the permeate volume, V_P (see

Eq. 1). The electrical *SEC* was similarly calculated by integrating and summing the recorded power *P* [kW] for each pump over time *t* [h] and then dividing by V_P (see Eq. 2).

$$\text{Hydraulic } SEC = \frac{\oint p_S . dV_S + \oint p_R . dV_R}{3600 . V_P} \quad (1)$$

$$\text{Electrical } SEC = \frac{\oint (P_S + P_R) . dt}{V_P} \quad (2)$$

$$\text{Pump efficiency}, \eta = \frac{Hydraulic\ SEC}{Electrical\ SEC} \quad (3)$$

As in previous studies [14, 31], data from the third cycle was analysed to allow the system to reach a steady state. Raw data are included as supplementary files.

3. Results

3.1. Comparison of batch vs semi-batch RO treating seawater

Despite several theoretical studies on seawater batch RO to our knowledge, no experimental results have yet been reported [13, 18, 25, 32, 33]. Here we test batch RO and compare it to semi-batch RO in treating seawater.

3.1.1. Applied pressure

In batch RO, the starting point of applied pressure for water permeation was lower than in semi-batch RO by about 21%. This difference can be attributed to lower salt retention in the batch process, where the initial internal system volume is much greater than in semi-batch, resulting in the dilution of retained salt. Throughout most of the process, the applied pressure in batch RO remained lower (see Fig. 4A). The applied pressure in batch mode increased from 47 to 110 bar while that of semi-batch RO rose from 60 to 107 bar. Although the final peak pressure was expected to be similar, the batch RO showed a slightly higher peak. This may be attributed to a better salt rejection in batch RO as opposed to the semi-batch RO (see section 3.2.3). The average applied pressure in batch RO was about 66.8 bar, below that of 79.4 bar in semi-batch RO, representing a 16% reduction (see Fig. 4B).

In semi-batch RO, internal volume remains constant while mass increases linearly with time (with nearly 100% salt rejection). Concentration and pressure thus grow linearly. In batch RO, mass remains constant, with linear reduction in volume over time with fixed permeate outflow. This causes concentration and pressure to rise hyperbolically at an accelerating rate (see Fig. 4A).

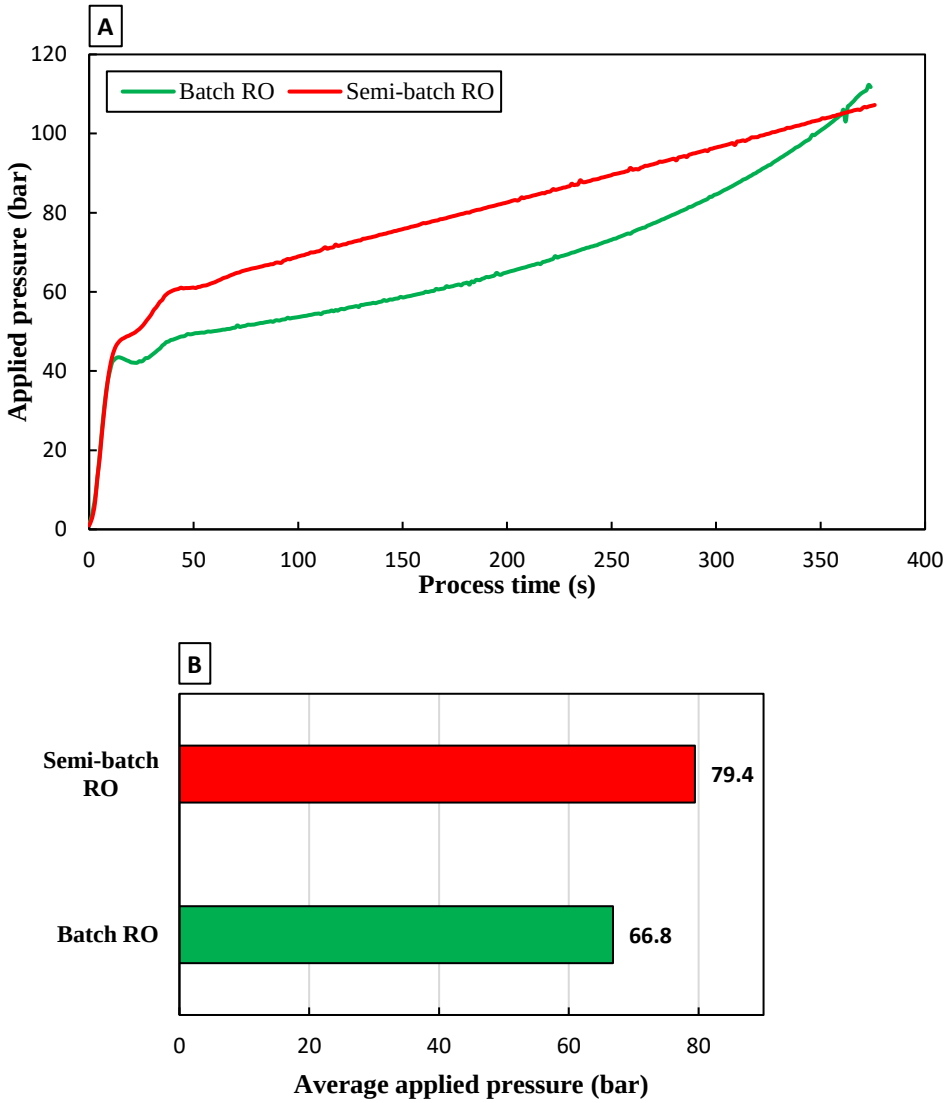

Fig. 4. Comparison of A) applied pressure variation, and B) average applied pressure of semi-batch RO ($V_b = 0$), and batch RO over a pressurization phase with seawater feed at $r = 0.655$ and $J_w = 10.5$ L/m^2/h.

3.1.2. Energy consumption

The lower applied pressure reduced *SEC* in batch RO *vs* semi-batch RO (see Fig. 5). For example, hydraulic *SEC* in batch mode was lowered by 13.4% from 2.62 down to 2.27 kWh/m^3. This is slightly less than the 16% reduction in average applied pressure because of parasitic power consumption by the recirculation pump (see Table S1). Regarding electrical *SEC*, the reduction was again smaller (about 10%, from 3.82 to 3.42 kWh/m^3) because of a better pump efficiency at the higher average pressures encountered in semi-batch mode. This points to the importance of optimised pump design and selection to suit the varying pressure requirements of batch RO.

Osmotic backflow has a negative effect on recovery and permeate output in both modes. Osmotic backflow was about 4.5 L; thus, approximately 13% of the output was lost. If this backflow could be eliminated, we could achieve higher recoveries (about 0.682) and lower *SECs*. For instance, without osmotic backflow, the hydraulic *SEC* of batch and semi-batch RO would drop to 2.0 and 2.31 kWh/m^3 while the electrical *SEC* would fall to 3.02 and 3.36

kWh/m^3 respectively. This corresponds to a 12% decrease in *SEC*. For the brackish water case, osmotic backflow is less of a problem because the cycles are longer and the output per cycle is much larger, such that osmotic backflow contributes only to a small fraction of the total output.

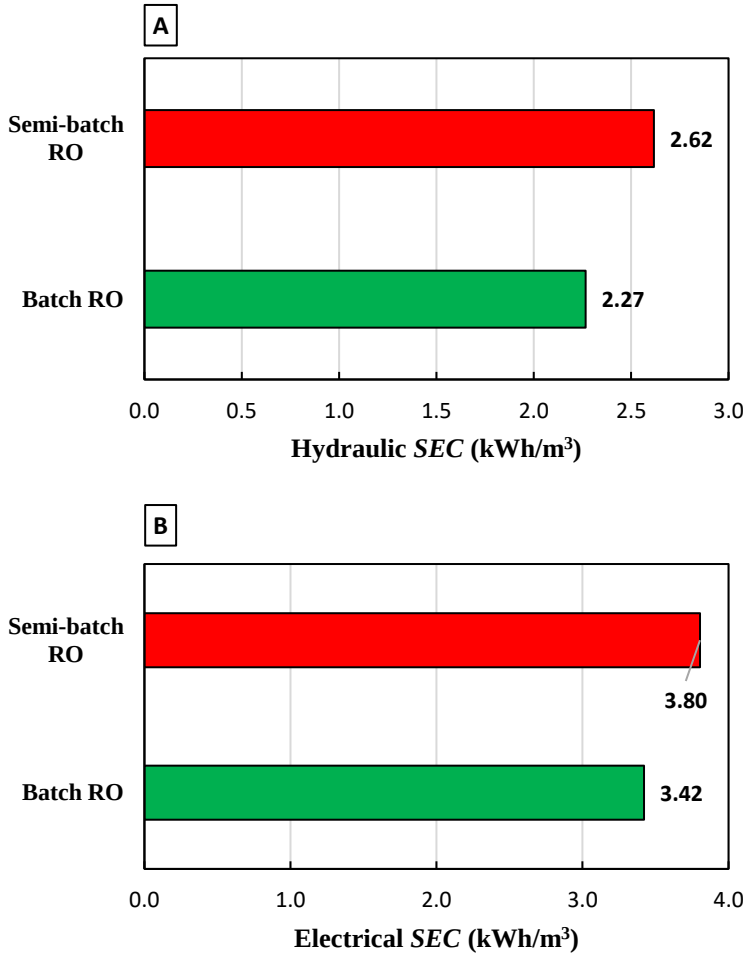

Fig. 5. Comparison of A) hydraulic and B) electrical *SEC* of semi-batch RO and batch RO ($V_b = 40$) with seawater feed, at $r = 0.655$, and $J_w = 10.5$ L/m^2/h.

3.1.3. Permeate quality

Fig. 6A shows the variation in permeate conductivity for batch and semi-batch RO during pressurization. Both systems showed a similar pattern, rapidly reaching an initial peak, followed by a sharp decrease to the lowest point. Subsequently, there was a gradual increase, albeit at a slower rate, as the internal concentration rose. Nonetheless, the permeate conductivity of batch RO was lower than that of semi-batch RO throughout permeate production. Excluding the initial peak, the permeate conductivity of batch RO ranged from 0.5 to 1 mS/cm, compared to 0.7 to 1.1 mS/cm for semi-batch. The initial peak could be excluded, for example, by diverting the permeate to the feed tank until its conductivity drops to its minimum value following the peak, and then collecting in the permeate tank as normal. Including the initial peak, however, the average permeate conductivities for batch and semi-batch RO were 0.75 and 0.96 mS/cm respectively (see Fig. 6B). Thus, the permeate quality of

batch RO was approximately 22% better than that of semi-batch RO. Nonetheless, the water produced by both systems falls within the acceptable range for both drinking and irrigation purposes. These permeate conductivities correspond to salt rejections of 0.985 and 0.981 for batch and semi-batch RO respectively, relative to the feed solution.

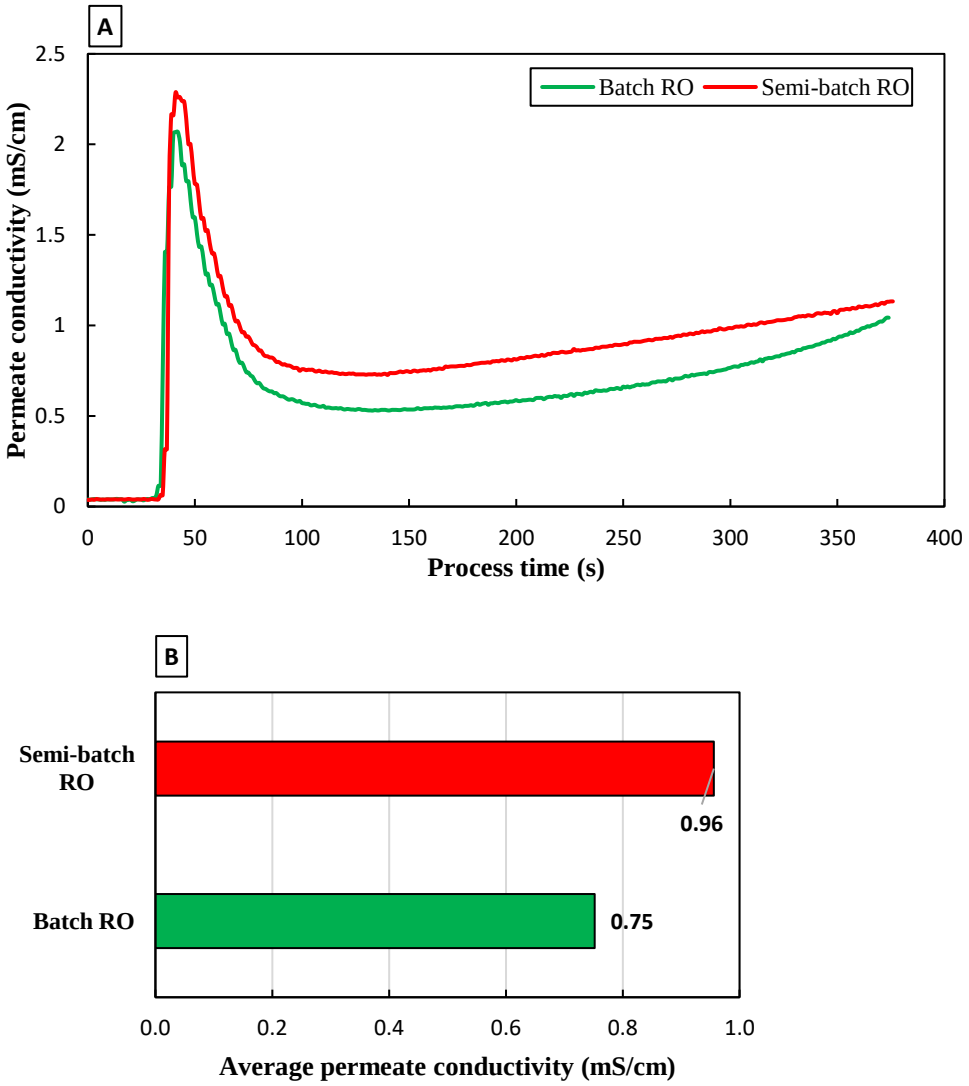

Fig. 6. Comparison of A) permeate conductivity variation, and B) average permeate conductivity of semi-batch RO ($V_b = 0$), and batch RO over a pressurization phase at $r = 0.655$, $J_w = 10.5$ L/m^2/h, seawater feed.

3.2. Comparison of HSBRO against semi-batch RO in treating brackish water

Brackish water experiments were carried out at recoveries of 0.9, 0.92 and 0.94. At such high recovery, pure batch operation would require a very large work exchange swept volume ($V_b >$ 150 L). Instead, hybrid mode was chosen with V_b of only 20 or 40 L thus providing a three-way comparison including the semi-batch RO baseline mode.

3.2.1. Applied pressure

Fig. 7A compares applied pressure throughout the pressurization phase. Although the final peak pressure was nearly identical across all three cases, the pressure variation leading to this peak diverged significantly. The starting pressure in hybrid mode was considerably lower than in semi-batch, while there was only a moderate gap in pressure between the cases of 40 and 20 L swept volume in hybrid mode. Water production in semi-batch mode started at about 47 bar and increased linearly with a steep slope until it peaked at about 100 bar. In hybrid mode with a batch volume of 20 and 40 L, it started at about 36 and 30 bar respectively and also peaked at about 101 bar. However, in hybrid mode, the applied pressure increased linearly at the semi-batch phase with a moderate slope (thanks to the work exchanger volume) and then at an increasing rate upon switching to the batch phase. This was theoretically predicted in the study by Li [34] and subsequently confirmed experimentally in this study. Li noted that although the initial and final applied pressures and concentrations for semi-batch RO and batch RO with varying cylinder sizes were almost similar, their temporal paths to reach to the final pressure differed. Our experimental findings align with this prediction (see Fig. 7A).

The average applied pressure in hybrid mode was much lower than in semi-batch mode in all experiments (Fig. 7B). For example, at recovery of 0.9, it reduced from 51.3 bar to 38 and 34 bar at V_b of 20 and 40 L respectively – a reduction of 26% and 34%. This gap increased with recovery, with corresponding reductions of 31% and 43% achieved at r = 0.94. These reductions were greater than observed with seawater feed in batch mode, where the recovery was limited to 0.655 and hybrid mode could not be used because of pressure limitations.

With the brackish feed, peak pressure was almost unaffected by the mode of operation, consistently reaching 67, 80 and 101 bar at recoveries of 0.90, 0.92, and 0.94 respectively. This means that, if we wanted to achieve such a high recovery using standard continuous RO, we would need to apply approximately such high pressures continuously, consuming more energy than in the hybrid or semi-batch mode.

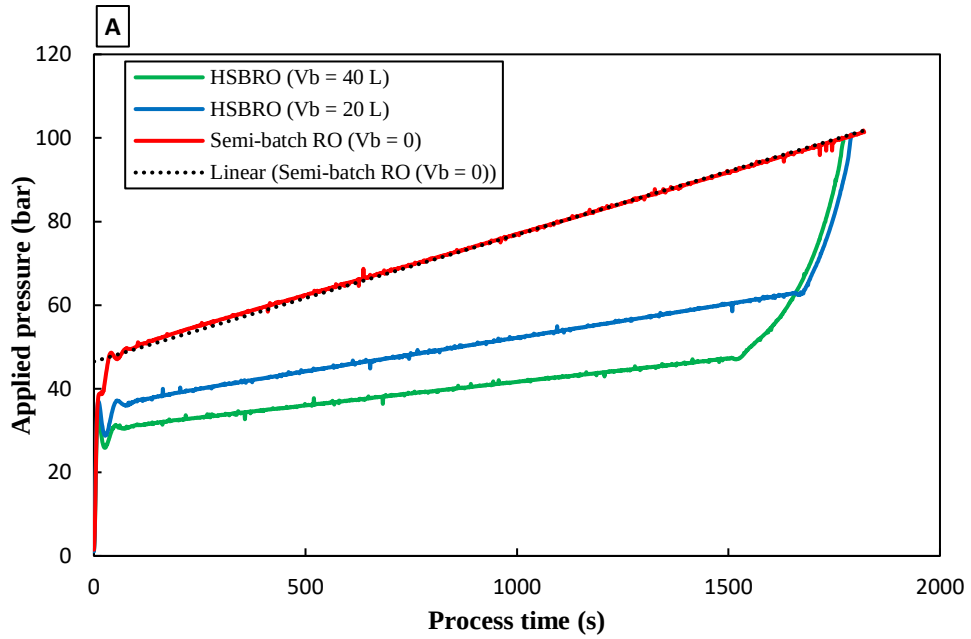

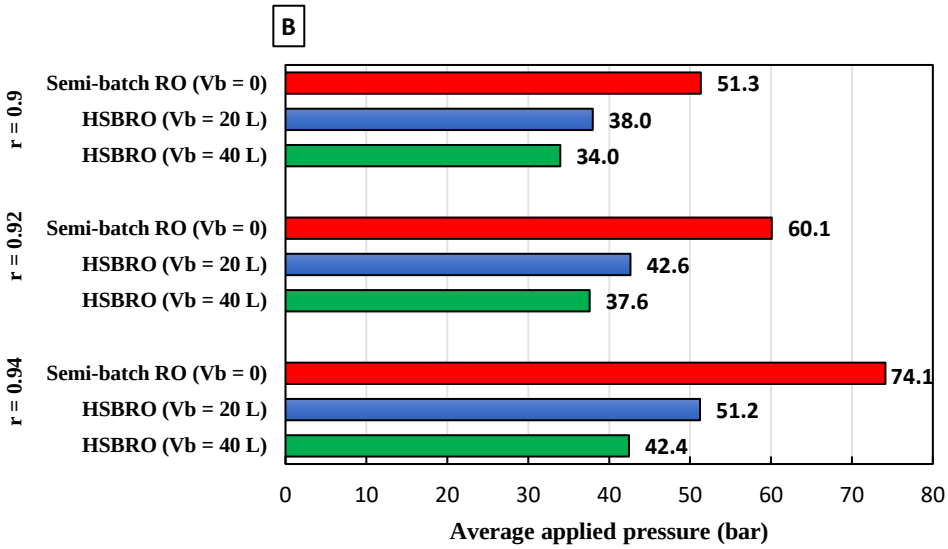

Fig. 7. Comparison of A) applied pressure variation, and B) average applied pressure of semi-batch RO ($V_b = 0$), and two cases of HSBRO (V_b = 20 and 40 L) at different recoveries, and J_w = 16.8 L/m^2/h, brackish water feed.

3.2.2. Energy consumption

Fig. 8A compares the hydraulic *SEC*, clearly demonstrating the advantage in energy efficiency of the hybrid system over semi-batch RO for treating brackish water. For instance, with V_b = 40 L, the hydraulic *SEC* of the hybrid system was 1.01, 1.10 and 1.23 kWh/m^3 at recovery of 0.9, 0.92, and 0.94 respectively – as such 32, 37 and 42% below semi-batch RO. Using a smaller swept volume of V_b = 20 L incured a slight penalty; for example, increasing hydraulic *SEC* back up to 1.48 kWh/m^3 at r = 0.94. Thus, the energy consumption gap between semi-batch RO and hybrid system widens as recovery increases, again highlighting more favourable results than with seawater feed.

Electrical *SEC* in hybrid mode was also lower than in semi-batch mode but by a smaller fraction. For instance, at r = 0.94, hybrid mode achieved a 42% reduction in hydraulic *SEC* compared to only 32% in electrical *SEC*. This difference was similar to that observed with the seawater feed and was also observed in earlier studies [14]. It shows that pump efficiency was not constant, in contrast to the assumptions made by the theoretical studies [13, 16, 35]. The high-pressure pump efficiency (i.e. hydraulic *SEC*/electrical *SEC*) was in the range of 60-65 % while that of the recirculation pump was only about 30-40 %.

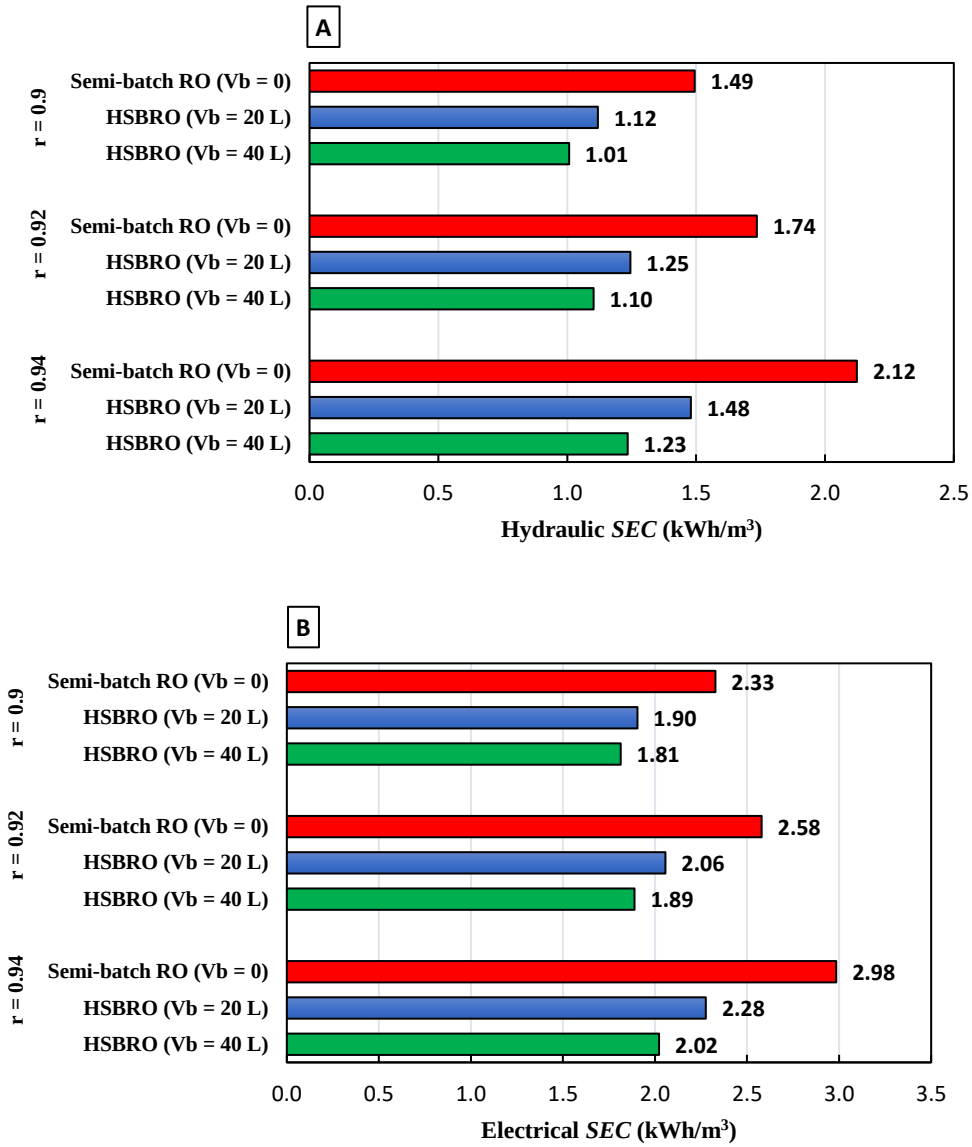

Fig. 8. Comparison of A) hydraulic and B) electrical *SEC* of semi-batch RO ($V_b = 0$), and two cases of HSBRO ($V_b \sim 20$ and 40 L) at different recoveries, and $J_w = 16.8$ L/m^2/h, brackish water feed.

3.2.3. Permeate quality and salt rejection

Fig. 9A compares how permeate conductivity varied with time over the pressurisation phase at $r = 0.94$. After the initial peak, the trends are similar to those in pressure, because increasing internal concentration affects pressure and permeate concentration similarly.

At $r = 0.94$, the average permeate conductivity produced by the hybrid system with $V_b = 40$ L was approximately half of the semi-batch RO system: 0.31 as opposed to 0.58 mS/cm. The average permeate conductivity of hybrid system with $V_b = 20$ L, was 20% higher compared to that of hybrid system with $V_b = 40$ L. The gap was smaller at lower recoveries of 0.92 and 0.9 (see Fig. 9B).

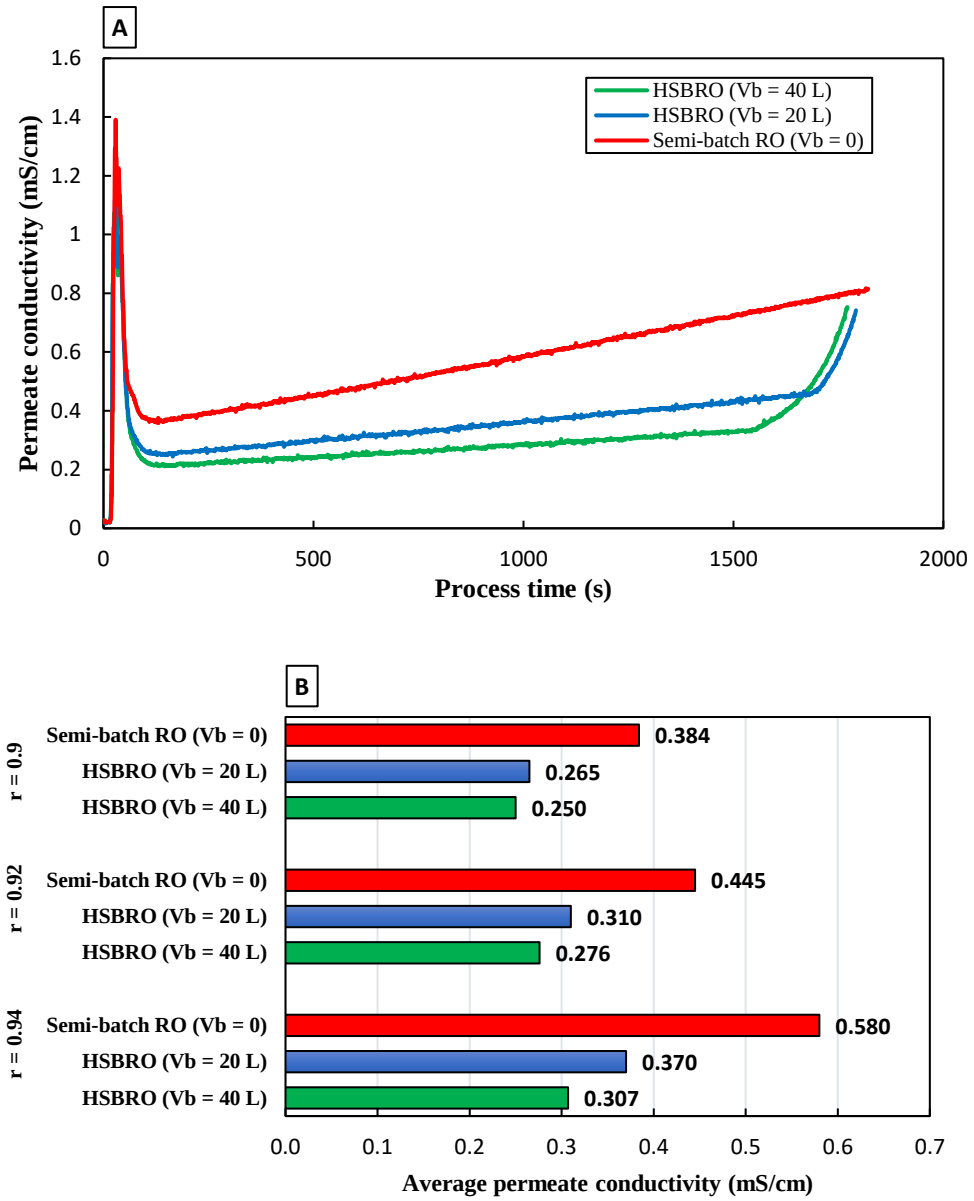

Fig. 9. Comparison of A) permeate conductivity variation, and B) average permeate conductivity of semi-batch RO ($V_b = 0$), and two cases of HSBRO ($V_b = 20$ and 40 L) at different recoveries, and $J_w = 16.8$ L/m^2/h, brackish water feed.

Fig. 10 compares the corresponding salt rejections. The total average salt rejection was in the range of 94 to 98% for all modes of operation and decreased with recovery. Nonetheless, salt rejection of hybrid system was higher than that of semi-batch RO. For instance, at recovery of 0.94, salt rejection in hybrid mode ($V_b = 40$ L) was 97% compared to only 94.3% in semi-batch mode.

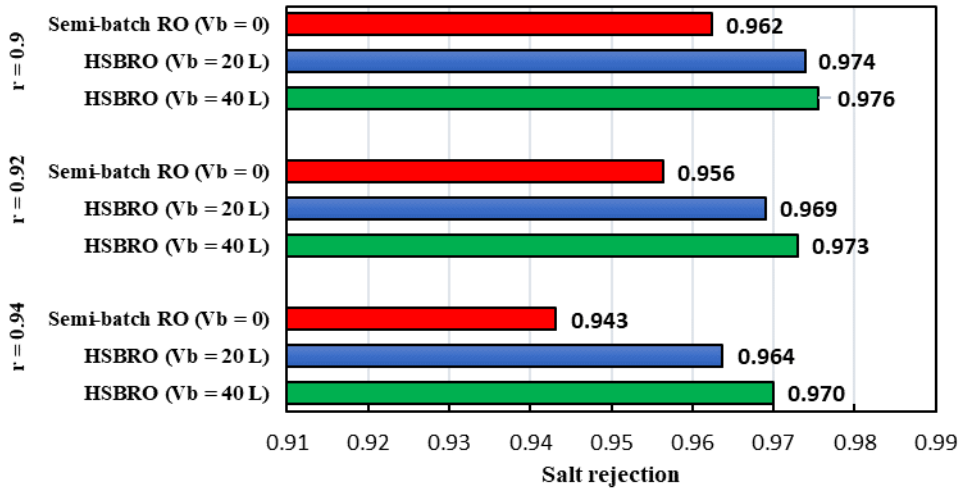

Fig. 10. Comparison of the average salt rejection of semi-batch RO ($V_b = 0$), and two cases of HSBRO ($V_b = 20$ and 40 L) at different recoveries, and $J_w = 16.8$ L/m^2/h, brackish water feed.

4. Discussion and conclusions

Next, we compare the experimental results against previous theoretical studies that compared the efficiency of batch RO technologies. Werber et al. [13] modelled batch and semi-batch RO in brackish water desalination at recovery of $r = 0.9$, and feed concentration of $c_{feed} = 5840$ mg/L (0.1M NaCl). Assuming a recirculation pump pressure drop of 0.1 bar, they calculated an *SEC* of about 0.4 kWh/m^3 for batch RO, down from 0.87 kWh/m^3 for semi-batch. This 54% reduction compares to only 32% reduction observed here. The likely reasons are the high membrane permeability of 3 L/m^2/h/bar, and high pump efficiency of 80% assumed in [13]. For the high-pressure membrane of the current study, the permeability is more likely around 1 L/m^2/h/bar [30] such that the frictional contribution to *SEC* is higher. This contribution is not affected by the choice of batch over semi-batch mode thus limiting the scope for *SEC* reduction. We also note that the high-pressure pump efficiency was lower at 60-65% in the current study.

Werber et al [13] also modelled the case of seawater desalination ($r = 0.5$, $c_{feed} = 35000$ mg/L). Interestingly, they predicted that semi-batch is more efficient than batch (with *SEC*s of 1.93 and 2.09 kWh/m^3 respectively). Our experiments have shown the opposite. This may be because their batch RO model assumed a non-pressurised vessel and ERD which introduced losses that were avoided in the free-piston design used here.

Also using a theoretical model, Park et al. [16] found that (at $r = 0.8$ and with a brackish feed of $c_{feed} = 3000$ mg/L), *SEC* of batch, hybrid and semi-batch RO were 0.386, 0.388, and 0.486 kWh/m^3, respectively. As such, the *SEC* of hybrid mode was 20% below that of semi-batch and marginally above that of the batch. However, at higher recoveries ($r > 0.89$), hybrid mode achieved lower *SEC* than batch, because it avoided the onerous transfer of fluid required to refill the large work exchanger of batch RO at high recoveries. Though the trend of these results agrees with the current study, a direct comparison is difficult because this study uses higher recoveries and did not include non-hybrid batch RO tests, because such tests would have required an impractically large work exchanger for brackish feed.

In an earlier study of a 25-bar system, Hosseinipour et al. [14] also predicted the effect of work exchanger volume in the hybrid mode. They found similar *SEC* values for batch and

hybrid modes with $V_b = 0.26V_{b0}$ (at $r = 0.94$, $c_{feed} = 1000$ mg/L, and $J_w = 18.9$ L/m^2/h). They predicted that reducing the work exchanger volume to $V_b = 0.15V_{b0}$ would result in a 7% increase in *SEC*. We similarly experimentally observed an 9% increase in *SEC* with a similar volume change. Nonetheless, it is important to note that the current study differed in terms of recovery ($r = 0.92$), feed concentration ($c_{feed} = 5000$ mg/L), water flux (16.8 L/m^2/h), and pressure (averaging about 38 bar compared to only 9 bar in [14]). Additionally, we employed a different membrane module with lower permeability. Thus, whereas the results agree generally, they are not directly comparable.

Qiu and Davies [36] reported hydraulic *SEC* of 0.26 and 0.17 kWh/m^3 for semi-batch and batch RO, respectively, while treating brackish water at $r = 0.8$, and $c_{feed} = 4000$ mg/L. These values are notably lower than those reported by Park et al. [16] primarily because the former did not account for most of the non-idealities such as membrane hydrodynamic losses. Additionally, they indicated a large gap between batch and semi-batch RO with a 34% reduction in *SEC* in contrast to the 20% reduction reported by Park et al. [16]. Comparing against these findings is difficult because, due to the limitation in work exchanger volume and pressure, the current study was unable to use high recoveries ($r > 0.7$) solely in batch RO mode, making hybrid operation necessary. Nevertheless, we observed a 32% reduction in hydraulic *SEC* at recovery of 0.9 which is consistent with previous findings.

Warsinger et al. [35] also conducted a theoretical comparison of batch and semi-batch RO, assuming pump efficiencies of 70%. At $r = 0.9$ and $c_{feed} = 3000$ mg/L, they predicted *SEC* of approximately 0.55 and 0.82 kWh/m^3 for batch and semi-batch RO, respectively. This prediction indicated a 33% reduction in *SEC* for the batch RO system, close to the reduction of 32% observed here when comparing hybrid RO with $V_b = 0.3V_{b0}$ against semi-batch RO. In our case, the comparison was made at the same recovery but with a higher feed concentration of $c_{feed} = 5000$ mg/L.

In their modelling study, Li [34] predicted that enhanced semi-batch RO (similar to batch RO with a free-piston design) exhibits comparable energy efficiency to the conventional multistage design but is approximately 30% more energy-efficient than the original semi-batch RO. The extent of energy savings further increases with the use of a smaller design flux. Moreover, they noted that the energy-saving advantage of the enhanced semi-batch over the original semi-batch becomes more evident as the recovery surpasses 0.9. This observation aligns closely with the trends observed in our experiments. In another theoretical study, Li et al. [37], predicted a SEC of approximately 0.433 kWh/m^3 for a three-stage system with a recovery of 0.9 and TDS < 1000 mg/L, while using booster pumps to improve uniformity of recovery and flux (predictions were conducted by assuming a pump efficiency of 80%). This SEC value is fairly comparable to those observed in batch RO system, as demonstrated in our previous study [14], where an electrical SEC of 0.456 kW/m^3 was recorded experimentally at a recovery of 0.95 and TDS of 1000 mg/L, albeit with a lower pump efficiency of only 60%.

Regarding future work, conducting a comparative experimental analysis between batch RO and continuous RO systems (e.g. single-stage and multi-stage) using the same equipment will provide a more accurate assessment of energy savings and performance parameters. In addition, while various studies have highlighted the energy efficiency advantages of batch RO compared to other methods, especially at high recovery rates, successful scaling up of this technology requires careful design and operation considerations. For instance, the availability of a

sufficiently large pressure vessel for use as the work exchanger presents a significant challenge. Therefore, there is a crucial need for comprehensive assessments and studies to evaluate the feasibility of scaling up batch RO for commercial viability.

In summary, depending on the operating conditions and assumptions used, the various modelling studies have predicted a 20-54% reduction in *SEC* for batch or hybrid mode as compared to semi-batch mode. Based on electrical *SEC*, this experimental study found reductions of 10% for seawater feed in batch mode, and 22-32% for brackish feed in hybrid mode. Because of pump characteristics, reductions in hydraulic *SEC* were greater, ranging from 13.4 to 42%. This confirms that *SEC* can be reduced significantly relative to semi-batch RO. The reduction could be further improved if a pump can be introduced that is optimised for the pressure variations in the batch RO process. Moreover, this study has shown the superior permeate quality obtained with batch and hybrid semi-batch/batch RO, which was not revealed by any of the earlier models or experiments. This study also highlights the need for more accurate models to represent the experimental results now available.

Acknowledgements

This project has received funding from the European Union's Horizon 2020 research and innovation programme under grant agreement No 958454 and from the Engineering and Physical Sciences Research Council (Grant Ref: EP/T025867/1).

Supplementary information

Table S1. A) Hydraulic, and B) electrical *SEC* (kWh/m^3) breakdown of semi-batch RO ($V_b = 0$), and batch RO over a pressurization phase at $r = 0.655$, and $J_w = 10.5$ L/m^2/h, seawater feed.

(A)	Supply pump				Recirc Pump				TOTAL
Phase / Mode	Semi-batch pressurization	Batch pressurization	Purge-refill	Total	Semi-batch pressurization	Batch pressurization	Purge-refill	Total	
Semi-batch	2.554	-	0.012	2.566	0.039	-	0.012	0.051	2.617
batch	-	2.155	0.035	2.19	-	0.04	0.035	0.075	2.265

(B)	Supply pump				Recirc Pump				TOTAL
Phase / Mode	Semi-batch pressurization	Batch pressurization	Purge-refill	Total	Semi-batch pressurization	Batch pressurization	Purge-refill	Total	
Semi-batch	3.447	-	0.202	3.649	0.141	-	0.014	0.155	3.804

batch	-	3.033	0.21	3.243	-	0.138	0.04	0.178	3.421

Table S2. A) Hydraulic, and B) electrical *SEC* (kWh/m^3) breakdown of semi-batch RO ($V_b = 0$), and two cases of HSBRO ($V_b = 20$ and 40 L) at $r = 0.94$, $J_w = 16.8$ L/m^2/h, brackish water feed.

(A)	Supply pump				Recirc Pump				TOTAL
Phase / Mode	Semi-batch pressurization	Batch pressurization	Purge-refill	Total	Semi-batch pressurization	Batch pressurization	Purge-refill	Total	
Semi-batch	2.1	-	0.001	2.101	0.022	-	0.001	0.023	2.124
Hybrid $V_b = 20$	1.285	0.17	0.001	1.455	0.021	0.002	0.001	0.024	1.479
Hybrid $V_b = 40$	0.933	0.275	0.001	1.209	0.02	0.004	0.001	0.025	1.234

(B)	Supply pump				Recirc Pump				TOTAL
Phase / Mode	Semi-batch pressurization	Batch pressurization	Purge-refill	Total	Semi-batch pressurization	Batch pressurization	Purge-refill	Total	
Semi-batch	2.877	-	0.022	2.899	0.084	-	0.001	0.085	2.984
Hybrid $V_b = 20$	1.938	0.231	0.022	2.191	0.076	0.007	0.002	0.085	2.276
Hybrid $V_b = 40$	1.522	0.392	0.022	1.936	0.069	0.013	0.004	0.086	2.022

References

[1] Y. Cohen, R. Semiat, A. Rahardianto, A perspective on reverse osmosis water desalination: Quest for sustainability, AIChE Journal, 63 (2017) 1771-1784.
[2] V.G. Gude, Desalination and sustainability–an appraisal and current perspective, Water research, 89 (2016) 87-106.
[3] B.D. Stanford, J.F. Leising, R.G. Bond, S.A. Snyder, Inland desalination: Current practices, environmental implications, and case studies in Las Vegas, NV, Sustainability science and engineering, 2 (2010) 327-350.
[4] K.M. Shah, I.H. Billinge, X. Chen, H. Fan, Y. Huang, R.K. Winton, N.Y. Yip, Drivers, challenges, and emerging technologies for desalination of high-salinity brines: A critical review, Desalination, 538 (2022) 115827.
[5] A. Khalil, S. Mohammed, R. Hashaikeh, N. Hilal, Lithium recovery from brine: Recent developments and challenges, Desalination, 528 (2022) 115611.
[6] M.O. Mavukkandy, C.M. Chabib, I. Mustafa, A. Al Ghaferi, F. AlMarzooqi, Brine management in desalination industry: From waste to resources generation, Desalination, 472 (2019) 114187.

[7] A. Panagopoulos, V. Giannika, Decarbonized and circular brine management/valorization for water & valuable resource recovery via minimal/zero liquid discharge (MLD/ZLD) strategies, Journal of Environmental Management, 324 (2022) 116239.
[8] A. Panagopoulos, Brine management (saline water & wastewater effluents): Sustainable utilization and resource recovery strategy through Minimal and Zero Liquid Discharge (MLD & ZLD) desalination systems, Chemical Engineering and Processing-Process Intensification, 176 (2022) 108944.
[9] T. Tong, M. Elimelech, The global rise of zero liquid discharge for wastewater management: drivers, technologies, and future directions, Environmental science & technology, 50 (2016) 6846-6855.
[10] S. Lin, Energy efficiency of desalination: fundamental insights from intuitive interpretation, Environmental science & technology, 54 (2019) 76-84.
[11] F.E. Ahmed, R. Hashaikeh, N. Hilal, Hybrid technologies: The future of energy efficient desalination–A review, Desalination, 495 (2020) 114659.
[12] K. Park, L. Burlace, N. Dhakal, A. Mudgal, N.A. Stewart, P.A. Davies, Design, modelling and optimisation of a batch reverse osmosis (RO) desalination system using a free piston for brackish water treatment, Desalination, 494 (2020) 114625.
[13] J.R. Werber, A. Deshmukh, M. Elimelech, Can batch or semi-batch processes save energy in reverse-osmosis desalination?, Desalination, 402 (2017) 109-122.
[14] E. Hosseinipour, S. Karimi, S. Barbe, K. Park, P.A. Davies, Hybrid semi-batch/batch reverse osmosis (HSBRO) for use in zero liquid discharge (ZLD) applications, Desalination, 544 (2022) 116126.
[15] T. Lee, A. Rahardianto, Y. Cohen, Multi-cycle operation of semi-batch reverse osmosis (SBRO) desalination, Journal of Membrane Science, 588 (2019) 117090.
[16] K. Park, P.A. Davies, A compact hybrid batch/semi-batch reverse osmosis (HBSRO) system for high-recovery, low-energy desalination, Desalination, 504 (2021) 114976.
[17] R.L. Stover, High recovery, low fouling, and low energy reverse osmosis, Desalination and Water Treatment, 57 (2016) 26501-26506.
[18] J. Swaminathan, E.W. Tow, R.L. Stover, J.H. Lienhard, Practical aspects of batch RO design for energy-efficient seawater desalination, Desalination, 470 (2019) 114097.
[19] M. Li, Cyclic simulation and energy assessment of closed-circuit RO (CCRO) of brackish water, Desalination, 545 (2023) 116149.
[20] T. Qiu, P.A. Davies, Comparison of configurations for high-recovery inland desalination systems, Water, 4 (2012) 690-706.
[21] M.H. Sharqawy, S.M. Zubair, J.H. Lienhard, Second law analysis of reverse osmosis desalination plants: An alternative design using pressure retarded osmosis, Energy, 36 (2011) 6617-6626.
[22] E. Hosseinipour, K. Park, L. Burlace, T. Naughton, P.A. Davies, A free-piston batch reverse osmosis (RO) system for brackish water desalination: Experimental study and model validation, Desalination, 527 (2022) 115524.
[23] E. Hosseinipour, E. Harris, H.A. El Nazer, Y.M. Mohamed, P.A. Davies, Desalination by batch reverse osmosis (RO) of brackish groundwater containing sparingly soluble salts, Desalination, 566 (2023) 116875.
[24] E. Hosseinipour, P. Davies, Effect of membrane properties on the performance of batch reverse osmosis (RO): The potential to minimize energy consumption, Desalination, (2024) 117378.
[25] Q.J. Wei, C.I. Tucker, P.J. Wu, A.M. Trueworthy, E.W. Tow, J.H. Lienhard, Impact of salt retention on true batch reverse osmosis energy consumption: experiments and model validation, Desalination, 479 (2020) 114177.
[26] A. Efraty, Closed circuit desalination series no-4: high recovery low energy desalination of brackish water by a new single stage method without any loss of brine energy, Desalination and water treatment, 42 (2012) 262-268.
[27] B. Schuetze, K. Rainwater, L. Song, Closed-concentrate circulation for high recovery and energy efficiency in small-scale brackish reverse osmosis, Journal of Environmental Engineering, 140 (2014) 04014012.
[28] H. Gu, M.H. Plumlee, M. Boyd, M. Hwang, J.C. Lozier, Operational optimization of closed-circuit reverse osmosis (CCRO) pilot to recover concentrate at an advanced water purification facility for potable reuse, Desalination, 518 (2021) 115300.
[29] Z. Gal, A. Efraty, CCD series no. 18: record low energy in closed-circuit desalination of ocean seawater with nanoH2O elements without ERD, Desalination and Water Treatment, 57 (2016) 9180-9189.
[30] S. Karimi, R. Engstler, E. Hosseinipour, F. Heinzler, M. Wagner, M. Piepenbrink, S. Barbe, P. Davies, High-Pressure Batch Reverse Osmosis (Ro) for Zero Liquid Discharge (Zld) in a Cr (Iii) Electroplating Process, Available at SSRN 4675842.
[31] S. Karimi, R. Engstler, E. Hosseinipour, M. Wagner, F. Heinzler, M. Piepenbrink, S. Barbe, P. Davies, High-pressure batch reverse osmosis (RO) for zero liquid discharge (ZLD) in a Cr (III) electroplating process, Desalination, (2024) 117479.
[32] A. Chougradi, F. Zaviska, A. Abed, J. Harmand, J.-E. Jellal, M. Heran, Batch reverse osmosis desalination modeling under a time-dependent pressure profile, Membranes, 11 (2021) 173.

[33] S. Cordoba, A. Das, J. Leon, J.M. Garcia, D.M. Warsinger, Double-acting batch reverse osmosis configuration for best-in-class efficiency and low downtime, Desalination, 506 (2021) 114959.
[34] M. Li, Effect of cylinder sizing on performance of improved closed-circuit RO (CCRO), Desalination, 561 (2023) 116688.
[35] D.M. Warsinger, E.W. Tow, K.G. Nayar, L.A. Maswadeh, J.H. Lienhard, Energy efficiency of batch and semi-batch (CCRO) reverse osmosis desalination, Water research, 106 (2016) 272-282.
[36] T. Qiu, P. Davies, Comparison of configurations for high-recovery inland desalination systems, Water. 4 (2012) 690–706, in.
[37] M. Li, N. Chan, J. Li, Novel dynamic and cyclic designs for ultra-high recovery waste and brackish water RO desalination, Chemical Engineering Research and Design, 179 (2022) 473-483.

Paper 7: Free-piston batch reverse osmosis (RO): modelling and scale-up

E. Hosseinipour[1*], P.A. Davies[1*]

[1]School of Engineering, University of Birmingham, Edgbaston, Birmingham, UK

* e.hosseinipour@bham.ac.uk and p.a.davies@bham.ac.uk

Graphical Abstract

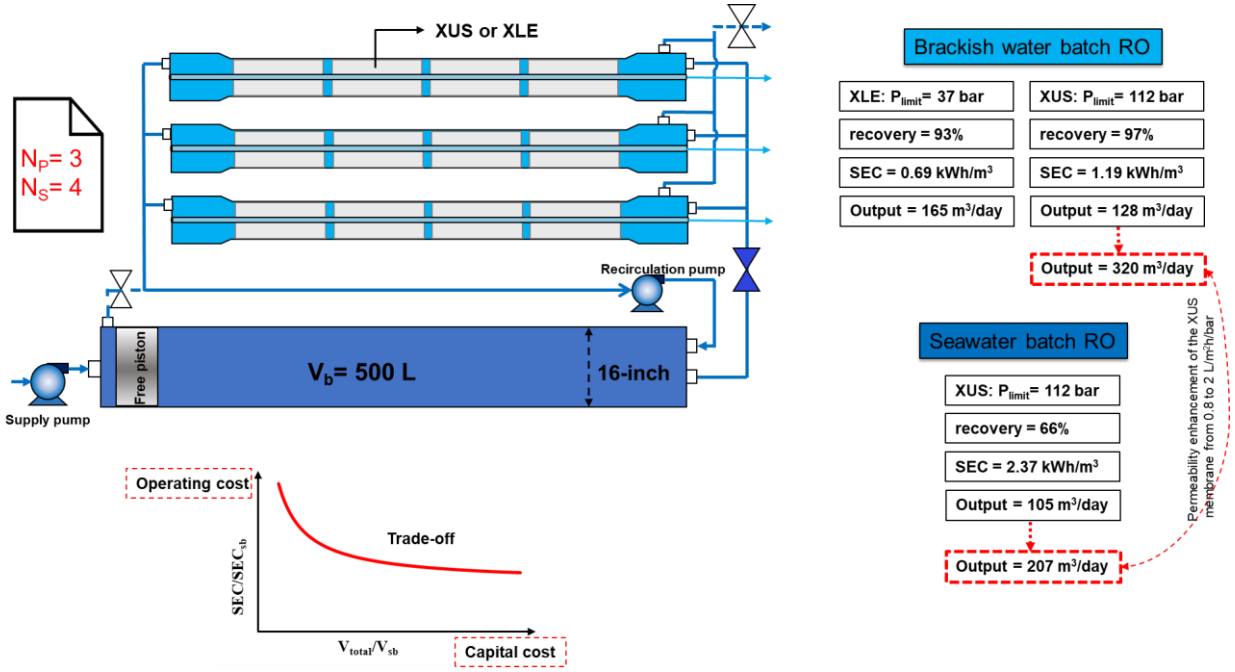

Abstract

Free-piston batch RO achieves excellent energy efficiency at high recovery, but current systems have outputs <25 m^3/day. Designing larger systems poses challenges like designing an appropriate work exchanger and optimizing membrane arrangements in series and/or parallel. This study calibrates a batch RO model against brackish and seawater experiments up to 112 bar and uses the model to predict performance on scale-up. Modelling up to 6 membranes in series predicts *SEC* of 1.11-1.5 kWh/m^3 at recirculation flow Q_r/Q_f = 4 with brackish water, with *SEC* becoming more sensitive to Q_r/Q_f as the number of membranes increases. Using a 500-L work exchanger, a batch RO system with twelve 8-inch membranes is designed. For brackish water (3000 mg/L) this system gives outputs of 165 and 128 m^3/day with *SEC* of 0.69 and 1.19 kWh/m^3 at recoveries of 0.93-0.97 with low- and high-pressure RO membranes, respectively - representing *SEC* reductions of 33 and 45% compared to semi-batch RO. For seawater, it gives 105 m^3/day with *SEC* of 2.37 kWh/m^3 at recovery of 0.66. High-permeability membranes would significantly enhance batch RO performance; for example, increasing permeability from 0.8 to 2 L/m^2/h/bar would boost output to 320 and 207 m^3/day in brackish and seawater desalination respectively.

Keywords: Batch RO, Scale up, High recovery, Energy efficiency, Membrane permeability.

Highlights:

- Detailed model validation using brackish and seawater experiments up to 112 bar.
- Batch RO scale-up: 12 membranes (N_S=4 and N_P=3) with a batch volume of 500 L.
- 165 and 105 m^3/day output with brackish and seawater, respectively.
- *SEC* of 1.2 and 2.4 kWh/m^3 at r=0.97 and 0.66 with brackish and seawater at scale.
- Improved permeability can nearly double output.

Nomenclature

Symbols

A_w	L/m^2/h/bar, Membrane permeability
A_m	m^2, Membrane area
C_d	-, Coefficient of discharge
c_{feed}	mg/L, Feed concentration
D	mm, Pipe diameter
f	-, Friction factor
J_w	L/m^2/h, Flux
L	-, Pipe length
L_m	m, Membrane length
N_d	-, Number of equivalent diameters added to unpurged section to represent minor losses
N_P	-, Number of elements in parallel
N_S	-, Number of elements in series
ΔP_m	kPa, Cross-flow pressure drop across RO membrane
$\Delta P_{orifice}$	kPa, Pressure drop across orifice
$\Delta P_{recirc,pipe}$	kPa, Pressure drop across pipe
Q_f	L/min, Feed flow from high-pressure supply pump
Q_r	L/min, Recirculation flow at brine outlet of RO module
r	-, Water recovery
R_s	-, Salt rejection
V_b	L, Swept volume of work exchanger
V_h	L, Volume of the pressure vessels housing the membranes
V_{total}	L, Total volume of pressure vessels comprising membrane housings and the work exchanger
v	m/s, Cross-flow velocity
ρ	kg/m^3, Density

Abbreviations

MLD/ZLD	Minimal/Zero Liquid Discharge
RO	Reverse Osmosis
SEC	Specific Energy Consumption
SI	Supporting Information
XLE	Membrane (FilmTec™ BW XLE-440)
XUS	Membrane (Dupont XUS180808)

1. Introduction

Reverse osmosis (RO) stands out as one of the most thermodynamically effective and economically viable methods for desalination [1, 2]. Among RO configurations, batch RO is an innovative approach noted for its high energy efficiency, particularly at high recovery [3]. This makes it especially interesting for minimal or zero liquid discharge (MLD/ZLD)

applications [4-6] and for brackish water desalination [7-10]. There is a growing interest in MLD/ZLD, particularly for decentralized water treatment [11-13]. Applications include treatment of wastewater from metal plating [6], textile industry [14], semiconductor industry [15], food processing industries [16, 17], hydroponic waste recycling [18], and mineral recovery such as lithium extraction [19-22]. Recent literature underscores the increasing needs to enhance water and solute recovery and extract valuable metals and chemicals from wastewater and desalination concentrates [23-25]. Batch RO systems could play a significant role in these areas. Developing innovative approaches, such as batch RO, is crucial to meet these needs, especially given European Union strategic priorities such as water resilience and circular economy [26]. So far, however, research in batch RO has been mostly limited to small-scale laboratory studies, where the output is less than 25 m^3/day. Even in decentralized water treatment applications, capacities of 1000 m^3/day or larger may be required. Therefore, there is a need to address the challenge of scaling up batch RO.

Unlike continuous RO, batch RO recovers water in multiple passes achieving more uniform flux distribution over the membrane [27-30]. In ideal batch RO, there is no spatial variation in quantities of flux, concentration or osmotic pressure; thus, the lowest thermodynamic energy consumption is theoretically possible [3, 31]. In reality, however, these quantities do vary somewhat over the RO membrane element, reducing the energy savings [8, 32]. This problem is minimized by decreasing the recovery per pass, i.e., by increasing the recirculation flow [8, 33]. However, scale up of batch RO is likely to need several membrane elements in series, which may aggravate losses associated with the recirculation flow. On the one hand, use of several elements in series is beneficial in reducing the number of vessels and amount of pipework. On the other hand, it requires an increased recirculation flow to maintain uniform flux, incurring higher energy consumption [34]. Thus, there is a trade-off between a simpler, low-cost design and a design that is more energy efficient [33]. In semi-batch RO applications, 3-4 membrane elements in series have been favoured [35-37], as opposed to 6-8 typically used in conventional continuous RO plants. For batch RO, however, experimental reports have so far been limited to just one element per vessel. Consequently, it is important to quantify batch RO performance with multiple elements in series to meet the scale up challenge.

The main approaches to batch RO use either: (1) atmospheric vessels with energy recovery devices, or (2) pressurized work exchanger vessels. In a theoretical study based on the first approach, Das et al. [38] introduced a design for zero downtime and scalability. They simulated such a design comprising five parallel trains each having five membranes in series (total of 25 membranes), to predict a plant capacity of 378.5 m^3/day with seawater feed (35000 mg/L NaCl). Key assumptions included membrane permeability of 3 L/m^2/h/bar, high recovery ratio per pass of 0.45, salt rejection of 99.4%, pump efficiencies of 80%, and a membrane pressure rating of 83 bar. The study calculated Specific Energy Consumption (*SEC*) of 2.12 kWh/m^3 (corresponding to a 2nd law efficiency of 48.2%) and overall system recovery of r = 0.51. Despite such favourable results, the study concluded that the proposed system still consumes ~7.6% more energy than designs using pressurised work exchangers at the conditions specified above. Free-piston batch RO design is one such design [3, 8].

Davies et al. [3] reported the first experimental study of free-piston batch RO. They constructed a prototype using readily available components and tested it with varying feed salinities (2000 to 5000 mg/L) and recovery ratios (0.17 to 0.71). The prototype consisted of one pressure vessel (i.e., work exchanger) housing free pistons of different lengths to vary the

recovery, and two pressure vessels in parallel each housing one 2.5-inch diameter membrane element (FilmTec™ BW30 with area of 2.6 m^2). The tests were conducted at fluxes of 7-23 $L/m^2/h$, resulting in output of 0.9-2.6 m^3/day. A limitation of this prototype was the interruption of output while the system refilled between cycles. Thus, this group designed a new configuration in which the work exchanger is double-acting, i.e., one side refills while the other side pressurizes. This allowed continuous output during the refill phase and boosted water production by about 25% compared to the earlier design, without increasing membrane area [7]. However, the double-acting arrangement was considered somewhat complex requiring 5 valves and 3 pumps. Therefore, this group opted instead to pursue a single-acting arrangement that combined the purge and refill stages to minimize downtime, while requiring only 3 valves and 2 pumps (see Fig. 1) [39].

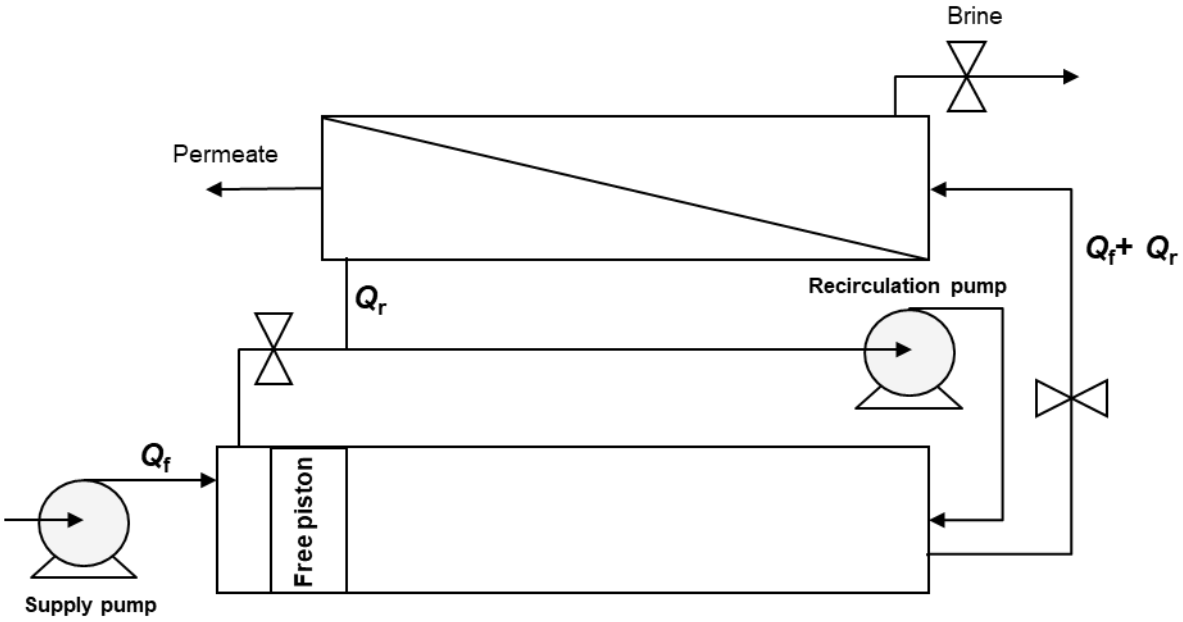

Fig. 1. Schematic of single-acting free-piston batch RO showing supply flow Q_f and recirculation flow Q_r.

Another type of pressurized work exchanger employs a flexible bladder instead of a free piston. Wei et al. [30] designed and operated the first bladder batch RO. In their bench-scale prototype, they used a single pressure vessel to house both bladder and membrane (Hydranautics ESPA-2514 with area of 0.47 m^2). They conducted their experiments at recovery < 0.55 (due to pressure limit of 10 bar), feed salinities of 2000-5000 mg/L and fluxes of 10-20 $L/m^2/h$, giving an output of 0.1-0.2 m^3/day.

Park et al. [8] designed a larger free-piston batch RO using an 8-inch RO membrane, intended for brackish water desalination at recovery of r = 0.8. This design was later constructed and tested with various feed solutions including NaCl solution [9, 40] and synthetic brackish groundwater [10] at different water fluxes (11-23 $L/m^2/h$) using 5 different membrane types each with surface area of 41 m^2. Output up to 22 m^3/day was achieved. Subsequent studies introduced the concept of hybrid semi-batch/batch RO which was designed to avoid need for excessively large work exchangers at recoveries > 0.8 [4, 5]. Following these studies, a high-pressure (120 bar) hybrid semi-batch/batch RO pilot was designed for the treatment of metal plating wastewater [6]. This pilot was also used for a direct experimental comparison of batch RO technologies for the first time [41]. A high-pressure membrane (Dupont XUS180808) with

active area of 30.6 m^2 was used at fluxes < 17 $L/m^2/h$ in this pilot, giving outputs up to 12 m^3/day. In summary, experimental studies of batch RO to date had outputs of only 0.1-22 m^3/day (see Table 1).

The scale of RO systems can vary greatly depending on specific application needs, environmental regulations, and the feedwater sources. The choice of scale for a project is influenced by factors such as population served, industrial demand, environmental constraints, and economic feasibility. For example, in reviewing brackish water desalination systems, Zhao et al. reported a wide range of capacities from 0.2 to 25,000 m^3/day [42].

Whereas the approach to scaling up conventional RO plants is well established, this is not the case for batch RO where several new issues arise. One issue relates to the need for a large work exchanger vessel (in the case of the free-piston or bladder design) especially at recoveries above about r = 0.8 [4, 5, 30]. For example, achieving a recovery of r = 0.95 through pure batch operation needs a work exchanger volume of approximately 300 L for only one 8-inch membrane. This translates to an excessive length of 9 or 4.5 m when employing an 8-inch or 16-inch diameter vessel, respectively, for the work exchanger. This would greatly increase the footprint and capital cost of the system. Additionally, longer pressure vessels increase the risk of inadequate mixing between the recirculating brine solution and the feed solution in the work exchanger, potentially leading to performance loss or necessitating higher recirculation flow and thus increasing *SEC*. This problem has been partially overcome with the introduction of hybrid semi-batch/batch RO, as noted above [4].

Another issue regards the pipework. In conventional RO, the layout and sizing of pipework is not critical, provided it is adequately sized to avoid frictional resistance which would otherwise increase the pumping energy. In batch RO, however, retention of salt from one cycle to the next makes it important to avoid oversizing [8, 9, 28, 30]. Therefore, the pipework must be optimised considering this trade-off between minimizing salt retention and flow resistance. For larger plants, which tend to require longer pipe runs, this trade-off may become more important.

Thus, in this study, the aim is to accurately predict scaled up performance of batch RO based on the single-acting free-piston design as described in [4, 8] (see Fig 1). This will be done with careful validation against a laboratory prototype rated at 120 bar. Using hybrid semi-batch/batch operation, water recovery up to r = 0.97 is achieved. Thus, the study will give a complete and reliable picture about scaling up free-piston batch RO, providing a guide for design selection and optimisation at outputs up to about 300 m^3/day which is more than 10 times larger than currently implemented.

Table 1. Experimental studies of batch RO and their outputs.

Work exchanger type	Year	Membrane area (m^2)	Approximate output (m^3/day)	Notes	References
Free-piston (single acting)	2016	2 × 2.6	0.9-2.6	The recovery ranged from 0.17 to 0.71, with the brackish feed water varying between 2000 and 5000 mg/L. Hydraulic SEC was reported.	[3]
Free-piston (double acting)	2016	8.7	3.2	Increased water production by 25% compared to the single-acting design. The recovery ranged from 0.7 to 0.8 when using brackish water.	[7]

Free-piston (single acting)	2018	3 × 2.6	3.8	The recovery achieved was 0.72 when using brackish water with a feed concentration of 2000 mg/L.	[39]
Bladder (low pressure)	2020	0.47	0.1-0.2	The recovery ranged from 0.3 to 0.5 when using brackish water with feed concentrations ranging from 2000 to 5000 mg/L. Hydraulic SEC was reported. Pressure limit of the system was 10 bar.	[30]
Free-piston (low pressure)	2022	41	10-22	The recovery was ranging from 0.8 to 0.95 when using brackish water with feed concentration ranging from 500 to 5000 mg/L. Electrical *SEC* of 0.4 to 0.8 kWh/m^3 was reported. Pressure limit of the system was 25 bar.	[5, 9, 10, 40]
Free-piston (high pressure)	2023	30.6	4-12	Recovery of 0.85 to 0.96 with brackish and seawater feed as well as electroplating wastewater. Electrical *SEC* < 3.5 kWh/m^3 was reported. Pressure limit of the system was 120 bar.	[6, 41]

2. Model development

The model presented in this paper has been developed by modifying an existing model to reflect features that are important in the scale up of the system.

2.1. Overview of existing model

The model has been developed through several iterations alongside the development of free-piston batch RO in Birmingham, UK. Recently, it has been validated against two prototypes at the University of Birmingham. The model initially developed by Park et al. [8] included most losses and led to a specific design recommendation for brackish water treatment. However, in experimental studies of the recommended design, Hosseinipour et al. [9] identified osmotic backflow (previously neglected) as an additional loss which they therefore incorporated into the model.

The next step was the development of hybrid semi-batch/batch RO, used to achieve recovery > 0.8 in a compact design. As with the non-hybrid batch RO, the initial model [4] of the hybrid system did not consider osmotic backflow and therefore had to be modified. Also, at very high recoveries, the assumption of 100% salt rejection was no longer a good approximation in calculating salt retention, peak pressure, and *SEC*. Thus, the modelling of salt retention was improved by adjusting for salt rejection, thus predicting *SEC* with < 3% error [5].

Further features of the modelling included representation of the longitudinal concentration gradient in the RO module by a linear approximation whereby the average concentration is assumed equal to the average of inlet and outlet concentrations [4, 5, 8, 9]. The typically high recirculation rate in the module (giving recovery per pass <33%) results in only a small increase in the applied pressure relative to the idealised case of infinite recirculation flow, thus justifying the approximation. The approach avoids the need to solve partial differential equations representing the non-steady behaviour of the batch RO system, which depends on both space and time variables. Instead, only explicit algebraic equations are used.

For a complete description of the existing model, the reader is referred to the works referenced above.

2.2. Modifications for frictional pressure losses affecting recirculation pump

On scaling up, the recirculation flow tends to increase, amplifying frictional pressure losses, and increasing the energy consumption of the recirculation pump. Some modifications have been made to the model to ensure that these losses are represented with sufficient accuracy. Frictional pressure losses depend on the flow path according to the phase of operation (see Fig. S1 and Table S1).

Pressure drop ΔP_m [kPa] along the membrane channel is caused by friction with the membrane surface and spacer element. As in our previous studies [4, 5, 8, 9], the correlation (Eq. 1) established by Haidari et al. [43] is employed for ΔP_m.

$$\Delta P_m = k \times v^{1.63} \times L_m \quad (1)$$

where v is the cross-flow velocity [m/s], and L_m [m] is the length of the membrane. Haidari used a constant k value of 791 but this has been modified based on experimental measurements in the current study. The cross-flow velocity was averaged between inlet and outlet.

The longest pipe section in the free-piston batch RO system is that either side of the recirculation pump, highlighted in red Fig. 5. In the current prototype at the University of Birmingham, this section has a length of 2.2 m. For scale up, to match the total membrane length, we added 1 m for each additional membrane element, such that the length becomes 7.2 m for 6 membranes in series. This length is important regarding both salt retention and pressure loss. Other pipe sections are less than 0.5 m in length, so for those shorter sections, pressure losses are calculated by considering them equivalent to an orifice of the same diameter as the internal diameter of the pipe. In this way, the exit loss from the pipe was represented. The pipe friction is calculated using a friction factor of f = 0.024 and an additional pipe length (L) equivalent to N_d = 75 times the pipe diameter (D = 21.2 mm in the case of existing pilot) is allowed for the total minor losses in bends and fittings. Thus, the equation for pressure drop in the recirculation pipe is:

$$\Delta P_{\text{recirc,pipe}} = \frac{f(L + N_d.D)}{D}\frac{\rho v^2}{2} \quad (2)$$

Friction factor may depend on Reynolds number (Re) which, in this study, ranged from about 50,000 to 150,000. Nonetheless, as there is only a weak dependency on Re (typically following the Blasius equation $f = 0.31\ Re^{-0.25}$) a constant value of f was adopted for simplicity. The diameter D was also increased on scale up. It was optimised by trial-and-error, while selecting from standard available diameters.

The Torricelli equation for flow through an orifice is used to represent pressure drop through valves or short pipe lengths, as follows:

$$\Delta P_{\text{orifice}} = \frac{\rho}{2}\left(\frac{v}{C_d}\right)^2 \quad (3)$$

where ν represents the velocity at the orifice, and C_d denotes the coefficient of discharge. As noted by Massey [44], C_d typically falls within the range of 0.6 to 0.7 and is adjusted to C_d= 0.62 in the model.

3. Model validation

Model validation measurements were carried out using the single-acting free-piston batch RO system and a DuPont XUS180808 membrane rated at 120 bar (henceforth referred to as XUS). The experimental equipment and method were as described previously [6, 41]. NaCl solution was used as feed.

3.1. Frictional pressure losses affecting recirculation pump

We conducted experiments to measure the pressure across the recirculation pump, at 4 different feed concentrations and over 3 phases of operation, giving 12 measurements in total. After adjusting three parameters (i.e., k in Eq. 1, the piston seal friction pressure, and the friction factor, f, in Eq. 2) we arrived at the modelling results in Table 2 which agree with the measured pressure drop with 0.5 to 7% error.

Though the value of k = 300 used for the XUS membrane differs significantly from the value of k = 791 used by Haidari et al. [43], we also observe a wide variation in the literature. For example, FilmTec™ RO membranes technical manual provides a value of k = 450 but without reference to any specific type of membrane [45]. Moreover, for membrane elements with thinner feed spacers, we experimentally observed higher values, such as k = 600 for FilmTec™ BW XLE-440 (with feed spacer thickness of 28 mil compared to 34 mil for the XUS; see Table S2 for the membrane properties taken from the manufacturer's datasheet). Using real data from a seawater desalination plant located in Persian Gulf having 7 membranes in series in each pressure vessel and operating at recovery of r = 0.4 and flux of 15 L/m^2/h, this value was about k = 370 (with feed spacer thickness of 34 mil). Therefore, we consider that the value of k = 300 is reliable for the XUS membrane.

Table 2. Comparison of experimental results and modelling predictions for the recirculation pump pressure drop over 3 phases of operation in the free-piston batch RO when using the XUS membrane. Parameters of $k = 300$ for the RO membrane pressure drop, piston friction pressure drop of 25 kPa, and pipe friction factor of $f = 0.024$ were used in the modelling.

Feed salinity (mg/L), c_{feed}	Recovery, r	Flow (L/min)		Recirculation pump pressure drop (kPa)						Hydraulic *SEC*			
				Experimental results			Modelling results (% of deviation)			Experimental results		Modelling results (% of deviation)	
		Supply pump, Q_f	Recirc pump, Q_r	Semi-batch	Batch	Purge-and-refill	Semi-batch	Batch	Purge-and-refill	Supply pump	Recirc pump	Supply pump	Recirc pump
4000	0.95	8.7	20	6.9	5.6	43.4	7.4 (6.7%)	5.3 (5.7%)	43.1 (0.7%)	1.298	0.007	1.250 (3.8%)	0.008
5000	0.94	6.1	23.3	7.5	6.3	42	7.9 (5.1%)	6.3 (0%)	42.6 (1.4%)	1.067	0.010	1.020 (4.6%)	0.012
5000	0.95	6.1	27.5	10.2	8.7	42	10.2 (0%)	8.4 (3.6%)	42.8 (1.9%)	1.165	0.015	1.105 (5.4%)	0.017
4000	0.95	8.7	36	17.1	16.4	43.3	17.7 (3.4%)	15.3 (7.2%)	43.1 (0.5%)	1.209	0.026	1.164 (3.9%)	0.026

3.2. Overall SEC

Having established the modelling of pipework losses, we next validate the whole system modelling for *SEC* taking into account membrane properties. This part of the modelling uses two additional adjustable parameters: (1) membrane permeability, adjusted to 0.8 L/m^2/h/bar and (2) salt rejection R_s adjusted to 0.985 and 0.96 for seawater and brackish water respectively, which was consistent with the experimental values.

In the case of a seawater feed, the experimentally measured hydraulic *SEC* matched closely the model prediction, with < 3% error observed across various fluxes at recovery r = 0.63 (Fig. 2). For brackish water feed, the corresponding error was < 4% (Fig. 3) based on tests at flux of 16.8 L/m^2/h and recovery of r = 0.952 (except at c_{feed} = 5000 mg/L when recovery was 0.942 due to the peak pressure limit).

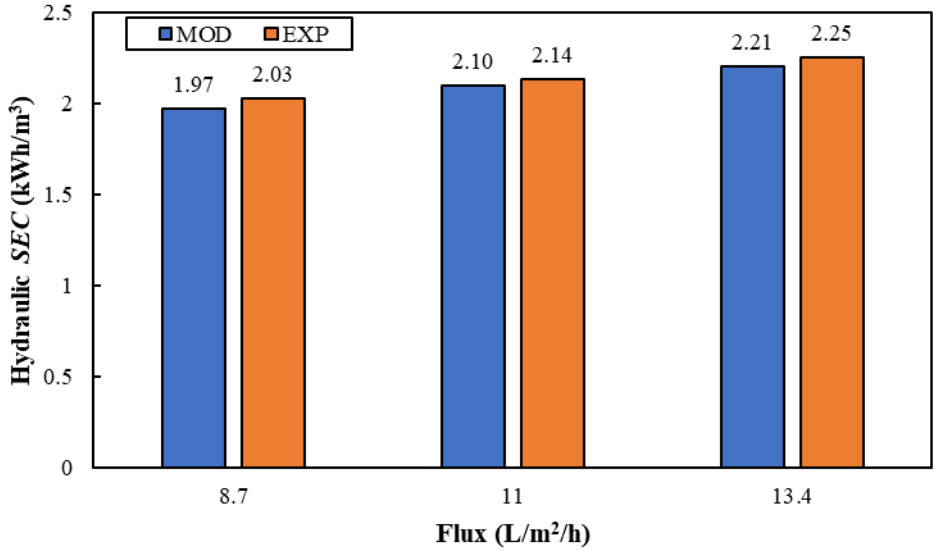

Fig. 2. Comparison of model predictions (MOD) and experimental measurements (EXP) of hydraulic *SEC* for seawater feed at recovery of r = 0.63 (XUS membrane). Experiments were conducted exclusively in batch mode because the recovery is low due to the high osmotic pressure of the feed, avoiding the need for the hybrid mode.

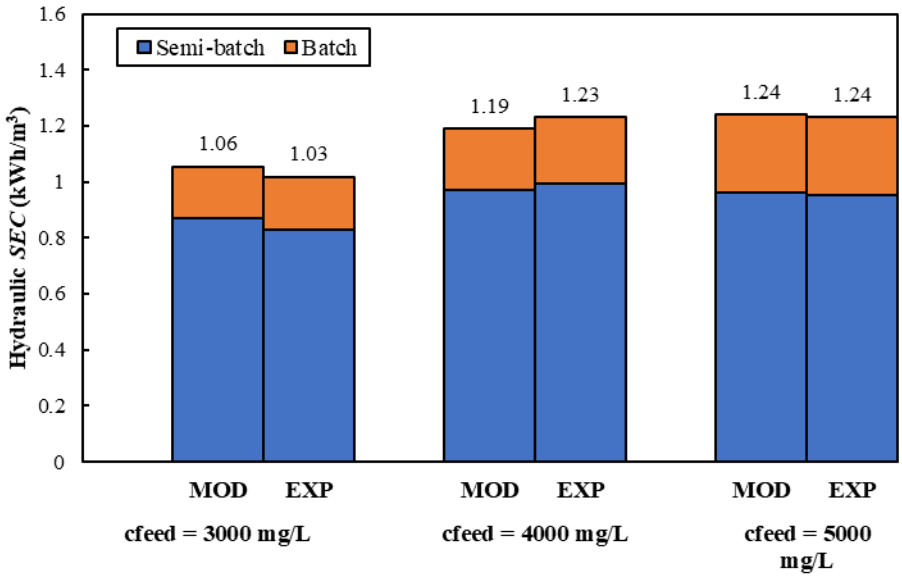

Fig. 3. Comparison of model predictions (MOD) and experimental measurements (EXP) of hydraulic *SEC* at different feed concentrations, J_w = 16.8 L/m^2/h, and recovery of r = 0.952 (except for c_{feed} = 5000 mg/L where r = 0.942). XUS membrane was used. Experiments were conducted in hybrid semi-batch/batch mode because achieving such a high recovery with a batch RO would require an impractically large work exchanger (approximately 300 L compared to the 40 L used here).

3.3. Effect of recirculation flow

Recirculation flow is quantified as the ratio Q_r/Q_f of the flow at the brine outlet divided by the feed flow from high-pressure supply pump (see Fig. 1). In a prior investigation [5], we examined the effect of recirculation flow in a low-pressure hybrid RO system in treating low-concentration NaCl solutions (c_{feed}=1000 mg/L). To minimise *SEC*, we optimised the recirculation flow as Q_r/Q_f = 2 (equivalent to a recovery per pass of 0.33). Here, we conducted a similar experiment to optimise Q_r/Q_f in the high-pressure system using values of Q_r/Q_f =2.3, 4.1 and 5.7 (corresponding to the recovery per pass of 0.15–0.3) at c_{feed} = 4000 mg/L, J_w = 16.8 L/m^2/h, and r = 0.954.

On increasing the recirculation flow while maintaining the feed flow at 8.8 L/min (i.e. increasing Q_r/Q_f) peak pressure decreased uniformly, whereas the total *SEC* initially decreased and then increased (Fig. 4A). For example, the peak pressure fell from 108 to 102 and then 100 bar, on increasing Q_r/Q_f from 2.3 to 4.1 and then 5.7 respectively; while hydraulic *SEC* decreased from 1.30 to 1.24 kWh/m^3 initially and then increased again to 1.27 kWh/m^3 (Fig. 4B). The main reason for the decreased peak pressure is that the recirculation flow promotes a uniform concentration in the feed channel transversally and longitudinally (i.e., decreasing the concentration polarization and longitudinal concentration gradients) which in turn decreases the required applied pressure (see also Table 3). In turn, this reduces the energy consumption of the supply pump. However, on increasing Q_r/Q_f, the recirculation pump energy consumption increases (Table 3). Hence there is a trade-off between supply pump energy saving and recirculation pump energy saving. Increasing Q_r/Q_f also improved permeate quality, reducing conductivity by 11% when almost doubling Q_r/Q_f. The model predicted hydraulic *SEC* and peak pressure within 4% of the above experimental values (Fig. 4).

Priorities of specific applications will determine the preference between achieving a slightly lower peak pressure with slightly higher energy consumption (operating at Q_r/Q_f approximately 5 to 6) or slightly lower energy consumption with a higher peak pressure (operating at Q_r/Q_f around 4).

Table 3. Experimental measurement of the effect of varying Q_r/Q_f ratio on the main parameters of the high-pressure free-piston batch RO including permeate quality, average pressure and *SEC*. Brackish water c_{feed} = 4000 mg/L, r = 0.954 and J_w = 16.8 L/m^2/h.

Q_r/Q_f	Permeate conductivity (mS/cm)	Rejection, R_s	Average applied pressure (bar)	Peak pressure (bar)	Hydraulic *SEC* (kWh/m^3)	Electrical *SEC* (kWh/m^3)		
						Supply pump	Recirc pump	Total
2.3	0.351	0.957	45.9	108.3	1.30	2.01	0.04	2.05
4.1	0.324	0.960	42.7	102.3	1.24	1.91	0.08	1.99
5.7	0.310	0.962	41.9	100.4	1.27	1.89	0.16	2.05

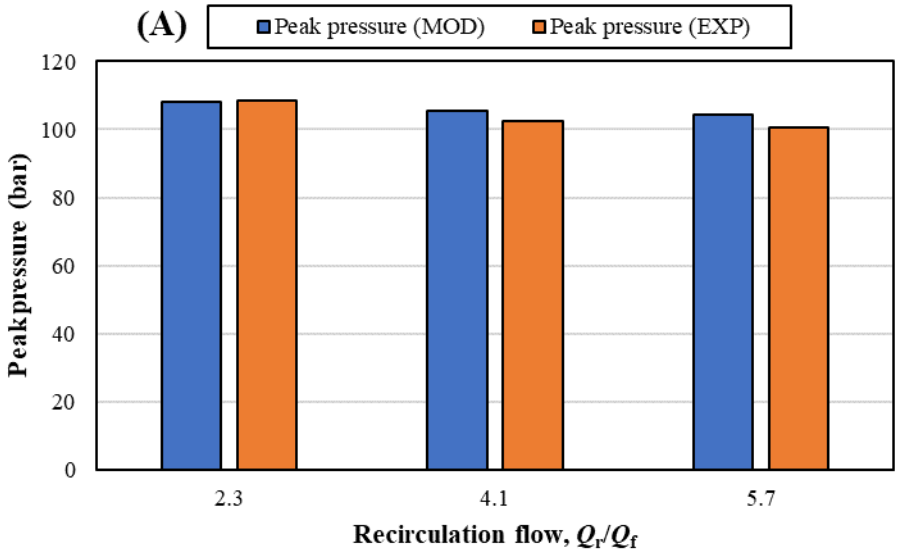

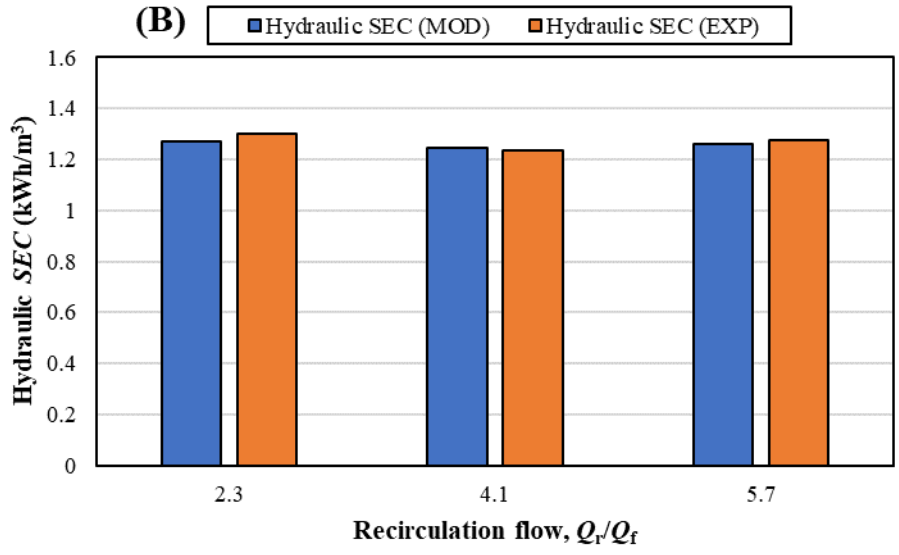

Fig. 4. Comparison of the model predictions (MOD) and experimental measurements (EXP) when varying the recirculation flow, A) peak pressure, and B) hydraulic *SEC*. Brackish water: c_{feed} = 4000 mg/L, r = 0.954 and J_w = 16.8 L/m^2/h. Hybrid semi-batch/batch RO operation.

4. Model predictions

Following the above validation and optimisation, this section uses the model to predict and optimise scale up for brackish and seawater feed. Table 4 shows baseline parameters used by default, as well as variations used in the scaled-up modelling.

Table 4. Parameters for the free-piston batch RO modelling, showing baseline (default) values and variations used for scale up (brackish and seawater feed).

Parameter	Brackish water feed		Seawater feed	
	Baseline	Scale up	Baseline	Scale up
Feed salinity, c_{feed} (mg/L)	3000	3000	35000	35000
Water recovery, r	0.97	0.93 and 0.97	0.66	0.66
Average water flux, J_w (L/m^2/h)	15	15	15	15
Membrane type	XUS	XUS, XLE	XUS	XUS
Number of elements in series, N_S	1	1 – 6	1	1 – 6
Number of elements in parallel, N_P	1	1 – 3	1	1 – 3
Total membrane area, A_m (m^2)	30.6	30.6 and 492	30.6	30.6 and 367.2
Membrane water permeability, A_w (L/m^2/h/bar)	0.8	0.8 and 4.6	0.8	0.8
Salt rejection, R_s	0.96	0.92 and 0.96	0.98	0.98
Q_r/Q_f (or recovery per pass ratio)	4 (0.2)	2 (0.33) – 8 (0.11)	4 (0.2)	2 (0.33) – 8 (0.11)
Supply (high-pressure) and recirculation pumps efficiency (%)	80	80	80	80
k value for membrane pressure drop (Eq. 1)	300	300 and 600	300	300
Maximum peak pressure used in the modelling (bar)	112	37 and 112*	112	112
Work exchanger volume (L), V_b	40	40 – 500	40	40 – 500
Pipe internal diameter (mm)*	21.2	21.2 – 80	21.2	21.2 – 80
Pipe length incorporating recirculation pump (m)*	2.2	2.2 – 7.2	2.2	2.2 – 7.2

*The length and diameter of the pipe in the recirculation loop was increased according to the number of membrane elements in series N_S. The length in the current prototype at University of Birmingham is 2.2 m with internal diameter of 21.2 mm. Consequently, we added 1 m to the pipe length for each additional membrane element of length 1 m. Standard pipe internal diameters of 21.2, 32, 44, 56, 68.3 and 80 mm were used for N_S= 1,2,3,4,5 and 6 elements in series, respectively. Peak pressure safety margin of 8 and 4 bar was considered for the XUS and XLE membranes respectively.

4.1. Effect of work exchanger size

As mentioned in section 2, it is important to consider the size of the work exchanger when scaling up. In this study, we assume that the work exchanger is constructed from a pressure vessel similar to those used to house the RO membranes. Thus, we define the total internal volume V_{total} of all pressure vessels as:

$$V_{total} = V_b + V_h \quad (4)$$

where V_b is the volume of work exchanger and V_h is the volume of the membrane housings (see Fig. 5). V_{total} is used as an indicator of system size. Then we define V_{total}/V_h as a parameter that varies from 1 in the semi-batch case (i.e., no work exchanger, V_b = 0, corresponding to minimum system size) to a maximum value that represents the batch RO case (corresponding to maximum system size). Hybrid semi-batch/batch RO lies anywhere between these two extremes.

Thus, Fig. 6 plots the effect of system size on *SEC* (normalised against semi-batch *SEC*) for brackish feed (c_{feed} = 3000 mg/L) in cases of N_s=1 and 4 membranes in series. It shows how energy efficiency improves with size. For example, at r = 0.97, increasing V_{total}/V_h from 1 to 3 decreases *SEC* dramatically (by 54%) thus showing the advantage of hybrid over pure-semi-batch RO. This advantage becomes even more pronounced as recovery increases. For example, at V_{total}/V_h = 2, the ratio of SEC/SEC_{sb} decreases from 0.69 to 0.54 when raising the recovery from 0.93 to 0.97 (see Fig. 6A). Nonetheless, increasing V_{total}/V_h above 3 yields little further benefit in decreasing *SEC,* suggesting that pure-batch RO is not advisable for high-recovery brackish water desalination.

Overall, Fig. 6 highlights a trade-off between a more compact design (i.e., smaller V_{total}/V_h) *vs*. higher energy efficiency. In other words, there is a trade-off involving capital cost vs operating cost. The suggested range of V_{total}/V_h = 2 to 3 corresponds to a work exchanger size 1 to 2 times that of the membrane housing.

We note that Hosseinipour et al. [41] recently investigated this trade-off by conducting experiments with two different work exchanger volumes (around 20 and 40 L) using the same prototype as in this study. Li [46] also provided theoretical evidence supporting these findings. He predicted that if the cylinder (i.e., the work exchanger in free-piston batch RO design) is removed from a proposed improved semi-batch RO design (i.e., the system returns to the standard semi-batch RO configuration) the energy consumption increases by 30%. He also predicted about 2% increase in energy consumption when cylinder is oversized or undersized.

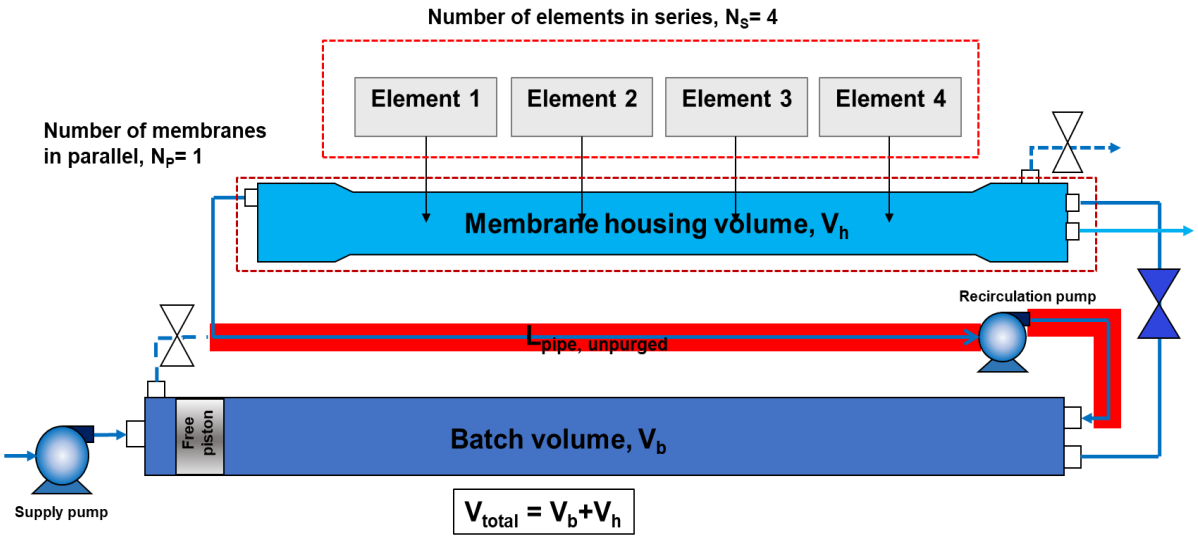

Fig. 5. Illustration of a free-piston batch RO system with labelled volumes. The red section highlights the pipeline length that remains unpurged during the flushing phase, resulting in higher salt retention and increased energy consumption.

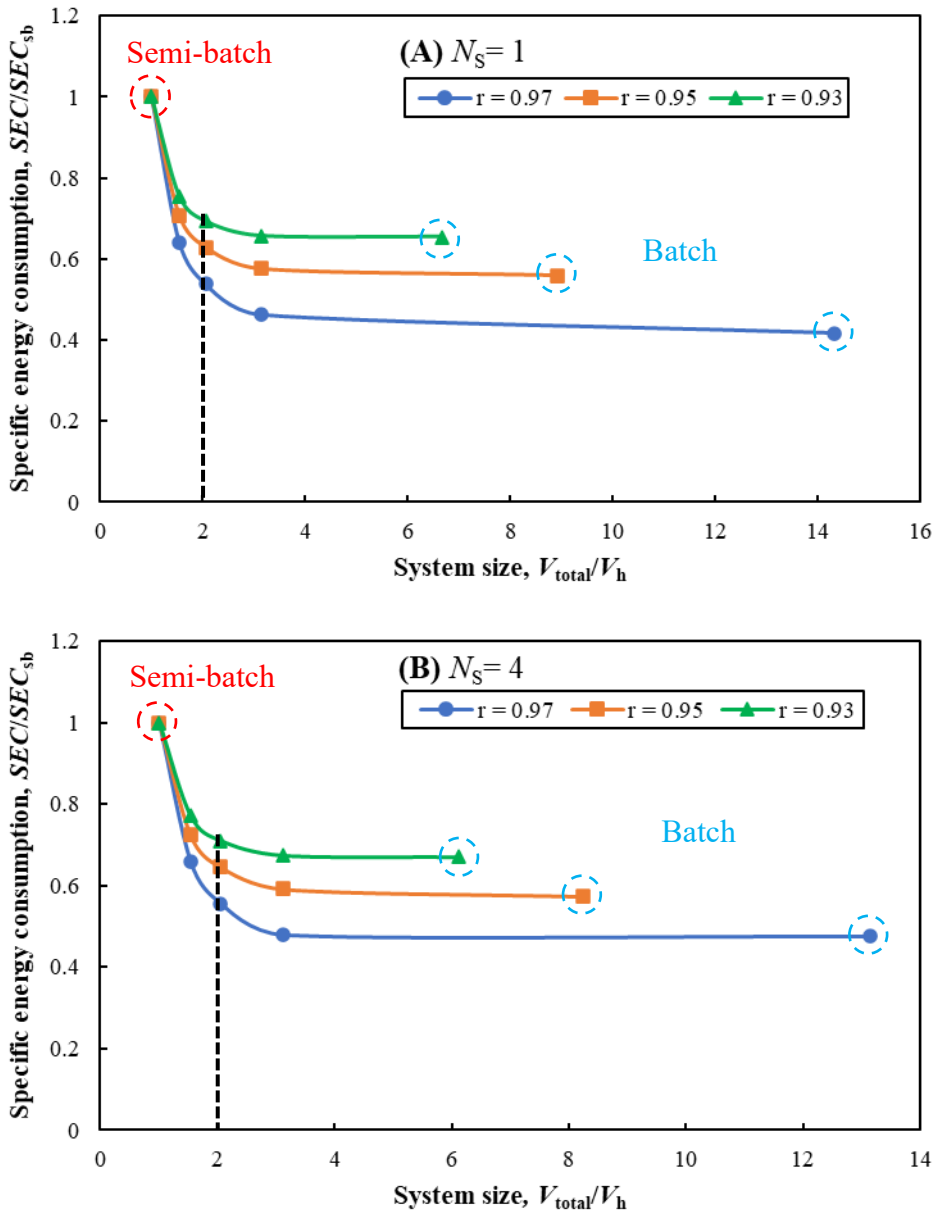

Fig. 6. Increasing work exchanger sizes increases system size but decreases energy consumption. Graph shows the effect of system size on *SEC* at three high recovery rates *r*, with c_{feed} = 3000 mg/L, Q_r/Q_f = 4, and J_w = 15 L/m^2/h using XUS membrane. A) one membrane, and B) four membranes in series (N_P = 1 in all cases). Values are normalised against the semi-batch case, for which in A) SEC_{sb}= 2.1, 1.5 and 1.25 kWh/m^3 at recoveries of *r* = 0.97, 0.95, and 0.93 respectively; and V_h ~ 40 L, and in B) SEC_{sb}= 2.25, 1.62 and 1.35 kWh/m^3 at recoveries of *r* = 0.97, 0.95, and 0.93 respectively; and V_h ~ 150 L. Thus, V_{total}/V_h = 2 and 3 represent respectively work exchanger volumes of 40 and 80 L in A, and 160 and 320 L in B. Vertical dotted lines correspond to baseline cases in Table 1 above.

4.2. Effect of number of membranes in series, N_S

In this subsection, we use the model to investigate the effect of varying the number of membranes in series N_S from 1 to 6 while keeping N_P = 1 (*i.e.,* without use of parallel membrane elements). The recirculation flow (Q_r/Q_f) is optimised.

4.2.1. Brackish water feed

Fig. 7 compares the hydraulic *SEC* of the recirculation and supply pumps, as well as the total hydraulic and electrical *SEC*, at recirculation flows Q_r/Q_f from 2 to 8. Increasing N_S increases *SEC* but less so at low recirculation flows. Recirculation flow affects the recirculation pump *SEC* much more than the supply pump *SEC*. Thus, the hydraulic *SEC* of the supply pump remains within the range of 1.05-1.3 kWh/m^3 while that of the recirculation pump increases from 0.02 to 1.4 kWh/m^3, when $N_s = 6$. This trend is most pronounced at high values of $Q_r/Q_f \geq 6$. Nonetheless, when $N_S \leq 4$ and $Q_r/Q_f \leq 5$, recirculation pump hydraulic *SEC* is < 0.2 kWh/m^3 (see Fig. 7B), contributing only to a small fraction of the total hydraulic *SEC*. For example, when $N_S = 4$ and $Q_r/Q_f = 4$, the recirculation pump accounts for only 12.5% of the total hydraulic *SEC*. This minor impact on the energy efficiency of the batch RO system at very high recoveries during scale-up means that good performance can be maintained.

With $N_S \leq 2$, Q_r/Q_f has only a weak effect on overall *SEC*. This is because the increase in *SEC* of the recirculation pump is offset by the decreased *SEC* of the supply pump. However, operating at a higher Q_r/Q_f could help decrease the peak pressure (by about 10-15%) and provide slightly better permeate quality (as shown in experimental results, see Table 3), while maintaining the *SEC* at a relatively consistent level. In contrast, with $N_S \geq 5$, operating at large recirculation flows ($Q_r/Q_f \geq 6$) has a greater impact on total *SEC*. Therefore, at $N_S \leq 3$, operation at Q_r/Q_f of 3 to 7 is recommended while for $N_S \geq 4$, it is better to operate at lower Q_r/Q_f (3 to 5) to minimize the *SEC*.

We also predict the total electrical *SEC* assuming 80% pump efficiency for both the recirculation and supply pumps as other modelling studies of batch RO [32, 33, 38]. With $Q_r/Q_f \leq 5$ and $N_S \leq 4$ at $r = 0.97$ (which is used later for the scale-up cases in the section 4.3), the total electrical *SEC* in brackish water is < 1.6 kWh/m^3 (see Fig. 7D). Considering that the recirculation pump efficiency may be lower than that of the supply pump, we conducted a sensitivity analysis to evaluate its impact on the total electrical *SEC*. Sensitivity to the recirculation pump efficiency is minimal at small scale and low recirculation flow rates but becomes much more noticeable as the recirculation flow increases. Therefore, recirculation pump efficiency becomes crucial in the scale-up, as flow rate is much higher and the recirculation pump's energy consumption constitutes a larger share of the system's total energy use. As an example, at $Q_r/Q_f = 4$, when recirculation pump efficiency decreases from 80 to 50%, the total electrical *SEC* will increase by 5% and 11% when $N_S = 4$ and $N_S = 6$, respectively. The detailed analysis can be found in the SI section 4.

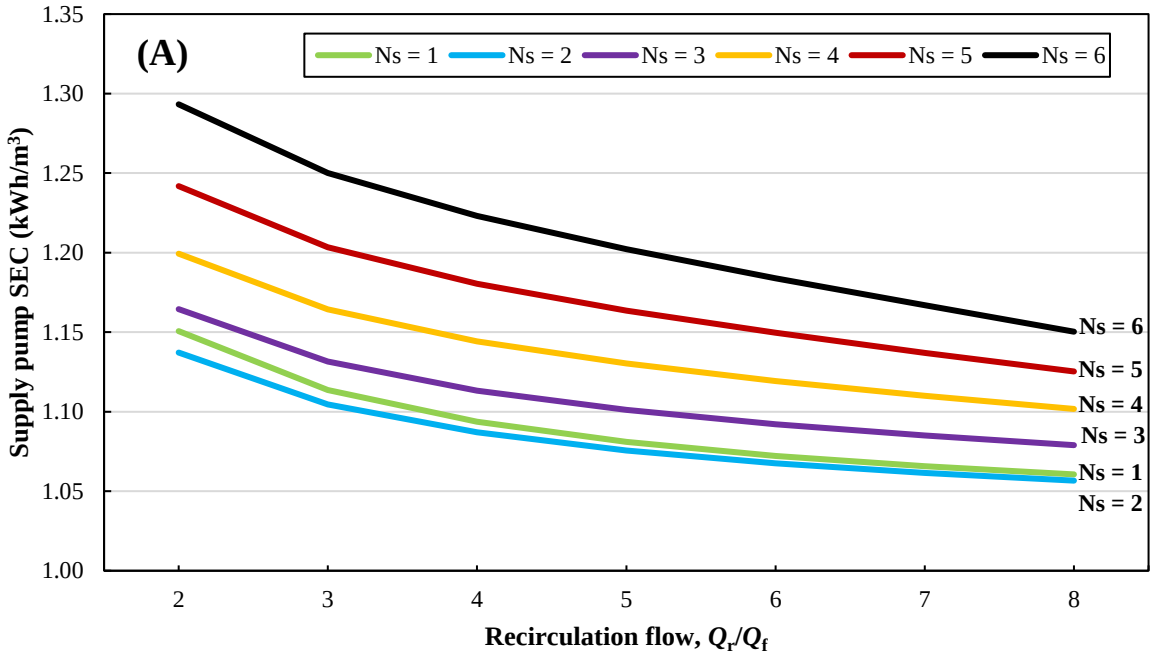
(A)
Ns = 1
Ns = 2
Ns = 3
Ns = 4
Ns = 5
Ns = 6
Supply pump SEC (kWh/m3)
1.35
1.30
1.25
1.20
1.15
1.10
1.05
1.00
2
3
4
5
6
7
8
Recirculation flow, Qr/Qf
Ns = 6
Ns = 5
Ns = 4
Ns = 3
Ns = 1
Ns = 2

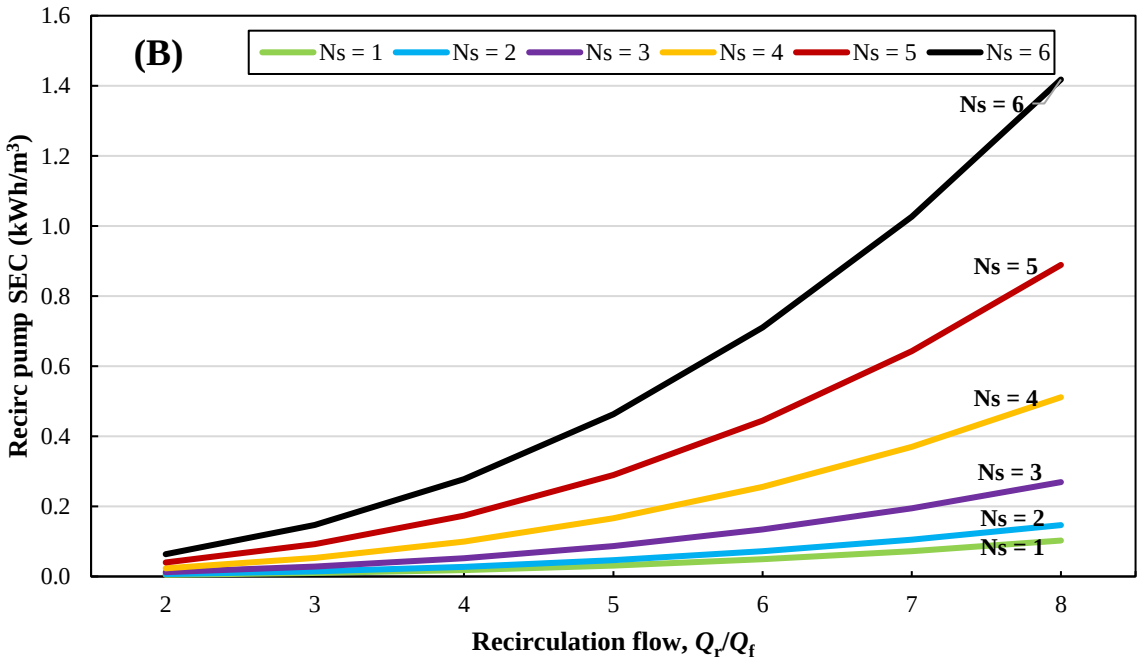
(B)
Ns = 1
Ns = 2
Ns = 3
Ns = 4
Ns = 5
Ns = 6
Recirc pump SEC (kWh/m3)
1.6
1.4
1.2
1.0
0.8
0.6
0.4
0.2
0.0
2
3
4
5
6
7
8
Recirculation flow, Qr/Qf
Ns = 6
Ns = 5
Ns = 4
Ns = 3
Ns = 2
Ns = 1

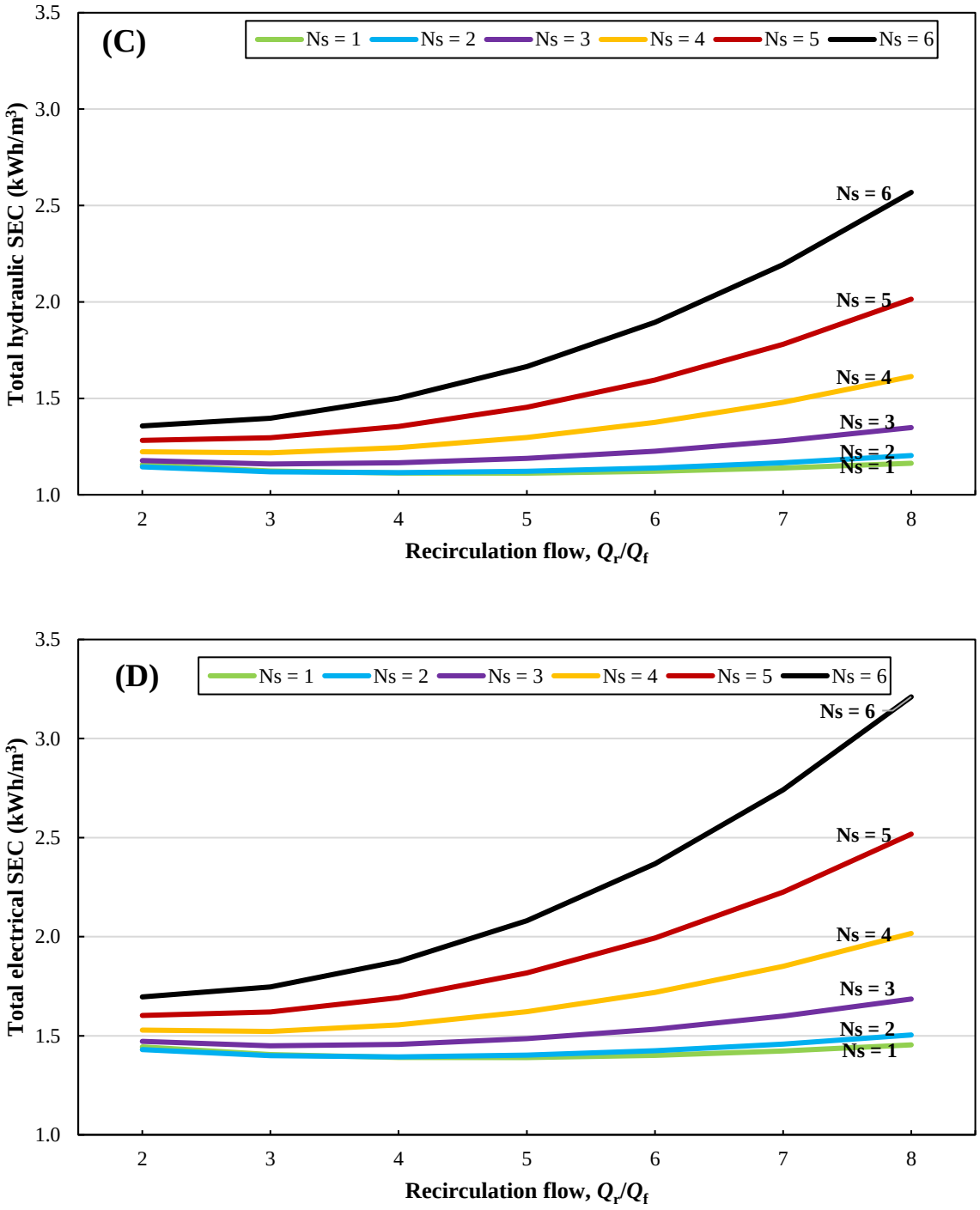

Fig. 7. *SEC* vs recirculation flow, according to number of membranes in series (N_S = 1 – 6), A) supply pump hydraulic *SEC*, B) recirculation pump hydraulic *SEC*, C) total hydraulic *SEC*, and D) total electrical *SEC* (assuming 80% pump efficiency for recirculation and supply pumps). N_P = 1. Brackish water, c_{feed} = 3000 mg/L, r = 0.97, and J_w = 15 L/m^2/h. Hybrid semi-batch/batch operation.

On increasing the number of membranes and the recirculation flow, we increase the diameter of the piping and valves to keep the flow velocity in the pipe in a standard range (see Table 4 footnote). Thus, the pressure drop in valves and piping remains almost unchanged, but the membrane cross-flow pressure drop rises, particularly in a greater degree in the cases of $N_S \geq 5$

(see Fig. 8). Simultaneously, the recirculation pump is required to transfer much larger volumes of brine during refill, resulting in an increase in its energy consumption ($E = \oint p_R . dV_R$).

Fig. 8 also compares membrane friction pressure drop for thick (Fig. 8A) and thin (Fig. 8B) feed spacers, according to recirculation flow and the number of membranes in series. Both cases show a greater rise in membrane friction pressure drop when $N_S \geq 5$ and $Q_r/Q_f \geq 5$, with this trend being more pronounced with thin feed spacers. Conversely, when $Q_r/Q_f \leq 5$ and $N_S \leq 4$, the membrane pressure drop remains under 100 kPa for thick feed spacers and under 200 kPa for thin feed spacers.

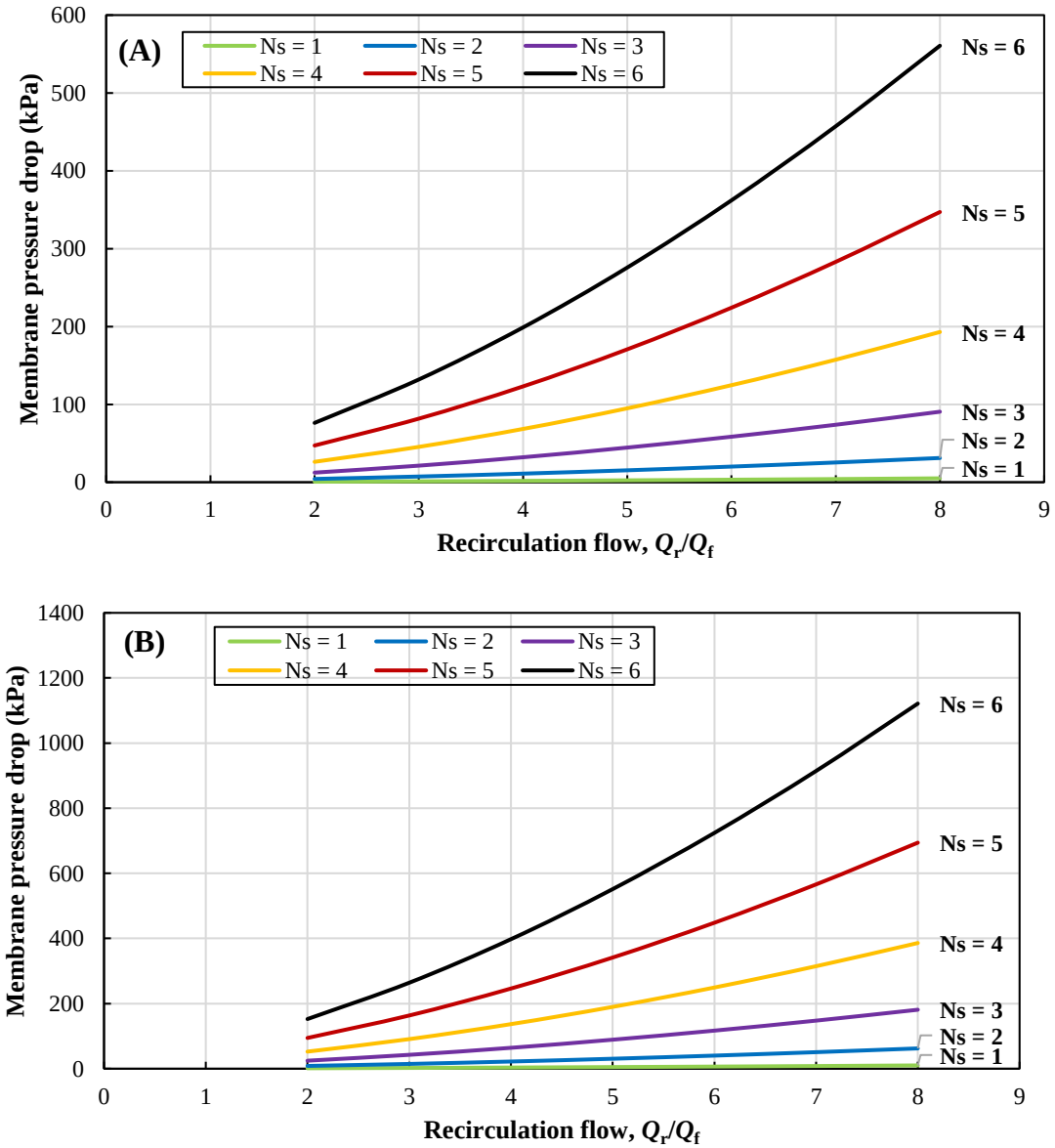

Fig. 8. Membrane cross-flow pressure drop as a function of recirculation flow at different number of membranes in series (N_S = 1 – 6, N_P=1) A) thick feed spacer [k = 300], and B) thin feed spacer [k = 600]. Brackish water, c_{feed} = 3000 mg/L, r = 0.97, and J_w = 15 L/m^2/h. Hybrid semi-batch/batch operation.

4.2.2. Seawater feed

The trends with seawater resemble those with brackish water feed. As the osmotic pressure of seawater is much higher, however, the recovery is much lower than with brackish water (r = 0.66 down from 0.97). Thus, the initial semi-batch phase is not used in the seawater case. Because of the increased pressure, supply pump *SEC* greatly exceeds recirculation pump *SEC*. For example, when $N_S = 4$ and $Q_r/Q_f = 4$, recirculation pump hydraulic *SEC* accounts for only 4.3% of the total *SEC*. Therefore, increasing the Q_r/Q_f value has less impact on the total hydraulic *SEC* compared to the brackish water case. For instance, with four membranes in series ($N_S = 4$), increasing Q_r/Q_f from 2 to 8 results in only a 19% increase in total hydraulic *SEC* compared to 48% with brackish water. Even with $N_S = 5$, operation at high Q_r/Q_f such as 6 increases the hydraulic *SEC* by only 15% compared to *SEC* at $Q_r/Q_f = 2$ (see Fig. 9C).

In the seawater case overall, *SEC* is insensitive to Q_r/Q_f up to $N_S = 3$. With $N_S \geq 4$ it is better to operate at $Q_r/Q_f \leq 6$ to avoid significant increase in *SEC*. With $Q_r/Q_f \leq 5$ and $N_S \leq 4$ at r = 0.66 (which is used later for the scale-up cases in the section 4.3), the total electrical *SEC* in seawater is < 3 kWh/m^3 (see Fig. 9D).

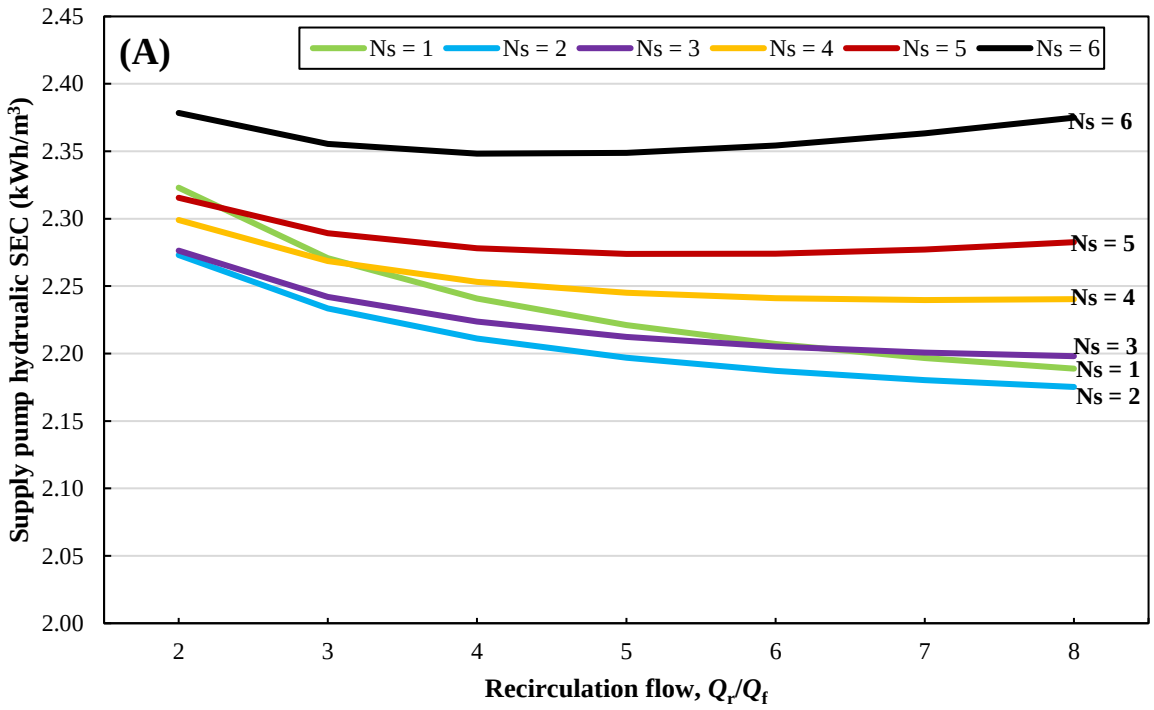

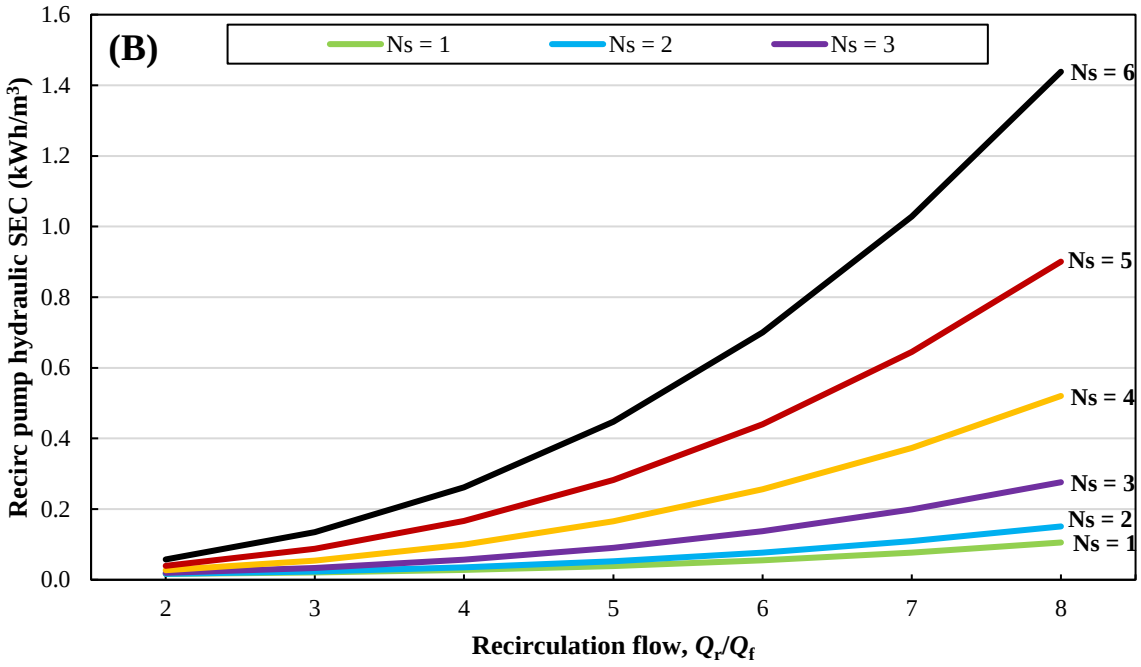
(B)
Ns = 1
Ns = 2
Ns = 3
Ns = 6
Ns = 5
Ns = 4
Ns = 3
Ns = 2
Ns = 1
Recirc pump hydraulic SEC (kWh/m³)
Recirculation flow, Q_r/Q_f

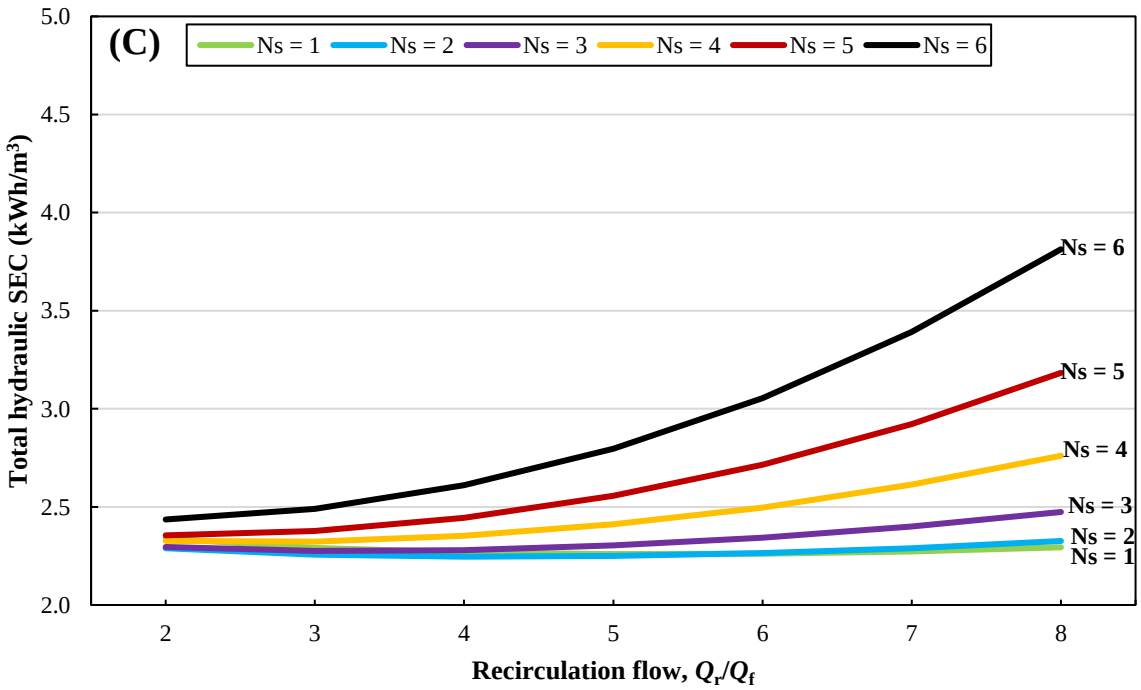
(C)
Ns = 1
Ns = 2
Ns = 3
Ns = 4
Ns = 5
Ns = 6
Total hydraulic SEC (kWh/m³)
Recirculation flow, Q_r/Q_f

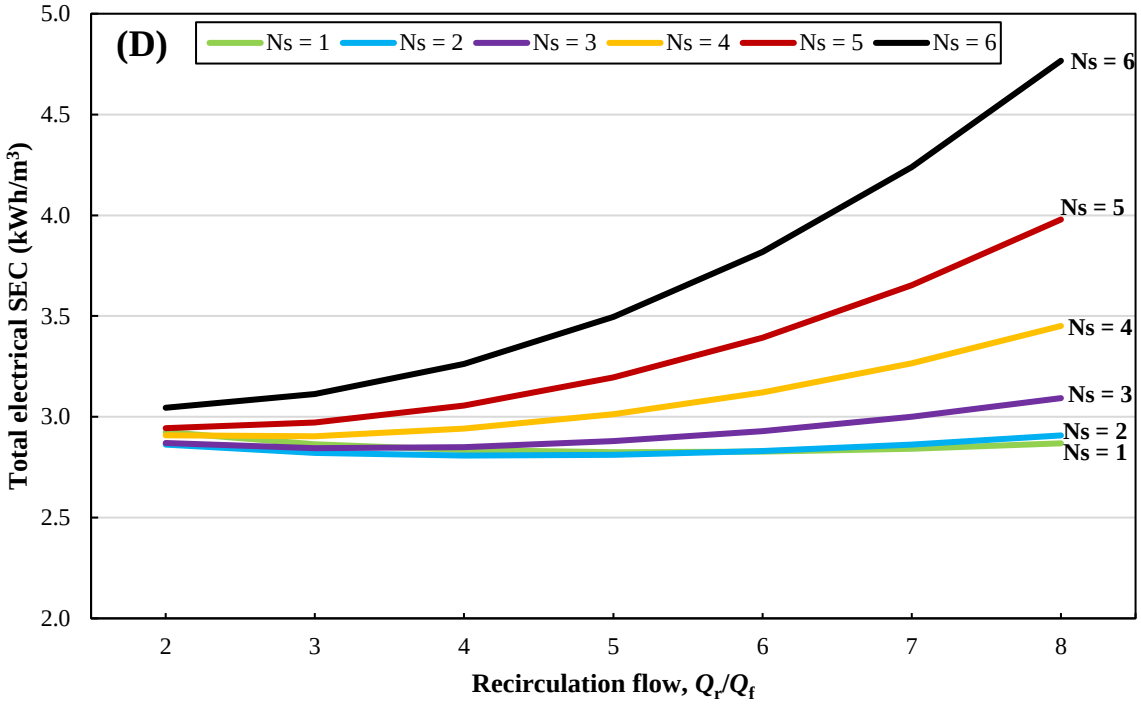

Fig. 9. *SEC* vs recirculation flow, according to number of membranes in series (N_S = 1 – 6), A) recirculation pump hydraulic *SEC*, B) supply pump hydraulic *SEC*, C) total hydraulic *SEC*, and D) total electrical *SEC* (assuming 80% pump efficiency for recirculation and supply pumps). N_P = 1. Seawater, c_{feed} = 35000 mg/L, r = 0.66, and J_w = 15 L/m^2/h, XUS membrane. Batch operation.

4.3. Free-piston batch RO scale-up: design examples

In this subsection, we provide specific scale up examples based on a standard 16-inch diameter × 4 m long pressure vessel as the work exchanger (giving volume of V_b = 500 L) along with multiple RO elements in parallel.

We consider two case studies, the first using feed concentrations of 3000 mg/L (representing brackish water) and the second using 35000 mg/L (representing seawater). We aim for maximum recovery, using either batch RO or hybrid semi-batch/batch RO as appropriate (see SI section 3 for modelling of maximum recovery with brackish water). More details regarding main parameters such as recovery, flux, rejection and permeability are given in Table 4.

By considering a ratio of V_{total}/V_h = 2 (similar to the pilot used in [6, 41]) and V_{total}/V_h = 3 (to minimize energy penalty by increasing the work exchanger volume as seen in Fig. 6), we estimate the required number of membranes. To accommodate these, we arrange them into several pressure vessels each containing 4 membranes in series.

4.3.1. Brackish water case study

When treating brackish water at V_{total}/V_h = 2, we initially estimated 13 RO membranes. Therefore, for practicality, we specify 12 membranes distributed across three pressure vessels connected in parallel (see Fig. 10A). At V_{total}/V_h = 3, 7 RO membranes were estimated. Thus, we specify 8 membranes accommodated in two parallel vessels (see Fig. 10B). Both arrangements are modelled for two different membrane types: (1) the XUS membrane, as assumed until now, and (2) the BW XLE-440 high-permeable brackish water RO element with

membrane permeability of 4.6 L/m^2/h/bar and pressure rating of 41 bar. The membrane permeabilities were experimentally verified in [40, 41]. Also, the constants used to calculate membrane cross-flow pressure drop are k = 300 and 600 for the XUS and XLE respectively as explained in section 3.1. Recirculation flow of $Q_r/Q_f = 4$ is chosen. To achieve high recovery, the system is operated in hybrid semi-batch/batch mode.

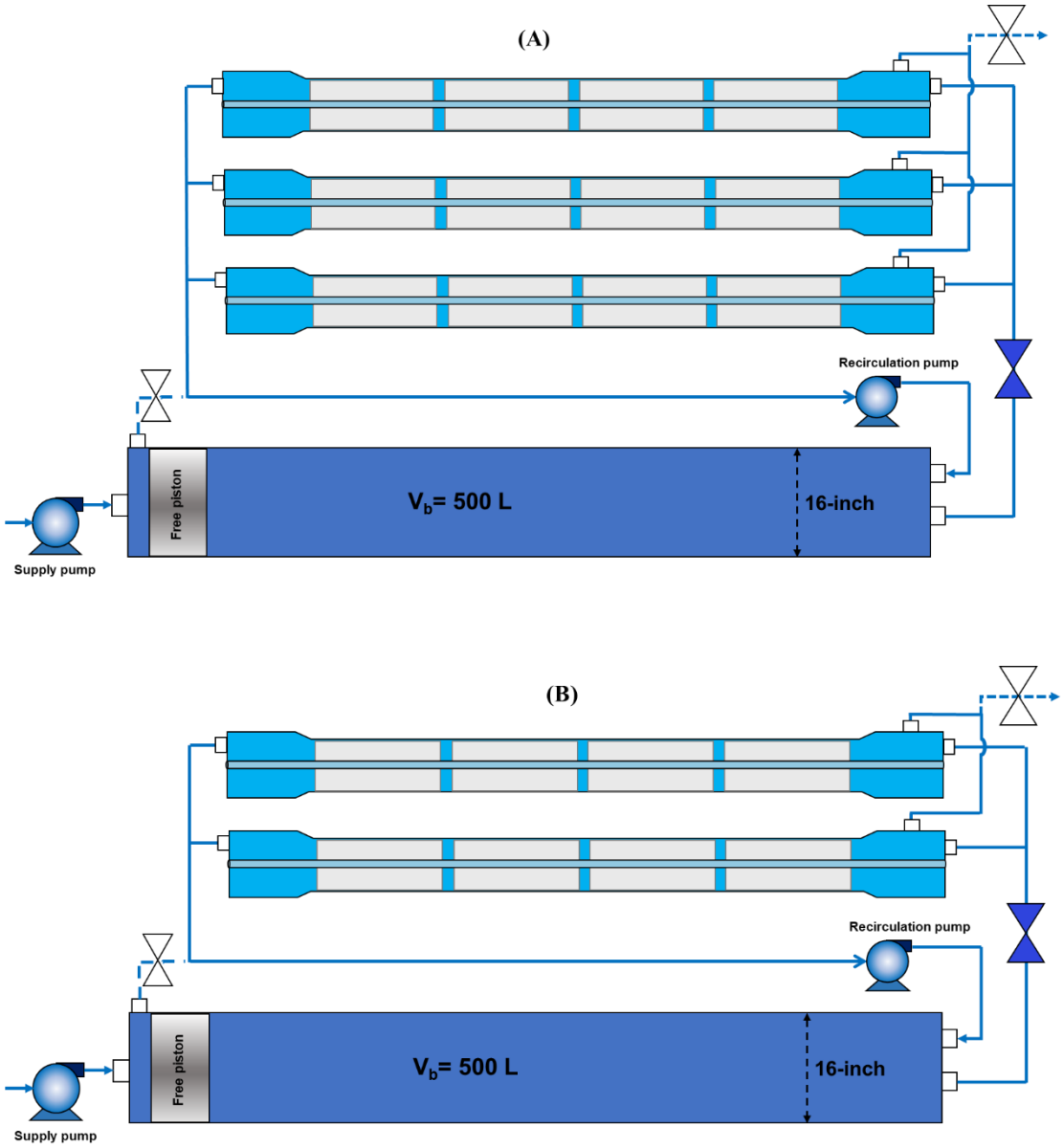

Fig. 10. Schematic of scaled-up free-piston batch RO configuration when using a 16-inch pressure vessel with a 4 m length as the work exchanger, for two cases: A) $V_{total}/V_h = 2$, requiring 12 membranes; B) $V_{total}/V_h = 3$, requiring 8 membranes.

Based on the modelling, recovery is restricted by the pressure limit of the membranes (see SI section 3). Thus, maximum recoveries of 0.93 and 0.97 are achievable for the XLE and XUS membranes respectively (see Table 5). In practice, recovery may be further restricted by the solubility of sparingly soluble salts in the feed, causing scaling. Nonetheless, recent studies have suggested that batch RO can avoid or delay scaling through mechanisms such as salinity cycling, osmotic backwash, flushing, and feed flow reversal [10, 47].

The XLE membrane element has 30% more active area than the XUS, giving more permeate output from the same number of elements. For example, in the case of using 12 elements, total membrane area is 492 and 367.2 m^2 for XLE and XUS, giving a permeate output of 165 and 128 m^3/day respectively (at recoveries of 0.93 and 0.97).

For the fixed work exchanger volume of V_b = 500 L, use of fewer membranes (corresponding to increased V_{total}/V_h) decreases *SEC* but at the expense of decreased output. Thus, when V_{total}/V_h = 2, the total hydraulic *SEC* is 0.69 and 1.19 kWh/m^3 for XLE and XUS respectively with outputs of 165 and 128 m^3/day. But on increasing to V_{total}/V_h = 3, *SEC* decreases by 9% for both types of membranes. However, this comes at the expense of a 34% reduction in permeate output, which may not justify the modest energy saving (Table 5).

In the case of semi-batch RO (V_{total}/V_h = 1) we predict hydraulic *SEC* of 1.03 and 0.996 kWh/m^3 when using 12 and 8 XLE membranes, respectively. In comparison, hybrid semi-batch/batch RO reduces *SEC* by 33% (V_{total}/V_h = 2) and 37% (V_{total}/V_h = 3). These reductions grow to 45 and 50% respectively for the XUS membrane.

Key factors that restrict higher outputs include the maximum pressure rating of the membranes, which limits the flux. Additionally, if membrane permeability were greater, the peak pressure would decrease, allowing us to operate at higher fluxes without reaching the pressure limit. For instance, if the permeability of the XUS membrane were 2 L/m²/h/bar instead of 0.8 L/m²/h/bar, flux could increase from 15 to 37.5 L/m²/h (assuming a maximum pressure of 112 bar). This would result in outputs of 320 m³/day and a hydraulic *SEC* of 1.735 kWh/m³ when using 12 membranes, translating to a 150% increase in output and only a 45% increase in *SEC*. These values underscore the critical role of membrane development to enhance permeability and increase burst pressure in the development and scale-up of batch RO.

An interesting observation also arises when comparing the *SEC* of the XLE membrane assuming the cross-flow pressure drop matches that of the XUS (i.e., assuming a constant value of k = 300 for the XLE instead of 600 in Eq. 1). Then, the *SEC* would decrease even further, dropping from 0.69 to 0.567 kWh/m^3 (an 18% reduction) and from 0.628 to 0.506 kWh/m^3 (a 19% reduction) when using 12 and 8 elements, respectively. The *SEC* reduction could be even more substantial if we operated at higher fluxes or higher Q_r/Q_f ratios, as these adjustments would increase the pressure drop. This underscores the significance of membrane spacer development in minimizing *SEC* in batch RO.

Second law efficiency was also calculated using the equation for the thermodynamic minimum SEC provided in [5]. For the cases mentioned in Table 5, we determined the minimum SEC and divided it by the total electrical SEC. For the XLE membrane, the second law efficiency was 21.2% and 23.3% for cases with 12 and 8 modules, respectively. These values decreased to 15.8% and 17.2% for the XUS membrane due to its lower permeability and higher electrical SEC (though it has a better rejection and higher recovery rate). However, it still remains higher than existing brackish water RO systems, which typically exhibit second law efficiencies ranging from 2% to 15% only [48].

Table 5. Details of a scaled up free-piston batch RO system using a 500 L work exchanger volume (a standard 16-inch diameter × 4 m long pressure vessel) when treating brackish NaCl feed with concentration of c_{feed}= 3000 mg/L, at J_w = 15 L/m^2/h and Q_r/Q_f = 4. Membrane permeability is adjusted to 0.8 and 4.6 L/m^2/h/bar for XUS and XLE membranes respectively while rejection is set to 0.96 and 0.92 (consistent with experimental results [40,

41]). The length and diameter of the pipe in the recirculation loop is 6.2 m and 56 mm respectively. Hybrid semi-batch/batch operation.

Feed conc. (mg/L) c_{feed}	Membrane type	V_{total}/V_h	No of elements	Total membrane area (m^2)	Recovery, r	Peak Pressure (bar)	Permeate output (m^3/day)	Hydraulic *SEC* (kWh/m^3)			Electrical *SEC* (kWh/m^3)		
								Supply pump	Recirc pump	Total	Supply pump	Recirc pump	Total
3000	XLE	2	12	492	0.93	37	165	0.353	0.337	0.690	0.441	0.421	0.862
		3	8	328			108	0.339	0.289	0.628	0.424	0.361	0.785
	XUS	2	12	367.2	0.97	108	128	1.051	0.142	1.193	1.314	0.177	1.491
		3	8	244.8			84	0.98	0.114	1.094	1.225	0.142	1.367

Permeate output could be further increased by employing multiple independent systems in parallel. As an illustration, to obtain 1000 m^3/day of permeate output about six systems using the XLE membrane would be needed. This approach may increase capital costs compared to conventional RO systems. Nonetheless, independent units may also improve reliability by providing backups.

4.3.2. Seawater case study

For the seawater case study, 12 membranes are used with three parallel pressure vessels giving $V_{total}/V_h = 2$ with V_b kept at 500 L, giving a recovery of 0.66 in batch mode (hybrid operation is avoided as this would lead to excess pressures). For maximum recovery, the high-pressure XUS membrane is used. The modelling results are summarised in Table 6.

With a peak pressure limit of 112 bar, we predict output of 105 m^3/day at a flux of 15 L/m^2/h. The hydraulic *SEC* is 2.371 kWh/m^3, down by 13.1% compared to 2.727 kWh/m^3 for semi batch, and electrical *SEC* is 2.963 kWh/m^3. We can achieve a high recovery rate (r = 0.66), which is advantageous in applications with high salinity, such as mineral recovery, and the energy consumption is competitive with conventional seawater desalination. However, low membrane permeability and osmotic backflow are the primary obstacles to achieving even greater energy efficiency.

Although most studies [32, 38] assumed permeability of 3 L/m^2/h/bar in their modelling, we use the experimentally validated value of only 0.8 L/m^2/h/bar. If we were to assume 2 or 4 L/m^2/h/bar, hydraulic *SEC* would reduce to 2.023 and 1.907 kWh/m^3 respectively (down by 15 and 20% from 2.371 kWh/m^3 at 0.8 L/m^2/h/bar). This would be accompanied by lower peak pressures of 102 and 98 bar respectively, allowing an increase in water flux and/or recovery if the same peak pressure were maintained. This, in turn, would increase permeate output. For instance, at a permeability of 2 L/m^2/h/bar, flux could be increased from 15 to 29.4 L/m^2/h, boosting the permeate output to 207 m^3/day at the cost of higher *SEC* of 2.656 kWh/m^3. This corresponds to doubling the permeate output while the *SEC* increases only by 12%. These findings again underline the potential for future enhancements in membrane permeability to enhance the energy efficiency and overall competitiveness of batch RO in high-pressure high-recovery seawater desalination, or other similar applications requiring a high concentration factor with saline feedwater.

Moreover, osmotic backflow is estimated at 4.5 L per element per cycle, i.e., 54 L for the 12-element system, resulting in a 12% loss of permeate output. If this backflow were eliminated, we could achieve higher recoveries or lower *SECs*. For the brackish water case, osmotic backflow is much less significant because the cycles are longer and with larger output. For

example, when using 12 XUS membranes with the brackish water, osmotic backflow sacrifices only 1% of total output.

The corresponding second law efficiency for the case detailed in Table 6 was 43.4%, significantly higher than the cases reported in the literature [49]. This efficiency is 2-3 times higher than the brackish water cases discussed in Table 5 because the feed salinity is much higher. Consequently, the impact of inefficiencies (such as membrane friction losses) in batch RO is much less.

Table 6. Details of a scaled up free-piston batch RO system using a 500 L work exchanger volume when treating NaCl feed concentration of 35,000 mg/L, representing seawater, at J_w = 15 L/m^2/h, Q_r/Q_f = 4 (or recovery per pass of 0.2) and rejection of 0.98. The length and diameter of the pipe in the recirculation loop was assumed at 6.2 m and 56 mm. Batch operation.

Feed conc. (mg/L), c_{feed}	Membrane type	V_{total}/V_h	No of elements	Total membrane area (m^2)	Recovery, r	Peak Pressure (bar)	Permeate output (m^3/day)	Hydraulic *SEC* (kWh/m^3)			Electrical *SEC* (kWh/m^3)		
								Supply pump	Recirc pump	Total	Supply pump	Recirc pump	Total
35000	XUS	2	12	367.2	0.66	112	105	2.227	0.143	2.371	2.784	0.179	2.963

While readily available 16-inch pressure vessels from the RO market are assumed in this study, further scale up may be achieved using other types of larger pressure vessel. Alternatively, large pressure vessels may be developed specifically for use in batch RO. This will likely depend on sufficient commercial uptake to justify investment in facilities and tooling for manufacturing.

5. Conclusions

A modelling and scale up study of batch RO has been conducted for brackish water and seawater feed represented respectively by 3000 mg/L and 35000 mg/L NaCl solutions. Special attention has been paid to modelling the energy usage of the recirculation pump which becomes more significant as the number of membrane elements increases. Transmembrane water flux is set at 15 L/m^2/h throughout. The key conclusions are:

1. Validation of the model against experiments shows agreement in *SEC* with error <4%.
2. Operating at up to 112 bar (*i.e.*, safely below the 120 bar limit of the experimental system) the maximum possible recovery is 0.97 and 0.66 with brackish and seawater respectively.
3. For brackish water, hybrid semi-batch/batch operation is recommended whereas for seawater pure batch operation is recommended.
4. The volume of the work exchanger should be about 1 to 2× the volume of the membrane pressure vessels because this achieves significant (31-54%) saving in *SEC* compared to semi-batch where no work exchanger is used. Larger work exchanger volume further reduces *SEC* but only marginally.
5. Arranging up to 4 membrane elements in series increases *SEC* only marginally (i.e., by <10%) provided the recirculation flow does not exceed 4× the flow from the supply pump. With 5 or 6 elements in series, *SEC* becomes more sensitive to increased recirculation flow, but the electrical *SEC* can be maintained below 1.5 kWh/m^3 with brackish water (r = 0.97) and 3 kWh/m^3 with seawater (r = 0.66) at such high recoveries.
6. Specific designs are proposed based on a 500-L work exchanger connected to parallel pressure vessels each housing four 8-inch membrane elements.

7. For brackish water feed, three parallel vessels (*i.e.*, 12 membrane elements) provide 165 m^3/day and 128 m^3/day of permeate output with XLE and XUS membranes respectively, achieving recoveries of 0.93 and 0.97 with hydraulic *SEC* of 0.69 and 1.19 kWh/m^3. These values represent *SEC* reductions of 33% and 45% compared to semi-batch RO. Assuming efficiency of 80% for the supply and recirculation pumps, this translates to electrical *SEC* of 0.862 and 1.487 kWh/m^3 for XLE and XUS membranes respectively.
8. Using a similar arrangement of 12 XUS membranes for seawater, at $r = 0.66$, batch RO provides 105 m^3/day permeate output, with hydraulic *SEC* of 2.37 kWh/m^3 (a 13% reduction compared to semi-batch) and electrical *SEC* of 2.962 kWh/m^3.
9. The second law efficiency of the scaled-up case study with seawater was 43.4%, approximately twice as high as the brackish water case study, which reached up to 23.3%. In the process of scaling up, the second law efficiency decreased but only slightly, by less than 5%.
10. Future high-permeability membranes (giving 2 L/m^2/h/bar as compared to 0.8 L/m^2/h/bar for the XUS) could enhance output by 150% and 97% with *SEC* penalty of 12% and 45% for brackish and seawater respectively, without exceeding the maximum pressure of 112 bar.

This study has been validated by means of a single-acting free piston batch RO system. However, we expect that the trends of the results will apply also to other types of batch RO system using pressurised vessels, such as double-acting systems or systems using bladders [30, 50]. This is because these systems all work by similar principles.

Though outputs above 300 m^3/day are difficult to achieve in a single unit using the suggested 16-inch pressure vessel as a work exchanger, larger outputs are possible using multiple units or custom-designed vessels to increase the work exchanger volume. In summary, while this work provides a solid foundation for scaling up free-piston batch RO systems, it does not set an upper limit on their size. Greater system sizes are conceivable, but addressing the challenges outlined in this study will require continued research, technological innovation, and comprehensive economic analysis.

Regarding future work, it is important to find efficient pumps specifically designed for the pressure variations in batch RO process. Additionally, developing modules with lower cross-flow pressure drop is beneficial for scaling up batch RO. As mentioned in section 4.2.1, pressure drop increases with system scale, impacting recirculation pump energy consumption. Exploring alternative pressure vessels for the work exchanger is also recommended. For example, adapting designs with larger diameters from other industries, or different geometries may provide alternatives beyond those available in the desalination market, permitting larger scale up factors. A comprehensive techno-economic analysis is also needed to assess the cost-benefit ratio of scaling up batch RO systems. This should include evaluating capital costs, operational expenses, and potential savings in energy and maintenance compared to conventional continuous RO systems.

Acknowledgements

This project has received funding from the Engineering and Physical Sciences Research Council, UK (Grant Ref: EP/T025867/1).

References

[1] N. Ghaffour, T.M. Missimer, G.L. Amy, Technical review and evaluation of the economics of water desalination: Current and future challenges for better water supply sustainability, Desalination, 309 (2013) 197-207.
[2] F.E. Ahmed, A. Khalil, N. Hilal, Emerging desalination technologies: Current status, challenges and future trends, Desalination, 517 (2021) 115183.
[3] P.A. Davies, J. Wayman, C. Alatta, K. Nguyen, J. Orfi, A desalination system with efficiency approaching the theoretical limits, Desalination and Water Treatment, 57 (2016) 23206-23216.
[4] K. Park, P.A. Davies, A compact hybrid batch/semi-batch reverse osmosis (HBSRO) system for high-recovery, low-energy desalination, Desalination, 504 (2021) 114976.
[5] E. Hosseinipour, S. Karimi, S. Barbe, K. Park, P.A. Davies, Hybrid semi-batch/batch reverse osmosis (HSBRO) for use in zero liquid discharge (ZLD) applications, Desalination, 544 (2022) 116126.
[6] S. Karimi, R. Engstler, E. Hosseinipour, M. Wagner, F. Heinzler, M. Piepenbrink, S. Barbe, P. Davies, High-pressure batch reverse osmosis (RO) for zero liquid discharge (ZLD) in a Cr (III) electroplating process, Desalination, (2024) 117479.
[7] P. Davies, A. Afifi, F. Khatoon, G. Kuldip, S. Javed, S. Khan, Double-acting batch-RO system for desalination of brackish water with high efficiency and high recovery, Desalination for the Environment–Clean Energy and Water, Rome, (2016) 23-25.
[8] K. Park, L. Burlace, N. Dhakal, A. Mudgal, N.A. Stewart, P.A. Davies, Design, modelling and optimisation of a batch reverse osmosis (RO) desalination system using a free piston for brackish water treatment, Desalination, 494 (2020) 114625.
[9] E. Hosseinipour, K. Park, L. Burlace, T. Naughton, P.A. Davies, A free-piston batch reverse osmosis (RO) system for brackish water desalination: Experimental study and model validation, Desalination, 527 (2022) 115524.
[10] E. Hosseinipour, E. Harris, H.A. El Nazer, Y.M. Mohamed, P.A. Davies, Desalination by batch reverse osmosis (RO) of brackish groundwater containing sparingly soluble salts, Desalination, 566 (2023) 116875.
[11] A.G. Capodaglio, A. Callegari, D. Cecconet, D. Molognoni, Sustainability of decentralized wastewater treatment technologies, Water Practice and Technology, 12 (2017) 463-477.
[12] A. Hafeez, Z. Shamair, N. Shezad, F. Javed, T. Fazal, S. ur Rehman, A.A. Bazmi, F. Rehman, Solar powered decentralized water systems: a cleaner solution of the industrial wastewater treatment and clean drinking water supply challenges, Journal of Cleaner Production, 289 (2021) 125717.
[13] V.G. Varma, S. Jha, L.H.K. Raju, R.L. Kishore, V. Ranjith, A review on decentralized wastewater treatment systems in India, Chemosphere, 300 (2022) 134462.
[14] N. Jahan, M. Tahmid, A.Z. Shoronika, A. Fariha, H. Roy, M.N. Pervez, Y. Cai, V. Naddeo, M.S. Islam, A comprehensive review on the sustainable treatment of textile wastewater: zero liquid discharge and resource recovery perspectives, Sustainability, 14 (2022) 15398.
[15] Z. Lv, H. Feng, R. Chen, B. Shen, H. Tao, Y. Ding, Y. Xia, Y. He, Y. Zhang, Simultaneous removal of fluorine and dissolved silica from semiconductor wastewater by an in-situ crystal nucleation method towards near-zero liquid discharge, Desalination, (2024) 117831.
[16] G. Mekuria, Dairy Wastewater Treatment through Synergies of the Biological and Hybrid Membrane: A Systematic Review, J. Environ. Inform. Lett, 8 (2022) 31-50.
[17] A. Bottino, G. Capannelli, A. Comite, C. Costa, R. Firpo, A. Jezowska, M. Pagliero, Treatment of olive mill wastewater through integrated pressure-driven membrane processes, Membranes, 10 (2020) 334.
[18] B. Martin-Gorriz, J.F. Maestre-Valero, B. Gallego-Elvira, P. Marín-Membrive, P. Terrero, V. Martínez-Alvarez, Recycling drainage effluents using reverse osmosis powered by photovoltaic solar energy in hydroponic tomato production: Environmental footprint analysis, Journal of Environmental Management, 297 (2021) 113326.
[19] N. van Linden, R. Shang, G. Stockinger, B. Heijman, H. Spanjers, Separation of natural organic matter and sodium chloride for salt recovery purposes in zero liquid discharge, Water Resources and Industry, 23 (2020) 100117.
[20] X. Liu, J. Ma, E. Li, J. Zhu, H. Chu, X. Zhou, Y. Zhang, Multistage membrane-integrated zero liquid discharge system for ultra-efficient resource recovery from steel industrial brine: Pilot-scale investigation and spatial membrane fouling, Journal of Membrane Science, 699 (2024) 122655.
[21] A. Panagopoulos, V. Giannika, Decarbonized and circular brine management/valorization for water & valuable resource recovery via minimal/zero liquid discharge (MLD/ZLD) strategies, Journal of Environmental Management, 324 (2022) 116239.

[22] A. Khalil, S. Mohammed, R. Hashaikeh, N. Hilal, Lithium recovery from brine: Recent developments and challenges, Desalination, 528 (2022) 115611.
[23] P. Goh, K. Wong, A. Ismail, Membrane technology: A versatile tool for saline wastewater treatment and resource recovery, Desalination, 521 (2022) 115377.
[24] J. Du, T.D. Waite, P. Biesheuvel, W. Tang, Recent advances and prospects in electrochemical coupling technologies for metal recovery from water, Journal of Hazardous Materials, 442 (2023) 130023.
[25] G. Naidu, L. Tijing, M.A. Johir, H. Shon, S. Vigneswaran, Hybrid membrane distillation: Resource, nutrient and energy recovery, Journal of Membrane Science, 599 (2020) 117832.
[26] D.-G.f.R.a.I. European Commission, Horizon Europe strategic plan 2025-2027., in, https://data.europa.eu/doi/10.2777/092911, 2024.
[27] M. Li, Y. Heng, J. Luo, Batch reverse osmosis: a new research direction in water desalination, Sci. Bull, 65 (2020) 1705-1708.
[28] M. Li, Effects of finite flux and flushing efficacy on specific energy consumption in semi-batch and batch reverse osmosis processes, Desalination, 496 (2020) 114646.
[29] A. Das, D.M. Warsinger, Batch counterflow reverse osmosis, Desalination, 507 (2021) 115008.
[30] Q.J. Wei, C.I. Tucker, P.J. Wu, A.M. Trueworthy, E.W. Tow, Impact of salt retention on true batch reverse osmosis energy consumption: experiments and model validation, Desalination, 479 (2020) 114177.
[31] T. Qiu, P.A. Davies, Comparison of configurations for high-recovery inland desalination systems, Water, 4 (2012) 690-706.
[32] J.R. Werber, A. Deshmukh, M. Elimelech, Can batch or semi-batch processes save energy in reverse-osmosis desalination?, Desalination, 402 (2017) 109-122.
[33] J. Swaminathan, E.W. Tow, R.L. Stover, Practical aspects of batch RO design for energy-efficient seawater desalination, Desalination, 470 (2019) 114097.
[34] M. Li, N. Chan, J. Li, Novel dynamic and cyclic designs for ultra-high recovery waste and brackish water RO desalination, Chemical Engineering Research and Design, 179 (2022) 473-483.
[35] Z. Gal, A. Efraty, CCD series no. 18: record low energy in closed-circuit desalination of ocean seawater with nanoH2O elements without ERD, Desalination and Water Treatment, 57 (2016) 9180-9189.
[36] A. Efraty, Closed circuit desalination series no-4: high recovery low energy desalination of brackish water by a new single stage method without any loss of brine energy, Desalination and water treatment, 42 (2012) 262-268.
[37] H. Gu, M.H. Plumlee, M. Boyd, M. Hwang, J.C. Lozier, Operational optimization of closed-circuit reverse osmosis (CCRO) pilot to recover concentrate at an advanced water purification facility for potable reuse, Desalination, 518 (2021) 115300.
[38] A. Das, A.K. Rao, S. Alnajdi, D.M. Warsinger, Pressure exchanger batch reverse osmosis with zero downtime operation, Desalination, 574 (2024) 117121.
[39] H. Abu Ali, M. Baronian, L. Burlace, P.A. Davies, S. Halasah, M. Hind, A. Hossain, C. Lipchin, A. Majali, M. Mark, Off-grid desalination for irrigation in the Jordan Valley, Desalination and Water Treatment, 168 (2019) 143-154.
[40] E. Hosseinipour, P. Davies, Effect of membrane properties on the performance of batch reverse osmosis (RO): The potential to minimize energy consumption, Desalination, 577 (2024) 117378.
[41] E. Hosseinipour, P. Davies, Direct experimental comparison of batch reverse osmosis (RO) technologies, Desalination, (2024) 117717.
[42] R. Zhao, S. Porada, P. Biesheuvel, A. Van der Wal, Energy consumption in membrane capacitive deionization for different water recoveries and flow rates, and comparison with reverse osmosis, Desalination, 330 (2013) 35-41.
[43] A. Haidari, S. Heijman, W. van der Meer, Visualization of hydraulic conditions inside the feed channel of Reverse Osmosis: A practical comparison of velocity between empty and spacer-filled channel, Water research, 106 (2016) 232-241.
[44] B. Massey, Mechanics of Fluids 4. th Edition, The English Language Book Society, (1980).
[45] D.W. Solutions, Filmtec™ reverse osmosis membranes, Technical Manual, Form, 399 (2010) 1-180.
[46] M. Li, Effect of cylinder sizing on performance of improved closed-circuit RO (CCRO), Desalination, 561 (2023) 116688.
[47] D.M. Warsinger, E.W. Tow, L.A. Maswadeh, G.B. Connors, J. Swaminathan, Inorganic fouling mitigation by salinity cycling in batch reverse osmosis, Water research, 137 (2018) 384-394.
[48] J.H. Lienhard, G.P. Thiel, D.M. Warsinger, L.D. Banchik, Low carbon desalination: status and research, development, and demonstration needs, report of a workshop conducted at the Massachusetts Institute of Technology in association with the Global Clean Water Desalination Alliance, (2016).
[49] J. Kim, K. Park, D.R. Yang, S. Hong, A comprehensive review of energy consumption of seawater reverse osmosis desalination plants, Applied Energy, 254 (2019) 113652.
[50] S. Cordoba, A. Das, J. Leon, J.M. Garcia, D.M. Warsinger, Double-acting batch reverse osmosis configuration for best-in-class efficiency and low downtime, Desalination, 506 (2021) 114959.

APPENDIX A. Author contributions

This appendix contains the co-author statements of my contributions.

Co-author statements

- **Philip A. Davies**

From: Philip Davies (Civil Engineering) <p.a.davies@bham.ac.uk>
Sent: Thursday, August 8, 2024 5:15 PM
To: Ebrahim Hosseinipour (Engineering) <e.hosseinipour@bham.ac.uk>
Subject: RE: Request for paper contribution statement

Dear Ebrahim,

I confirm the accuracy of the author contribution statement below

Good luck with your submission,

Kind regards
Philip

Philip Davies
Professor of Water Technology
School of Engineering
College of Engineering and Physical Sciences
p.a.davies@bham.ac.uk
0121 414 2826

UNIVERSITY OF BIRMINGHAM

From: Ebrahim Hosseinipour (Engineering) <e.hosseinipour@bham.ac.uk>
Sent: Thursday, August 8, 2024 5:13 PM
To: Philip Davies (Civil Engineering) <p.a.davies@bham.ac.uk>
Subject: Request for paper contribution statement

Dear Philip,

As you kindly assisted me through the process, I am in the final steps of submitting my thesis for the Award of a PhD by Published Work at the University of Birmingham. As part of the formal submission requirements, I need to provide a statement from you confirming my contribution to our co-authored paper(s):

1. Hosseinipour E, Park K, Burlace L, Naughton T, Davies PA. A free-piston batch reverse osmosis (RO) system for brackish water desalination: Experimental study and model validation. Desalination. 2022 Apr1;527:115524. https://doi.org/10.1016/j.desal.2021.115524.

2. Hosseinipour E, Davies PA. Effect of membrane properties on the performance of batch reverse osmosis (RO): The potential to minimize energy consumption. Desalination. 2024 May 18;577:117378. https://doi.org/10.1016/j.desal.2024.117378.

3. Hosseinipour E, Harris E, El Nazer HA, Mohamed YM, Davies PA. Desalination by batch reverse osmosis (RO) of brackish groundwater containing sparingly soluble salts. Desalination. 2023 Nov 15;566:116875. https://doi.org/10.1016/j.desal.2023.116875.

4.Hosseinipour E, Karimi S, Barbe S, Park K, Davies PA. Hybrid semi-batch/batch reverse osmosis (HSBRO) for use in zero liquid discharge (ZLD) applications. Desalination. 2022 Dec 15;544:116126. https://doi.org/10.1016/j.desal.2022.116126.

5. Karimi S, Engstler R, Hosseinipour E, Wagner M, Heinzler F, Piepenbrink M, Barbe S, Davies PA. High-pressure batch reverse osmosis (RO) for zero liquid discharge (ZLD) in a Cr (III) electroplating process. Desalination. 2024 Jul 1;580:117479. https://doi.org/10.1016/j.desal.2024.117479.

6. Hosseinipour E, Davies PA. Direct experimental comparison of batch reverse osmosis (RO) technologies. Desalination. 2024 Aug19; 583: 117717. https://doi.org/10.1016/j.desal.2024.117717.

7. Hosseinipour, Ebrahim, and Philip Davies. "Free-Piston Batch Reverse Osmosis (Ro): Modelling and Scale-Up." *Available at SSRN 4854851*.

To streamline this process, I have drafted a statement below outlining my contributions. I would be grateful if you could review the statement and confirm your agreement simply by responding to this email (e.g., by writing '*I confirm the accuracy of the author contribution statement below*'). Alternatively, if you feel any amendments are necessary, please feel free to adjust the text as you see fit.

Statement of Author Contribution

I, **Philip A. Davies**, confirm that **Ebrahim Hosseinipour** was the first author of the paper(s) above, on which I was a co-author. As the first author, Ebrahim was responsible for designing the study, conducting experiments, analyzing data, writing the manuscript, and addressing the reviewers' comments. He also ensured that all co-authors reviewed and approved the manuscript before publication.

Thank you for your support and collaboration.

Best regards,
Ebrahim Hosseinipour

- **Kiho Park**

From: 박기호 <kiho138@hanyang.ac.kr>
Sent: Thursday, August 8, 2024 4:25 PM
To: Ebrahim Hosseinipour (Engineering) <e.hosseinipour@bham.ac.uk>
Cc: Philip Davies (Civil Engineering) <p.a.davies@bham.ac.uk>
Subject: Re: Request for paper contribution statement

Dear Ebrahim,

I, **Kiho Park**, confirm that **Ebrahim Hosseinipour** was the first author of the paper(s) above, on which I was a co-author. As the first author, Ebrahim was responsible for designing the study, conducting experiments, analyzing data, writing the manuscript, and addressing the reviewers' comments. He also ensured that all co-authors reviewed and approved the manuscript before publication.

If you have any further questions and requests, please do not hesitate to contact me.

Kind regards
Kiho
PS.) Good luck!!

2024년 8월 8일 (목) 오후 10:00, Ebrahim Hosseinipour <e.hosseinipour@bham.ac.uk>님이 작성:

Dear Kiho,

As you may be aware, I am currently in the process of submitting my thesis for the Award of a PhD by Published Work at the University of Birmingham. As part of the formal submission requirements, I need to provide a statement from you confirming my contribution to our co-authored paper(s):

1. Hosseinipour E, Park K, Burlace L, Naughton T, Davies PA. A free-piston batch reverse osmosis (RO) system for brackish water desalination: Experimental study and model validation. Desalination. 2022 Apr 1;527:115524. https://doi.org/10.1016/j.desal.2021.115524.

2. Hosseinipour E, Karimi S, Barbe S, Park K, Davies PA. Hybrid semi-batch/batch reverse osmosis (HSBRO) for use in zero liquid discharge (ZLD) applications. Desalination. 2022 Dec 15;544:116126. https://doi.org/10.1016/j.desal.2022.116126.

To streamline this process, I have drafted a statement below outlining my contributions. I would be grateful if you could review the statement and confirm your agreement simply by responding to this email (e.g., by writing '*I confirm the accuracy of the author contribution statement below*'). Alternatively, if you feel any amendments are necessary, please feel free to adjust the text as you see fit.

Statement of Author Contribution

I, **Kiho Park**, confirm that **Ebrahim Hosseinipour** was the first author of the paper(s) above, on which I was a co-author. As the first author, Ebrahim was responsible for designing the study, conducting experiments, analyzing data, writing the manuscript, and addressing the reviewers' comments. He also ensured that all co-authors reviewed and approved the manuscript before publication.

Thank you for your support and collaboration.

Best regards,
Ebrahim Hosseinipour

- **Tim Naughton**

From: Tim Naughton <Tim.Naughton@salinitysolutions.co.uk>
Sent: Friday, August 9, 2024 9:34 AM
To: Ebrahim Hosseinipour (Engineering) <e.hosseinipour@bham.ac.uk>
Cc: Philip Davies (Civil Engineering) <p.a.davies@bham.ac.uk>
Subject: RE: Request for paper contribution statement

Hi Ebrahim,

Exiting times!

I, Tim Naughton, confirm that Ebrahim Hosseinipour was the first author of the paper above, on which I was a co-author. As the first author, Ebrahim was responsible for designing the study, conducting experiments, analyzing data, writing the manuscript, and addressing the reviewers' comments. He also ensured that all co-authors reviewed and approved the manuscript before publication.

If you need anything else let me know.

Kind regards,
Tim Naughton
Technical Director, Founder
+44 7770 858 420
Tim.Naughton@salinitysolutions.co.uk

From: Ebrahim Hosseinipour <e.hosseinipour@bham.ac.uk>
Sent: Thursday, August 8, 2024 2:00 PM
To: Tim Naughton <Tim.Naughton@salinitysolutions.co.uk>
Cc: Philip Davies (Civil Engineering) <p.a.davies@bham.ac.uk>
Subject: Request for paper contribution statement

Dear Tim,

As you may be aware, I am currently in the process of submitting my thesis for the Award of a PhD by Published Work at the University of Birmingham. As part of the formal submission requirements, I need to provide a statement from you confirming my contribution to our co-authored paper(s):

Hosseinipour E, Park K, Burlace L, Naughton T, Davies PA. A free-piston batch reverse osmosis (RO) system for brackish water desalination: Experimental study and model validation. Desalination. 2022 Apr 1;527:115524. https://doi.org/10.1016/j.desal.2021.115524.

To streamline this process, I have drafted a statement below outlining my contributions. I would be grateful if you could review the statement and confirm your agreement simply by responding to this email (e.g., by writing '*I confirm the accuracy of the author contribution statement below*'). Alternatively, if you feel any amendments are necessary, please feel free to adjust the text as you see fit.

Statement of Author Contribution

I, **Tim Naughton**, confirm that **Ebrahim Hosseinipour** was the first author of the paper above, on which I was a co-author. As the first author, Ebrahim was responsible for designing the study, conducting experiments, analyzing data, writing the manuscript, and addressing the reviewers' comments. He also ensured that all co-authors reviewed and approved the manuscript before publication.

Thank you for your support and collaboration.

Best regards,
Ebrahim Hosseinipour

- **Liam Burlace**

From: Liam Burlace <liam.burlace@salinitysolutions.co.uk>
Sent: Thursday, August 8, 2024 2:49 PM
To: Ebrahim Hosseinipour (Engineering) <e.hosseinipour@bham.ac.uk>
Cc: Philip Davies (Civil Engineering) <p.a.davies@bham.ac.uk>
Subject: RE: Request for paper contribution statement

Good afternoon Ebrahim,

Congrats on making it to this stage of the PhD process, I can confirm that your contribution described in the author contribution statement below to be completely accurate.

All the best with the final few steps.

Kind regards

Liam Burlace
Technology Manager
+44 7446 788760
liam.burlace@salinitysolutions.co.uk

From: Ebrahim Hosseinipour <e.hosseinipour@bham.ac.uk>
Sent: Thursday, August 8, 2024 2:00 PM
To: Liam Burlace <liam.burlace@salinitysolutions.co.uk>
Cc: Philip Davies (Civil Engineering) <p.a.davies@bham.ac.uk>
Subject: Request for paper contribution statement

Dear Liam,

As you may be aware, I am currently in the process of submitting my thesis for the Award of a PhD by Published Work at the University of Birmingham. As part of the formal submission requirements, I need to provide a statement from you confirming my contribution to our co-authored paper(s):

Hosseinipour E, Park K, Burlace L, Naughton T, Davies PA. A free-piston batch reverse osmosis (RO) system for brackish water desalination: Experimental study and model validation. Desalination. 2022 Apr 1;527:115524. https://doi.org/10.1016/j.desal.2021.115524.

To streamline this process, I have drafted a statement below outlining my contributions. I would be grateful if you could review the statement and confirm your agreement simply by responding to this email (e.g., by writing '*I confirm the accuracy of the author contribution statement below*'). Alternatively, if you feel any amendments are necessary, please feel free to adjust the text as you see fit.

Statement of Author Contribution

I, **Liam Burlace**, confirm that **Ebrahim Hosseinipour** was the first author of the paper above, on which I was a co-author. As the first author, Ebrahim was responsible for designing the study, conducting experiments, analyzing data, writing the manuscript, and addressing the reviewers' comments. He also ensured that all co-authors reviewed and approved the manuscript before publication.

Thank you for your support and collaboration.

Best regards,
Ebrahim Hosseinipour

- **Stephan Barbe**

From: Stéphan Barbe <stephan.barbe@th-koeln.de>
Sent: Friday, August 9, 2024 10:04 AM
To: Ebrahim Hosseinipour (Engineering) <e.hosseinipour@bham.ac.uk>
Cc: Philip Davies (Civil Engineering) <p.a.davies@bham.ac.uk>
Subject: Aw: Request for paper contribution statement

Dear Ebrahim,

I confirm the accuracy of the author contribution statement below.

Sincerely
Stéphan

>>> Ebrahim Hosseinipour <e.hosseinipour@bham.ac.uk> 09.08.2024, 09:00 >>>

Dear Stephan,

As you may be aware, I am currently in the process of submitting my thesis for the Award of a PhD by Published Work at the University of Birmingham. As part of the formal submission requirements, I need to provide a statement from you confirming my contribution to our co-authored paper(s):

1. Hosseinipour E, Karimi S, Barbe S, Park K, Davies PA. Hybrid semi-batch/batch reverse osmosis (HSBRO) for use in zero liquid discharge (ZLD) applications. Desalination. 2022 Dec 15;544:116126. https://doi.org/10.1016/j.desal.2022.116126.
2. Karimi S, Engstler R, Hosseinipour E, Wagner M, Heinzler F, Piepenbrink M, Barbe S, Davies PA. High-pressure batch reverse osmosis (RO) for zero liquid discharge (ZLD) in a Cr (III) electroplating process. Desalination. 2024 Jul 1;580:117479. https://doi.org/10.1016/j.desal.2024.117479.

To streamline this process, I have drafted a statement below outlining my contributions. I would be grateful if you could review the statement and confirm your agreement simply by responding to this email (e.g., by writing '*I confirm the accuracy of the author contribution statement below*'). Alternatively, if you feel any amendments are necessary, please feel free to adjust the text as you see fit.

Statement of Author Contribution

I, **Stephan Barbe**, confirm that **Ebrahim Hosseinipour** was the first author of paper 1 and second author of paper 2 above, on which I was a co-author. As the first and second author, Ebrahim was responsible for designing the study, conducting experiments, analyzing data, writing the manuscript, and addressing the reviewers' comments. He also ensured that all co-authors reviewed and approved the manuscript before publication.

Thank you for your support and collaboration.

Best regards,
Ebrahim Hosseinipour

- **Somayeh Karimi**

From: Somayeh Karimi (Civil Engineering) <s.karimi@bham.ac.uk>
Sent: Saturday, August 10, 2024 7:10 PM
To: Ebrahim Hosseinipour (Engineering) <e.hosseinipour@bham.ac.uk>

Cc: Philip Davies (Civil Engineering) <p.a.davies@bham.ac.uk>
Subject: Re: Request for paper contribution statement

Hi Ebrahim,

I confirm the accuracy of the author contribution statement below.

Best regards,
Somayeh

From: Ebrahim Hosseinipour (Engineering) <e.hosseinipour@bham.ac.uk>
Sent: Friday, August 9, 2024 10:30:00 AM
To: Somayeh Karimi (Civil Engineering) <s.karimi@bham.ac.uk>
Cc: Philip Davies (Civil Engineering) <p.a.davies@bham.ac.uk>
Subject: Request for paper contribution statement

Dear Somayeh,

As you may be aware, I am currently in the process of submitting my thesis for the Award of a PhD by Published Work at the University of Birmingham. As part of the formal submission requirements, I need to provide a statement from you confirming my contribution to our co-authored paper(s):

1. Hosseinipour E, Karimi S, Barbe S, Park K, Davies PA. Hybrid semi-batch/batch reverse osmosis (HSBRO) for use in zero liquid discharge (ZLD) applications. Desalination. 2022 Dec 15;544:116126. https://doi.org/10.1016/j.desal.2022.116126.

2. Karimi S, Engstler R, Hosseinipour E, Wagner M, Heinzler F, Piepenbrink M, Barbe S, Davies PA. High-pressure batch reverse osmosis (RO) for zero liquid discharge (ZLD) in a Cr (III) electroplating process. Desalination. 2024 Jul 1;580:117479. https://doi.org/10.1016/j.desal.2024.117479.

To streamline this process, I have drafted a statement below outlining my contributions. I would be grateful if you could review the statement and confirm your agreement simply by responding to this email (e.g., by writing '*I confirm the accuracy of the author contribution statement below*'). Alternatively, if you feel any amendments are necessary, please feel free to adjust the text as you see fit.

Statement of Author Contribution

I, **Somayeh Karimi**, confirm that **Ebrahim Hosseinipour** was the first author of paper 1 and the second author of paper 2 above, on which I was a co-author. As the first and second author, Ebrahim was responsible for designing the study, conducting experiments, analyzing data, writing the manuscript, and addressing the reviewers' comments. He also ensured that all co-authors reviewed and approved the manuscript before publication.

Thank you for your support and collaboration.

Best regards,
Ebrahim Hosseinipour

- **Roxanne Engstler**

From: Roxanne Engstler <roxanne.engstler@th-koeln.de>
Sent: Friday, August 9, 2024 10:37 AM
To: Ebrahim Hosseinipour (Engineering) <e.hosseinipour@bham.ac.uk>
Subject: RE: Request for paper contribution statement

Hello Ebrahim,

I confirm the accuracy of the author contribution statement below.

Best regards,
Roxanne Engstler.

M. Sc. Roxanne Engstler
Wissenschaftliche Mitarbeiterin
T: +49 214 32831 4719
E: roxanne.engstler@th-koeln.de

From: Ebrahim Hosseinipour <e.hosseinipour@bham.ac.uk>
Sent: Freitag, 9. August 2024 09:00
To: roxanne.engstler@th-koeln.de
Cc: Philip Davies <p.a.davies@bham.ac.uk>
Subject: Request for paper contribution statement

Dear Roxanne,

As you may be aware, I am currently in the process of submitting my thesis for the Award of a PhD by Published Work at the University of Birmingham. As part of the formal submission requirements, I need to provide a statement from you confirming my contribution to our co-authored paper(s):

Karimi S, Engstler R, Hosseinipour E, Wagner M, Heinzler F, Piepenbrink M, Barbe S, Davies PA. High-pressure batch reverse osmosis (RO) for zero liquid discharge (ZLD) in a Cr (III) electroplating process. Desalination. 2024 Jul 1;580:117479. https://doi.org/10.1016/j.desal.2024.117479.

To streamline this process, I have drafted a statement below outlining my contributions. I would be grateful if you could review the statement and confirm your agreement simply by responding to this email (e.g., by writing '*I confirm the accuracy of the author contribution*

statement below'). Alternatively, if you feel any amendments are necessary, please feel free to adjust the text as you see fit.

Statement of Author Contribution

I, **Roxanne Engstler**, confirm that **Ebrahim Hosseinipour** was a co-author of the paper above, on which I was a co-author as well. Ebrahim was responsible for assisting in the study design, conducting experiments, analyzing data, and writing the manuscript.

Thank you for your support and collaboration.

Best regards,
Ebrahim Hosseinipour

- **Felix Heinzler**

From: Heinzler Dr.-Ing. Felix A. <Felix.Heinzler@bia-group.com>
Sent: Friday, August 9, 2024 10:30 AM
To: Ebrahim Hosseinipour (Engineering) <e.hosseinipour@bham.ac.uk>
Subject: Re: Request for paper contribution statement

Good morning,

No Problem and as always an absolute pleasure working with you!

Statement of Author Contribution

I, **Felix Heinzler**, confirm that **Ebrahim Hosseinipour** was a co-author of the paper above, on which I was a co-author as well. Ebrahim was responsible for assisting in the study design, conducting experiments, analyzing data, and writing the manuscript.

Best regards,

Felix
Mit freundlichen Grüßen / Kind regards
i. V. Dr.-Ing. Felix A. Heinzler
Leitung Entwicklung und Prozesstechnik
Head of Development and Processing Technologies

Die Oberfläche

From: Ebrahim Hosseinipour <e.hosseinipour@bham.ac.uk>
Sent: Friday, August 9, 2024 9:00:00 AM

To: Heinzler Dr.-Ing. Felix A. <Felix.Heinzler@bia-group.com>
Cc: Philip Davies <p.a.davies@bham.ac.uk>
Subject: Request for paper contribution statement

Dear Felix,

As you may be aware, I am currently in the process of submitting my thesis for the Award of a PhD by Published Work at the University of Birmingham. As part of the formal submission requirements, I need to provide a statement from you confirming my contribution to our co-authored paper(s):

Karimi S, Engstler R, Hosseinipour E, Wagner M, Heinzler F, Piepenbrink M, Barbe S, Davies PA. High-pressure batch reverse osmosis (RO) for zero liquid discharge (ZLD) in a Cr (III) electroplating process. Desalination. 2024 Jul 1;580:117479. https://doi.org/10.1016/j.desal.2024.117479.

To streamline this process, I have drafted a statement below outlining my contributions. I would be grateful if you could review the statement and confirm your agreement simply by responding to this email (e.g., by writing '*I confirm the accuracy of the author contribution statement below*'). Alternatively, if you feel any amendments are necessary, please feel free to adjust the text as you see fit.

Statement of Author Contribution

I, **Felix Heinzler**, confirm that **Ebrahim Hosseinipour** was a co-author of the paper above, on which I was a co-author as well. Ebrahim was responsible for assisting in the study design, conducting experiments, analyzing data, and writing the manuscript.

Thank you for your support and collaboration.

Best regards,
Ebrahim Hosseinipour

- **Marc Piepenbrink**

From: Piepenbrink Marc <Marc.Piepenbrink@bia-group.com>
Sent: Friday, August 9, 2024 8:56 AM
To: Ebrahim Hosseinipour (Engineering) <e.hosseinipour@bham.ac.uk>
Subject: AW: Request for paper contribution statement

Hello Ebrahim,

herewith I confirm the accuracy of the author contribution statement below:

Karimi S, Engstler R, Hosseinipour E, Wagner M, Heinzler F, Piepenbrink M, Barbe S, Davies PA. High-pressure batch reverse osmosis (RO) for zero liquid discharge (ZLD) in a Cr (III) electroplating process. Desalination. 2024 Jul 1;580:117479. https://doi.org/10.1016/j.desal.2024.117479.

Statement of Author Contribution

I, **Marc Piepenbrink**, confirm that **Ebrahim Hosseinipour** was a co-author of the paper above, on which I was a co-author as well. Ebrahim was responsible for assisting in the study design, conducting experiments, analyzing data, and writing the manuscript.

Best regards and good luck for the Award,

Marc
Mit freundlichen Grüßen / Kind regards
i. A. Marc Piepenbrink
Entwicklung und Prozesstechnik
Development and Processing Technologies

Von: Ebrahim Hosseinipour <e.hosseinipour@bham.ac.uk>
Gesendet: Freitag, 9. August 2024 09:00
An: Piepenbrink Marc <Marc.Piepenbrink@bia-group.com>
Cc: Philip Davies <p.a.davies@bham.ac.uk>
Betreff: Request for paper contribution statement

Dear Mark,

As you may be aware, I am currently in the process of submitting my thesis for the Award of a PhD by Published Work at the University of Birmingham. As part of the formal submission requirements, I need to provide a statement from you confirming my contribution to our co-authored paper(s):

Karimi S, Engstler R, Hosseinipour E, Wagner M, Heinzler F, Piepenbrink M, Barbe S, Davies PA. High-pressure batch reverse osmosis (RO) for zero liquid discharge (ZLD) in a Cr (III) electroplating process. Desalination. 2024 Jul 1;580:117479. https://doi.org/10.1016/j.desal.2024.117479.

To streamline this process, I have drafted a statement below outlining my contributions. I would be grateful if you could review the statement and confirm your agreement simply by responding to this email (e.g., by writing '*I confirm the accuracy of the author contribution statement below*'). Alternatively, if you feel any amendments are necessary, please feel free to adjust the text as you see fit.

Statement of Author Contribution

I, **Marc Piepenbrink**, confirm that **Ebrahim Hosseinipour** was a co-author of the paper above, on which I was a co-author as well. Ebrahim was responsible for assisting in the study design, conducting experiments, analyzing data, and writing the manuscript.

Thank you for your support and collaboration.

Best regards,
Ebrahim Hosseinipour

- **Marvin Wagner**

From: Wagner Marvin <Marvin.Wagner@bia-group.com>
Sent: Monday, August 12, 2024 9:47 AM
To: Ebrahim Hosseinipour (Engineering) <e.hosseinipour@bham.ac.uk>
Cc: Philip Davies (Civil Engineering) <p.a.davies@bham.ac.uk>
Subject: AW: Request for paper contribution statement

Dear Ebrahim,

you're welcome, here's my statement of author contribution:

Karimi S, Engstler R, Hosseinipour E, Wagner M, Heinzler F, Piepenbrink M, Barbe S, Davies PA. High-pressure batch reverse osmosis (RO) for zero liquid discharge (ZLD) in a Cr (III) electroplating process. Desalination. 2024 Jul 1;580:117479. https://doi.org/10.1016/j.desal.2024.117479.

I, **Marvin Wagner**, confirm that **Ebrahim Hosseinipour** was a co-author of the paper above, on which I was a co-author as well. Ebrahim was responsible for assisting in the study design, conducting experiments, analyzing data, and writing the manuscript.

Mit freundlichen Grüßen / Kind regards
i. A. Marvin Wagner
Entwicklung und Prozesstechnik
Development and Processing Technologies

Die Oberfläche

Von: Ebrahim Hosseinipour <e.hosseinipour@bham.ac.uk>
Gesendet: Freitag, 9. August 2024 09:00
An: Wagner Marvin <Marvin.Wagner@bia-group.com>
Cc: Philip Davies <p.a.davies@bham.ac.uk>
Betreff: Request for paper contribution statement

Dear Marvin,

As you may be aware, I am currently in the process of submitting my thesis for the Award of a PhD by Published Work at the University of Birmingham. As part of the formal submission requirements, I need to provide a statement from you confirming my contribution to our co-authored paper(s):

Karimi S, Engstler R, Hosseinipour E, Wagner M, Heinzler F, Piepenbrink M, Barbe S, Davies PA. High-pressure batch reverse osmosis (RO) for zero liquid discharge (ZLD) in a Cr (III) electroplating process. Desalination. 2024 Jul 1;580:117479. https://doi.org/10.1016/j.desal.2024.117479.

To streamline this process, I have drafted a statement below outlining my contributions. I would be grateful if you could review the statement and confirm your agreement simply by responding to this email (e.g., by writing '*I confirm the accuracy of the author contribution statement below*'). Alternatively, if you feel any amendments are necessary, please feel free to adjust the text as you see fit.

Statement of Author Contribution

I, **Marvin Wagner**, confirm that **Ebrahim Hosseinipour** was a co-author of the paper above, on which I was a co-author as well. Ebrahim was responsible for assisting in the study design, conducting experiments, analyzing data, and writing the manuscript.

Thank you for your support and collaboration.

Best regards,
Ebrahim Hosseinipour

- **Ellie Harris**

From: Ellie Harris <ellie.a.harris@gmail.com>
Sent: Monday, August 12, 2024 9:55 AM
To: Ebrahim Hosseinipour (Engineering) <e.hosseinipour@bham.ac.uk>
Cc: Philip Davies (Civil Engineering) <p.a.davies@bham.ac.uk>
Subject: Re: Request for paper contribution statement

Dear Ebrahim,

I confirm the accuracy of the author contribution statement below.

I, **Ellie Harris**, confirm that **Ebrahim Hosseinipour** was the first author of the paper above, on which I was a co-author. As the first author, Ebrahim was responsible for designing the study, conducting experiments, analyzing data, writing the manuscript, and addressing the reviewers' comments. He also ensured that all co-authors reviewed and approved the manuscript before publication.

Kind regards,
Ellie

On Mon, Aug 12, 2024 at 9:52 AM Ebrahim Hosseinipour <e.hosseinipour@bham.ac.uk> wrote:

Dear Ellie,

I am currently in the process of submitting my thesis for the Award of a PhD by Published Work at the University of Birmingham. As part of the formal submission requirements, I need to provide a statement from you confirming my contribution to our co-authored paper(s):

Hosseinipour E, Harris E, El Nazer HA, Mohamed YM, Davies PA. Desalination by batch reverse osmosis (RO) of brackish groundwater containing sparingly soluble salts. Desalination. 2023 Nov 15;566:116875. https://doi.org/10.1016/j.desal.2023.116875.

To streamline this process, I have drafted a statement below outlining my contributions. I would be grateful if you could review the statement and confirm your agreement simply by responding to this email (e.g., by writing '*I confirm the accuracy of the author contribution statement below*'). Alternatively, if you feel any amendments are necessary, please feel free to adjust the text as you see fit.

Statement of Author Contribution

I, **Ellie Harris**, confirm that **Ebrahim Hosseinipour** was the first author of the paper above, on which I was a co-author. As the first author, Ebrahim was responsible for designing the study, conducting experiments, analyzing data, writing the manuscript, and addressing the reviewers' comments. He also ensured that all co-authors reviewed and approved the manuscript before publication.

Thank you for your support and collaboration.

Best regards,
Ebrahim Hosseinipour

- **Prof. Hosam El Nazer**

From: Dr hosam El Nazer <dr_hosamnazer@yahoo.com>
Sent: Monday, August 12, 2024 10:02 PM
To: Ebrahim Hosseinipour (Engineering) <e.hosseinipour@bham.ac.uk>
Cc: Philip Davies (Civil Engineering) <p.a.davies@bham.ac.uk>
Subject: Re: Request for paper contribution statement

Dear Ebrahim Hosseinipour

I hope everything is going well.
I enclose the required signed statement.

Best of Luck.
Statement of author contribution

I, **Prof Hosam El Nazer**, affirm that **Ebrahim Hosseinipour** served as the primary author of the above-mentioned article, in which I participated as a co-author. Ebrahim played a pivotal role in every stage of the research process. He was responsible for conceptualizing and

designing the study, developing the experimental protocols, and carrying out the necessary experiments. He meticulously analyzed the collected data, ensuring the integrity and accuracy of the results.

Ebrahim also took the lead in drafting the manuscript, synthesizing the findings into a coherent narrative, and articulating the significance of the research. Throughout the peer review process, he was diligent in addressing the reviewers' comments, making necessary revisions, and ensuring that the paper met the required standards for publication.

Furthermore, Ebrahim coordinated with all co-authors to review and provide feedback on the manuscript, ensuring that everyone was in agreement with the content and conclusions before the final submission. His leadership and dedication were instrumental in bringing the research to fruition and ensuring its successful publication.

Prof. Dr. Hossam El Nazer
Professor of Water Technology/Photocatalysis
Photochemistry Dept.
Chemical Industries Research Institute
National Research Centre,
33 El Bohouth St. (Former El-Tahrir st.)
Dokki-Giza - Egypt - P.O. 12622
Email: dr_hosamnazer@yahoo.com ,
he.abdelfattah@nrc.sci.eg
Tel: (002) 0122 7331952

On Sunday, August 11, 2024 at 10:00:28 AM GMT+3, Ebrahim Hosseinipour <e.hosseinipour@bham.ac.uk> wrote:

Dear Prof. El Nazer,

I am currently in the process of submitting my thesis for the Award of a PhD by Published Work at the University of Birmingham. As part of the formal submission requirements, I need to provide a statement from you confirming my contribution to our co-authored paper(s):

Hosseinipour E, Harris E, El Nazer HA, Mohamed YM, Davies PA. Desalination by batch reverse osmosis (RO) of brackish groundwater containing sparingly soluble salts. Desalination. 2023 Nov 15;566:116875. https://doi.org/10.1016/j.desal.2023.116875.

To streamline this process, I have drafted a statement below outlining my contributions. I would be grateful if you could review the statement and confirm your agreement simply by responding to this email (e.g., by writing '*I confirm the accuracy of the author contribution statement below*'). Alternatively, if you feel any amendments are necessary, please feel free to adjust the text as you see fit.

Statement of Author Contribution

I, **Hosam El Nazer**, confirm that **Ebrahim Hosseinipour** was the first author of the paper above, on which I was a co-author. As the first author, Ebrahim was responsible for designing the study, conducting experiments, analyzing data, writing the manuscript, and addressing the reviewers' comments. He also ensured that all co-authors reviewed and approved the manuscript before publication.

Thank you for your support and collaboration.

Best regards,
Ebrahim Hosseinipour

- **Prof. Yasser Mahmoud A. Mohamed**

From: Yasser Mahmoud <y.m.a.mohamed@outlook.com>
Sent: Wednesday, August 14, 2024 7:23 AM
To: Ebrahim Hosseinipour (Engineering) <e.hosseinipour@bham.ac.uk>
Subject: Re: Request for paper contribution statement

Dear Dr. Ebrahim Hosseinipour,

Based on your request for signing statement of author contribution, please find the attached file.
Thanks for cooperation,

Best regards
Yasser

Attached file

"To whom it may concern"

Statement of Author Contribution

Concerning published article that have been cited as follows: Hosseinipour E, Harris E, El Nazer HA, Mohamed YM, Davies PA. "Desalination by batch reverse osmosis (RO) of brackish groundwater containing sparingly soluble salts." Desalination. 2023 Nov 15; 566: 116875. https://doi.org/10.1016/j.desal.2023.116875.

I, **Prof. Dr. Yasser Mahmoud A. Mohamed**, confirm that **Ebrahim Hosseinipour** was the first author of the paper above mentioned article, on which I was a co-author. As the first author, Ebrahim was responsible for designing the research study, conducting experiments, interpreting data, writing the manuscript, and addressing on the reviewers' comments. He also ensured that all co-authors had reviewed and approved the manuscript before publication.

Sincerely yours,

Prof. Dr. Yasser M. A. Mohamed

Yasser M. A. Mohamed
Professor
Photochemistry Department
Chemical Industries Research Insistitute
National Research Centre
El-Tahrir Street, Dokki, Giza
P. O. 12622

Egypt
Mobile number: 002-01009550514
E-mail: y.m.a.mohamed@outlook.com
https://scholar.google.com/citations?user=GGchnsgAAAAJ&hl=en

From: Ebrahim Hosseinipour <e.hosseinipour@bham.ac.uk>
Sent: Sunday, August 11, 2024 7:00 AM
To: y.m.a.mohamed@outlook.com <y.m.a.mohamed@outlook.com>
Cc: Philip Davies <p.a.davies@bham.ac.uk>
Subject: Request for paper contribution statement

Dear Prof. Mohamed,

I am currently in the process of submitting my thesis for the Award of a PhD by Published Work at the University of Birmingham. As part of the formal submission requirements, I need to provide a statement from you confirming my contribution to our co-authored paper(s):

Hosseinipour E, Harris E, El Nazer HA, Mohamed YM, Davies PA. Desalination by batch reverse osmosis (RO) of brackish groundwater containing sparingly soluble salts. Desalination. 2023 Nov 15;566:116875. https://doi.org/10.1016/j.desal.2023.116875.

To streamline this process, I have drafted a statement below outlining my contributions. I would be grateful if you could review the statement and confirm your agreement simply by responding to this email (e.g., by writing '*I confirm the accuracy of the author contribution statement below*'). Alternatively, if you feel any amendments are necessary, please feel free to adjust the text as you see fit.

Statement of Author Contribution

I, **Yasser Mahmoud A. Mohamed**, confirm that **Ebrahim Hosseinipour** was the first author of the paper above, on which I was a co-author. As the first author, Ebrahim was responsible for designing the study, conducting experiments, analyzing data, writing the manuscript, and addressing the reviewers' comments. He also ensured that all co-authors reviewed and approved the manuscript before publication.

Thank you for your support and collaboration.

Best regards,
Ebrahim Hosseinipour